NANOPARTICLE-MEDIATED SIGNALING REWIRING AND REPROGRAMMING OF IMMUNE RESPONSES

EDITED BY: David Pozo and Francisco Javier Quintana
PUBLISHED IN: Frontiers in Immunology

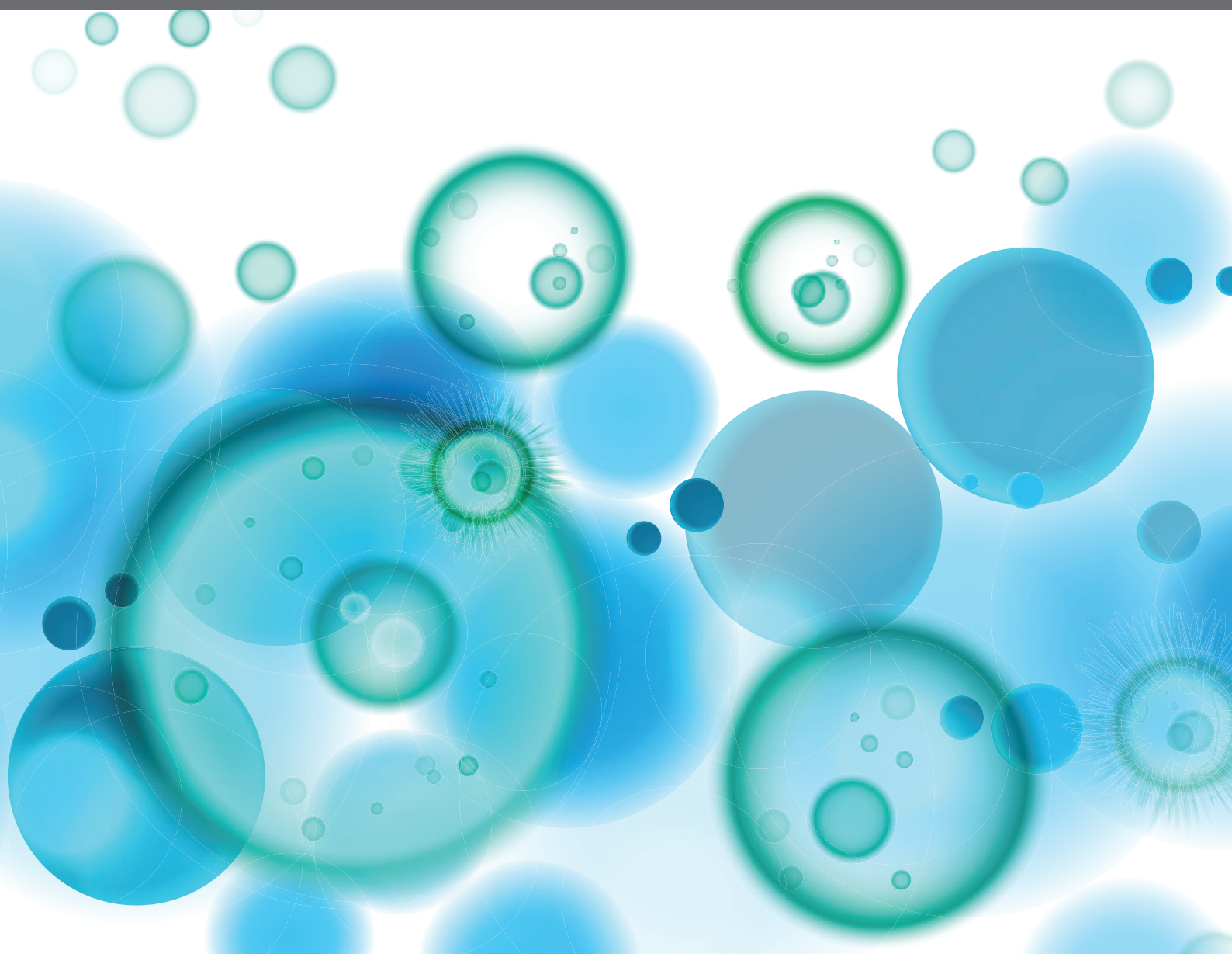

frontiers Research Topics

ISSN 1664-8714
ISBN 978-2-88976-318-4
DOI 10.3389/978-2-88976-318-4

About Frontiers

Frontiers is more than just an open-access publisher of scholarly articles: it is a pioneering approach to the world of academia, radically improving the way scholarly research is managed. The grand vision of Frontiers is a world where all people have an equal opportunity to seek, share and generate knowledge. Frontiers provides immediate and permanent online open access to all its publications, but this alone is not enough to realize our grand goals.

Frontiers Journal Series

The Frontiers Journal Series is a multi-tier and interdisciplinary set of open-access, online journals, promising a paradigm shift from the current review, selection and dissemination processes in academic publishing. All Frontiers journals are driven by researchers for researchers; therefore, they constitute a service to the scholarly community. At the same time, the Frontiers Journal Series operates on a revolutionary invention, the tiered publishing system, initially addressing specific communities of scholars, and gradually climbing up to broader public understanding, thus serving the interests of the lay society, too.

Dedication to Quality

Each Frontiers article is a landmark of the highest quality, thanks to genuinely collaborative interactions between authors and review editors, who include some of the world's best academicians. Research must be certified by peers before entering a stream of knowledge that may eventually reach the public - and shape society; therefore, Frontiers only applies the most rigorous and unbiased reviews.
Frontiers revolutionizes research publishing by freely delivering the most outstanding research, evaluated with no bias from both the academic and social point of view. By applying the most advanced information technologies, Frontiers is catapulting scholarly publishing into a new generation.

What are Frontiers Research Topics?

Frontiers Research Topics are very popular trademarks of the Frontiers Journals Series: they are collections of at least ten articles, all centered on a particular subject. With their unique mix of varied contributions from Original Research to Review Articles, Frontiers Research Topics unify the most influential researchers, the latest key findings and historical advances in a hot research area! Find out more on how to host your own Frontiers Research Topic or contribute to one as an author by contacting the Frontiers Editorial Office: frontiersin.org/about/contact

NANOPARTICLE-MEDIATED SIGNALING REWIRING AND REPROGRAMMING OF IMMUNE RESPONSES

Topic Editors:
David Pozo, University of Seville, Spain
Francisco Javier Quintana, Harvard Medical School, United States

Dr. Quintana is the founder of AnTolRx. The other Topic Editor declares no competing interests.

Citation: Pozo, D., Quintana, F. J., eds. (2022). Nanoparticle-Mediated Signaling Rewiring and Reprogramming of Immune Responses. Lausanne: Frontiers Media SA. doi: 10.3389/978-2-88976-318-4

Table of Contents

frontiers | Frontiers in Immunology

EDITORIAL
published: 12 May 2022
doi: 10.3389/fimmu.2022.927733

Editorial: Nanoparticle-Mediated Signaling Rewiring and Reprogramming of Immune Responses

Francisco J. Quintana[1,2]* *and David Pozo*[3,4]*

[1] Ann Romney Center for Neurologic Diseases, Brigham and Women's Hospital, Harvard Medical School, Boston, MA, United States, [2] Broad Institute of Massachusetts Institute of Technology (MIT) and Harvard, Cambridge, MA, United States, [3] Department of Medical Biochemistry, Molecular Biology and Immunology, The University of Seville School of Medicine, Seville, Spain, [4] CABIMER-Andalusian Center for Molecular Biology and Regenerative Medicine, Seville-University Pablo de Olavide (UPO)-University of Seville-Consejo Superior de Investigaciones Científicas (CSIC), Seville, Spain

Keywords: cell signalling, autoimmunity, inflammation, reprogramming, personalized medicine, immunotherapy, nanoparticles, immunoregulation

Editorial on the Research Topic

Nanoparticle-Mediated Signaling Rewiring and Reprogramming of Immune Responses

Recent advances on the molecular mechanisms that control immune cells are at the core of the development of better immunomodulatory therapies. For example, these mechanisms may enable T cell manipulation interventions to treat and prevent autoimmune disease by rewiring T cells towards an anti-inflammatory phenotype. Indeed, it has been recently reported that metabolic sensing in immune cells is coupled to signal transduction pathways that control cell fate. These phenomena have been linked to the onset and/or progression of several diseases such as multiple sclerosis, rheumatoid arthritis, diabetes or Alzheimer's disease, and also exploited therapeutically to develop cancer immunotherapies (1–4). Unifying our understanding of the molecular pathways that control the immune response might identify novel efficacious interventions to reprogram immune cells for therapeutic purposes in diseases associated with immune dysregulation. However, two important challenges limit the clinical translation of our current knowledge on the regulation of the immune response by small molecules which could provide the basis for novel immunotherapeutic drugs. First, the absence of mechanisms to control the specificity of these reprogramming approaches, resulting in off-target effects. Second, limitations associated to the short half-life and/or low bioavailability of immune-modulatory small molecules.

Nanomaterial-based approaches offer a platform for novel immunotherapeutic approaches. In this sense, nanoparticle (NP) delivery systems are gaining momentum because they allow the development of precision-based medicines for the reprogramming and dynamic rewiring of signalling pathways in immune cells. Even without a well-defined cell-targeting strategy, several studies have shown the feasibility of reprogramming inflammatory immune cells after i.v administration of different nanoparticles based only on their physical properties (5–7). For example, it is possible to differentially reprogram immune cells to favor their homing to injured locations to promote neuroprotection or to reduce their recruitment to inflamed areas and limit immunopathology. Immune-reprogramming NPs have been shown to redirect suppressive macrophages to act as anti-tumor effector cells, and without the described side-effects linked to checkpoint inhibitors. Indeed, several clinical trials are underway to bring immune-reprogramming NPs to patients and there is a critical mass of proof-of-concept studies on

OPEN ACCESS

Edited and reviewed by:
Francesca Granucci,
University of Milano-Bicocca, Italy

***Correspondence:**
Francisco J. Quintana
fquintana@bwh.harvard.edu
David Pozo
david.pozo@cabimer.es

Specialty section:
This article was submitted to Molecular Innate Immunity, a section of the journal Frontiers in Immunology

Received: *24 April 2022*
Accepted: *26 April 2022*
Published: *12 May 2022*

Citation:
Quintana FJ and Pozo D (2022) Editorial: Nanoparticle-Mediated Signaling Rewiring and Reprogramming of Immune Responses. Front. Immunol. 13:927733. doi: 10.3389/fimmu.2022.927733

nanoparticles tailored with different biological and chemical strategies to modify the response of immune cells (8, 9). Also, NP reprogramming of macrophages and T-cell mediated responses is having a major impact on the development of new methods for cancer immunotherapy (10, 11). In this Research Topic, we have gathered articles covering novel and significant aspects about the connection between NPs and functional immune responses, providing a series of updated and insightful views of the potential mechanisms involved. More specifically, we have arranged this special issue into three broad subjects, as follows: (A) NP-based reprogramming to promote infection resolution. (B) NP-based reprogramming in cancer immunotherapy; (C) NP-based reprogramming of immune memory.

NP-BASED REPROGRAMMING TO PROMOTE INFECTION RESOLUTION

Beyond the bactericidal or bacteriostatic effects that were described in the early days of nanomedicine, an interesting field of research is related to the long-term effect of NP exposure on trained innate immunity (12, 13). Swartzwelter et al. report how gold nanoparticles (AuNPs) loaded with different microbial molecules differentially reprogram macrophage responses which downregulate or exacerbate innate immune memory. Although the molecular mechanisms underlying how AuNPs modulate innate memory are unknown, it appears to be defined by the pathogenic agent and the individual's immune history, independently of the primary response elicited by AuNPs. An often understudied issue is the linking of initiation, progression and resolution of inflammation with the effect of NPs on functional responses by macrophages. Sun et al. describe a tryptophan-containing hexapeptide-coated AuNP with opposite immunomodulatory activities in resting and TLR-stimulated macrophages, targeting NF-κB or IRAK downstream signalling, respectively. Korshoj et al. provide an insightful review on how to tackle chronic infections in the central nervous system by modulating macrophage/microglia polarization using different NP platforms. Finally, Ernst and Puntes comment on the role of oxidative metabolism in macrophage function and the potential of regulatory interventions trough cerium oxide NPs. Interestingly, it is worth mentioning that inorganic or metallic core NPs are attracting more attention compared to the reluctance they triggered a few years ago because of their potential toxicity.

NP-BASED REPROGRAMMING IN CANCER IMMUNOTHERAPY

The review by Mulens-Arias et al. provides a comprehensive account of our current understanding on the effects of Iron Oxide Nanoparticles (IONPs) on macrophage reprogramming in the tumour microenvironment, including effects on the interactions between malignant and non-transformed cells. Garland et al. explore the capacity of cytosolic double-stranded DNA to promote antitumor immunity by activating the cytosolic DNA sensor cyclic-GMP-AMP synthase (cGAS) and its downstream effector, stimulator of interferon genes (STING), which drive the production of type I interferons and other inflammatory cytokines. A major bottleneck to activate the cGAS/STING cytosolic pathway with double-stranded DNA is the combination of both deoxyribonuclease activity and endosomal escape, which forced the development of direct STING activators. To overcome the limitation of a non-physiological stimulation of cGAS-STING signaling, Garland et al. identified in a DNA library screening a DNA-based polymeric nanoparticle with enhanced features in terms of stability and functional activation of the cGAS-STING pathway. *In vitro* and *in vivo* experiments demonstrated the feasibility of directly targeting cGAS to reprogram macrophages in tumors, opening new venues for cancer immunotherapy. Alongside, Dey et al. provide further information on the impact of nucleic acid cargo in cationic lipid-based delivery systems aimed to induce macrophage and dendritic cell modulation. Finally, Makhijani and McGaha review the role of exosomes in myeloid immune cells. These nano-sized vesicles of endosomal origin (30-150 nm in diameter) are the smallest type of extracellular vesicles, whose role in cancer immunology and inflammatory/autoimmune diseases has only recently started to be fully appreciated.

NP-BASED REPROGRAMMING IN ADAPTIVE IMMUNE MEMORY

The review by Solé and Santamaría focuses on the reprogramming capabilities of NPs to generate antigen-specific T-regulatory type 1 (Tr1)-like cells. They pay special attention to Tr1-like cell heterogeneity and its potential molecular characterization. By using dendritic mesoporous silica nanoparticles, An et al. report the synthesis and characterization of a peptide-based delivery platform as a vaccination strategy towards foot-and-mouth disease virus. Also in the field of modified platforms for new vaccination strategies, Feola et al. exploit oncolytic viruses as *in situ* cancer vaccines. In this work, they developed an alternative approach to generate oncolytic adenovirus functionalised with tumour antigens in order to obtain sustained T cell responses while avoiding non-scalable procedures.

AUTHOR CONTRIBUTIONS

Authors listed have made a direct and intellectual contribution to the editorial and approved for publication.

FUNDING

DP is supported by the Regional Ministry of Transformación Económica, Industria, Conocimiento y Universidades, PAID2020, CTS677 to DP) and the Spanish Government Ministry of Science and Innovation of Spain [RTI2018-098432-B-I00, co-funded by the European Regional Development Fund (ERDF), a way to build Europe]. FQ is supported by the National Institutes of Health, the Progressive Multiple Sclerosis Alliance and the National Multiple Sclerosis Society.

REFERENCES

1. Heim CE, Bosch ME, Yamada KJ, Aldrich AL, Chaudhari SS, Klinkebiel D, et al. Lactate Production by Staphylococcus Aureus Biofilm Inhibits HDAC11 to Reprogramme the Host Immune Response During Persistent Infection. *Nat Microbiol* (2020) 5:1271–84. doi: 10.1038/S41564-020-0756-3
2. Leal-Lasarte M, Mannini B, Chiti F, Vendruscolo M, Dobson CM, Roodveldt C, et al. Distinct Responses of Human Peripheral Blood Cells to Different Misfolded Protein Oligomers. *Immunology* (2021) 164:358–71. doi: 10.1111/imm.13377
3. Lee HG, Wheeler MA, Quintana FJ. Function and Therapeutic Value of Astrocytes in Neurological Diseases. *Nat Rev Drug Discov* (2022) 21: 339–58. doi: 10.1038/S41573-022-00390-X
4. Serra P, Santamaria P. Antigen-Specific Therapeutic Approaches for Autoimmunity. *Nat Biotechnol* (2019) 37:238–51. doi: 10.1038/s41587-019-0015-4
5. Park J, Zhang Y, Saito E, Gurczynski SJ, Moore BB, Cummings BJ, et al. Intravascular Innate Immune Cells Reprogrammed *via* Intravenous Nanoparticles to Promote Functional Recovery After Spinal Cord Injury. *Proc Natl Acad Sci USA* (2019) 116:14947–54. doi: 10.1073/PNAS.1820276116
6. Yeste A, Takenaka MC, Mascanfroni ID, Nadeau M, Kenison JE, Patel B, et al. Tolerogenic Nanoparticles Inhibit T Cell-Mediated Autoimmunity Through SOCS2. *Sci Signal* (2016) 9(433):ra61. doi: 10.1126/SCISIGNAL.AAD0612
7. Kenison JE, Jhaveri A, Li Z, Khadse N, Tjon E, Tezza S, et al. Tolerogenic Nanoparticles Suppress Central Nervous System Inflammation. *Proc Natl Acad Sci USA* (2020) 117:32017–28. doi: 10.1073/PNAS.2016451117
8. Shemesh CS, Hsu JC, Hosseini I, Shen BQ, Rotte A, Twomey P, et al. Personalized Cancer Vaccines: Clinical Landscape, Challenges, and Opportunities. *Mol Ther* (2021) 29:555–70. doi: 10.1016/J.YMTHE.2020.09.038
9. Wang N, Wang S, Wang X, Zheng Y, Yang B, Zhang J, et al. Research Trends in Pharmacological Modulation of Tumor-Associated Macrophages. *Clin Transl Med* (2021) 11:e288. doi: 10.1002/CTM2.288
10. Wang H, Najibi AJ, Sobral MC, Seo BR, Lee JY, Wu D, et al. Biomaterial-Based Scaffold for *In Situ* Chemo-Immunotherapy to Treat Poorly Immunogenic Tumors. *Nat Commun* (2020) 11(1):5696. doi: 10.1038/S41467-020-19540-Z
11. Krienke C, Kolb L, Diken E, Streuber M, Kirchhoff S, Bukur T, et al. A Noninflammatory mRNA Vaccine for Treatment of Experimental Autoimmune Encephalomyelitis. *Science* (2021) 371:145–53. doi: 10.1126/SCIENCE.AAY3638
12. Swartzwelter BJ, Fux AC, Johnson L, Swart E, Hofer S, Hofstätter N, et al. The Impact of Nanoparticles on Innate Immune Activation by Live Bacteria. *Int J Mol Sci* (2020) 21:1–22. doi: 10.3390/IJMS21249695
13. Italiani P, della Camera G, Boraschi D. Induction of Innate Immune Memory by Engineered Nanoparticles in Monocytes/Macrophages: From Hypothesis to Reality. *Front Immunol* (2020) 11:566309. doi: 10.3389/FIMMU.2020.566309

Conflict of Interest: The authors declare that the research was conducted in the absence of any commercial or financial relationships that could be construed as a potential conflict of interest.

frontiers in Immunology

REVIEW
published: 09 June 2021
doi: 10.3389/fimmu.2021.693709

The Use of Iron Oxide Nanoparticles to Reprogram Macrophage Responses and the Immunological Tumor Microenvironment

Vladimir Mulens-Arias[1], *José Manuel Rojas*[2] *and Domingo F. Barber*[1]*

[1] Department of Immunology and Oncology, and NanoBiomedicine Initiative, Centro Nacional de Biotecnología (CNB)-CSIC, Madrid, Spain, [2] Centro de Investigación en Sanidad Animal, Centro Nacional Instituto de Investigación y Tecnología Agraria y Alimentaria (CISA-INIA)-CSIC, Valdeolmos, Madrid, Spain

The synthesis and functionalization of iron oxide nanoparticles (IONPs) is versatile, which has enhanced the interest in studying them as theranostic agents over recent years. As IONPs begin to be used for different biomedical applications, it is important to know how they affect the immune system and its different cell types, especially their interaction with the macrophages that are involved in their clearance. How immune cells respond to therapeutic interventions can condition the systemic and local tissue response, and hence, the final therapeutic outcome. Thus, it is fundamental to understand the effects that IONPs have on the immune response, especially in cancer immunotherapy. The biological effects of IONPs may be the result of intrinsic features of their iron oxide core, inducing reactive oxygen species (ROS) and modulating intracellular redox and iron metabolism. Alternatively, their effects are driven by the nanoparticle coating, for example, through cell membrane receptor engagement. Indeed, exploiting these properties of IONPs could lead to the development of innovative therapies. In this review, after a presentation of the elements that make up the tumor immunological microenvironment, we will review and discuss what is currently known about the immunomodulatory mechanisms triggered by IONPs, mainly focusing on macrophage polarization and reprogramming. Consequently, we will discuss the implications of these findings in the context of plausible therapeutic scenarios for cancer immunotherapy.

Keywords: iron oxide nanoparticles, nanoparticle–macrophage interaction, macrophage polarization, tumor associated macrophages, therapeutic applications

OPEN ACCESS

Edited by:
David Pozo,
University of Seville, Spain

Reviewed by:
Diana Caballero-Hernández,
Universidad Autónoma de Nuevo León, Mexico
Ceren Ciraci,
Istanbul Technical University, Turkey

***Correspondence:**
Domingo F. Barber
dfbarber@cnb.csic.es

Specialty section:
This article was submitted to Molecular Innate Immunity, a section of the journal Frontiers in Immunology

Received: *11 April 2021*
Accepted: *24 May 2021*
Published: *09 June 2021*

Citation:
Mulens-Arias V, Rojas JM and Barber DF (2021) The Use of Iron Oxide Nanoparticles to Reprogram Macrophage Responses and the Immunological Tumor Microenvironment. Front. Immunol. 12:693709. doi: 10.3389/fimmu.2021.693709

INTRODUCTION

The highly innovative field of nanotheranostics has been expanding now for more than two decades, with easy-to-scale nanomaterials emerging as potential candidates to treat a variety of pathologies, such as cancer (1–4), autoimmune diseases (5, 6) or neurodegenerative disorders (7, 8). The therapeutic interest in nanomaterials, and particularly in nanoparticles, is in part kindled by the chemical and physical versatility of these materials. Nanoparticles can be functionalized with targeting moieties (9) or drugs (10), and their surface can be built for specific biomolecule release using molecular domains responsive to stimuli like pH (11, 12) or reactive oxygen species (ROS (13,

14). In addition, they also possess physical properties associated with their core that can be exploited, such as magnetism (15) and plasmon coupling (16).

Iron oxide nanoparticles (IONPs) are of particular therapeutic interest due to their magnetic properties and their flexibility for surface functionalization. IONPs have been used as contrast agents and as heat-inducers through the application of an external magnetic field (17, 18). Their versatility in terms of surface functionalization means they can target diverse molecules and they can be used to ensure the correct localized delivery of different cargos, such as drugs, RNAs, cytokines or antibodies (15). Importantly, IONPs also exhibit intrinsic biological activity in cellular systems, including the immune system, which can be exploited to broaden their therapeutic potential. This review will first outline the main characteristics of the tumor microenvironment (TME), emphasizing the influence of tumor-associated macrophages (TAMs), and subsequently, we will address the impact that IONPs have on macrophage reprogramming and the implications of this for cancer immunotherapy.

IMMUNOLOGICAL TUMOR MICROENVIRONMENT

Cancer is a complex and heterogeneous disease that involves the dysregulation of various cell processes, such as metabolism (19), proliferation (20), intracellular pH dynamics (21), redox signaling (22), and migration/invasion (23, 24). The complexity of this disease is also reflected by the different ecosystems that constitute a permissive TME (25, 26). A close inspection of the TME reveals a network of cellular and non-cellular components that provide the signals that control tumor cell survival, proliferation, angiogenesis, immune evasion and metastasis. We can divide the TME landscape into three ecosystems: 1) the cellular compartment; 2) the soluble factors; and 3) the extracellular matrix (ECM: **Figure 1** and **Table 1**). The tumor niche is a very dynamic 3D structure in which stromal cells play a crucial role in regulating different stages of tumor development and in which there is also an intricate interplay among these cells. The TME cell ecosystem also includes a

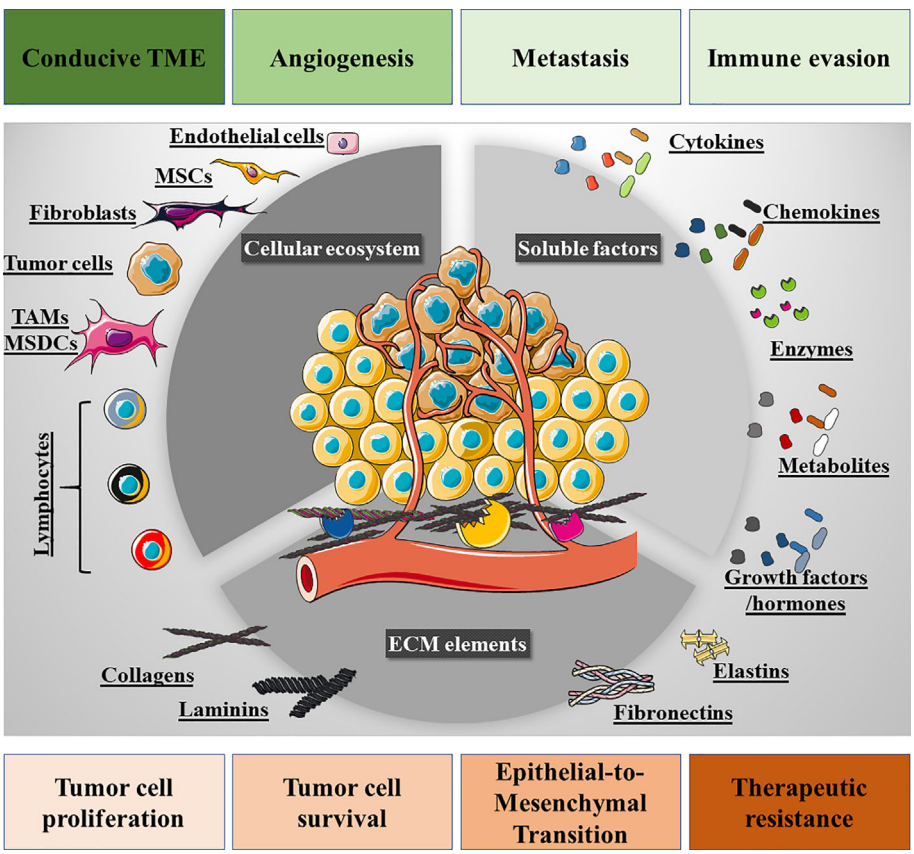

FIGURE 1 | Overview of the tumor microenvironment (TME). Three ecosystems contribute to the TME: firstly, the cellular ecosystem that is composed of immune cells (lymphoid and myeloid), fibroblasts, mesenchymal stem cells (MSCs), pericytes, endothelial cells, and tumor cells. Secondly, the cell-to-cell membrane interactions and soluble secreted factors that participate in the intricate interplay among these cells, *e.g.*, cytokines, chemokines, growth factors, hormones, proteolytic enzymes, and metabolites. Thirdly, the extracellular matrix (ECM) bed on which the cellular ecosystem resides, also providing biological signals to the tumor and stromal cells through ECM-derived peptides and the structural domains of its proteins. The interplay of these signaling networks and ecosystems promotes tumor cell proliferation, survival, epithelial-to-mesenchymal transition, drug resistance and loco-regional modulation, such that the TME is conducive to tumor cell invasion and metastatic spreading, angiogenesis and immune cell evasion.

TABLE 1 | Examples of TME ecosystems and their implications in the progression of three significant cancers: breast, lung and colorectal.

Tumor	Component	Implications
Breast tumors	Cancer-associated fibroblasts (CAFs)	Tumor invasion through stromatogenesis (27) Tumor EMT through TGF-β1 (28, 29) Self-renewal of breast cancer stem cells (30) Tumor progression through growth factors, e.g., SDF-1 (31), FGF-β (32) Tumor progression through cytokines and chemokines, e.g., CXCL14 (33), CXCL16 (34), IL-4 & IL-6 (35), IL-33 (36)
Breast tumors	Mesenchymal stem cells (MSCs)	Immunosuppression through the CCL5/PD-L1 axis (37) Enhanced tumor progression through CCL5 and IL-6 (38)
Lung tumors	CAFs	Chemoresistance through upregulation of TNFSF4 (39) and/or ANXA3 (40) Immunosuppression by modulating TIM (41) Enhanced growth and invasion through VCAM-1 secretion (42) and induction of PD-L1 (43)
Colorectal cancers	CAFs	Enhanced metastasis through HGF (44) Chemoresistance through exosomal lncRNA H19 (45) Enhanced tumor cell migration/invasion through Wnt2 (46), IL-33 (47), CLEC3B (48) and/or SNAIL-1 (49)
Colorectal cancers	Pericytes	Enhanced tumor cell invasion through the TGF-β1/IGFBP-3 axis (50)
Colorectal cancers	MSCs	Enhanced tumor progression through IL-8 (51), TGF-β1/CXCR4 (52), CCL5/β-catetin/Slug (53)

plethora of non-immune stromal cell types, such as cancer-associated fibroblasts (CAFs (54), mesenchymal stem cells (MSCs), pericytes, adipocytes, endothelial and vascular cells. Notably, these cells exhibit a high degree of plasticity and they may originate through trans-differentiation. For instance, breast cancer CAFs may stem from resident fibroblasts, from breast epithelial cells *via* the epithelial-to-mesenchymal transition (EMT) or from pericytes in the perivascular niche (55, 56). CAFs may also be derived from bone marrow-derived mesenchymal stem cells (BM-MSCs), as PDGFR-α^-, $CD45^-$, $CD34^-$ BM-MSCs are recruited into primary breast tumors to differentiate into α-SMA^+, PDGFR-α^-, $CD45^-$, $CD34^-$ CAFs (57). This fact highlights the complex transcriptional reprogramming that many stromal cells go through, suggesting that the cellular ecosystem in the TME is in constant transcriptional flux (58, 59). Indeed, this dynamic transcriptional program is likely to constantly redefine the immunological landscape of the TME.

The TME is also comprised of tumor-infiltrating immune cells, both innate immune cells (monocytes, macrophages, and NK cells) and adaptive immune cells (T and B cells), that define the tumor immune microenvironment (TIME). Dynamic communication takes place within this ecosystem that are mediated by cell-to-cell contacts and cell-derived soluble factors. The intermediates derived from stromal and tumor cells, such as cytokines, chemokines, and ROS, promote immune evasion by inducing $CD8^+$ T cell anergy/exhaustion, T regulatory (Tregs) cells, suppressor dendritic cells (DCs), and M2 macrophage differentiation (60). As a result, tumors escape immune surveillance and they adopt a metastatic phenotype through modulation of the EMT, enhanced angiogenesis and ECM degradation.

The non-cellular TME network is comprised of ECM components [*e.g.*, collagens (61), fibronectin (62), elastin (63), and laminin (64)], and soluble cellular derivatives [*e.g.*, cytokines, chemokines (65), hormones (66), metabolites (67, 68) and growth factors (69)]. This non-cellular network is responsible for cell-to-cell crosstalk, ultimately shaping the pro-malignant environment.

However, the immunological landscape within the TME has emerged as a crucial variable for cancer progression and treatment, and understanding the TIME has become a critical step in designing efficient immunotherapies for cancer. Indeed, the TIME defines the prognosis of cancer patients (70, 71) and their therapeutic response to immunotherapies like checkpoint inhibitors (72, 73), T-cell transfer (74), or therapeutic vaccines (75). Driven by tumor cell plasticity, the TIME is a dynamic system where diverse innate and adaptive immune cells co-exist, continually changing over time in response to the reprogramming of tumor cell transcription (**Figure 2**). To better comprehend the TIME's influence on cancer prognosis, the TIME can be divided into the T cell-inflammatory microenvironment and non-T cell-inflammatory microenvironment. The first of these is characterized by the infiltration of T cell subsets and macrophages, whereas the second is mainly composed of TAMs. Of all immune cells, TAMs play a pivotal role in defining the tumor immunological landscape and thus, they have been the target of various therapeutic approaches.

Immunosuppressive Tumor-Associated Macrophages

TAMs are tumor-enriched immunosuppressor cells that exert a pivotal influence on tumor progression and metastasis. Since their first description 30 years ago (76), TAMs have been characterized as potent pro-tumorigenic agents that act primarily by modulating the natural (and induced) anti-tumor response, ECM remodeling, and inducing angiogenesis, not only leading to tumor cell survival and proliferation but also, to their dissemination (**Figure 3**). It is currently accepted that the TAM phenotype resembles the alternatively activated macrophage M2 phenotype (Arginase 1^+, $CD163^+$, $CD206^+$, $CD209^+$, $FIZZ1^+$, and $Ym1/2^+$), which can be subdivided into four subtypes: M2a, M2b, M2c, and M2d (77). These subtypes are generated by the stimuli triggering macrophage differentiation and some specific phenotypic markers (**Table 2**). However, it is generally accepted that TAMs retain a high degree of plasticity, permitting several different subtypes to co-exist simultaneously and their trans-differentiation into each different subtype depending on the TME signals available.

In general, blood monocytes infiltrate the TME, and along with the tumor-resident macrophages, they represent a source of TAMs. In this context, tumor cells shape the macrophage's immunosuppressive phenotype by secreting anti-inflammatory

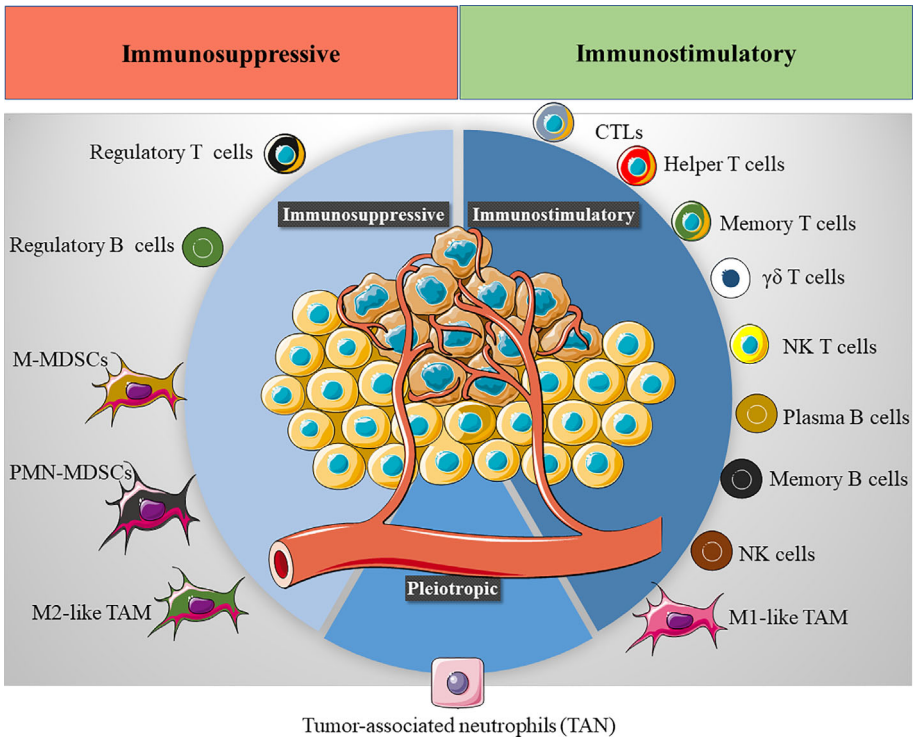

FIGURE 2 | The tumor immune microenvironment (TIME). Several immune cells are found in the TIME, exhibiting either an immunostimulatory (CTLs, cytotoxic T cells, helper T cells, memory T cells, γδ T cells, NK T cells, plasma B cells, memory B cells, NK cells and M1-like TAMs) or immunosuppressive phenotype (Tregs cells, regulatory B cells, M-MDSCs, monocytic monocyte-derived suppressor cells, PMN-MDSCs, polymorphonuclear monocyte-derived suppressor cells and M2-like TAMs). The final immunological response in the TME will depend on the balance between these immunomodulatory populations.

interleukins and other metabolites. The TAMs then inhibit tumor-infiltrating T cells directly through receptor-ligand cognates [*e.g.*, PD-1:PD-L1 (84)] or by releasing anti-inflammatory cytokines (IL-10, TGF-β1, and IL-6). Concomitantly, the TAMs can produce different proteolytic enzymes such as metalloproteinases (MMPs), cathepsins, and disintegrin and metalloproteinase-like proteases (ADAMs), thereby producing a profound ECM remodeling. Consequently, the ECM becomes conducive to invasion, and it facilitates tumor cell dissemination into the surrounding tissue and peripheral circulation. TAMs can further enhance tumor invasiveness by inducing angiogenesis, mediated by various cytokines and growth factors like VEGF-A (85) and IL-8 (86). Since TAMs are involved in tumor progression, the induction of a specific phenotype that switches these cells towards a pro-immunogenic profile has been proposed as an attractive therapeutic tool to enhance local anti-tumor immune responses.

The modulation of TAM activity is a plausible and promising therapeutic approach to combat tumors when combined with cancer immunotherapies. Indeed, multiple drugs that modulate the pro-tumor activity of TAMs have been tested, including bisphosphonates (87) and zoledronic acid (88) in particular, or chemotherapeutic drugs like docetaxel and cyclophosphamide (89). While zoledronic acid can revert the M2 TAM phenotype in breast tumors into an M1-like phenotype or induce TAM apoptosis, the chemotherapeutic drugs can promote an M1-phenotype that secretes pro-inflammatory cytokines like IL-12, thus driving an anti-tumor effect. In this context, nanoparticles that modulate TAM activity, particularly IONPs, provide new and innovative tools to prolong anti-tumor responses *in situ*.

INTRINSIC MODULATION OF THE TIME BY IRON OXIDE NANOPARTICLES (IONPS)

IONPs have been studied extensively as an effective magnetic nanocarrier for various cargos, such as drugs (15), cytokines (90, 91), siRNAs (92), and adjuvants (93). There are several motives for the increasing interest in IONPs as nanocarriers. First, the IONP core responds to an external electromagnetic field that permits their use in applications like magnetic targeting, magnetic resonance imaging (MRI) or the induction of local hyperthermia. Second, mammalian cells have efficient iron metabolism that can prevent the cells from suffering iron-related toxicity. Third, the IONP surface provides a chemical interface that can be easily modified with a number of polymers and moieties, which when combined with the high surface-to-volume ratio, facilitate the delivery of wide range of cargoes.

However, IONPs also produce interesting intrinsic biological effects that provide added therapeutic benefits to IONP-based

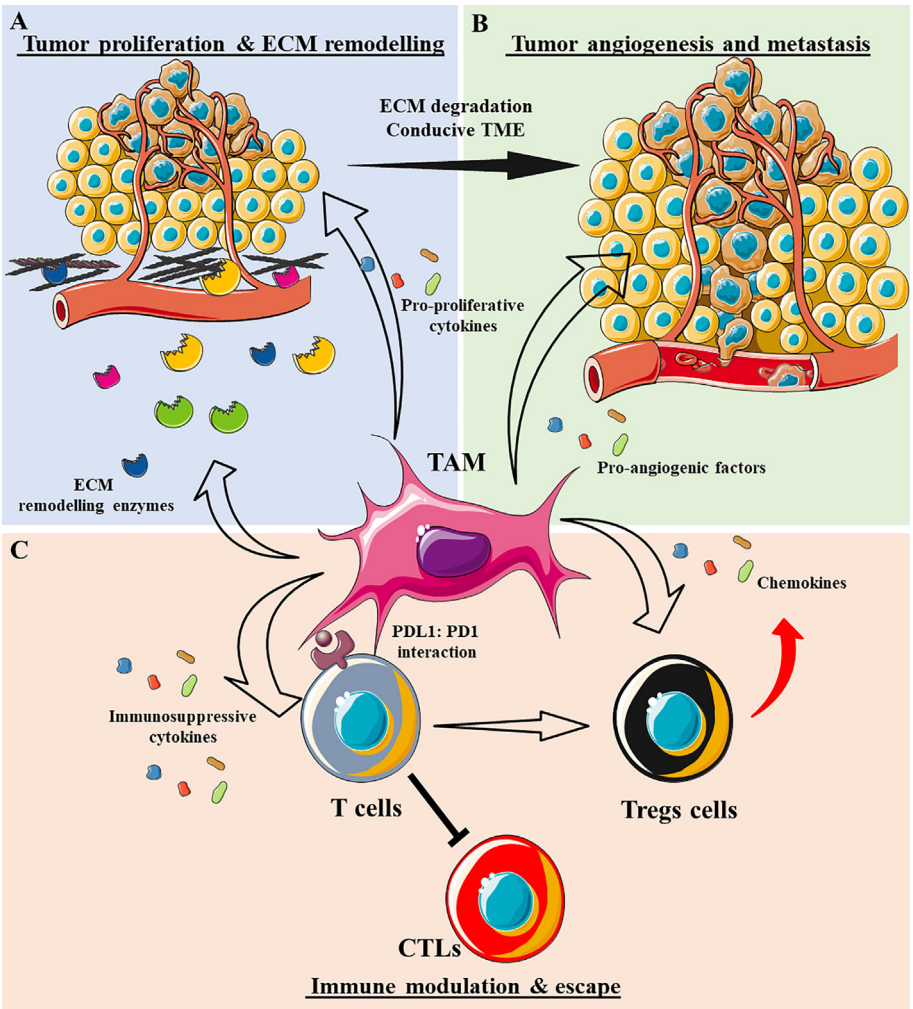

FIGURE 3 | The role of tumor-associated macrophages (TAMs) in shaping the tumor microenvironment (TME). **(A)** TAMs secrete a plethora of enzymes that degrade ECM components, such as metalloproteinases (MMPs), cathepsins, disintegrin and metalloproteinase (ADAM)-family proteases, and tissue inhibitors of metalloproteinases (TIMPs). As a result, the ECM becomes destructured and conducive to tumor cell invasion. TAMs also secrete cytokines that support tumor cell proliferation, e.g., TGF-β1, IL-10, IL-6, IL-1β, and EGF. **(B)** TAMs secrete various pro-angiogenic factors that induce vessel formation, *e.g.*, VEGF-A, bFGF, IL-6, and TNFα. Together with ECM degradation, tumor angiogenesis permits the systemic dissemination of tumor cells. **(C)** TAMs adopt an immunosuppressive phenotype by secreting many anti-inflammatory cytokines/chemokines, *e.g.*, IL-10, TGF-β1, CCL17, CCL18, and CCL22, inhibiting cytotoxic T cells (CTLs) and attracting or differentiating T cells into regulatory T cells. TAMs can also exhaust CTLs by direct engagement of anti-inflammatory cognates receptors like PD1-PD-L1.

TABLE 2 | | M2 macrophage subtypes and their involvement in tumor development.

M2 Subtype	Stimuli	Phenotype	Functions
M2a	IL-4/IL13	IL-10, TGF-β1, IL-1R agonist	To promote a Th2 response and tumor cell invasiveness (78, 79)
M2b	IL-1β, immune complexes and LPS	IL-1, IL-6, IL-10, TNFα	Pro-Th2 activity, tumor progression and immunotherapy resistance (80)
M2c	IL-10, TGF-β1, glucocorticoids	IL-10, TGF-β1	ECM remodeling and to promote tumor migration/invasion (81, 82)
M2d	IL-6, adenosine	IL-10, IL-12, TNFα, TGF-β1	Tumor progression and invasion (83)

nanomedicines. We demonstrated that polyethyleneimine (PEI)-coated IONPs can inhibit the migration and invasion of tumor cells (94), and impair angiogenesis (95). More importantly, the intrinsic biological effects of IONPs arise from their surface coating and the surrounding protein corona, as well as the free intracellular iron derived from IONP degradation. While IONP surface microdomains are primarily involved in the nanoparticle's interaction with cell membrane receptors, soluble factors, and intracellular components, the released intracellular iron actively changes the intracellular redox status

through the Fenton reaction (96), modulating several iron-regulated genes. Since macrophages contribute to the TIME, their interaction with IONPs can define the theranostic outcome and provide an invaluable tool to reprogram the phenotype of TAMs. The most recent findings on how IONPs affect macrophage activation are summarized in **Table 3**.

To understand how IONPs affect macrophage polarization, we have to consider the internalization process as at least three different steps, during which IONPs can engage with different signaling cascades: 1) IONP interaction with the cell membrane; 2) endocytosis and endolysosomal trafficking; and 3) IONP degradation. In each step the IONPs are exposed to diverse biological milieu and ultimately, this determines the indirect or direct engagement that drives macrophage transcriptional reprogramming and shifts in phenotype. This effect on transcriptional reprogramming of macrophages has been assessed by several groups whereby key transcription factors such as STAT family (107) and c-Fos/c-Jun complex (107) are upregulated upon IONP treatment. Noteworthy, IONPs appear to induce a variety of transcription factors related to MAPK pathways and the innate response, including the TLR-AP-1 signaling pathway (108). This complex reprogramming was revealed by Liu Y et al., who observed that the DMSA-coated IONPs engaged the activation of the signaling pathways mentioned above (107). Therefore, the IONPs can trigger a multifactorial transcription reprogramming of macrophages where several signaling pathways are involved.

It is important to note that among the transcriptional reprogramming that IONPs can induce in macrophages, some are related to cell death processes such as apoptosis, ferroptosis, and autophagy. The balance between all signaling pathways activated by a particular IONPs will determine the macrophage fate. In this review, we focus on the transcriptional reprogramming of macrophage response in terms of the immune response and suggest other comprehensive and recent studies on the toxicity of IONPs that can be more thorough in this sense (109, 110).

The coating of IONPs influences their interaction with cell membrane-associated proteins like receptors, thereby triggering signaling cascades that can activate macrophages. As such, IONPs with a positively charged coating consistently polarize macrophages towards a M1-like phenotype. Indeed, when macrophages are treated with PEI-coated IONPs, a straightforward program of M1 activation occurs, enhancing co-stimulatory receptors like CD40, CD80, and CD86, along with the secretion of the pro-inflammatory cytokine, IL-12 (101). When analyzing the transcriptional reprogramming induced by PEI-coated IONPs, several pro-inflammatory genes were seen to be upregulated (i.e., *Il1b*, *Tnfa*, *Ccl2* and *Il6*). However, the most exciting finding was the involvement of the toll-like receptor 4 (TLR-4) in PEI-coated IONP-induced macrophage activation (101). The PEI polymer appears to engage TLR-4 activation, stimulating the mitogen-activating protein kinase (MAPK). Two commercially available IONPs (carboxydextran-coated Resovist and carboxylmethyl-dextran coated feraheme) have also been demonstrated to induce macrophage activation through TLR-4 engagement, indicating that different IONP coatings can activate macrophages in this way, although activation by these IONPs induces autophagy (102). Other effects of IONPs were at least partly associated with different TLRs, including the cell membrane TLR2, TLR4, and TLR6, and the intracellular TLR8. Indeed, IONP size influences TLR activation as a relatively small IONP (10 nm) can enhance TLR2, TLR6, TLR4, and TLR8-induced cytokine secretion in peripheral blood, whereas a larger IONP (30 nm) only affects TLR2 and TLR6-dependent cytokine secretion (108). Although a direct interaction between the IONPs and the cell surface TLRs has yet to be demonstrated, the dependence of cytokine enhancement on the formation of a complex between TLR4/MD2 and the CD14 co-receptor suggests that a physical interaction between the TLR4 complex and IONPs could be responsible for the increase in TLR4 activity. However, elsewhere IONPs were shown to interfere with TLR4 agonist activation, suggesting that this mechanism could depend on the type of IONP (111).

In addition, it has been shown that IONPs with opposite surface charges promote similar macrophage repolarization. Two opposite charged IONPs induced an M1-like phenotype in RAW 264.7 macrophages, although negatively charged IONPs appeared to be more potent in promoting this effect (98) and neutral IONPs have a negligible impact. The crucial role that such M1-differentiated macrophages can play within the TIME was also addressed and there was significant tumor growth retardation when $IONP^+$ or $IONP^-$ treated macrophages were co-inoculated with HT1080 human fibrosarcoma cells, reflecting the anti-tumor effect of these repolarized M1-like macrophages (98).

IONP morphology also plays a critical role in determining the degree of macrophage activation. Using IONPs with four distinct morphologies (octopod, plate, cube, and spherical), yet with a comparable aspect ratios and surface charge, the IONPs with an octopod or plate morphology were seen to significantly activate the inflammasome, as measured by IL-1β secretion (112). More importantly, this dependence on morphology appeared to be related to the nanoparticle's capacity to induce ROS production. IONP size also affected the extent of inflammasome activation in macrophages, with spherical IONPs of ~30 nm inducing significantly more IL-1β release than larger spherical IONPs of ~80 and 120 nm (113). ROS production appears to be a common molecular mechanism for the effect of IONPs on macrophage activation, although this result also seems to depend on lysosomal destabilization and may reflect another common phenomenon. The involvement of ROS in IONP-induced macrophage activation is related to the central role these metabolites play in macrophage cell biology as short-lived second messengers. ROS mediate the oxidation of thiol groups in several proteins, altering their structure and hence, their function. The MAPK pathway is ROS-sensitive and it regulates several biological processes like cell proliferation, apoptosis, and the innate immune response. In this regard, ROS have been implicated in the induction and maintenance of an M1-like status of macrophages through the activation of NFκB and p38 MAPK signaling. In the former situation, ROS trigger the phosphorylation of the NFκB inhibitor, IκB, thereby activating NFκB (114). In the latter, ROS induce the phosphorylation of the apoptosis signaling-regulating kinase 1

TABLE 3 | | Example of the effects of iron oxide nanoparticles on macrophage polarization.

Iron oxide nanoparticles	Cell model	Mechanisms	Effects exerted
PLGA@Fe_3O_4 & CD206-Ab-PLGA@Fe_3O_4 (97)	*In vitro:* IL-4-stimulated RAW 264.7 cells *In vivo:* tumor model 4T1	ROS production	↑TNFα, iNOS, IL-1β ↓Arg1, IL-10, TGF-β1 ↑$CD86^+$ (M1) TAMs *in vivo*
Negative charged SPION Neutral charged SPION (PEG-coated) Positive charged SPION (98)	*In vitro:* RAW 264.7 cells *In vivo:* tumor model HT1080	ROS production	↑TNFα, iNOS ↓IL-10, VEGF ↓Tumor growth
Ferumoxytol (Feraheme™) (99)	*In vitro*: Co-culture RAW 264.7/MMTV-PyMT tumor cells *In vivo: tumor model MMTV-PyMT* *In vivo metastasis: tumor model KP1*	Tumor cell apoptosis	↑Pro-M1 genes (*TNFA, INOS, CD86, ARG1*) ↓Pro-M2 genes (*IL10, CD206*) ↓Tumor growth and lung/liver metastases-*in vivo* ↑M1 macrophage polarization *in vivo*
4-nm amphiphilic (PMA)@Fe_3O_4 (100)	*In vitro:* RAW 264.7 cells	Vacuolization, lysosomal damage	↑Pro-M1 genes (*TNFA, CD86, NFKB*) ↓Pro-M2 genes (*CD206*)
Polyethyleneimine@Fe_3O_4 (101)	*In vitro:* RAW 264.7 cells, mouse peritoneal macrophages, THP1 cells	TLR4 activation, ROS production	↑IL-12, IL-10, CD80, CD86, CD40, I-A/I-E ↑MAPK activation
Resovist™ & Ferumoxytol (Feraheme™) (102)	*In vitro:* Bone marrow-derived macrophages (BMDMs) *In vivo*: liver	TLR4 activation	↑Pro-inflammatory factors ↑Autophagy
DMSA@SPION, APS@SPION, & AD@SPION (103)	*In vitro:* M2 Macrophages: IL-4-*stimulated* Bone marrow-derived macrophages (BMDMs) and PMA-stimulated THP1	ROS production	↑IL-10 ↑MAPK activation ↑Cell invasion ↓Cell migration
Resovist™ (104)	*In vitro:* M2 Macrophages: IL-4/IL-13-*stimulated* PMA-differentiated THP1		Induce a shift towards a M1 phenotype ↑CD86, TNF-α, Ferritin, Cathepsin L
2-kDa PEG@SPIONs (105)	*In vitro:* LPS-stimulated RAW 264.7 cells	Inhibition of TLR4 signaling	↓IL-6, TNFα, iNOS
100 nm large maghemite (Fe_2O_3) nanoparticles (106)	*In vitro:* J774A.1 cells	Iron uptake & Fenton reactions	↓Phagocytic rate ↓LPS-dependent response

(ASK1) and the downstream activation of the p38 MAPK (115). However, ROS can either activate or inhibit NFκB in a context-dependent manner, highlighting the need to characterize the effect of IONP-triggered ROS production on NFκB activation in a cell-type and context-dependent manner (116). In addition to MAPK, the phosphoinositide-3 kinase (PI3K) is also regulated by ROS, sensitizing macrophages to hormone, cytokine, and growth factor signaling (117).

IONP phagocytosis can lead to autophagy, as is the case for the two FDA-approved IONPs, resovist and ferumoxytol that induce the appearance of an early autophagic vacuole and eventually, IONPs-containing double-membrane autophagic vacuoles, small internal vesicles, and cellular and membrane debris (102). These events were accompanied by the accumulation of LC3 puncta and overexpression of the p62/SQSTM1-positive sequestosome (118–120). In accordance with the involvement of TLRs in this effect, the TLR4-p38-Nrf2 pathway appears to mediate IONP-induced autophagy as opposed to the classic autophagy machinery dependent on ATG5/12. Indeed, pre-treatment with the TLR4 signaling inhibitor, CLI-095, prevented IONP-loaded macrophages from inducing the aforementioned structural changes (102).

Importantly, each macrophage phenotype expresses different factors involved in iron metabolism, reflected in their distinct iron sensitivity (121). For instance, M2-polarized THP1 macrophages internalize significantly more IONPs than M1-polarized and M0 macrophages, leading to a higher T1 signal in M2 macrophages and a higher T2* signal in M0 macrophages (122). In turn, internalized IONPs could also exert effects on polarization and iron metabolism. Indeed, our group demonstrated that DMSA-, APS-, and aminodextran-coated IONPs shifted iron metabolism towards an iron-sequestering status in M2-like macrophages (103). In the light of the above, we can propose a general overview of the events induced by IONPs that precipitates macrophage activation (**Figure 4**).

IONPs have also been used to track microglia and assayed as a potential nanocarrier in brain tumors. Microglia are highly phagocytic cells found entirely in the central nervous system (CNS) where they protect the nervous tissue from debris and damaged CNS structures and from viruses, microorganisms, and tumors (123–126). Therefore, like macrophages, microglia can phagocytose IONPs and react to them. In this sense, Wu HY et al. found that the carboxydextran-coated IONP (Resovist^{TM}) counteract the LPS-induced microglia activation by directly decrease IL-1β secretion (127), suggesting IONPs can protect CNS from an exacerbated inflammation. However, other reports pinpoint the involvement of IONPs in recruiting and activating microglia in CNS structures such as the olfactory bulb, hippocampus, and striatum. Indeed, Wang Y et al. found that Fe_2O_3 IONPs administered intranasally promote the recruitment of microglia into the above CNS structures and induced microglia activation and proliferation, with ROS and nitric oxide (NO) production, as a possible defense mechanism against foreign particulates (128). Thus, IONPs appear to change CNS immunological microenvironment toward an inflammatory or anti-inflammatory phenotype, highlighting the need to comprehend these effects in the context of brain tumors.

THERAPEUTIC IRON OXIDE NANOPARTICLE-ENABLED MODULATION OF TIME

We have discussed the activation of macrophages by IONPs and the molecular mechanisms mediating these effects. Considering the intrinsic biological activity of IONPs on macrophages, their application in therapeutic and prophylactic vaccination schemes has emerged as an attractive therapeutic approach to treat cancer. This approach relies on the possibility of combining the carrier capacity of IONPs with their by-stander activation of macrophages within the TIME. A general overview of IONP-based vaccine designs highlights the use of IONPs as an antigen carrier (primarily associated with the tumor cells)with the possible addition of adjuvant and/or a targeting moiety.

The use of IONPs as an antigen carrier in a vaccination schedule takes advantage of the intrinsic capacity of the IONPs to drive macrophages or DCs towards a pro-inflammatory phenotype. Consequently, antigen internalization, intracellular processing, and restricted major histocompatibility complex (MHC) presentation to T cells within an inflammatory microenvironment will elicit a robust immune response against the antigen-expressing tumor cells. A simple vaccine formulation has been tested by loading ovalbumin (OVA) onto IONPs, demonstrating that this formulation could activate bone marrow-derived dendritic cells (BMDCs) and RAW 264.7 macrophages. However, the most exciting finding was that prophylactic or therapeutic injection of three doses of this preparation delayed OVA-expressing B16 tumor cell growth.

Interestingly, OVA-coated IONPs effectively prevented lung metastasis from OVA-expressing cells (129). Likewise, the sole conjugation of OVA alone with IONPs was sufficient to elicit potent DC and macrophage activation, and to reduce the OVA-expressing CT26 tumor burden *in vivo* (130). This anti-tumor effect appeared to be mediated by the induction of pro-inflammatory cytokines like IL-6, TNF-α, and IFN-γ.

Other studies have addressed the potential of the IONPs as carriers of tumor-associated antigens in vaccine designs. For example, the administration of self-assembled MUC1 lipo(glycol) peptide-coated IONPs elicited a strong antibody response, prompting an antibody profile able to recognize the MUC1-expressing tumor cell line, MCF7 (131). In this scenario, the anti-tumor effect seems more likely to be related to the enhanced activation of plasma B cells due to the high number of lipo (glycol)peptide copies presented on the IONP surface. However, we cannot rule out a direct effect on macrophages or DCs.

It is desirable that macrophage-based anti-tumor therapy induces naive macrophages to adopt a M1 phenotype and that it switches the resident M2 program into a M1 phenotype, ensuring a pro-inflammatory and anti-tumor TIME. It was seen that hyaluronic acid-modified IONPs or bare IONPs trigger the production of ROS and pro-inflammatory cytokines (132). Consequently, IONP-treated macrophages exerted an anti-tumor effect on the murine 4T1 breast-tumor cell line in a cell contact-independent manner, inducing active caspase 3 and inhibiting cell proliferation. Notably, hyaluronic acid-modified

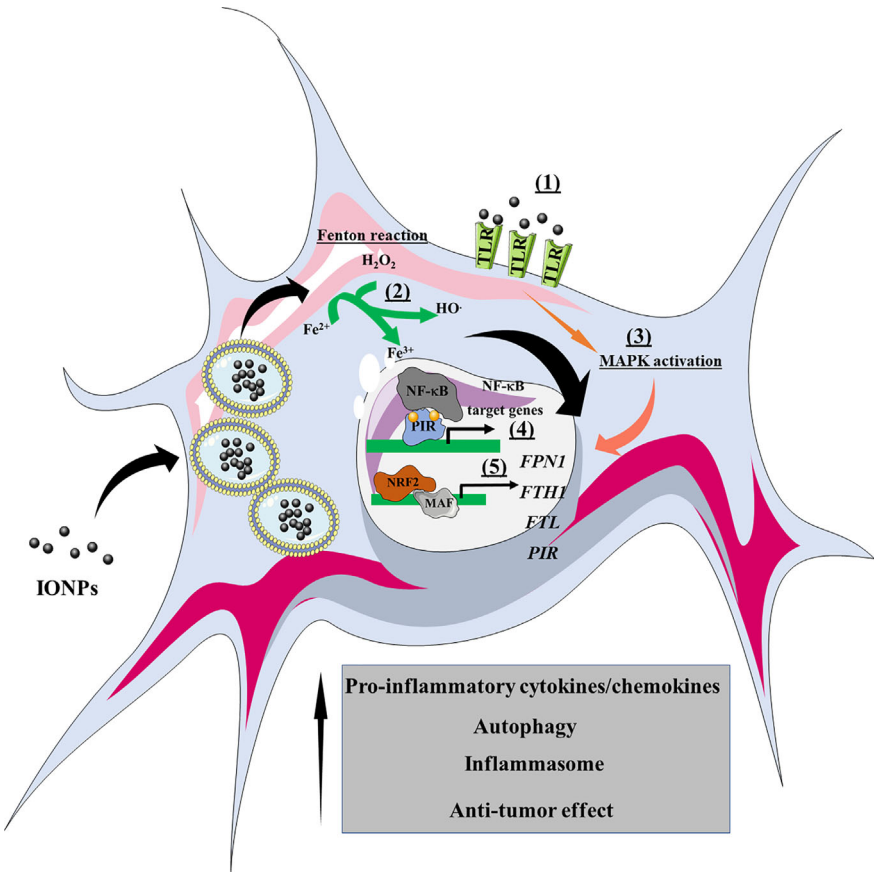

FIGURE 4 | Overview of the effects of IONPs on macrophage polarization. The IONPs can interact with cell surface receptors such as TLRs (1), leading to activation of the MAPK signaling pathway. Once internalized by macrophages, the IONPs are enclosed within endolysosomes where they are biodegraded. Consequently, atomic iron is released into the cytoplasm, where it engages the Fenton reaction and produces ROS (2). As a result, transcriptional reprogramming is triggered, such as that involving NF-κB (e.g., cytokines, chemokines) and NRF2 target genes (e.g., iron metabolism). NRF2, nuclear factor (erythroid-derived 2)-like 2; PIR, Pirin; *FPN1*, ferroportin-1; *FTH1*, ferritin heavy chain; *FTL*, ferritin light chain; MAPK, mitogen-activated protein kinases; MAF, musculoaponeurotic fibrosarcoma.

IONPs induced M1 macrophages resistant to M2-inducing factors and M2-to-M1 macrophage reversion (132). IONP intracellular degradation also increases the labile iron pool, providing another element that can modulate the TIME. It was shown that red blood cells (RBCs) were responsible for the presence of iron-loaded macrophages nesting in the invasive margins of non-small lung cell tumors, which were in turn correlated with a smaller tumor size (133). Indeed, hemolytic RBCs triggered TAM polarization toward a M1-like phenotype, as evident by the expression of M1 marker transcripts (*Il6, Nos2*, and *Tnfa*) and their increased anti-tumor activity (133). More importantly, IONPs injected intravenously in Lewis lung carcinoma (LLC)-bearing mice accumulated within F4/80 macrophages and reduced tumor growth, indicating that these IONPs have a similar effect reverting M2 macrophages to a M1 phenotype (133).

Advantages have also been reported when a combination of antigen-coated IONPs and adjuvant-coated IONPs is used therapeutically. While IONPs were initially used as antigen carriers, adjuvant and nanoparticle association enhanced the adjuvant effect on the respective signaling pathway. Indeed, co-delivery of polyIC-R837@mPEG-PL-OA-IONPs (as TLR3-7 agonists) and OVA@mPEG-PL-OA-IONPs (as antigen) delayed tumor growth in OVA-expressing B16-bearing animals and led to tumor-free survival in some individuals, probably through an enhanced agonist effect on TLR signaling. The increase in the ferroptosis process induced by IONP-derived iron further promoted an antitumoral TME, indicating that the IONPs provide not only transport but also an intrinsic potential to change the TME toward an anti-tumor phenotype (134). **Table 4** summarizes the most recent approaches using IONPs in anti-tumor vaccination regimens.

CONCLUSIONS

IONPs have been studied intensively in recent decades to exploit their magnetic and surface chemical features. However, only recently has attention been drawn to their intrinsic immunomodulatory properties, especially their effects on macrophages. These effects are particularly important in the context of cancer immunotherapy as IONPs can provide an efficient vehicle for antigen delivery and elicit a

TABLE 4 | Use of IONPs in vaccine formulation.

Nano-formulation	Tumor model	Effects
Ovalbumin@Fe_3O_4 (129)	Murine melanoma OVA-expressing B16	Bone marrow-derived DC maturation Therapeutic and prophylactic inhibition of tumor growth Therapeutic and prophylactic attenuation of lung metastasis
OVA@Fe_3O_4 (130)	Murine colon carcinoma OVA-expressing CT26	Murine dendritic cell (DC2.4) and macrophage (RAW 264.7) activation (increased IL-6, TNF-α and IFN-γ) Therapeutic anti-tumor effect (reduced CT26 tumor growth and increased serum IL-6, TNF-α and IFN-γ)
OVA/CpG/anti-DEC205 Ab@Fe_2O_3 (135)	Murine melanoma OVA-expressing B16	*In vivo* targeting of $CD8^+$ DCs *In vivo* B16 tumor arrest
Hsp70@SPION (136)	Murine C6 glioma	DCs, tumor lysate and Hsp70@SPION co-treatment arrests glioma tumor growth
MUC1 Lipoglycopeptide@SPION (131)	MCF7	Multivalent engagement of antibody-producing B cells. Generation of a strong antibody response *in vivo*. Tumor cell recognition and cell death by immunized sera.
Co-delivery of micellar OVA@phospholipid-PEG-IONP & LOS@ phospholipid-PEG-IONP (137)	OVA-expressing B16-F10	Increased IL-6 and reduced LOS cytotoxicity Prophylactic anti-tumor effect & synergetic effect with PD-L1 inhibitor
Co-delivery of polyIC-R837@mZnSPION & OVA@mZnSPION (93)	OVA-expressing B16-F10	Micellar ZnSPION enhances TLR3/7 agonist effects Prophylactic and therapeutic anti-tumor effect & synergetic effect with PD-L1 inhibitor
Co-delivery of polyIC-R837@mPEG-PL-OA-IONP & OVA@mPEG-PL-OA-IONP (134)	OVA-expressing B16-F10	Enhances TLR agonist effects on DCs Improves the tumor-free rate over time Synergistic effects with immunostimulatory antibodies (anti-OX40 & anti-PD-L1)

potent immune response, reprogramming TAMs toward an immunogenic phenotype. Two main molecular mechanisms can explain the intrinsic immunomodulatory effect of IONPs: 1) the production of ROS and consequently, the modulation of redox-sensitive signaling pathways; and 2) the direct engagement and activation of immune response-related receptors, such as TLRs, inducing transcriptional reprogramming in macrophages. The use of IONPs can provide a reliable platform to reprogram the typical M2-TAM phenotype toward a pro-immunogenic phenotype, synergizing with currently used immunotherapies like checkpoint inhibitors to mount a potent anti-tumor immune response both locally and systemically.

AUTHOR CONTRIBUTIONS

VM-A, JR, and DB conceived and designed the review. VM-A and JR wrote sections of the manuscript, and prepared the figures and tables. DB coordinated, critically revised, modified and completed the manuscript. All authors contributed to the article and approved the submitted version.

FUNDING

VM-A is a post-doctoral scholar working under a Juan de la Cierva-Incorporación Contract (IJCI-2017-31447) from the Spanish Ministry of Science and Innovation. The European Commission-funded VetBioNet INFRAIA-731014 project supports JR. This work was supported in part by grants from the Spanish Ministry of Science and Innovation (SAF-2017-82223-R and PID-2020-112685RB-100 to DB). DFB group is part of the Network "Nanotechnology in Translational Hyperthermia" (HIPERNANO, RED2018-102626-T) supported by the Spanish Ministry of Science and Innovation.

ACKNOWLEDGMENTS

We thank members of the laboratories led by Domingo F Barber (CNB-CSIC, Madrid) and María del Puerto Morales (ICMM-CSIC, Madrid) for helpful comments and discussion. The authors are also grateful to Mark Sefton (BiomedRed SL) for English language editing of the manuscript.

REFERENCES

1. Habibi N, Quevedo DF, Gregory JV, Lahann J. Emerging Methods in Therapeutics Using Multifunctional Nanoparticles. *WIREs Nanomed Nanobiotechnol* (2020) e1625. doi: 10.1002/wnan.1625
2. Khan AU, Khan M, Cho MH, Khan MM. Selected Nanotechnologies and Nanostructures for Drug Delivery, Nanomedicine and Cure. *Bioprocess Biosyst Eng* (2020) 43:1339–57. doi: 10.1007/s00449-020-02330-8
3. Wicki A, Witzigmann D, Balasubramanian V, Huwyler J. Nanomedicine in Cancer Therapy: Challenges, Opportunities, and Clinical Applications. *J Controlled Release* (2015) 200:138–57. doi: 10.1016/j.jconrel.2014.12.030
4. Hare JI, Lammers T, Ashford MB, Puri S, Storm G, Barry ST. Challenges and Strategies in Anti-Cancer Nanomedicine Development: An Industry Perspective. *Adv Drug Delivery Rev* (2017) 108:25–38. doi: 10.1016/j.addr.2016.04.025
5. Gharagozloo M, Majewski S, Foldvari M. Therapeutic Applications of Nanomedicine in Autoimmune Diseases: From Immunosuppression to Tolerance Induction. *Nanomed: Nanotechnol Biol Med* (2015) 11:1003–18. doi: 10.1016/j.nano.2014.12.003
6. Qamar N, Arif A, Bhatti A, John P. Nanomedicine: An Emerging Era of Theranostics and Therapeutics for Rheumatoid Arthritis. *Rheumatology* (2019) 58:1715–21. doi: 10.1093/rheumatology/kez286

7. Poovaiah N, Davoudi Z, Peng H, Schlichtmann B, Mallapragada S, Narasimhan B, et al. Treatment of Neurodegenerative Disorders Through the Blood–Brain Barrier Using Nanocarriers. *Nanoscale* (2018) 10:16962–83. doi: 10.1039/C8NR04073G
8. Ramanathan S, Archunan G, Sivakumar M, Tamil Selvan S, Fred AL, Kumar S, et al. Theranostic Applications of Nanoparticles in Neurodegenerative Disorders. *Int J Nanomed* (2018) 13:5561–76. doi: 10.2147/IJN.S149022
9. Steichen SD, Caldorera-Moore M, Peppas NA. A Review of Current Nanoparticle and Targeting Moieties for the Delivery of Cancer Therapeutics. *Eur J Pharm Sci* (2013) 48:416–27. doi: 10.1016/j.ejps.2012.12.006
10. Amreddy N, Babu A, Muralidharan R, Panneerselvam J, Srivastava A, Ahmed R, et al. "Chapter Five - Recent Advances in Nanoparticle-Based Cancer Drug and Gene Delivery". In: KD Tew and PB Fisher, editors. *Advances in Cancer Research*. Academic Press. (2018) 137 p. 115–70. doi: 10.1016/bs.acr.2017.11.003
11. Deirram N, Zhang C, Kermaniyan SS, Johnston APR, Such GK. Ph-Responsive Polymer Nanoparticles for Drug Delivery. *Macromol Rapid Commun* (2019) 40:1800917. doi: 10.1002/marc.201800917
12. Karimi M, Eslami M, Sahandi-Zangabad P, Mirab F, Farajisafiloo N, Shafaei Z, et al. pH-Sensitive Stimulus-Responsive Nanocarriers for Targeted Delivery of Therapeutic Agents. *WIREs Nanomed Nanobiotechnol* (2016) 8:696–716. doi: 10.1002/wnan.1389
13. Xu X, Saw PE, Tao W, Li Y, Ji X, Bhasin S, et al. Ros-Responsive Polyprodrug Nanoparticles for Triggered Drug Delivery and Effective Cancer Therapy. *Adv Mater* (2017) 29:1700141. doi: 10.1002/adma.201700141
14. Lv X, Zhu Y, Ghandehari H, Yu A, Wang Y. An ROS-responsive and Self-Accelerating Drug Release Nanoplatform for Overcoming Multidrug Resistance. *Chem Commun* (2019) 55:3383–6. doi: 10.1039/C9CC00358D
15. Vangijzegem T, Stanicki D, Laurent S. Magnetic Iron Oxide Nanoparticles for Drug Delivery: Applications and Characteristics. *Expert Opin Drug Delivery* (2019) 16:69–78. doi: 10.1080/17425247.2019.1554647
16. Xia H, Gao Y, Yin L, Cheng X, Wang A, Zhao M, et al. Light-Triggered Covalent Coupling of Gold Nanoparticles for Photothermal Cancer Therapy. *ChemBioChem* (2019) 20:667–71. doi: 10.1002/cbic.201800648
17. Berry SL, Walker K, Hoskins C, Telling ND, Price HP. Nanoparticle-Mediated Magnetic Hyperthermia is an Effective Method for Killing the Human-Infective Protozoan Parasite Leishmania Mexicana In Vitro. *Sci Rep* (2019) 9:1059. doi: 10.1038/s41598-018-37670-9
18. Faraj AA, Luciani N, Kolosnjaj-Tabi J, Mattar E, Clement O, Wilhelm C, et al. Real-Time High-Resolution Magnetic Resonance Tracking of Macrophage Subpopulations in a Murine Inflammation Model: A Pilot Study With a Commercially Available Cryogenic Probe. *Contrast Media Mol Imaging* (2013) 8:193–203. doi: 10.1002/cmmi.1516
19. Nagarajan SR, Butler LM, Hoy AJ. The Diversity and Breadth of Cancer Cell Fatty Acid Metabolism. *Cancer Metab* (2021) 9:2. doi: 10.1186/s40170-020-00237-2
20. Chen Q, Gao J, Zhao Y, Hou R. Long non-Coding RNA Lbx2-AS1 Enhances Glioma Proliferation Through Downregulating Microrna-491-5p. *Cancer Cell Int* (2020) 20:411. doi: 10.1186/s12935-020-01433-2
21. Czowski BJ, Romero-Moreno R, Trull KJ, White KA. Cancer and Ph Dynamics: Transcriptional Regulation, Proteostasis, and the Need for New Molecular Tools. *Cancers (Basel)* (2020) 12:2760. doi: 10.3390/cancers12102760
22. Kaweme NM, Zhou S, Changwe GJ, Zhou F. The Significant Role of Redox System in Myeloid Leukemia: From Pathogenesis to Therapeutic Applications. *Biomark Res* (2020) 8:63–3. doi: 10.1186/s40364-020-00242-z
23. Ruan Z, Deng H, Liang M, Xu Z, Lai M, Ren H, et al. Overexpression of Long non-Coding RNA00355 Enhances Proliferation, Chemotaxis, and Metastasis in Colon Cancer Via Promoting GTF2B-mediated Itga2. *Transl Oncol* (2021) 14:100947–7. doi: 10.1016/j.tranon.2020.100947
24. Hudson LG, Gillette JM, Kang H, Rivera MR, Wandinger-Ness A. Ovarian Tumor Microenvironment Signaling: Convergence on the Rac1 Gtpase. *Cancers (Basel)* (2018) 10:358. doi: 10.3390/cancers10100358
25. Bhat AA, Yousuf P, Wani NA, Rizwan A, Chauhan SS, Siddiqi MA, et al. Tumor Microenvironment: An Evil Nexus Promoting Aggressive Head and Neck Squamous Cell Carcinoma and Avenue for Targeted Therapy. *Signal Transduct Targeted Ther* (2021) 6:12. doi: 10.1038/s41392-020-00419-w
26. Song SG, Kim S, Koh J, Yim J, Han B, Kim YA, et al. Comparative Analysis of the Tumor Immune-Microenvironment of Primary and Brain Metastases of non-Small-Cell Lung Cancer Reveals Organ-Specific and EGFR Mutation-Dependent Unique Immune Landscape. *Cancer Immunol Immunother* (2021). doi: 10.1007/s00262-020-02840-0
27. Giatromanolaki A, Sivridis E, Koukourakis MI. The Pathology of Tumor Stromatogenesis. *null* (2007) 6:639–45. doi: 10.4161/cbt.6.5.4198
28. Lebrun J-J. The Dual Role of Tgfβ in Human Cancer: From Tumor Suppression to Cancer Metastasis. *ISRN Mol Biol* (2012) 2012:381428–8. doi: 10.5402/2012/381428
29. Principe DR, Doll JA, Bauer J, Jung B, Munshi HG, Bartholin L, et al. Tgf-β: Duality of Function Between Tumor Prevention and Carcinogenesis. *J Natl Cancer Inst* (2014) 106:djt369–9. doi: 10.1093/jnci/djt369
30. Wang B, Xi C, Liu M, Sun H, Liu S, Song L, et al. Breast Fibroblasts in Both Cancer and Normal Tissues Induce Phenotypic Transformation of Breast Cancer Stem Cells: A Preliminary Study. *PeerJ* (2018) 6:e4805–5. doi: 10.7717/peerj.4805
31. Orimo A, Gupta PB, Sgroi DC, Arenzana-Seisdedos F, Delaunay T, Naeem R, et al. Stromal Fibroblasts Present in Invasive Human Breast Carcinomas Promote Tumor Growth and Angiogenesis Through Elevated Sdf-1/CXCL12 Secretion. *Cell* (2005) 121:335–48. doi: 10.1016/j.cell.2005.02.034
32. Suh J, Kim D-H, Lee Y-H, Jang J-H, Surh Y-J. Fibroblast Growth factor-2, Derived From Cancer-Associated Fibroblasts, Stimulates Growth and Progression of Human Breast Cancer Cells Via FGFR1 Signaling. *Mol Carcinogene* (2020) 59:1028–40. doi: 10.1002/mc.23233
33. Sjöberg E, Meyrath M, Milde L, Herrera M, Lövrot J, Hägerstrand D, et al. A Novel Ackr2-Dependent Role of Fibroblast-Derived CXCL14 in Epithelial-to-Mesenchymal Transition and Metastasis of Breast Cancer. *Clin Cancer Res* (2019) 25:3702. doi: 10.1158/1078-0432.CCR-18-1294
34. Allaoui R, Bergenfelz C, Mohlin S, Hagerling C, Salari K, Werb Z, et al. Cancer-Associated Fibroblast-Secreted CXCL16 Attracts Monocytes to Promote Stroma Activation in Triple-Negative Breast Cancers. *Nat Commun* (2016) 7:13050–0. doi: 10.1038/ncomms13050
35. Liao D, Luo Y, Markowitz D, Xiang R, Reisfeld RA. Cancer Associated Fibroblasts Promote Tumor Growth and Metastasis by Modulating the Tumor Immune Microenvironment in a 4T1 Murine Breast Cancer Model. *PloS One* (2009) 4:e7965–5. doi: 10.1371/journal.pone.0007965
36. Shani O, Vorobyov T, Monteran L, Lavie D, Cohen N, Raz Y, et al. Fibroblast-Derived IL33 Facilitates Breast Cancer Metastasis by Modifying the Immune Microenvironment and Driving Type 2 Immunity. *Cancer Res* (2020) 80:5317. doi: 10.1158/0008-5472.CAN-20-2116
37. Aboulkheyr Es H, Bigdeli B, Zhand S, Aref AR, Thiery JP, Warkiani ME. Mesenchymal Stem Cells Induce PD-L1 Expression Through the Secretion of CCL5 in Breast Cancer Cells. *J Cell Physiol* (2020) 3918–28. doi: 10.1002/jcp.30135
38. Gallo M, Frezzetti D, Roma C, Chicchinelli N, Barbieri A, Arra C, et al. RANTES and IL-6 Cooperate in Inducing a More Aggressive Phenotype in Breast Cancer Cells. *Oncotarget* (2018) 9:17543–53. doi: 10.18632/oncotarget.24784
39. Li Y, Chen Y, Miao L, Wang Y, Yu M, Yan X, et al. Stress-Induced Upregulation of TNFSF4 in Cancer-Associated Fibroblast Facilitates Chemoresistance of Lung Adenocarcinoma Through Inhibiting Apoptosis of Tumor Cells. *Cancer Lett* (2021) 497:212–20. doi: 10.1016/j.canlet.2020.10.032
40. Wang L, Li X, Ren Y, Geng H, Zhang Q, Cao L, et al. Cancer-Associated Fibroblasts Contribute to Cisplatin Resistance by Modulating ANXA3 in Lung Cancer Cells. *Cancer Sci* (2019) 110:1609–20. doi: 10.1111/cas.13998
41. Xiang H, Ramil CP, Hai J, Zhang C, Wang H, Watkins AA, et al. Cancer-Associated Fibroblasts Promote Immunosuppression by Inducing Ros-Generating Monocytic Mdscs in Lung Squamous Cell Carcinoma. *Cancer Immunol Res* (2020) 8:436. doi: 10.1158/2326-6066.CIR-19-0507
42. Zhou Z, Zhou Q, Wu X, Xu S, Hu X, Tao X, et al. VCAM-1 Secreted From Cancer-Associated Fibroblasts Enhances the Growth and Invasion of Lung Cancer Cells Through AKT and MAPK Signaling. *Cancer Lett* (2020) 473:62–73. doi: 10.1016/j.canlet.2019.12.039
43. Inoue C, Miki Y, Saito R, Hata S, Abe J, Sato I, et al. Pd-L1 Induction by Cancer-Associated Fibroblast-Derived Factors in Lung Adenocarcinoma Cells. *Cancers (Basel)* (2019) 11:1257. doi: 10.3390/cancers11091257
44. Zhang R, Qi F, Shao S, Li G, Feng Y. Human Colorectal Cancer-Derived Carcinoma Associated Fibroblasts Promote CD44-mediated Adhesion of Colorectal Cancer Cells to Endothelial Cells by Secretion of HGF. *Cancer Cell Int* (2019) 19:192–2. doi: 10.1186/s12935-019-0914-y

45. Ren J, Ding L, Zhang D, Shi G, Xu Q, Shen S, et al. Carcinoma-Associated Fibroblasts Promote the Stemness and Chemoresistance of Colorectal Cancer by Transferring Exosomal lncRNA H19. *Theranostics* (2018) 8:3932–48. doi: 10.7150/thno.25541
46. Aizawa T, Karasawa H, Funayama R, Shirota M, Suzuki T, Maeda S, et al. Cancer-Associated Fibroblasts Secrete Wnt2 to Promote Cancer Progression in Colorectal Cancer. *Cancer Med* (2019) 8:6370–82. doi: 10.1002/cam4.2523
47. Landskron G, de la Fuente López M, Dubois-Camacho K, Díaz-Jiménez D, Orellana-Serradell O, Romero D, et al. Interleukin 33/ST2 Axis Components Are Associated to Desmoplasia, a Metastasis-Related Factor in Colorectal Cancer. *Front Immunol* (2019) 10:1394. doi: 10.3389/fimmu.2019.01394
48. Zhu H-F, Zhang X-H, Gu C-S, Zhong Y, Long T, Ma Y-D, et al. Cancer-Associated Fibroblasts Promote Colorectal Cancer Progression by Secreting CLEC3B. *Cancer Biol Ther* (2019) 20:967–78. doi: 10.1080/15384047.2019.1591122
49. Stanisavljevic J, Loubat-Casanovas J, Herrera M, Luque T, Peña R, Lluch A, et al. Snail1-Expressing Fibroblasts in the Tumor Microenvironment Display Mechanical Properties That Support Metastasis. *Cancer Res* (2015) 75:284. doi: 10.1158/0008-5472.CAN-14-1903
50. Navarro R, Tapia-Galisteo A, Martín-García L, Tarín C, Corbacho C, Gómez-López G, et al. Tgf-β-Induced IGFBP-3 is a Key Paracrine Factor From Activated Pericytes That Promotes Colorectal Cancer Cell Migration and Invasion. *Mol Oncol* (2020) 14:2609–28. doi: 10.1002/1878-0261.12779
51. Ma X, Liu J, Yang X, Fang K, Zheng P, Liang X, et al. Mesenchymal Stem Cells Maintain the Stemness of Colon Cancer Stem Cells Via interleukin-8/mitogen-activated Protein Kinase Signaling Pathway. *Exp Biol Med (Maywood)* (2020) 245:562–75. doi: 10.1177/1535370220910690
52. Tan H-X, Xiao Z-G, Huang T, Fang Z-X, Liu Y, Huang Z-C. Cxcr4/Tgf-β1 Mediated Self-Differentiation of Human Mesenchymal Stem Cells to Carcinoma-Associated Fibroblasts and Promoted Colorectal Carcinoma Development. *Cancer Biol Ther* (2020) 21:248–57. doi: 10.1080/15384047.2019.1685156
53. Chen K, Liu Q, Tsang LL, Ye Q, Chan HC, Sun Y, et al. Human MSCs Promotes Colorectal Cancer Epithelial-Mesenchymal Transition and Progression Via CCL5/β-Catenin/Slug Pathway. *Cell Death Dis* (2017) 8:e2819–9. doi: 10.1038/cddis.2017.138
54. Giorello MB, Borzone FR, Labovsky V, Piccioni FV, Chasseing NA. Cancer-Associated Fibroblasts in the Breast Tumor Microenvironment. *J Mammary Gland Biol Neoplasia* (2021). doi: 10.1007/s10911-020-09475-y
55. Bartoschek M, Oskolkov N, Bocci M, Lövrot J, Larsson C, Sommarin M, et al. Spatially and Functionally Distinct Subclasses of Breast Cancer-Associated Fibroblasts Revealed by Single Cell RNA Sequencing. *Nat Commun* (2018) 9:5150. doi: 10.1038/s41467-018-07582-3
56. Elwakeel E, Brüggemann M, Fink AF, Schulz MH, Schmid T, Savai R, et al. Phenotypic Plasticity of Fibroblasts During Mammary Carcinoma Development. *Int J Mol Sci* (2019) 20:4438. doi: 10.3390/ijms20184438
57. Raz Y, Cohen N, Shani O, Bell RE, Novitskiy SV, Abramovitz L, et al. Bone Marrow-Derived Fibroblasts are a Functionally Distinct Stromal Cell Population in Breast Cancer. *J Exp Med* (2018) 215:3075–93. doi: 10.1084/jem.20180818
58. Hass R, von der Ohe J, Ungefroren H. Impact of the Tumor Microenvironment on Tumor Heterogeneity and Consequences for Cancer Cell Plasticity and Stemness. *Cancers (Basel)* (2020) 12:3716. doi: 10.3390/cancers12123716
59. Najafi M, Mortezaee K, Majidpoor J. Stromal Reprogramming: A Target for Tumor Therapy. *Life Sci* (2019) 239:117049. doi: 10.1016/j.lfs.2019.117049
60. Zhou J, Tang Z, Gao S, Li C, Feng Y, Zhou X. Tumor-Associated Macrophages: Recent Insights and Therapies. *Front Oncol* (2020) 10:188. doi: 10.3389/fonc.2020.00188
61. Chen D, Liu Z, Liu W, Fu M, Jiang W, Xu S, et al. Predicting Postoperative Peritoneal Metastasis in Gastric Cancer With Serosal Invasion Using a Collagen Nomogram. *Nat Commun* (2021) 12:179. doi: 10.1038/s41467-020-20429-0
62. Zhong C, Tao B, Tang F, Yang X, Peng T, You J, et al. Remodeling Cancer Stemness by Collagen/Fibronectin Via the AKT and CDC42 Signaling Pathway Crosstalk in Glioma. *Theranostics* (2021) 11:1991–2005. doi: 10.7150/thno.50613
63. Li J, Xu X, Jiang Y, Hansbro NG, Hansbro PM, Xu J, et al. Elastin is a Key Factor of Tumor Development in Colorectal Cancer. *BMC Cancer* (2020) 20:217–7. doi: 10.1186/s12885-020-6686-x
64. Huang C, Chen J. Laminin−332 Mediates Proliferation, Apoptosis, Invasion, Migration and Epithelial−to−Mesenchymal Transition in Pancreatic Ductal Adenocarcinoma. *Mol Med Rep* (2021) 23:11. doi: 10.3892/mmr.2020.11649
65. Hussain S, Peng B, Cherian M, Song JW, Ahirwar DK, Ganju RK. The Roles of Stroma-Derived Chemokine in Different Stages of Cancer Metastases. *Front Immunol* (2020) 11:598532. doi: 10.3389/fimmu.2020.598532
66. Contreras-Zárate MJ, Cittelly DM. Sex Steroid Hormone Function in the Brain Niche: Implications for Brain Metastatic Colonization and Progression. *Cancer Rep* (2020) n/a:e1241. doi: 10.1002/cnr2.1241
67. Li X, Berg NK, Mills T, Zhang K, Eltzschig HK, Yuan X. Adenosine at the Interphase of Hypoxia and Inflammation in Lung Injury. *Front Immunol* (2021) 11:604944. doi: 10.3389/fimmu.2020.604944
68. Haferkamp S, Drexler K, Federlin M, Schlitt HJ, Berneburg M, Adamski J, et al. Extracellular Citrate Fuels Cancer Cell Metabolism and Growth. *Front Cell Dev Biol* (2020) 8:602476. doi: 10.3389/fcell.2020.602476
69. Souza JL, Martins-Cardoso K, Guimarães IS, de Melo AC, Lopes AH, Monteiro RQ, et al. Interplay Between EGFR and the Platelet-Activating Factor/Paf Receptor Signaling Axis Mediates Aggressive Behavior of Cervical Cancer. *Front Oncol* (2020) 10:557280. doi: 10.3389/fonc.2020.557280
70. Miyake M, Hori S, Owari T, Oda Y, Tatsumi Y, Nakai Y, et al. Clinical Impact of Tumor-Infiltrating Lymphocytes and PD-L1-Positive Cells as Prognostic and Predictive Biomarkers in Urological Malignancies and Retroperitoneal Sarcoma. *Cancers (Basel)* (2020) 12:3153. doi: 10.3390/cancers12113153
71. Fusco N, Vaira V, Righi I, Sajjadi E, Venetis K, Lopez G, et al. Characterization of the Immune Microenvironment in Malignant Pleural Mesothelioma Reveals Prognostic Subgroups of Patients. *Lung Cancer* (2020) 150:53–61. doi: 10.1016/j.lungcan.2020.09.026
72. Vilariño N, Bruna J, Bosch-Barrera J, Valiente M, Nadal E. Immunotherapy in NSCLC Patients With Brain Metastases. Understanding Brain Tumor Microenvironment and Dissecting Outcomes From Immune Checkpoint Blockade in the Clinic. *Cancer Treat Rev* (2020) 89:1–10. doi: 10.1016/j.ctrv.2020.102067
73. Baba Y, Nomoto D, Okadome K, Ishimoto T, Iwatsuki M, Miyamoto Y, et al. Tumor Immune Microenvironment and Immune Checkpoint Inhibitors in Esophageal Squamous Cell Carcinoma. *Cancer Sci* (2020) 111:3132–41. doi: 10.1111/cas.14541
74. Effern M, Glodde N, Braun M, Liebing J, Boll HN, Yong M, et al. Adoptive T Cell Therapy Targeting Different Gene Products Reveals Diverse and Context-Dependent Immune Evasion in Melanoma. *Immunity* (2020) 53:564–580.e9. doi: 10.1016/j.immuni.2020.07.007
75. Osborne N, Sundseth R, Burks J, Cao H, Liu X, Kroemer AH, et al. Gastrin Vaccine Improves Response to Immune Checkpoint Antibody in Murine Pancreatic Cancer by Altering the Tumor Microenvironment. *Cancer Immunol Immunother* (2019) 68:1635–48. doi: 10.1007/s00262-019-02398-6
76. Stein M, Keshav S, Harris N, Gordon S. Interleukin 4 Potently Enhances Murine Macrophage Mannose Receptor Activity: A Marker of Alternative Immunologic Macrophage Activation. *J Exp Med* (1992) 176:287–92. doi: 10.1084/jem.176.1.287
77. Ferrante CJ, Pinhal-Enfield G, Elson G, Cronstein BN, Hasko G, Outram S, et al. The Adenosine-Dependent Angiogenic Switch of Macrophages to an M2-like Phenotype is Independent of Interleukin-4 Receptor Alpha (IL-4Rα) Signaling. *Inflammation* (2013) 36:921–31. doi: 10.1007/s10753-013-9621-3
78. Little AC, Pathanjeli P, Wu Z, Bao L, Goo LE, Yates JA, et al. Il-4/Il-13 Stimulated Macrophages Enhance Breast Cancer Invasion Via Rho-Gtpase Regulation of Synergistic Vegf/Ccl-18 Signaling. *Front Oncol* (2019) 9:456. doi: 10.3389/fonc.2019.00456
79. Grugan KD, McCabe FL, Kinder M, Greenplate AR, Harman BC, Ekert JE, et al. Tumor-Associated Macrophages Promote Invasion While Retaining Fc-Dependent Anti-Tumor Function. *J Immunol* (2012) 189:5457. doi: 10.4049/jimmunol.1201889
80. Liu Y, Ji X, Kang N, Zhou J, Liang X, Li J, et al. Tumor Necrosis Factor α Inhibition Overcomes Immunosuppressive M2b Macrophage-Induced Bevacizumab Resistance in Triple-Negative Breast Cancer. *Cell Death Dis* (2020) 11:993–3. doi: 10.1038/s41419-020-03161-x
81. Steitz AM, Steffes A, Finkernagel F, Unger A, Sommerfeld L, Jansen JM, et al. Tumor-Associated Macrophages Promote Ovarian Cancer Cell Migration

by Secreting Transforming Growth Factor Beta Induced (TGFBI) and Tenascin C. *Cell Death Dis* (2020) 11:249–9. doi: 10.1038/s41419-020-2438-8
82. Sousa S, Brion R, Lintunen M, Kronqvist P, Sandholm J, Mönkkönen J, et al. Human Breast Cancer Cells Educate Macrophages Toward the M2 Activation Status. *Breast Cancer Res* (2015) 17:101–1. doi: 10.1186/s13058-015-0621-0
83. Cao W, Peters JH, Nieman D, Sharma M, Watson T, Yu J. Macrophage Subtype Predicts Lymph Node Metastasis in Oesophageal Adenocarcinoma and Promotes Cancer Cell Invasion In Vitro. *Br J Cancer* (2015) 113:738–46. doi: 10.1038/bjc.2015.292
84. Shima T, Shimoda M, Shigenobu T, Ohtsuka T, Nishimura T, Emoto K, et al. Infiltration of Tumor-Associated Macrophages is Involved in Tumor Programmed Death-Ligand 1 Expression in Early Lung Adenocarcinoma. *Cancer Sci* (2020) 111:727–38. doi: 10.1111/cas.14272
85. Verheul HMW, Pinedo HM. The Role of Vascular Endothelial Growth Factor (VEGF) in Tumor Angiogenesis and Early Clinical Development of VEGFReceptor Kinase Inhibitors. *Clin Breast Cancer* (2000) 1:S80–4. doi: 10.3816/CBC.2000.s.015
86. Tan PHS, Chia SS, Toh SL, Goh JCH, Nathan SS. The Dominant Role of IL-8 as an Angiogenic Driver in a Three-Dimensional Physiological Tumor Construct for Drug Testing. *Tissue Eng Part A* (2014) 20:1758–66. doi: 10.1089/ten.TEA.2013.0245
87. Rogers TL, Holen I. Tumour Macrophages as Potential Targets of Bisphosphonates. *J Transl Med* (2011) 9:177–7. doi: 10.1186/1479-5876-9-177
88. Veltman JD, Lambers MEH, van Nimwegen M, Hendriks RW, Hoogsteden HC, Hegmans JPJJ, et al. Zoledronic Acid Impairs Myeloid Differentiation to Tumour-Associated Macrophages in Mesothelioma. *Br J Cancer* (2010) 103:629–41. doi: 10.1038/sj.bjc.6605814
89. Khan KA, Ponce de Léon JL, Benguigui M, Xu P, Chow A, Cruz-Muñoz W, et al. Immunostimulatory and Anti-Tumor Metronomic Cyclophosphamide Regimens Assessed in Primary Orthotopic and Metastatic Murine Breast Cancer. *NPJ Breast Cancer* (2020) 6:29. doi: 10.1038/s41523-020-0171-1
90. Mejías R, Pérez-Yagüe S, Gutiérrez L, Cabrera LI, Spada R, Acedo P, et al. Dimercaptosuccinic Acid-Coated Magnetite Nanoparticles for Magnetically Guided In Vivo Delivery of Interferon Gamma for Cancer Immunotherapy. *Biomaterials* (2011) 32:2938–52. doi: 10.1016/j.biomaterials.2011.01.008
91. Jin L, Wang Q, Chen J, Wang Z, Xin H, Zhang D. Efficient Delivery of Therapeutic siRNA by Fe(3)O(4) Magnetic Nanoparticles Into Oral Cancer Cells. *Pharmaceutics* (2019) 11:615. doi: 10.3390/pharmaceutics11110615
92. Cristofolini T, Dalmina M, Sierra JA, Silva AH, Pasa AA, Pittella F, et al. Multifunctional Hybrid Nanoparticles as Magnetic Delivery Systems for siRNA Targeting the HER2 Gene in Breast Cancer Cells. *Mater Sci Eng: C* (2020) 109:110555. doi: 10.1016/j.msec.2019.110555
93. Bocanegra Gondan AI, Ruiz-de-Angulo A, Zabaleta A, Gómez Blanco N, Cobaleda-Siles BM, García-Granda MJ, et al. Effective Cancer Immunotherapy in Mice by polyIC-imiquimod Complexes and Engineered Magnetic Nanoparticles. *Biomaterials* (2018) 170:95–115. doi: 10.1016/j.biomaterials.2018.04.003
94. Mulens-Arias V, Rojas JM, Pérez-Yagüe S, Morales M del P, Barber DF. Polyethylenimine-Coated SPION Exhibits Potential Intrinsic Anti-Metastatic Properties Inhibiting Migration and Invasion of Pancreatic Tumor Cells. *J Controlled Release* (2015) 216:78–92. doi: 10.1016/j.jconrel.2015.08.009
95. Mulens-Arias V, Rojas JM, Sanz-Ortega L, Portilla Y, Pérez-Yagüe S, Barber DF. Polyethylenimine-Coated Superparamagnetic Iron Oxide Nanoparticles Impair In Vitro and In Vivo Angiogenesis. *Nanomed: Nanotechnol Biol Med* (2019) 21:102063. doi: 10.1016/j.nano.2019.102063
96. Akatsuka S, Yamashita Y, Ohara H, Liu Y-T, Izumiya M, Abe K, et al. Fenton Reaction Induced Cancer in Wild Type Rats Recapitulates Genomic Alterations Observed in Human Cancer. *PloS One* (2012) 7:e43403–3. doi: 10.1371/journal.pone.0043403
97. Zhou Y, Que K-T, Tang H-M, Zhang P, Fu Q-M, Liu Z-J. Anti-CD206 Antibody-Conjugated Fe(3)O(4)-based PLGA Nanoparticles Selectively Promote Tumor-Associated Macrophages to Polarize to the Pro-Inflammatory Subtype. *Oncol Lett* (2020) 20:298–8. doi: 10.3892/ol.2020.12161
98. Zhang W, Cao S, Liang S, Tan CH, Luo B, Xu X, et al. Differently Charged Super-Paramagnetic Iron Oxide Nanoparticles Preferentially Induced M1-Like Phenotype of Macrophages. *Front Bioeng Biotechnol* (2020) 8:537. doi: 10.3389/fbioe.2020.00537
99. Zanganeh S, Hutter G, Spitler R, Lenkov O, Mahmoudi M, Shaw A, et al. Iron Oxide Nanoparticles Inhibit Tumour Growth by Inducing Pro-Inflammatory Macrophage Polarization in Tumour Tissues. *Nat Nanotechnol* (2016) 11:986–94. doi: 10.1038/nnano.2016.168
100. Cheng J, Zhang Q, Fan S, Zhang A, Liu B, Hong Y, et al. The Vacuolization of Macrophages Induced by Large Amounts of Inorganic Nanoparticle Uptake to Enhance the Immune Response. *Nanoscale* (2019) 11:22849–59. doi: 10.1039/C9NR08261A
101. Mulens-Arias V, Rojas JM, Pérez-Yagüe S, Morales MP, Barber DF. Polyethylenimine-Coated SPIONs Trigger Macrophage Activation Through TLR-4 Signaling and ROS Production and Modulate Podosome Dynamics. *Biomaterials* (2015) 52:494–506. doi: 10.1016/j.biomaterials.2015.02.068
102. Jin R, Liu L, Zhu W, Li D, Yang L, Duan J, et al. Iron Oxide Nanoparticles Promote Macrophage Autophagy and Inflammatory Response Through Activation of Toll-Like Receptor-4 Signaling. *Biomaterials* (2019) 203:23–30. doi: 10.1016/j.biomaterials.2019.02.026
103. Rojas JM, Sanz-Ortega L, Mulens-Arias V, Gutiérrez L, Pérez-Yagüe S, Barber DF. Superparamagnetic Iron Oxide Nanoparticle Uptake Alters M2 Macrophage Phenotype, Iron Metabolism, Migration and Invasion. *Nanomed: Nanotechnol Biol Med* (2016) 12:1127–38. doi: 10.1016/j.nano.2015.11.020
104. Laskar A, Eilertsen J, Li W, Yuan X-M. SPION Primes THP1 Derived M2 Macrophages Towards M1-like Macrophages. *Biochem Biophys Res Commun* (2013) 441:737–42. doi: 10.1016/j.bbrc.2013.10.115
105. Chen Y, Zeng Z, Ying H, Wu C, Chen S. Superparamagnetic Iron Oxide Nanoparticles Attenuate Lipopolysaccharide-Induced Inflammatory Responses Through Modulation of Toll-Like Receptor 4 Expression. *J Appl Toxicol* (2020) 40:1067–75. doi: 10.1002/jat.3967
106. Dalzon B, Torres A, Reymond S, Gallet B, Saint-Antonin F, Collin-Faure V, et al. Influences of Nanoparticles Characteristics on the Cellular Responses: The Example of Iron Oxide and Macrophages. *Nanomater (Basel)* (2020) 10:E266. doi: 10.3390/nano10020266
107. Liu Y, Chen Z, Gu N, Wang J. Effects of DMSA-coated Fe3O4 Magnetic Nanoparticles on Global Gene Expression of Mouse Macrophage RAW264.7 Cells. *Toxicol Lett* (2011) 205:130–9. doi: 10.1016/j.toxlet.2011.05.1031
108. Wolf-Grosse S, Mollnes TE, Ali S, Stenvik J, Nilsen AM. Iron Oxide Nanoparticles Enhance Toll-like Receptor-Induced Cytokines in a Particle Size- and Actin-Dependent Manner in Human Blood. *Nanomedicine* (2018) 13:1773–85. doi: 10.2217/nnm-2017-0362
109. Frtús A, Smolková B, Uzhytchak M, Lunova M, Jirsa M, Kubinová Š, et al. Analyzing the Mechanisms of Iron Oxide Nanoparticles Interactions With Cells: A Road From Failure to Success in Clinical Applications. *J Controlled Release* (2020) 328:59–77. doi: 10.1016/j.jconrel.2020.08.036
110. Malhotra N, Lee J-S, Liman RAD, Ruallo JMS, Villaflores OB, Ger T-R, et al. Potential Toxicity of Iron Oxide Magnetic Nanoparticles: A Review. *Molecules* (2020) 25:3159. doi: 10.3390/molecules25143159
111. Grosse S, Stenvik J, Nilsen AM. Iron Oxide Nanoparticles Modulate Lipopolysaccharide-Induced Inflammatory Responses in Primary Human Monocytes. *Int J Nanomed* (2016) 11:4625–42. doi: 10.2147/IJN.S113425
112. Liu L, Sha R, Yang L, Zhao X, Zhu Y, Gao J, et al. Impact of Morphology on Iron Oxide Nanoparticles-Induced Inflammasome Activation in Macrophages. *ACS Appl Mater Interfaces* (2018) 10:41197–206. doi: 10.1021/acsami.8b17474
113. Chen S, Chen S, Zeng Y, Lin L, Wu C, Ke Y, et al. Size-Dependent Superparamagnetic Iron Oxide Nanoparticles Dictate Interleukin-1β Release From Mouse Bone Marrow-Derived Macrophages. *J Appl Toxicol* (2018) 38:978–86. doi: 10.1002/jat.3606
114. Narayanan A, Amaya M, Voss K, Chung M, Benedict A, Sampey G, et al. Reactive Oxygen Species Activate Nfκb (p65) and p53 and Induce Apoptosis in RVFV Infected Liver Cells. *Virology* (2014) 449:270–86. doi: 10.1016/j.virol.2013.11.023
115. Wang Y, Zeigler MM, Lam GK, Hunter MG, Eubank TD, Khramtsov VV, et al. The Role of the NADPH Oxidase Complex, P38 MAPK, and Akt in Regulating Human Monocyte/Macrophage Survival. *Am J Respir Cell Mol Biol* (2007) 36:68–77. doi: 10.1165/rcmb.2006-0165OC

116. Lingappan K. Nf-κb in Oxidative Stress. *Curr Opin Toxicol* (2018) 7:81–6. doi: 10.1016/j.cotox.2017.11.002
117. Schieber M, Chandel NS. Ros Function in Redox Signaling and Oxidative Stress. *Curr Biol* (2014) 24:R453–62. doi: 10.1016/j.cub.2014.03.034
118. Liu X, Gal J, Zhu H. Sequestosome 1/p62: A Multi-Domain Protein With Multi-Faceted Functions. *Front Biol* (2012) 7:189–201. doi: 10.1007/s11515-012-1217-z
119. Seibenhener ML, Babu JR, Geetha T, Wong HC, Krishna NR, Wooten MW. Sequestosome 1/P62 Is a Polyubiquitin Chain Binding Protein Involved in Ubiquitin Proteasome Degradation. *Mol Cell Biol* (2004) 24:8055. doi: 10.1128/MCB.24.18.8055-8068.2004
120. Yang H, Ni H-M, Guo F, Ding Y, Shi Y-H, Lahiri P, et al. Sequestosome 1/P62 Protein is Associated With Autophagic Removal of Excess Hepatic Endoplasmic Reticulum in Mice. *J Biol Chem* (2016) 291:18663–74. doi: 10.1074/jbc.M116.739821
121. Recalcati S, Locati M, Marini A, Santambrogio P, Zaninotto F, De Pizzol M, et al. Differential Regulation of Iron Homeostasis During Human Macrophage Polarized Activation. *Eur J Immunol* (2010) 40:824–35. doi: 10.1002/eji.200939889
122. Zini C, Venneri MA, Miglietta S, Caruso D, Porta N, Isidori AM, et al. USPIO-Labeling in M1 and M2-polarized Macrophages: An In Vitro Study Using a Clinical Magnetic Resonance Scanner. *J Cell Physiol* (2018) 233:5823–8. doi: 10.1002/jcp.26360
123. Bolte AC, Lukens JR. Neuroimmune Cleanup Crews in Brain Injury. *Trends Immunol* (2021) 42:480–94. doi: 10.1016/j.it.2021.04.003
124. Cayre M, Falque M, Mercier O, Magalon K, Durbec P. Myelin Repair: From Animal Models to Humans. *Front Cell Neurosci* (2021) 15:604865. doi: 10.3389/fncel.2021.604865
125. Stoessel MB, Majewska AK. Little Cells of the Little Brain: Microglia in Cerebellar Development and Function. *Trends Neurosci* (2021) doi: 10.1016/j.tins.2021.04.001
126. Lanza M, Casili G, Campolo M, Paterniti I, Colarossi C, Mare M, et al. Immunomodulatory Effect of Microglia-Released Cytokines in Gliomas. *Brain Sci* (2021) 11:466. doi: 10.3390/brainsci11040466
127. Wu H-Y, Chung M-C, Wang C-C, Huang C-H, Liang H-J, Jan T-R. Iron Oxide Nanoparticles Suppress the Production of IL-1beta Via the Secretory Lysosomal Pathway in Murine Microglial Cells. *Particle Fibre Toxicol* (2013) 10:46. doi: 10.1186/1743-8977-10-46
128. Wang Y, Wang B, Zhu M-T, Li M, Wang H-J, Wang M, et al. Microglial Activation, Recruitment and Phagocytosis as Linked Phenomena in Ferric Oxide Nanoparticle Exposure. *Toxicol Lett* (2011) 205:26–37. doi: 10.1016/j.toxlet.2011.05.001
129. Luo L, Iqbal MZ, Liu C, Xing J, Akakuru OU, Fang Q, et al. Engineered Nano-Immunopotentiators Efficiently Promote Cancer Immunotherapy for Inhibiting and Preventing Lung Metastasis of Melanoma. *Biomaterials* (2019) 223:119464. doi: 10.1016/j.biomaterials.2019.119464
130. Zhao Y, Zhao X, Cheng Y, Guo X, Yuan W. Iron Oxide Nanoparticles-Based Vaccine Delivery for Cancer Treatment. *Mol Pharmaceut* (2018) 15:1791–9. doi: 10.1021/acs.molpharmaceut.7b01103
131. Sungsuwan S, Yin Z, Huang X. Lipopeptide-Coated Iron Oxide Nanoparticles as Potential Glycoconjugate-Based Synthetic Anticancer Vaccines. *ACS Appl Mater Interfaces* (2015) 17535–44. doi: 10.1021/acsami.5b05497
132. Li C-X, Zhang Y, Dong X, Zhang L, Liu M-D, Li B, et al. Artificially Reprogrammed Macrophages as Tumor-Tropic Immunosuppression-Resistant Biologics to Realize Therapeutics Production and Immune Activation. *Adv Mater* (2019) 31:1807211. doi: 10.1002/adma.201807211
133. Costa da Silva M, Breckwoldt MO, Vinchi F, Correia MP, Stojanovic A, Thielmann CM, et al. Iron Induces Anti-Tumor Activity in Tumor-Associated Macrophages. *Front Immunol* (2017) 8:1479. doi: 10.3389/fimmu.2017.01479
134. Ruiz-de-Angulo A, Bilbao-Asensio M, Cronin J, Evans SJ, Clift MJD, Llop J, et al. Chemically Programmed Vaccines: Iron Catalysis in Nanoparticles Enhances Combination Immunotherapy and Immunotherapy-Promoted Tumor Ferroptosis. *iScience* (2020) 23:1–18. doi: 10.1016/j.isci.2020.101499
135. Shen L, Krauthäuser S, Fischer K, Hobernik D, Abassi Y, Dzionek A, et al. Vaccination With Trifunctional Nanoparticles That Address CD8+ Dendritic Cells Inhibits Growth of Established Melanoma. *Nanomedicine* (2016) 11:2647–62. doi: 10.2217/nnm-2016-0174
136. Shevtsov MA, Nikolaev BP, Yakovleva LY, Parr MA, Marchenko YY, Eliseev I, et al. 70-kDa Heat Shock Protein Coated Magnetic Nanocarriers as a Nanovaccine for Induction of Anti-Tumor Immune Response in Experimental Glioma. *J Controlled Release* (2015) 220:329–40. doi: 10.1016/j.jconrel.2015.10.051
137. Traini G, Ruiz-de-Angulo A, Blanco-Canosa JB, Zamacola Bascarán K, Molinaro A, Silipo A, et al. Cancer Immunotherapy of TLR4 Agonist–Antigen Constructs Enhanced With Pathogen-Mimicking Magnetite Nanoparticles and Checkpoint Blockade of PD-L1. *Small* (2019) 15:1803993. doi: 10.1002/smll.201803993

Conflict of Interest: The authors declare that their research was conducted in the absence of any commercial or financial relationships that could be construed as a potential conflict of interest.

frontiers in Immunology

ORIGINAL RESEARCH
published: 16 June 2021
doi: 10.3389/fimmu.2021.684612

In Vivo Sustained Release of Peptide Vaccine Mediated by Dendritic Mesoporous Silica Nanocarriers

Weiteng An[1], *Sira Defaus*[2]*, *David Andreu*[2] *and Pilar Rivera-Gil*[1]*

[1] Integrative Biomedical Materials and Nanomedicine Laboratory, Department of Experimental and Health Sciences, Universitat Pompeu Fabra, Barcelona, Spain, [2] Proteomics and Protein Chemistry Unit, Department of Experimental and Health Sciences, Universitat Pompeu Fabra, Barcelona, Spain

Mesoporous silica nanoparticles have drawn increasing attention as promising candidates in vaccine delivery. Previous studies evaluating silica-based vaccine delivery systems concentrated largely on macromolecular antigens, such as inactivated whole viruses. In this study, we synthesized dendritic mesoporous silica nanoparticles (DMSNs), and we evaluated their effectiveness as delivery platforms for peptide-based subunit vaccines. We encapsulated and tested *in vivo* an earlier reported foot-and-mouth disease virus (FMDV) peptide vaccine (B_2T). The B_2T@DMSNs formulation contained the peptide vaccine and the DMSNs without further need of other compounds neither adjuvants nor emulsions. We measured *in vitro* a sustained release up to 930 h. B_2T@DMSNs-57 and B_2T@DMSNs-156 released 23.7% (135 μg) and 22.8% (132 μg) of the total B_2T. The formation of a corona of serum proteins around the DMSNs increased the B_2T release up to 61% (348 μg/mg) and 80% (464 μg/mg) for B_2T@DMSNs-57 and B_2T@DMSNs-156. *In vitro* results point out to a longer sustained release, assisted by the formation of a protein corona around DMSNs, compared to the reference formulation (i.e., B_2T emulsified in Montanide). We further confirmed *in vivo* immunogenicity of B_2T@DMSNs in a particle size-dependent manner. Since B_2T@DMSNs elicited specific immune responses in mice with high IgG production like the reference B_2T@Montanide™, self-adjuvant properties of the DMSNs could be ascribed. Our results display DMSNs as efficacious nanocarriers for peptide-based vaccine administration.

Keywords: dendritic mesoporous silica nanoparticles, peptide vaccines, sustained and controlled release, foot-and-mouth disease virus, nanovaccine, immunogenicity, adjuvancy

OPEN ACCESS

Edited by:
David Pozo,
University of Seville, Spain

Reviewed by:
Even Fossum,
Oslo University Hospital, Norway
Xin Li,
China Agricultural University, China

***Correspondence:**
Pilar Rivera-Gil
pilar.rivera@upf.edu
Sira Defaus
sira.defaus@upf.edu

Specialty section:
This article was submitted to Molecular Innate Immunity, a section of the journal Frontiers in Immunology

Received: *23 March 2021*
Accepted: *24 May 2021*
Published: *16 June 2021*

Citation:
An W, Defaus S, Andreu D and Rivera-Gil P (2021) In Vivo Sustained Release of Peptide Vaccine Mediated by Dendritic Mesoporous Silica Nanocarriers. Front. Immunol. 12:684612. doi: 10.3389/fimmu.2021.684612

INTRODUCTION

Peptide-based vaccines are considered an attractive alternative strategy to overcome many of the limitations of conventional (inactivated, attenuated) whole virus-based vaccines (1–3). They present advantages such as reduced toxicity, good definition of T- and B-cell epitopes for targeted immune responses, cost-effective scale up manufacturing processes, easy handling, storage, and transport (1, 4, 5). These advantages have prompted the progress of many peptide-based vaccines to different preclinical and clinical stages (1, 6, 7). Nevertheless, peptide-based vaccines tend to be poorly

immunogenic usually requiring adjuvants, multivalency, and/or delivery systems to become more effective *in vivo*. Adjuvants of different kinds, such as aluminum hydroxide, mineral salts, water-oil emulsions, or liposome-based formulations have been developed to enhance efficacy (7). Although these strategies can boost to a certain extent the low immunogenicity of peptide-based vaccines, only a limited number are approved for human and animal applications due to their not well-established mode of action, as well as to other related toxicity and safety issues (8, 9).

In the last decade, the field of nanovaccines has gained maturity (10–13). Nanoparticles, especially synthetic ones made of polymers, phospholipids, metal, carbon, or silica (14) among other compositions have been extensively studied for vaccine applications ref (1, 9, 15, 16). Within the variety of nanomaterials used for vaccine delivery, mesoporous silica nanoparticles (MSNs), especially dendritic mesoporous silica nanoparticles (DMSNs), are emerging as promising vaccine delivery platforms because of their versatile formulation, boosting abilities, lack of side effects, and depot effect. They have unique central-radial pore structures with large pore sizes (17–19) and are characterized by low cross-linking silica frameworks with fast degradability rate *in vivo* (20). Studies on DMSNS show their enhanced loading capacity, sustained release profile, easy surface functionalization, and potential adjuvant activity (21, 22). Furthermore, DMSNs have shown effective immune potentiation *in vivo*, inducing strong humoral and cellular immune responses against target antigens (23–25). The majority of studies on MSNs-based vaccine delivery systems are focused on carrying large-size immunogens, such as bacterial recombinants, viral capsid proteins and OVA- and BSA-conjugated model vaccines (26–29), whereas few papers explore their use to carry smaller biomolecules, such as peptides in subunit vaccines.

In this study, we extend the use of DMSNs to delivery platforms for peptide-based vaccines and evaluate their *in vivo* effectiveness. We have encapsulated a peptide construct named B_2T, which confers full protection against foot-and-mouth disease virus (FMDV) in swine (30, 31). Previous publications of the authors have shown that inclusion of a T-cell epitope in the B_2T construct provides a rather powerful T-cell response (lymphoproliferation, γ-interferon production) (31–33). B_2T is currently administered emulsified with Montanide™ ISA 50V2 W/O (water in oil) (*i.e.*, B_2T@Montanide™). This formulation has some drawbacks. For instance, there are several studies reporting unacceptable local reactions toward the Montanide adjuvant (34). Moreover, Montanide requires a dedicated emulsification procedure for each antigen which add complexity to its industrial production (35). To overcome these challenges, we have explored the use of DMSNs loaded with B_2T as nanovaccine against FMDV. Briefly, we have synthesized DMSNs of different sizes (57 ± 9 nm and 156 ± 10 nm) and have loaded them with B_2T, naming the resulting nanoformulation B_2T@DMSNs. Both sizes exhibited high B_2T loading capacities (570 μg/mg for DMSNs-57 and 580 μg/mg for DMSNs-156) and an *in vitro* sustained B_2T release profile over 930 h. Furthermore, RAW 264.7 macrophage cells efficiently internalized the fluorescent version of both nanoformulations in a size-dependent manner. Finally, we have confirmed a specific immune response with high IgG production upon vaccination of outbred Swiss mice (Swiss ICR-CD1) with two doses of B_2T@DMSNs, obtaining similar antibody titers than those elicited by the previous gold standard B_2T@Montanide™.

MATERIALS AND METHODS

For a detailed description of the procedures and more results, we refer the readers to the **Supporting Information File**.

Synthesis and Characterization of DMSNs-57 and DMSNs-156

The DMSNs with a diameter of 156 nm (designated as DMSNs-156) were synthesized using a modified version of a previously reported method (17). Briefly, 136 mg TEA were added to 50 mL Milli-Q water and stirred at 500 rpm, 80°C for 0.5 h. Then, 760 mg CTAB and 250 mg sodium salicylate (NaSal) was added to the above solution and stirred for another 1 h. Next, 4 ml TEOS was added dropwise to the solution under stirring, which continued overnight. The products were collected by centrifugation at 12,000 rpm for 10 min and washed three times with ethanol. Then, the collected products were extracted three times with 80 ml of methanol solution containing 4.5 ml of HCl (37%) at 65°C for 6 h to remove the template. Finally, the nanoparticles were dried in vacuum at room temperature overnight. DMSNs with a diameter of 57 nm (designated as DMSNs-57) were synthesized following the abovementioned method except for decreasing the amount of structure directing agent NaSal from 250 to 83 mg.

The structure of both DMSNs types was imaged with a transmission electron microscope (TEM, JEOL JEM1010) at an acceleration voltage of 80 kV. TEM specimens were prepared by evaporating one drop of ethanolic nanoparticle solution on Ted Pella Formvar carbon-coated copper grids. The z-potential and hydrodynamic diameter of the samples was determined in a Malvern Zetasizer ZS instrument at 25°C. Samples were dispersed in water and transferred into disposable polystyrene cuvette. The given values are the average of triplicate readings.

See de **Supplementary File** (section *§SI-1.1*) for complementary information.

B_2T Synthesis

The dendrimeric B_2T immunogen was produced as described earlier (31), by conjugation of 2 copies of the B-cell epitope moiety to a maleimide-functionalized T-cell epitope. The conjugation reaction was clean and practically quantitative, and the resulting branched peptide was satisfactorily characterized by HPLC and mass spectrometry. See section *§SI-1.2* for complementary information and section *§SI-2.1* for the synthesis of fluoro-B_2T@DMSNs.

B_2T Loading in DMSNs-57 and DMSNs-156 and Quantification of Peptide Loading

We followed the same methodology to load B_2T into both DMSNs sizes. The resulting products were named, B_2T@DMSNs-57 and B_2T@DMSNs-156. Briefly, 1.5 mg B_2T and 2.0 mg DMSNs were mixed in 2.0 mL DPBS buffer solution (pH 7.4) and then properly dispersed by sonication for 5 min. The resulting mixture was gently shaken at 200 rpm for 5 h at RT. Afterward, the products were separated by centrifugation at 12,000 rpm for 10 min and washed twice with PBS. B_2T encapsulation efficiency (EE%) was defined as follows:

$$B_2T \text{ encapsulation efficiency } (EE\,\%) = (\textit{weight of loaded } B_2T / \textit{weight of total } B_2T) \times 100\,\%$$

where the amount of loaded B_2T was determined by subtracting the free B_2T in the supernatant from the total amount, and the amount of free B_2T in the supernatant was calculated based on the B_2T calibration curve obtained in DPBS (section *§SI-1.3*, **Figure SI-3**). See section *§SI-1.4* for complementary information on the impact of key parameters (ionic strength, peptide structure, and DMSNs charge) on the loading efficiencies, and section *§SI-2.1* for the loading of fluoro-B_2T into DMSNs.

B_2T Calibration Curve

A B_2T stock solution (1,000 μg/ml) was prepared by dissolving 2 mg lyophilized B_2T powder in 2 ml DPBS. From this stock solution serial dilutions in DPBS (31.3, 62.5, 125, 250, and 500 μg/ml) were prepared and measured on a Biochrom™ Ultrospec 2100 Pro UV/Vis spectrophotometer using a quartz cuvette with a 1-cm path length (with DPBS as blank). The calibration curve was constructed by plotting the absorbance at 225 nm against the corresponding B_2T concentrations. See section *§SI-1.3* for complementary information.

B_2T Release Kinetics From the DMSNs

Release experiments were carried out in 1.5 ml Eppendorf tubes containing 1.0 mg DMSNs loaded with B_2T and 1.0 ml DPBS (pH 7.4). Samples were gently shaken at 37°C and, at predetermined time points, the suspension was centrifuged at 12,000 rpm for 10 min. We took the supernatant and measure the absorbance (225 nm) of B_2T released. The procedure was repeated for each time point and for both DMSNs. Fresh DPBS (same volume than aliquot of supernatant taken) was added to redisperse the pellet. All release measurements were performed in duplicate.

Imaging the Cellular Uptake of B_2T@DMSNs

RAW 264.7 cells in RPMI 1640 medium (containing 2 mM L-glutamine, 10% heat-inactivated FBS, and 1% penicillin and streptomycin) were seeded in Ibidi μ-slide 8 well at a density of 5.0×10^4 cells/well. Cells were incubated at 37°C in an atmosphere of 5% CO_2 for 24 h. Then, 30 μg/ml of fluoro-B_2T@DMSNs was added to the cells. Following 0.5, 1, 2, 4, 8, and 16 h incubation, cells were washed three times with PBS, and fresh growth medium containing CellMask deep red plasma membrane was added and incubated for 8 min. After three washes with PBS, fresh PBS was added, and cells were imaged by confocal laser scanning microscopy (CLSM). See section *§SI-2.2* for complementary information.

Flow Cytometry Analysis of Cellular Uptake

RAW 264.7 cells were seeded in six-well plates in RPMI 1640 medium (containing 2 mM L-glutamine, 10% heat-inactivated FBS, and 1% penicillin and streptomycin) at a density of 1.0×10^6 cells/well. Cells were incubated at 37°C in an atmosphere of 5% CO_2 for 24 h. Then, 30 μg/ml fluoro-B_2T@DMSNs was added. Following 0.5, 1, 2, 4, 8, and 16 h incubation, cells were washed three times with PBS, new PBS was added, and cells were carefully detached from the plates with a Falcon cell scraper. The collected cells were transferred to tubes, were placed in ice, and the nuclear dye, DAPI was added to a final concentration of 1.0 μg/ml, and incubated for 2 min. The labelled cells were then measured by flow cytometry (FC) in a BD LSRFortessa X-50 flow cytometer. The mean fluorescence intensity (MFI) and percentage of cells with a positive fluorescent signal compared to the control (untreated cells) were determined on 5,000 gated single-living cells. FACS data were processed by the method described in section *§SI-2.3*.

Mice Immunization

Experiments were carried out in the animal facility of the CSIC Center for Research and Development (CID-CSIC), in agreement with EU (Directive 2010/63/EU on the protection of animals used for scientific purposes) and domestic (Real Decreto 53/2013) regulations. The protocol to produce antibodies was in accordance with institutional guidelines under a license from the local government (DAAM 7463) and was approved by the Institutional Animal Care and Use Committee at the CID-CSIC.

All formulations were prepared on the day of injection. Mice were randomized into groups and inoculated by two subcutaneous injections over the interscapular area at day 0 and day 21. All mice were euthanized at day 40 by carbon dioxide inhalation. Animals were monitored three times per week for health during the study.

To assess immunogenicity of B_2T@DMSNs in mice, two trials were performed (section *§SI-3)*. In the first one, mice were divided into three groups as shown in **Table SI-1**. The first group was the positive control group (4 mice) which was immunized with 200 μl of Montanide ISA 50V2 emulsion containing 100 μg B_2T (B_2T@Montanide™), following earlier studies (30); the second (six mice) and third (four mice) groups were the sample groups. The second group was treated with 100 μg B_2T loaded in DMSNs-156 (B_2T@DMSNs-156) in 200 μl DPBS, and the third group was treated with the same amount of DMSNs alone (163 μg DMSNs-156) in 200 μl DPBS. All groups were boosted at day 21. Blood samples were collected before vaccination (day 0) and at days 14, 20 (pre-boost), and 40 (euthanize, sample obtained by cardiac puncture). In the second trial, aimed at assessing the impact of DMSNs size on

mice immunization, mice were divided into three groups as shown in **Table SI-2**. The first group was again the positive control group (B_2T@Montanide™; three mice). The second (five mice) group was treated with the formulation B_2T@DMSNs-57 and the third (five mice) group with B_2T@DMSNs-156. All mice were treated with the same dose of peptide vaccine (100 μg B_2T). Blood sample collection was extended until day 80, to study the long-term immune effect of B_2T@DMSNs.

Detection of Specific Anti-B_2T Antibodies by ELISA

Specific antibodies were detected by enzyme-linked immunosorbent assay (ELISA). 96-well Costar® plates were coated with 50 μl B_2T (15.4 μg/ml) in bicarbonate/carbonate coating buffer (0.05 M, pH 9.6) and incubated at 4°C overnight. After washing three times with DPBS, 50 μl of diluted serums (two-fold dilution series of each collected serum sample were prepared, starting at 1/150, and each dilution sample in duplicate) were incubated for 1 h at 37°C, followed by four DPBS washes. Pre-immune sera from mice were used as negative controls. Next, 50 μl of a 1:4,000 dilution of HRP-labeled rabbit anti-mouse IgG were added and incubated for 1 h at 37°C followed by five washings with DPBS. Then, 100 μl of TMB substrate solution was added for 20 min at RT in the dark. Finally, the reaction was stopped by adding 100 μl of 1 M H_2SO_4. The optical density (OD) of the samples was measured in an ELISA reader (BioRad, CA, USA) at 450 nm. Titers in a log10 scale were expressed as the reciprocal of the last dilution giving the absorbance recorded in the control wells (serum at day 0) plus 2 SD. See section *§SI-3.2* for complementary information on the individual response of each mice to the treatment.

Statistical Analysis

Differences among B_2T@DMSNs-immunized groups in B_2T-antibody titers were analyzed by one-way ANOVA, followed by Tukey's post-hoc comparisons tests. Values are cited in the text as means ± SD. All p values are two-sided, and p values < 0.05 were considered significant. Statistical analyses were conducted using GraphPad Prism Software 5.0 (San Diego, CA, USA).

RESULTS

DMSNs Synthesis and Physicochemical Characterization

TEM measurements showed that both types of DMSNs have an inorganic core diameter of 57 ± 9 nm (DMSNs-57) and 156 ± 10 nm (DMSNs-156) (**Figure 1A, B**; *§SI-1.1*, **Figures SI-1A–D**). DLS measurements indicated that the averaged hydrodynamic diameter of DMSNs-57 was 75 nm with a polydispersity index (PDI) of 0.060 and the averaged hydrodynamic diameter of DMSNs-156 was 227 nm with a PDI of 0.061 (**Figure 1C**; §SI-1.1, **Figure SI-1.E**). The low PDIs for both nanoparticles demonstrate excellent monodispersity and uniformity which are consistent with TEM images. As expected, the DLS measurement showed higher size values for the DMSNs than those measured by TEM. This is due to the DMSNs' surface hydration in aqueous solution (36). The z-potential values of DMSNs-57 and DMSNs-156 were -30.2 mV and -37.1 mV, respectively (**Figure 1C**). These results indicate colloidal stability and homogenous size distribution.

Loading B_2T Vaccine Into Differently Sized DMSNs (B_2T@DMSNs) and *In Vitro* Characterization of B_2T Release Kinetics

After synthesizing DMSNs-57 and DMSNs-156, we performed their loading with the B_2T peptide vaccine (see section *§SI-1.2*, **Figure SI-2** for B_2T structure). The B_2T amount loaded into both types of DMSNs was quantified based on its absorbance at 225 nm (section *§SI-1.3*, **Figure SI-3A**) and using a calibration curve (section *§SI-1.3*, **Figure SI-3B**). We quantified 1.14 mg and 1.16 mg of B_2T loaded in 2.0 mg of DMSNs-57 and DMSNs-156, respectively. The loading capacities were 570 μg/mg DMSNs for DMSNs-57 and 580 μg/mg DMSNs for DMSNs-156, and the encapsulation efficiencies (EE%) reached 76% and 77%, respectively. Regardless the differences in DMSNs sizes, we measured similar loading efficiencies. We attribute this to their close z-potential values and to the equivalent hydrogen bonds and polar interactions with the peptide (37). The high B_2T loading capacities obtained are probably related to the strong electrostatic interaction between the anionic DMSNs and the positively charged B_2T (pI 10.88) in DPBS (pH 7.4) and to the DMSNs central-radial pore structures with large surface areas (17, 18).

We performed the loading under different conditions (section *§SI-1.4*) (38, 39) to evaluate the impact of ionic strength (**Figure SI-4**), peptide (cargo) structure (dendrimer *vs.* linear) (**Figure SI-5**) and DMSNs charge (**Figure SI-6**) on the loading efficiency of the DMSNs. We used, for comparison, 168 nm solid silica nanoparticles (SNSs-168) (**Figures SI-4** and **SI-5**). Results on section *§SI-1.4* (**Figures SI-4, SI-5, SI-6**) displayed that the higher the ionic strength, the more B_2T was loaded into all silica nanoparticles. Being DMSNs more efficient than SNSs. The trend was maintained for the dendrimer B_2T and a linear control peptide (O PanAsia B epitope B) regardless of DMSNs charge. Up to 5× ionic strength, DMSNs-156 were more efficiently loading the peptide. Note that within this work the ionic strength was set at 1×. Furthermore, we observed that our synthesized, negatively charged DMSNs were significantly more effective in loading the B_2T peptide than their positively charged counterparts (**Figure SI-6**).

Next, we investigated the B_2T release kinetics from the DMSNs. To this end B_2T@DMSNs were dispersed in a saline buffer (1× DPBS). At given time points, we collected the supernatants after centrifugation, we measured their absorbance at 225 nm and with help of the calibration curve (**Figure SI-3.B**), we quantified the amount of B_2T released from the DMSNs. **Figure 2** shows a sustained release of B_2T up to 1000 h (41 days). After 700 h, the release curve reached a plateau. Both B_2T@DMSNs-57 and B_2T@DMSNs-156 showed similar release kinetics. The B_2T amount released in B_2T@DMSNs-57

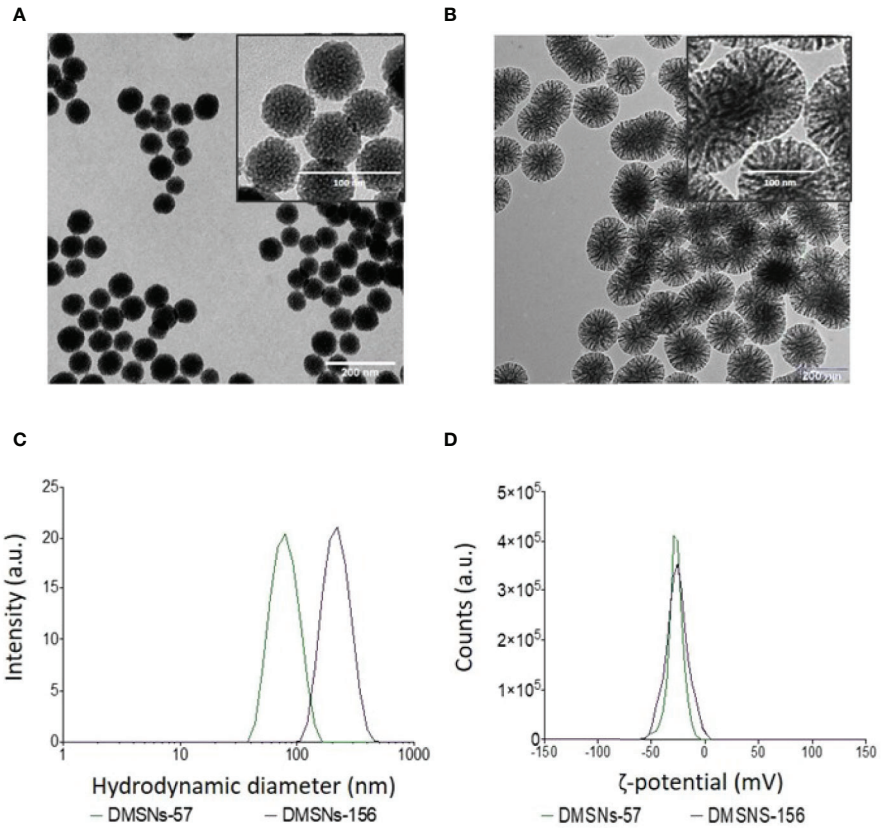

FIGURE 1 | TEM and DLS analysis of DMSNs-57 and DMSNs-156. TEM image of 57 nm DMSNs **(A)** and of 156 nm DMSNs **(B)**. Scale bar, 200 nm. The insets show the DMSNs with higher magnification revealing the dendritic structure. Scale bar, 100 nm. **(C)** DMSNs-57 and DMSNs-156 hydrodynamic size (75 ± 9 nm and 156 ± 10 nm) and **(D)** ζ-potential values (-30.2 and -37.1 mV).

and B_2T@DMSNs-156 corresponds to 23.7% (135 μg) and 22.8% (132 μg) of the total amount loaded.

Albumin is one of the most frequent proteins in physiological fluids and a major component of the protein corona of biomedical nanomaterials dispersed in such fluids (40–44). It is also known that the protein corona formed on nanoparticles is a dynamic system. Following typical nanoparticle behavior, we expected a protein corona around our DMSNs upon their *in vivo* administration. We therefore wanted to elucidate the impact of the protein corona on the B_2T release kinetics (**Figure 2**). To this end, we dispersed the B_2T@DMSNs in medium containing albumin (BSA 250 μg/ml in DPBS), allowed the DMSNs to build their protein corona and measured the B_2T release (section *§SI-1.5*) following the procedure described before. We took advantage of the distinct absorption peaks for B_2T at 225 nm (section *§SI-1.3*) and for albumin at 280 nm (section *§SI-1.5*, **Figure SI-7**) to build calibration curves. In this case we could also track changes on the protein corona formed around the B_2T@DMSNs. Our methodology enabled the concomitant quantification of the release of both components, B_2T and albumin, from the DMSNs to the medium. We validated this technology with HPLC (section *§SI-1.5*, **Figure SI-8**). Then we quantified the B_2T release from the protein coated DMSNs (**Figure 2**) and correlated the results with the amount of albumin released from the protein corona (section *§SI-1.5*, **Figure SI-9**).

After the formation of the protein corona, B_2T release increased 158% on B_2T@DMSNs-57 and 252% on B_2T@DMSNs-156. This corresponds to 61% (348 μg/mg) and 80% (464 μg/mg) of the total B_2T loaded within B_2T@DMSNs-57 and B_2T@DMSNs-156, respectively. It seems evident, that the presence of BSA significantly enhances B_2T release. We ascribed this effect to a competitive interaction towards the DMSNs in favor of BSA resulting in B_2T displacement and release (45, 46). To prove this, we monitored the changes of BSA concentration in the dispersed medium in the presence of the DMSNs (**Figure SI-9**). As seen in **Figure SI-9**, during the first 66.5 hours, both B_2T@DMSNs-57 and B_2T@DMSNs-156 kept absorbing BSA from the medium, probably due to forming BSA protein corona on DMSNs, which resulted in lower BSA concentrations (< 250 μg/mL) in the supernatants. Afterwards, the BSA level in both formations kept fluctuating around 250 μg/ml (initial concentration added) which points out to an absence of protein corona around the DMSNs. Although longer

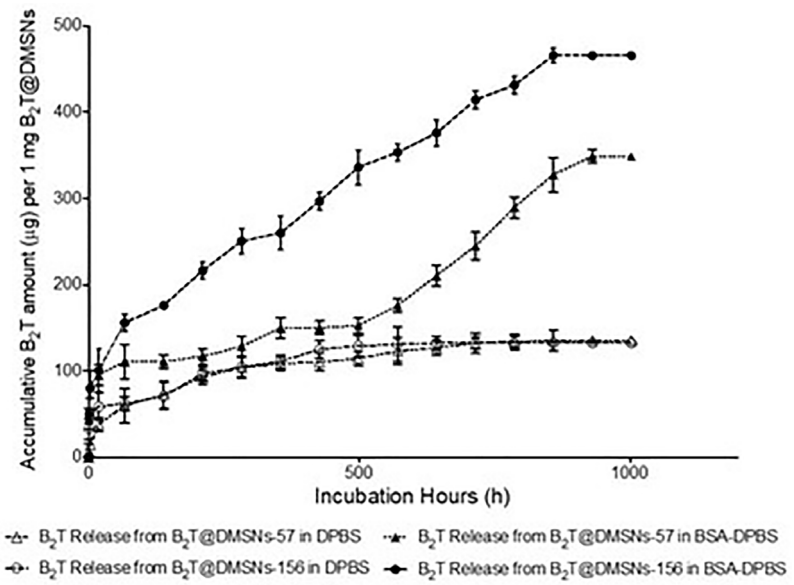

FIGURE 2 | B_2T release profiles from B_2T@DMSNs-57 and from B_2T@DMSNs-156 dispersed in DPBS or BSA-DPBS. After each time point, the supernatants were collected for UV-vis analysis and the pellets were redispersed in the same volume of medium. The procedure was repeated during 1,000 h.

experiments would be required to draw a conclusion, these results may indicate a long-term sustained release promoted by the DMSNs. At any rate, they confirm vaccine release from the DMSNs in physiological complex media as the one in the cell.

Internalization of B_2T@DMSNs by Macrophages

Cellular uptake of antigens by innate immune cells provides antigen-processing and subsequent costimulatory signals that are crucial to trigger acquired immune responses, especially for low immunogenic peptide antigens. Macrophage-like RAW 264.7 cells (47) are often used to study cellular responses to microbes and their products (48). We selected this cell model to assess *in vitro* cellular internalization of our nanoformulations, using 1 mg DMSNs-57 and 1 mg DMSNs-156 loaded with 200 μg B_2T labeled with a dye (*i.e.*, fluoro-B_2T) (see section §SI-2 and **Figure SI-10**). Similar to other nanoparticles (49), cellular uptake of fluoro-B_2T@DMSNs occurred in a size-dependent manner (**Figure 3**). The maximum uptake level was observed after 4 h for the fluoro-B_2T@DMSNs-57 (57 nm size) and after 8 h for the fluoro-B_2T@DMSNs-156 (156 nm size) (**Figures 3A, B**, and §SI-2 and **Figures SI-11, SI-12** and **SI-13**). During the first 4 h, the amount of B_2T@DMSNs-57 interacting with the cells was approximately two times the amount of B_2T@DMSNs-156 (**Figure 3B**). We can conclude that at least after an acute exposure, the smaller DMSNs-57 are faster internalized by RAW 264.7 cells than larger DMSNs-156. It is noteworthy that after the cellular uptake reached the maximum value, longer incubation times resulted in reduced uptake values. We suppose that it is due to the fast cell growth and division of RAW 264.7 cells (50) which resulted in the "dilution effect" of fluorescence intensity per cell.

Sustained Mice Immunogenicity Provided by B_2T@DMSNs

We next validated B_2T@DMSNs performance by testing *in vivo* their immunogenicity. To this end, we performed two sets of vaccination trials in mice (see section §SI-3 for a detailed description). In both trials, we injected subcutaneously samples containing the same amount of B_2T antigen (100 μg) at day 0 and boosted with the same dose at day 21. We performed an ELISA to detect specific anti-B_2T antibodies in sera collected following the schedule shown in **Tables SI-1** and **SI-2** (section §SI-2). In the first trial (**Table SI-1** and **Figure 4**), mice were vaccinated with B_2T@Montanide™ (positive control), B_2T@DMSNs-156, and bare DMSNs-156 (negative control). Results in **Figure 4** show that B_2T@DMSNs treatment elicits a consistent response with all treated mice, presenting an increase in anti-B_2T IgG production values after the boost (day 40). Although the anti-B_2T IgG level from B_2T@DMSNs-156 is slightly lower than B_2T@Montanide, these results confirm that B_2T@DMSNs-156 successfully stimulates anti-B_2T–specific immune response in mice. On the contrary, as expected, no enhancement of the immune response was found in mice treated with bare DMSNs-156.

Once we confirmed the immunogenic effect of B_2T@DMSNs and considering their long-time sustained release profile obtained *in vitro* (**Figure 2**), we performed a second trial (section §SI-2, **Table SI-2**). In this case, mice vaccinated with either B_2T@DMSNs-57 or B_2T@DMSNs-156 particle sizes were subjected to a longitudinal analysis of serum-IgG responses up to 80 days. As shown in **Figure 5**, anti-B_2T IgG titers were clearly boosted up among all tested formulations at day 40, although this time we also detected serum-IgG responses in some mice

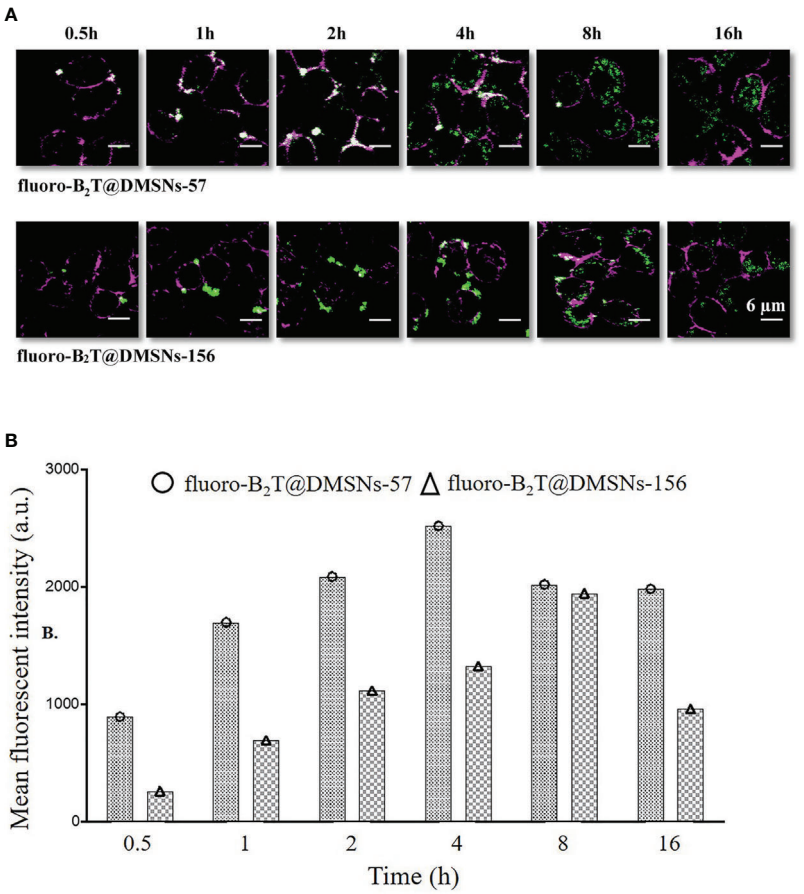

FIGURE 3 | RAW 264.7 macrophage cellular interactions of fluoro-B_2T@DMSNs-57 and fluoro-B_2T@DMSNs-156. **(A)** CLSM images showing a time- and DMSNs size-dependent internalization. (Note: Green correspond to BodiFluor-488 conjugated to the B_2T loaded within the DMSNs whereas the magenta color corresponds to the dye, cell mask deep red used to stain the plasma membrane of the cells). (*cf.* §SI-11, **Figures SI-11, SI-12**, and **SI-16**) **(B)** Flow cytometry analysis of cellular interactions. The columns represent the mean fluorescence intensity of fluoro-B_2T@DMSNs-57 and fluoro-B_2T@DMSNs-156. (*cf.* §SI-2.3, **Figures SI–13**).

immunized with B_2T@DMSNs-156 already at day 20 before the boost. We do not have a clear explanation for these different results between trials, so we attribute it to the intrinsic variability of *in vivo* studies (section §SI-3, **Figures SI-14, SI-15**, and **SI-16**). B_2T@DMSNs-57 and B_2T@DMSNs-156 showed slightly lower post-boosting titers than the positive control, B_2T@Montanide™. However, in the case of the B_2T@DMSNs-57 mice group, their serum titers increased over time until reaching comparable IgG levels to the positive control group at days 60 and 80 with high consistency among individuals. These results with the DMSNs-57 formulation are in consonance with published works reporting nanoparticle traffic to the draining lymph node in a size-dependent manner, with small 20~50 nm nanoparticles being more efficiently drained than bigger ones (9, 23, 25). We can confirm the efficiency of DMSNs to induce sustained Ab responses in a size dependent manner comparable to the emulsified version B_2T@Montanide™, pointing to demonstrable adjuvant properties of DMSNs. Finally, it is worth noting that, as not all B_2T is released from the DMSNs at day 80, one could possibly expect a sustained immunogenic effect beyond that time point.

CONCLUSIONS

Biopharmaceutical companies are now actively focused on the development of sustained release drug delivery systems, in view of their inherent benefits. Sustained release formulations designed to maintain the required therapeutic concentrations over an extended period of time present several advantages over conventional dosage forms, including less frequent drug dose, reduced concentration fluctuations, minimal side effects, reduced healthcare costs, improved efficiency and/or immune responses (51, 52). In this context, DMSNs are gaining increasing interest as effective delivery system because they are tunable, exhibit high loading capacity for therapeutic agents, and their release can be controlled. In this work, we evaluate the applicability of these nanocarriers in vaccination and long-term protection using a peptide-based vaccine with

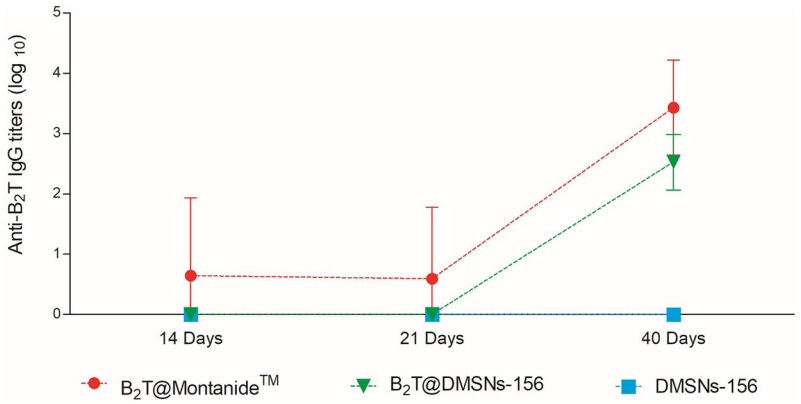

FIGURE 4 | *In vivo* functional validation. ELISA-determined anti-B_2T peptide responses of mice vaccinated with B_2T@Montanide™ (red circle, n=4), B_2T@DMSNs-156nm (green down triangle, n=6), DMSNs-156nm (blue squares, n=4) from sera collected at days 14, 21 (pre-boost) and 40 (post-boost) post-immunization. Each point depicts mean antibody titers (calculated as described in Materials and methods) ± SD for each group. No individual spontaneous reactivity was observed in the titers determined at day 0. (*cf.* §SI-3; **Table SI-1**, and **Figures SI-14, SI-15**, and **SI-16**).

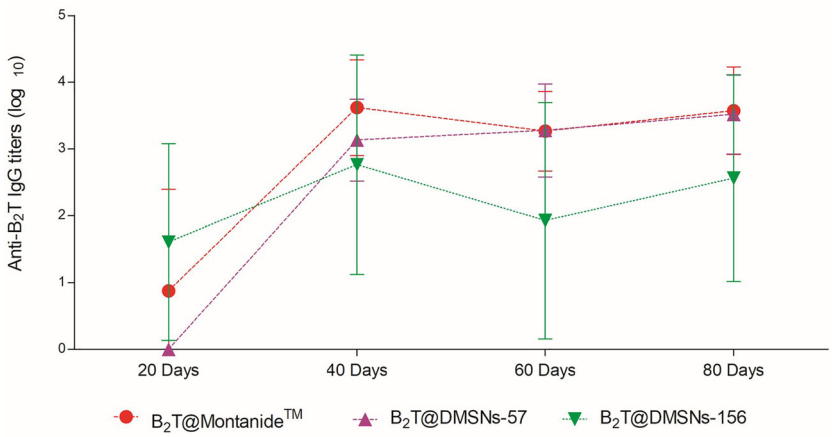

FIGURE 5 | Sustained *in vivo* immune response performed by the DMSNs. ELISA-determined anti-B_2T peptide responses obtained in vaccination trial II (**Table SI-2**) of mice vaccinated with B_2T@Montanide™ (red circle, n=3), B_2T@DMSNs-57nm (purple up triangle, n=5) and B_2T@DMSNs-156nm (green down triangle, n=5) from sera collected on the indicated days post-immunization (20, 40, 60, and 80 pi). Each point depicts mean antibody titers (calculated as described in Materials and methods) ± SD for each group. No individual spontaneous reactivity was observed in the titers determined at day 0. (*cf.* §SI-3; **Table SI-2, and Figures SI-14, SI-15, and SI-16**).

previously reported protective immunity against FMDV. Our results demonstrate that DMSNs are colloidally stable and monodisperse, with high loading capacities for a bioactive peptide such as B2T, besides being reported as non-toxic (53–56). The B_2T@DMSNs resulting formulations present long-term sustained *in vitro* release properties, enhanced in the presence of BSA. Tracking a fluoro-labeled version of B_2T within DMSNs formulations we could observed acute differences (within 16 h) in the internalization of the B_2T@DMSNs by macrophage cells in a size dependent manner. Finally, the effectivity of B_2T@DMSNs as nanovaccine was validated *in vivo* by comparing the inmunogenic response to that of the positive control B_2T@Montanide™. Mice vaccination trials showed that both DMSNs formulations increased specific B_2T antibody titers in a similar manner. However, results revealed a trend toward higher antibody titers in the animal group immunized with DMSNs of smaller particle size (57 nm) in agreement with previous literature (57, 58). Taken together, these results indicate that DMSNs is an excellent carrier for peptide vaccine which favors the internalization of the antigen by immune cell. Besides, they also delay or slown down their *in vivo* release, finally leading to a long-lasting sustained immune response activation. Therefore, DMSNs may be a suitable vaccine delivery system alternative to conventional adjuvanted vaccines not only for whole viruses or protein antigens but also for synthetic peptide-based subunit candidates.

DATA AVAILABILITY STATEMENT

The original contributions presented in the study are included in the article/**Supplementary Material**. Further inquiries can be directed to the corresponding author.

ETHICS STATEMENT

The animal study was reviewed and approved by DAAM 7463.

AUTHOR CONTRIBUTIONS

WA contributed to the design of the synthesis study, to data analysis, and wrote the first draft. SD contributed to the design of the *in vivo* study, and to its data analysis. DA contributed to the design of the *in vivo* study. PR contributed to the conception and design of the study, to data analysis and wrote the manuscript. All authors contributed to the article and approved the submitted version.

FUNDING

This research was funded by Spanish Ministry of Science, Innovation and Universities (grants AGL2014-48923-C2 and AGL2017-84097-C2-2-R to DA) as well as by Generalitat de Catalunya (grant 2009SGR492 to DA).

ACKNOWLEDGMENTS

PRG acknowledges The Gneralitat de Catalunya (2017SGR 1054 - AGAUR) and the Ministry of Science, Innovation and Universities (MICINN) and the AEI (AEI-PID2019-106755RB-I00, RYC-2012-10059, MDM-2014-0370-04, CTQ2013-45433-P [FEDER], MAT2016-75362-C3-2-R, AEI-SAF2015-73052-EXP) for financial support. PR and WA thank the China Scholarship Council (201694910800) for the PhD fellowship of WA. The ICTS "NANOBIOSIS", and particularly the Custom Antibody Service (CAbS, IQAC-CSIC, CIBER-BBN), is acknowledged for the assistance and support on animal experiments. We thank the UPF/CRG Flow Cytometry Unit (PRBB, Barcelona) for help with the flow cytometry analysis.

SUPPLEMENTARY MATERIAL

The Supplementary Material for this article can be found online at: https://www.frontiersin.org/articles/10.3389/fimmu.2021.684612/full#supplementary-material

REFERENCES

1. Li W, Joshi MD, Singhania S, Ramsey KH, Murthy AK. Peptide Vaccine: Progress and Challenges. *Vaccines* (2014) 2:515–36. doi: 10.3390/vaccines2030515
2. Fujita Y, Taguchi H. *Nanoparticle-Based Peptide Vaccines*. Oxford, United Kingdom; Cambridge, MA: William Andrew is an imprint of Elsevier (2017). doi: 10.1016/B978-0-323-39981-4.00008-7
3. Moynihan KD, Holden RL, Mehta NK, Wang C, Karver MR, Dinter J, et al. Enhancement of Peptide Vaccine Immunogenicity by Increasing Lymphatic Drainage and Boosting Serum Stability. *Cancer Immunol Res* (2018) 6 (9):1025–38. doi: 10.1158/2326-6066.CIR-17-0607
4. Sesardic D. Synthetic Peptide Vaccines. *J Med Microbiol* (1993) 39:241–2. doi: 10.18097/pbmc20115701014
5. Blanco E, Andreu D, Sobrino F. Peptide Vaccines Against Foot-and-Mouth Disease Virus. *Curr Res Emerg Trends* (2017), 317–32. doi: 10.21775/9781910190517.13
6. Bezu L, Kepp O, Cerrato G, Pol J, Fucikova J, Spisek R, et al. Trial Watch: Peptide-Based Vaccines in Anticancer Therapy. *Oncoimmunology* (2018) 7: e1511506. doi: 10.1080/2162402X.2018.1511506
7. Azmi F, Fuaad AAHA, Skwarczynski M, Toth I. Recent Progress in Adjuvant Discovery for Peptide-Based Subunit Vaccines. *Hum Vaccines Immunother* (2014) 10:778–96. doi: 10.4161/hv.27332
8. Awate S, Babiuk LA, Mutwiri G. Mechanisms of Action of Adjuvants. *Front Immunol* (2013) 4:1-10. doi: 10.3389/fimmu.2013.00114
9. Chattopadhyay S, Chen JY, Chen HW, Jack Hu CM. Nanoparticle Vaccines Adopting Virus-Like Features for Enhanced Immune Potentiation. *Nanotheranostics* (2017) 1:244–60. doi: 10.7150/ntno.19796
10. Gregory AE, Titball R, Williamson D. Vaccine Delivery Using Nanoparticles. *Front Cell Infect Microbiol* (2013) 3:13. doi: 10.3389/fcimb.2013.00013
11. Peek LJ, Middaugh CR, Berkland C. Nanotechnology in Vaccine Delivery. *Adv Drug Deliv Rev* (2008) 60:915–28. doi: 10.1016/j.addr.2007.05.017
12. Gheibi Hayat SM, Darroudi M. Nanovaccine: A Novel Approach in Immunization. *J Cell Physiol* (2019) 234:12530–6. doi: 10.1002/jcp.28120
13. Zhao L, Seth A, Wibowo N, Zhao C-XX, Mitter N, Yu C, et al. Nanoparticle Vaccines. *Vaccine* (2014) 32:327–37. doi: 10.1016/j.vaccine.2013.11.069
14. Fenollosa R, Garcia-Rico E, Alvarez S, Alvarez R, Yu X, Rodriguez I, et al. Silicon Particles as Trojan Horses for Potential Cancer Therapy. *J Nanobiotechnol* (2014) 12:1–10. doi: 10.1186/s12951-014-0035-7
15. Rivera Gil P, Hühn D, del Mercato LL, Sasse D, Parak WJ. Nanopharmacy: Inorganic Nanoscale Devices as Vectors and Active Compounds. *Pharmacol Res* (2010) 62:115–25. doi: 10.1016/j.phrs.2010.01.009
16. Taki A, Smooker P. Small Wonders—The Use of Nanoparticles for Delivering Antigen. *Vaccines* (2015) 3:638–61. doi: 10.3390/vaccines3030638
17. Yang Y, Bernardi S, Song H, Zhang J, Yu M, Reid JC, et al. Anion Assisted Synthesis of Large Pore Hollow Dendritic Mesoporous Organosilica Nanoparticles: Understanding the Composition Gradient. *Chem Mater* (2016) 28:704–7. doi: 10.1021/acs.chemmater.5b03963
18. Lu Y, Yang Y, Gu Z, Zhang J, Song H, Xiang G, et al. Glutathione-Depletion Mesoporous Organosilica Nanoparticles as a Self-Adjuvant and Co-delivery Platform for Enhanced Cancer Immunotherapy. *Biomaterials* (2018) 175:82–92. doi: 10.1016/j.biomaterials.2018.05.025
19. Cha BG, Jeong JH, Kim J. Extra-Large Pore Mesoporous Silica Nanoparticles Enabling Co-Delivery of High Amounts of Protein Antigen and Toll-Like Receptor 9 Agonist for Enhanced Cancer Vaccine Efficacy. *ACS Cent Sci* (2018) 4:484–92. doi: 10.1021/acscentsci.8b00035
20. Shen D, Yang J, Li X, Zhou L, Zhang R, Li W, et al. Biphase Stratification Approach to Three-Dimensional Dendritic Biodegradable Mesoporous Silica Nanospheres. *Nano Lett* (2014) 14:923–32. doi: 10.1021/nl404316v
21. Mody KT, Popat A, Mahony D, Cavallaro AS, Yu C, Mitter N. Mesoporous Silica Nanoparticles as Antigen Carriers and Adjuvants for Vaccine Delivery. *Nanoscale* (2013) 5:5167–79. doi: 10.1039/c3nr00357d
22. Xu C, Lei C, Yu C. Mesoporous Silica Nanoparticles for Protein Protection and Delivery. *Front Chem* (2019) 7:290. doi: 10.3389/fchem.2019.00290
23. Manolova V, Flace A, Bauer M, Schwarz K, Saudan P, Bachmann MF. Nanoparticles Target Distinct Dendritic Cell Populations According to Their Size. *Eur J Immunol* (2008) 38:1404–13. doi: 10.1002/eji.200737984

24. Bachmann MF, Jennings GT. Vaccine Delivery: A Matter of Size, Geometry, Kinetics and Molecular Patterns. *Nat Rev Immunol* (2010) 10:787–96. doi: 10.1038/nri2868
25. Reddy ST, van der Vlies AJ, Simeoni E, Angeli V, Randolph GJ, O'Neil CP, et al. Exploiting Lymphatic Transport and Complement Activation in Nanoparticle Vaccines. *Nat Biotechnol* (2007) 25:1159–64. doi: 10.1038/nbt1332
26. de Pádua Oliveira DC, de Barros ALB, Belardi RM, de Goes AM, de Oliveira Souza BK, Soares DCF. Mesoporous Silica Nanoparticles as a Potential Vaccine Adjuvant Against Schistosoma Mansoni. *J Drug Deliv Sci Technol* (2016) 35:234–40. doi: 10.1016/J.JDDST.2016.07.002
27. Virginio VG, Bandeira NC, Leal FMDA, Lancellotti M, Zaha A, Ferreira HB. Assessment of the Adjuvant Activity of Mesoporous Silica Nanoparticles in Recombinant Mycoplasma Hyopneumoniae Antigen Vaccines. *Heliyon* (2017) 3(1):e00225. doi: 10.1016/J.HELIYON.2016.E00225
28. Zhao L, Mahony D, Cavallaro AS, Zhang B, Zhang J, Deringer JR, et al. Immunogenicity of Outer Membrane Proteins VirB9-1 and VirB9-2, A Novel Nanovaccine Against Anaplasma Marginale. *PloS One* (2016) 11:e0154295. doi: 10.1371/journal.pone.0154295
29. Bai M, Dong H, Su X, Jin Y, Sun S, Zhang Y, et al. Hollow Mesoporous Silica Nanoparticles as Delivery Vehicle of Foot-and-Mouth Disease Virus-Like Particles Induce Persistent Immune Responses in Guinea Pigs. *J Med Virol* (2019) 91:941–8. doi: 10.1002/jmv.25417
30. Blanco E, Cubillos C, Moreno N, Bárcena J, de la Torre BG, Andreu D, et al. B Epitope Multiplicity and B/T Epitope Orientation Influence Immunogenicity of Foot-and-Mouth Disease Peptide Vaccines. *Clin Dev Immunol* (2013) 2013. doi: 10.1155/2013/475960
31. Blanco E, Guerra B, de la Torre BG, Defaus S, Dekker A, Andreu D, et al. Full Protection of Swine Against Foot-and-Mouth Disease by a Bivalent B-Cell Epitope Dendrimer Peptide. *Antiviral Res* (2016) 129:74–80. doi: 10.1016/j.antiviral.2016.03.005
32. de León P, Cañas-Arranz R, Defaus S, Torres E, Forner M, Bustos MJ, et al. Swine T-Cells and Specific Antibodies Evoked by Peptide Dendrimers Displaying Different FMDV T-Cell Epitopes. *Front Immunol* (2021) 11:621537. doi: 10.3389/fimmu.2020.621537
33. Defaus S, Forner M, Cañas-Arranz R, de León P, Bustos MJ, Rodríguez-Pulido M, et al. Designing Functionally Versatile, Highly Immunogenic Peptide-Based Multiepitopic Vaccines Against Foot-and-Mouth Disease Virus. *Vaccines (Basel)* (2020) 8(3):406. doi: 10.3390/vaccines8030406
34. Wu Y, Ellis RD, Shaffer D, Fontes E, Malkin EM, Mahanty S, et al. Phase 1 Trial of Malaria Transmission Blocking Vaccine Candidates Pfs25 and Pvs 25 Formulated With Montanide ISA 51. *PloS One* (2008) 3(7):e2636. doi: 10.1371/journal.pone.0002636
35. Reed SG, Bertholet S, Coler RN, Friede M. New Horizons in Adjuvants for Vaccine Development. *Trends Immunol* (2009) 30:23–32. doi: 10.1016/j.it.2008.09.006
36. Lin YS, Haynes CL. Synthesis and Characterization of Biocompatible and Size-Tunable Multifunctional Porous Silica Nanoparticles. *Chem Mater* (2009) 21:3979–86. doi: 10.1021/cm901259n
37. Patwardhan SV, Emami FS, Berry RJ, Jones SE, Naik RR, Deschaume O, et al. Chemistry of Aqueous Silica Nanoparticle Surfaces and the Mechanism of Selective Peptide Adsorption. *J Am Chem Soc* (2012) 134(14):6244–56. doi: 10.1021/ja211307u
38. Rivera-Gil P, Jimenez De Aberasturi D, Wulf V, Pelaz B, Del Pino P, Zhao Y, et al. The Challenge to Relate the Physicochemical Properties of Colloidal Nanoparticles to Their Cytotoxicity. *Acc Chem Res* (2013) 46:743–9. doi: 10.1021/ar300039j
39. Schweiger C, Hartmann R, Zhang F, Parak WJ, Kissel TH, Rivera-Gil P. Quantification of the Internalization Patterns of Superparamagnetic Iron Oxide Nanoparticles With Opposite Charge. *J Nanobiotechnol* (2012) 10:28. doi: 10.1186/1477-3155-10-28
40. Zamora-Perez P, Tsoutsi D, Xu R, Rivera-Gil P. Hyperspectral-Enhanced Dark Field Microscopy for Single and Collective Nanoparticle Characterization in Biological Environments. *Mater (Basel)* (2018) 11 (2):243. doi: 10.3390/ma11020243
41. Mahmoudi M, Meng J, Xue X, Liang XJ, Rahman M, Pfeiffer C, et al. Interaction of Stable Colloidal Nanoparticles With Cellular Membranes. *Biotechnol Adv* (2014) 32:679–92. doi: 10.1016/j.biotechadv.2013.11.012
42. Chanana M, Rivera-Gil P, Correa-Duarte MA, Liz-Marzán LM, Parak WJ. Physicochemical Properties of Protein-Coated Gold Nanoparticles in Biological Fluids and Cells Before and After Proteolytic Digestion, Angew. *Chemie - Int Ed* (2013) 52:4179–83. doi: 10.1002/anie.201208019
43. Bros M, Nuhn L, Simon J, Moll L, Mailänder V, Landfester K, et al. The Protein Corona as a Confounding Variable of Nanoparticle-Mediated Targeted Vaccine Delivery. *Front Immunol* (2018) 9:1760. doi: 10.3389/fimmu.2018.01760
44. Ge C, Tian J, Zhao Y, Chen C, Zhou R, Chai Z. Towards Understanding of Nanoparticle–Protein Corona. *Arch Toxicol* (2015) 89:519–39. doi: 10.1007/s00204-015-1458-0
45. Ozboyaci M, Kokh DB, Corni S, Wade RC. Modeling and Simulation of Protein-Surface Interactions: Achievements and Challenges. *Q Rev Biophys 49* (2016) 49:e4. doi: 10.1017/S0033583515000256
46. Ge C, Du J, Zhao L, Wang L, Liu Y, Li D, et al. Binding of Blood Proteins to Carbon Nanotubes Reduces Cytotoxicity. *Proc Natl Acad Sci USA* (2011) 108:16968–73. doi: 10.1073/pnas.1105270108
47. Hartley JW, Evans LH, Green KY, Naghashfar Z, Macias AR, Zerfas PM, et al. Expression of Infectious Murine Leukemia Viruses by RAW264.7 Cells, a Potential Complication for Studies With a Widely Used Mouse Macrophage Cell Line. *Retrovirology* (2008) 5:6–11. doi: 10.1186/1742-4690-5-1
48. Berghaus LJ, Moore JN, Hurley DJ, Vandenplas ML, Fortes BP, Wolfert MA, et al. Innate Immune Responses of Primary Murine Macrophage-Lineage Cells and RAW 264.7 Cells to Ligands of Toll-Like Receptors 2, 3, and 4. *Comp Immunol Microbiol Infect Dis* (2010) 33:443–54. doi: 10.1016/j.cimid.2009.07.001
49. Kastl L, Sasse D, Wulf V, Hartmann R, Mircheski J, Ranke C, et al. Multiple Internalization Pathways of Polyelectrolyte Multilayer Capsules Into Mammalian Cells. *ACS Nano* (2013) 7:6605–18. doi: 10.1021/nn306032k
50. Assanga I. Cell Growth Curves for Different Cell Lines and Their Relationship With Biological Activities. *Int J Biotechnol Mol Biol Res* (2013) 4:60–70. doi: 10.5897/ijbmbr2013.0154
51. Demento SL, Cui W, Criscione JM, Stern E, Tulipan J, Kaech SM, et al. Role of Sustained Antigen Release From Nanoparticle Vaccines in Shaping the T Cell Memory Phenotype. *Biomaterials* (2012) 33:4957–64. doi: 10.1016/j.biomaterials.2012.03.041
52. Men Y, Gander B, Merkle HP, Corradin G. Induction of Sustained and Elevated Immune Responses to Weakly Immunogenic Synthetic Malarial Peptides by Encapsulation in Biodegradable Polymer Microspheres. *Vaccine* (1996) 14:1442–50. doi: 10.1016/S0264-410X(96)00074-6
53. Liu T, Li L, Teng X, Huang X, Liu H, Chen D, et al. Single and Repeated Dose Toxicity of Mesoporous Hollow Silica Nanoparticles in Intravenously Exposed Mice. *Biomaterials* (2011) 32:1657–68. doi: 10.1016/j.biomaterials.2010.10.035
54. Fu C, Liu T, Li L, Liu H, Chen D, Tang F. The Absorption, Distribution, Excretion and Toxicity of Mesoporous Silica Nanoparticles in Mice Following Different Exposure Routes. *Biomaterials* (2013) 34:2565–75. doi: 10.1016/j.biomaterials.2012.12.043
55. He X, Nie H, Wang K, Tan W, Wu X, Zhang P. In Vivo Study of Biodistribution and Urinary Excretion of Surface-Modified Silica Nanoparticles. *Anal Chem* (2008) 80:9597–603. doi: 10.1021/ac801882g
56. He Q, Zhang Z, Gao F, Li Y, Shi J. In Vivo Biodistribution and Urinary Excretion of Mesoporous Silica Nanoparticles: Effects of Particle Size and Pegylation. *Small* (2011) 7:271–80. doi: 10.1002/smll.201001459
57. Toda T, Yoshino S. Enhancement of Ovalbumin-Specific Th1, Th2, and Th17 Immune Responses by Amorphous Silica Nanoparticles. *Int J Immunopathol Pharmacol* (2016) 29:408–20. doi: 10.1177/0394632016656192
58. An M, Li M, Xi J, Liu H. Silica Nanoparticle as a Lymph Node Targeting Platform for Vaccine Delivery. *ACS Appl Mater Interfaces* (2017) 9:23466–75. doi: 10.1021/acsami.7b06024

Conflict of Interest: The authors declare that the research was conducted in the absence of any commercial or financial relationships that could be construed as a potential conflict of interest.

frontiers in Immunology

PERSPECTIVE
published: 23 June 2021
doi: 10.3389/fimmu.2021.670931

The Prospect of Nanoparticle Systems for Modulating Immune Cell Polarization During Central Nervous System Infection

*Lee E. Korshoj[1], Wen Shi[2], Bin Duan[2] and Tammy Kielian[1]**

[1] Department of Pathology and Microbiology, University of Nebraska Medical Center, Omaha, NE, United States, [2] Mary & Dick Holland Regenerative Medicine Program, Division of Cardiology, Department of Internal Medicine, University of Nebraska Medical Center, Omaha, NE, United States

The blood-brain barrier (BBB) selectively restricts the entry of molecules from peripheral circulation into the central nervous system (CNS) parenchyma. Despite this protective barrier, bacteria and other pathogens can still invade the CNS, often as a consequence of immune deficiencies or complications following neurosurgical procedures. These infections are difficult to treat since many bacteria, such as *Staphylococcus aureus*, encode a repertoire of virulence factors, can acquire antibiotic resistance, and form biofilm. Additionally, pathogens can leverage virulence factor production to polarize host immune cells towards an anti-inflammatory phenotype, leading to chronic infection. The difficulty of pathogen clearance is magnified by the fact that antibiotics and other treatments cannot easily penetrate the BBB, which requires extended regimens to achieve therapeutic concentrations. Nanoparticle systems are rapidly emerging as a promising platform to treat a range of CNS disorders. Nanoparticles have several advantages, as they can be engineered to cross the BBB with specific functionality to increase cellular and molecular targeting, have controlled release of therapeutic agents, and superior bioavailability and circulation compared to traditional therapies. Within the CNS environment, therapeutic actions are not limited to directly targeting the pathogen, but can also be tailored to modulate immune cell activation to promote infection resolution. This perspective highlights the factors leading to infection persistence in the CNS and discusses how novel nanoparticle therapies can be engineered to provide enhanced treatment, specifically through modulation of immune cell polarization.

Keywords: central nervous system, infection, biofilm, immunometabolism, nanoparticles, blood-brain barrier, leukocytes, microglia

OPEN ACCESS

Edited by:
David Pozo,
University of Seville, Spain

Reviewed by:
Karita Haapasalo,
University of Helsinki, Finland
Emma Harriet Wilson,
University of California, Riverside, United States

****Correspondence:***
Tammy Kielian
tkielian@unmc.edu

Specialty section:
This article was submitted to Molecular Innate Immunity, a section of the journal Frontiers in Immunology

Received: *22 February 2021*
Accepted: *03 June 2021*
Published: *23 June 2021*

Citation:
Korshoj LE, Shi W, Duan B and Kielian T (2021) The Prospect of Nanoparticle Systems for Modulating Immune Cell Polarization During Central Nervous System Infection. Front. Immunol. 12:670931. doi: 10.3389/fimmu.2021.670931

INTRODUCTION

The blood-brain barrier (BBB) represents a double-edged sword in the context of central nervous system (CNS) infectious diseases. On the one hand, tight junctions between brain capillary endothelial cells, reinforced with astrocyte end feet and pericytes, act as a defense to restrict pathogen invasion into the CNS from the periphery (1, 2). However, the same tight junctions also

hinder the delivery of therapeutics to the brain parenchyma in situations where the BBB is breached. A wide range of bacteria, viruses, fungi, and parasites can traverse the BBB with neurotropism for CNS meningeal, ventricular, and parenchymal compartments (1–3). These pathogens are responsible for severe clinical conditions including meningitis, encephalitis, and pyogenic infections. Patients with CNS infections often require lengthy hospitalization, critical care support, complex diagnostic tests, and invasive treatment procedures. Globally, more than 1.2 million individuals are affected by meningitis annually, with bacterial meningitis responsible for 120,000 deaths (4, 5). Many of the pathogens that invade the CNS are opportunistic and exploit patients with primary immune deficiencies that worsen disease severity (6, 7). Other CNS infections can arise from complications following neurosurgical procedures, such as craniotomy and cerebrospinal fluid (CSF) shunt placement (8–10). The expanded use of therapeutics targeting immune effector mechanisms, such as monoclonal antibodies to inhibit cytokine action or leukocyte trafficking, can increase susceptibility to CNS infection (11–13). In the CNS, pathogens can tightly regulate virulence factor and metabolite production to promote their survival (3, 14–16). In bacterial strains such as *Staphylococcus aureus*, this includes biofilm formation and antibiotic tolerance (17). Additionally, host-pathogen crosstalk can polarize immune cells towards an anti-inflammatory phenotype to promote chronic infection. Although CNS infections are generally less frequent compared to the periphery, their high morbidity and mortality rates necessitate better understanding and management to improve patient outcomes.

Treatments for CNS infection depend on the suspected pathogen, but one commonality exists – time is essential. As infections can be rapidly fatal, it is imperative that therapeutic interventions are initiated as soon as a diagnosis is made. For drugs, CNS entry is dependent on size, charge, lipophilicity, plasma protein binding, affinity for active transport mechanisms at the BBB, as well as edema and CSF flow (18). With these stringent requirements, it is no surprise that the BBB is the bottleneck of the pharmaceutical industry for CNS therapeutics. Around 98% of brain-targeting drug candidates have impeded ability to pass the BBB, including new classes of biotherapies such as RNAs (19, 20). Current treatment options for many bacterial, fungal, and viral pathogens are highly empirical due to a lack of clinical trial-based evidence and few approved therapies (3). Administration routes are also empirical, and due to the difficulty in achieving therapeutic concentrations of compounds in the CNS following intravenous injection, more invasive transcranial delivery is often required. This includes intrathecal and intraventricular injection of anti-infection agents dosed as high as 10-fold in excess of the minimum inhibitory concentration to achieve clearance, and ventricular catheters must be maintained for 24-48 h or substantially longer (21). A growing number of CNS infections with multi-drug resistant (MDR) bacteria such as *Acinetobacter baumannii*, *Pseudomonas aeruginosa*, and *Klebsiella pneumoniae* present a serious problem as these superbugs are only sensitive to select classes of polymyxin last-resort antibiotics, severely limiting treatment options (22). Further complicating treatment is that many drugs, such as the antibiotics for MDR bacteria, are associated with neurotoxicity due to the need for high therapeutic concentrations, non-specific targeting, and only small amounts of drug reaching the infection site within the CNS. As such, treatments must include neuroprotective agents to alleviate harmful side effects.

Engineered nanoparticle systems have emerged as a promising therapeutic path to circumvent BBB restrictions and provide targeted delivery of drugs to the CNS (23, 24). Additionally, the concept of using immunometabolic modulation to treat neurological disorders such as Alzheimer's disease (AD), Parkinson's disease (PD), and multiple sclerosis (MS) has gained traction in recent years (25, 26). We believe that using nanoparticle delivery systems with immunometabolic therapies could provide a paradigm shift for the successful treatment of life-threatening CNS infections. This approach has the potential as a dual-action therapeutic bolstering the host defenses and synergizing with anti-infection agents, ultimately improving patient outcomes (**Figure 1**).

PATHOGENIC AND IMMUNE CHARACTERISTICS OF CNS INFECTIONS

Mechanisms of Pathogen Entry Into the CNS

A variety of routes facilitate pathogen entry into the CNS (4). One common path is through the meninges and CSF. Bacterial species including *Streptococcus pneumoniae* and *Listeria monocytogenes* access the blood and CSF after colonization in the nasopharynx or gastrointestinal tract, respectively (27, 28). Once in the subarachnoid space, interactions between bacterial and host proteins facilitate invasion into the CNS parenchyma. For example, *S. pneumoniae* uses the adhesion molecule RrgA to bind the polymeric immunoglobulin receptor plgR or platelet-associated cell adhesion molecule (PECAM)-1 on endothelial cells (27). *L. monocytogenes* uses the internalin InlF to interact with the cytoplasmic intermediate filament protein vimentin that is also expressed on the surface of brain endothelial cells (28). Fungal invasion of the CNS can also occur through the CSF in cases of congenital, acquired, or drug-mediated T cell dysfunction (29, 30). Direct infection and replication inside BBB endothelial cells provides another route for pathogen entry to the CNS. For example, Zika virus is known to have tropism for vascular endothelial cells though mechanisms involving the AXL tyrosine kinase receptor family, and the protozoan *Toxoplasma gondii* utilizes parasite adhesion microneme protein-2 (MIC2) for growth in brain endothelial cells (31, 32). Upon replication, these pathogens are released into the CNS parenchyma after endothelial cell lysis. Microbes can also use host endocytic machinery to reach the CNS *via* transcytosis. For example, *S. pneumoniae* can cross endothelial barriers by clathrin- and caveolae-mediated micropinocytosis (33). West Nile virus (WNV) can invade the CNS through the use of lipid rafts and caveolae-facilitated endocytosis (34). Fungal species such as *Cryptococcus neoformans*

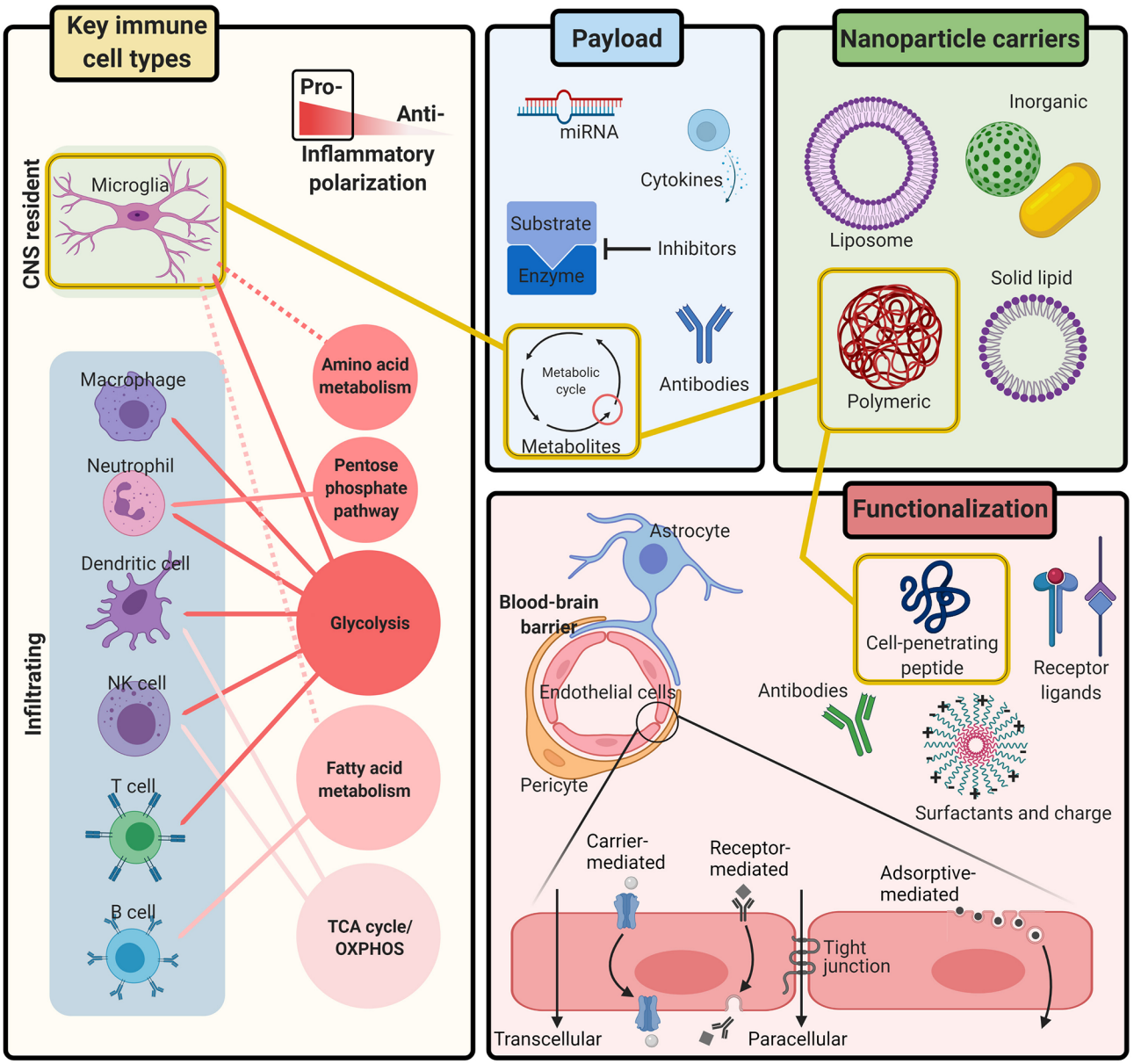

FIGURE 1 | Integrating immunometabolism and nanoparticle systems for the treatment of CNS infection. Immune activation is controlled by the metabolic pathways needed to generate the energy and intermediates required for effector responses. Research continues to uncover the metabolic pathways that regulate inflammatory polarization of all **Key immune cell types** during CNS infection, including microglia and infiltrating leukocytes. **Nanoparticle carriers** can be engineered with different **Functionalization** to safely, and non-invasively transport therapeutic **Payloads** across the BBB to the CNS with a variety of tunable compositions, chemical ligands, and physiological characteristics. Together, nanoparticle systems provide a multi-tool kit of customizable parts for delivering immunometabolic modulating therapies to targeted cells in the CNS. Figure created with BioRender.

also leverage host proteins for transcytosis, including cysteinyl leukotrienes and the glycoprotein receptor CD44 (35). Another notable entry route to the CNS for pathogens is *via* a "Trojan-horse" mechanism, whereby microbes are transported across the BBB within phagocytic leukocytes (36, 37). Research has demonstrated that WNV is carried to the brain *via* infected neutrophils, and CNS infection with *T. gondii* is associated with migration of infected monocytes and dendritic cells (DCs) (38, 39). Finally, foreign bodies introduced into the CNS provide direct routes for pathogen colonization, often leading to infection with skin flora such as *S. aureus* or *S. epidermidis* (40, 41). Later, we will discuss how the same biological mechanisms exploited by pathogens to enter the CNS can be used for designing new classes of nanoparticle therapeutics with enhanced BBB permeability.

The Host Immune Response to CNS Infection

The immune response to pathogen invasion of the CNS is an organized and dynamic process. Microbes are sensed by microglia and astrocytes in the CNS parenchyma as well as macrophages within the choroid plexus, meninges, and perivascular space (42, 43). Activation occurs through the recognition of pathogen-associated molecular patterns (PAMPs) by a range of pattern recognition receptors (PRRs), the most well studied being the Toll-like receptor (TLR) family (44, 45). Microglial and CNS macrophage activation in response to TLR stimulation is characterized by increased major histocompatibility complex class II (MHCII) and costimulatory molecule (CD80 and CD86) expression. Additionally, pro-inflammatory cytokines and chemokines including TNF-α, IL-1β, CCL2, and CCL5 are secreted concomitant with nitric oxide and reactive oxygen species (ROS) production. Changes in phagocytosis, cell motility, and proliferation are also observed. These attributes serve to limit pathogen expansion, and recruit and activate peripheral blood leukocytes into the CNS to mitigate the infection. Ideally, activation is tightly regulated and short-lived before resolving into a homeostatic state characterized by the secretion of anti-inflammatory signals, including IL-10 and transforming growth factor-beta (TGF-β) that support neurorepair (44, 46, 47). Given the high mortality rates associated with CNS infections, it is clear that immune activation can become dysregulated, leading to bystander damage of surrounding normal brain parenchyma and increased disease severity.

In recent years, the rapidly expanding field of immunometabolism has demonstrated that immune activation is controlled by the metabolic pathways needed to generate the energy and intermediates required for effector responses (26, 48, 49). The major pathways identified to date that dictate leukocyte function include glycolysis, the tricarboxylic acid (TCA) cycle, oxidative phosphorylation (OXPHOS), fatty acid oxidation and synthesis (FAO and FAS, respectively), the pentose phosphate pathway (PPP), and amino acid metabolism (50). During normal resting conditions, leukocytes tend to display a basal activity of all major metabolic pathways. Glucose is converted to pyruvate to fuel the TCA cycle and generate adenosine triphosphate (ATP) for energy as well as nicotinamide adenine dinucleotide (NADH) and flavin adenine dinucleotide ($FADH_2$) as electron donors for OXPHOS. Upon activation, cells undergo metabolic reprogramming characteristic of altered fuel consumption, modified mitochondrial structure and dynamics, preferential use of specific metabolic pathways, and metabolite flux (48–50). In response to pro-inflammatory signals, many leukocytes undergo Warburg metabolism that is typified by increased glycolysis under aerobic conditions (51). This glycolytic bias enhances the synthesis of nucleotides, amino acids, fatty acids, and other metabolic intermediates to promote proliferation and cytokine production, including rapid ATP generation. Cells in an anti-inflammatory state tend to favor OXPHOS since their biosynthetic demands are less pronounced. However, it is important to note that the concept of metabolic bias is not an "all-or-none" phenomenon but instead exists on a spectrum since metabolic pathways are highly integrated (50). Furthermore, unique metabolic pathways have been linked to specific cell types, revealing another layer of complexity (52–54). Metabolic programming is also highly dependent on substrate availability. This provides an opportunity for pathogens to manipulate host defenses through substrate competition that can ultimately suppress pro-inflammatory responses by biasing leukocytes towards an anti-inflammatory state (55, 56). For example, *S. aureus* biofilm promotes an anti-inflammatory milieu through depletion of key nutrients such as glucose, preferential recruitment of granulocytic-myeloid-derived suppressor cells (G-MDSCs), and release of lactate to drive production of the anti-inflammatory cytokine IL-10 (57). The CNS has a distinct nutrient environment compared to the periphery, which likely influences the immunometabolic status of resident microglia and infiltrating leukocytes during infection. While comprising only 2% of the total body mass, the brain utilizes approximately 25% of the glucose consumed by the human body (58). Under conditions of diminished glucose supply, such as infection or ischemia, CNS cells can adapt to use alternative energy sources generated from FAO or glutaminolysis (53). The concept of metabolically reprograming cells to promote infection clearance presents an exciting therapeutic opportunity. To realize this idea, it is important to understand the relationships between inflammatory polarization and metabolic status for the various immune cell populations within the CNS and how this changes in the context of infection.

Immunometabolism of Glial and Leukocyte Populations

The key players in controlling CNS infections are resident microglia and macrophage populations along with infiltrating leukocytes. These cell types share many similarities in terms of TLR usage but also significant heterogeneity in effector functions. Microglia originate from the primitive yolk sac during development and comprise 5-10% of the total cell population in the brain parenchyma (59). During normal steady-state conditions, microglia survey the brain parenchyma detecting neuronal activity and maintain homeostasis through synaptic pruning, clearance of apoptotic cells, and regulating neurogenesis (60, 61). In response to pro-inflammatory stimuli, microglia undergo Warburg metabolism, shifting from OXPHOS in the resting state to aerobic glycolysis (62, 63). As a result, specific metabolite transporters and glycolytic genes are upregulated, notably the glucose transporter GLUT-1 and hexokinase, respectively, leading to protein acetylation due to acetyl-CoA accumulation and release of IL-1β. Further, superoxide generation is used to kill pathogens, and it is suggested that histone deacetylase (HDAC) activity links epigenetic changes with metabolism (25, 62). Non-immune cells, such as CNS resident astrocytes and oligodendrocytes also play key metabolic roles to support neuron homeostasis. Under physiological conditions, astrocytes provide neurons with metabolic substrates for neurotransmission, maintain neural electrical activity, and support energy balance and synaptic pruning (64, 65). Upon activation, astrocytes have been shown to undergo aerobic glycolysis to promote pro-inflammatory signals (54, 63). Oligodendrocytes form the lipid-rich myelin supporting

the propagation of neuronal action potentials, where cells respond to glutamatergic signals by increasing glycolysis to support axonal energy metabolism (26, 66). The metabolic changes that occur in astrocytes and oligodendrocytes during CNS infection and how this shapes neuronal survival remain to be determined.

Infiltrating leukocytes are the other key contributors to CNS infection. Macrophages, neutrophils, DCs, and natural killer (NK) cells are rapidly recruited into the infected CNS where they can influence glial activation through release of inflammatory cytokines and other factors such as ROS (25, 26, 67–69). Macrophages and monocytes are found in the CNS meningeal and perivascular interfaces as well as the infected brain and experience a metabolic shift from OXPHOS to glycolysis upon pro-inflammatory activation, similar to microglia (70–72). The most comprehensive immunometabolic studies to date have been conducted on macrophages, wherein two major breakpoints in the TCA cycle result in succinate and citrate accumulation and nitric oxide, IL-6, and IL-1β production. Citrate accumulation also leads to the generation of itaconate, which exerts bactericidal activity (73). However, chronic production of itaconate can elicit anti-inflammatory effects and, as such, this balance must be tightly regulated. Similar to macrophages, pro-inflammatory DCs exhibit a metabolic shift towards glycolysis; however, DCs continue to use the TCA cycle for generating ATP as opposed to heavily relying on glycolysis which differs from macrophages (74, 75). There are numerous DC subsets, and it is important to recognize that each may undergo unique metabolic programs during activation in a context-dependent manner (76). Activated neutrophils favor glycolysis as well as the PPP to produce NADPH for redox reactions. Their low mitochondrial abundance reflects their reduced reliance on OXPHOS (77). NK cells do not experience a glycolytic bias upon activation but instead enhance both glycolysis and OXPHOS, where glucose remains the primary fuel (78). With regard to adaptive immunity, T cells also play important roles in many CNS infectious diseases, ranging from cytotoxic activity during viral infections to promoting innate immunity through the release of cytokines such as IFN-γ and IL-17 (79). Like their innate counterparts, T cell activation is highly dependent on glycolytic metabolism for their effector functions. However, metabolic variability exists for dictating T cell subset fate. For example, the OXPHOS pathway is important for Th17 differentiation, and the absence of OXPHOS during differentiation leads to regulatory T cell (Treg) development (79, 80). B cells are rather unique in their metabolic program compared to other immune cells, relying heavily on FAO and minimally on glycolysis (81, 82). There are few reports on the role of B cells during CNS infections, but available evidence shows important contributions for pathogen neutralization by enhanced opsonophagocytosis and complement activation (83). The metabolic diversity of infiltrating leukocytes during CNS infectious diseases and how this shapes not only their intrinsic properties but also extrinsic effects on surrounding leukocytes and resident glia represents a complex scenario, and one that is ripe for interrogation to exploit pathways that promote infection resolution without excessive bystander damage to normal brain parenchyma.

Modulating Immune Cell Polarization

Extensive evidence has shown that immune cell polarization is linked to metabolism, supporting the idea of manipulating metabolism as a means to direct immune cells towards pathways that promote infection clearance, which has been coined metabolic reprogramming (50). Most current research into immune modulation in the CNS has targeted inflammation associated with AD, PD, and MS; however, the same concepts can be leveraged for CNS infectious diseases. In the context of neurodegenerative disorders, T cell activation has been targeted to attenuate chronic inflammation. Initial work showed that inhibition of glycolysis limited T cell pathogenicity by favoring Treg development (84, 85). Tetramerization of pyruvate kinase M2, the enzyme catalyzing the last step in glycolysis, inhibited the glycolytic activity of pro-inflammatory T cells to ameliorate experimental autoimmune encephalomyelitis (EAE), the mouse model of MS (86). Other work demonstrated that the TCA derivative itaconate also reduced EAE severity by suppressing T cell and microglial activation (87). Further studies have shown metabolic polarization effects in T cells with cytokines such as IFN-β and targeting mitochondrial respiratory chain enzymes (88, 89). A growing body of literature is beginning to uncover the mechanisms driving microglial plasticity in the brain, where the mechanistic target of rapamycin (mTOR) pathway has been identified and has clear links with metabolism (90). As critical metabolic nodes emerge, a variety of approaches relying on pharmacological agents, cytokines, lipid messengers, and microRNAs have all been shown to be effective metabolic modulating agents (91).

Insights into how metabolic status may shape CNS immune activation can also be drawn from research in the periphery, where much focus has been on macrophages. Studies have uncovered mechanisms behind mitochondrial repurposing during activation, and how resulting mitochondrial reactive oxygen species (mtROS) production can be blocked to promote anti-inflammatory states (92). Other work has demonstrated that metabolic reprogramming of monocytes *via* the OXPHOS inhibitor oligomycin reduced bacterial burden in a *S. aureus* biofilm model of prosthetic joint infection (93). The effectiveness of this treatment resulted from inhibiting the anti-inflammatory OXPHOS bias, shifting cells towards a pro-inflammatory glycolytic state to promote biofilm clearance. Pertinent to CNS infection, similar immune-based approaches have been used with exogenous application of IL-1β or grafted pro-inflammatory macrophages, both of which lowered bacterial burden in a *S. aureus* biofilm model of craniotomy infection (94, 95). As another layer of complexity, a recent study demonstrated the influence of microenvironment in shaping immunomodulatory attributes, where macrophage expression of glycolytic markers was suppressed upon migration into the brain parenchyma (71). More specifically, lactate dehydrogenase A (LDHA; converts pyruvate to lactate) and monocarboxylate transporter 4 (MCT-4; exports lactate from glycolytic cells) expression was significantly reduced in macrophages that invaded the brain parenchyma in EAE, whereas these molecules were elevated in macrophages associated with perivascular cuffs. This suggests a failure of macrophages to

maintain their pro-inflammatory properties upon entering the CNS, which the authors attributed to differences in metabolic demand. While a specific mechanism for this reprogramming is unknown, it could be influenced by local nutrient or metabolite availability, such as lactate itself, which is known to be produced by astrocytes and oligodendrocytes for supporting proper axonal function (58, 96), or it may provide balance to the local inflammatory response. Collectively, these findings support the idea that immune cell function could be tailored by modulating metabolism to overcome deficiencies in CNS metabolites, such that infiltrating leukocytes remain in a pro-inflammatory state to fight infection.

The aforementioned examples reflect only a small amount of the growing literature on metabolic modulation. Ongoing work continues to identify molecular agents targeting aspects of key metabolic pathways. Overall, strong evidence supports the use of metabolic modulation therapy for controlling immune cell activation states and effector functions (84–86, 89, 91, 94). The heterogeneity between different cell types highlights the need to uniquely target select immune populations. Additionally, more work should aim to investigate how immunometabolic therapies can synergize with existing anti-infection drugs to enhance clearance from the CNS. Such an immunometabolic approach to treating CNS infections has potential to improve disease outcomes, depending on the availability of suitable delivery mechanisms.

THE PROSPECT OF NANOPARTICLE SYSTEMS FOR MODULATING IMMUNE CELL POLARIZATION

Shortcomings of Current CNS Infection Treatments

As previously discussed, the BBB is a cooperative interaction between brain capillary endothelial cells, astrocytes, and pericytes that maintains brain homeostasis and controls nutrient influx into the parenchyma. Transport through the BBB can occur through a variety of routes, generally classified as passive transport, carrier-mediated, and vesicular trafficking (**Figure 1**) (97). Passive transport is mostly limited to small substances. Small hydrophilic compounds may pass paracellularly through the tight junctions between endothelial cells likely by means of transient relaxation of the junctions, while small lipophilic substances can use transcellular passive diffusion to reach the brain (97). Carrier-mediated transport exploits diverse solute transporters for traversing the BBB, such as those for glucose or amino acids. Receptor-mediated and adsorptive-mediated transport utilize antibody binding or plasma proteins for crossing *via* endocytosis and pinocytosis (98).

Expectedly, delivery of anti-infection agents to the CNS is strongly hindered by the BBB, and more invasive transcranial delivery *via* intrathecal and intraventricular injection is often used as a bypass (99, 100). However, bypass strategies are complicated by limited drug diffusion, which reduces biodistribution to the target location in the parenchyma. Osmotic disruption of the BBB with vasoactive substances, exposure to high intensity focused ultrasound, and electromagnetic pulses have also been explored to improve drug permeability to the CNS (101–103). However, BBB disruption can lead to unwanted entry of other molecules into the CNS or drugs becoming trapped in brain endothelial cells rather than distributing to target sites. Engineered nanoparticles represent a promising approach to improve non-invasive delivery of CNS therapeutics by ferrying drugs across the BBB. Nanoparticles can be designed to perform multiple, targeted functions aimed at both the pathogen and host, and their biodegradable properties have the added advantage of self-clearance (20, 23, 24, 100).

Design Variables of Nanoparticle Therapies

Nanoparticles are small structures ranging from 1 to 1000 nm in diameter. They can be generated by a wide array of biodegradable and non-biodegradable substances and readily modified to deliver therapeutic agents, as discussed in the following sections (24). There are several approaches for transporting nanoparticles across the BBB, all facilitated by harnessing the physiological properties of endogenous molecules required for proper brain function (98, 104). For example, carrier-mediated transport allows nanoparticles to use essential nutrient transporters, such as GLUT-1 for glucose and L1 and y+ for large amino acids. Through adsorptive-mediated transcytosis, electrostatic interactions between cationic ligands and negatively charged endothelial cell membranes lead to vesicle-based endocytosis. Perhaps the most effective approach, receptor-mediated transcytosis, relies on luminal plasma membrane receptors of endothelial cells for endocytosis. Examples include the lactoferrin and transferrin receptors (LfR and TfR, respectively), low density lipoprotein receptor-related protein 1 and 2 (LRP-1 and -2), insulin receptor, and folate receptor (98, 104).

To exploit the endogenous transport machinery of the BBB, nanoparticles must be designed to mimic physiologically active compounds. Several key characteristics can be leveraged to optimize nanoparticle entry into the CNS. First, nanoparticle size is crucial for endocytosis, with a critical limit of approximately 200 nm or less for efficient cellular uptake *via* clathrin-mediated endocytosis (23, 105). Charge is another important factor affecting both internalization and circulation time. Due to the net negative charge on endothelial cell membranes, positively charged nanoparticles can more readily use adsorptive transcytosis. On the contrary, neutral and negatively charged nanoparticles remain in circulation longer because of reduced protein adsorption. Zwitterionic nanoparticles can provide a balance between uptake and circulation requirements (106). Functionalization through incorporation of surface ligands provides the most flexibility to engineered nanoparticles. The main objective in selecting surface ligands is increasing BBB passage and cell-specific targeting through carrier- and receptor-mediated transcytosis. Studies have demonstrated the ability to decorate particles with ligands for GLUT-1, albumin transporters, LfRs and TfRs, and more (107–110). The use of cell-penetrating peptides as surface ligands can be used to bypass endocytosis, leading to direct nanoparticle entry to the cytoplasm (111). Studies have also demonstrated the use of

ligands such as insulin for targeting affected brain regions in neurodegenerative and neuropsychiatric disorders (105). Not only the ligand itself, but its density or avidity are also important factors, as too many high affinity ligands can hinder endocytosis by anchoring nanoparticles to cell membranes (110).

Intravenous injection is the most widely utilized route for nanoparticle administration. However, the rapid clearance of particles from circulation can limit the concentrations reaching the CNS (23). New non-invasive routes of administration are being explored to improve CNS bioavailability. Intranasal delivery is a major alternative route, which could facilitate direct nose-to-brain delivery in a matter of minutes *via* olfactory and trigeminal nerves (112–117). The functional diversity and customization possibilities in designing CNS-targeting nanoparticles makes them multi-tool kits with options for tailoring transport routes, targets, and payload release kinetics. Researchers continue to discern the relative importance of the variables governing nanoparticle characteristics and how one property may modify another attribute (118). One such study examining these relationships determined that for the specific polymeric nanoparticles used, the most influential parameter for efficient BBB penetration was the surfactant type, whereas size and zeta potential had little impact (119). Continued efforts advancing CNS-targeting nanoparticles will only enhance their potential for personalized medicine applications.

Nanoparticles for the CNS

Significant work has identified a wide range of polymeric, lipid-based, cell-derived, and inorganic nanoparticles as viable therapeutic options to promote CNS uptake. While most of the current research and select examples discussed below have focused on cancer, neuroinflammation, and neurodegenerative diseases, the same nanoparticle systems can be leveraged to treat CNS infections by simply changing the therapeutic payload. Both *in vitro* and *in vivo* studies have been conducted to demonstrate the vast potential of nanoparticle therapeutics. While *in vitro* systems are useful for isolating specific research variables and uncovering transport mechanisms, the use of *in vivo* models provides much greater measures of physiological relevance (97). The fact that a majority of the examples described below are from *in vivo* models shows the exciting success of many nanoparticle systems and the impending progression toward clinical trials.

Polymers, both artificially- and naturally-derived, have received the most attention for CNS delivery (24, 100, 120). The most widely used polymer is poly(D,L-lactide-co-glycolic acid) (PLGA), which is FDA approved and can undergo hydrolysis within the body to form biocompatible metabolites (121). PLGA nanoparticles have proven effective at increasing the half-life and stability of drugs such as the chemotherapeutic agent cisplatin, in comparison to the raw drug counterpart (122). Another study demonstrated that PLGA encapsulation of the anti-inflammatory and anti-oxidant compound curcumin dramatically improved BBB permeability and stimulated hippocampal neurogenesis to reduce cognitive decline in a rat model of AD (123). PLGA can also be conjugated and functionalized for specific targeting. In one example, researchers used Lf-conjugated polyethylene glycol (PEG)-PLGA nanoparticles containing the peptide urocortin to increase blood circulation time and promote specific uptake in the striatum and substantia nigra as a neuroprotective therapeutic for PD (124, 125).

Poly(alkyl cyanoacrylate) (PACA) is another nanoparticle polymer with proven ability to cross the BBB. PACA nanoparticles can be coated with surfactants for improved BBB permeability and have demonstrated promise as potential AD therapeutics from *in vitro* studies showing limited effects on vascular homeostasis and inflammatory response (126). Poly(butyl cyanoacrylate) (PBCA) nanoparticles are closely related to PACA, but degrade more rapidly in the body due to their higher water solubility (127). Other classes of biocompatible polymers include copolymer-poly (methylmethacrylate-sulfopropylmethacrylate) (PMMA-SPM), which have been loaded with anti-retroviral drugs for transport across the BBB (128). Natural polymers such as chitosan have also been explored as nanoparticle materials with CNS permeability. Tripolyphosphate cross-linked chitosan nanoparticles delivered the anti-inflammatory compound piperine to the CNS following intranasal administration in a rat model of sporadic dementia, which reduced inflammation by decreasing TNF-α and activated caspase-3 concomitant with increased superoxide dismutase activity (129). Another study used chitosan-coated lipid nanoparticle carriers conjugated to the transactivator of transcription (TAT) cell-penetrating peptide to enhance CNS delivery of glial cell-derived neurotrophic factor (GDNF) in a mouse model of PD, leading to decreased dopaminergic neuron loss and improved motor function (130).

Lipid-based nanoparticles include solid lipid and nanoemulsions, both of which are biocompatible, stable, and BBB-permeable (131, 132). Solid lipid nanoparticles consist of glycerides, waxes, and fatty acids stabilized with emulsifiers, and nanoemulsions are similar but with a liquid lipid core. Both are best suited for carrying lipophilic and hydrophobic drugs. A recent study used solid lipid nanoparticles loaded with doxorubicin for treating glioblastoma, which demonstrated excellent tumor cell toxicity (131).

Cell-derived nanoparticles consist of liposomes and exosomes. Liposomes have an aqueous core surrounded by a phospholipid bilayer, making them suitable for both hydrophobic and hydrophilic drugs. Phase III clinical trials are underway using cytarabine-carrying liposomes for treatment of neoplastic meningitis. The liposomal nanoparticles showed increased therapeutic concentrations of cytarabine in the CSF for up to 14 days post-administration (133). Another study has used cationic nanoliposomes with TfR-affinity ligands to deliver oligonucleotides and siRNA to the brain within 6 hours following intravenous injection. These nanoparticles reduced neuroinflammation when the siRNA targeted TNF-α (132). Exosomes are small vesicles secreted from all cell types that contain a wide range of biological molecules, including surface proteins, ligands, cytokines, and RNAs. They are beginning to be studied for therapeutic applications based on their ability to be loaded with drugs, BBB permeability, and potential for nasal administration (134).

Other unique nanoparticle formulations continue to be developed (135, 136). For example, biodegradable anti-TfR

monoclonal antibody (OX26)-PEGylated selenium nanoparticles were shown to suppress pathological inflammation and oxidative metabolism associated with cerebral stroke (137). Additionally, inorganic gold nanoparticles with varying surface ligands have shown promise for treating CNS bacterial infections due to both the inherent bactericidal properties of gold and conjugated antibiotics (138). The nanoparticle examples noted here merely represent a small snapshot of the wealth of possibilities for designing therapeutic carriers for improved treatment of CNS infections.

Cell-Specific Targeting With Nanoparticles

A final goal of nanoparticle therapies is cell-specific targeting (139, 140). In the context of CNS parenchymal infection, microglia represent a logical candidate. For microglial specificity, nanoparticles can leverage receptor-targeting ligands and the inherent phagocytic properties of microglia, while maintaining biocompatibility (140). An early study of microglial targeting used liposomal nanoparticles modified with the TLR4 ligand lipopolysaccharide (LPS), which significantly increased uptake of the encapsulated drug compared to non-targeted liposomes (141). In a later study, ceria-zirconia nanoparticles decorated with CD11b antibody showed preferential uptake by microglia compared to other cell types in the brain and higher internalization compared to nanoparticles conjugated to an isotype-matched control antibody (142). Other promising surface receptors exist to target microglia, including triggering receptor expressed on myeloid cells 2 (TREM2), Tmem119, and P2RY12 (143). Recent work has highlighted the significant transcriptional heterogeneity of leukocyte subpopulations within the CNS during *S. aureus* craniotomy infection, including microglia (144). The tunability of nanoparticle systems has exciting potential to target this diversity within a given cell type, where typical molecular therapies fall short. Of note, several of the receptors that have been exploited to deliver nanoparticles to microglia are also expressed on macrophages and neutrophils that infiltrate the CNS during infection. Therefore, targeting a single cell type with these receptors is unlikely. However, with the increasing abundance of next-generation sequencing datasets for CNS diseases, including infection, the identification of receptors that are enriched on a given phagocyte population is likely. Ultimately, nanoparticles targeting all of the key immune cell populations would fully complement the multi-tool kit of carriers for precisely modulating metabolic activity for the treatment of CNS infections.

DISCUSSION

Many bacteria, viruses, fungi, and parasites can invade the CNS and cause severe meningitis, encephalitis, and pyogenic infections. These conditions can become exceedingly dangerous as pathogens can acquire drug resistance, form biofilm, and leverage virulence factors that disrupt the host immune response and reprogram immune cells towards an anti-inflammatory bias. These challenges are exacerbated by the fact that therapeutic agent delivery to the CNS is hindered by the BBB, the same defense meant to exclude harmful pathogens. As such, treatment of CNS infections remains highly empirical and difficult, relying on extended and/or invasive delivery of anti-infection agents often with deleterious side effects.

We propose that together, the fields of immunometabolism and nanotechnology have the potential for a paradigm shift in novel treatments for CNS infections (**Figure 1**). The rapidly expanding field of immunometabolism has demonstrated that immune activation is controlled by the metabolic pathways needed to generate the energy and intermediates required for effector responses. The metabolic pathways that elicit pro-inflammatory activity have been described for all the key immune players in CNS infection, including microglia and infiltrating leukocytes but primarily in the context of neurodegeneration. It remains to be determined whether similar metabolic programs are observed during infection, which may differ based on nutrient competition with the pathogen. A variety of pharmacological agents, cytokines, lipid messengers, and microRNAs have been shown to modulate metabolism and could serve as potential therapeutics. In the realm of nanotechnology, nanoparticles can be engineered with a host of tunable structures, chemical ligands, and physiological characteristics to safely, and non-invasively deliver therapeutics to the CNS by transporting drugs across the BBB. Nanoparticle applications and design will continue to improve with increased knowledge of the precise interactions between structure, BBB penetration, and efficacy. Overall, merging therapeutic approaches with metabolic modulating agents and nanoparticles as delivery vehicles warrants the need for more focused research efforts given the promise for improving patient outcomes associated with CNS infections.

Research into metabolic reprogramming in the CNS to date has mainly focused on AD, PD, and MS, but more emphasis should be placed on infectious diseases, particularly in the current era of increasing antimicrobial resistance. Compared to peripheral tissues, the use of nanoparticles is especially important for CNS infections because of the BBB exclusivity. In the periphery, the major objective of nanoparticle usage is to target specific cell types and enhance cellular uptake of the drug or payload. In the CNS, these same attributes hold with the additional requirement of BBB penetration, which adds complexity to any potential therapeutic application. Nanoparticle-mediated metabolic modulation therapy could bolster endogenous cellular effector mechanisms to better fight infections compared to the introduction of compounds with harmful side effects throughout the CNS and periphery. Alongside future work into nanoparticle-based treatments for CNS infections, we anticipate the need for more long-term studies to address potential nanoparticle toxicity. Finally, we predict that the most effective nanoparticle therapeutics for CNS infections will be realized in a combinational platform leveraging not only metabolic modulation but also nanoparticle-encapsulated or intravenous anti-infection agents. The optimal metabolic modulation therapy may also not take the form of a

single re-polarization event, but instead a series of controlled toggling between pro- and anti-inflammatory states to adjust to the temporal nature of inflammation as the infection subsides.

AUTHOR CONTRIBUTIONS

LK drafted the manuscript. WS, BD, and TK reviewed and revised the manuscript. All authors contributed to the article and approved the submitted version.

FUNDING

The Kielian laboratory is supported by NIH grants R01 NS107369 and 3P01AI083211 (Project 4 to TK) and a Nebraska Research Institute Collaborative Grant (to TK and BD).

ACKNOWLEDGMENTS

We apologize to authors whose work could not be cited due to space constraints.

REFERENCES

1. Forrester JV, McMenamin PG, Dando SJ. CNS Infection and Immune Privilege. *Nat Rev Neurosci* (2018) 19(11):655–71. doi: 10.1038/s41583-018-0070-8
2. Klein RS, Hunter CA. Protective and Pathological Immunity During Central Nervous System Infections. *Immunity* (2017) 46(6):891–909. doi: 10.1016/j.immuni.2017.06.012
3. Beckham JD, Tyler KL. Neuro-Intensive Care of Patients With Acute CNS Infections. *Neurotherapeutics* (2012) 9(1):124–38. doi: 10.1007/s13311-011-0086-5
4. Cain MD, Salimi H, Diamond MS, Klein RS. Mechanisms of Pathogen Invasion Into the Central Nervous System. *Neuron* (2019) 103(5):771–83. doi: 10.1016/j.neuron.2019.07.015
5. Doran KS, Fulde M, Gratz N, Kim BJ, Nau R, Prasadarao N, et al. Host-Pathogen Interactions in Bacterial Meningitis. *Acta Neuropathol* (2016) 131 (2):185–209. doi: 10.1007/s00401-015-1531-z
6. Bowen LN, Smith B, Reich D, Quezado M, Nath A. HIV-Associated Opportunistic CNS Infections: Pathophysiology, Diagnosis and Treatment. *Nat Rev Neurol* (2016) 12(11):662–74. doi: 10.1038/nrneurol.2016.149
7. Weidauer S, Wagner M, Enkirch SJ, Hattingen E. CNS Infections in Immunoincompetent Patients: Neuroradiological and Clinical Features. *Clin Neuroradiol* (2020) 30(1):9–25. doi: 10.1007/s00062-019-00837-6
8. Cheatle J, Aldrich A, Thorell WE, Boska MD, Kielian T. Compartmentalization of Immune Responses During Staphylococcus Aureus Cranial Bone Flap Infection. *Am J Pathol* (2013) 183(2):450–8. doi: 10.1016/j.ajpath.2013.04.031
9. de Morais S DB, Kak G, Menousek JP, Kielian T. Immunopathogenesis of Craniotomy Infection and Niche-Specific Immune Responses to Biofilm. *Front Immunol* (2021) 12:625467. doi: 10.3389/fimmu.2021.625467
10. Jorgensen J, Williams C, Sarang-Sieminski A. Hydrocephalus and Ventriculoperitoneal Shunts: Modes of Failure and Opportunities for Improvement. *Crit Rev BioMed Eng* (2016) 44(1-2):91–7. doi: 10.1615/CritRevBiomedEng.2016017149
11. Bloomgren G, Richman S, Hotermans C, Subramanyam M, Goelz S, Natarajan A, et al. Risk of Natalizumab-Associated Progressive Multifocal Leukoencephalopathy. *New Engl J Med* (2012) 366(20):1870–80. doi: 10.1056/NEJMoa1107829
12. Lai Y, Dong C. Therapeutic Antibodies That Target Inflammatory Cytokines in Autoimmune Diseases. *Int Immunol* (2016) 28(4):181–8. doi: 10.1093/intimm/dxv063
13. Schwab N, Schneider-Hohendorf T, Wiendl H. Therapeutic Uses of Anti-Alpha4-Integrin (Anti-VLA-4) Antibodies in Multiple Sclerosis. *Int Immunol* (2015) 27(1):47–53. doi: 10.1093/intimm/dxu096
14. Yamada KJ, Kielian T. Biofilm-Leukocyte Cross-Talk: Impact on Immune Polarization and Immunometabolism. *J Innate Immun* (2019) 11(3):280–8. doi: 10.1159/000492680
15. Dando SJ, Mackay-Sim A, Norton R, Currie BJ, St John JA, Ekberg JA, et al. Pathogens Penetrating the Central Nervous System: Infection Pathways and the Cellular and Molecular Mechanisms of Invasion. *Clin Microbiol Rev* (2014) 27(4):691–726. doi: 10.1128/CMR.00118-13
16. Herold R, Schroten H, Schwerk C. Virulence Factors of Meningitis-Causing Bacteria: Enabling Brain Entry Across the Blood-Brain Barrier. *Int J Mol Sci* (2019) 20(21):5393. doi: 10.3390/ijms20215393
17. Schilcher K, Horswill AR. Staphylococcal Biofilm Development: Structure, Regulation, and Treatment Strategies. *Microbiol Mol Biol Rev* (2020) 84(3): e00026–19. doi: 10.1128/MMBR.00026-19
18. Nau R, Sorgel F, Eiffert H. Penetration of Drugs Through the Blood-Cerebrospinal Fluid/Blood-Brain Barrier for Treatment of Central Nervous System Infections. *Clin Microbiol Rev* (2010) 23(4):858–83. doi: 10.1128/CMR.00007-10
19. Pardridge WM. Why is the Global CNS Pharmaceutical Market So Under-Penetrated? *Drug Discovery Today* (2002) 7(1):5–7. doi: 10.1016/S1359-6446(01)02082-7
20. Reynolds JL, Mahato RI. Nanomedicines for the Treatment of CNS Diseases. *J Neuroimmune Pharmacol* (2017) 12(1):1–5. doi: 10.1007/s11481-017-9725-x
21. Ziai WC, Lewin JJ. 3rd. Improving the Role of Intraventricular Antimicrobial Agents in the Management of Meningitis. *Curr Opin Neurol* (2009) 22(3):277–82. doi: 10.1097/wco.0b013e32832c1396
22. Velkov T, Dai C, Ciccotosto GD, Cappai R, Hoyer D, Li J. Polymyxins for CNS Infections: Pharmacology and Neurotoxicity. *Pharmacol Ther* (2018) 181:85–90. doi: 10.1016/j.pharmthera.2017.07.012
23. Ceña V, Játiva P. Nanoparticle Crossing of Blood–Brain Barrier: A Road to New Therapeutic Approaches to Central Nervous System Diseases. *Nanomedicine* (2018) 13(13):1513–6. doi: 10.2217/nnm-2018-0139
24. DeMarino C, Schwab A, Pleet M, Mathiesen A, Friedman J, El-Hage N, et al. Biodegradable Nanoparticles for Delivery of Therapeutics in CNS Infection. *J Neuroimmune Pharmacol* (2017) 12(1):31–50. doi: 10.1007/s11481-016-9692-7
25. Kaushik DK, Yong VW. Metabolic Needs of Brain-Infiltrating Leukocytes and Microglia in Multiple Sclerosis. *J Neurochem* (2020) 1–11. doi: 10.1111/jnc.15206
26. Runtsch MC, Ferrara G, Angiari S. Metabolic Determinants of Leukocyte Pathogenicity in Neurological Diseases. *J Neurochem* (2020) 1–23. doi: 10.1111/jnc.15169
27. Iovino F, Engelen-Lee JY, Brouwer M, van de Beek D, van der Ende A, Valls Seron M, et al. Pigr and PECAM-1 Bind to Pneumococcal Adhesins Rrga and Pspc Mediating Bacterial Brain Invasion. *J Exp Med* (2017) 214(6):1619–30. doi: 10.1084/jem.20161668
28. Ghosh P, Halvorsen EM, Ammendolia DA, Mor-Vaknin N, O'Riordan MXD, Brumell JH, et al. Invasion of the Brain by Listeria Monocytogenes is Mediated by Inlf and Host Cell Vimentin. *mBio* (2018) 9(1):e00160-18. doi: 10.1128/mBio
29. Engelhardt B, Vajkoczy P, Weller RO. The Movers and Shapers in Immune Privilege of the CNS. *Nat Immunol* (2017) 18(2):123–31. doi: 10.1038/ni.3666
30. Snarr BD, Drummond RA, Lionakis MS. It's All in Your Head: Antifungal Immunity in the Brain. *Curr Opin Microbiol* (2020) 58:41–6. doi: 10.1016/j.mib.2020.07.011
31. Richard AS, Shim BS, Kwon YC, Zhang R, Otsuka Y, Schmitt K, et al. AXL-Dependent Infection of Human Fetal Endothelial Cells Distinguishes Zika Virus From Other Pathogenic Flaviviruses. *Proc Natl Acad Sci USA* (2017) 114(8):2024–9. doi: 10.1073/pnas.1620558114
32. Harker KS, Jivan E, McWhorter FY, Liu WF, Lodoen MB. Shear Forces Enhance Toxoplasma Gondii Tachyzoite Motility on Vascular Endothelium. *mBio* (2014) 5(2):e01111–13. doi: 10.1128/mBio.01111-13

33. Loh LN, Gao G, Tuomanen EI. Dissecting Bacterial Cell Wall Entry and Signaling in Eukaryotic Cells: An Actin-Dependent Pathway Parallels Platelet-Activating Factor Receptor-Mediated Endocytosis. *mBio* (2017) 8 (1):e02030-16. doi: 10.1128/mBio.02030-16
34. Hasebe R, Suzuki T, Makino Y, Igarashi M, Yamanouchi S, Maeda A, et al. Transcellular Transport of West Nile Virus-Like Particles Across Human Endothelial Cells Depends on Residues 156 and 159 of Envelope Protein. *BMC Microbiol* (2010) 10(165):1–10. doi: 10.1186/1471-2180-10-165
35. Jong A, Wu CH, Gonzales-Gomez I, Kwon-Chung KJ, Chang YC, Tseng HK, et al. Hyaluronic Acid Receptor CD44 Deficiency is Associated With Decreased Cryptococcus Neoformans Brain Infection. *J Biol Chem* (2012) 287(19):15298–306. doi: 10.1074/jbc.M112.353375
36. Santiago-Tirado FH, Doering TL. False Friends: Phagocytes as Trojan Horses in Microbial Brain Infections. *PloS Pathog* (2017) 13(12):e1006680. doi: 10.1371/journal.ppat.1006680
37. Santiago-Tirado FH, Onken MD, Cooper JA, Klein RS, Doering TL. Trojan Horse Transit Contributes to Blood-Brain Barrier Crossing of a Eukaryotic Pathogen. *mBio* (2017) 8(1):e02183-16. doi: 10.1128/mBio.02183-16
38. Bai F, Kong KF, Dai J, Qian F, Zhang L, Brown CR, et al. A Paradoxical Role for Neutrophils in the Pathogenesis of West Nile Virus. *J Infect Dis* (2010) 202(12):1804–12. doi: 10.1086/657416
39. Courret N, Darche S, Sonigo P, Milon G, Buzoni-Gatel D, Tardieux I. CD11c- and CD11b-Expressing Mouse Leukocytes Transport Single Toxoplasma Gondii Tachyzoites to the Brain. *Blood* (2006) 107(1):309–16. doi: 10.1182/blood-2005-02-0666
40. Gutierrez-Murgas Y, Snowden JN. Ventricular Shunt Infections: Immunopathogenesis and Clinical Management. *J Neuroimmunol* (2014) 276(1-2):1–8. doi: 10.1016/j.jneuroim.2014.08.006
41. Tunkel AR, Hasbun R, Bhimraj A, Byers K, Kaplan SL, Scheld WM, et al. 2017 Infectious Diseases Society of America's Clinical Practice Guidelines for Healthcare-Associated Ventriculitis and Meningitis. *Clin Infect Dis* (2017) 64(6):e34–65. doi: 10.1093/cid/ciw861
42. Li L, Acioglu C, Heary RF, Elkabes S. Role of Astroglial Toll-Like Receptors (Tlrs) in Central Nervous System Infections, Injury and Neurodegenerative Diseases. *Brain Behav Immun* (2021) 91:740–55. doi: 10.1016/j.bbi.2020.10.007
43. Mariani MM, Kielian T. Microglia in Infectious Diseases of the Central Nervous System. *J Neuroimmune Pharmacol* (2009) 4(4):448–61. doi: 10.1007/s11481-009-9170-6
44. Heneka MT, Kummer MP, Latz E. Innate Immune Activation in Neurodegenerative Disease. *Nat Rev Immunol* (2014) 14(7):463–77. doi: 10.1038/nri3705
45. Hanke ML, Kielian T. Toll-Like Receptors in Health and Disease in the Brain: Mechanisms and Therapeutic Potential. *Clin Sci* (2011) 121(9):367–87. doi: 10.1042/CS20110164
46. Burmeister AR, Marriott I. The Interleukin-10 Family of Cytokines and Their Role in the CNS. *Front Cell Neurosci* (2018) 12:458. doi: 10.3389/fncel.2018.00458
47. Sochocka M, Diniz BS, Leszek J. Inflammatory Response in the CNS: Friend or Foe? *Mol Neurobiol* (2017) 54(10):8071–89. doi: 10.1007/s12035-016-0297-1
48. Pearce EJ, Pearce EL. Immunometabolism in 2017: Driving Immunity: All Roads Lead to Metabolism. *Nat Rev Immunol* (2018) 18(2):81–2. doi: 10.1038/nri.2017.139
49. Pearce EL, Pearce EJ. Metabolic Pathways in Immune Cell Activation and Quiescence. *Immunity* (2013) 38(4):633–43. doi: 10.1016/j.immuni.2013.04.005
50. O'Neill LA, Kishton RJ, Rathmell J. A Guide to Immunometabolism for Immunologists. *Nat Rev Immunol* (2016) 16(9):553–65. doi: 10.1038/nri.2016.70
51. DeBerardinis RJ, Chandel NS. We Need to Talk About the Warburg Effect. *Nat Metab* (2020) 2(2):127–9. doi: 10.1038/s42255-020-0172-2
52. Belanger M, Allaman I, Magistretti PJ. Brain Energy Metabolism: Focus on Astrocyte-Neuron Metabolic Cooperation. *Cell Metab* (2011) 14(6):724–38. doi: 10.1016/j.cmet.2011.08.016
53. Bernier LP, York EM, MacVicar BA. Immunometabolism in the Brain: How Metabolism Shapes Microglial Function. *Trends Neurosci* (2020) 43 (11):854–69. doi: 10.1016/j.tins.2020.08.008
54. Vainchtein ID, Molofsky AV. Astrocytes and Microglia: In Sickness and in Health. *Trends Neurosci* (2020) 43(3):144–54. doi: 10.1016/j.tins.2020.01.003
55. Lehman MK, Nuxoll AS, Yamada KJ, Kielian T, Carson SD, Fey PD. Protease-Mediated Growth of Staphylococcus Aureus on Host Proteins is Opp3 Dependent. *mBio* (2019) 10(2):e02553–18. doi: 10.1128/mBio.02553-18
56. Potter AD, Butrico CE, Ford CA, Curry JM, Trenary IA, Tummarakota SS, et al. Host Nutrient Milieu Drives an Essential Role for Aspartate Biosynthesis During Invasive Staphylococcus Aureus Infection. *Proc Natl Acad Sci USA* (2020) 117(22):12394–401. doi: 10.1073/pnas.1922211117
57. Heim CE, Bosch ME, Yamada KJ, Aldrich AL, Chaudhari SS, Klinkebiel D, et al. Lactate Production by Staphylococcus Aureus Biofilm Inhibits HDAC11 to Reprogramme the Host Immune Response During Persistent Infection. *Nat Microbiol* (2020) 5(10):1271–84. doi: 10.1038/s41564-020-0756-3
58. Mergenthaler P, Lindauer U, Dienel GA, Meisel A. Sugar for the Brain: The Role of Glucose in Physiological and Pathological Brain Function. *Trends Neurosci* (2013) 36(10):587–97. doi: 10.1016/j.tins.2013.07.001
59. Ginhoux F, Greter M, Leboeuf M, Nandi S, See P, Gokhan S, et al. Fate Mapping Analysis Reveals That Adult Microglia Derive From Primitive Macrophages. *Science* (2010) 330(6005):841–5. doi: 10.1126/science.1194637
60. Li Q, Barres BA. Microglia and Macrophages in Brain Homeostasis and Disease. *Nat Rev Immunol* (2018) 18(4):225–42. doi: 10.1038/nri.2017.125
61. Prinz M, Jung S, Priller J. Microglia Biology: One Century of Evolving Concepts. *Cell* (2019) 179(2):292–311. doi: 10.1016/j.cell.2019.08.053
62. Lauro C, Limatola C. Metabolic Reprograming of Microglia in the Regulation of the Innate Inflammatory Response. *Front Immunol* (2020) 11:493. doi: 10.3389/fimmu.2020.00493
63. Lynch MA. Can the Emerging Field of Immunometabolism Provide Insights Into Neuroinflammation? *Prog Neurobiol* (2020) 184:101719. doi: 10.1016/j.pneurobio.2019.101719
64. Matias I, Morgado J, Gomes FCA. Astrocyte Heterogeneity: Impact to Brain Aging and Disease. *Front Aging Neurosci* (2019) 11:59. doi: 10.3389/fnagi.2019.00059
65. Sofroniew MV. Astrocyte Reactivity: Subtypes, States, and Functions in CNS Innate Immunity. *Trends Immunol* (2020) 41(9):758–70. doi: 10.1016/j.it.2020.07.004
66. Saab AS, Tzvetavona ID, Trevisiol A, Baltan S, Dibaj P, Kusch K, et al. Oligodendroglial NMDA Receptors Regulate Glucose Import and Axonal Energy Metabolism. *Neuron* (2016) 91(1):119–32. doi: 10.1016/j.neuron.2016.05.016
67. Cragnolini AB, Lampitella G, Virtuoso A, Viscovo I, Panetsos F, Papa M, et al. Regional Brain Susceptibility to Neurodegeneration: What is the Role of Glial Cells? *Neural Regener Res* (2020) 15(5):838–42. doi: 10.4103/1673-5374.268897
68. Greenhalgh AD, David S, Bennett FC. Immune Cell Regulation of Glia During CNS Injury and Disease. *Nat Rev Neurosci* (2020) 21(3):139–52. doi: 10.1038/s41583-020-0263-9
69. Prinz M, Priller J. The Role of Peripheral Immune Cells in the CNS in Steady State and Disease. *Nat Neurosci* (2017) 20(2):136–44. doi: 10.1038/nn.4418
70. Jha AK, Huang SC, Sergushichev A, Lampropoulou V, Ivanova Y, Loginicheva E, et al. Network Integration of Parallel Metabolic and Transcriptional Data Reveals Metabolic Modules That Regulate Macrophage Polarization. *Immunity* (2015) 42(3):419–30. doi: 10.1016/j.immuni.2015.02.005
71. Kaushik DK, Bhattacharya A, Mirzaei R, Rawji KS, Ahn Y, Rho JM, et al. Enhanced Glycolytic Metabolism Supports Transmigration of Brain-Infiltrating Macrophages in Multiple Sclerosis. *J Clin Invest* (2019) 129 (8):3277–92. doi: 10.1172/JCI124012
72. Devanney NA, Stewart AN, Gensel JC. Microglia and Macrophage Metabolism in CNS Injury and Disease: The Role of Immunometabolism in Neurodegeneration and Neurotrauma. *Exp Neurol* (2020) 329:113310. doi: 10.1016/j.expneurol.2020.113310
73. Luan HH, Medzhitov R. Food Fight: Role of Itaconate and Other Metabolites in Antimicrobial Defense. *Cell Metab* (2016) 24(3):379–87. doi: 10.1016/j.cmet.2016.08.013
74. Everts B, Amiel E, Huang SC, Smith AM, Chang CH, Lam WY, et al. TLR-Driven Early Glycolytic Reprogramming *Via* the Kinases TBK1-Ikkvarepsilon Supports the Anabolic Demands of Dendritic Cell Activation. *Nat Immunol* (2014) 15(4):323–32. doi: 10.1038/ni.2833
75. Krawczyk CM, Holowka T, Sun J, Blagih J, Amiel E, DeBerardinis RJ, et al. Toll-Like Receptor-Induced Changes in Glycolytic Metabolism Regulate

Dendritic Cell Activation. *Blood* (2010) 115(23):4742–9. doi: 10.1182/blood-2009-10-249540
76. Macri C, Pang ES, Patton T, O'Keeffe M. Dendritic Cell Subsets. *Semin Cell Dev Biol* (2018) 84:11–21. doi: 10.1016/j.semcdb.2017.12.009
77. Injarabian L, Devin A, Ransac S, Marteyn BS. Neutrophil Metabolic Shift During Their Lifecycle: Impact on Their Survival and Activation. *Int J Mol Sci* (2019) 21(1):287. doi: 10.3390/ijms21010287
78. Keppel MP, Saucier N, Mah AY, Vogel TP, Cooper MA. Activation-Specific Metabolic Requirements for NK Cell IFN-Gamma Production. *J Immunol* (2015) 194(4):1954–62. doi: 10.4049/jimmunol.1402099
79. Bantug GR, Galluzzi L, Kroemer G, Hess C. The Spectrum of T Cell Metabolism in Health and Disease. *Nat Rev Immunol* (2018) 18(1):19–34. doi: 10.1038/nri.2017.99
80. Shin B, Benavides GA, Geng J, Koralov SB, Hu H, Darley-Usmar VM, et al. Mitochondrial Oxidative Phosphorylation Regulates the Fate Decision Between Pathogenic Th17 and Regulatory T Cells. *Cell Rep* (2020) 30 (6):1898–909 e4. doi: 10.1016/j.celrep.2020.01.022
81. Jellusova J. The Role of Metabolic Checkpoint Regulators in B Cell Survival and Transformation. *Immunol Rev* (2020) 295(1):39–53. doi: 10.1111/imr.12855
82. Weisel FJ, Mullett SJ, Elsner RA, Menk AV, Trivedi N, Luo W, et al. Germinal Center B Cells Selectively Oxidize Fatty Acids for Energy While Conducting Minimal Glycolysis. *Nat Immunol* (2020) 21(3):331–42. doi: 10.1038/s41590-020-0598-4
83. Fillatreau S. Novel Regulatory Functions for Toll-Like Receptor Activated B Cells During Intracellular Bacterial Infection. *Immunol Rev* (2011) 240:52–71. doi: 10.1111/j.1600-065X.2010.00991.x
84. Gerriets VA, Kishton RJ, Nichols AG, Macintyre AN, Inoue M, Ilkayeva O, et al. Metabolic Programming and PDHK1 Control CD4+ T Cell Subsets and Inflammation. *J Clin Invest* (2015) 125(1):194–207. doi: 10.1172/JCI76012
85. Shi LZ, Wang R, Huang G, Vogel P, Neale G, Green DR, et al. HIF1alpha-Dependent Glycolytic Pathway Orchestrates a Metabolic Checkpoint for the Differentiation of TH17 and Treg Cells. *J Exp Med* (2011) 208(7):1367–76. doi: 10.1084/jem.20110278
86. Angiari S, Runtsch MC, Sutton CE, Palsson-McDermott EM, Kelly B, Rana N, et al. Pharmacological Activation of Pyruvate Kinase M2 Inhibits CD4(+) T Cell Pathogenicity and Suppresses Autoimmunity. *Cell Metab* (2020) 31 (2):391–405 e8. doi: 10.1016/j.cmet.2019.10.015
87. Kuo PC, Weng WT, Scofield BA, Paraiso HC, Brown DA, Wang PY, et al. Dimethyl Itaconate, an Itaconate Derivative, Exhibits Immunomodulatory Effects on Neuroinflammation in Experimental Autoimmune Encephalomyelitis. *J Neuroinflamm* (2020) 17(1):138. doi: 10.1186/s12974-020-01768-7
88. Haghikia A, Faissner S, Pappas D, Pula B, Akkad DA, Arning L, et al. Interferon-Beta Affects Mitochondrial Activity in CD4+ Lymphocytes: Implications for Mechanism of Action in Multiple Sclerosis. *Mult Scler* (2015) 21(10):1262–70. doi: 10.1177/1352458514561909
89. Klotz L, Eschborn M, Lindner M, Liebmann M, Herold M, Janoschka C, et al. Teriflunomide Treatment for Multiple Sclerosis Modulates T Cell Mitochondrial Respiration With Affinity-Dependent Effects. *Sci Trans Med* (2019) 11:eaao5563. doi: 10.1126/scitranslmed.aao5563
90. Hu Y, Mai W, Chen L, Cao K, Zhang B, Zhang Z, et al. Mtor-Mediated Metabolic Reprogramming Shapes Distinct Microglia Functions in Response to Lipopolysaccharide and ATP. *Glia* (2020) 68(5):1031–45. doi: 10.1002/glia.23760
91. Fumagalli M, Lombardi M, Gressens P, Verderio C. How to Reprogram Microglia Toward Beneficial Functions. *Glia* (2018) 66(12):2531–49. doi: 10.1002/glia.23484
92. Mills EL, Kelly B, Logan A, Costa ASH, Varma M, Bryant CE, et al. Succinate Dehydrogenase Supports Metabolic Repurposing of Mitochondria to Drive Inflammatory Macrophages. *Cell* (2016) 167(2):457–70 e13. doi: 10.1016/j.cell.2016.08.064
93. Yamada KJ, Heim CE, Xi X, Attri KS, Wang D, Zhang W, et al. Monocyte Metabolic Reprogramming Promotes Pro-Inflammatory Activity and Staphylococcus Aureus Biofilm Clearance. *PloS Pathog* (2020) 16(3): e1008354. doi: 10.1371/journal.ppat.1008354
94. Aldrich A, Kuss MA, Duan B, Kielian T. 3D Bioprinted Scaffolds Containing Viable Macrophages and Antibiotics Promote Clearance of Staphylococcus Aureus Craniotomy-Associated Biofilm Infection. *ACS Appl Mater Interfaces* (2019) 11(13):12298–307. doi: 10.1021/acsami.9b00264
95. Aldrich AL, Heim CE, Shi W, Fallet RW, Duan B, Kielian T. TLR2 and Caspase-1 Signaling are Critical for Bacterial Containment But Not Clearance During Craniotomy-Associated Biofilm Infection. *J Neuroinflamm* (2020) 17(1):114. doi: 10.1186/s12974-020-01793-6
96. Barros LF. Metabolic Signaling by Lactate in the Brain. *Trends Neurosci* (2013) 36(7):396–404. doi: 10.1016/j.tins.2013.04.002
97. Barar J, Rafi MA, Pourseif MM, Omidi Y. Blood-Brain Barrier Transport Machineries and Targeted Therapy of Brain Diseases. *Bioimpacts* (2016) 6 (4):225–48. doi: 10.15171/bi.2016.30
98. Saeedi M, Eslamifar M, Khezri K, Dizaj SM. Applications of Nanotechnology in Drug Delivery to the Central Nervous System. *BioMed Pharmacother* (2019) 111:666–75. doi: 10.1016/j.biopha.2018.12.133
99. Pardridge WM. The Blood-Brain Barrier: Bottleneck in Brain Drug Development. *NeuroRX* (2005) 2:3–14. doi: 10.1602/neurorx.2.1.3
100. Poupot R, Bergozza D, Fruchon S. Nanoparticle-Based Strategies to Treat Neuro-Inflammation. *Materials* (2018) 11(2): 270. doi: 10.3390/ma11020270
101. McDannold N, Vykhodtseva N, Hynynen K. Blood-Brain Barrier Disruption Induced by Focused Ultrasound and Circulating Preformed Microbubbles Appears to be Characterized by the Mechanical Index. *Ultrasound Med Biol* (2008) 34(5):834–40. doi: 10.1016/j.ultrasmedbio.2007.10.016
102. Meairs S. Facilitation of Drug Transport Across the Blood-Brain Barrier With Ultrasound and Microbubbles. *Pharmaceutics* (2015) 7(3):275–93. doi: 10.3390/pharmaceutics7030275
103. Yang LL, Zhou Y, Tian WD, Li HJ, Kang Chu L, Miao X, et al. Electromagnetic Pulse Activated Brain Microglia *Via* the P38 MAPK Pathway. *Neurotoxicology* (2016) 52:144–9. doi: 10.1016/j.neuro.2015.12.008
104. Banks WA. From Blood-Brain Barrier to Blood-Brain Interface: New Opportunities for CNS Drug Delivery. *Nat Rev Drug Discovery* (2016) 15 (4):275–92. doi: 10.1038/nrd.2015.21
105. Betzer O, Shilo M, Opochinsky R, Barnoy E, Motiei M, Okun E, et al. The Effect of Nanoparticle Size on the Ability to Cross the Blood–Brain Barrier: An In Vivo Study. *Nanomedicine* (2017) 12(3):1533–46. doi: 10.2217/nnm-2017-0022
106. Ou H, Cheng T, Zhang Y, Liu J, Ding Y, Zhen J, et al. Surface-Adaptive Zwitterionic Nanoparticles for Prolonged Blood Circulation Time and Enhanced Cellular Uptake in Tumor Cells. *Acta Biomater* (2018) 65:339–48. doi: 10.1016/j.actbio.2017.10.034
107. Lin T, Zhao P, Jiang Y, Tang Y, Jin H, Pan Z, et al. Blood-Brain-Barrier-Penetrating Albumin Nanoparticles for Biomimetic Drug Delivery *Via* Albumin-Binding Protein Pathways for Antiglioma Therapy. *ACS Nano* (2016) 10(11):9999–10012. doi: 10.1021/acsnano.6b04268
108. Liu DZ, Cheng Y, Cai RQ, Wang Bd WW, Cui H, Liu M, et al. The Enhancement of Siplk1 Penetration Across BBB and its Anti Glioblastoma Activity *In Vivo* by Magnet and Transferrin Co-Modified Nanoparticle. *Nanomedicine* (2018) 14(3):991–1003. doi: 10.1016/j.nano.2018.01.004
109. Martinez-Veracoechea FJ, Frenkel D. Designing Super Selectivity in Multivalent Nano-Particle Binding. *Proc Natl Acad Sci USA* (2011) 108 (27):10963–8. doi: 10.1073/pnas.1105351108
110. Wiley DT, Webster P, Gale A, Davis ME. Transcytosis and Brain Uptake of Transferrin-Containing Nanoparticles by Tuning Avidity to Transferrin Receptor. *Proc Natl Acad Sci USA* (2013) 110(21):8662–7. doi: 10.1073/pnas.1307152110
111. Lindgren M, Hällbrink M, Prochiantz A, Langel Ü. Cell-Penetrating Peptides. *TiPS* (2000) 21:99–103. doi: 10.1016/S0165-6147(00)01447-4
112. Khan AR, Liu M, Khan MW, Zhai G. Progress in Brain Targeting Drug Delivery System by Nasal Route. *J Control Release* (2017) 268:364–89. doi: 10.1016/j.jconrel.2017.09.001
113. Sonvico F, Clementino A, Buttini F, Colombo G, Pescina S, Staniscuaski Guterres S, et al. Surface-Modified Nanocarriers for Nose-to-Brain Delivery: From Bioadhesion to Targeting. *Pharmaceutics* (2018) 10(1):34. doi: 10.3390/pharmaceutics10010034
114. Srikanth M, Kessler JA. Nanotechnology-Novel Therapeutics for CNS Disorders. *Nat Rev Neurol* (2012) 8(6):307–18. doi: 10.1038/nrneurol.2012.76
115. Ham AS, Cost MR, Sassi AB, Dezzutti CS, Rohan LC. Targeted Delivery of PSC-RANTES for HIV-1 Prevention Using Biodegradable Nanoparticles. *Pharm Res* (2009) 26(3):502–11. doi: 10.1007/s11095-008-9765-2
116. Rao KS, Reddy MK, Horning JL, Labhasetwar V. TAT-Conjugated Nanoparticles for the CNS Delivery of Anti-HIV Drugs. *Biomaterials* (2008) 29(33):4429–38. doi: 10.1016/j.biomaterials.2008.08.004

117. Wen Z, Yan Z, Hu K, Pang Z, Cheng X, Guo L, et al. Odorranalectin-Conjugated Nanoparticles: Preparation, Brain Delivery and Pharmacodynamic Study on Parkinson's Disease Following Intranasal Administration. *J Control Release* (2011) 151(2):131–8. doi: 10.1016/j.jconrel.2011.02.022
118. Kreuter J. Drug Delivery to the Central Nervous System by Polymeric Nanoparticles: What do We Know? *Adv Drug Delivery Rev* (2014) 71:2–14. doi: 10.1016/j.addr.2013.08.008
119. Voigt N, Henrich-Noack P, Kockentiedt S, Hintz W, Tomas J, Sabel BA. Surfactants, Not Size or Zeta-Potential Influence Blood-Brain Barrier Passage of Polymeric Nanoparticles. *Eur J Pharm Biopharm* (2014) 87 (1):19–29. doi: 10.1016/j.ejpb.2014.02.013
120. Vinogradov SV, Batrakova EV, Kabanov AV. Nanogels for Oligonucleotide Delivery to the Brain. *Bioconjugate Chem* (2004) 15:50–60. doi: 10.1021/bc034164r
121. Kumari A, Yadav SK, Yadav SC. Biodegradable Polymeric Nanoparticles Based Drug Delivery Systems. *Colloids Surf B Biointerfaces* (2010) 75(1):1–18. doi: 10.1016/j.colsurfb.2009.09.001
122. Avgoustakisa K, Beletsia A, Panagia Z, Klepetsanisa P, Karydasb AG, Ithakissios DS. PLGA–Mpeg Nanoparticles of Cisplatin: *In Vitro* Nanoparticle Degradation, *In Vitro* Drug Release and *In Vivo* Drug Residence in Blood Properties. *J Controlled Release* (2002) 79:123–35. doi: 10.1016/S0168-3659(01)00530-2
123. Tiwari SK, Agarwal S, Seth B, Yadav A, Nair S, Bhatnagar P, et al. Curcumin-Loaded Nanoparticles Potently Induce Adult Neurogenesis and Reverse Cognitive Deficits in Alzheimer's Disease Model *Via* Canonical Wnt/β-Catenin Pathway. *ACS Nano* (2014) 8(1):76–103. doi: 10.1021/nn405077y
124. Hu K, Shi Y, Jiang W, Han J, Huang S, Jiang X. Lactoferrin Conjugated PEG-PLGA Nanoparticles for Brain Delivery: Preparation, Characterization and Efficacy in Parkinson's Disease. *Int J Pharm* (2011) 415(1-2):273–83. doi: 10.1016/j.ijpharm.2011.05.062
125. Li H, Tong Y, Bai L, Ye L, Zhong L, Duan X, et al. Lactoferrin Functionalized PEG-PLGA Nanoparticles of Shikonin for Brain Targeting Therapy of Glioma. *Int J Biol Macromol* (2018) 107(Pt A):204–11. doi: 10.1016/j.ijbiomac.2017.08.155
126. Orlando A, Re F, Sesana S, Rivolta I, Panariti A, Brambilla D, et al. Effect of Nanoparticles Binding Beta-Amyloid Peptide on Nitric Oxide Production by Cultured Endothelial Cells and Macrophages. *Int J Nanomed* (2013) 8:1335–47. doi: 10.2147/IJN.S40297
127. Aslund AKO, Berg S, Hak S, Morch Y, Torp SH, Sandvig A, et al. Nanoparticle Delivery to the Brain - by Focused Ultrasound and Self-Assembled Nanoparticle-Stabilized Microbubbles. *J Control Release* (2015) 220(Pt A):287–94. doi: 10.1016/j.jconrel.2015.10.047
128. Kuo YC, Lee CL. Methylmethacrylate-Sulfopropylmethacrylate Nanoparticles With Surface RMP-7 for Targeting Delivery of Antiretroviral Drugs Across the Blood-Brain Barrier. *Colloids Surf B Biointerfaces* (2012) 90:75–82. doi: 10.1016/j.colsurfb.2011.09.048
129. Elnaggar YSR, Etman SM, Abdelmonsif DA, Abdallah OY. Intranasal Piperine-Loaded Chitosan Nanoparticles as Brain-Targeted Therapy in Alzheimer's Disease: Optimization, Biological Efficacy, and Potential Toxicity. *J Pharm Sci* (2015) 104(10):3544–56. doi: 10.1002/jps.24557
130. Hernando S, Herran E, Figueiro-Silva J, Pedraz JL, Igartua M, Carro E, et al. Intranasal Administration of TAT-Conjugated Lipid Nanocarriers Loading GDNF for Parkinson's Disease. *Mol Neurobiol* (2018) 55(1):145–55. doi: 10.1007/s12035-017-0728-7
131. Battaglia L, Gallarate M, Peira E, Chirio D, Muntoni E, Biasibetti E, et al. Solid Lipid Nanoparticles for Potential Doxorubicin Delivery in Glioblastoma Treatment: Preliminary *In Vitro* Studies. *J Pharm Sci* (2014) 103(7):2157–65. doi: 10.1002/jps.24002
132. Kim SS, Rait A, Garrido-Sanabria ER, Pirollo KF, Harford JB, Chang EH. Nanotherapeutics for Gene Modulation That Prevents Apoptosis in the Brain and Fatal Neuroinflammation. *Mol Ther* (2018) 26(1):84–94. doi: 10.1016/j.ymthe.2017.10.003
133. Phuphanich S, Maria B, Braeckman R, Chamberlain M. A Pharmacokinetic Study of Intra-CSF Administered Encapsulated Cytarabine (Depocyt) for the Treatment of Neoplastic Meningitis in Patients With Leukemia, Lymphoma, or Solid Tumors as Part of a Phase III Study. *J Neurooncol* (2007) 81(2):201–8. doi: 10.1007/s11060-006-9218-x
134. Aryani A, Denecke B. Exosomes as a Nanodelivery System: A Key to the Future of Neuromedicine? *Mol Neurobiol* (2016) 53(2):818–34. doi: 10.1007/s12035-014-9054-5
135. Patel MM, Patel BM. Crossing the Blood-Brain Barrier: Recent Advances in Drug Delivery to the Brain. *CNS Drugs* (2017) 31(2):109–33. doi: 10.1007/s40263-016-0405-9
136. Monsalve Y, Tosi G, Ruozi B, Belletti D, Vilella A, Zoli M, et al. PEG-G-Chitosan Nanoparticles Functionalized With the Monoclonal Antibody OX26 for Brain Drug Targeting. *Nanomedicine* (2015) 10(11):1735–50. doi: 10.2217/nnm.15.29
137. Amani H, Habibey R, Shokri F, Hajmiresmail SJ, Akhavan O, Mashaghi A, et al. Selenium Nanoparticles for Targeted Stroke Therapy Through Modulation of Inflammatory and Metabolic Signaling. *Sci Rep* (2019) 9 (1):6044. doi: 10.1038/s41598-019-42633-9
138. Rizvi SMD, Hussain T, Ahmed ABF, Alshammari TM, Moin A, Ahmed MQ, et al. Gold Nanoparticles: A Plausible Tool to Combat Neurological Bacterial Infections in Humans. *BioMed Pharmacother* (2018) 107:7–18. doi: 10.1016/j.biopha.2018.07.130
139. Poupot R, Goursat C, Fruchon S. Multivalent Nanosystems: Targeting Monocytes/Macrophages. *Int J Nanomed* (2018) 13:5511–21. doi: 10.2147/IJN.S146192
140. Zhao N, Francis NL, Calvelli HR, Moghe PV. Microglia-Targeting Nanotherapeutics for Neurodegenerative Diseases. *APL Bioeng* (2020) 4 (3):030902. doi: 10.1063/5.0013178
141. Wiley NJ, Madhankumar AB, Mitchell RM, Neely EB, Rizk E, Douds GL, et al. Lipopolysaccharide Modified Liposomes for Amyotropic Lateral Sclerosis Therapy: Efficacy in SOD1 Mouse Model. *Adv Nanoparticles* (2012) 01(03):44–53. doi: 10.4236/anp.2012.13007
142. Choi B, Soh M, Manandhar Y, Kim D, Han SI, Baik S, et al. Highly Selective Microglial Uptake of Ceria-Zirconia Nanoparticles for Enhanced Analgesic Treatment of Neuropathic Pain. *Nanoscale* (2019) 11(41):19437–47. doi: 10.1039/c9nr02648g
143. Provenzano F, Perez MJ, Deleidi M. Redefining Microglial Identity in Health and Disease at Single-Cell Resolution. *Trends Mol Med* (2021) 27(1):47–59. doi: 10.1016/j.molmed.2020.09.001
144. Aldrich AL, Horn CM, Heim CE, Korshoj LE, Kielian T. Transcriptional Diversity and Niche-Specific Distribution of Leukocyte Populations During Staphylococcus Aureus Craniotomy-Associated Biofilm Infection. *J Immunol* (2021) 206:751–65. doi: 10.4049/jimmunol.2001042

Conflict of Interest: The authors declare that the research was conducted in the absence of any commercial or financial relationships that could be construed as a potential conflict of interest.

frontiers in Immunology

REVIEW
published: 15 July 2021
doi: 10.3389/fimmu.2021.684240

Re-Programming Autoreactive T Cells Into T-Regulatory Type 1 Cells for the Treatment of Autoimmunity

Patricia Solé[1] *and Pere Santamaria*[1,2]*

[1] Institut D'Investigacions Biomèdiques August Pi i Sunyer, Barcelona, Spain, [2] Julia McFarlane Diabetes Research Centre (JMDRC) and Department of Microbiology, Immunology and Infectious Diseases, Snyder Institute for Chronic Diseases and Hotchkiss Brain Institute, Cumming School of Medicine, University of Calgary, Calgary, AB, Canada

Systemic delivery of peptide-major histocompatibility complex (pMHC) class II-based nanomedicines can re-program cognate autoantigen-experienced CD4+ T cells into disease-suppressing T-regulatory type 1 (TR1)-like cells. In turn, these TR1-like cells trigger the formation of complex regulatory cell networks that can effectively suppress organ-specific autoimmunity without impairing normal immunity. In this review, we summarize our current understanding of the transcriptional, phenotypic and functional make up of TR1-like cells as described in the literature. The true identity and direct precursors of these cells remain unclear, in particular whether TR1-like cells comprise a single terminally-differentiated lymphocyte population with distinct transcriptional and epigenetic features, or a collection of phenotypically different subsets sharing key regulatory properties. We propose that detailed transcriptional and epigenetic characterization of homogeneous pools of TR1-like cells will unravel this conundrum.

Keywords: T-regulatory type 1 (TR1) cells, peptide-MHC class II-coated nanoparticles, T-cell reprogramming, interleukin 10 (IL10), autoimmune disease, therapy

OPEN ACCESS

Edited by:
Francisco Javier Quintana, Harvard Medical School, United States

Reviewed by:
Mohan Maddur, Pfizer, United States
Nikolina Mihaylova, Bulgarian Academy of Sciences, Bulgaria

****Correspondence:***
Pere Santamaria
psantama@ucalgary.ca

Specialty section:
This article was submitted to Molecular Innate Immunity, a section of the journal Frontiers in Immunology

Received: *23 March 2021*
Accepted: *22 June 2021*
Published: *15 July 2021*

Citation:
Solé P and Santamaria P (2021) Re-Programming Autoreactive T Cells Into T-Regulatory Type 1 Cells for the Treatment of Autoimmunity. Front. Immunol. 12:684240. doi: 10.3389/fimmu.2021.684240

INTRODUCTION

Interleukin 10 (IL-10)-producing regulatory T cells (Tregs) are key to immune homeostasis and play opposing roles in autoimmunity versus cancer. While the FoxP3+ Treg cell subset has been thoroughly described, FoxP3 and CD25 double-negative T cells producing IL-10 in the context of low IL-4 secretion are generally known as T-regulatory type 1 (TR1) cells (1). Given the lack of specificity of these phenotypic descriptors, the literature has considered as TR1-like cells what appears to be a rather heterogeneous collection of cell types (1), thus clouding our understanding of the true lineage identity of this regulatory T-cell subset. Production of IL-10, coupled to the expression of Latency-Associated Peptide (LAP), Lymphocyte Activation Gene 3 (LAG-3) or CCR5 and Programmed cell death protein 1 (PD-1) in the absence of CD25, or CD4+ cells lacking IL-7R expression, as well as cells induced by vitamin D3 or CD46-stimulation are some of the examples of cell types identified as TR1 (1, 2). Recently, co-expression of CD49b and LAG-3, accompanied by the expression of ICOS and PD-1, has been associated, in both humans and mice, with TR1-ness (3, 4), but these markers are not sufficiently specific or sensitive. Other surface markers have been

found to be variably upregulated by IL-10-producing T-cell subsets (5–8), including Cytotoxic T-Lymphocyte antigen 4 (CTLA-4), T-cell immunoglobulin and mucin-domain containing-3 (TIM-3) or TIGIT, as well as transcription factors (TFs) like T-bet, Aryl hydrocarbon receptor (AhR) or Nuclear Factor Interleukin 3-regulated (Nfil3).

Because of the lack of specific markers, it remains unclear whether the various IL-10 producing 'TR1-like' subsets correspond to multiple different cell types, or to cells at different stages of differentiation. Many studies implicating a role for Treg/TR1 cells in the therapeutic activity of various immunotherapies have often done so solely based on an increase in IL-10 expression by splenic CD4+ T cells. It is entirely possible that the various phenotypes associated to IL-10-producing FoxP3-negative CD4+ T-cell subsets correspond to cells at different stages of TR1 cell differentiation, or to distinct subsets of terminally differentiated cells with distinct phenotypic and/or functional properties. Unfortunately, the transcriptional and epigenetic profiles associated with true TR1-ness remain incompletely defined, a fact compounded by our incomplete knowledge on the developmental biology of the TR1 subset(s).

We have shown that treatment of various mouse models of autoimmune disease with nanoparticles (NPs) coated with disease-relevant peptide-major histocompatibility complex class II (pMHCII) molecules (9) suppresses organ inflammation and disease progression without impairing systemic immunity (10–12). This approach has shown clear therapeutic efficacy in animal models of type 1 diabetes (T1D), experimental autoimmune encephalomyelitis (EAE), collagen-induced arthritis (11), as well as primary biliary cholangitis (PBC), primary sclerosing cholangitis (PSC) and autoimmune hepatitis (AIH) (12, 13). pMHCII-NP therapy triggers the formation and expansion of TR1-like CD4+ T cells from autoantigen-experienced CD4+ T-cell precursors of as yet undefined identity. pMHCII-NPs bind directly to TCRs on cognate T cells, resulting in prolonged pMHCII-TCR interactions, the assembly of large TCR microclusters on such T cells, and rapid, robust and prolonged TCR signaling. In turn, this results in the acquisition of immunoregulatory properties, including the upregulation of the cytokines IL-10, IL-21 and Transforming Growth Factor β (TGF-β) (but neither IL-2 nor IL-4), the co-inhibitory receptors LAG-3, CTLA-4 and PD-1, the Inducible T-cell Costimulator (ICOS) and the transcription factors T-bet and c-Maf, among others, in the absence of FoxP3 expression (**Figure 1**).

Here, we review our current understanding of the phenotype, function and development of TR1-like cells in different experimental settings, including pMHCII-NP-treated mice. We identify knowledge gaps and propose that detailed transcriptional and epigenetic characterization of homogeneous pools of TR1-like cells will help define both, a true state of

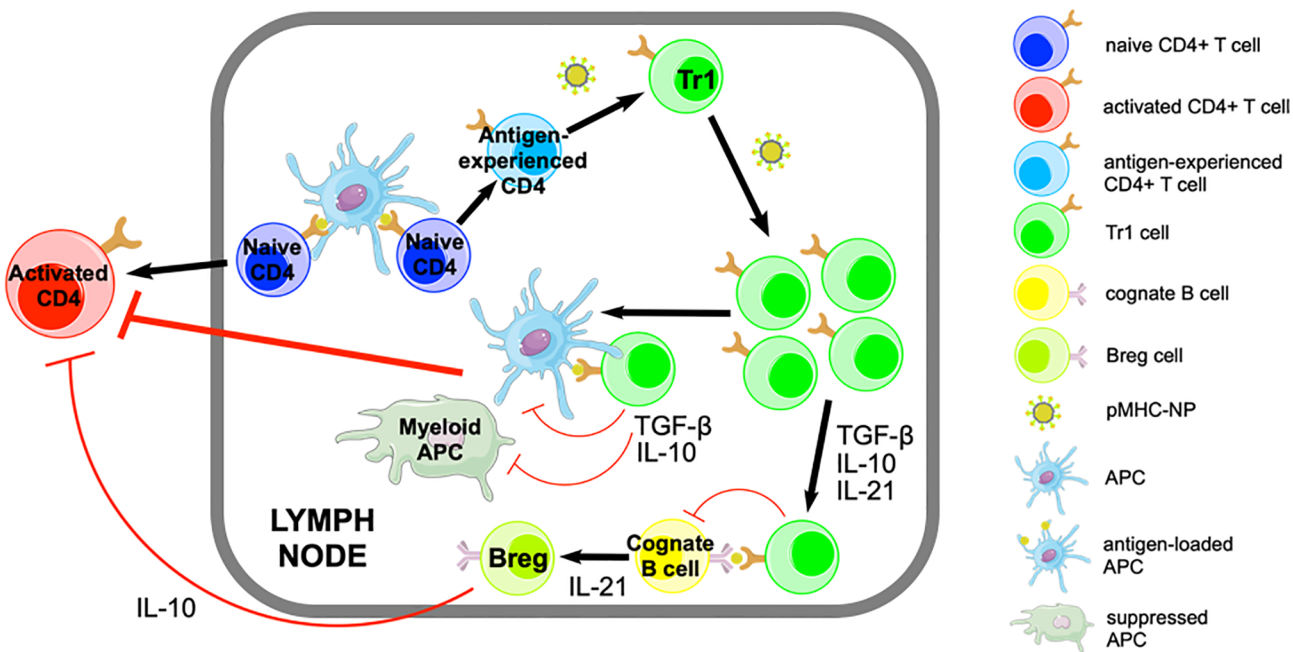

FIGURE 1 | Pharmacodynamic activity of pMHCII-NPs. pMHCII-NPs target autoantigen-experienced CD4+ T cells and induce their differentiation into memory TR1-like cells followed by their systemic expansion. This process involves IFN-γ and IL-10 signaling, but does not require IL-27. pMHCII-NP-induced TR1-like cells carry out their regulatory function by suppressing other autoreactive T-cell specificities *via* IL-10, IL-21 and TGF-β. IL-10 and TGF-β have immunosuppressive effects on autoantigen-loaded APCs, inhibiting their proinflammatory function and thus avoiding the activation of other non-cognate autoreactive T cells. pMHCII-NP-induced TR1-like cells can also interact with cognate B-cells, promoting their differentiation into Bregs in part *via* IL-21. Figure adapted from Clemente-Casares et al. (11).

TR1-ness as well as the identity of the TR1-poised cell precursors that give rise to TR1-like cells.

A BRIEF HISTORICAL PERSPECTIVE

The TR1 cell subset was first described in 1997 by Groux et al. (14). Previously, others (15, 16) had described a suppressor T-cell population that secreted IL-10 and protected patients against graft-versus-host disease (GvHD). This population displayed a cytokine profile that was distinct from those of common T-helper cell subsets, and involved the expression of IL-10, IL-5, TGF-β, and IFN-γ in the absence of IL-4 or IL-2 secretion (17). In 1997, TR1 cells were generated *in vitro* and their suppressive activity was documented both *in vitro* and *in vivo*, in a model of colitis.

Currently, all the regulatory CD4+ T cells that are FoxP3-negative and secrete IL-10 and low levels or no IL-4 are considered to be 'TR1'. Unfortunately, this characterization lacks specificity and likely includes phenotypically, functionally and developmentally heterogeneous T cells. This is compounded by the variety of protocols that can trigger the formation of IL-10-producing cells with regulatory properties. In some cases, TR1-like cells were generated from naive CD4+ T cells. For example, *in vitro* TCR stimulation of human naive CD4+/CD45RA+ T cells in the context of IL-10 secreted by dendritic cells (DCs) triggered their conversion into anergic, IL-10- and TGF-β-expressing T cells capable of suppressing effector T cells (14, 18). Likewise, *in vitro* culture of murine CD4+/CD44–/CD62L+ T cells with IL-10 or IL-27 can induce their differentiation into IL-10 producing TR1-like cells [reviewed in (19)]. Other lines of experimentation have suggested that IL-10-producing TR1-like cells can also be generated from memory CD4+ T cells, in the absence of polarizing cytokines in the culture (20, 21). In mice, induction of transplantation tolerance *via* anti-CD45RB mAb therapy is associated with the presence of antigen-specific IL-10-producing CD4+ T cells in the memory T-cell compartment (22, 23). There are also data supporting the view that TR1-like cells can develop from differentiated T-helper cell subsets. For example, Gagliani et al. provided evidence suggesting that a fraction of the regulatory T cells that are found in the gut arise from Th17 cells and display a TR1-like phenotype, including the production of IL-10 and some IFN-γ, and the expression of CD49b and LAG-3, while lacking expression of IL-4 and CCR6 (24). Moreover, there is also evidence that culture of Th17 cells in the presence of IL-27 and TGF-β can trigger the formation of IL-10-producing TR1-like cells *in vitro* (24, 25). Likewise, stimulation of Th1 cells with CXCL12 *in vitro* (26), or in the context of malaria infection (27), can promote their differentiation into CD4+/CD25–/FoxP3–/IL-10+ T cells. Human allergen-specific Th2 cells can also differentiate into IL-10-producing CD49b+/LAG3+ cells with regulatory properties (28, 29).

Unfortunately, these various 'TR1-like' cell types of different developmental origin were not thoroughly characterized at the phenotypic, transcriptional or functional levels. Accordingly, whether the various TR1-like cells that were generated in these studies correspond to one or several different cell types, or to cells at different stages of differentiation, remains unclear.

DISTINCT PHENOTYPES

Several surface phenotypes have been attributed to TR1-like cells (**Table 1**). Whether all these subsets correspond to one single, incompletely characterized population, or comprise a collection of phenotypically and/or functionally distinct subsets remains to be determined.

LAP+/CD25–/CD4+ T Cells

CD4+ CD25+ Treg cells express TGF-β on their surface and one of their mechanisms of suppression involves TGF-β recognition by target cells upon cell-to-cell contact (47). Weiner et al. reported a population of regulatory T cells that suppressed murine colitis in a TGF-β-dependent manner, but where CD25-negative and LAP-positive (30). LAP is the amino-terminal domain of the TGF-β precursor peptide that contains the TGF-β peptide within its latent complex (48). CD4+/CD25–/LAP+ cells are positive for thrombospondin, which can convert latent TGF-β to its active form. CD4+/CD25–/LAP+ cells represent ~3-5% of murine splenocytes and express high levels of TGF-β and IL-10, as well as IL-2, IL-4 and IFN-γ. A similar population was generated after oral anti-CD3 treatment and had a suppressive effect against autoimmune encephalomyelitis (31).

NKG2D+/CD25–/CD4+ T Cells

A small population of human CD4+ T cells that produce IL-10 and TGF-β express the natural killer receptor NKG2D. These cells are FoxP3-, CD103- and LAG-3-negative. They also express Fas ligand (FasL), which appears to be a main contributor of suppression by inhibiting the growth of bystander T cells (32). Although these T cells can be found in the peripheral blood of healthy individuals (~1-3%), they appear to increase substantially in cancer patients (to ~6-70%). They have also been described in patients with rheumatoid arthritis (33). One ligand of the NKG2D receptor is the MHC class I-related chain A (MICA), which is upregulated in tissues undergoing inflammation or in epithelial tumors. The role of NKG2D with regards to the immunoregulatory properties of these cells remains unclear.

CD127^{low}/CD25–/CD4+ T Cells

The IL-7 receptor (IL-7R) α-chain (CD127) is important for the survival of conventional CD4+ T cells (49) but is expressed at low levels in CD4+CD25+ T cells (50). Häringer et al. found a population of adaptive Treg cells that were CD25-, FoxP3- and IL-7R-negative. These cells comprised ~1% of the total CD4+ population from human peripheral blood. They expressed low levels of Bcl-2 and high levels of Ki-67 and ICOS, suggesting that they had been recently activated, and had a suppressive function mediated primarily by the secretion of IL-10 in response to potent T-cell receptor stimuli (34). However, only 10% of this T-cell pool produced IL-10 upon stimulation, compatible with the

TABLE 1 | Summary of phenotypes ascribed to TR1-like cells.

Markers	*Where*	*Phenotype*	*Species*	*Reference*
LAP+/CD25–/CD4+	~3-5% of murine splenocytes	High levels of TGF-β and IL-10, IL-2, IL-4 and IFN-γ	Mouse	(30)
	After oral anti-CD3 treatment	Suppressive effect in autoimmune encephalomyelitis	Mouse	(31)
NKG2D+/CD25–/CD4+	In peripheral blood of healthy individuals (~1-3%). Increased in cancer (~6-70%)		Human	(32)
	In patients with rheumatoid arthritis		Human	(33)
CD127^{low}/CD25–/CD4+	~1% of CD4+ of human PBMCs	Low levels of Bcl-2 and high levels of Ki-67 and ICOS Secretion of IL-10 upon TCR engagement	Human	(34)
CD49b+/CD25–/CD4+	In mice	Secretion of IL-10 TGF-β and IFN-γ. Anti-diabetogenic and anti-arthritogenic	Mouse	(35–38)
LAG-3+/CD25–/CD4+	In the spleen (2%), lymph nodes (1%) and Peyer's patches (PP) (8%)	Anergic upon TCR ligation, secrete IL-10 and IFN-γ, and low amounts of IL-2 and IL-4. Expression of Egr-2 and Blimp-1	Human	(39)
CD49b+/LAG-3+/ CD25–/CD4+	Peripheral blood	IL-10 producing suppressive cells	Human/ mouse	(3)
CCR5+/PD-1+/ CD25–/CD4+	Lamina propria	Secretion of IL-10- and IFN-γ. Expression of LAG-3 upon stimulation	Human	(2, 40)
CD44^{hi}/CD62L^{lo}/IL-7R–/ LAG-3+/CD49b+/ LAP+	Spleen and draining lymph nodes of pMHCII-NP-treated mice	Secretion of IL-10, IL-21, TGF-β and IFN-γ, but no IL-2, IL-4 or IL-17. Expression of c-Maf, T-bet and Blimp-1.	Mouse	(11)
Other markers				
TIGIT			Mouse	(5)
TIM-3			Mouse	(8)
CD226			Human/ mouse	(3, 41)
ROG			Mouse	(42)
Egr-2			Mouse	(43)
c-Maf and AhR	IL-27-induced TR1-like cells		Mouse	(44, 45)
IRF4	Activin-A stimulated human TR1-like cells		Human	(46)
LXR			Human	(7)
Bhlhe40			Human	(7)

presence of a small subset of TR1-like cells within the CD25–/FoxP3–/IL-7R– pool.

CD49b+/CD25–/CD4+ T Cells

Several studies have identified a population of CD4+ T cells with regulatory activity that express CD49b. These cells had anti-diabetogenic (35) and anti-arthritogenic properties in mice (36), were both FoxP3– and CD25– and secreted the regulatory cytokines IL-10 and TGF-β, as well as IFN-γ. In later studies, it was shown that these T cells suppressed CD8+ T-cell responses and IFN-γ production by CD4+ T cells, presumably *via* IL-10 (37, 38).

LAG-3+/CD25–/CD4+ T Cells

LAG-3 is known to suppress T-cell proliferation (51). Despite being required for the maximal regulatory activity of conventional CD4+CD25+ Treg cells, LAG-3 protein can hardly be detected on the surface of CD4+CD25+ T cells. In contrast, LAG-3 was found to be expressed by a subset of CD4+ CD25– T cells (39) found at low frequencies in the spleen (2%) and lymph nodes (1%) but at higher frequencies in Peyer's patches (PP) (8%). These T cells are anergic upon TCR ligation, but they secrete high quantities of IL-10, moderate amounts of IFN-γ and low amounts of IL-2 and IL-4. These cells do not express FoxP3 and, unlike CD4+/CD25–/LAP+ cells, express low levels of CD103 and LAP. They are further characterized by expression of the Early response gene 2 (Egr-2), a transcription factor that is a negative regulator of T-cell activation, inducing an anergic state (52). These CD4+/CD25–/LAG-3+ cells were also found to express the *Prdm1* gene, encoding the B lymphocyte-induced maturation protein (Blimp)-1.

CD49b+/LAG-3+/CD25–/CD4+ T Cells

In 2013, Gagliani et al. provided evidence indicating that co-expression of LAG-3 and CD49b can be used to enumerate human and mouse TR1-like cells (3). CD49b had been previously described as a marker for regulatory CD25– T cells, but cannot be used in isolation to identify this T-cell subset, because it can also be expressed by Th17 cells and certain memory CD4+ T-cell subsets (53). Likewise, LAG-3 is associated with T-cell activation and IL-10 production, but its expression is not unique to any particular T-cell subset; it can be upregulated by conventional T cells upon activation and is also expressed by FoxP3+ Tregs (51).

CCR5+/PD-1+/CD25–/CD4+ T Cells

Geginat and coworkers used the C-C chemokine receptor type 5 (CCR5) and PD-1 as markers to purify TR1-like IL-10- and IFN-γ-producing cells from the human intestine (2, 40). They demonstrated that the majority of IL-10+/CD4+/CD25–/IL-7R– T cells found in the lamina propria co-expressed CCR5+ and PD-1+ (2). Despite expressing *Lag3* mRNA, only a small percentage of cells displayed LAG-3 protein in the steady state. *In vitro* stimulation triggered the upregulation of surface LAG-3 protein expression (2).

Other Markers

TR1-like cells express several other surface molecules and transcription factors, albeit none of them specifically. For example, both murine and human IL-10 producing TR1-like cells can express the immune checkpoint molecules TIGIT (5) and TIM-3 (8), but conventional FoxP3+ Treg cells and T-follicular regulatory (Tfr) cells (54, 55) can also express these markers. CD226, presumably involved in the cytotoxic activity of at least some TR1-like cells, is another example of such lack of specificity (3, 41).

With regards to transcription factors, ROG (the repressor of GATA-3), a regulator of Th differentiation and cytokine production upon activation (56), has also been described in TR1-like cells (42). Since expression of Egr-2 in CD4+ T cells induces IL-10 production by binding to the Blimp-1 promoter (57), Okamura et al. proposed that this transcription factor might be involved in the acquisition of a suppressor phenotype by CD4+/CD25–/LAG-3+ T cells (43). However, purified TR1-like cells from the gut of anti-CD3 mAb-treated mice, as well as those induced *in vitro*, express levels of Egr-2 that are no different than those seen in effector T cells (3). Likewise, the transcription factors c-Maf and AhR, which are expressed by IL-27-induced TR1 cells and bind to the *Il10* promoter in TR1 cells (44, 45), are also expressed by non-TR1 cell types, including human and murine Th17 subsets (58, 59). The interferon regulatory factor 4 (IRF4) is yet another non-TR1 cell-specific transcription factor that presumably plays a role in the developmental biology of TR1-like cells, as a downstream effector of the inducible tyrosine kinase (ITK) (60). Since IRF4 regulates Blimp-1, it is probably involved in the regulation of IL-10 expression in these cells, along with other transcription factors. Activin A-induced IRF4 activation has been suggested to promote human TR1-like cell formation *in vitro* (46). The liver X receptor (LXR) and Bhlhe40 are other transcription factors found to be expressed in at least some TR1-like cells (7).

pMHCII-NP-Induced TR1-Like Cells

When compared to other TR1-like subsets, the IL-10-producing $CD44^{hi}/CD62L^{lo}$/IL-7R–/CD25–/FoxP3– TR1-like cells that arise *in vivo* in response to pMHCII-NP therapy co-express several of the markers previously identified in different TR1-like cell subsets, including LAG-3, CD49b, ICOS, LAP, c-Maf, T-bet, and Blimp-1. These cells produce the cytokines IL-10, IL-21 and, to a lesser extent, IFN-γ, but no or very low levels of IL-2, IL-4 or IL-17 (11). Thus, these cells appear to embody the phenotypic properties of most other TR1-like cells, begging the question of whether different IL-10-expressing CD4+CD25– TR1-like cell subsets, as described in the literature, correspond to one single cell subset rather than to a phenotypically heterogenous collection of distinct cell types.

MECHANISMS OF ACTION

In order to affect regulatory activity, TR1 cells need to be activated by antigen recognition. Upon activation, they target effector T cells and/or professional APCs *via* cytokines, direct cell contact, metabolic disruption and/or cytolysis (**Figure 2**). Although TCR activation is antigen-specific, TR1-mediated suppression of APCs or neighboring T cells is antigen-agnostic (bystander immunoregulation).

Interleukin 10

Upon activation, TR1 cells secrete the immunoregulatory cytokines IL-10 and TGF-β (**Figure 2**). IL-10 has effects on different cell populations. Although IL-10 expression is a hallmark of TR1-like cells, this cytokine can also be produced by other CD4+ T-cell subsets, as well as CD8+ T cells, macrophages, DCs and B cells (61). IL-10 suppresses T-cell responses by inhibiting T-cell proliferation (62) and cytokine production by effector T cells, including IL-2, IFN-γ, IL-4, IL-5 and TNF-α. Moreover, IL-10 can downregulate MHC class II and costimulatory molecule expression in APCs, and reduce the production of pro-inflammatory cytokines (IL-1α and -β, IL-6, IL-12, IL-18, and TNF-α) and chemokines (CCL2, CCL5, CCL12, CXCL2, CXCL10, and IL-8) by these APCs (61). In humans, IL-10 can elicit the generation of tolerogenic DCs by upregulating immunoglobulin-like transcripts 3 and 4 (ILT3, ILT4) and the non-classical HLA-G molecule (63). On B-cells, IL-10 promotes proliferation, MHC II expression and isotype switching to IgG4 (64). IL-10 also amplifies regulatory T-cell formation. IL-10 stimulation of CD4+ T cells can induce the expression of IL-10, T-cell anergy or TR1-like cell differentiation in a STAT3-dependent manner. STAT3 promotes IL-10 expression and represses pro-inflammatory cytokine expression (65). It is unclear whether the phenotype of full-fledged (i.e. fully differentiated) TR1-like cells is stable. However, pMHCII-NP-induced, antigen-specific TR1-like cells can persist for several months post-treatment withdrawal without any obvious loss of key phenotypic properties or acquisition of pathogenic activity (11).

Transforming Growth Factor β

Like IL-10, TGF-β inhibits APC function and T-cell proliferation, differentiation and cytokine production (**Figure 2**). TGF-β suppresses T-cell proliferation by inhibiting IL-2 production and downregulating cyclins while upregulating cyclin-dependent kinase (CDK) inhibitors. It also inhibits the differentiation of both CD4+ and CD8+ T cells into effectors, by inhibiting master transcriptional regulators of each phenotype (GATA-3, T-bet, IL-12Rβ2). The main effect of TGF-β on APCs involves inhibition of their maturation, in part by upregulating indoleamine 2,3-dioxygenase (IDO) expression and by inhibiting MyD88-mediated TLR signaling (66). As shown in (11, 12), the therapeutic effects of pMHCII-NP-induced TR1-like cells are dependent on IL-10 and TGF-β. The blockade of these cytokines with monoclonal antibodies abrogates the suppression of autoantigen crosspresentation by pMHCII-NP-expanded TR1-like cells and thus the therapeutic properties of pMHCII-NP treatment in several models, including T1D, EAE and liver autoimmunity.

Costimulatory and Co-Inhibitory Molecules

TR1-like cells can also inhibit APCs in a cell contact-dependent manner upon engagement of co-inhibitory receptors such as

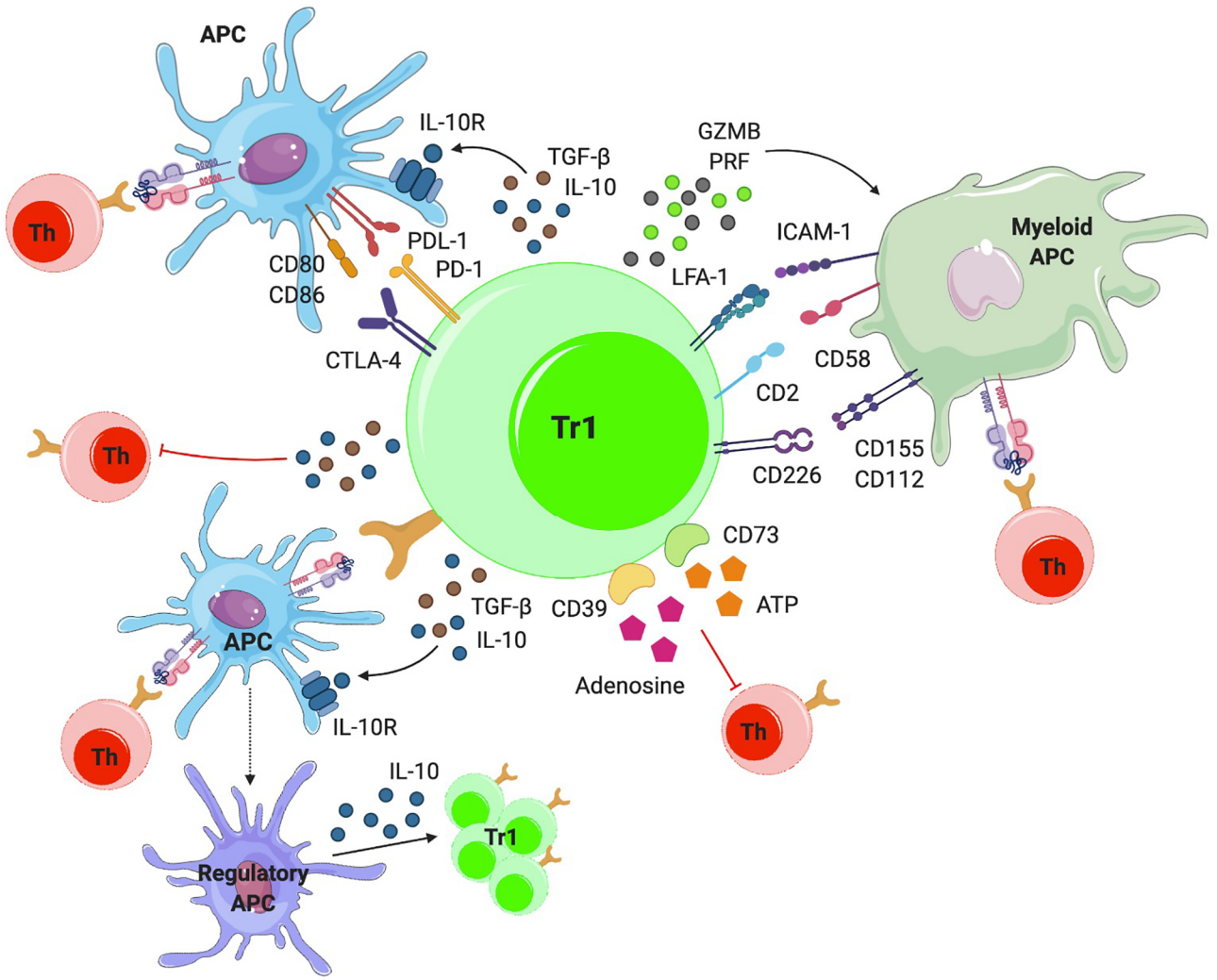

FIGURE 2 | Mechanisms of action. TR1-like cells can suppress effector T cells directly or indirectly, by modulating the phenotype and function of APCs *via* IL-10 and TGF-β. IL-10 also induces a regulatory phenotype in APCs, by triggering the upregulation of tolerogenic molecules (i.e. ILT3, ILT4 and HLA-G) and the production of IL-10, further amplifying TR1-like cell formation. TR1-like cells can also make direct cell-to-cell contacts with APCs *via* cell surface CTLA-4 and PD-1, inhibiting APC-induced effector T-cell activation. TR1-like cells can kill myeloid APCs *via* granzyme-B (GZMB) and perforin (PRF). In addition, they can suppress T-cell activation *via* metabolic disruption.

CTLA-4, PD-1, LAG-3 or TIGIT and the costimulatory molecule ICOS (**Figure 2**).

Like other members of the CD28 family, CTLA-4 can bind CD80/86, but it does so with higher affinity than the co-stimulatory molecule CD28. In the presence of CTLA-4, CD80/86 engagement by CD28 on T cells is inhibited. In addition, CTLA-4 can signal into T cells through Src homology region 2-contatining protein tyrosine phosphatase 2 (SHP-2), dephosphorylating TCR and CD28 signaling intermediates and promoting T-cell inactivation (67). However, engagement of CTLA-4 on T cells by its ligands on APCs can also have inhibitory effects on the latter, such as by triggering the downregulation of CD80 and CD86 (68–70), or by upregulating IDO expression by APCs (71).

LAG-3 is another negative regulator of T-cell activation. This molecule is structurally similar to CD4 and binds MHC class II molecules with higher affinity than CD4 (39). Okazaki's work has recently shown that LAG-3 does not universally bind to all MHC class II molecules, but rather recognizes stable pMHC class II complexes (72). LAG-3 signals intracellularly, transducing inhibitory signals that hinder T-cell activation (72). Inhibitory signals through the LAG-3 intracytoplasmic region are mediated by a *FXXL* motif in the membrane-proximal region and the EX repeat in the C-terminal region (73). In addition, the LAG-3-pMHCII interaction inhibits DC activation (74).

PD-1 is a co-inhibitory receptor that belongs to the Ig superfamily containing ITIM and ITSM motifs and signals after interacting with its ligands PD-L1 or PD-L2. PD-L1 is

expressed on leukocytes, non-hematopoietic cells and non-lymphoid tissues, and can be induced in parenchymal cells by inflammatory cytokines (e.g. IFN-γ) or tumorigenic signaling pathways. PD-L1 expression is also found on different tumor types and is associated with an increased number of tumor-infiltrating lymphocytes (TILs) and poor prognosis. PD-L2 is primarily expressed on professional APCs (DCs and monocytes) but can be induced in other immune and non-immune cell types. PD-1 has a higher binding affinity for PD-L2 than for PD-L1, a difference that might be responsible for the differential contributions of these two ligands to immune responses. It has an inhibitory function similar to that of CTLA-4, by recruiting SHP-1 and SHP-2 phosphatases, reducing T-cell activation and inducing Treg differentiation (75). There is also emerging evidence for 'reverse signaling' through PD-L into DCs. PD-1 binding to PD-L2 decreases the expression of DC maturation markers, such as CD40, CD80 and CD86, and increases IL-10 production by DCs, resulting in a suppressive DC phenotype (76).

TIGIT is another immune checkpoint inhibitor that interferes with the activation of T and NK cells. It has an extracellular IgV domain and an intracellular ITT domain that recruits SHIP-1 to mediate T-cell inactivation (77). TIGIT competes with the immunoactivator receptor CD226 (DNAM-1) for the same ligands: CD155 (poliovirus receptor, PVR) and CD112 (Nectin-2 or PVRL2), expressed on APCs, T cells and some non-hematopoietic cell types like tumor cells (78). TIGIT binding to its ligands on APCs has an effect on DC cytokine production, inducing IL-10 expression and inhibiting the expression of IL-12, reducing T-cell activation (79).

ICOS is a costimulatory molecule with structural homology to CD28 and CTLA-4 that binds to ICOS-L on DCs, B cells, and macrophages. ICOS-ICOS-L engagement regulates antigen presentation and secretion of regulatory cytokines such as IL-10 by APCs (80–82).

Metabolic Disruption

TR1-like cells can also inhibit effector T cells *via* metabolic disruption mechanisms, similar to those used by FoxP3+ Tregs. In TR1-like cells, the main proteins involved in this process are the ectoenzymes ectonucleoside triphosphate diphosphohydrolase 1 (CD39) and ecto-5'-nucleotidase (CD73). These enzymes hydrolyze extracellular 5'-adenosine triphosphate (ATP) to adenosine, disrupting the metabolic state of T cells. ATP released during T-cell activation (83) has an effect on T-cell and APC activation (**Figure 2**). First, CD39 degrades ATP and ADP into AMP (84), which is then further degraded to adenosine by CD73 (85). Adenosine can bind to A_{2A} receptors, inhibiting T-cell proliferation and cytokine production of effector T cells (86). Binding of adenosine to these receptors on APCs inhibits their maturation and the secretion of pro-inflammatory cytokines, while inducing the secretion of IL-10 (87).

Killing

Another mechanism *via* which TR1-like cells can inhibit T-cell responses is by killing APCs, particularly APCs of myeloid origin. TR1-like cells can express both granzyme A and B proteins, which, together with perforin, mediate cell-mediated cytotoxicity (88) (**Figure 2**). In humans, granzyme expression has been shown to be induced by IL-10 signaling (89). Unlike NK-mediated killing, which takes place when target cells lack or downregulate MHC class I, TR1-mediated cytolysis is antigen-dependent and only takes place when there is TCR engagement with cognate pMHC on the APC (it also requires recognition of other surface molecules expressed by the APC, including CD54 (ICAM-1), CD58, CD155 and CD112) (41). In addition to direct effects on the activation of antigen-specific CD4+ T-cell responses, APC killing indirectly impairs the activation of bystander T cells. Although pMHCII-NP-induced TR1-like cells can express granzymes, they lack cytolytic activity against peptide-pulsed B-cells or DC cells (11).

DRIVERS OF TR1-LIKE CELL FORMATION

TCR Signaling

TCR stimulation is essential, but not sufficient for the generation of TR1-like cells. pMHC multimers (90–92) or superantigens (93, 94) have been found to induce IL-10-production in some T-cell populations, although it is not clear whether the resulting cells were *bona fide* TR1-like cells. Several studies have suggested that the strength of the TCR interaction plays an important role; high avidity interactions favor IL-10 production (95), in particular the number of IL-10-producing cells and the cells' suppressive properties (96). The dose of antigen appears to play a lesser role, as high doses of ligands were not enough to induce IL-10 unless they were administered simultaneously with IL-12 (97, 98). Nevertheless, repeated high-dose stimulation was indeed sufficient to induce IL-10. One study pointed to Nfil3 as a transcription factor involved in the upregulation of IL-10 production in response to repeated antigenic stimulation (99). However, as noted above, it is unclear whether these cells were true TR1-like cells or simply Th1 cells that have acquired the ability to produce IL-10. Singha et al. have shown that the ability of pMHCII-NP to elicit TR1 cell formation is dependent on high pMHCII densities onto the NPs. High densities promote sustained pMHC-NP-TCR interactions and formation of TCR microclusters, amplifying the duration and magnitude of TCR signaling, which is associated with their pro-TR1-like cell-differentiation properties (9).

Interleukin 10

IL-10 has been associated with the induction and maintenance of TR1-like cells (14, 100), although some studies have suggested that it is dispensable (101). In the absence of IL-10 (in *Il10* gene knockout mice) pMHCII-based nanomedicines could readily trigger the expansion of cognate T cells, but these cells upregulated IL-4, suggesting a role for IL-10 in the acquisition of the full-fledged TR1-like cell phenotype (11). Tolerogenic DCs are the main source of IL-10 *in vivo* and they may play a role in the induction of TR1-like cells under physiological conditions (102, 103). Indeed, human IL-10-producing DCs have the ability to induce TR1-like cell differentiation *in vitro* in an IL-10-dependent manner (63, 104).

Interleukin 27

IL-27, largely produced by activated APCs (105), can support the generation of IL-10-producing TR1-like cells and CD8+ T cells (106, 107). It is a member of the IL-12 family and is a heterodimer composed by the Epstein-Barr virus-induced gene 3 (Ebi3)-encoded IL-12-related p40 and the IL-27 p28 (or IL-27α) chains. IL-27 binds to the IL-27 receptor (IL-27R) on DCs, monocytes, macrophages, T and B lymphocytes, NK cells, mast cells, and endothelial cells. This receptor is a heterodimer composed by the orphan cytokine receptor WSX-1 (also known as T-cell cytokine receptor (TCCR)) and a signal-transducing chain, the glycoprotein 130 (gp130).

IL-27 has inhibitory effects on Th1, Th2 and Th17 subsets as well as on APCs (108–110). Several studies have shown that it is capable of inducing both murine (111, 112) and human (106, 113) IL-10-producing T cells. Signaling through the IL-27R primarily induces STAT1 and STAT3 activation, promoting the expression of AhR and c-Maf transcription factors, which in turn control IL-10 and IL-21 production, hallmarks of the TR1-like cell phenotype (44). STAT3 further upregulates Egr-2, which as noted above contributes to IL-10 production by promoting Blimp-1 expression (57) (**Figure 3**).

Notwithstanding the positive role of IL-27-IL-27R signaling in TR1-like cell differentiation *in vitro*, pMHCII-NP-induced TR1-like cell formation *in vivo* is IL-27R-independent (11).

Interleukin 21

IL-21 is a type I cytokine that is produced by antigen-stimulated CD4+ T cells as well as NKT cells, and it has pleiotropic effects targeting T, B, NK, and myeloid cells (114). IL-21 binds to a heterodimeric receptor that is composed by the IL-21Rα chain (115) and the common cytokine receptor γ_c chain and signals through STAT3 and, to a lesser extent, STAT1 and STAT5. IL-21 plays a critical role in the regulation of Ig production and in the differentiation of B-cells into antibody-producing plasma cells (116, 117), in part by inducing T-follicular helper (TFH) cells (118), and has been implicated in the promotion of CD8+ T-cell and NK cell responses (119). IL-21 can also have negative effects on immune responses, such as by inducing B-cell apoptosis (120) and inhibiting DC maturation and function (121). c-Maf, expressed by TR1-like cells, contributes to IL-21 expression (59), and IL-27 promotes IL-21 expression in TR1-like cells by upregulating c-Maf (44). Furthermore, IL-21 functions as an autocrine growth factor that facilitates the expansion and homeostasis of IL-27-derived TR1-like cells (44), in part by promoting the upregulation of IL-10 (122) and, in turn, c-Maf expression. Like their IL-27-induced counterparts, pMHCII-NP-induced TR1-like cells express and secrete high levels of IL-21 upon recognition of cognate pMHCII on professional APCs (11, 123), which then plays a critical role in the TR1-like cell-induced differentiation of conventional B-cells into IL-10/IL-35-producing Breg cells and in the recruitment/re-programming of neutrophils into myeloid-derived suppressor-like cells, as downstream effectors of pMHCII-NP-induced immunoregulation (11, 123).

Inducible Costimulator

The ICOS molecule, a member of the B7 superfamily, is a glycosylated disulfide-linked homodimer that is expressed by certain T-cell subsets, including TFH- and TR1-like cells, upon productive TCR ligation. The ICOS-L is expressed on a wide range of lymphoid and non-lymphoid cells types, including APCs (124). ICOS signaling has been implicated in IL-10 production (80), as well as in IL-6-induced TFH cell specification (125, 126), although it can also stimulate the production of Th1 and Th2 cytokines *in vivo*. There is also evidence that c-Maf is a downstream target of ICOS engagement (59, 127), suggesting that ICOS engagement on TR1-like cells plays a role in the stabilization of the TR1-like cell phenotype, in part by sustaining IL-21 and IL-10 expression.

Interleukin 6

IL-6 is a pleotropic cytokine with both pro- and anti-inflammatory effects. It has been associated with the development/progression of certain autoimmune diseases, such as EAE, rheumatoid arthritis and psoriasis (128–130), in part by promoting Th17, TFH and B-cell responses (131). However, it has suppressive effects on the development of T1D, dextran sodium sulfate (DSS)-induced colitis and inflammatory bone destruction (132–134). IL-6, together with TGF-β, was found to induce expression of IL-10 in Th17 cells without suppressing IL-17 production (112, 135). It has also been shown that IL-6 can upregulate IL-21 production and, together with IL-2, can induce IL-10 expression and thus promote TR1-like cell generation (136), even in the absence of IL-27 or TGF-β. It is worth noting that IL-6 shares certain structural homology with IL-27 and that, like IL-27, binds to the gp130 receptor. Both cytokines signal through STAT1 and STAT3. IL-6 can upregulate the TR1-like transcription factors c-Maf, AhR and IRF4 which, as noted above, play a role in IL-10 and IL-21 production (136).

Type I Interferons

The type I interferons IFN-α and -β, constitute the first barrier against viral infections by inducing an 'antiviral state' in target cells which seeks to blunt protein synthesis, degrade mRNA and promote cell death in order to prevent viral replication. Type I interferons also induce upregulation of MHC I and adhesion molecules to enhance cytotoxic T lymphocyte (CTL)-mediated killing of virus-infected cells. However, IFN-α also has anti-inflammatory properties, such as the suppression of IL-8 and IL-1 production or the upregulation of the IL-1R antagonist (IL-1RA). By signaling *via* STAT1, STAT2 and STAT3 (137, 138), type I IFNs can promote the expression of IL-10 by CD4+ T cells (139–142), including memory T cells. When administered with anti-CD3 and IL-10, IFN-α promoted the development of TR1-like cells (100).

Interleukin 2 and Interleukin 15

IL-2 and IL-15 function as T-cell growth factors (143, 144). IL-15 was initially shown to play a critical role in the preservation of the memory repertoire, by preventing T-cell apoptosis (145) and promoting the survival of resting memory T cells (146, 147).

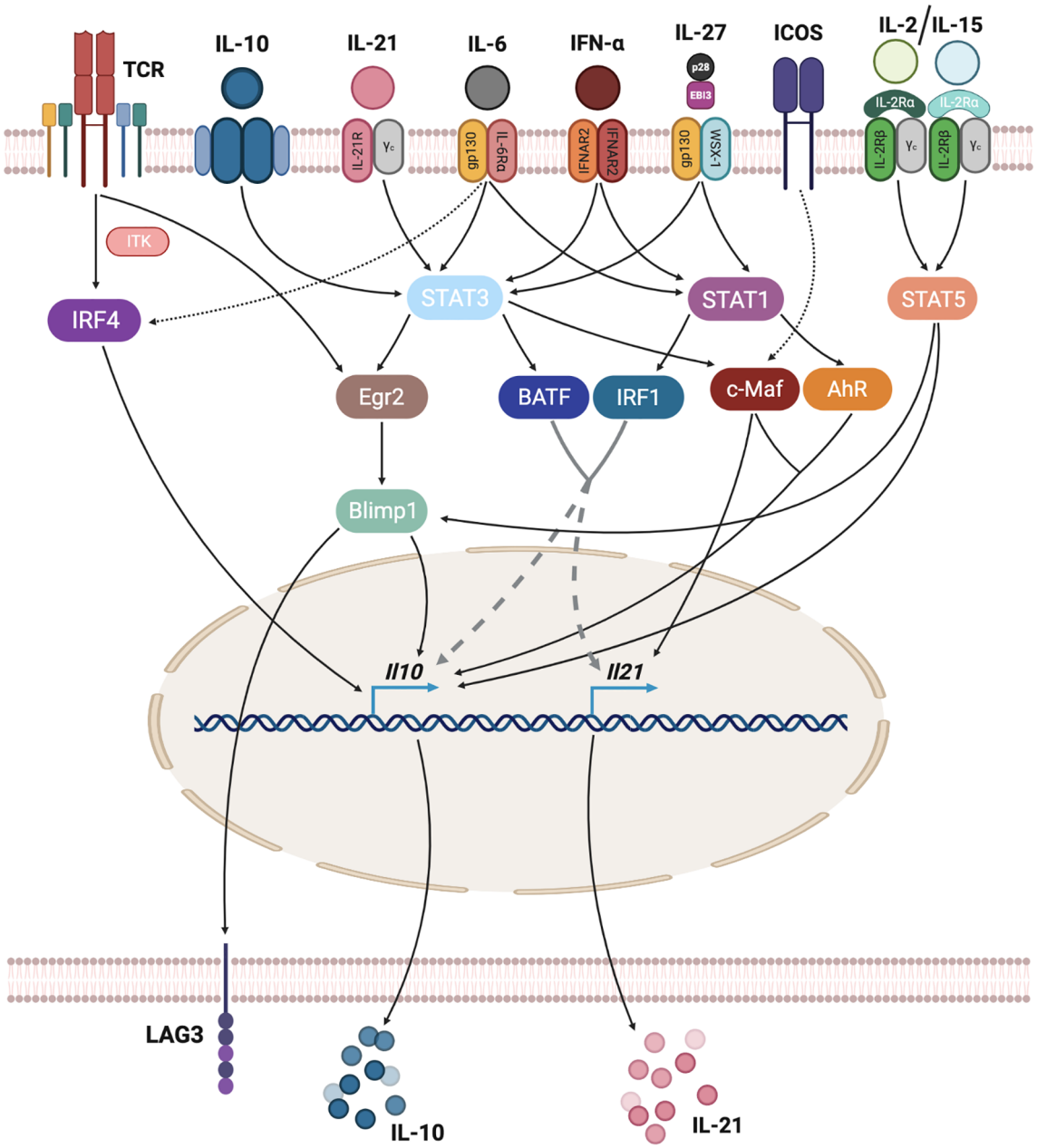

FIGURE 3 | Transcriptional regulation of TR1-like cell formation. TR1-like cell differentiation requires the integration of different stimuli. TCR signaling, through IRF4, can activate IL-10 expression. Many cytokines, including IL-10, IL-21, IL-6, type-I interferons and IL-27 signal *via* STAT1 and/or STAT3 proteins, activating several transcription factors that regulate IL-10 and IL-21 expression. ICOS signaling is also a direct regulator of IL-21 expression, while IL-2 or IL-15 cytokines can induce IL-10 directly *via* STAT5 binding to *Il10* or *via* STAT5-mediated activation of Blimp-1.

Some years later, Bacchetta et al. described IL-15 as a growth factor capable of inducing and supporting TR1-like cell proliferation in the absence of TCR ligation (148). Culture of TR1-like cell clones with IL-15 supported their *in vitro* proliferation. A recent report has suggested that IL-15 may inhibit the production of IL-10 by DCs, thus preventing the generation of IL-10-producing CD4+ T cells (149).

The IL-15R shares its β and γ chains with the IL-2R (150, 151). Although similar, IL-2 and IL-15 have non-overlapping functions. While IL-2 is mainly produced by T cells and plays a major role in the homeostasis of IL-2Rα (CD25)-expressing T cells, like activated T cells or nTregs (143, 152), IL-15 is produced during the innate immune response by cell types other than T cells (151). Stimulation with IL-2 can reverse clonal anergy

(153). IL-2 and other γ-chain cytokines, such as IL-15 or IL-21, signal through STAT5. The presence of a STAT5-responsive intronic enhancer in the *Il10* locus suggests that these cytokines might also contribute to IL-10 expression by CD4+ T cells (154, 155).

Role of Antigenic Experience and TR1-Relevant Cytokines in pMHCII-NP-Induced TR1 Cell Formation

The pMHCII-NP-induced TR1 population specifically develops from autoantigen-experienced precursors (11). For example, whereas diabetic NOD.*G6pc2*$^{-/-}$ mice (which lack IGRP) responded to BDC2.5mi/IA^{g7}-NPs like wild-type NOD mice, they did not respond to IGRP$_{4-22}$/IA^{g7}-NPs. *In vitro*, BDC2.5 TCR-transgenic anti-CD3/anti-CD28 mAb-activated but not naïve T cells upregulate both CD49b, LAG-3 and IL-10 in response to BDC2.5mi/IA^{g7}-NPs, indicating that ligation of cognate TCRs by NP-bound pMHCII complexes can trigger these events only in antigen-experienced cells.

Studies using diabetic NOD.*Ifng*$^{-/-}$ and NOD.*Il10*$^{-/-}$ mice revealed that development of the TR1 precursors and/or TR1-like cells that expand in response to this therapy requires IFN-γ in addition to IL-10 (11). The memory-like phenotype and the upregulation of T-bet mRNA in the expanded TR1-like cells, coupled with the inability of pMHC-NPs to trigger expansion of cognate TR1-like cells in non-diseased mice or NOD.*Ifng*$^{-/-}$ mice suggested that the TR1 precursors might be autoantigen-experienced effector/memory T cells of an as yet unknown identity.

As noted above, although IL-27 plays a role in the induction of TR1-like cells from naive T-cell precursors, where it triggers expression of the transcription factor c-Maf, IL-21 and ICOS (44), IL-27 is dispensable for pMHCII-NP-induction of TR1-like cells (11). Since, unlike IL-27, pMHC class II-NPs can only trigger TR1-like cell formation from antigen-experienced but not naive T cells (11), these observations are compatible with the possibility that pMHCII-NPs operate downstream of IL-27.

The specific roles of ICOS, IL-2, IL-6, IL-15 and type I IFNs in the development of pMHCII-NP-induced TR1-like cells remains to be determined.

TRANSCRIPTIONAL REGULATION

Transcription factors translate different TR1-like cell-promoting stimuli into transcriptional regulation of key TR1-like cell genes, thus playing a critical role in TR1-like cell specification (**Figure 3**).

IRF4

The IL-2 inducible T-cell kinase (ITK) plays an essential role in T-cell activation, differentiation and function in response to TCR ligation (156). Although the lack of ITK impairs the development of IL-27-induced TR1-like cells, constitutive expression of the IRF4 (a downstream target of ITK signaling) overcomes this effect (60). Of note, IRF4 expression has been linked to the expression of IL-4 and IL-10 in Th2 cells (157), IL-21, Blimp-1 and Bcl-6 in TFH cells (158) and IL-10 expression in Treg cells (159) or Th1 cells (157).

c-Maf and AhR

c-Maf has context-dependent effects on IL-4, IL-10 and IL-21 expression. c-Maf positively regulates IL-4 production in both TFH and Th2 cells (160, 161), induces IL-21 expression in both TFH and Th17 cells (59) and contributes to the expression of CXCR5 (162). c-Maf is expressed early on during IL-27-induced TR1-like cell induction, and its expression progressively increases with time (44). IL-27 stimulation also upregulates the expression of AhR, implicated in FoxP3+ Treg and Th17 differentiation (44). c-Maf and AhR have been shown to transactivate both *Il10* and *Il21* gene expression in TR1-like cells (45).

Egr-2 and Blimp-1

Egr-2 is a transcription factor that plays a role in T-cell anergy (163) and has been associated with the acquisition of regulatory activity by CD4+ T cells (52). Egr-2 expression can be induced by TCR ligation in the absence of costimulation, as well as by IL-27 stimulation (via STAT3). In turn, Egr-2 promotes IL-10 and LAG-3 expression *via* Blimp-1 (57).

The Blimp-1 protein, encoded by the *Prdm1* gene, is a zinc finger-containing transcriptional regulator of plasma cell differentiation (164), but has also been implicated in IL-10 production by CD4+ T cells (165), including both TR1-like (25, 57, 166) and FoxP3+ Treg cells (159).

IRF1 and BATF

Whereas IL-27R signaling promotes TR1-like cell formation, in part *via* the transcription factors c-Maf, AhR, Egr-2 and Blimp-1, access of these transcription factors to their binding sites on target genes, such as *Il10* or *Il21*, is enabled by pioneering transcription factors, such as BATF and IRF1 (167). BATF had been previously defined as a pioneer factor for Th2, Th17 and effector CD8+ T-cell differentiation, by modifying the chromatin landscape of precursor cells (168–172). BATF also plays a role in TFH differentiation, by regulating Bcl-6 and c-Maf expression (173).

Other Transcription Factors

Other transcription factors, such as Eomes (174, 175) and Rora (176), have also been proposed to transactivate the *Il10* gene in CD4+ T cells in a context-dependent manner. For example, Eomes requires co-expression of T-bet, the key Th1 transcription factor.

Figure 3 summarizes the main stimuli leading to TR1-like cell induction, integrating transcriptional regulation of the key TR1-associated genes, *Il10* and *Il21*.

Although pMHCII-NP-induced, antigen-specific TR1-like cells can persist for several months post-treatment withdrawal without any obvious loss of key phenotypic properties or acquisition of pathogenic activity, the cues responsible for their homeostatic survival remain unclear. Cytokines produced by the TR1-like cells themselves or by downstream regulatory cell types (e.g. Breg cells), including IL-10, IL-21 and IL-35, may play a role. Studies employing cell-specific cytokine receptor knock-out mice should help address this knowledge gap.

IL-10 UPREGULATION *VERSUS* TR1-NESS

To date, the TR1-ness of specific T-cell types has generally been ascribed to IL-10 expression. However, IL-10 can be expressed by differentiated Th subsets without the need to invoke a true TR1/regulatory phenotype.

For instance, whereas the *Il10* locus lies in a closed conformation in naive CD4+ T cells (177), all differentiated T-helper subsets expose accessible regions along the locus (178), together with deposition of H3K4me3 in the absence of H3K27me3 marks (171, 179), promoting a transcriptionally-competent state. The chromatin remodeling processes that lead to a poised or active *Il10* transcription state in Th subsets is mediated by pioneering transcription factors.

In TR1-like cells, BATF and IRF1 are thought to function as pioneering factors responsible for eliciting some of the chromatin accessibility changes that are required for TR1-like cell differentiation. Only after certain loci, such as *Il10*, become accessible, other TR1-like cell-associated transcription factors, such as AhR and c-Maf, can then bind the *Il10* promoter (167). In Th17 cells, BATF, in association with IRF4, induces *Il10* transcription (180). IRF4 is also involved in eliciting *Il10* expression in Th2 (157, 181) and Treg cells (159). STAT proteins also contribute to *Il10* expression in various Th cell subsets, such as by priming the locus with H3K4me1. STAT4, and STAT6 and GATA-3, induce IL-10 production in Th1 and Th2 cells, respectively (98, 182). GATA-3 induces H3 and H4 acetylation and an increase in chromatin accessibility in the *Il10* locus (183). In Tregs, FoxP3 regulates IL-10 expression, but this process is independent of DNA binding (184). Rather, FoxP3 recruits HAT1 complexes to the locus where they induce the acetylation of H4K5 and H5K12 at the *Il10* promoter, making it more permissive for STAT3 binding (185). Nfil3 is another transcription factor linked to IL-10 production in Th1, Th2, Treg and NK cells, by promoting acetylation of H3 in the *Il10* locus (99). In contrast, in both Th1 and Th2 cells, Ets1 suppresses IL-10 production, by recruiting the de-acetylase HDAC1 to the *Il10* promoter and enhancer regions (186, 187). Importantly, transcription factors involved in T-helper subset specification, such as T-bet, GATA-3 or RORγt can enhance IL-10 expression.

Thus, IL-10 expression *per se* is not a cell subset- but rather a functional state-defining property and IL-10 expression can co-exist with an effector cell program within a given T-cell subset.

A ROLE FOR EPIGENETIC REMODELING OF THE CHROMATIN IN TR1-LIKE CELL FORMATION?

Transcriptional features alone do not invariably define a final differentiated cell state. Like in other T-cell developmental or differentiation steps, cell fate decisions require both transcriptional changes and epigenetic remodeling of the chromatin.

For example, during development, the epigenome of the parental gametes progressively evolves to acquire the specific epigenome of the zygote (188). The chromatin of the zygote further undergoes additional waves of epigenetic changes, including DNA demethylation and methylation, modifications in histones, and changes in chromatin accessibility (189, 190). Epigenetic reprogramming is also essential for differentiation of embryonic stem cells (ESCs) into distinct cell populations (190–192). Pluripotent cells display an open chromatin configuration that is progressively restricted during development (193), accompanied by an increase in DNA methylation and the redistribution of histone marks. The gene expression changes that are associated with such chromatin remodeling processes are not unique to the germline and also take place in somatic cells in response to stimuli. For example, cytokine stimulation induces chromatin changes in APCs, such as DCs or macrophages (194). This phenomenon has also been reported for cytokine-challenged pancreatic β-cells (195), where cytokine stimulation triggers the appearance of new regulatory elements (neo-IREs).

It is becoming increasingly clear that susceptibility of the chromatin to undergo certain epigenetic modifications is affected by the underlying nucleotide sequence. A significant number of disease-associated single nucleotide polymorphisms (SNPs) lie in fact in non-coding, regulatory regions (196). For example, T1D-associated variants appear to be enriched in T- and B-cell enhancers (196, 197), in some cases promoting a three dimensional chromatin architecture that facilitates changes in gene expression in immune cells that might be able to promote the autoimmune pathology (198). Type 2 diabetes (T2D) is another example of a disease whose genetic susceptibility is commonly associated with non-coding variants (199, 200). In this case, many risk variants locate in enhancers or super-enhancers of genes involved in islet cell function and differentiation (201–204).

T cells are known to undergo extensive epigenome remodeling in response to activation/differentiation cues, enabling the acquisition of phenotypic and functional stability (**Figure 4**). The first epigenetic decision takes place when the T-cell fate is defined in developing thymocytes (205). T-cell activation (206) and T-helper cell polarization also involve epigenetic modifications along with changes in transcription factor expression. For example, Th1 development involves the upregulation of STAT1 in response to IFN-γ and IL-27, leading to the expression of T-bet, which upregulates the expression of IFN-γ, H2.0-like homeobox (HLX) transcription factors and Runt-related transcription factor 3 (Runx3), and suppresses the expression of GATA-3 (207–209). In turn, T-bet and Runx3 repress the *Il4* gene to prevent Th2 differentiation. The *Ifng* gene harbors multiple regulatory elements around the locus, including enhancers at conserved non-coding sequences and an insulator. This locus is found in a poised, de-methylated state marked by bivalent histone modifications (poised for either expression or silencing) in naive CD4+ T cells, which produce low levels of this cytokine. Th1 differentiation involves H3K4me2, H3 and H4 acetylation and the creation of accessible chromatin at regulatory elements within the *Ifng* locus, together with loss of H3K27me3 throughout the locus, followed by DNA demethylation (210–213). T-bet transactivates expression of *Ifng* by binding to its promoter as well as several enhancers and by recruiting histone

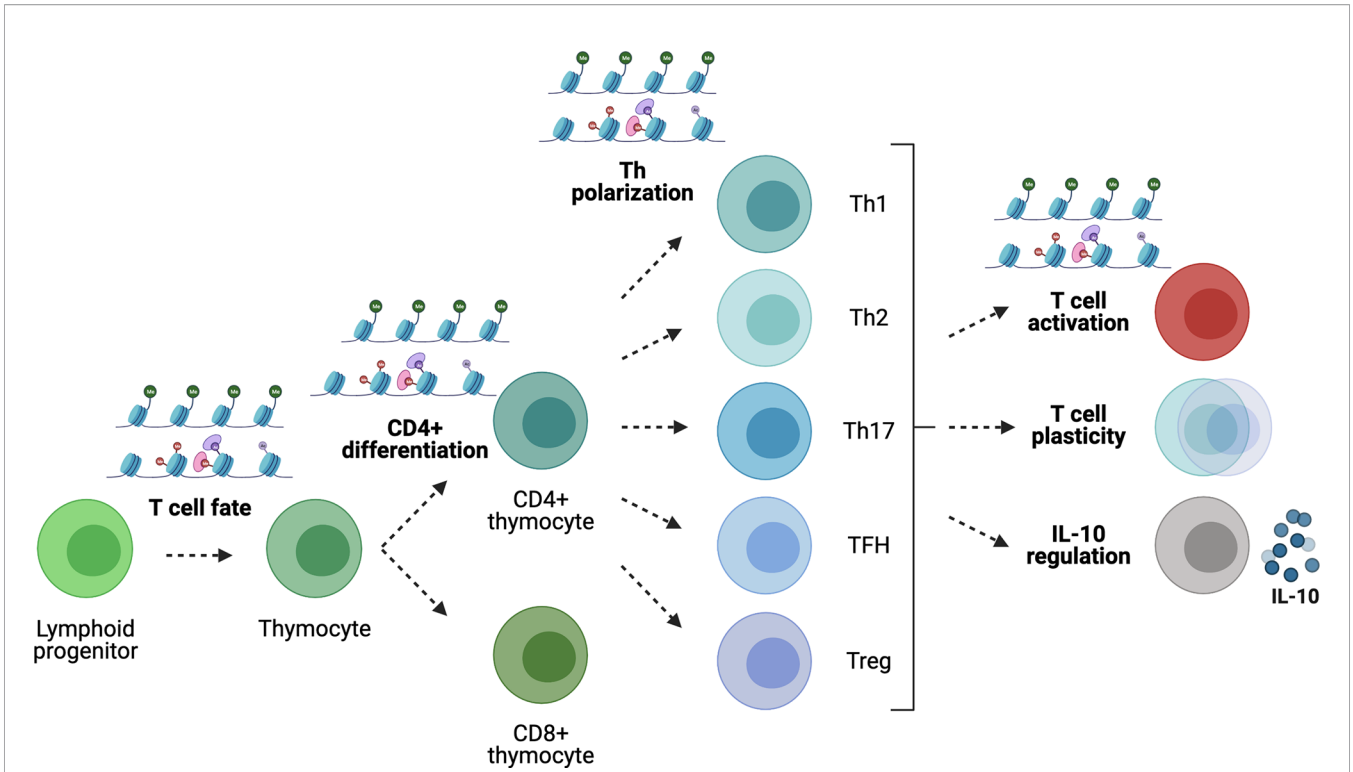

FIGURE 4 | Gene regulation in T cells. Epigenetic modifications play key roles during T-cell development, differentiation and Th polarization. In the periphery, the epigenome regulates Th cell lineage stability/plasticity as well as IL-10 expression competency.

acetyltransferases (HATs) (214) and histone demethylases (HDMs) (215).

In contrast, activation of the Th2 program results in the loss of permissive histone modifications and H3K27 trimethylation along the *Ifng* locus, coupled to DNA methylation (210, 216, 217). The Th2 program is induced by IL-4-mediated activation of STAT6, which in turn activates GATA-3 (218). GATA-3 induces the expression of c-Maf, regulating IL-4 expression, and together with STAT6 enhances the transcription of *Il4*, *Il5* and *Il13* (218). In mice, *Il4*, *Il5* and *Il13* (encoding Th2 cytokines), together with the *Rad50* gene, co-localize near a Locus Control Region (LCR). Expression of the *Il4* gene is regulated by enhancers (overlapping with DNAse I hypersensitive sites) that bind NFAT and Th2-promoting transcription factors. In naive T cells, there are few accessibility and histone modifications at these DNAse I hypersensitive sites, and the cytokine gene promoters and enhancers are hyper-methylated (219). Upon Th2-polarizing stimulation, the loci acquire permissive histone modifications and lose H3K27me3 (220, 221). In Th1 cells, the Th2-cytokine locus is all covered with H3K27me3 (222). GATA-3 induces most of these epigenetic modifications, as it can recruit HATs and histone H3K4 methyltransferases (218, 223), inhibit histone deacetylases (HDACs) (224) and DNA (cytosine-5)-methyltransferase 1 (DNMT1) (219, 225), and recruit chromatin-remodeling factors (226). In addition, the *Ifng* locus in Th2 cells is silenced by H3K27me3 deposition (217).

TGF-β induction of Th17 and Treg lineage formation represents another example. This cytokine induces both the expression of FoxP3 and retinoic-acid-receptor-related orphan receptor-γt (RORγt) (227–230). The context determines if the Treg or the Th17 program is induced: in the absence of IL-6, FoxP3 inhibits RORγt and leads to Treg formation. If IL-6 is present, STAT3 is activated, inhibiting the expression of FoxP3 and enhancing Th17 formation. IL-17A and IL-17F are both co-expressed by Th17 cells and the genes encoding these cytokines co-localize and may be regulated by shared regulatory elements. The *Il17* locus contains eight different gene regulatory elements (231). When naïve CD4+ T cells are cultured under Th17-polarizing conditions, STAT3 (227) and RORγt (232) induce the appearance of permissive H3 acetylation changes in the *Il17a* and *Il17f* gene regulatory elements (231), enabling their expression.

The fate of TFH and non-TFH (Th1, Th2, Th17) effector cells is regulated by Bcl-6 and Blimp-1, which are reciprocal regulators of each other (233). Bcl-6 binds promoters and enhancers regulating genes involved in T-cell migration (Ebi2, CCR6, CCR7, S1pr1, Klf-2, PSGL-1, CXCR5, CXCR4, PD-1 and SAP) (126, 234). Ascl-2 also controls TFH differentiation by upregulating CXCR5 and CXCR4, while downregulating CCR7 and PSGL-1 expression. The *Bcl6* locus in TFH cells displays positive histone modifications, but it also contains permissive marks in Th1, Th2 and Th17 cells (235). Other TFH-related genes, such as c-Maf, BATF and IRF4, are also associated with H3K4me3 in all subsets. In contrast, the *Ascl2* locus is uniquely

marked with the active chromatin mark H3K4me3 in TFH cells. *Prdm1* (encoding BLIMP-1), which is downregulated in TFH cells, displays bivalent modifications, allowing re-programming between TFH and other Th effector subsets (236).

Acquisition of Treg-cell-specific epigenetic marks during thymocyte development (237, 238), along with FoxP3 expression, determines the regulatory phenotype of nTregs (239). Once in the periphery, Treg cells can be divided into subpopulations that locate in different tissues, and each acquires an additional level of epigenetic modification that defines a tissue-specific epigenetic footprint (240). The expression of some Treg-function associated molecules, such as CTLA-4 or CD25, is clearly associated with DNA de-methylation and can occur in the absence of FoxP3. In contrast, expression of *Il2*, *Ifng* or *Zap70* is lost if FoxP3 is not present. Several regulatory elements control *Foxp3* gene expression (237). The *Foxp3* promoter is de-methylated upon TCR signaling, facilitating the binding of FoxP3-inducing transcription factors (241).

Moreover, there is increasing evidence that Th subsets are plastic. To name a few examples, T-cell populations have been described that stably express both T-bet and GATA-3 and produce both IFN-γ and IL-4 (242), produce both Th1 and Th17 cytokines (243, 244), or have a Th1/Th17 phenotype but can switch to Th2 during helminth infections (245). This observed plasticity can be regulated by different mechanisms. First, certain environmental stimuli may be able to modify epigenetic marks responsible for maintaining lineage stability; for example, prolonged activation of Treg cells *in vitro* can lead to demethylation of the *Rorc* locus in FoxP3+ Tregs and allow IL-17 production (246). Second, Th subsets display an intrinsic plasticity potential. Although the various lineage-specific cytokines present active histone marks in the corresponding cell lineages and repressive marks in the others, some transcription factors are not so strictly marked. For example, in Th1 cells, *Tbx21*, encoding T-bet, bears activating H3K4me3 marks in the promoter. In other Th cell subsets, on the other hand, the *Tbx21* promoter bears bivalent modifications. Likewise, the *Gata3* promoter carries H3K4me3 marks in Th2 cells, but bivalent marks in other Th cell subsets. The same is true for *Rorc* or *Bcl6* genes in non-Th17 or non-TFH cells, respectively (235, 247). Third, polarized T-cell types might represent stable lineages yet comprise a continuum of different epigenotypes with differential susceptibility for lineage conversion in response to external signals.

To date, the study of TR1-like cell specification is largely based on phenotypic and transcriptional studies. Based on the data summarized above, it is reasonable to suspect that the cues responsible for TR1-like cell formation operate on a precursor cell type that either has a TR1-poised epigenome or responds to TR1-inducing signals by undergoing further epigenetic modifications enabling the acquisition of a stable TR1-like cell phenotype, including DNA hypomethylation (248–250). Thus, detailed characterization of TR1-like cells at the transcriptional and epigenetic levels, including analysis of their chromatin status, three-dimensional structure and interactions, as well as DNA methylation status (**Table 2**), should provide unique clues about the true identity of this cell lineage and the identity of their cellular precursors.

CONCLUDING REMARKS

Currently, TR1-like cells are defined as a regulatory CD4+ T-cell subset that lacks FoxP3 expression (unlike conventional FoxP3+ Treg cells) and secretes IL-10 and low levels or no IL-4. However, this Treg cell subset lacks cell-specific markers and their developmental origin remains a mystery. Moreover, the signaling, genetic and epigenetic mechanisms that are responsible for the acquisition of the TR1-like cell phenotype *in vivo* remain unclear.

We posit that detailed transcriptional and epigenetic studies will enable a better understanding of the role of this T-cell subset in immunity, autoimmunity and cancer, the identification of biomarkers capable of accurately track its development *in vivo*, as well as a detailed understanding of gene regulatory mechanisms responsible for TR1-like cell specification. In turn, this will help pinpoint specific areas of the genome that might be impacted by genetic polymorphisms associated with susceptibility and/or resistance to specific immune-mediated diseases, and the development and testing of compounds capable of triggering the formation of antigen-specific TR1-like cells *in vivo*, for therapeutic purposes.

TR1 cell formation in response to pMHCII-NPs afford a unique opportunity to address the above knowledge gaps. These compounds trigger the formation of relatively large numbers of mono-specific TR1-like cells, thus enabling this type of studies with unprecedented resolution. Transcriptional studies at the

TABLE 2 | Summary of epigenetic modifications and their effects on gene expression.

Epigenetic modification	*Found in*	*Relation to gene transcription*	*Study methods*
Chromatin accessibility	Promoters and GREs	Activating	ATAC-seq DNAse-seq MNase-seq
H3K27ac	Active enhancers and TSS	Activating	
H3K4me3	TSS	Activating	
H3K4me1	Gene body Primed enhancers	Activating	ChIP-seq Cut&Run
H3K27me3	Bivalent/inactive enhancers, promoters and intergenic regions	Repressing	Cut&Tag
H3K9me3	Constitutive heterochromatin	Repressing	
DNA methylation	Enhancers, promoters, gene body (CpG rich regions)	Repressing	Bisulfite sequencing

bulk and single cell levels should help determine the homogeneity or heterogeneity of the resulting cognate T-cell pools, and pinpoint developmentally-related cell subsets with poised TR1-like cell transcriptional programs. Epigenetic studies shall include screening for histone modifications, chromatin accessibility and 3D chromatin maps, to enumerate the genome-wide distribution of active promoters and enhancers, define the epigenomic architecture underpinning the TR1-like cell state, describe the various steps underlying TR1-like cell re-programming, identify key TR1-like cell epigenetic signatures, and potentially expose new targets for therapeutic intervention.

Collectively, these studies should provide a comprehensive set of functional, phenotypic, transcriptional and epigenetic markers capable of specifically identifying TR1 cells. These markers would likely play a pivotal role in guiding the clinical translation of compounds capable of promoting TR1 cell formation *in vivo* for the treatment of autoimmunity, including pMHCII-based nanomedicines. They should also prove useful to enumerate the contribution of this cell type to tumor progression in the context of cancer.

AUTHOR CONTRIBUTIONS

PSo and PSa co-wrote the manuscript. All authors contributed to the article and approved the submitted version.

FUNDING

The authors' work is funded by the Canadian Institutes of Health Research (CIHR), Diabetes Canada, REEM (Red Española de Esclerosis Múltiple), the Praespero Foundation, the Ministerio de Economia y Competitividad of Spain (MINECO; RD16/0015/0020), and Generalitat de Catalunya (SGR and CERCA Programmes). The JMDRC is supported by Diabetes Canada.

ACKNOWLEDGMENTS

We thank the members of the PSa's laboratories for their contributions.

REFERENCES

1. Fujio K, Okamura T, Yamamoto K. The Family of IL-10-Secreting CD4+T Cells. In: *Advances in Immunology*. Elsevier Inc. (2010). p. 99–130. doi: 10.1016/S0065-2776(10)05004-2
2. Alfen JS, Larghi P, Facciotti F, Gagliani N, Bosotti R, Paroni M, et al. Intestinal IFN-γ–Producing Type 1 Regulatory T Cells Coexpress CCR5 and Programmed Cell Death Protein 1 and Downregulate IL-10 in the Inflamed Guts of Patients With Inflammatory Bowel Disease. *J Allergy Clin Immunol* (2018) 142:1537–47.e8. doi: 10.1016/j.jaci.2017.12.984
3. Gagliani N, Magnani CF, Huber S, Gianolini ME, Pala M, Licona-Limon P, et al. Coexpression of CD49b and LAG-3 Identifies Human and Mouse T Regulatory Type 1 Cells. *Nat Med* (2013) 19:739–46. doi: 10.1038/nm.3179
4. Roncarolo MG, Gregori S, Bacchetta R, Battaglia M, Gagliani N. The Biology of T Regulatory Type 1 Cells and Their Therapeutic Application in Immune-Mediated Disease. *Immunity* (2018) 49:1004–19. doi: 10.1016/j.immuni.2018.12.001
5. Burton BR, Britton GJ, Fang H, Verhagen J, Smithers B, Sabatos-Peyton CA, et al. Sequential Transcriptional Changes Dictate Safe and Effective Antigen-Specific Immunotherapy. *Nat Commun* (2014) 5:4741. doi: 10.1038/ncomms5741
6. White AM, Wraith DC. Tr1-Like T Cells - An Enigmatic Regulatory T Cell Lineage. *Front Immunol* (2016) 7:355. doi: 10.3389/fimmu.2016.00355
7. Brockmann L, Soukou S, Steglich B, Czarnewski P, Zhao L, Wende S, et al. Molecular and Functional Heterogeneity of IL-10-Producing CD4+ T Cells. *Nat Commun* (2018) 9:5457. doi: 10.1038/s41467-018-07581-4
8. Zhu C, Sakuishi K, Xiao S, Sun Z, Zaghouani S, Gu G, et al. An IL-27/NFIL3 Signaling Axis Drives Tim-3 and IL-10 Expression and T Cell Dysfunction. *Nat Commun* (2015) 6:1–14. doi: 10.1038/ncomms7072
9. Singha S, Shao K, Yang Y, Clemente-Casares X, Solé P, Clemente A, et al. Peptide–MHC-Based Nanomedicines for Autoimmunity Function as T-Cell Receptor Microclustering Devices. *Nat Nanotechnol* (2017) 12:701–10. doi: 10.1038/nnano.2017.56
10. Tsai S, Shameli A, Yamanouchi J, Clemente-Casares X, Wang J, Serra P, et al. Reversal of Autoimmunity by Boosting Memory-Like Autoregulatory T Cell. *Immunity* (2010) 32:568–80. doi: 10.1016/j.immuni.2010.03.015
11. Clemente-Casares X, Blanco J, Ambalavanan P, Yamanouchi J, Singha S, Fandos C, et al. Expanding Antigen-Specific Regulatory Networks to Treat Autoimmunity. *Nature* (2016) 530:434–40. doi: 10.1038/nature16962
12. Umeshappa CS, Singha S, Blanco J, Shao K, Nanjundappa RH, Yamanouchi J, et al. Suppression of a Broad Spectrum of Liver Autoimmune Pathologies by Single Peptide-MHC-Based Nanomedicines. *Nat Commun* (2019) 10:1–17. doi: 10.1038/s41467-019-09893-5
13. Umeshappa CS, Mbongue J, Singha S, Mohapatra S, Yamanouchi J, Lee JA, et al. Ubiquitous Antigen-Specific T Regulatory Type 1 Cells Variably Suppress Hepatic and Extrahepatic Autoimmunity. *J Clin Invest* (2020) 130:1823–9. doi: 10.1172/JCI130670
14. Groux H, O'Garra A, Bigler M, Rouleau M, Antonenko S, de Vries JE. Roncarolo MG. A CD4+ T-Cell Subset Inhibits Antigen-Specific T-Cell Responses and Prevents Colitis. *Nature* (1997) 389:737–42. doi: 10.1038/39614
15. Roncarolo MG, Yssel H, Touraine JL, Betuel H, De Vries JE, Spits H. Autoreactive T Cell Clones Specific for Class I and Class II HLA Antigens Isolated From a Human Chimera. *J Exp Med* (1988) 167:1523–34. doi: 10.1084/jem.167.5.1523
16. Vieira P, De Waal-Malefyt R, Dang MN, Johnson KE, Kastelein R, Fiorentino DF, et al. Isolation and Expression of Human Cytokine Synthesis Inhibitory Factor cDNA Clones: Homology to Epstein-Barr Virus Open Reading Frame BCRF. *Proc Natl Acad Sci USA* (1991) 88:1172–6. doi: 10.1073/pnas.88.4.1172
17. Bacchetta R, Bigler M, Touraine JL, Parkman R, Tovo PA, Abrams J, et al. High Levels of Interleukin 10 Production *In Vivo* Are Associated With Tolerance in SCID Patients Transplanted With HLA Mismatched Hematopoietic Stem Cells. *J Exp Med* (1994) 179:493–502. doi: 10.1084/jem.179.2.493
18. Bacchetta R, Gregori S, Serafini G, Sartirana C, Schulz U, Zino E, et al. Molecular and Functional Characterization of Allogantigen Specific Anergic T Cells Suitable for Cell Therapy. *Haematologica* (2010) 95:2134–43. doi: 10.3324/haematol.2010.025825
19. Roncarolo MG, Gregori S, Bacchetta R, Battaglia M. Tr1 Cells and the Counter-Regulation of Immunity: Natural Mechanisms and Therapeutic Applications. *Curr Top Microbiol Immunol* (2014) 380:39–68. doi: 10.1007/978-3-662-43492-5_3
20. Bollyky PL, Wu RP, Falk BA, Lord JD, Long SA, Preisinger A, et al. ECM Components Guide IL-10 Producing Regulatory T-Cell (TR1) Induction From Effector Memory T-Cell Precursors. *Proc Natl Acad Sci USA* (2011) 108:7938–43. doi: 10.1073/pnas.1017360108
21. Yao Y, Vent-Schmidt J, McGeough MD, Wong M, Hoffman HM, Steiner TS, et al. Tr1 Cells, But Not Foxp3 + Regulatory T Cells, Suppress NLRP3 Inflammasome Activation *via* an IL-10–Dependent Mechanis. *J Immunol* (2015) 195:488–97. doi: 10.4049/jimmunol.1403225
22. Gagliani N, Gregori S, Jofra T, Valle A, Stabilini A, Rothstein DM, et al. Rapamycin Combined With Anti-CD45RB mAB and IL-10 or With G-CSF

Induces Tolerance in a Stringent Mouse Model of Islet Transplantation. *PloS One* (2011) 6:1–12. doi: 10.1371/journal.pone.0028434
23. Gagliani N, Jofra T, Valle A, Stabilini A, Morsiani C, Gregori S, et al. Transplant Tolerance to Pancreatic Islets Is Initiated in the Graft and Sustained in the Spleen. *Am J Transplant* (2013) 13:1963–75. doi: 10.1111/ajt.12333
24. Gagliani N, Amezcua Vesely MC, Iseppon A, Brockmann L, Xu H, Palm NW, et al. TH17 Cells Transdifferentiate Into Regulatory T Cells During Resolution of Inflammation. *Nature* (2015) 523:221–5. doi: 10.1038/nature14452
25. Heinemann C, Heink S, Petermann F, Vasanthakumar A, Rothhammer V, Doorduijn E, et al. IL-27 and IL-12 Oppose Pro-Inflammatory IL-23 in CD4+ T Cells by Inducing Blimp1. *Nat Commun* (2014) 5:1–13. doi: 10.1038/ncomms4770
26. Meiron M, Zohar Y, Anunu R, Wildbaum G, Karin N. CXCL12 (SDF-1α) Suppresses Ongoing Experimental Autoimmune Encephalomyelitis by Selecting Antigen-Specific Regulatory T Cells. *J Exp Med* (2008) 205:2643–55. doi: 10.1084/jem.20080730
27. Lönnberg T, Svensson V, James KR, Fernandez-Ruiz D, Sebina I, Montandon R, et al. Single-Cell RNA-Seq and Computational Analysis Using Temporal Mixture Modeling Resolves TH1/TFH Fate Bifurcation in Malaria. *Sci Immunol* (2017) 2(9):eaal2192. doi: 10.1126/sciimmunol.aal2192
28. Pacciani V, Gregori S, Chini L, Corrente S, Chianca M, Moschese V, et al. Induction of Anergic Allergen-Specific Suppressor T Cells Using Tolerogenic Dendritic Cells Derived From Children With Allergies to House Dust Mites. *J Allergy Clin Immunol* (2010) 125:727–36. doi: 10.1016/j.jaci.2009.12.004
29. Pellerin L, Jenks JA, Chinthrajah S, Dominguez T, Block W, Zhou X, et al. Peanut-Specific Type 1 Regulatory T Cells Induced *In Vitro* From Allergic Subjects Are Functionally Impaired. *J Allergy Clin Immunol* (2018) 141:202–213.e8. doi: 10.1016/j.jaci.2017.05.045
30. Oida T, Zhang X, Goto M, Hachimura S, Totsuka M, Kaminogawa S, et al. CD4+ CD25– T Cells That Express Latency-Associated Peptide on the Surface Suppress CD4+ CD45RB High -Induced Colitis by a TGF-β-Dependent Mechanis. *J Immunol* (2003) 170:2516–22. doi: 10.4049/jimmunol.170.5.2516
31. Ochi H, Abraham M, Ishikawa H, Frenkel D, Yang K, Basso AS, et al. Oral CD3-Specific Antibody Suppresses Autoimmune Encephalomyelitis by Inducing CD4+CD25–LAP+ T Cells. *Nat Med* (2006) 12:627–35. doi: 10.1038/nm1408
32. Groh V, Smythe K, Dai Z, Spies T. Fas Ligand-Mediated Paracrine T Cell Regulation by the Receptor NKG2D in Tumor Immunity. *Nat Immunol* (2006) 7:755–62. doi: 10.1038/ni1350
33. Groh V, Brühl A, El-Gabalawy H, Nelson JL, Spies T. Stimulation of T Cell Autoreactivity by Anomalous Expression of NKG2D and Its MIC Ligands in Rheumatoid Arthritis. *Proc Natl Acad Sci USA* (2003) 100:9452–7. doi: 10.1073/pnas.1632807100
34. Häringer B, Lozza L, Steckel B, Geginat J. Identification and Characterization of IL-10/IFN-γ-Producing Effector-Like T Cells With Regulatory Function in Human Blood. *J Exp Med* (2009) 206:1009–17. doi: 10.1084/jem.20082238
35. Gonzalez A, Andre-Schmutz I, Carnaud C, Mathis D, Benoist C. Damage Control, Rather Than Unresponsiveness, Effected by Protective DX5+T Cells in Autoimmune Diabetes. *Nat Immunol* (2001) 2:1117–25. doi: 10.1038/ni738
36. Charbonnier L-M, van Duivenvoorde LM, Apparailly F, Cantos C, Han WGH, Noël D, et al. Immature Dendritic Cells Suppress Collagen-Induced Arthritis by In Vivo Expansion of CD49b + Regulatory T Cell. *J Immunol* (2006) 177:3806–13. doi: 10.4049/jimmunol.177.6.3806
37. Han WGH, Schuurhuis DH, Fu N, Camps M, van Duivenvoorde LM, Louis-Plence P, et al. DC-Induced CD8+ T-Cell Response Is Inhibited by MHC Class II-Dependent DX5+CD4+ Treg. *Eur J Immunol* (2009) 39:1765–73. doi: 10.1002/eji.200838842
38. El Bannoudi H, Han WGH, Stoop JN, Louis-Plence P, Huizinga TWJ, Toes REM. DX5+CD4+ T Cells Modulate CD4+ T-Cell Response *via* Inhibition of IL-12 Production by DC. *Eur J Immunol* (2013) 43:439–46. doi: 10.1002/eji.201242796
39. Workman CJ, Rice DS, Dugger KJ, Kurschner C, Vignali DAA. Phenotypic Analysis of the Murine CD4-Related Glycoprotein, CD223 (LAG-3). *Eur J Immunol* (2002) 32:2255–63. doi: 10.1002/1521-4141(200208)32:8<2255::AID-IMMU2255>3.0.CO;2-A
40. Facciotti F, Gagliani N, Häringer B, Alfen JS, Penatti A, Maglie S, et al. IL-10-Producing Forkhead Box Protein 3-Negative Regulatory T Cells Inhibit B-Cell Responses and Are Involved in Systemic Lupus Erythematosus. *J Allergy Clin Immunol* (2016) 137:318–21. doi: 10.1016/j.jaci.2015.06.044
41. Magnani CF, Alberigo G, Bacchetta R, Serafini G, Andreani M, Roncarolo MG, et al. Killing of Myeloid APCs *via* HLA Class I, CD2 and CD226 Defines a Novel Mechanism of Suppression by Human Tr1 Cells. *Eur J Immunol* (2011) 41:1652–62. doi: 10.1002/eji.201041120
42. Cobbold SP, Nolan KF, Graca L, Castejon R, Le Moine A, Frewin M, et al. Regulatory T Cells and Dendritic Cells in Transplantation Tolerance: Molecular Markers and Mechanisms. *Immunol Rev* (2003) 196:109–24. doi: 10.1046/j.1600-065X.2003.00078.x
43. Okamura T, Fujio K, Shibuya M, Sumitomo S, Shoda H, Sakaguchi S, et al. CD4+CD25-LAG3+ Regulatory T Cells Controlled by the Transcription Factor Egr-2. *Proc Natl Acad Sci* (2009) 106:13974–9. doi: 10.1073/pnas.0906872106
44. Pot C, Jin H, Awasthi A, Liu SM, Lai C-Y, Madan R, et al. Cutting Edge: IL-27 Induces the Transcription Factor C-Maf, Cytokine IL-21, and the Costimulatory Receptor ICOS That Coordinately Act Together to Promote Differentiation of IL-10-Producing Tr1 Cell. *J Immunol* (2009) 183:797–801. doi: 10.4049/jimmunol.0901233
45. Apetoh L, Quintana FJ, Pot C, Joller N, Xiao S, Kumar D, et al. The Aryl Hydrocarbon Receptor Interacts With C-Maf to Promote the Differentiation of Type 1 Regulatory T Cells Induced by IL-27. *Nat Immunol* (2010) 11:854–61. doi: 10.1038/ni.1912
46. Tousa S, Semitekolou M, Morianos I, Banos A, Trochoutsou AI, Brodie TM, et al. Activin-A Co-Opts IRF4 and AhR Signaling to Induce Human Regulatory T Cells That Restrain Asthmatic Responses. *Proc Natl Acad Sci USA* (2017) 114:2891–900. doi: 10.1073/pnas.1616942114
47. Nakamura K, Kitani A, Strober W. Cell Contact-Dependent Immunosuppression by CD4+CD25+ Regulatory T Cells Is Mediated by Cell Surface-Bound Transforming Growth Factor β. *J Exp Med* (2001) 194:629–44. doi: 10.1084/jem.194.5.629
48. Nakajima U, Miyazono K, Kato M, Takase M, Yamagishi T, Nakamura H. Extracellular Fibrillar Structure of Latent Tgfβ Binding Protein-1: Role in Tgfβ-Dependent Endothelial-Mesenchymal Transformation During Endocardial Cushion Tissue Formation in Mouse Embryonic Heart. *J Cell Biol* (1997) 136:193–204. doi: 10.1083/jcb.136.1.193
49. Bradley LM, Haynes L, Swain SL. IL-7: Maintaining T-Cell Memory and Achieving Homeostasis. *Trends Immunol* (2005) 26:172–6. doi: 10.1016/j.it.2005.01.004
50. Liu W, Putnam AL, Xu-yu Z, Szot GL, Lee MR, Zhu S, et al. CD127 Expression Inversely Correlates With FoxP3 and Suppressive Function of Human CD4+ T Reg Cells. *J Exp Med* (2006) 203:1701–11. doi: 10.1084/jem.20060772
51. Huang C-TT, Workman CJ, Flies D, Pan X, Marson AL, Zhou G, et al. Role of LAG-3 in Regulatory T Cells. *Immunity* (2004) 21:503–13. doi: 10.1016/j.immuni.2004.08.010
52. Safford M, Collins S, Lutz MA, Allen A, Huang CT, Kowalski J, et al. Egr-2 and Egr-3 Are Negative Regulators of T Cell Activation. *Nat Immunol* (2005) 6:472–80. doi: 10.1038/ni1193
53. Kassiotis G, Gray D, Kiafard Z, Zwirner J, Stockinger B. Functional Specialization of Memory Th Cells Revealed by Expression of Integrin CD49. *J Immunol* (2006) 177:968–75. doi: 10.4049/jimmunol.177.2.968
54. Gupta S, Thornley TB, Gao W, Larocca R, Turka LA, Kuchroo VK, et al. Allograft Rejection Is Restrained by Short-Lived TIM 3^+ $PD1^+$ $Foxp3^+$ Treg. *J Clin Invest* (2012) 122:2395–404. doi: 10.1172/JCI45138
55. Wu H, Chen Y, Liu H, Xu LL, Teuscher P, Wang S, et al. Follicular Regulatory T Cells Repress Cytokine Production by Follicular Helper T Cells and Optimize IgG Responses in Mice. *Eur J Immunol* (2016) 46:1152–61. doi: 10.1002/eji.201546094
56. Miaw SC, Choi A, Yu E, Kishikawa H, Ho IC. ROG, Repressor of GATA, Regulates the Expression of Cytokine Genes. *Immunity* (2000) 12:323–33. doi: 10.1016/s1074-7613(00)80185-5
57. Iwasaki Y, Fujio K, Okamura T, Yanai A, Sumitomo S, Shoda H, et al. Egr-2 Transcription Factor Is Required for Blimp-1-Mediated IL-10 Production in

IL-27-Stimulated CD4+T Cells. *Eur J Immunol* (2013) 43:1063–73. doi: 10.1002/eji.201242942
58. Veldhoen M, Hirota K, Westendorf AM, Buer J, Dumoutier L, Renauld J-C, et al. The Aryl Hydrocarbon Receptor Links TH17-Cell-Mediated Autoimmunity to Environmental Toxins. *Nature* (2008) 453:106–9. doi: 10.1038/nature06881
59. Bauquet AT, Jin H, Paterson AM, Mitsdoerffer M, Ho I-CC, Sharpe AH, et al. The Costimulatory Molecule ICOS Regulates the Expression of C-Maf and IL-21 in the Development of Follicular T Helper Cells and TH -17 Cells. *Nat Immunol* (2009) 10:167–75. doi: 10.1038/ni.1690
60. Huang W, Solouki S, Koylass N, Zheng S-GG, August A. ITK Signalling *via* the Ras/IRF4 Pathway Regulates the Development and Function of Tr1 Cells. *Nat Commun* (2017) 8:15871. doi: 10.1038/ncomms15871
61. Moore KW, de Waal Malefyt R, Coffman RL, O'Garra A. Interleukin-10 and the Interleukin-10 Receptor. *Annu Rev Immunol* (2001) 19:683–765. doi: 10.1146/annurev.immunol.19.1.683
62. Taga K, Tosato G. IL-10 Inhibits Human T Cell Proliferation and IL-2 Production. *J Immunol* (1992) 148:1143–8.
63. Gregori S, Tomasoni D, Pacciani V, Scirpoli M, Battaglia M, Magnani CF, et al. Differentiation of Type 1 T Regulatory Cells (Tr1) by Tolerogenic DC-10 Requires the IL-10-Dependent ILT4/HLA-G Pathway. *Blood* (2010) 116:935–44. doi: 10.1182/blood-2009-07-234872
64. Satoguina JS, Weyand E, Larbi J, Hoerauf A. T Regulatory-1 Cells Induce IgG4 Production by B Cells: Role of IL-10. *J Immunol* (2005) 174:4718–26. doi: 10.4049/jimmunol.174.8.4718
65. Murray PJ. The Primary Mechanism of the IL-10-Regulated Antiinflammatory Response Is to Selectively Inhibit Transcription. *Proc Natl Acad Sci USA* (2005) 102:8686–91. doi: 10.1073/pnas.0500419102
66. Bourque J, Hawiger D. Immunomodulatory Bonds of the Partnership Between Dendritic Cells and T Cells. *Crit Rev Immunol* (2018) 38:379–401. doi: 10.1615/CritRevImmunol.2018026790
67. Lee KM, Chuang E, Griffin M, Khattri R, Hong DK, Zhang W, et al. Molecular Basis of T Cell Inactivation by CTLA-4. *Science* (1998) 282:2263–6. doi: 10.1126/science.282.5397.2263
68. Serra P, Amrani A, Yamanouchi J, Han B, Thiessen S, Utsugi T, et al. CD40 Ligation Releases Immature Dendritic Cells From the Control of Regulatory CD4+CD25+ T Cell. *Immunity* (2003) 19:877–89. doi: 10.1016/S1074-7613(03)00327-3
69. Oderup C, Cederbom L, Makowska A, Cilio CM, Ivars F. Cytotoxic T Lymphocyte Antigen-4-Dependent Down-Modulation of Costimulatory Molecules on Dendritic Cells in CD4+ CD25+ Regulatory T-Cell-Mediated Suppression. *Immunology* (2006) 118:240–9. doi: 10.1111/j.1365-2567.2006.02362.x
70. Cederbom L, Hall H, Ivars F. Stimulatory Molecules on Antigen-Presenting Cell. *Cell* (2000) 30:1538–43. doi: 10.1002/1521-4141(200006)30:6<1538::AID-IMMU1538>3.0.CO;2-X
71. Finger EB, Bluestone JA. When Ligand Becomes Receptor — Tolerance via B7 Signaling on DC. *Nat Immunol* (2002) 3:1056–7. doi: 10.1038/ni1102-1056
72. Maruhashi T, Okazaki II mi, Sugiura D, Takahashi S, Maeda TK, Shimizu K, et al. LAG-3 Inhibits the Activation of CD4 + T Cells That Recognize Stable pMHCII Through Its Conformation-Dependent Recognition of pMHCII. *Nat Immunol* (2018) 19:1415–26. doi: 10.1038/s41590-018-0217-9
73. Maeda TK, Sugiura D, Okazaki II mi, Maruhashi T, Okazaki T. Atypical Motifs in the Cytoplasmic Region of the Inhibitory Immune Co-Receptor LAG-3 Inhibit T Cell Activation. *J Biol Chem* (2019) 294:6017–26. doi: 10.1074/jbc.RA119.007455
74. Liang B, Workman C, Lee J, Chew C, Dale BM, Colonna L, et al. Regulatory T Cells Inhibit Dendritic Cells by Lymphocyte Activation Gene-3 Engagement of MHC Class II. *J Immunol* (2008) 180:5916–26. doi: 10.4049/jimmunol.180.9.5916
75. Sharpe AH, Pauken KE. The Diverse Functions of the PD1 Inhibitory Pathway. *Nat Rev Immunol* (2018) 18:153–67. doi: 10.1038/nri.2017.108
76. Sharpe AH, Wherry EJ, Ahmed R, Freeman GJ. The Function of Programmed Cell Death 1 and Its Ligands in Regulating Autoimmunity and Infection. *Nat Immunol* (2007) 8:239–45. doi: 10.1038/ni1443
77. Liu S, Zhang H, Li M, Hu D, Li C, Ge B, et al. Recruitment of Grb2 and SHIP1 by the ITT-Like Motif of TIGIT Suppresses Granule Polarization and Cytotoxicity of NK Cells. *Cell Death Differ* (2013) 20:456–64. doi: 10.1038/cdd.2012.141
78. Zhang B, Zhao W, Li H, Chen Y, Tian H, Li L, et al. Immunoreceptor TIGIT Inhibits the Cytotoxicity of Human Cytokine-Induced Killer Cells by Interacting With CD155. *Cancer Immunol Immunother* (2016) 65:305–14. doi: 10.1007/s00262-016-1799-4
79. Yu X, Harden K, Gonzalez LC, Francesco M, Chiang E, Irving B, et al. The Surface Protein TIGIT Suppresses T Cell Activation by Promoting the Generation of Mature Immunoregulatory Dendritic Cells. *Nat Immunol* (2009) 10:48–57. doi: 10.1038/ni.1674
80. Hutloff A, Dittrich AM, Beier KC, Eljaschewitsch B, Kraft R, Anagnostopoulos I, et al. ICOS Is an Inducible T-Cell Co-Stimulator Structurally and Functionally Related to CD28. *Nature* (1999) 397:263–6. doi: 10.1038/16717
81. Witsch EJ, Peiser M, Hutloff A, Bchner K, Dorner BG, Jonuleit H, et al. ICOS and CD28 Reversely Regulate IL-10 on Re-Activation of Human Effector T Cells With Mature Dendritic Cells. *Eur J Immunol* (2002) 32:2680–6. doi: 10.1002/1521-4141(200209)32:9<2680::AID-IMMU2680>3.0.CO;2-6
82. Dong C, Juedes AE, Temann UA, Shresta S, Allison JP, Ruddle NH, et al. ICOS Co-Stimulatory Receptor Is Essential for T-Cell Activation and Function. *Nature* (2001) 409:97–101. doi: 10.1038/35051100
83. Junger WG. Immune Cell Regulation by Autocrine Purinergic Signalling. *Nat Rev Immunol* (2011) 11:201–12. doi: 10.1038/nri2938
84. Colgan SP, Eltzschig HK, Eckle T, Thompson LF. Physiological Roles for Ecto-5′-Nucleotidase (CD73). *Purinergic Signal* (2006) 2:351–60. doi: 10.1007/s11302-005-5302-5
85. Allard B, Longhi MS, Robson SC, Stagg J. The Ectonucleotidases CD39 and CD73: Novel Checkpoint Inhibitor Targets. *Immunol Rev* (2017) 276:121–44. doi: 10.1111/imr.12528
86. Mandapathil M, Lang S, Gorelik E, Whiteside TL. Isolation of Functional Human Regulatory T Cells (Treg) From the Peripheral Blood Based on the CD39 Expression. *J Immunol Methods* (2009) 346:55–63. doi: 10.1016/j.jim.2009.05.004
87. Ben Addi A, Lefort A, Hua X, Libert F, Communi D, Ledent C, et al. Modulation of Murine Dendritic Cell Function by Adenine Nucleotides and Adenosine: Involvement of the A2B Receptor. *Eur J Immunol* (2008) 38:1610–20. doi: 10.1002/eji.200737781
88. Grossman WJ, Verbsky JW, Tollefsen BL, Kemper C, Atkinson JP, Ley TJ. Differential Expression of Granzymes A and B in Human Cytotoxic Lymphocyte Subsets and T Regulatory Cells. *Blood* (2004) 104:2840–8. doi: 10.1182/blood-2004-03-0859
89. Kawamura K, Kadowaki N, Kitawaki T, Uchiyama T. Virus-Stimulated Plasmacytoid Dendritic Cells Induce CD4+ Cytotoxic Regulatory T Cells. *Blood* (2006) 107:1031–8. doi: 10.1182/blood-2005-04-1737
90. Casares S, Hurtado A, McEvoy RC, Sarukhan A, von Boehmer H, Brumeanu TD. Down-Regulation of Diabetogenic CD4+ T Cells by a Soluble Dimeric Peptide-MHC Class II Chimera. *Nat Immunol* (2002) 3:383–91. doi: 10.1038/ni770
91. Masteller EL, Warner MR, Ferlin W, Judkowski V, Wilson D, Glaichenhaus N, et al. Peptide-MHC Class II Dimers as Therapeutics to Modulate Antigen-Specific T Cell Responses in Autoimmune Diabete. *J Immunol* (2003) 171:5587–95. doi: 10.4049/jimmunol.171.10.5587
92. Li L, Yi Z, Wang B, Tisch R. Suppression of Ongoing T Cell-Mediated Autoimmunity by Peptide-MHC Class II Dimer Vaccinatio. *J Immunol* (2009) 183:4809–16. doi: 10.4049/jimmunol.0901616
93. Grundström S, Cederbom L, Sundstedt A, Scheipers P, Ivars F. Superantigen-Induced Regulatory T Cells Display Different Suppressive Functions in the Presence or Absence of Natural CD4 + CD25 + Regulatory T Cells *In Vivo*. *J Immunol* (2003) 170:5008–17. doi: 10.4049/jimmunol.170.10.5008
94. Taylor AL, Llewelyn MJ. Superantigen-Induced Proliferation of Human CD4 + CD25 – T Cells Is Followed by a Switch to a Functional Regulatory Phenotyp. *J Immunol* (2010) 185:6591–8. doi: 10.4049/jimmunol.1002416
95. Metzler B, Wraith DC. Inhibition of Experimental Autoimmune Encephalomyelitis by Inhalation But Not Oral Administration of the Encephalitogenic Peptide: Influence of MHC Binding Affinity. *Int Immunol* (1993) 5:1159–65. doi: 10.1093/intimm/5.9.1159

96. Gabryšová L, Wraith DC. Antigenic Strength Controls the Generation of Antigen-Specific IL-10-Secreting T Regulatory Cells. *Eur J Immunol* (2010) 40:1386–95. doi: 10.1002/eji.200940151
97. Chang HD, Helbig C, Tykocinski L, Kreher S, Koeck J, Niesner U, et al. Expression of IL-10 in Th Memory Lymphocytes Is Conditional on IL-12 or IL-4, Unless the IL-10 Gene is Imprinted by GATA-3. *Eur J Immunol* (2007) 37:807–17. doi: 10.1002/eji.200636385
98. Saraiva M, Christensen JR, Veldhoen M, Murphy TL, Murphy KM, O'Garra A. Interleukin-10 Production by Th1 Cells Requires Interleukin-12-Induced STAT4 Transcription Factor and ERK MAP Kinase Activation by High Antigen Dos. *Immunity* (2009) 31:209–19. doi: 10.1016/j.immuni.2009.05.012
99. Motomura Y, Kitamura H, Hijikata A, Matsunaga Y, Matsumoto K, Inoue H, et al. The Transcription Factor E4BP4 Regulates the Production of IL-10 and IL-13 in CD4+ T Cells. *Nat Immunol* (2011) 12:450–9. doi: 10.1038/ni.2020
100. Levings MK, Sangregorio R, Galbiati F, Squadrone S, de Waal Malefyt R, Roncarolo M-G. IFN-α and IL-10 Induce the Differentiation of Human Type 1 T Regulatory Cell. *J Immunol* (2001) 166:5530–9. doi: 10.4049/jimmunol.166.9.5530
101. Maynard CL, Harrington LE, Janowski KM, Oliver JR, Zindl CL, Rudensky AY, et al. Regulatory T Cells Expressing Interleukin 10 Develop From Foxp3+ and Foxp3- Precursor Cells in the Absence of Interleukin 10. *Nat Immunol* (2007) 8:931–41. doi: 10.1038/ni1504
102. Levings MK, Gregori S, Tresoldi E, Cazzaniga S, Bonini C, Roncarolo MG. Differentiation of Tr1 Cells by Immature Dendritic Cells Requires IL-10 But Not CD25+CD4+ Tr Cells. *Blood* (2005) 105:1162–9. doi: 10.1182/blood-2004-03-1211
103. Shiokawa A, Tanabe K, Tsuji NM, Sato R, Hachimura S. IL-10 and IL-27 Producing Dendritic Cells Capable of Enhancing IL-10 Production of T Cells are Induced in Oral Tolerance. *Immunol Lett* (2009) 125:7–14. doi: 10.1016/j.imlet.2009.05.002
104. Comi M, Amodio G, Gregori S. Interleukin-10-Producing DC-10 Is a Unique Tool to Promote Tolerance Via Antigen-Specific T Regulatory Type 1 Cell. *Front Immunol* (2018) 9:682. doi: 10.3389/fimmu.2018.00682
105. Pflanz S, Timans JC, Cheung J, Rosales R, Kanzler H, Gilbert J, et al. IL-27, a Heterodimeric Cytokine Composed of EBI3 and P28 Protein, Induces Proliferation of Naive CD4+T Cells. *Immunity* (2002) 16:779–90. doi: 10.1016/S1074-7613(02)00324-2
106. Murugaiyan G, Mittal A, Lopez-Diego R, Maier LM, Anderson DE, Weiner HL. IL-27 Is a Key Regulator of IL-10 and IL-17 Production by Human CD4 + T Cell. *J Immunol* (2009) 183:2435–43. doi: 10.4049/jimmunol.0900568
107. Sun J, Dodd H, Moser EK, Sharma R, Braciale TJ. CD4+ T Cell Help and Innate-Derived IL-27 Induce Blimp-1-Dependent IL-10 Production by Antiviral CTL. *Nat Immunol* (2011) 12:327–35. doi: 10.1038/ni.1996
108. Wang S, Miyazaki Y, Shinozaki Y, Yoshida H. Augmentation of Antigen-Presenting and Th1-Promoting Functions of Dendritic Cells by WSX-1(IL-27r) Deficienc. *J Immunol* (2007) 179:6421–8. doi: 10.4049/jimmunol.179.10.6421
109. Yoshimoto T, Yoshimoto T, Yasuda K, Mizuguchi J, Nakanishi K. IL-27 Suppresses Th2 Cell Development and Th2 Cytokines Production From Polarized Th2 Cells: A Novel Therapeutic Way for Th2-Mediated Allergic Inflammatio. *J Immunol* (2007) 179:4415–23. doi: 10.4049/jimmunol.179.7.4415
110. Batten M, Li J, Yi S, Kljavin NM, Danilenko DM, Lucas S, et al. Interleukin 27 Limits Autoimmune Encephalomyelitis by Suppressing the Development of Interleukin 17-Producing T Cells. *Nat Immunol* (2006) 7:929–36. doi: 10.1038/ni1375
111. Awasthi A, Carrier Y, Peron JPS, Bettelli E, Kamanaka M, Flavell RA, et al. A Dominant Function for Interleukin 27 in Generating Interleukin 10-Producing Anti-Inflammatory T Cells. *Nat Immunol* (2007) 8:1380–9. doi: 10.1038/ni1541
112. Stumhofer JS, Silver JS, Laurence A, Porrett PM, Harris TH, Turka LA, et al. Interleukins 27 and 6 Induce STAT3-Mediated T Cell Production of Interleukin 10. *Nat Immunol* (2007) 8:1363–71. doi: 10.1038/ni1537
113. Wang H, Meng R, Li Z, Yang B, Liu Y, Huang F, et al. IL-27 Induces the Differentiation of Tr1-Like Cells From Human Naive CD4+T Cells *via* the Phosphorylation of STAT1 and STAT3. *Immunol Lett* (2011) 136:21–8. doi: 10.1016/j.imlet.2010.11.007
114. Spolski R, Leonard WJ. Interleukin-21: Basic Biology and Implications for Cancer and Autoimmunit. *Annu Rev Immunol* (2008) 26:57–79. doi: 10.1146/annurev.immunol.26.021607.090316
115. Parrish-Novak J, Dillon SR, Nelson A, Hammond A, Sprecher C, Gross JA, et al. Interleukin 21 and Its Receptor Are Involved in NK Cell Expansion and Regulation of Lymphocyte Function. *Nature* (2000) 408:57–63. doi: 10.1038/35040504
116. Ozaki K, Spolski R, Feng CG, Qi CF, Cheng J, Sher A, et al. A Critical Role for IL-21 in Regulating Immunoglobulin Production. *Science* (2002) 298:1630–4. doi: 10.1126/science.1077002
117. Ozaki K, Spolski R, Ettinger R, Kim H-P, Wang G, Qi C-F, et al. Regulation of B Cell Differentiation and Plasma Cell Generation by IL-21, A Novel Inducer of Blimp-1 and Bcl-6. *J Immunol* (2004) 173:5361–71. doi: 10.4049/jimmunol.173.9.5361
118. Vogelzang A, McGuire HM, Yu D, Sprent J, Mackay CR, King C. A Fundamental Role for Interleukin-21 in the Generation of T Follicular Helper Cell. *Immunity* (2008) 29:127–37. doi: 10.1016/j.immuni.2008.06.001
119. Zeng R, Spolski R, Finkelstein SE, Oh SK, Kovanen PE, Hinrichs CS, et al. Synergy of IL-21 and IL-15 in Regulating CD8+ T Cell Expansion and Function. *J Exp Med* (2005) 201:139–48. doi: 10.1084/jem.20041057
120. Jin H, Carrio R, Yu A, Malek TR. Distinct Activation Signals Determine Whether IL-21 Induces B Cell Costimulation, Growth Arrest, or Bim-Dependent Apoptosi. *J Immunol* (2004) 173:657–65. doi: 10.4049/jimmunol.173.1.657
121. Brandt K, Bulfone-Paus S, Foster DC, Rückert R. Interleukin-21 Inhibits Dendritic Cell Activation and Maturation. *Blood* (2003) 102:4090–8. doi: 10.1182/blood-2003-03-0669
122. Spolski R, Kim H-P, Zhu W, Levy DE, Leonard WJ. IL-21 Mediates Suppressive Effects *via* Its Induction of IL-10. *J Immunol* (2009) 182:2859–67. doi: 10.4049/jimmunol.0802978
123. Umeshappa CS, Solé P, Surewaard BGJ, Mohopatra S, Yamanouchi J, Uddin MM, et al. Liver-Specific T-Regulatory Type 1 Cells Program Local Neutrophils to Suppress Hepatic Autoimmunity *via* Cram. *Cell Rep* (2021) 34(13):108919. doi: 10.1016/j.celrep.2021.108919
124. Greenwald RJ, Freeman GJ, Sharpe AH. The B7 Family Revisite. *Annu Rev Immunol* (2005) 23:515–48. doi: 10.1146/annurev.immunol.23.021704.115611
125. Nurieva RI, Chung Y, Hwang D, Yang XO, Kang HS, Ma L, et al. Generation of T Follicular Helper Cells Is Mediated by Interleukin-21 But Independent of T Helper 1, 2, or 17 Cell Lineage. *Immunity* (2008) 29:138–49. doi: 10.1016/j.immuni.2008.05.009.Generation
126. Choi YS, Kageyama R, Eto D, Escobar TC, Johnston RJ, Monticelli L, et al. ICOS Receptor Instructs T Follicular Helper Cell Versus Effector Cell Differentiation *via* Induction of the Transcriptional Repressor Bcl6. *Immunity* (2011) 34:932–46. doi: 10.1016/j.immuni.2011.03.023
127. Nurieva RI, Duong J, Kishikawa H, Dianzani U, Rojo JM, Ho IC, et al. Transcriptional Regulation of Th2 Differentiation by Inducible Costimulator. *Immunity* (2003) 18:801–11. doi: 10.1016/S1074-7613(03)00144-4
128. Serada S, Fujimoto M, Mihara M, Koike N, Ohsugi Y, Nomura S, et al. IL-6 Blockade Inhibits the Induction of Myelin Antigen-Specific Th17 Cells and Th1 Cells in Experimental Autoimmune Encephalomyelitis. *Proc Natl Acad Sci USA* (2008) 105:9041–6. doi: 10.1073/pnas.0802218105
129. Fonseca JE, Santos MJ, Canhão H, Choy E. Interleukin-6 as a Key Player in Systemic Inflammation and Joint Destruction. *Autoimmun Rev* (2009) 8:538–42. doi: 10.1016/j.autrev.2009.01.012
130. Lindroos J, Svensson L, Norsgaard H, Lovato P, Moller K, Hagedorn PH, et al. IL-23-Mediated Epidermal Hyperplasia Is Dependent on IL-6. *J Invest Dermatol* (2011) 131:1110–8. doi: 10.1038/jid.2010.432
131. Hiramatsu Y, Suto A, Kashiwakuma D, Kanari H, Kagami S, Ikeda K, et al. C-Maf Activates the Promoter and Enhancer of the IL-21 Gene, and TGF-β Inhibits C-Maf-Induced IL-21 Production in CD4 + T Cells. *J Leukoc Biol* (2010) 87:703–12. doi: 10.1189/jlb.0909639
132. Dicosmo BF, Picarella D, Ravell RA. Local Production of Human IL-6 Promotes Insulitis But Retards the Onset of Insulin-Dependent Diabetes Mellitus in Non-Obese Diabetic Mice. *Int Immunol* (1994) 6:1829–37. doi: 10.1093/intimm/6.12.1829
133. Grivennikov S, Karin E, Terzic J, Mucida D, Yu GY, Vallabhapurapu S, et al. IL-6 and Stat3 Are Required for Survival of Intestinal Epithelial Cells And Development of Colitis-Associated Cance. *Cancer Cell* (2009) 15:103–13. doi: 10.1016/j.ccr.2009.01.001

134. Balto K, Sasaki H, Stashenko P. Interleukin-6 Deficiency Increases Inflammatory Bone Destruction. *Infect Immun* (2001) 69:744–50. doi: 10.1128/IAI.69.2.744-750.2001
135. McGeachy MJ, Bak-Jensen KS, Chen Y, Tato CM, Blumenschein W, McClanahan T, et al. TGF-β and IL-6 Drive the Production of IL-17 and IL-10 by T Cells and Restrain TH-17 Cell-Mediated Pathology. *Nat Immunol* (2007) 8:1390–7. doi: 10.1038/ni1539
136. Jin JO, Han X, Yu Q. Interleukin-6 Induces the Generation of IL-10-Producing Tr1 Cells and Suppresses Autoimmune Tissue Inflammation. *J Autoimmun* (2013) 40:28–44. doi: 10.1016/j.jaut.2012.07.009
137. Novick D, Cohen B, Rubinstein M. The Human Interferon α β Receptor: Characterization and Molecular Cloning. *Cell* (1994) 77:391–400. doi: 10.1016/0092-8674(94)90154-6
138. Guarda G, Braun M, Staehli F, Tardivel A, Mattmann C, Förster I, et al. Type I Interferon Inhibits Interleukin-1 Production and Inflammasome Activatio. *Immunity* (2011) 34:213–23. doi: 10.1016/j.immuni.2011.02.006
139. Hu X, Paik PK, Chen J, Yarilina A, Kockeritz L, Lu TT, et al. IFN-γ Suppresses IL-10 Production and Synergizes With TLR2 by Regulating GSK3 and CREB/AP-1 Protein. *Immunity* (2006) 24:563–74. doi: 10.1016/j.immuni.2006.02.014
140. Garcia CA, Benakanakere MR, Alard P, Kosiewicz MM, Kinane DF, Martin M. Antigenic Experience Dictates Functional Role of Glycogen Synthase Kinase-3 in Human CD4 + T Cell Response. *J Immunol* (2008) 181:8363–71. doi: 10.4049/jimmunol.181.12.8363
141. Aman MJ, Tretter T, Eisenbeis I, Bug G, Decker T, Aulitzky WE, et al. Interferon-Alpha Stimulates Production of Interleukin-10 in Activated CD4+ T Cells and Monocytes. *Blood* (1996) 87:4731–6. doi: 10.1182/blood.V87.11.4731.bloodjournal87114731
142. McRae BL, Semnani RT, Hayes MP, van Seventer GA. Type I IFNs Inhibit Human Dendritic Cell IL-12 Production and Th1 Cell Development. *J Immunol* (1998) 160:4298–304.
143. Ma A, Boone DL, Lodolce JP. The Pleiotropic Functions of Interleukin 15: Not So Interleukin 2-Like After All. *J Exp Med* (2000) 191:753–5. doi: 10.1084/jem.191.5.753
144. Waldmann T, Tagaya Y, Bamford R. Interleukin-2, Interleukin-15, and Their Receptors. *Int Rev Immunol* (1998) 16:205–26. doi: 10.3109/08830189809042995
145. Bulfone-Paus S, Ungureanu D, Pohl T, Lindner G, Paus R, Rückert R, et al. Interleukin-15 Protects From Lethal Apoptosis *In Vivo*. *Nat Med* (1997) 3:1124–8. doi: 10.1038/nm1097-1124
146. Ku CC, Murakami M, Sakamoto A, Kappler J, Marrack P. Control of Homeostasis of CD8+ Memory T Cells by Opposing Cytokines. *Science* (2000) 288:675–8. doi: 10.1126/science.288.5466.675
147. Tough DF, Sun S, Zhang X, Sprent J. Stimulation of Memory T Cells by Cytokines. *Vaccine* (2000) 18:1642–8. doi: 10.1016/S0264-410X(99)00500-9
148. Bacchetta R, Sartirana C, Levings MK, Bordignon C, Narula S, Roncarolo MG. Growth and Expansion of Human T Regulatory Type 1 Cells Are Independent From TCR Activation But Require Exogenous Cytokines. *Eur J Immunol* (2002) 32:2237–45. doi: 10.1002/1521-4141(200208)32:8<2237::AID-IMMU2237>3.0.CO;2-2
149. Chow KPN, Lee JM, Qiu JT, Liao SK, Lin SC, Hsu SL, et al. Enhanced IL-10 Production by CD4 + T Cells Primed in IL-15rα-Deficient Mice. *Eur J Immunol* (2011) 41:3146–56. doi: 10.1002/eji.201141746
150. Giri JG, Kumaki S, Ahdieh M, Friend DJ, Loomis A, Shanebeck K, et al. Identification and Cloning of a Novel IL-15 Binding Protein That Is Structurally Related to the Alpha Chain of the IL-2 Receptor. *EMBO J* (1995) 14:3654–63. doi: 10.1002/j.1460-2075.1995.tb00035.x
151. Waldmann TA, Tagaya Y. The Multifaced Regulation of Interleukin-15 Expression an the Role of This Cytokine in NK Cell Differentiation and Host Response to Intracellular Pathogens. *Annu Rev Immunol* (1999) 17:19–49. doi: 10.1146/annurev.immunol.17.1.19
152. Papiernik M. Natural CD4+ CD25+ Regulatory T Cells. Their Role in the Control of Superantigen Responses. *Immunol Rev* (2001) 182:180–9. doi: 10.1034/j.1600-065X.2001.1820114.x
153. Anderson PO, Sundstedt A, Yazici Z, Minaee S, Woolf R, Nicolson K, et al. IL-2 Overcomes the Unresponsiveness But Fails to Reverse the Regulatory Function of Antigen-Induced T Regulatory Cell. *J Immunol* (2005) 174:310–9. doi: 10.4049/jimmunol.174.1.310
154. Tsuji-Takayama K, Suzuki M, Yamamoto M, Harashima A, Okochi A, Otani T, et al. The Production of IL-10 by Human Regulatory T Cells Is Enhanced by IL-2 Through a STAT5-Responsive Intronic Enhancer in the IL-10 Locu. *J Immunol* (2008) 181:3897–905. doi: 10.4049/jimmunol.181.6.3897
155. Kasprzycka M, Zhang Q, Witkiewicz A, Marzec M, Potoczek M, Liu X, et al. γc-Signaling Cytokines Induce a Regulatory T Cell Phenotype in Malignant CD4 + T Lymphocyte. *J Immunol* (2008) 181:2506–12. doi: 10.4049/jimmunol.181.4.2506
156. Andreotti AH, Schwartzberg PL, Joseph RE, Berg LJ. T-Cell Signaling Regulated by the Tec Family Kinase, It. *Cold Spring Harb Perspect Biol* (2010) 2:1–22. doi: 10.1101/cshperspect.a002287
157. Ahyi A-NN, Chang H-C, Dent AL, Nutt SL, Kaplan MH. IFN Regulatory Factor 4 Regulates the Expression of a Subset of Th2 Cytokine. *J Immunol* (2009) 183:1598–606. doi: 10.4049/jimmunol.0803302
158. Kwon H, Thierry-Mieg D, Thierry-Mieg J, Kim HP, Oh J, Tunyaplin C, et al. Analysis of Interleukin-21-Induced Prdm1 Gene Regulation Reveals Functional Cooperation of STAT3 and IRF4 Transcription Factor. *Immunity* (2009) 31:941–52. doi: 10.1016/j.immuni.2009.10.008
159. Cretney E, Xin A, Shi W, Minnich M, Masson F, Miasari M, et al. The Transcription Factors Blimp-1 and IRF4 Jointly Control the Differentiation and Function of Effector Regulatory T Cells. *Nat Immunol* (2011) 12:304–12. doi: 10.1038/ni.2006
160. Kim JI, Ho IC, Grusby MJ, Glimcher LH. The Transcription Factor C-Maf Controls the Production of Interleukin-4 But Not Other Th2 Cytokines. *Immunity* (1999) 10:745–51. doi: 10.1016/S1074-7613(00)80073-4
161. Zhu J, Yamane H, Paul WE. Differentiation of Effector CD4 T Cell Population. *Annu Rev Immunol* (2010) 28:445–89. doi: 10.1146/annurev-immunol-030409-101212
162. Kroenke MA, Eto D, Locci M, Cho M, Davidson T, Haddad EK, et al. Bcl6 and Maf Cooperate To Instruct Human Follicular Helper CD4 T Cell Differentiatio. *J Immunol* (2012) 188:3734–44. doi: 10.4049/jimmunol.1103246
163. Harris JE, Bishop KD, Phillips NE, Mordes JP, Greiner DL, Rossini AA, et al. Early Growth Response Gene-2, a Zinc-Finger Transcription Factor, Is Required for Full Induction of Clonal Anergy in CD4 + T Cell. *J Immunol* (2004) 173:7331–8. doi: 10.4049/jimmunol.173.12.7331
164. Crotty S, Johnston RJ, Schoenberger SP. Effectors and Memories: Bcl-6 and Blimp-1 in T and B Lymphocyte Differentiation. *Nat Immunol* (2010) 11:114–20. doi: 10.1038/ni.1837
165. Martins G, Calame K. Regulation and Functions of Blimp-1 in T and B Lymphocyte. *Annu Rev Immunol* (2008) 26:133–69. doi: 10.1146/annurev.immunol.26.021607.090241
166. Neumann C, Heinrich F, Neumann K, Junghans V, Mashreghi MF, Ahlers J, et al. Role of Blimp-1 in Programing Th Effector Cells Into IL-10 Producers. *J Exp Med* (2014) 211:1807–19. doi: 10.1084/jem.20131548
167. Karwacz K, Miraldi ER, Pokrovskii M, Madi A, Yosef N, Wortman I, et al. Critical Role of IRF1 and BATF in Forming Chromatin Landscape During Type 1 Regulatory Cell Differentiation. *Nat Immunol* (2017) 18:412–21. doi: 10.1038/ni.3683
168. Schraml BU, Hildner K, Ise W, Lee WL, Smith WAE, Solomon B, et al. The AP-1 Transcription Factor Batf Controls T H 17 Differentiation. *Nature* (2009) 460:405–9. doi: 10.1038/nature08114
169. Ellyard JI, Vinuesa CG. A BATF-Ling Connection Between B Cells and Follicular Helper T Cells. *Nat Immunol* (2011) 12:519–20. doi: 10.1038/ni.2042
170. Betz BC, Jordan-Williams KL, Wang C, Kang SG, Liao J, Logan MR, et al. Batf Coordinates Multiple Aspects of B and T Cell Function Required for Normal Antibody Responses. *J Exp Med* (2010) 207:933–42. doi: 10.1084/jem.20091548
171. Ciofani M, Madar A, Galan C, Sellars M, Mace K, Pauli F, et al. A Validated Regulatory Network for Th17 Cell Specification. *Cell* (2012) 151:289–303. doi: 10.1016/j.cell.2012.09.016
172. Kurachi M, Barnitz RA, Yosef N, Odorizzi PM, Diiorio MA, Lemieux ME, et al. The Transcription Factor BATF Operates as an Essential Differentiation Checkpoint in Early Effector CD8 + T Cells. *Nat Immunol* (2014) 15:373–83. doi: 10.1038/ni.2834
173. Ise W, Kohyama M, Schraml BU, Zhang T, Schwer B, Basu U, et al. The Transcription Factor BATF Controls the Global Regulators of Class-Switch

Recombination in Both B Cells and T Cells. *Nat Immunol* (2011) 12:536–43. doi: 10.1038/ni.2037
174. Zhang P, Lee JS, Gartlan KH, Schuster IS, Comerford I, Varelias A, et al. Eomesodermin Promotes the Development of Type 1 Regulatory T (TR1) Cells. *Sci Immunol* (2017) 2. doi: 10.1126/sciimmunol.aah7152
175. Dejean AS, Joulia E, Walzer T. The Role of Eomes in Human CD4 T Cell Differentiation: A Question of Context. *Eur J Immunol* (2019) 49:38–41. doi: 10.1002/eji.201848000
176. Farez MFF, Mascanfroni IDD, Méndez-Huergo SPP, Yeste A, Murugaiyan G, Garo LPP, et al. Melatonin Contributes to the Seasonality of Multiple Sclerosis Relapse. *Cell* (2015) 162:1338–52. doi: 10.1016/j.cell.2015.08.025
177. Im SH, Hueber A, Monticelli S, Kang KH, Rao A. Chromatin-Level Regulation of the IL10 Gene in T Cells. *J Biol Chem* (2004) 279:46818–25. doi: 10.1074/jbc.M401722200
178. Miraldi ER, Pokrovskii M, Watters A, Castro DM, De Veaux N, Hall JA, et al. Leveraging Chromatin Accessibility for Transcriptional Regulatory Network Inference in T Helper 17 Cell. *Genome Res* (2019) 29:449–63. doi: 10.1101/gr.238253.118
179. Wei L, Vahedi G, Sun HW, Watford WT, Takatori H, Ramos HL, et al. Discrete Roles of STAT4 and STAT6 Transcription Factors in Tuning Epigenetic Modifications and Transcription During T Helper Cell Differentiation. *Immunity* (2010) 32:840–51. doi: 10.1016/j.immuni.2010.06.003
180. Li P, Spolski R, Liao W, Wang L, Murphy TL, Murphy KM, et al. BATF-JUN Is Critical for IRF4-Mediated Transcription in T Cells. *Nature* (2012) 490:543–6. doi: 10.1038/nature11530
181. Lee CG, Hwang W, Maeng KE, Kwon HK, So JS, Sahoo A, et al. IRF4 Regulates IL-10 Gene Expression in CD4+ T Cells Through Differential Nuclear Translocation. *Cell Immunol* (2011) 268:97–104. doi: 10.1016/j.cellimm.2011.02.008
182. Vahedi G, Takahashi H, Nakayamada S, Sun HW, Sartorelli V, Kanno Y, et al. STATs Shape the Active Enhancer Landscape of T Cell Populations. *Cell* (2012) 151:981–93. doi: 10.1016/j.cell.2012.09.044
183. Shoemaker J, Saraiva M, O'Garra A. GATA-3 Directly Remodels the IL-10 Locus Independently of IL-4 in CD4 + T Cell. *J Immunol* (2006) 176:3470–9. doi: 10.4049/jimmunol.176.6.3470
184. Samstein RM, Arvey A, Josefowicz SZ, Peng X, Reynolds A, Sandstrom R, et al. Foxp3 Exploits a Pre-Existent Enhancer Landscape for Regulatory T Cell Lineage Specification. *Cell* (2012) 151:153–66. doi: 10.1016/j.cell.2012.06.053
185. Hossain DMS, Panda AK, Manna A, Mohanty S, Bhattacharjee P, Bhattacharyya S, et al. FoxP3 Acts as a Cotranscription Factor With STAT3 in Tumor-Induced Regulatory T Cell. *Immunity* (2013) 39:1057–69. doi: 10.1016/j.immuni.2013.11.005
186. Lee C-G, Kwon H-K, Sahoo A, Hwang W, So J-S, Hwang J-S, et al. Interaction of Ets-1 With HDAC1 Represses IL-10 Expression in Th1 Cell. *J Immunol* (2012) 188:2244–53. doi: 10.4049/jimmunol.1101614
187. Grenningloh R, Bok YK, Ho IC. Ets-1, A Functional Cofactor of T-Bet, is Essential for Th1 Inflammatory Responses. *J Exp Med* (2005) 201:615–26. doi: 10.1084/jem.20041330
188. Lee MT, Bonneau AR, Giraldez AJ. Zygotic Genome Activation During the Maternal-To-Zygotic Transitio. *Annu Rev Cell Dev Biol* (2014) 30:581–613. doi: 10.1146/annurev-cellbio-100913-013027
189. Tang WWC, Kobayashi T, Irie N, Dietmann S, Surani MA. Specification and Epigenetic Programming of the Human Germ Line. *Nat Rev Genet* (2016) 17:585–600. doi: 10.1038/nrg.2016.88
190. Weinberger L, Ayyash M, Novershtern N, Hanna JH. Dynamic Stem Cell States: Naive to Primed Pluripotency in Rodents and Humans. *Nat Rev Mol Cell Biol* (2016) 17:155–69. doi: 10.1038/nrm.2015.28
191. Hackett JA, Azim Surani M. Regulatory Principles of Pluripotency: From the Ground State Up. *Cell Stem Cell* (2014) 15:416–30. doi: 10.1016/j.stem.2014.09.015
192. Smith ZD, Meissner A. DNA Methylation: Roles in Mammalian Development. *Nat Rev Genet* (2013) 14:204–20. doi: 10.1038/nrg3354
193. Stergachis AB, Neph S, Reynolds A, Humbert R, Miller B, Paige SL, et al. Developmental Fate and Cellular Maturity Encoded in Human Regulatory DNA Landscapes. *Cell* (2013) 154:888–903. doi: 10.1016/j.cell.2013.07.020
194. Ostuni R, Piccolo V, Barozzi I, Polletti S, Termanini A, Bonifacio S, et al. Latent Enhancers Activated by Stimulation in Differentiated Cells. *Cell* (2013) 152:157–71. doi: 10.1016/j.cell.2012.12.018
195. Ramos-Rodríguez M, Raurell-Vila H, Colli ML, Alvelos MI, Subirana-Granés M, Juan-Mateu J, et al. The Impact of Proinflammatory Cytokines on the β-Cell Regulatory Landscape Provides Insights Into the Genetics of Type 1 Diabetes. *Nat Genet* (2019) 51:1588–95. doi: 10.1038/s41588-019-0524-6
196. Onengut-Gumuscu S, Chen WM, Burren O, Cooper NJ, Quinlan AR, Mychaleckyj JC, et al. Fine Mapping of Type 1 Diabetes Susceptibility Loci and Evidence for Colocalization of Causal Variants With Lymphoid Gene Enhancers. *Nat Genet* (2015) 47:381–6. doi: 10.1038/ng.3245
197. Farh KKH, Marson A, Zhu J, Kleinewietfeld M, Housley WJ, Beik S, et al. Genetic and Epigenetic Fine Mapping of Causal Autoimmune Disease Variants. *Nature* (2015) 518:337–43. doi: 10.1038/nature13835
198. Fasolino M, Goldman N, Wang W, Cattau B, Zhou Y, Petrovic J, et al. Genetic Variation in Type 1 Diabetes Reconfigures the 3D Chromatin Organization of T Cells and Alters Gene Expressio. *Immunity* (2020) 52:257–74.e11. doi: 10.1016/j.immuni.2020.01.003
199. Flannick J, Florez JC. Type 2 Diabetes: Genetic Data Sharing to Advance Complex Disease Research. *Nat Rev Genet* (2016) 17:535–49. doi: 10.1038/nrg.2016.56
200. Fuchsberger C, Flannick J, Teslovich TM, Mahajan A, Agarwala V, Gaulton KJ, et al. The Genetic Architecture of Type 2 Diabetes. *Nature* (2016) 536:41–7. doi: 10.1038/nature18642
201. Whyte WA, Orlando DA, Hnisz D, Abraham BJ, Lin CY, Kagey MH, et al. Master Transcription Factors and Mediator Establish Super-Enhancers at Key Cell Identity Genes. *Cell* (2013) 153:307–19. doi: 10.1016/j.cell.2013.03.035
202. Gaulton KJ, Nammo T, Pasquali L, Simon JM, Giresi PG, Fogarty MP, et al. A Map of Open Chromatin in Human Pancreatic Islets. *Nat Genet* (2010) 42:255–9. doi: 10.1038/ng.530
203. Pasquali L, Gaulton KJ, Rodríguez-Seguí SA, Mularoni L, Miguel-Escalada I, Akerman I, et al. Pancreatic Islet Enhancer Clusters Enriched in Type 2 Diabetes Risk-Associated Variants. *Nat Genet* (2014) 46:136–43. doi: 10.1038/ng.2870
204. Miguel-Escalada I, Bonàs-Guarch S, Cebola I, Ponsa-Cobas J, Mendieta-Esteban J, Atla G, et al. Human Pancreatic Islet Three-Dimensional Chromatin Architecture Provides Insights Into the Genetics of Type 2 Diabetes. *Nat Genet* (2019) 51:1137–48. doi: 10.1038/s41588-019-0457-0
205. Sellars M, Huh JR, Day K, Issuree PD, Galan C, Gobeil S, et al. Regulation of DNA Methylation Dictates Cd4 Expression During the Development of Helper and Cytotoxic T Cell Lineages. *Nat Immunol* (2015) 16:746–54. doi: 10.1038/ni.3198
206. Bevington SL, Cauchy P, Piper J, Bertrand E, Lalli N, Jarvis RC, et al. Inducible Chromatin Priming Is Associated With the Establishment of Immunological Memory in T Cells. *EMBO J* (2016) 35:515–35. doi: 10.15252/embj.201592534
207. Djuretic IM, Levanon D, Negreanu V, Groner Y, Rao A, Ansel KM. Transcription Factors T-Bet and Runx3 Cooperate to Activate Ifng and Silence Il4 in T Helper Type 1 Cells. *Nat Immunol* (2007) 8:145–53. doi: 10.1038/ni1424
208. Mullen AC, Hutchins AS, High FA, Lee HW, Sykes KJ, Chodosh LA, et al. Hlx Is Induced by and Genetically Interacts With T-Bet to Promote Heritable THI Gene Induction. *Nat Immunol* (2002) 3:652–8. doi: 10.1038/ni807
209. Usui T, Preiss JC, Kanno Y, Zheng JY, Bream JH, O'Shea JJ, et al. T-Bet Regulates Th1 Responses Through Essential Effects on GATA-3 Function Rather Than on IFNG Gene Acetylation and Transcription. *J Exp Med* (2006) 203:755–66. doi: 10.1084/jem.20052165
210. Schoenborn JR, Dorschner MO, Sekimata M, Santer DM, Shnyreva M, Fitzpatrick DR, et al. Comprehensive Epigenetic Profiling Identifies Multiple Distal Regulatory Elements Directing Transcription of the Gene Encoding Interferon-γ. *Nat Immunol* (2007) 8:732–42. doi: 10.1038/ni1474
211. Hatton RD, Harrington LE, Luther RJ, Wakefield T, Janowski KM, Oliver JR, et al. A Distal Conserved Sequence Element Controls Ifng Gene Expression by T Cells and NK Cell. *Immunity* (2006) 25:717–29. doi: 10.1016/j.immuni.2006.09.007

212. Lee DU, Avni O, Chen L, Rao A. A Distal Enhancer in the Interferon-γ (IFN-γ) Locus Revealed by Genome Sequence Comparison. *J Biol Chem* (2004) 279:4802–10. doi: 10.1074/jbc.M307904200
213. Shnyreva M, Weaver WM, Blanchette M, Taylor SL, Tompa M, Fitzpatrick DR, et al. Evolutionarily Conserved Sequence Elements That Positively Regulate IFN-γ Expression in T Cells. *Proc Natl Acad Sci USA* (2004) 101:12622–7. doi: 10.1073/pnas.0400849101
214. Chen GY, Osada H, Santamaria-Babi LF, Kannagi R. Interaction of GATA-3/T-Bet Transcription Factors Regulates Expression of Sialil Lewis X Homing Receptors on Th1/Th2 Lymphocytes. *Proc Natl Acad Sci USA* (2006) 103:16894–9. doi: 10.1073/pnas.0607926103
215. Miller SA, Huang AC, Miazgowicz MM, Brassil MM, Weinmann AS. Coordinated But Physically Separable Interaction With H3K27-Demethylase and H3K4-Methyltransferase Activities Are Required for T-Box Protein-Mediated Activation of Developmental Gene Expression. *Genes Dev* (2008) 22:2980–93. doi: 10.1101/gad.1689708
216. Jones B, Chen J. Inhibition of IFN-γ Transcription by Site-Specific Methylation During T Helper Cell Development. *EMBO J* (2006) 25:2443–52. doi: 10.1038/sj.emboj.7601148
217. Chang S, Aune TM. Dynamic Changes in Histone-Methylation "Marks" Across the Locus Encoding Interferon-γ During the Differentiation of T Helper Type 2 Cells. *Nat Immunol* (2007) 8:723–31. doi: 10.1038/ni1473
218. Ansel KM, Djuretic I, Tanasa B, Rao A. Regulation of Th2 Differentiation and Il4 Locus Accessibility. *Annu Rev Immunol* (2006) 24:607–56. doi: 10.1146/annurev.immunol.23.021704.115821
219. Tykocinski LO, Hajkova P, Chang HD, Stamm T, Sözeri O, Löhning M, et al. A Critical Control Element for Interleukin-4 Memory Expression in T Helper Lymphocytes. *J Biol Chem* (2005) 280:28177–85. doi: 10.1074/jbc.M502038200
220. Avni O, Lee D, Macian F, Szabo SJ, Glimcher LH, Rao A. Th Cell Differentiation is Accompanied by Dynamic Changes in Histone Acetylation of Cytokine Genes. *Nat Immunol* (2002) 3:643–51. doi: 10.1038/ni808
221. Fields PE, Kim ST, Flavell RA. Cutting Edge: Changes in Histone Acetylation at the IL-4 and IFN-γ Loci Accompany Th1/Th2 Differentiation. *J Immunol* (2002) 169:647–50. doi: 10.4049/jimmunol.169.2.647
222. Koyanagi M, Baguet A, Martens J, Margueron R, Jenuwein T, Bix M. EZH2 and Histone 3 Trimethyl Lysine 27 Associated With Il4 and Il13 Gene Silencing in TH1 Cells. *J Biol Chem* (2005) 280:31470–7. doi: 10.1074/jbc.M504766200
223. Yamashita M, Hirahara K, Shinnakasu R, Hosokawa H, Norikane S, Kimura MY, et al. Crucial Role of MLL for the Maintenance of Memory T Helper Type 2 Cell Response. *Immunity* (2006) 24:611–22. doi: 10.1016/j.immuni.2006.03.017
224. Hutchins AS, Mullen AC, Lee HW, Sykes KJ, High FA, Hendrich BD, et al. Gene Silencing Quantitatively Controls the Function of a Developmental Trans-Activator. *Mol Cell* (2002) 10:81–91. doi: 10.1016/S1097-2765(02)00564-6
225. Makar KW, Pérez-Melgosa M, Shnyreva M, Weaver WM, Fitzpatrick DR, Wilson CB. Active Recruitment of DNA Methyltransferases Regulates Interleukin 4 in Thymocytes and T Cells. *Nat Immunol* (2003) 4:1183–90. doi: 10.1038/ni1004
226. Wurster AL, Pazin MJ. BRG1-Mediated Chromatin Remodeling Regulates Differentiation and Gene Expression of T Helper Cell. *Mol Cell Biol* (2008) 28:7274–85. doi: 10.1128/mcb.00835-08
227. Ivanov II, Zhou L, Littman DR. Transcriptional Regulation of Th17 Cell Differentiation. *Semin Immunol* (2007) 19:409–17. doi: 10.1016/j.smim.2007.10.011
228. McGeachy MJ, Cua DJ. Th17 Cell Differentiation: The Long and Winding Roa. *Immunity* (2008) 28:445–53. doi: 10.1016/j.immuni.2008.03.001
229. Zhou L, Lopes JE, Chong MMW, Ivanov II, Min R, Victora GD, et al. TGF-β-Induced Foxp3 Inhibits TH17 Cell Differentiation by Antagonizing Rorγt Function. *Nature* (2008) 453:236–40. doi: 10.1038/nature06878
230. Dong C. TH17 Cells in Development: An Updated View of Their Molecular Identity and Genetic Programming. *Nat Rev Immunol* (2008) 8:337–48. doi: 10.1038/nri2295
231. Akimzhanov AM, Yang XO, Dong C. Chromatin Remodeling of Interleukin-17 (IL-17)-IL-17F Cytokine Gene Locus During Inflammatory Helper T Cell Differentiation. *J Biol Chem* (2007) 282:5969–72. doi: 10.1074/jbc.C600322200
232. Yang XO, Pappu BP, Nurieva R, Akimzhanov A, Kang HS, Chung Y, et al. T Helper 17 Lineage Differentiation Is Programmed by Orphan Nuclear Receptors Rorα and Rorγ. *Immunity* (2008) 28:29–39. doi: 10.1016/j.immuni.2007.11.016
233. Johnston RJ, Poholek AC, DiToro D, Yusuf I, Eto D, Barnett B, et al. Bcl6 and Blimp-1 Are Reciprocal and Antagonistic Regulators of T Follicular Helper Cell Differentiation. *Science* (2009) 325:1006–10. doi: 10.1126/science.1175870
234. Poholek AC, Hansen K, Hernandez SG, Eto D, Chandele A, Weinstein JS, et al. In Vivo Regulation of Bcl6 and T Follicular Helper Cell Development. *J Immunol* (2010) 185:313–26. doi: 10.4049/jimmunol.0904023
235. Lu KT, Kanno Y, Cannons JL, Handon R, Bible P, Elkahloun AG, et al. Functional and Epigenetic Studies Reveal Multistep Differentiation and Plasticity of In Vitro-Generated and In Vivo-Derived Follicular T Helper Cell. *Immunity* (2011) 35:622–32. doi: 10.1016/j.immuni.2011.07.015
236. Cannons JL, Lu KT, Schwartzberg PL. T Follicular Helper Cell Diversity and Plasticity. *Trends Immunol* (2013) 34:200–7. doi: 10.1016/j.it.2013.01.001
237. Kitagawa Y, Ohkura N, Kidani Y, Vandenbon A, Hirota K, Kawakami R, et al. Guidance of Regulatory T Cell Development by Satb1-Dependent Super-Enhancer Establishment. *Nat Immunol* (2017) 18:173–83. doi: 10.1038/ni.3646
238. Toker A, Engelbert D, Garg G, Polansky JK, Floess S, Miyao T, et al. Active Demethylation of the Foxp3 Locus Leads to the Generation of Stable Regulatory T Cells Within the Thymus. *J Immunol* (2013) 190:3180–8. doi: 10.4049/jimmunol.1203473
239. Ohkura N, Hamaguchi M, Morikawa H, Sugimura K, Tanaka A, Ito Y, et al. T Cell Receptor Stimulation-Induced Epigenetic Changes and Foxp3 Expression Are Independent and Complementary Events Required for Treg Cell Development. *Immunity* (2012) 37:785–99. doi: 10.1016/j.immuni.2012.09.010
240. Delacher M, Imbusch CD, Weichenhan D, Breiling A, Hotz-Wagenblatt A, Träger U, et al. Genome-Wide DNA-Methylation Landscape Defines Specialization of Regulatory T Cells in Tissues. *Nat Immunol* (2017) 18:1160–72. doi: 10.1038/ni.3799
241. Liu B, Tahk S, Yee KM, Fan G, Shuai K. The Ligase PIAS1 Restricts Natural Regulatory T Cell Differentiation by Epigenetic Repression. *Science* (2010) 330:521–5. doi: 10.1126/science.1108297
242. Hegazy AN, Peine M, Helmstetter C, Panse I, Fröhlich A, Bergthaler A, et al. Interferons Direct Th2 Cell Reprogramming to Generate a Stable GATA-3 +T-Bet+ Cell Subset With Combined Th2 and Th1 Cell Function. *Immunity* (2010) 32:116–28. doi: 10.1016/j.immuni.2009.12.004
243. Hirota K, Duarte JH, Veldhoen M, Hornsby E, Li Y, Cua DJ, et al. Fate Mapping of IL-17-Producing T Cells in Inflammatory Responses. *Nat Immunol* (2011) 12:255–63. doi: 10.1038/ni.1993
244. Dominguez-Villar M, Baecher-Allan CM, Hafler DA. Identification of T Helper Type 1-Like, Foxp3+ Regulatory T Cells in Human Autoimmune Disease. *Nat Med* (2011) 17:673–5. doi: 10.1038/nm.2389
245. Panzer M, Sitte S, Wirth S, Drexler I, Sparwasser T, Voehringer D. Rapid In Vivo Conversion of Effector T Cells Into Th2 Cells During Helminth Infectio. *J Immunol* (2012) 188:615–23. doi: 10.4049/jimmunol.1101164
246. Schmidl C, Hansmann L, Andreesen R, Edinger M, Hoffmann P, Rehli M. Epigenetic Reprogramming of the RORC Locus During In Vitro Expansion Is a Distinctive Feature of Human Memory But Not Naïve Tre. *Eur J Immunol* (2011) 41:1491–8. doi: 10.1002/eji.201041067
247. Wei G, Wei L, Zhu J, Zang C, Hu-Li J, Yao Z, et al. Global Mapping of H3K4me3 and H3K27me3 Reveals Specificity and Plasticity in Lineage Fate Determination of Differentiating CD4+ T Cell. *Immunity* (2009) 30:155–67. doi: 10.1016/j.immuni.2008.12.009
248. Barnett KR, Decato BE, Scott TJ, Hansen TJ, Chen B, Attalla J, et al. ATAC-Me Captures Prolonged DNA Methylation of Dynamic Chromatin Accessibility Loci During Cell Fate Transition. *Mol Cell* (2020) 77:1–15. doi: 10.1016/j.molcel.2020.01.004
249. Kornberg RD, Lorch Y. Chromatin Structure and Transcription. *Annu Rev Cell Biol* (1992) 8:563–87. doi: 10.1146/annurev.cb.08.110192.003023
250. Mellor J. The Dynamics of Chromatin Remodeling at Promoters. *Mol Cell* (2005) 19:147–57. doi: 10.1016/j.molcel.2005.06.023

Conflict of Interest: PSa is scientific founder of Parvus Therapeutics Inc. and has a financial interest in the company.

The remaining author declares that the research was conducted in the absence of any commercial or financial relationships that could be construed as a potential conflict of interest.

frontiers in Immunology

ORIGINAL RESEARCH
published: 23 August 2021
doi: 10.3389/fimmu.2021.722411

Tuning the Immunostimulation Properties of Cationic Lipid Nanocarriers for Nucleic Acid Delivery

Arindam K. Dey[1,2], *Adrien Nougarède*[1,3], *Flora Clément*[1,2,4], *Carole Fournier*[1,2], *Evelyne Jouvin-Marche*[1,2], *Marie Escudé*[1,3], *Dorothée Jary*[1,3], *Fabrice P. Navarro*[1,3] *and Patrice N. Marche*[1,2*]

[1] Univ. Grenoble Alpes, St Martin d'Hères, France, [2] Institute for Advanced Biosciences, Research Center INSERM U1209, CNRS UMR5309, La Tronche, France, [3] CEA, LETI, Division for Biology and Healthcare Technologies, Microfluidic Systems and Bioengineering Lab, Grenoble, France, [4] Univ. Grenoble Alpes, CEA, INSERM, IRIG, Biomics, Grenoble, France

Nonviral systems, such as lipid nanoparticles, have emerged as reliable methods to enable nucleic acid intracellular delivery. The use of cationic lipids in various formulations of lipid nanoparticles enables the formation of complexes with nucleic acid cargo and facilitates their uptake by target cells. However, due to their small size and highly charged nature, these nanocarrier systems can interact *in vivo* with antigen-presenting cells (APCs), such as dendritic cells (DCs) and macrophages. As this might prove to be a safety concern for developing therapies based on lipid nanocarriers, we sought to understand how they could affect the physiology of APCs. In the present study, we investigate the cellular and metabolic response of primary macrophages or DCs exposed to the neutral or cationic variant of the same lipid nanoparticle formulation. We demonstrate that macrophages are the cells affected most significantly and that the cationic nanocarrier has a substantial impact on their physiology, depending on the positive surface charge. Our study provides a first model explaining the impact of charged lipid materials on immune cells and demonstrates that the primary adverse effects observed can be prevented by fine-tuning the load of nucleic acid cargo. Finally, we bring rationale to calibrate the nucleic acid load of cationic lipid nanocarriers depending on whether immunostimulation is desirable with the intended therapeutic application, for instance, gene delivery or messenger RNA vaccines.

Keywords: nanostructured lipid carrier, antigen presenting cells, nucleic acid delivery, immunotoxicity assessment, surface charge (zeta potential)

OPEN ACCESS

Edited by:
David Pozo,
University of Seville, Spain

Reviewed by:
Girdhari Lal,
National Centre for Cell Science, India
Vladimir Mulens-Arias,
Pompeu Fabra University, Spain

****Correspondence:***
Patrice N. Marche
patrice.marche@inserm.fr

Specialty section:
This article was submitted to Molecular Innate Immunity, a section of the journal Frontiers in Immunology

Received: *08 June 2021*
Accepted: *04 August 2021*
Published: *23 August 2021*

Citation:
Dey AK, Nougarède A, Clément F, Fournier C, Jouvin-Marche E, Escudé M, Jary D, Navarro FP and Marche PN (2021) Tuning the Immunostimulation Properties of Cationic Lipid Nanocarriers for Nucleic Acid Delivery. Front. Immunol. 12:722411. doi: 10.3389/fimmu.2021.722411

INTRODUCTION

In recent years, advances in field of nanotechnology have demonstrated potential for precision medicine. For instance, lipid nanoparticles (LNPs) can be used for the targeted delivery of therapeutic molecules, increasing their bioavailability and pharmacokinetic properties beyond the Lipinski rules (1). Indeed, the development of nucleic acid therapeutics has long been hampered by

the inherent hydrophilic nature, large size, and poor membrane permeability of nucleic acids (2). LNPs can be a potent alternative to viral-mediated nucleic acid delivery, with an extensive range of applications such as RNA interference (RNAi) therapy or RNA-based vaccines through intracellular delivery, respectively, of short interfering RNA (siRNA) or messenger RNA (mRNA) (3).

One of the primary advantages associated with LNPs is their biocompatibility that enables their use *in vivo* for human therapy (4, 5). LNPs are made of two major components: a lipid phase and a water phase containing surfactants. LNPs are generally divided into liposomes with an aqueous core or other LNPs; the latter could be solid lipid nanoparticles (SLNs) with a solid core and nanostructured lipid carriers (NLCs) featuring a core that is a mixture of solid and molten lipids (6). This subclass of LNPs was initially designed to improve the colloidal stability of lipid carriers and increase the drug payload into the core by controlling the release profile (7). Moreover, they are considered advantageous because their manufacturing processes can be easily scaled up for large production (8).

Due to the nature of their lipid core, these particles are not well adapted for nucleic acid encapsulation. The loading of biomacromolecules such as siRNA or mRNA, therefore, occurs through the association with their shell either by chemical modifications of Polyethylene glycol (PEG) residues (9) or by incorporation of cationic lipids at the level of phospholipid monolayer, thus allowing electrostatic interactions with negatively charged nucleic acids (9–12). The most chosen cationic lipids are quaternised cationic lipids, such as Dioleoyl-3-trimethylammonium propane (DOTAP), which are added to the formulation at the appropriate ratio (13). The NLCs with DOTAP present thereby a globally positive charge; thus, their toxicity and their impact on the immune systems need to be assessed. A previous study has reported that positively charged nanocarriers induce some systemic toxicity and pro-inflammatory effects (14). The microenvironment is known to drive distinct antigen-presenting cell (APC) fates by affecting functions of macrophages and dendritic cells (DCs) by activating different metabolic pathways. For example, while lipopolysaccharides (LPS) classically activated macrophages (M1), displaying pro-inflammatory activity, rely on glycolysis, Interleukin 4 (IL-4) alternatively activated macrophages (M2), displaying anti-inflammatory activity, primarily utilise fatty acid oxidation (FAO) and oxidative phosphorylation (OXPHOS) (15). DCs, like macrophages, respond differently in the presence of LPS and IL4 (16).

The exposition to cationic lipid carriers (cNLCs) has been shown to affect the functions of APCs. For instance, cNLCs were shown to activate bone-marrow-derived dendritic cells (BMDCs) partially by inducing the expression of two costimulatory molecules, CD80 and CD86, but without inducing the secretion of pro-inflammatory cytokines (17).

DOTAP itself could interact directly with ligands on the surface of the immune system (18). In the cationic NLCs formulation, we describe here that the phospholipid layer incorporating cationic lipids is covered by a dense PEGylated coating that contributes to the stability and also is known to reduce the interaction with proteins and other biological entities (14, 19, 20).

Moreover, how the positive charge of lipid particles modulates the metabolic fitness of APCs and how this is related to the cellular function have not yet been elucidated. Therefore, understanding the impact of positively charged particles on immune responses and particularly on APCs metabolism, fate and cytokine secretion is crucial to control the use of nanocarriers fully.

In the present study, we analysed the effect of NLCs surface charge on primary APCs using BMDCs and bone-marrow-derived macrophages (BMDMs), as cellular models. We evaluated the impact of neutral lipid carriers (nNLCs) and cNLCs on the secretion of different signalling factors and mitochondrial metabolism and glycolysis. Furthermore, we used negatively charged siRNA to reverse the net charge on cNLCs and evaluate the effect of different surface charges on cell function.

MATERIALS AND METHODS

Cell Culture

The murine macrophage cell line (J774.1A) was purchased from ATCC; the cells were cultured in Dulbecco's modified Eagle's medium (DMEM) supplemented with 10% fetal bovine serum and 1% penicillin-streptomycin.

As previously described (21), BMDCs were generated from the bone marrow extracted from C57BL/6 mice (Charles River, l'Arbresle, France). Bone marrow cells were isolated by flushing from the tibia and femur. Erythrocytes and GR1 positives cells were removed by incubating with Ly-6G/Ly-6C (BD Pharmingen, #553125) and TER-119 (BD Pharmingen, #553672) antibodies, and the remaining negatively sorted cells were isolated using Dynabeads isolation kit (ThermoFisher, #11047) by magnetic cell sorting; then the remaining negatively sorted cells were resuspended at 5×10^5 cells/ml in complete Iscove's modified Dulbecco's medium supplemented with Granulocyte-macrophage colony-stimulating factor (GM-CSF) (PeproTech, #315-03), FLT-3L (PeproTech, #250-31L) and Interleukin 6 (IL-6) (Peprotech, #216-16) according to **Table 1**. The transformation of the progenitors into fully active DCs was performed over a 10-day time frame.

Abbreviations: APCs, antigen presenting cells; DCs, dendritic cells; LNPs, Lipid nano particles; RNAi, RNA interference; siRNA, small interfering RNA, mRNA, messenger RNA; SLN, solid lipid nanoparticles; NLCs, nanostructured lipid carriers; PEG, polyethylene glycol; DOTAP, Dioleoyl-3-trimethylammonium propane; M1, pro-inflammatory macrophages; M2, anti-inflammatory macrophages; BMDCs, bone marrow derived dendritic cells; BMDMs, bone marrow derived macrophages; cNLCs, cationic lipid carrier; CD, cluster of differentiation; FAO, fatty acid oxidation; ECAR, extracellular acidification rate; IL, interleukin; PDI, polydispersity index; DLS, dynamic light scattering; ELS, electrophoretic light scattering; SD, standard deviation; CBA, cytometric Bead Array; LDH, lactate dehydrogenase; LPS, lipopolysaccharide; LC, lipid nanocarrier; OCR, oxygen consumption rate; OXPHOS, oxidative phosphorylation; NLC,nano structured lipid carrier; cNLCs, cationic nanostructured lipid carriers; nNLCs, neutral nanostructured lipid carriers; NPs, nano particles; ROS, reactive oxygen species; SLN, solid lipid nanoparticles; TNF, tumor necrosis factor.

TABLE 1 | Concentration of GM-CSF, FLT-3L and IL-6 for BMDCs culture.

Cells are cultured in a 100-mm TC-treated cell culture dish with 15 mL culture media						
		Day 0	Day 3	Day 5	Day 7	Day 10
Cell concentration		0.6 x 10^6/mL	0.5 x 10^6/mL	0.5 x 10^6/mL	0.5 x 10^6/mL	According to cell plating
Supplement	IL-6	5 ng/mL	2.5 ng/mL	2.5 ng/mL	–	–
	FLT-3L	50 ng/mL	40 ng/mL	30 ng/mL	25 ng/mL	25 ng/mL
	GM-CSF	5 ng/mL	5 ng/mL	5 ng/mL	5 ng/mL	5 ng/mL

Culture of BMDCs: BMDCs were seeded into a 100-mm TC-treated cell culture dish with 15 mL culture media. Culture media is supplemented with variable concentrations of GM-CSF, FLT-3L and IL-6 on day 0, day 3, day 5, day 7 and day 10 to harvest fully differentiated BMDCs on day 11.

BMDMs were also generated from bone marrow extracted from C57BL/6 mice as previously described (22). Briefly, the erythrocytes were removed by the RBC lysis buffer, and the remaining cells were cultured in a complete DMEM with 20% L929 (Sigma, #85011425) in conditioned medium (source of macrophage colony-stimulating factor) for 7 days.

Cationic and Neutral Lipid Nanocarriers

nNLCs and cNLCs were prepared as described in the previous study (23). Briefly, for nNLCs, a lipid phase was prepared containing triglycerides (Suppocire NB, Gattefossé and super-refined soybean oil, Croda Uniqema) and phospholipids (Lipoid SPC3, Lipoid). For cNLCs, the same lipid phase supplemented with the cationic lipid DOTAP (1,2-dioleoyl-3-trimethylammonium-propane chloride, Avanti Polar Lipids) and fusogenic lipid DOPE (1,2-dioleoyl-sn-glycero-3-phosphoethanolamine, Avanti Polar Lipids) were used. When indicated, Dil lipophilic dye (D282, ThermoFisher) was added to the lipid phase to enable fluorescence detection of nNLCs. A second aqueous phase containing the PEGylated surfactant PEG-40 Stearate (Myrj S40, Croda Uniqema) was prepared in Phosphate-buffered saline (PBS) (#806552, Sigma). Both lipid and aqueous phases were mixed together through high-frequency sonication. Lipid nanoparticles are purified by dialysing in 100 volumes of LNP buffer: 154 mM NaCl, 10 mM HEPES, and pH 7.4 using endotoxin-free ultra-pure water (TMS-011-A, Sigma) and 12–14 kDa MW cut-off membranes (ZelluTrans/Roth T3). Finally, the LNP solution was sterilised by filtrating through a 0.22-µm millipore membrane. A putative structure depicting each component of cNLCs and nNLCs is presented in **Supplementary Figure 1**.

Nanoparticle Uptake Assay

For nanoparticle uptake assays, 0.5 x 10^5 cells/mL of BMDCs and BMDMs were seeded into a 4-well Lab-Tek chambered coverslip. After 24 h of growth, the cells were incubated with both Dil-labelled nanocarriers, cNLCs and nNLCs, for 24 h at 37°C with 5% CO_2. Nanocarrier accumulation inside cells was monitored by time-lapse microscopy using a spinning disk confocal microscope (Andromeda, TILL-FEI). The Dil-labelled nanocarriers were visualised using the lipophilic dye excitation wavelength of 514 nm while plasma membranes were labelled with FITC-conjugated cholera toxin (Sigma, C1655) and visualised at the excitation wavelength of 488 nm. After acquisition, the images were processed in Icy 2.0.3.0 software, and spectral deconvolution was performed using NIS 5.20.01 software.

Physical Characterisation of NLCs

The hydrodynamic diameter and polydispersity index (PDI) of the NLCs were determined by dynamic light scattering (DLS), and the zeta potential was determined by electrophoretic light scattering (ELS) using a Zetasizer Nano ZS instrument (Malvern). The hydrodynamic diameter and PDI were measured with a dispersion of 1 mg/mL NLCs in PBS while the zeta potential was measured with a dispersion of 1 mg/mL NLCs in 1 mM NaCl. Each assay was performed in three replications at 25°C. A table showing the size, PDI and zeta potential of both NLCs is documented in **Supplementary Figure 1**.

Complexation of cNLCs With Nucleic Acid

In the complexation of cNLCs with model nucleic acid, all-star negative control siRNA (siMock) was carried out in PBS. The required volume for siMock was calculated according to the desired N/P ratios (ratio of positively-chargeable polymer amine (N = nitrogen) groups to negatively-charged nucleic acid phosphate (P) groups) at a constant concentration of the cNLCs nanocarrier (100 µg/mL). The cNLCs carrier and diluted siMock were gently homogenised by pipetting and kept for 10 min at room temperature before immediate use for downstream experiments.

Incubation With Nanoparticles

For cell culture, 12, 24 and 96 cell culture microplates manufactured by Falcon® or seahorse XFe96 were used. Cells were seeded at a concentration of 10^6 cells/mL and cultured for 24 h. They were incubated for 24 h with nNLCs or cNLCs at a concentration ranging from 20 to 100 µg/mL. Cells were subsequently washed and stimulated with LPS (2 µg/mL) or IL-4 (20 ng/mL) for another 24 h. Finally, the impact of the two nanocarriers on BMDMs and BMDCs was assayed using various parameters, such as viability, phagocytosis, activation, cytokine secretion, nitric oxide (NO) production, reactive oxygen species (ROS) production and glycolysis or mitochondrial metabolism.

Toxicity Assessment

Toxicity was measured by quantifying the cell viability using the CytoTox-ONE™ Homogeneous Membrane Integrity Assay kit (Promega, G7891) according to the manufacturer's protocol. Briefly, the lysis solution (2 µl of lysis solution per 100 µl original volume) was used as a positive control for lactate dehydrogenase (LDH) release. A volume of 100 µL of CytoTox-ONE™ reagent was added to each well, before homogenisation on a shaker for 30 seconds and followed by

incubation for another 10 min in the dark. After that, stop solution (50 µL) was added to each well, and the plate was placed on the shaker for another 10 seconds. Finally, their fluorescence was recorded at an excitation wavelength of 560 nm and an emission wavelength of 590 nm using a CLARIOstar® microplate reader (BMG LABTECH).

Phagocytosis Assay

Nanocarrier-exposed macrophages (BMDMs and J774.1A cells) and BMDCs were incubated at a ratio of 10 microspheres per cell for 6 h with 1.0-µm FluoSpheres® carboxylate-modified microspheres (ThermoFisher, F8851) labelled with a red fluorescent dye (580 nm excitation and 605 nm emission). Cells were analysed by flow cytometry with an Accuri C6 instrument (Becton-Dickinson), and the analysis was performed by the FCS Express V5 software (*De Novo* Software).

Cell Activation

Nanocarrier-exposed BMDCs and BMDMs were stimulated for 24 h using 2µg/mL LPS from *Escherichia coli*. Supernatants were collected for downstream cytokine immunoassay. After blocking the Fc receptor (BD Pharmingen, 553142) to reduce nonspecific binding, BMDCs and BMDMs were stained for APC/Cy7 conjugated CD11b (Ozyme, BLE101226) and PE/Cy7 conjugated CD11c (Ozyme, BLE117318) or PE/Cy7 conjugated CD11b (Ozyme, BLE101216) and APC/Fire™ 750 conjugated F4/80 (Ozyme, BLE123152), respectively. To evaluate the cell activation, BMDCs and BMDMs were stained with Alexa Fluor® 488 conjugated anti-IAb (Ozyme, BLE116410) and PE conjugated CD86 (Ozyme, BLE105008) antibodies. In both cases, live cells were selected by negative 7-aminoactinomycin D (7AAD; BD Pharmingen, 559925) staining and analysed by flow cytometry using an LSR II instrument (Becton-Dickinson). The proportion of activated cells was quantified using FCS Express V5 software.

Cytokine Immunoassays

Cytokine production was measured from cell culture supernatants with cytometric bead array (CBA; BD Pharmingen, 552364) using a mouse inflammation kit against IL-6, IL-12p70, MCP-1, TNFα, IL-10 and IFNγ. Results were acquired by flow cytometry using a BD LSR II instrument and analysed with FCAP Array Software v3.0 (BD Pharmingen, 652099).

NO and ROS Production

NO produced by BMDMs and BMDCs was determined by measuring nitrite concentration in cell culture media by Griess assay. Briefly, 50 µL of cell supernatant was transferred to a 96-well plate and incubated with an equal volume of sulphanilamide (Sigma, S9251) and N-alpha-naphthyl-ethylenediamine (Sigma, 222488) solutions, respectively, for 10 min each, protected from light. Optical density was measured at 540 nm using a CLARIOstar® microplate reader, and sample nitrite concentration was determined using a standard curve. ROS production by BMDMs and BMDCs was determined by ROS-Glo™ H_2O_2 assay kit (Promega, G8821). The cells were cultured at 5 x 10^4 cell/mL concentration in a 96-well plate, exposed to nanocarriers for 24 h and stimulated with 2 µg/mL of LPS. A volume of 20 µL of H_2O_2 substrate solution was added to each well before 6 h of ROS production measurement. ROS production measurement was performed by adding 100 µL of ROS-Glo™ detection solution per well, before 20 min of incubation at 22°C followed by luminescence using a CLARIOstar® microplate reader.

Metabolic Flux Analysis

For mature BMDCs (on day 10), 1.5 x 10^5 cells per well were seeded into seahorse culture plate (Agilent, 102416-100) precoated with Cell-Tak (Corning, 354240) to enable BMDCs adherence, in complete culture media supplemented with GM-CSF (5 ng/mL) and FLT-3L (25 ng/mL). For mature BMDMs (on day 7), 0.8 x 10^5 cells per well were seeded into seahorse culture plate as described in the previous study (24). A graphical representation of the experiment design is presented in **Supplementary Figure 2**.

Statistical Analysis

Results are expressed as mean values ± standard deviation (SD). Statistical analysis was performed using GraphPad Prism version 8.4.2. Data were analysed by one-way ANOVA and Tukey's multiple comparison test to analyse the difference between different groups. P-values below 0.05 were considered as significant and indicated as follows: *P ≤ 0.05, **P ≤ 0.01, ***P ≤ 0.001, and ****P ≤ 0. 0001 as compared with untreated cells (not exposed to NLCs).

RESULTS

nNLCs and cNLCs Do Not Induce Cell Toxicity and Are Efficiently Internalised by APCs

We first investigated whether the exposure of nNLCs and cNLCs is toxic for APCs *in vitro*, using a macrophage cell line (J774.1A) or primary untransformed cells extracted from bone marrow: macrophages (BMDMs) and DCs (BMDCs). Cells were exposed to nNLCs or cNLCs with concentrations ranging from 0 to 250 µg/mL and measured toxicity (**Figure 1A**). Among all the tested cells, BMDCs were most susceptible to both nNLCs and cNLCs exposure, and all the tested conditions exhibited more than 80% of cell viability. Therefore, for subsequent experiments, we chose 20 and 100 µg/mL as low and high standard doses, respectively, without adverse effects, that is, higher than 80% of cell viability after 24 h of incubation.

Next, we assayed the internalisation of both nNLCs and cNLCs by two primary cell types: BMDCs and BMDMs that are more physiologically relevant than any immune cell lines. The analysis of the time dependent engulfment of both NLCs showed that the maximum of uptake was reached after 1h for both BMDCs (**Figure 1B**) and BMDMs (**Figure 1C**). Staining the cell membrane of APCs with FITC conjugated cholera toxin showed both the nanocarriers were internalised into BMDCs (**Figure 1D**) and BMDMs (**Figure 1E**) within a 24-h time frame. Therefore, from these first experiments, we can conclude that

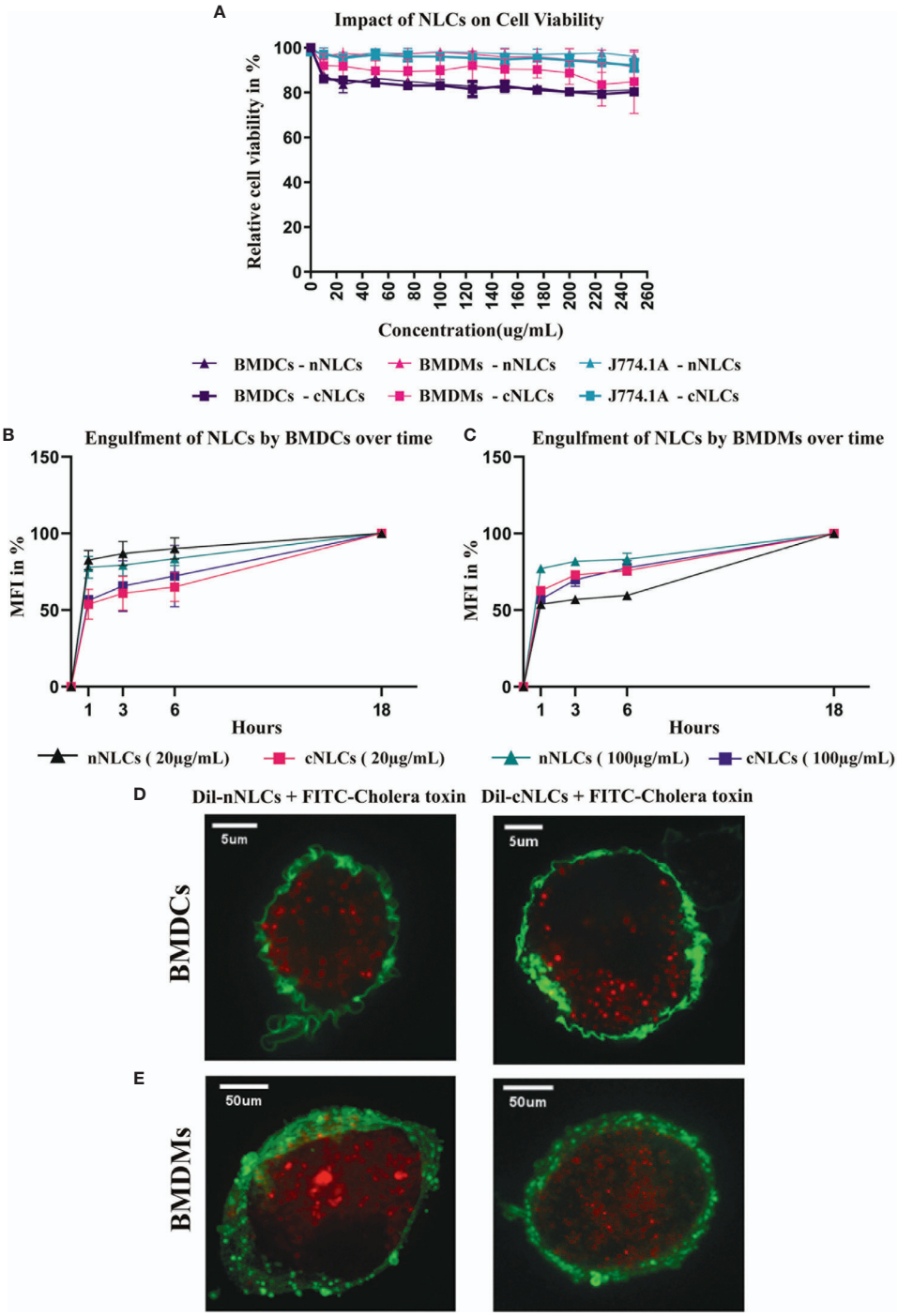

FIGURE 1 | nNLCs and cNLCs do not induce cell toxicity and are efficiently internalised by APCs **(A)** Cell viability (LDH release assay) of BMDCs, BMDMs and J774.1A cells was analysed after exposure to different concentrations of nNLCs and cNLCs nanocarriers for 24 h. Data are displayed as mean ± SD and normalised to the untreated cells (N = 3 independent experiments). Time-dependent engulfment of both cNLCs and nNLC in BMDCs **(B)** and BMDMs **(C)**. After APCs exposure to 20 and 100 µg/ml of DiI labeled nNLCs or DiI labeled cNLCs nanocarriers for 1, 3, 6, 18 h cells were analysed by flow cytometry. Data are displayed as mean ± SD and presented as % of max MFI (at 18h) (N = 3 independent experiments). Confocal microscopy analysis of nNLCs and cNLCs uptake in **(D)** BMDCs and **(E)** BMDMs. After APCs exposure to 100 µg/ml of nNLCs or cNLCs nanocarriers for 24 h, cell membranes were labelled with FITC-conjugated cholera toxin (green), and nNLCs and cNLCs are observed by excitation of DiI fluorescent dye (red). Images were acquired using a confocal spinning-disk microscope. The images displayed were representative of the majority of cells observed.

these two nanocarriers were not toxic up to a 250-µg/mL concentration, while they were both efficiently internalised by APCs.

nNLCs and cNLCs Are Internalised by APCs Without Affecting Their Phagocytic Capacity

Accumulation of nanocarriers into phagocytic APCs opens the question of whether their functions could be altered, such as phagocytosis, which is one of the primary features of APCs. The phagocytic capacity of BMDCs or BMDMs was assessed by counting the number of engulfed microspheres per cell by flow cytometry. This parameter was not altered by either the neutral or the cationic nanocarrier supporting that the phagocytic capacity of both APCs was not modified by any type of nanocarrier (**Figures 2A–D**). Moreover, we noticed that the phagocytic capacity of BMDMs was 20% higher than that of BMDCs (**Figures 2B, D**).

We also verified the impact of the nanocarriers on the phagocytic capacity of J774.1A cells, a well-characterised macrophage cell line for phagocytosis analysis (25). Similarly, we did not observe a significant change in phagocytic capacity between the nanocarrier treated cells or control cells. These results obtained with the J774.1A cell line were consistent with what we observed in the primary cells (**Supplementary Figures 3A, B**).

cNLCs but Not nNLCs Can Increase LPS Activation of BMDMs

BMDCs were identified by CD11b and CD11c expressions (26) whereas BMDMs were marked by CD11b and F4/80 expressions (27) (see the gating strategy in **Supplementary Figure 4**). Activation of BMDCs and BMDMs was evaluated by the frequency of CD86 and MHC-II double-positive cells. After LPS stimulation, the frequency of $CD86^+$ and $MHC\text{-}II^+$ in BMDCs increased from 27.83% to 75.9% (**Figure 3A** and **Table 2**) while no significative changes were observed in BMDMs (**Figure 3B**).

Exposure to increasing concentrations of nNLCs or cNLCs did not significantly alter LPS-induced double expression of CD86 and MHC-II in BMDCs. In the case of unstimulated BMDMs activation, CD86 and MHC-II double-positive cell percentage was not altered when exposed to nNLCs but decreased significantly when exposed to cNLCs at the highest dose from 19.6% to 9.79%. In the case of unactivated BMDMs, the percentage of CD86 positive cells remained unaltered when exposed to nNLCs (**Table 2**). Altogether, our data highlight that both nanocarriers do not activate BMDCs, but cNLCs slightly alter the activation of BMDMs. BMDCs, on exposure to both nanocarriers, maintained their capacity to respond to LPS activation. However, in the case of LPS-stimulated BMDMs, exposure to cNLCs significantly increased the percentage of

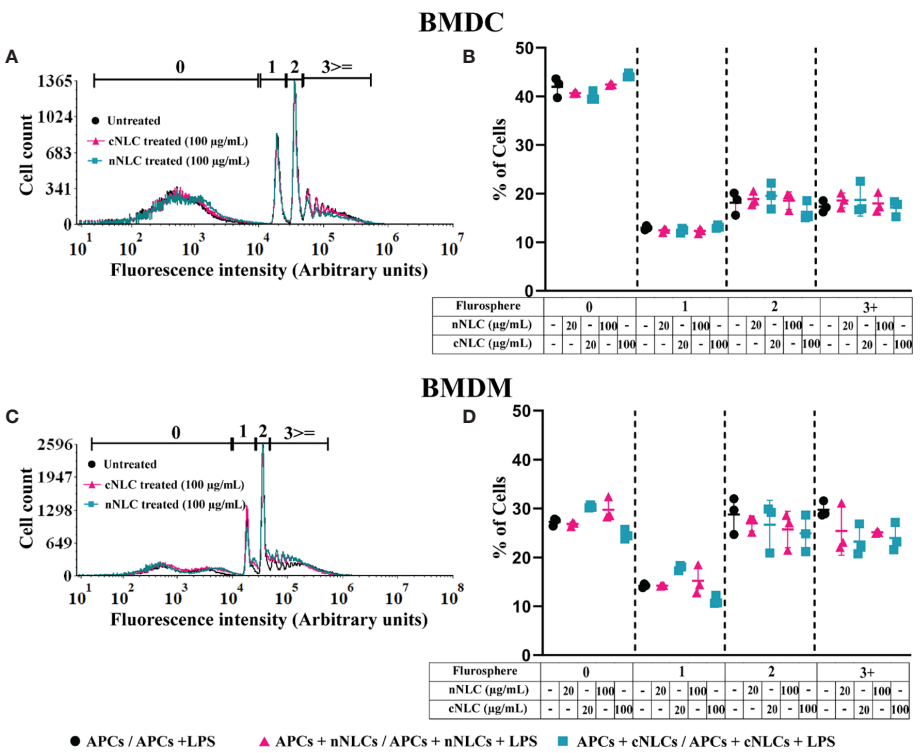

FIGURE 2 | Phagocytic capacity of APCs exposed to nNLCs or cNLCs. BMDCs and BMDMs were exposed to nNLCs and cNLCs nanocarriers at 20 and 100 µg/mL for 24 h, then incubated with fluorescent microspheres for 6 h and subsequently analysed by flow cytometry. The repartition of the cells in the 1st, 2nd, 3rd and 4th peak corresponds to 0, 1, 2 and 3 or more beads internalisation, respectively. Overlaid histograms are shown in **(A)** for BMDCs and **(C)** for BMDMs. The proportion of cells in each peak was analysed for **(B)** BMDCs and **(D)** BMDMs. Data are displayed as mean ± SD (N = 3 independent experiments).

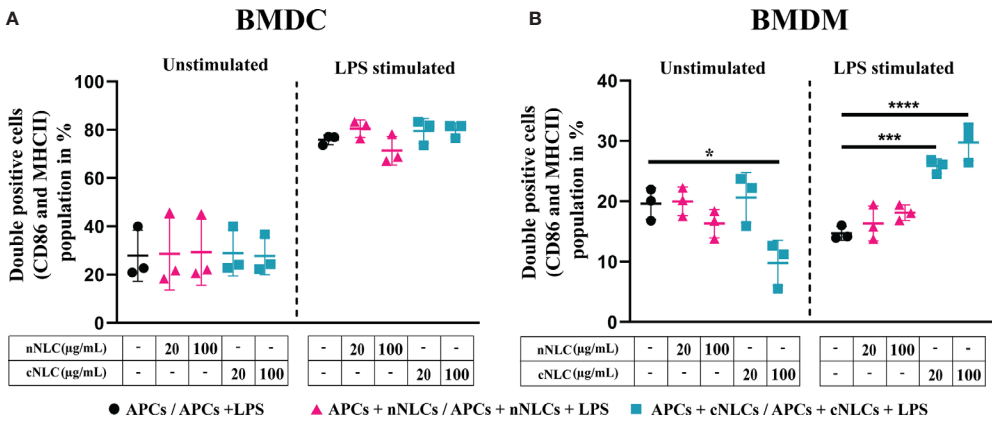

FIGURE 3 | Expression of activation surface marker in APCs following exposure to nNLCs or cNLCs. BMDCs **(A)** and BMDMs **(B)** were exposed to nNLCs or cNLCs for 24 h, followed by LPS stimulation for an additional 24 h. Percentage of double-positive (CD86 and MHC-II) BMDCs and CD86 positive BMDMs were determined, with gating on CD11b and Cd11c positive cells for BMDCs and CD11b and F4/80 positive cells for BMDMs. Data are displayed as mean ± SD (N = 3 independent experiments), and the statistical significance between nanocarrier treated or untreated groups was performed by one-way ANOVA test using Tukey's multiple comparisons test. *P ≤ 0.05; ***P ≤ 0.001; and ****P ≤ 0.0001.

activated BMDMs from 14.69% to 29.76%, while it remained the same with the nNLCs (**Figure 3B** and **Table 2**). This suggests that exposure to nanocarriers alone is not sufficient to activate both BMDCs and BMDMs. However, in LPS-stimulated BMDMs, exposure to cNLCs increased the frequency of $CD86^+$ and $MHC\text{-}II^+$ activated cells. Internalisation of both lipid nanocarriers, neutral and cationic ones, is not sufficient to activate both BMDCs and BMDMs, although exposure to cNLCs enhanced the ability of BMDMs to respond to LPS stimulation.

cNLCs and nNLCs Can Alter the Production of Signalling Molecules by APCs

The capacity to produce different soluble factors, including signalling proteins such as cytokines or chemokines and other small molecular mediators such as NO and ROS, is a hallmark of APCs activation.

Having demonstrated that exposure to cNLCs could alter the activation of BMDMs in response to LPS, we wondered what would be the impact of both nanocarriers on cytokine secretion. We observed that both nanocarriers did not induce cytokine secretion in unstimulated BMDCs and BMDMs (**Figures 4A–D**, left panel), except the highest dose of cNLCs but not nNLCs, which significantly increased the production of the MCP-1 chemokine in unstimulated BMDCs and to a lesser extend in unstimulated BMDMs (**Figures 4E, F**, left panel).

Upon LPS stimulation of APCs, nNLCs exposure did not alter IL-6 production by both BMDCs and BMDMs. However, exposure to cNLCs significantly increased IL-6 production by BMDMs (**Figure 4B**, right panel) but not by BMDCs (**Figure 4A**, right panel). In the case of BMDCs, both nNLCs and cNLCs decreased TNF-α production at 100 µg/mL (**Figure 4C**, right panel). For BMDMs, TNF-α production was only increased at 100 µg/mL of cNLCs but not for BMDCs (**Figure 4D**, right panel). We also observed that treatment with cNLCs but not nNLCs significantly increased MCP-1 production in both LPS-stimulated BMDCs and BMDMs (**Figures 4E, F**, right panel).

Two other important secretory molecules, NO and ROS productions were evaluated in the culture supernatant of APCs by Griess assay and H_2O_2 quantification, respectively. In absence

TABLE 2 | Percentage of activated APCs with or without NLCs treatment.

Double positive (CD86 and MHC-II) cells population percentage (mean ± SD)	BMDCs		BMDMs	
	Unstimulated	LPS-stimulated	Unstimulated	LPS-stimulated
Cells	27.83 ± 8.58	75.9 ± 1.62	19.6 ± 2.13	14.69 ± 0.93
Cells + nNLCs (20 ug/mL)	28.61 ± 12.22	80.51 ± 2.97	19.98 ± 1.92	16.32 ± 2.35
Cells + nNLCs (100 ug/mL)	29.3 ± 11.21	71.38 ± 4.85	16.3 ± 1.90	18.1 ± 1.05
Cells + cNLCs (20 ug/mL)	28.97 ± 7.79	79.57 ± 4.27	20.61 ± 3.39	25.84 ± 0.98
Cells + cNLCs (100 ug/mL)	27.74 ± 6.37	79.91 ± 2.39	9.79 ± 3.07	29.76 ± 2.45

Expression of activation surface marker of APCs. Expression of activation marker of BMDCs and BMDMs after exposure to nNLCs and cNLCs for 24 h, followed by LPS stimulation for another 24 h. Percentage of double-positive (CD86 and MHC-II) APCs were analysed. Prior to analyse, BMDCs were gated on $CD11b^+$ and $Cd11c^+$; BMDMs were gated on $CD11b^+$ and $F4/80^+$; and the data are presented in tabular form. Results are mean ± SD of 3 independent experiments.

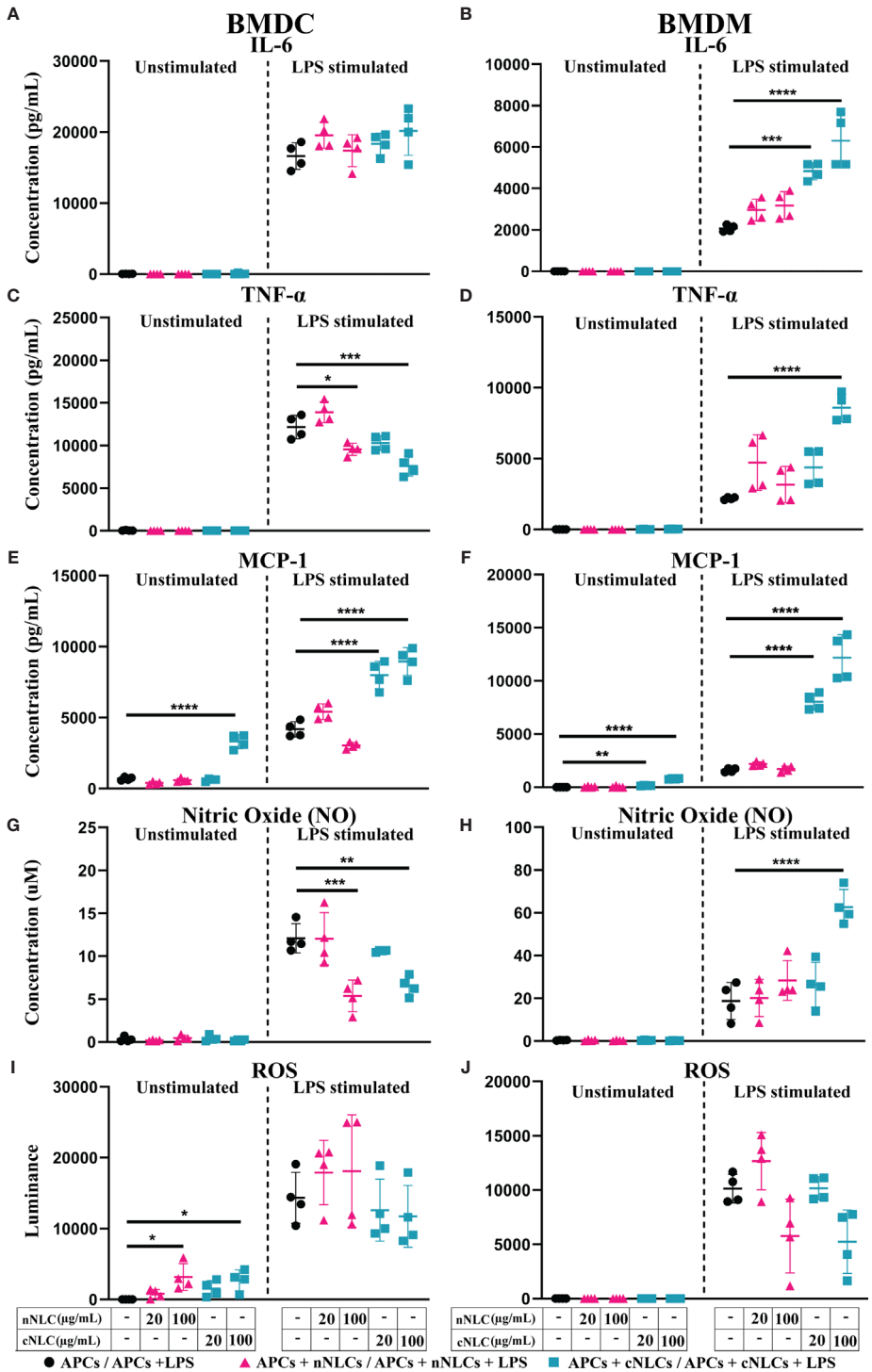

FIGURE 4 | Secretions of signalling factors by APCs in response to nNLCs or cNLCs. Relative cytokine and chemokine concentration in the supernatant of BMDCs and BMDMs exposed to nNLCs or cNLCs and activated or not by LPS was determined by immunoassay. Secretion of the IL-6 cytokine in **(A)** BMDCs and **(B)** BMDMs; the TNFα cytokine in **(C)** BMDCs and **(D)** BMDMs and the chemokine MCP-1 in **(E)** BMDCs and **(F)** BMDMs. Relative NO concentration in the supernatant of BMDCs **(G)** and BMDMs **(H)** cells exposed to nNLCs or cNLCs and activated or not by LPS was determined by Griess assay. ROS production by BMDCs **(I)** and BMDMs **(J)** cells exposed to nNLCs or cNLCs and activated or not by LPS was determined by ROS-Glo^{TM} H_2O_2 assay. Data are displayed as mean ± SD (N = 4 independent experiments), and the statistical significance between nanocarrier treated or untreated groups was performed by one-way ANOVA test using Tukey's multiple comparisons test. *P ≤ 0.05; **P ≤ 0.01; ***P ≤ 0.001; and ****P ≤ 0.0001.

of LPS stimulation, we did not observe a production of NO by BMDCs and BMDMs in response to both nanocarriers (**Figures 4G, H**, left panel) although ROS production was detected by BMDCs treated with 100 μg/mL of either nNLCs or cNLCs but not in BMDMs (**Figures 4I, J**, left panel). In LPS-stimulated conditions, both nNLCs and cNLCs at highest dose decreased NO production by BMDCs (**Figure 4G**, right panel), while the only cNLCs were responsible for increasing NO production in BMDMs (**Figure 4H**, right panel). After stimulation by LPS, both APCs produced increased quantities of ROS, but its production was not significantly altered by exposure to both nanocarriers (**Figures 4I, J**, right panel). These results indicate that BMDCs and BMDMs are differently affected by neutral or cationic nanocarriers regarding their capacity to produce NO and ROS and depending on activation stimuli.

Overall, nNLCs have only limited influence on the productions of signalling molecules, whereas cNLCs display significant effects, especially for inflammatory signals. The influence of cNLCs is clearly demonstrated in activated BMDMs by the increases of IL-6, TNF-α, MCP-1 secretions and NO production. Both nNLCs and cNLCs share most of their features such as their same size and composition; therefore, their major difference resides in their surface charge. This led us to hypothesise that this difference in the surface charge may be responsible for different effects driven by these two nanoparticles on APCs.

nNLCs and cNLCs Have a Significant Impact on the Mitochondrial Metabolism of BMDMs but Not on That of BMDCs

As cellular metabolism plays a key role in different functions of APCs, we sought to determine the effect of differentially charged LNCs on mitochondrial metabolism. For instance, pro-inflammatory stimuli by LPS are known to trigger a metabolic switch that would enhance glycolysis, whereas enhanced FAO and mitochondrial OXPHOS are hallmarks of IL-4-induced anti-inflammatory activity in immune cells.

Upon exposition to both nanocarriers, no alteration in the basal respiration, maximal respiration capacity, spare respiratory capacity, nonmitochondrial oxygen consumption and coupling efficiency (**Supplementary Figures 5A, C, E** and **Figures 6A, C**), proton leak or ATP production (**Figures 5A, C**) were found in unstimulated or stimulated BMDCs.

In BMDMs, exposure to both nanocarriers increased basal respiration and nonmitochondrial oxygen consumption of unstimulated cells at 100 μg/mL, as well as the nonmitochondrial oxygen consumption of LPS-stimulated cells treated with the nNLCs (**Supplementary Figures 5B** and **6B**). Treatment with 100 μg/mL of cNLCs significantly increased the proton leak, Adenosine triphosphate (ATP) production, basal respiration, maximal respiration capacity, spare respiratory capacity and nonmitochondrial oxygen consumption (**Figures 5B, D** and **Supplementary Figures 4B, D, F,** and **5B**) in unstimulated or IL-4-stimulated BMDMs whereas the nNLCs did only slightly increase basal respiration and nonmitochondrial oxygen consumption (**Supplementary Figures 5A** and **6A**).

It is to be noted that both nanocarriers did not impair the coupling efficiency of unstimulated or stimulated BMDMs (**Supplementary Figure 6B**).

As a whole, our results demonstrate that the cNLCs have a more important effect on BMDMs' metabolism compared with the nNLCs, while both nanocarriers have little effect on the metabolism of BMDCs.

nNLCs and cNLCs Alter the Glycolysis of BMDMs and Not of BMDCs

Considering the alterations of the mitochondrial metabolism induced by the cNLCs and to a lesser extent the nNLCs, we sought to investigate their effects on the glycolytic profile of APCs as LPS-stimulated cells are mostly dependent on glycolysis. To evaluate the different glycolytic parameters of BMDCs and BMDMs, cells were first pretreated with different concentrations of both nanocarriers and then stimulated with LPS or IL-4 for 24 h. After stimulation, the extracellular acidification rate (ECAR) was measured using the glyco stress assay.

Unlike for BMDCs that did not show any alteration in glycolysis (**Figure 5E**) or glycolytic capacity (**Supplementary Figure 7A**), BMDMs' glycolysis (**Figure 5F**) and glycolytic capacities (**Supplementary Figure 7B**) were increased in both unstimulated and stimulated conditions when exposed to 100 μg/mL of cNLCs. However, exposure to nNLCs did not induce any alteration in glycolysis or glycolytic capacity in BMDMs regardless of stimulating conditions (**Figure 5F** and **Supplementary Figure 7B**).

The combination of these results reveals that the cationic but not the nNLCs at the highest concentration alter the glycolytic profile in BMDMs. Conversely, both nanocarriers have no effect on glycolysis in BMDCs.

Reversing the Surface Charge With a Nucleic Acid Cargo Prevents Adverse Effects of cNLCs on APCs

As previous experiments have pointed out, at 100 μg/mL, cNLCs had a more dramatic effect on BMDMs' physiology than nNLCs; we wondered whether the surface charge could explain the differences observed.

This led us to investigate whether we could reverse the phenotype observed on APCs by reversing the surface charge of the cNLCs with a nucleic acid cargo, here a negative control siRNA (siMock). We used different surface charges by fine-tuning the ratio of the positively charged amine groups of cNLCs nanocarriers (N = NH^{3+} group) relative to the negatively charged phosphate groups (P) from each phosphodiester bonds within the nucleic acid sequence, hence called N/P ratio. After complexation between siRNA and cNLCs nanocarriers, the zeta potential and hydrodynamic diameter of these nanocomplexes were measured. Naked cNLCs showed a zeta potential of 45.80 ± 3.8 mV in 1 mM NaCl while increasing amounts of the nucleic acid cargo and thus decreasing the N/P ratio lead to lower the zeta potential values down to –9.97 ± 0.94 mV, while naked nNLCs was measured at –16.50 ± 0.53 mV (**Figure 6A**). It is to be noted that the complexation of cNLCs with different quantities of siRNA did not significantly alter the size of the nanocomplexes (**Figure 6B**).

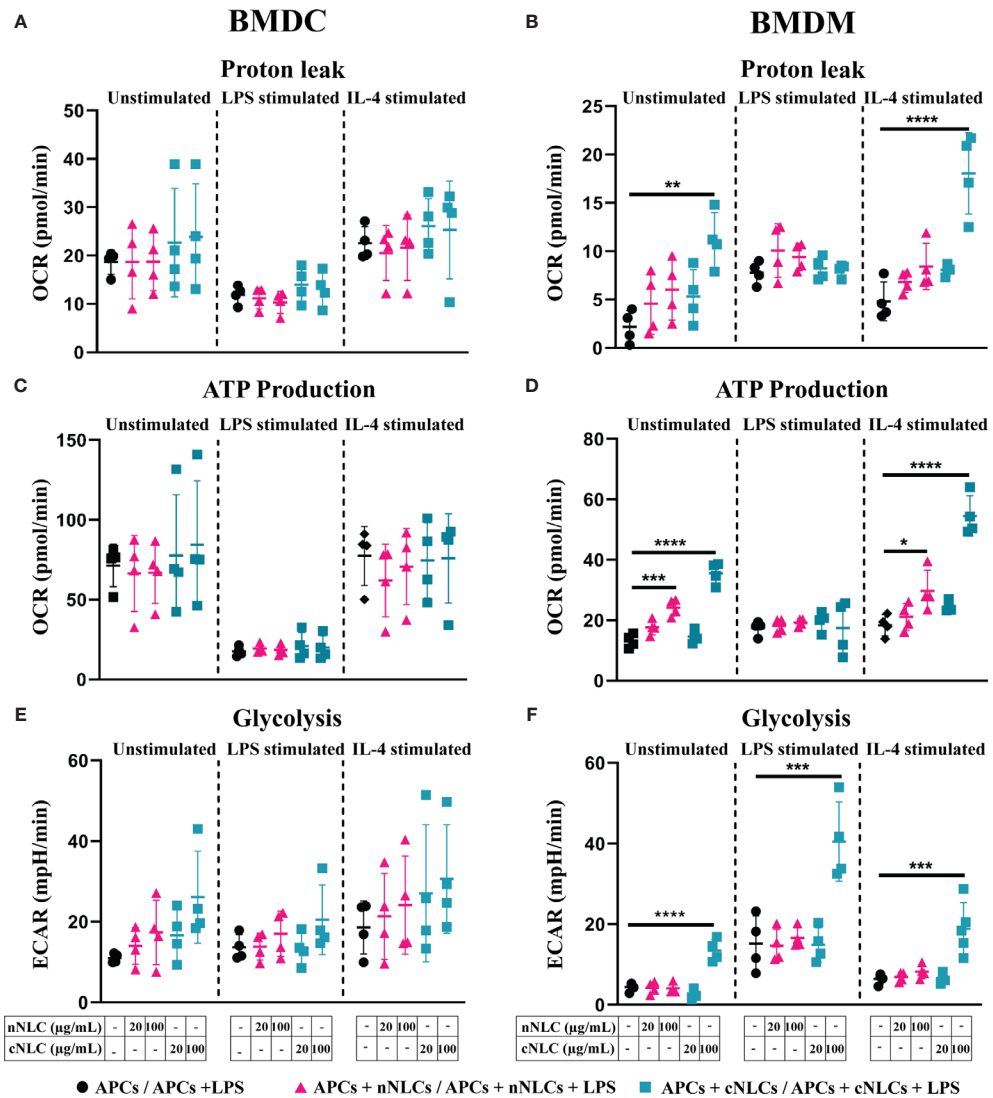

FIGURE 5 | Mitochondrial metabolism in naïve, classically activated or alternatively activated APCs in response to nNLCs or cNLCs. **(A, B)** Proton leak, **(C, D)** ATP production and **(E, F)** glycolysis in BMDCs and BMDMs, respectively, were measured after exposure to cNLCs or nNLCs for 24 h and activated by LPS or IL-4 for another 24 h. Oxygen consumption rate (OCR) and ECAR were quantified using a seahorse XF analyser. Data were normalised by cell number based on cell count (Hoechst 33342 staining) and are displayed as mean ± SD (N = 4 independent experiments). The statistical significance between nanocarrier treated or untreated groups was performed by one-way ANOVA test using Tukey's multiple comparisons test. *P ≤ 0.05; **P ≤ 0.01; ***P ≤ 0.001; and ****P ≤ 0.0001.

Using different N/P ratios, we generated nanocarriers with different zeta potentials that we subsequently used to investigate their effects on BMDMs functions. An experimental design of metabolic flux analysis for reversal of nanocarrier surface charge is depicted in **Supplementary Figure 8**. BMDMs were exposed to 100 µg/mL of cNLCs nanocarrier, cNLCs-siRNA nanocomplexes at N/P 8 to N/P 1 or nNLCs nanocarrier. The culture supernatants were collected, and the secretion of pro-inflammatory cytokines (IL-6, TNFα) or chemokine (MCP-1) was quantified by immunoassay. IL-6 and TNFα productions by LPS-stimulated BMDMs were correlated to the zeta potential of the nanocarriers (**Figures 6C, D**), that is, the productions were maximum with cNLCs and decreased when cNLCs are complexed to siRNA reaching at N/P ratio 1 a similar level than the one obtained with nNLCs. The production of NO and MCP-1 by LPS-activated BMDMs also decreased with lower N/P ratios but to a lesser extent than for IL-6 and TNFα (**Figure 6E** and **Supplementary Figure 9A**).

To analyse the effect of the surface charge on glycolysis, we measured ECAR in BMDMs exposed to nanocomplexes at different N/P ratios and then stimulated or not with LPS. Both unstimulated and LPS-stimulated BMDMs showed a decrease in both glycolysis and glycolytic capacities with decreasing zeta potential and almost down to the same values as that of the nNLCs for the unstimulated cells (**Figure 6F** and **Supplementary Figure 9C**).

Next, we analysed the effect of the surface charge on the mitochondrial metabolism of BMDMs, by measuring the OCR in

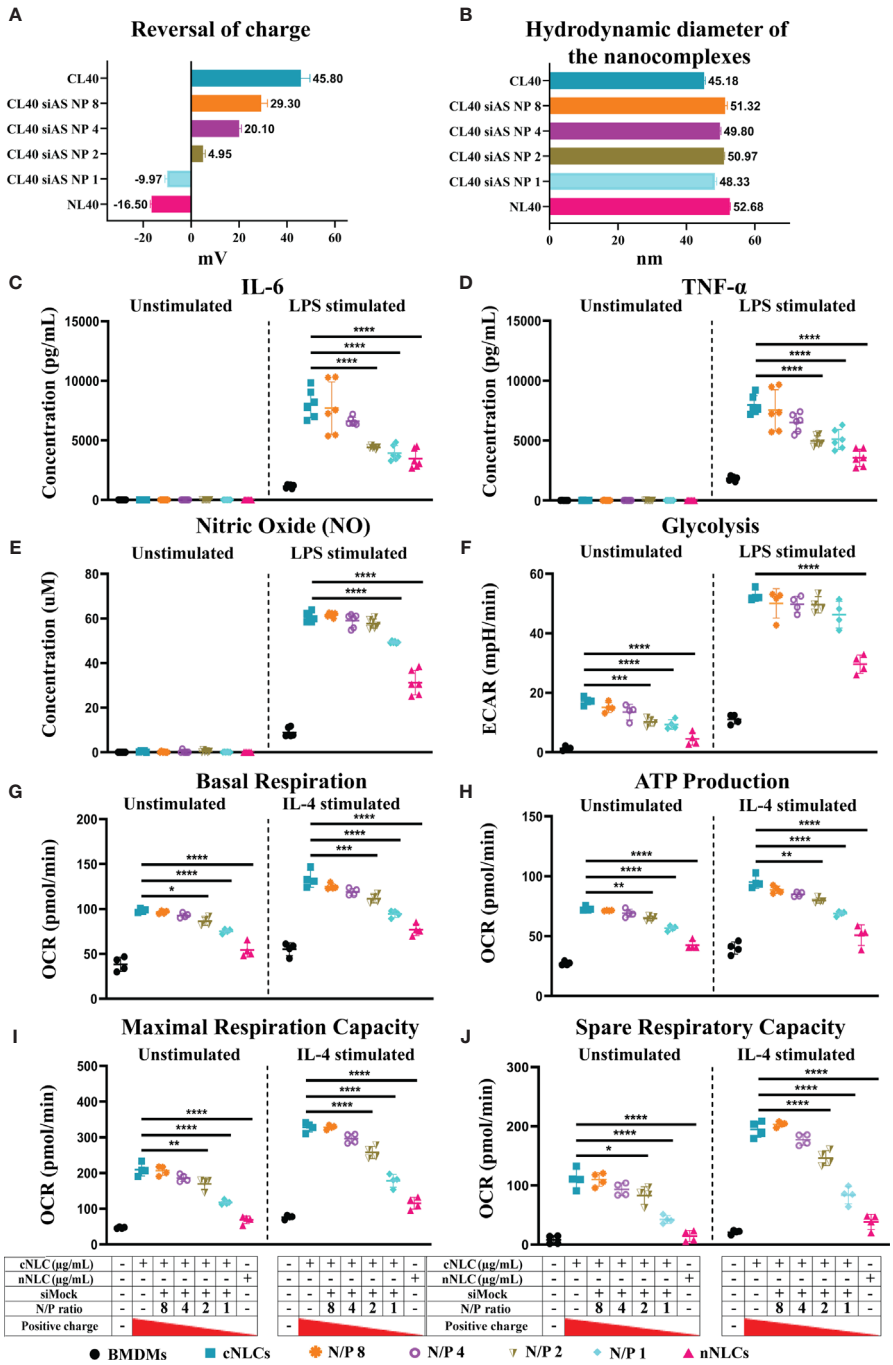

FIGURE 6 | Reversing the surface charge with a nucleic acid cargo prevent adverse effects of cNLCs on APCs. **(A)** The zeta potential measurement of cNLCs complexes with siRNA at different N/P ratios was performed on a zetasizer instrument by ELS in 1 mM NaCl. **(B)** The hydrodynamic diameter of cNLCs complexes with siRNA at different N/P ratios was measured on a zetasizer instrument by DLS in PBS buffer. **(C)** IL-6 and **(D)** TNFα secretion was quantified from the supernatant of BMDMs exposed to 100 μg/mL of cNLCs complexes with siRNA at different N/P ratios and activated or not by LPS. **(E)** NO concentration in the supernatant of BMDMs exposed to 100 μg/mL of cNLCs complexes with siRNA at different N/P ratios and activated or not by LPS was determined by Griess assay. **(F)** Glycolysis in BMDMs exposed to 100 μg/mL of cNLCs complexes with siRNA at different N/P ratios and activated or not by LPS was determined by ECAR. **(G)** Basal respiration, **(H)** ATP production, **(I)** maximal respiration capacity and **(J)** spare respiratory capacity in BMDMs exposed to 100 μg/mL of cNLCs alone or complexes with siRNA at different N/P ratios and activated or not by IL-4 was determined by OCR. OCR and ECAR were quantified using a seahorse XF analyser. Data were normalised by cell number based on cell count (Hoechst 33342 staining) and are displayed as mean ± SD (N = 4 or 6 independent experiments). The statistical significance between nanocarrier treated or untreated groups was performed by one-way ANOVA test using Tukey's multiple comparisons test. *P ≤ 0.05; **P ≤ 0.01; ***P ≤ 0.001; and ****P ≤ 0.0001.

BMDMs exposed to nanocomplexes at different N/P ratios and then stimulated or not with IL-4. The exposure to differently charged nanocarriers showed a decrease in basal respiration, maximal respiration capacity, ATP production, spare respiratory capacity and proton leak correlated with a decrease in zeta potential in both unstimulated and IL-4-stimulated BMDMs (**Figures 6G–J** and **Supplementary Figure 8B**). However, the effect of differently charged nanocarriers on both unstimulated and IL-4-stimulated BMDMs was not statistically significant for nonmitochondrial oxygen consumption and percentage of coupling efficiency (**Supplementary Figures 9D, E**).

Altogether, these results revealed that decreasing zeta potential, hence the surface charge of the cNLCs, was able to reverse their effect on the different cellular functions of primary BMDMs upon both pro- and anti-inflammatory stimulations. Moreover, using a range of N/P ratios representing the surface charge of the nanocarriers, we demonstrated that the alteration of the BMDMs physiology was proportional to the overall net surface charge of nucleic acid-loaded LNPs.

DISCUSSION

Lipid-based nanocarriers are promising delivery systems for imaging (28), gene therapy including nucleic acids delivery (29) such as siRNA transfection (13, 30) or mRNA vaccine delivery (31), drug delivery (32), adjuvant delivery system (33) and other biomedical applications.

Nanoparticles composed of cationic lipids have a strong capacity for binding and condensing nucleic acid by electrostatic interactions at the level of the phospholipid layer and deliver the payload across cellular membranes within the target cell cytoplasm (34). However, when designing a lipid-based nanocarrier, the composition of the lipids defines the protein corona around the nanocarrier that is closely linked with the activation of the immune system leading to undesired side effects and biodistribution (35, 36). It is well known that different components of lipid-based carriers such as DOPE and DOTAP facilitate the formation of protein corona eventually causing undesired side effects (37). One of the most efficient ways to reduce the nanocarrier-protein interaction and formation of protein corona is wrapping the nanocarrier with linear chains of PEG (38). PEGylation acts not only as an anti-opsonisation strategy but also as a thermodynamic shield that reduces nonspecific protein adsorption (39, 40). As our cNLCs contain DOPE and DOTAP, they were covered with 2 kDa PEG chains to limit the adsorption of proteins and direct interaction with plasma membrane as shown in a previous study (41), although preserving their capacity of the complexation with nucleic acids. However, it remains to assess the effects of cNLCs on different immune cells to precisely manage their future uses.

To understand the effect of differently charged NLCs, we opted for *ex vivo* experiments as an alternative to *in vivo* experiments, allowing for more regulated manipulation of cell functions and processes. Although cell lines have played a crucial role in scientific progress for decades, researchers are now increasingly skeptical when interpreting data generated from cell lines only. Factors such as misrepresented and contaminated cell lines have triggered a strong interest in primary cells (42, 43). In our study, to be closer to the physiological conditions, we conducted our experiments on BMDMs and BMDCs. Based on the results presented here, in unstimulated BMDCs and BMDMs, NLCs had very few effects on the cellular production of soluble factors. Interestingly, after LPS stimulation, macrophages and DCs responded differently when treated with cNLCs and nNLCs. In the case of BMDMs, after LPS stimulation, cNLCs at high concentration provoked an enhanced immune response by increasing the production of different secretory pro-inflammatory molecules including IL-6, TNF-α, and MCP-1, while nNLCs did not. However, in the case of BMDCs, we observe a reduction in TNF-α secretion by nNLCs and cNLCs exposed LPS-stimulated. Under LPS stimulation, cNLC-exposed BMDCs and BMDMs increase their production of MCP-1. MCP-1 is one of the essential chemokines that governs the migration and infiltration of monocyte and macrophage (44). Elevations of MCP-1 production have been reported after the exposure of several nanomaterials such as gold NPs on BMDMs and BMDCs (24) or nickel NPs on mesothelial cells (45). Hence, MCP-1 may be considered as a sensitive indicator of NPs exposure. MCP-1 is known to be associated with some inflammatory chronic diseases such as rheumatoid arthritis (46) or allergic asthma development (47). Therefore, it is important to consider the MCP-1 level when using cNLCs *in vivo* administration that might facilitate the emigration of immature myeloid cells at the site of exposure and promote inflammation.

To assess the influence of NLCs on the metabolism of BMDMs and BMDCs, we polarised these cells with either LPS or IL-4. While LPS-activated pro-inflammatory cells undergo a metabolic switch to enhanced glycolysis (48, 49), IL-4 induces alternatively activated cells towards an anti-inflammatory response, which would then rely mostly on FAO and mitochondrial OXPHOS (50). As a result, altered metabolism is not only a characteristic of macrophage cell functions but also a prerequisite for a proper response to an immune stimulus. We demonstrated that both NLCs did not alter the basal mitochondrial respiration of BMDCs. However, in the case of BMDMs, basal respiration increased when exposed to the highest concentration used with both NLCs, indicating that the concentration of either neutral or cationic cargo must be finely determined. While no metabolic change was observed in BMDCs, they showed an increase of glycolysis and mitochondrial respiration specific of positive cNLCs. A previous study has shown a positive association between the glycolytic and the secretory activities in macrophages; however, the same was evaluated under LPS stimulation (49). In unstimulated conditions with cNLCs exposure, we did not observe this coupling, probably because the cNLCs-induced increase of glycolysis is not high enough to drive secretory adaptations as observed in cNLCs-treated BMDMs under LPS stimulation. It is noteworthy that LPS-activated BMDMs rely on mitochondrial respiration. Based on these results obtained *in vitro*, we can assume that positive charge of cNLCs *in vivo* would not significantly affect the basal level of unstimulated DCs or macrophages secretory activity, hence preventing

unintended immune responses (suppression or activation) and subsequent harmful outcomes (cancer or autoimmunity).

For our investigations, we used two NLCs with similar composition and size but solely differing by their zeta potentials. Therefore, the effects on the cellular functions of APCs observed only with cNLCs may be linked to their respective charge. This could be explained by three hypotheses: 1) the lipid composition of the NLCs (35), 2) the net surface charge of NLCs (51) and 3) the protein corona around NLCs (37, 52). Previous studies showed that solid lipid NLCs were efficiently phagocytosed by macrophages but cationic NLCs led to increased cytotoxic effects than neutral equivalents supporting the influence of the charge on APC fate (53). An example of the effect of the charge on the activation of DCs was provided in the study of cationic hydrogel rod-shaped NLCs, which were more efficient than anionic equivalent NLCs in inducing specific immune responses (54). However, influence of cationic charge of NLCs on DC activation is not universal; for instance, both some cationic PLGA-based NLCs did not provoke significant activation of BMDCs from mice (55). Other parameters like the nature of the components of the NLCs must be considered such as DOTAP which induces pro-inflammatory effect (56) and used in lipid NLCs as adjuvant for vaccine purpose (57). Altogether, these studies highlight the difficulty in defining general rules in the reactivity of APCs after exposure to NLCs that results from the huge variety of NLCs, the diversity of APCs and the great sensitivity of APCs to their environment.

Here, we demonstrate that reversing the net charge of positively charged lipid NLCs by complexing with negatively charged RNA, can reverse the effect of charged carriers on different cellular functions. For this, we studied the effect of the charge of the nanocarrier using BMDMs as a cellular model since they appeared to be the most affected cells by the exposure to cNLCs. By modifying the net surface charge of the cNLCs using siRNA at different N/P ratios, we observed that the increase of the production of pro-inflammatory secretory molecules (IL-6, TNF-α, MCP-1 and NO) was proportional to the net surface charge of the lipid nanocarriers. In parallel, metabolic parameters, including basal respiration, maximal respiration capacity, ATP production, spare respiratory capacity and proton leak, were also modulated accordingly to the charge of the lipid nanocarriers. These results show that the effects of positively charged nanocarriers, such as cNLCs, can be reversed by the complexation of negatively charged ligands, such as RNA, proportionally to the net charge of the resulting nanocarrier. Different applications could then be developed with cNLCs associated with RNA, including RNAi therapeutics as well as mRNA delivery for vaccinal purposes, even in the context of immune disorders.

Several studies reported some effects of the charge of nanoparticles on cell behaviour. For instance, N-Arginine-N-octyl chitosan is used to synthesise pH-sensitive charge-reversal lysosomolytic nanocarriers, which could reduce the potential toxicity of the nanocarrier as well as increase the drug delivery efficiency (58). Moreover, it has been shown that that charge-reversal nanocarriers enhanced gene delivery to the tumor site (59). Furthermore, researchers demonstrated that the use of chitosan and the pH-responsive charge-reversible polymer enhanced the siRNA delivery (60). Here, our results highlight that fine-tuning of the surface charge of cationic NLCs with an oppositely charged biomaterial, for instance, nucleic acid, could prevent immunostimulation properties of the cationic carrier and has to be kept in mind for the future use of such carriers for therapeutic applications. Overall, using the same cationic lipid nanocarrier with tunable surface charge, we propose that positive charge is one of the major factors responsible for the alteration of the immune response.

CONCLUSION

In conclusion, both BMDCs and BMDMs responded differently when exposed to the cationic or neutral variation of the same lipid nanocarriers. Therefore, it is highly relevant to include both cell types in the case of immunotoxicity analysis. We demonstrated that both nanocarriers, at low concentration, did not significantly alter several functions of both APCs. However, the cationic nanocarrier, at the highest concentration, induced alterations of some functions of APCs. We demonstrated that this effect on APCs was dependent on the net positive charge surface charge of the lipid carrier that could be offset by loading nucleic acid cargo that mediated reversal of the charge. Finally, we propose that tuning the nucleic acid load, hence, the surface charge of NLCs is critical to their use for therapy and prevent the alteration of immune cell response to stimuli.

DATA AVAILABILITY STATEMENT

The raw data supporting the conclusions of this article will be made available by the authors, without undue reservation.

AUTHOR CONTRIBUTIONS

AD, AN, FC, CF, FN, and PM wrote the manuscript. AN, DJ, ME, and FN synthesized the nanoparticles and performed their physico-chemical characterization. AD, CF, and PM designed and performed cell experiments. FC, EJ-M, FN, and PM analysed the data and reviewed the study. All authors contributed to the article and approved the submitted version.

FUNDING

This work was supported by INSERM and CEA. This project has received funding from the European Union's Horizon 2020 research and innovation program H2020 "NEWDEAL" (grant agreement No. 720905). AD, AN, and FC were supported by a fellowship from H2020 NEWDEAL project.

ACKNOWLEDGMENTS

The authors acknowledge the staff of the animal facility of IAB, C. Charrat for technical support, M. Pezet for confocal

and flow cytometry analysis, S. Blanchet for her expertise in SeaHorse analysis, Z. Macek-Jilkova for stimulating discussions. This publication reflects only the author's view and the Commission is not responsible for any use that may be made of the information it contains.

SUPPLEMENTARY MATERIAL

The Supplementary Material for this article can be found online at: https://www.frontiersin.org/articles/10.3389/fimmu.2021.722411/full#supplementary-material

REFERENCES

1. Yousefi N, Tufenkji N. Probing the Interaction Between Nanoparticles and Lipid Membranes by Quartz Crystal Microbalance With Dissipation Monitoring. *Front Chem* (2016) 4:46. doi: 10.3389/fchem.2016.00046
2. Stoddard BL, Khvorova A, Corey DR, Dynan WS, Fox KR. Editorial: Nucleic Acids Research and Nucleic Acid Therapeutics. *Nucleic Acids Res* (2018) 46 (4):1563–4. doi: 10.1093/nar/gky059
3. Xue HY, Guo P, Wen WC, Wong HL. Lipid-Based Nanocarriers for RNA Delivery. *Curr Pharm Des* (2015) 21(22):3140–7. doi: 10.2174/1381612821666150531164540
4. Chira S, Jackson CS, Oprea I, Ozturk F, Pepper MS, Diaconu I, et al. Progresses Towards Safe and Efficient Gene Therapy Vectors. *Oncotarget* (2015) 6(31):30675–703. doi: 10.18632/oncotarget.5169
5. Hu B, Zhong L, Weng Y, Peng L, Huang Y, Zhao Y, et al. Therapeutic siRNA: State of the Art. *Signal Transduction Targeted Ther* (2020) 5(1):101. doi: 10.1038/s41392-020-0207-x
6. Mehnert W, Mäder K. Solid Lipid Nanoparticles: Production, Characterization and Applications. *Advanced Drug Deliv Rev* (2001) 47 (2):165–96. doi: 10.1016/S0169-409X(01)00105-3
7. zur Mühlen A, Schwarz C, Mehnert W. Solid Lipid Nanoparticles (SLN) for Controlled Drug Delivery – Drug Release and Release Mechanism. *Eur J Pharmaceutics Biopharmaceutics* (1998) 45(2):149–55. doi: 10.1016/S0939-6411(97)00150-1
8. Müller RH, Radtke M, Wissing SA. Solid Lipid Nanoparticles (SLN) and Nanostructured Lipid Carriers (NLC) in Cosmetic and Dermatological Preparations. *Adv Drug Deliv Rev* (2002) 54 Suppl 1:S131–55. doi: 10.1016/S0169-409X(02)00118-7
9. Kim HR, Kim IK, Bae KH, Lee SH, Lee Y, Park TG. Cationic Solid Lipid Nanoparticles Reconstituted From Low Density Lipoprotein Components for Delivery of siRNA. *Mol Pharmaceutics* (2008) 5(4):622–31. doi: 10.1021/mp8000233
10. del Pozo-Rodríguez A, Delgado D, Solinís MA, Gascón AR, Pedraz JL. Solid Lipid Nanoparticles: Formulation Factors Affecting Cell Transfection Capacity. *Int J Pharmaceutics* (2007) 339(1):261–8. doi: 10.1016/j.ijpharm.2007.03.015
11. Taratula O, Kuzmov A, Shah M, Garbuzenko OB, Minko T. Nanostructured Lipid Carriers as Multifunctional Nanomedicine Platform for Pulmonary Co-Delivery of Anticancer Drugs and siRNA. *J Control Release* (2013) 171 (3):349–57. doi: 10.1016/j.jconrel.2013.04.018
12. Resnier P, LeQuinio P, Lautram N, André E, Gaillard C, Bastiat G, et al. Efficient *In Vitro* Gene Therapy With PEG siRNA Lipid Nanocapsules for Passive Targeting Strategy in Melanoma. *Biotechnol J* (2014) 9(11):1389–401. doi: 10.1002/biot.201400162
13. Bruniaux J, Gidrol X, Navarro YGF, Sulpice E, Texier-Nogues I. *Formulation for the Delivery of Nucleotide Sequences That Can Modulate Endogenous Interfering Rna Mechanisms*. Commissariat Energie Atomique (2014). Available at: https://patents.google.com/patent/WO2014032953A1.
14. Kedmi R, Ben-Arie N, Peer D. The Systemic Toxicity of Positively Charged Lipid Nanoparticles and the Role of Toll-Like Receptor 4 in Immune Activation. *Biomaterials* (2010) 31(26):6867–75. doi: 10.1016/j.biomaterials.2010.05.027
15. Stunault MI, Bories G, Guinamard RR, Ivanov S. Metabolism Plays a Key Role During Macrophage Activation. *Mediators Inflamm* (2018) 2018:2426138. doi: 10.1155/2018/2426138
16. Wculek SK, Khouili SC, Priego E, Heras-Murillo I, Sancho D. Metabolic Control of Dendritic Cell Functions: Digesting Information. *Front Immunol* (2019) 10:775. doi: 10.3389/fimmu.2019.00775
17. Vangasseri DP, Cui Z, Chen W, Hokey DA, Falo LDJr., Huang L. Immunostimulation of Dendritic Cells by Cationic Liposomes. *Mol Membr Biol* (2006) 23(5):385–95. doi: 10.1080/09687860600790537
18. de Groot AM, Thanki K, Gangloff M, Falkenberg E, Zeng X, van Bijnen DCJ, et al. Immunogenicity Testing of Lipidoids *In Vitro* and *In Silico*: Modulating Lipidoid-Mediated TLR4 Activation by Nanoparticle Design. *Mol Ther Nucleic Acids* (2018) 11:159–69. doi: 10.1016/j.omtn.2018.02.003
19. Nel AE, Mädler L, Velegol D, Xia T, Hoek EMV, Somasundaran P, et al. Understanding Biophysicochemical Interactions at the Nano–Bio Interface. *Nat Materials* (2009) 8(7):543–57. doi: 10.1038/nmat2442
20. Blanco E, Shen H, Ferrari M. Principles of Nanoparticle Design for Overcoming Biological Barriers to Drug Delivery. *Nat Biotechnol* (2015) 33 (9):941–51. doi: 10.1038/nbt.3330
21. Faure M, Villiers CL, Marche PN. Normal Differentiation and Functions of Mouse Dendritic Cells Derived From RAG-Deficient Bone Marrow Progenitors. *Cell Immunol* (2004) 228(1):8–14. doi: 10.1016/j.cellimm.2004.04.002
22. Chen J, Ellert-Miklaszewska A, Garofalo S, Dey AK, Tang J, Jiang Y, et al. Synthesis and Use of an Amphiphilic Dendrimer for siRNA Delivery Into Primary Immune Cells. *Nat Protoc* (2021) 16(1):327–51. doi: 10.1038/s41596-020-00418-9
23. Courant T, Bayon E, Reynaud-Dougier HL, Villiers C, Menneteau M, Marche PN, et al. Tailoring Nanostructured Lipid Carriers for the Delivery of Protein Antigens: Physicochemical Properties *Versus* Immunogenicity Studies. *Biomaterials* (2017) 136:29–42. doi: 10.1016/j.biomaterials.2017.05.001
24. Dey AK, Gonon A, Pécheur E-I, Pezet M, Villiers C, Marche PN. Impact of Gold Nanoparticles on the Functions of Macrophages and Dendritic Cells. *Cells* (2021) 10(1):96. doi: 10.3390/cells10010096
25. Luo Y, Cook E, Fries BC, Casadevall A. Phagocytic Efficacy of Macrophage-Like Cells as a Function of Cell Cycle and Fcgamma Receptors (FcgammaR) and Complement Receptor (CR)3 Expression. *Clin Exp Immunol* (2006) 145 (2):380–7. doi: 10.1111/j.1365-2249.2006.03132.x
26. Li H, Zhang GX, Chen Y, Xu H, Fitzgerald DC, Zhao Z, et al. CD11c+CD11b+ Dendritic Cells Play an Important Role in Intravenous Tolerance and the Suppression of Experimental Autoimmune Encephalomyelitis. *J Immunol* (2008) 181(4):2483–93. doi: 10.4049/jimmunol.181.4.2483
27. Zhang X, Goncalves R, Mosser DM. The Isolation and Characterization of Murine Macrophages. *Curr Protoc Immunol* (2008) 14:14.1. doi: 10.1002%2F0471142735.im1401s83
28. Navarro FP, Mittler F, Berger M, Josserand V, Gravier J, Vinet F, et al. Cell Tolerability and Biodistribution in Mice of Indocyanine Green-Loaded Lipid Nanoparticles. *J BioMed Nanotechnol* (2012) 8(4):594–604. doi: 10.1166/jbn.2012.1422
29. Hibbitts A, Lucía A, Serrano-Sevilla I, De Matteis L, McArthur M, de la Fuente JM, et al. Co-Delivery of Free Vancomycin and Transcription Factor Decoy-Nanostructured Lipid Carriers can Enhance Inhibition of Methicillin Resistant Staphylococcus Aureus (MRSA). *PloS One* (2019) 14(9):e0220684. doi: 10.1371/journal.pone.0220684
30. Tezgel Ö., Szarpak-Jankowska A, Arnould A, Auzély-Velty R, Texier I. Chitosan-Lipid Nanoparticles (CS-LNPs): Application to siRNA Delivery. *J Colloid Interface Sci* (2018) 510:45–56. doi: 10.1016/j.jcis.2017.09.045
31. Zhang C, Maruggi G, Shan H, Li J. Advances in mRNA Vaccines for Infectious Diseases. *Front Immunol* (2019) 10:594. doi: 10.3389/fimmu.2019.00594
32. Hinger D, Navarro F, Käch A, Thomann JS, Mittler F, Couffin AC, et al. Photoinduced Effects of M-Tetrahydroxyphenylchlorin Loaded Lipid Nanoemulsions on Multicellular Tumor Spheroids. *J Nanobiotechnol* (2016) 14(1):68. doi: 10.1186/s12951-016-0221-x
33. Bayon E, Morlieras J, Dereuddre-Bosquet N, Gonon A, Gosse L, Courant T, et al. Overcoming Immunogenicity Issues of HIV P24 Antigen by the Use of Innovative Nanostructured Lipid Carriers as Delivery Systems: Evidences in Mice and non-Human Primates. *NPJ Vaccines* (2018) 3(1):46. doi: 10.1038/s41541-018-0086-0

34. Elouahabi A, Ruysschaert J-M. Formation and Intracellular Trafficking of Lipoplexes and Polyplexes. *Mol Ther* (2005) 11(3):336–47. doi: 10.1016/j.ymthe.2004.12.006
35. Caracciolo G, Pozzi D, Capriotti AL, Cavaliere C, Piovesana S, Amenitsch H, et al. Lipid Composition: A "Key Factor" for the Rational Manipulation of the Liposome–Protein Corona by Liposome Design. *RSC Adv* (2015) 5(8):5967–75. doi: 10.1039/C4RA13335H
36. Moore TL, Rodriguez-Lorenzo L, Hirsch V, Balog S, Urban D, Jud C, et al. Nanoparticle Colloidal Stability in Cell Culture Media and Impact on Cellular Interactions. *Chem Soc Rev* (2015) 44(17):6287–305. doi: 10.1039/C4CS00487F
37. Caracciolo G, Pozzi D, Capriotti AL, Cavaliere C, Laganà A. Effect of DOPE and Cholesterol on the Protein Adsorption Onto Lipid Nanoparticles. *J Nanoparticle Res* (2013) 15(3):1498. doi: 10.1007/s11051-013-1498-4
38. Vonarbourg A, Passirani C, Saulnier P, Benoit JP. Parameters Influencing the Stealthiness of Colloidal Drug Delivery Systems. *Biomaterials* (2006) 27 (24):4356–73. doi: 10.1016/j.biomaterials.2006.03.039
39. Satulovsky J, Carignano MA, Szleifer I. Kinetic and Thermodynamic Control of Protein Adsorption. *Proc Natl Acad Sci* (2000) 97(16):9037. doi: 10.1073/pnas.150236197
40. Szleifer I. Protein Adsorption on Surfaces With Grafted Polymers: A Theoretical Approach. *Biophys J* (1997) 72(2 Pt 1):595–612. doi: 10.1016/S0006-3495(97)78698-3
41. Wheeler JJ, Palmer L, Ossanlou M, MacLachlan I, Graham RW, Zhang YP, et al. Stabilized Plasmid-Lipid Particles: Construction and Characterization. *Gene Ther* (1999) 6(2):271–81. doi: 10.1038/sj.gt.3300821
42. ATCC. Cell Line Misidentification: The Beginning of the End. *Nat Rev Cancer* (2010) 10(6):441–8. doi: 10.1038/nrc2852
43. Lorsch JR, Collins FS, Lippincott-Schwartz J. Cell Biology. Fixing Problems With Cell Lines. *Sci (New York N.Y.)* (2014) 346(6216):1452–3. doi: 10.1126/science.1259110
44. Deshmane SL, Kremlev S, Amini S, Sawaya BE. Monocyte Chemoattractant Protein-1 (MCP-1): An Overview. *J Interferon Cytokine research: Off J Int Soc Interferon Cytokine Res* (2009) 29(6):313–26. doi: 10.1089/jir.2008.0027
45. Glista-Baker EE, Taylor AJ, Sayers BC, Thompson EA, Bonner JC. Nickel Nanoparticles Enhance Platelet-Derived Growth Factor-Induced Chemokine Expression by Mesothelial Cells *via* Prolonged Mitogen-Activated Protein Kinase Activation. *Am J Respir Cell Mol Biol* (2012) 47(4):552–61. doi: 10.1165/rcmb.2012-0023OC
46. Rantapää-Dahlqvist S, Boman K, Tarkowski A, Hallmans G. Up Regulation of Monocyte Chemoattractant Protein-1 Expression in Anti-Citrulline Antibody and Immunoglobulin M Rheumatoid Factor Positive Subjects Precedes Onset of Inflammatory Response and Development of Overt Rheumatoid Arthritis. *Ann Rheumatic Dis* (2007) 66(1):121. doi: 10.1136/ard.2006.057331
47. Ip WK, Wong CK, Lam CWK. Interleukin (IL)-4 and IL-13 Up-Regulate Monocyte Chemoattractant Protein-1 Expression in Human Bronchial Epithelial Cells: Involvement of P38 Mitogen-Activated Protein Kinase, Extracellular Signal-Regulated Kinase 1/2 and Janus Kinase-2 But Not C-Jun NH2-Terminal Kinase 1/2 Signalling Pathways. *Clin Exp Immunol* (2006) 145(1):162–72. doi: 10.1111/j.1365-2249.2006.03085.x
48. Van den Bossche J, Baardman J, de Winther MP. Metabolic Characterization of Polarized M1 and M2 Bone Marrow-Derived Macrophages Using Real-Time Extracellular Flux Analysis. *J Vis Exp* (2015) (105):53424. doi: 10.3791/53424
49. Kelly B, O'Neill LAJ. Metabolic Reprogramming in Macrophages and Dendritic Cells in Innate Immunity. *Cell Res* (2015) 25(7):771–84. doi: 10.1038/cr.2015.68
50. O'Neill LA, Pearce EJ. Immunometabolism Governs Dendritic Cell and Macrophage Function. *J Exp Med* (2016) 213(1):15–23. doi: 10.1084/jem.20151570
51. Fröhlich E. The Role of Surface Charge in Cellular Uptake and Cytotoxicity of Medical Nanoparticles. *Int J Nanomed* (2012) 7:5577–91. doi: 10.2147/IJN.S36111
52. Henriksen-Lacey M, Christensen D, Bramwell VW, Lindenstrøm T, Agger EM, Andersen P, et al. Comparison of the Depot Effect and Immunogenicity of Liposomes Based on Dimethyldioctadecylammonium (DDA), 3β-[N-(N′,N′-Dimethylaminoethane)carbomyl] Cholesterol (DC-Chol), and 1,2-Dioleoyl-3-Trimethylammonium Propane (DOTAP): Prolonged Liposome Retention Mediates Stronger Th1 Responses. *Mol Pharmaceutics* (2011) 8(1):153–61. doi: 10.1021/mp100208f
53. Erni C, Suard C, Freitas S, Dreher D, Merkle HP, Walter E. Evaluation of Cationic Solid Lipid Microparticles as Synthetic Carriers for the Targeted Delivery of Macromolecules to Phagocytic Antigen-Presenting Cells. *Biomaterials* (2002) 23(23):4667–76. doi: 10.1016/S0142-9612(02)00216-8
54. Fromen CA, Robbins GR, Shen TW, Kai MP, Ting JPY, DeSimone JM. Controlled Analysis of Nanoparticle Charge on Mucosal and Systemic Antibody Responses Following Pulmonary Immunization. *Proc Natl Acad Sci* (2015) 112(2):488. doi: 10.1073/pnas.1422923112
55. Barillet S, Fattal E, Mura S, Tsapis N, Pallardy M, Hillaireau H, et al. Immunotoxicity of Poly (Lactic-Co-Glycolic Acid) Nanoparticles: Influence of Surface Properties on Dendritic Cell Activation. *Nanotoxicology* (2019) 13 (5):606–22. doi: 10.1080/17435390.2018.1564078
56. Vasievich EA, Chen W, Huang L. Enantiospecific Adjuvant Activity of Cationic Lipid DOTAP in Cancer Vaccine. *Cancer Immunol Immunother* (2011) 60(5):629–38. doi: 10.1007/s00262-011-0970-1
57. Erasmus JH, Khandhar AP, Guderian J, Granger B, Archer J, Archer M, et al. A Nanostructured Lipid Carrier for Delivery of a Replicating Viral RNA Provides Single, Low-Dose Protection Against Zika. *Mol Ther* (2018) 26 (10):2507–22. doi: 10.1016/j.ymthe.2018.07.010
58. Sun M, Li J, Zhang C, Xie Y, Qiao H, Su Z, et al. Arginine-Modified Nanostructured Lipid Carriers With Charge-Reversal and pH-Sensitive Membranolytic Properties for Anticancer Drug Delivery. *Adv Healthc Mater* (2017) 6(8). doi: 10.1002/adhm.201600693
59. Chen X, Liu L, Jiang C. Charge-Reversal Nanoparticles: Novel Targeted Drug Delivery Carriers. *Acta Pharm Sinica B* (2016) 6(4):261–7. doi: 10.1016/j.apsb.2016.05.011
60. Han L, Zhao J, Zhang X, Cao W, Hu X, Zou G, et al. Enhanced siRNA Delivery and Silencing Gold-Chitosan Nanosystem With Surface Charge-Reversal Polymer Assembly and Good Biocompatibility. *ACS Nano* (2012) 6 (8):7340–51. doi: 10.1021/nn3024688

Conflict of Interest: The authors declare that the research was conducted in the absence of any commercial or financial relationships that could be construed as a potential conflict of interest.

frontiers in Immunology

ORIGINAL RESEARCH
published: 30 September 2021
doi: 10.3389/fimmu.2021.750128

The Modulatory Activity of Tryptophan Displaying Nanodevices on Macrophage Activation for Preventing Acute Lung Injury

Liya Sun[1†], Rui Wang[1†], Chenchen Wu[2], Jiameng Gong[1], Huiqiang Ma[1], Shan-Yu Fung[3] and Hong Yang[1*]*

[1] School of Biomedical Engineering and The Province and Ministry Co-Sponsored Collaborative Innovation Center for Medical Epigenetics, Tianjin Medical University, Tianjin, China, [2] Department of Pharmacology, School of Basic Medical Sciences, Tianjin Medical University, Tianjin, China, [3] Key Laboratory of Immune Microenvironment and Disease of the Ministry of Education and Department of Immunology, School of Basic Medical Sciences, Tianjin Medical University, Tianjin, China

OPEN ACCESS

Edited by:
David Pozo,
University of Seville, Spain

Reviewed by:
Guankui Wang,
University of Colorado Anschutz Medical Campus, United States
Charles E. McCall,
Wake Forest Baptist Medical Center, United States

***Correspondence:**
Hong Yang
hongyang@tmu.edu.cn;
hongyang36@gmail.com
Shan-Yu Fung
shanefung@tmu.edu.cn

[†]These authors have contributed equally to this work

Specialty section:
This article was submitted to Molecular Innate Immunity, a section of the journal Frontiers in Immunology

Received: *30 July 2021*
Accepted: *15 September 2021*
Published: *30 September 2021*

Citation:
Sun L, Wang R, Wu C, Gong J, Ma H, Fung SY and Yang H (2021) The Modulatory Activity of Tryptophan Displaying Nanodevices on Macrophage Activation for Preventing Acute Lung Injury. Front. Immunol. 12:750128. doi: 10.3389/fimmu.2021.750128

Macrophages play an important role in the initiation, progression and resolution of inflammation in many human diseases. Effective regulation of their activation and immune responses could be a promising therapeutic strategy to manage various inflammatory conditions. Nanodevices that naturally target macrophages are ideal agents to regulate immune responses of macrophages. Here we described a special tryptophan (Trp)-containing hexapeptide-coated gold nanoparticle hybrid, PW, which had unique immunomodulatory activities on macrophages. The Trp residues enabled PW higher affinity to cell membranes, and contributed to inducing mild pro-inflammatory responses of NF-κB/AP-1 activation. However, in the presence of TLR stimuli, PW exhibited potent anti-inflammatory activities through inhibiting multiple TLR signaling pathways. Mechanistically, PW was internalized primarily through micropinocytosis pathway into macrophages and attenuated the endosomal acidification process, and hence preferentially affected the endosomal TLR signaling. Interestingly, PW could induce the expression of the TLR negative regulator IRAK-M, which may also contribute to the observed TLR inhibitory activities. In two acute lung injury (ALI) mouse models, PW could effectively ameliorate lung inflammation and protect lung from injuries. This work demonstrated that nanodevices with thoughtful design could serve as novel immunomodulatory agents to manage the dysregulated inflammatory responses for treating many chronic and acute inflammatory conditions, such as ALI.

Keywords: immunomodulatory nanoparticles, acute lung injury, Toll-like receptor, peptide, gold nanoparticle, trained immunity

INTRODUCTION

Understanding the interactions between nanodevices and the immune system is pivotal to guide nanomaterial design for better biomedical application outcome. When the nanodevices are introduced into the body, they will inevitably encounter the immune system, and may trigger the innate and adaptive immune responses for good or bad. In the field of nanomedicine, majority of

the efforts have been focusing on designing "inert" or "invisible" nanodevices to escape elimination by the immune system to achieve prolonged circulation and less immunogenicity. For example, polyethylene glycol (PEG) has been widely used to modify the nanodrug carriers to avoid serum protein adsorption and reduce phagocytosis by immune cells (1–3); CD47 protein is introduced on the surface of the nanodevices to serve as the "don't eat me" signal (4, 5). However, with increasing understanding of the roles of specific immune cells in the pathophysiological process of human diseases, the phagocytotic properties of innate immune cells to grasp nanodevices could be conversely advantageous for modulation of immune reactions, opening new avenues to treat inflammatory disorders that currently lack of an effective cure.

In contrast to the "immune inert" purpose, the use of nanodevices to modulate innate and adaptive immune responses has sparked significant interests in recent years. For instance, studies have shown that the internalization of the Syk inhibitor (piceatannol)-loaded albumin nanoparticles into neutrophils can block the pro-inflammatory responses of activated neutrophils, serving as a new treatment for diseases associated with exaggerated neutrophil activation (6). A PEGylated polyphenol-based antioxidant, rosmarinic acid (RA), was designed to form nanoparticles (RANPs) to preferentially target the inflamed colon in colitis mice, and significantly reduce colon inflammation by scavenging the reactive oxygen species (ROS) (7). On the other hand, nucleic acid-based Toll-like receptor (TLR) ligands were encapsulated into liposomes to serve as potent adjuvants to boost anti-tumor immune responses (8). Interestingly, "drug-free" nanoparticles (i.e., do not carry any therapeutic agent) have been newly discovered with potent immune modulatory activities. A luminol-conjugated β-cyclodextrin based nanoparticle (LCD NP) was synthesized to effectively inhibit the inflammatory responses, oxidative stress and migration of neutrophils and macrophages to treat acute and chronic inflammatory disorders (9). These findings are encouraging that with proper design, nanoparticles could regulate immune responses, aiding to new immunotherapies to treat various diseases.

Previously, we discovered a "drug-free" peptide-gold nanoparticle (GNP) hybrid, P12, with novel anti-inflammatory activities (10–12). P12 was made of hexapeptides (CLPFFD) wrapping around the surface of a 13-nm GNP. It effectively inhibited multiple TLR signaling pathways in THP-1-derived macrophages and human peripheral blood mononuclear cells (PBMC), and exhibited potent anti-inflammatory activity in a lipopolysaccharide (LPS)-induced acute lung injury (ALI) mouse model (13). This unique bioactivity of P12 was attributed to its surface property associated with the amino acid characteristics in the modifying peptides (10).

Among the 20 natural amino acids, tryptophan (Trp, W) is one of the abundant amino acid residues in the membrane proteins, preferentially in the transmembrane region, suggesting its membrane anchoring property (14). Such a membrane anchoring process involves different interactions between the Trp residues and the lipid bilayer of the membrane. These interactions include the H-bonding, cation-π interaction, and hydrophobic interaction between Trp and the lipid phosphatidylcholine (PC). Thus, the use of Trp-containing peptides modifying the GNP surface may provide attractive properties aiding to the regulation of TLR signaling *in vitro* and *in vivo*.

In this study, we formulated the Trp-containing peptide (CLPWWD) coated GNP hybrid (designated as PW) and investigated its anti-inflammatory activity as well as the possible mechanism(s) of actions *in vitro* and *in vivo*. First, the inhibitory effects of PW on various TLR signaling pathways were confirmed. The global transcriptomic analysis was then applied to obtain the profile of gene expression altered by PW on the regulation of inflammatory responses with/without LPS stimulation. Mechanistically, the inhibitory activity of PW was associated with its endosomal pH modulatory activity. In addition, the up-regulated inhibitory signaling of IRAK-M by PW treatment may also contribute to its novel anti-inflammatory activities. Lastly, the *in vivo* therapeutic efficacy of PW was assessed using two ALI mouse models. This research provides knowledge of understanding the interactions between bioactive nanoparticles with the innate immune system *in vitro* and *in vivo*. It also helps develop immune modulatory nanodevices as a new generation of anti-inflammatory nanomedicine for human inflammatory diseases.

MATERIALS AND METHODS

Materials

Gold(III) chloride trihydrate (99.9%), phorbol myristate acetate (PMA), LPS (E-coli O111:B4, for mice), chloroquine (CHQ), wortmannin, fucoidan, mannan, genistein, methyl-β-cyclodextrin (MβCD), chlorpromazine (CPZ) and SP600125 were purchased from Sigma (Sant-Louis, MO, USA). Cytochalasin D (CytoD) and filipin III (filipin) were purchased from Cayman (Ann Arbor, MI, USA), while Nystatin was from MCE (Monmouth, NJ, USA). Peptides were synthesized from Nanjing Jietai Biological Company (Nanjing, China). The human monocytic THP-1 cell line was obtained from ATCC (Rockefeller, MD, USA). THP-1 reporter cell lines (XB and ISG), LPS-EK (LPS from E. coli K12, for cells), Poly I/C (high molecular weight, HMW), resiquimod (R848), Pam3CSK4, Zeocin and QUANTI-Blue™ solution were purchased from InvivoGen (San Diego, CA, USA). RPMI 1640 medium, phosphate buffered saline (PBS) and fetal bovine serum (FBS) were purchased from Biological Industries (Kibbutz Beit Haemek, Israel). L-glutamine and sodium pyruvate were from Gibco (Grand Island, NY, USA). MTS assay was purchased from Promega (Madison, WI, USA). Human ELISA kits (MCP-1, TNF-α and IL-6) and mouse IL-10 ELISA kits were purchased from Invitrogen (Grand Island, NY, USA). Human ELISA kit IL-12/IL-23 p40 was purchased from R&D Systems (Minneapolis, MN, USA). Tris buffered saline (TBS), Liu stain and red blood cell (RBC) lysis buffer were purchased from Solarbio (Beijing, China). The primary antibodies against phosphorylated p65

(#3033S), IRF3 (#4947S) and STAT1 (#9167S), IκBα (#9242S), β-actin (#8457S), IRF7 (#13014S) and IRAK-M (#4369S) as well as the HRP conjugated anti-rabbit (#7074S) antibodies were purchased from Cell Signaling Technology (Boston, MA, USA). The RIPA lysis buffer, Halt protease and phosphatase inhibitor cocktail, the Coomassie Plus (Pierce) of Bradford assay and pHrodo red-labeled 10,000 MW dextran were from Thermo Fisher Scientific (Waltham, MA, USA). Bovine serum albumin (BSA) was purchased from Genview (Houston, TX, USA). Tween 20, sodium citrate tribasic dihydrate and cholesterol were purchased from Sangon Biotech (Shanghai, China). Soy Lecithin was obtained from Tywei (Shanghai, China). RNeasy Plus Mini kit for total RNA extraction was obtained from Qiagen (Hilden, Germany). Cy5-PEG5000-SH was obtained from Ponsurebio (Shanghai, China). 3,3′-dioctadecyloxacarbocyanine perchlorate (DiO) and 2-(4-Amidinophenyl)-6-indolecarbamidine dihydrochloride (DAPI) were purchased from Beyotime (Shanghai, China).

Methods

Fabrication of Peptide-GNP Hybrids

Bare gold nanoparticles (GNPs) were synthesized based on the literature and our previous work (10, 15). The pepide-GNP hybrids were prepared by mixing 1 volume of different peptide solutions (CLPWWD, CLPFFD, CLPLLD, CLPIID, CLPAAD, CLPSSD and CLPTTD at a concentration of 1 mM) with 10 volumes of bare GNPs and kept in dark for at least 24 h. For fluorescent nanoparticles (PW-Cy5), one volume of peptide stock solution (1 mM) containing 1% Cy5-PEG5000-SH (molar ratio) was mixed with ten volumes of synthesized GNP solution. The peptide-GNP solution was filtered through a syringe filter (0.22 μm, Millipore, Billerica, MA, USA) and washed three times with sterile PBS to remove unbound peptide ligands by centrifugation (14,000 rpm for 30 minutes at 4°C). The peptide GNPs were resuspended in PBS or cell culture medium at the desired concentrations prior to the cell culture experiments or animal studies.

Liposome Fabrication

Liposomes were prepared by the method of thin film hydration and then purified by centrifugation (14000 rpm, 1 h, 4°C). Briefly, the soy lecithin (180 mg) and cholesterol (60 mg) were dissolved in 20 mL of the chloroform-methanol mixture (3:1, v/v). The thin lipid film was formed by rotary evaporation at 37°C. The lipids were re-hydrated in PBS (15 mL), and the suspension was dispersed by ultrasound, followed by filtering through a 0.22 μm microporous membrane (Millipore, Billerica, MA, USA). The liposomes were stored at 4°C prior to use.

Characterization of Peptide-GNP Hybrids and Their Interaction With Liposomes

The morphology of the hybrid PW and the mixtures of liposomes with PW or PT were imaged on a transmission electron microscope (TEM) (HT7700, Hitachi, Tokyo, Japan) with an accelerating voltage of 80 kV. The hydrodynamic diameter and Zeta potential of the bare GNPs and PW were determined by using the Zetasizer instrument (Nano-ZS, Malvern, Worcestershire, UK).

Cell Culture and Treatments

The THP-1 cells were cultured in the complete RPMI 1640 medium containing 10% FBS, 2 mM L-glutamine and 1 mM sodium pyruvate with 5% CO_2 at 37°C. The complete culture medium was supplemented with Zeocin (200 or 100 μg/mL) as the selection medium for THP-1-XBlue cells or THP-1-ISG cells, respectively. These cells were seeded into culture plates with the addition of PMA (50 ng/mL) for 24 h to differentiate into macrophages; they were then washed twice with PBS and rested for 48 h prior to further experiments.

The seeded macrophages were treated with the hybrids, different TLR ligands (LPS, Pam3CSK4 and poly I/C) or both the hybrid and TLR stimulus for various time periods; the culture medium and the cells lysates were collected for further analysis. For R848 stimulation, THP-1 monocytes were seeded in a cell culture plate overnight and then treated with PW and R848 (10 μg/mL) for 24 h before further analysis.

Cell Viability Test

The derived macrophages (1×10^5 cells/well) were seeded into a 96-well plate and treated with PW for 24 h. MTS reagent (20 μL/well) was directly added to each well and incubated for 1-2 h. The absorbance at 490 nm was recorded on a microplate reader (TECAN, Mannedorf, Zurich, Switzerland). The percentage of viable cells was estimated in comparison to the untreated group as 100%.

Reporter Cell Assay by QUANTI-Blue

The derived macrophages or THP-1 monocytes (1×10^5 cells/well) were seeded in a 96-well flat- or U-bottom plate, respectively. After treatments, the culture media were collected and centrifuged to remove the hybrids. The supernatants (20 μL) were transferred into a new 96-well plate and mixed with the QUANTI-Blue solution (180 μL) and incubated at 37°C for 1-2 h for the color development. The color change was quantified by measuring the absorbance at 655 nm on a microplate reader (TECAN, Mannedorf, Zurich, Switzerland) to examine NF-κB/AP-1 or IRF activation.

Immunoblotting Analysis

THP-1 monocytes (1×10^6 cells/well) were seeded into a 12-well plate and differentiated into macrophages. After various treatments, cells were lysed in ice-cold RIPA lysis buffer. The total protein concentration of the lysates was quantified and adjusted prior to the protein separation by 10% SDS-PAGE. The separated proteins were transferred to PVDF membranes (Immobilon-P, Millipore, Billerica, MA, USA). The membranes were blocked and blotted with primary antibodies against β-actin, IκBα, p-p65, p-IRF3, p-STAT1, IRF7 and IRAK-M at 4°C overnight. They were then blotted with HRP labelled secondary antibody for 1 h at room temperature, and imaged by the chemiluminescence method (ECL, Millipore, Billerica, MA, USA) on a ChemiDoc MP imaging system (Bio-Rad, Hercules,

CA, USA). The protein band densitometry was analyzed using ImageJ software (NIH, Bethesda, MD, USA).

Cytokine Analysis

THP-1 monocytes (5×10^5 cells/well) were seeded into a 24-well plate and differentiated into macrophages. After various treatments for 24 h, the culture medium was centrifuged (14000 rpm, 4°C, 30 min), and the supernatant was collected for the analysis of different cytokines by ELISA following the manufacturer's instructions.

Confocal Fluorescence Imaging

THP-1 cells (2.4×10^5 cells/well) were seeded in a 20 mm glass bottom dish (NEST, Wuxi, China) and differentiated into macrophages. To assess the endosomal acidification, cells were incubated with pHrodo red-labeled dextran (10,000 MW, 10 μg/mL) and PW (200, 100 and 50 nM) or chloroquine (30 μM) for 5 h and processed for confocal imaging. To examine the uptake of PW in macrophages, cells were incubated with Cy5-labelled PW (PW-Cy5, 10 nM) for 5 h, and the cell membrane and nucleus were then stained with DiO and DAPI, respectively. Cells were washed with PBS and imaged on a confocal microscope (LSM900, Leica Microsystems Inc., Wetzlar, Hessen, Germany). The fluorescence of pHrodo red (ex: 565 nm; em: 585 nm) and Cy5 (ex: 640 nm; em: 670 nm) in the cells was quantified by the ImageJ software. For each condition, at least 30 cells were quantified with three independent repeats.

Cellular Uptake Analysis

To analyze the endocytotic pathways of entry of PW, THP-1-derived macrophages were pre-treated with various endocytotic inhibitors 30 min prior to the addition of the PW-Cy5 (10 nM) for 5 h. These inhibitors included CytoD (3 μM) and wortmannin (10 μM) for macropinocytosis, fucoidan (25 μg/mL) for scavenger receptor-mediated endocytosis, mannan (500 μg/mL) for mannose receptor-mediated endocytosis, genistein (200 μM), nystatin (10 μM), MβCD (5 mM) and filipin (10 μM) for caveolae/lipid raft-mediated endocytosis, and CPZ (10 μM) for clathrin-mediated endocytosis. After treatments, cells were collected, washed and fixed by 4% paraformaldehyde for 15 min. They were washed and resuspended in 0.9% NaCl solution containing 0.1 M NaOH (to remove PW-Cy5 adsorbed on the membrane surface). After final wash step, cells were resuspended in PBS for flow cytometric analysis.

RNA-Seq Analysis

THP-1 monocytes (2×10^6 cells/well) were seeded into a 12-well plate and differentiated into macrophages. After various treatments (Unstim, PW, LPS and LPS-PW) for 4 h, the total RNA was extracted using RNeasy mini kit and assessed by a Nanodrop Lite Spectrophotometer (Thermo Scientific™, Waltham, MA, USA) for the purity. The RNA-Seq was done using Illumina Novaseq 6000 platform by Novogene Co., LTD (Beijing, China).

Differential expression analysis was performed using the DESeq2 R package (1.26.0). Genes with the criteria of an adjusted p-value < 0.05, |log2 (fold change)| > 0.5 or 2 were assigned as differentially expressed. The pheatmap R package (1.0.12) was used to produce heatmaps of differentially expressed genes (DEGs) between groups: PW vs. Unstim and LPS-PW vs. LPS. The ggplot2 R package (3.3.5) was used to generate volcano plots of DEGs.

ClusterProfiler R package (3.14.3) was used to perform the KEGG pathway enrichment analysis. KEGG pathways with adjusted p-values < 0.05 were considered statistical significance in the enrichment analysis. The most enriched 20 KEGG pathways were shown in the bar graph. ClueGO (2.5.8), a plug-in of Cytoscape, was used to show the enriched DEGs in the most significant KEGG pathways with a p value < 0.05 as the cut-off criterion.

Acute Lung Injury Murine Model

C57BL/6 wild-type male mice (6-8 weeks from SPF Biotechnology Co., Ltd, Beijing, China) were used to replicate the ALI mouse model by intratracheal LPS administration. All the surgical procedure was done under the 1% sodium pentobarbital anesthesia (45 mg/kg) through intraperitoneal injection. PW (1.25 nmol/kg) was given through intratracheal injection 2 h before LPS (10 mg/kg) challenge. Mice were sacrificed 24 h after LPS challenge for the analyses of lung inflammation and injury. All mouse studies were performed according to the guidelines of the Institutional Animal Care and Use Committee of Tianjin Medical University.

BALF Collection and Differential Cell Counting

At the end of the ALI model, mice were under tracheotomy, and ice-cold sterile PBS (0.8 mL) was injected through the trachea to the lung twice. The bronchoalveolar lavage fluid (BALF) was collected 30 s after injection, and centrifuged at 1000 rpm for 10 min at 4°C. The supernatants were stored at −80°C for cytokine analysis. The cell pellets were processed with 4% RBC lysis buffer and resuspended in PBS for total cell counting on a hemocytometer. Aliquots of the cell suspensions were cytospined onto a glass slide, stained with Liu stain, and imaged on an up-right microscope (ECLIPSE Ni-U, Nikon, Tokyo, Japan) for differential cell counting. A total of at least 300 cells were counted for each sample.

Lung Injury Score and W/D Ratio

In a different set of experiment, the left lung was collected, fixed in 4% paraformaldehyde, dehydrated and embedded in paraffin for histopathological sectioning. The tissue sections were stained with hematoxylin and eosin (H&E) and imaged on an up-right microscope (ECLIPSE Ni-U, Nikon, Tokyo, Japan). For each sample, at least 20 images at 400x amplification were blindly scored by three independent researchers on the five histopathological features: alveolar neutrophils, interstitial neutrophils, hyaline membranes, proteinaceous debris, and alveolar septal thickening (16). The remaining lungs were processed for the analysis of W/D ratio as follows. The fresh lung tissues were first weighed, and wrapped in aluminum foil for drying in an oven at 60°C for 48 h. They were weighed again, and the weight ratio was calculated to obtain the W/D ratio.

Statistical Analysis

All statistical analysis was carried out using GraphPad Prism 7.0. All data are expressed as means ± SEM, and a p-value of < 0.05 was considered statistically significant. For comparison between two groups, the student t-test was used, whereas one way ANOVA with Bonferroni correction was performed for multiple comparison among groups.

RESULTS

Synthesis and Characterization of the Peptide-GNP Hybrid PW

We previously developed a novel anti-inflammatory peptide-GNP hybrid (P12) that can inhibit multiple TLR signaling pathways without carrying any drug compound (10). P12 was made of a hexapeptide (CLPFFD) shell and a 13-nm GNP core. We demonstrated that the FF region in the peptide sequence plays an important role for TLR inhibition, and the hydrophobicity of this region contributes to the potency of such inhibitory activity (11). Among 20 natural amino acids, tryptophan (W) has a hydrophobic side chain and preferentially interacts with cell membrane; hence, it would be very interesting to know whether the replacement of FF with WW could render different immunomodulatory activities of P12. Accordingly, the CLPWWD hexapeptide was used to coat the GNP to obtain a new hybrid designated as PW (**Figure 1A**). The size and morphology of the PW were characterized by transmission electron microscopy (TEM). As shown in **Figure 1B**, the PW was monodispersed with a uniform spherical structure; its hydrodynamic diameter was analyzed to range from 11.2 ± 0.5 to 68.6± 5.0 with the peak size of 26.0 nm (PDI: 0.13 ± 0.01) by dynamic light scattering (DLS) (**Figure 1C**), which was 9.4 nm larger than the bare GNP (the peak size of 16.6 nm, range from 7.9 ± 0.3 to 34.4 ± 1.5; PDI: 0.04 ± 0.01), suggesting that the formation of the peptide coating on the GNP surface. The PW had a zeta-potential of −30.6 ± 2.1 mV, slightly less negative than the bare GNP (−36.0 ± 2.4 mV) (**Figure 1D**). However, this quite negative zeta-potential value was essential for the stability of PW in aqueous solution. In fact, PW was stable even in PBS solution while the bare GNP formed aggregates indicated by the solution color as well as the optical absorption at 519 nm (**Figure 1E**). These results suggested that peptide coating on the GNP surface significantly improved the stability of GNPs at the physiological condition.

Based on the optical characteristics of Trp that has a strong absorbance at 280 nm wavelength, we were able to estimate the number of Trp-containing peptide molecules conjugated on the

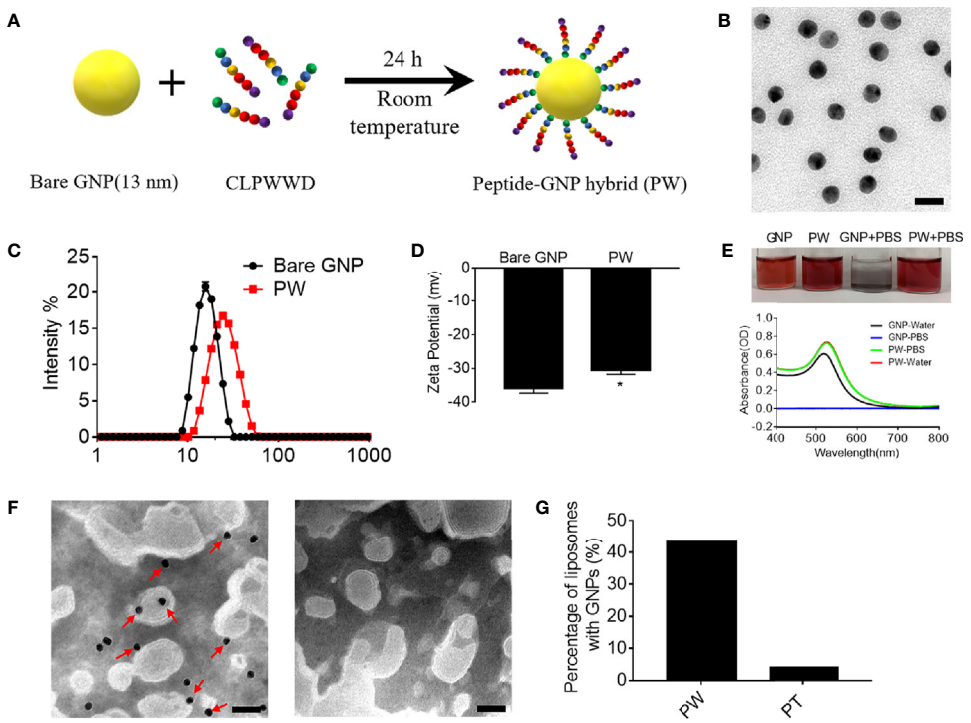

FIGURE 1 | Preparation of the peptide-GNP hybrid PW and its physicochemical characterization. **(A)** A schematic diagram of the synthesis of the peptide-GNP hybrid PW. **(B)** The TEM image of PW; scale bar = 20 nm. **(C)** The size distribution of the bare GNP and PW. **(D)** The zeta-potential of the bare GNP and PW. **(E)** The photograph (top) and UV-Vis spectra (bottom) showing the stability of bare GNP and PW in water and PBS. **(F)** The TEM images of the nano-hybrids PW (left) and PT (right, coated with the peptide CLPTTD) with liposomes showing that PW tends to interact with liposomes, but the control nano-hybrid PT does not; scale bar = 50 nm, PW, PT = 5 nM, phospholipid = 1.67 mg/mL. **(G)** The percentage of liposomes interacting with the nanohybrids; over 200 liposomal vesicles were counted. N ≥ 3, *p < 0.05.

GNP surface. It was found that each PW had approximately 1483 ± 344 peptides coating on the GNP surface.

To examine whether PW preferentially interacts with the cell membrane, we used liposomes as the artificial cell membrane and observed their interactions by TEM. A control hybrid PT, which W was replaced with the non-membrane anchoring amino acid threonine (T), was employed for comparison. As shown in **Figure 1F**, there were more nanoparticles (PW) observed on the liposome membranes (indicated by the red arrows), but none of PT were seen (right panel). These images were further quantified to show that more than 43% of liposomes had PW on the membranes, significantly higher than that (< 4%) for PT (**Figure 1G**). These observations suggested that PW had a stronger membrane affinity due to the membrane anchoring property of the Trp residues.

The Immunomodulatory Activity of PW to Macrophages

Macrophages are important phagocytic immune cells in initiating pro-inflammatory responses for the host defense against pathogens and participating in the pathogenesis of many diseases. To study how PW influences the immune responses of macrophages, we employed the human monocytic THP-1-derived macrophages with/without the reporter system of the transcription factors NF-κB/AP-1 (THP-1 XBlue cells) and IRF (THP-1 Blue ISG cells). First, we confirmed that PW had no effect on the viability of macrophages up to 200 nM (**Figure 2A**). Using the two reporter cells, we found that PW itself could mildly activate NF-κB/AP-1, but much less than the strong TLR4 agonist LPS (10 ng/mL) (**Figure 2B**); such an effect was not observed on the activation of IRF (**Figure 2C**). These observations were further confirmed at the protein level, where NF-κB was activated by PW as indicated by the increase in the phosphorylation of the NF-κB subunit p65 (p-p65) and the degradation of the NF-κB inhibitor unit IκBα, while PW had no effects on the phosphorylation of IRF3 (p-IRF3) for IRF3 activation (**Figures 2D, E**). Furthermore, PW at a higher concentration of 200 nM was able to induce the production of the pro-inflammatory cytokine TNF-α (**Figure 2F**). Together, these results suggested that PW alone could trigger the pro-inflammatory responses of macrophages.

Interestingly, when macrophages were activated by LPS, PW treatment on the contrary inhibited the activation of both NF-κB/AP-1 and IRF in a concentration dependent manner (**Figures 2G, H**). Such inhibition was also verified by immunoblotting (**Figures 2I–L**), where the LPS-induced phosphorylation of p65 and IRF3 as well as the degradation of IκBα were decreased by PW (indicated by red arrows). Moreover, PW was able to reduce the production of many pro-inflammatory cytokines, including IL-6, IL-12/IL-23p40, TNF-α and MCP-1, triggered by LPS stimulation (**Figure 2M**). Surprisingly, neither the peptide nor the GNPs alone could activate NF-κB/AP-1 of resting macrophages or reduce the activation of NF-κB/AP-1 of LPS stimulated macrophages (**Supplementary Figure S1**). Only when the peptide and GNP formed nano-hybrids did they exhibit immunomodulatory activities. These results demonstrated that PW itself seemed to activate macrophages and induce mild pro-inflammatory responses, but under strong inflammatory stimulation by LPS, PW instead exhibited potent anti-inflammatory activity. Such an opposite effect of PW makes it an interesting and unique class of immunomodulatory nanoparticles.

Preferential Inhibition of Endosomal TLR Signaling Pathways by PW

Next, we would like to address whether the inhibitory activity of PW was specific to TLR4. Among all known TLRs, we investigated the effects of PW on the cell surface TLR2 and the endosomal TLRs 3 and 7/8 (**Figure 3A**). We found that PW had no effects on the activation of NF-κB/AP-1 stimulated by the TLR1/2 ligand Pam3CSK4 (**Figure 3B**). However, PW treatment significantly reduced the activation of NF-κB/AP-1 and IRF triggered by the TLR3 ligand Poly I/C as well as the TLR7/8 ligand R848 in a concentration-dependent fashion (**Figures 3C–F**). In addition, PW was able to inhibit the secretion of IL-6, TNF-α and MCP-1 upon R848 stimulation (**Supplementary Figure S2**). These results indicated that PW had a relatively broad inhibitory activity preferentially on the endosomal TLR pathways.

Transcriptomic Analysis by RNA-Seq to Define the Immunomodulatory Activities of PW on Macrophages

To better define the pro-inflammatory and anti-inflammatory activity of PW, the high-throughput RNA-Seq analysis was conducted to obtain the transcriptomic profiles of PW treatment on the macrophages in the absence and presence of the LPS stimulation. The differential gene expression profiles of PW were visualized on the heat map (**Figure 4A**), where top 79 differentially expressed genes (DEGs) were displayed. PW induced 57 genes with > 2 folds of expression changes in comparison with the unstimulated control group. Interestingly, under LPS stimulation, PW was able to decrease 19 LPS up-regulated genes to the level similar to the unstimulated control group. The volcano plots showed all the gene expression pattern and highlighted the top 10 up- or down-regulated DEGs (**Figures 4B, C**). Collectively, the transcriptome analysis showed that the PW alone had mild pro-inflammatory effects, but exhibited significant anti-inflammatory activity in the presence of LPS stimulation.

The KEGG pathway enrichment analysis identified 20 and 17 significantly enriched pathways in the PW vs. Unstim group and the LPS-PW *vs*. LPS group, respectively (**Figures 4D, E**). PW treatment alone up-regulated the immune-related signaling pathways, such as Toll-like receptor signaling pathways, NF-κB signaling pathways, and viral infection-related signaling pathways (**Figure 4D**). However, with the LPS stimulation, PW in contrast down-regulated those immune-related signaling pathways including Toll-like receptor signaling pathways and NF-κB signaling pathways (**Figure 4E**). These up- and down-regulated pathways and essential genes were plotted into the pathway

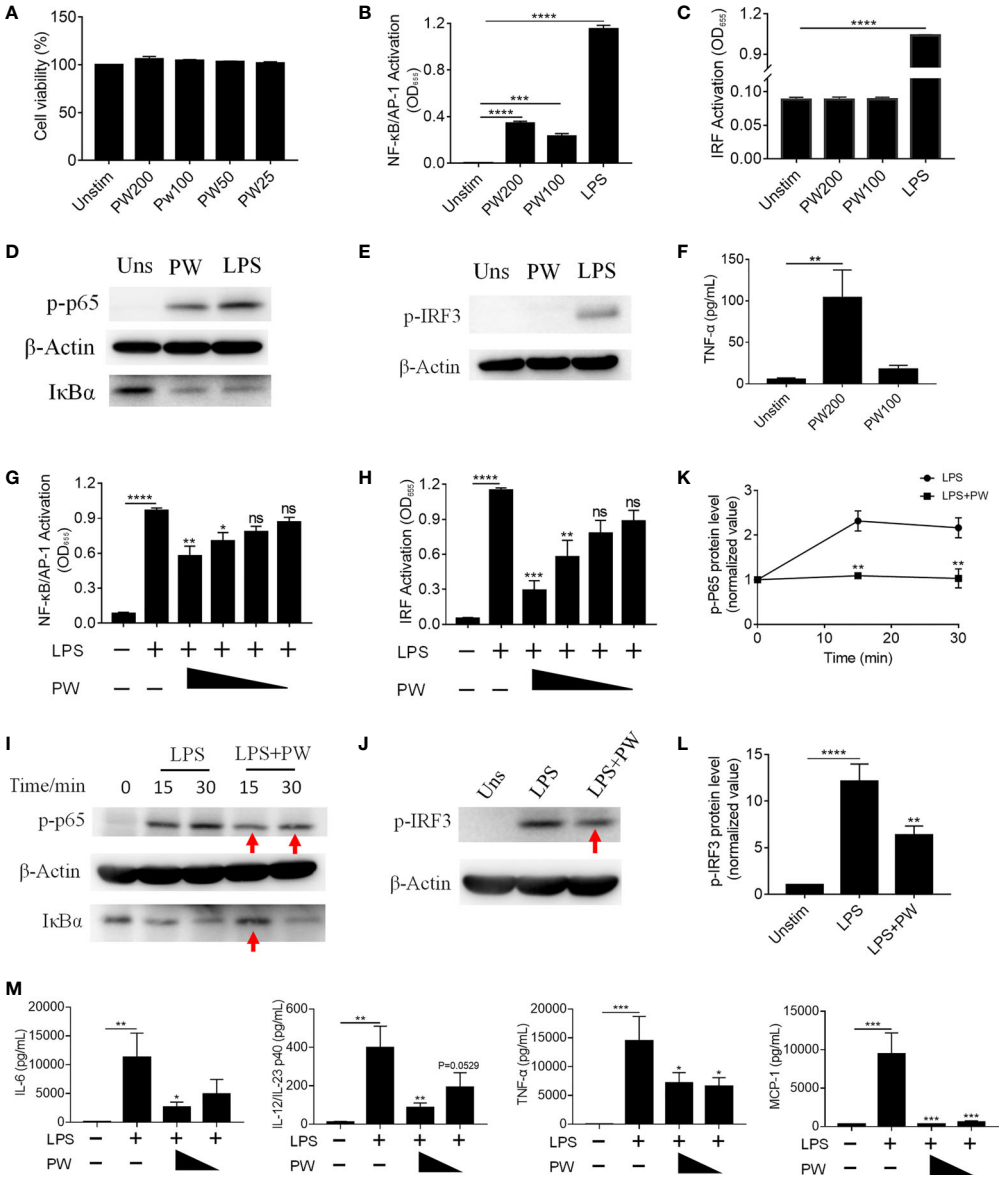

FIGURE 2 | The immunomodulatory activity of PW on TLR4 signaling in THP-1-derived macrophages. **(A)** The effect of the PW treatment on the cell viability measured by the MTS assay; PW concentrations: 200, 100, 50 and 25 nM. **(B, C)** The effect of PW treatment alone on the activation of NF-κB/AP-1 **(B)** and IRF **(C)** in the THP-1 reporter cell-derived macrophages. **(D, E)** Immunoblotting validating the effect of PW (200 nM) on the phosphorylation of p65 (p-p65) and degradation of IκBα at 1 h for NF-κB activation **(D)** and the phosphorylation of IRF3 (p-IRF3) at 1 h for IRF activation **(E)** in THP-1-derived macrophages; β-actin as the internal control. **(F)** TNF-α production induced by PW at 100 and 200 nM. **(G, H)** The inhibition of LPS-induced activation of NF-κB/AP-1 **(G)** and IRF **(H)** by PW with various concentrations (200, 100, 50 and 25 nM) in the THP-1 reporter cell-derived macrophages. **(I, J)** Immunoblotting confirming the inhibitory effect of PW (200 nM) on the LPS-induced phosphorylation of p65 (p-p65) and degradation of IκBα for NF-κB activation **(I)** and the phosphorylation of IRF3 (p-IRF3) at 1 h for IRF activation **(J)**; β-actin as the internal control; the time course of p65 phosphorylation **(K)** and the IRF3 phosphorylation **(L)** were quantified from **(I)** and **(J)**, respectively. **(M)** Inhibition of IL-6, IL-12/IL-23p40, TNF-α and MCP-1 production upon 24 h LPS stimulation by PW (200 and 100 nM) in THP-1-derived macrophages. N ≥ 3, LPS = 10 ng/mL, ns, not significant, *p < 0.05, **p < 0.01, ***p < 0.001, ****p < 0.0001 *vs*. LPS.

networks as shown in **Figures 4F, G**. In the networks, many cytokine genes were found to be elevated in PW vs. Unstim group, while the STAT1 and IRF7 transcription factors as well as the primary adaptor protein in TLR pathway MyD88 were down regulated in the LPS-PW vs. LPS group. The changes in the phosphorylation of STAT1 and IRF7 expression were confirmed by immunoblotting (**Figures 4H, I**). The reporter assay, cytokine measurements and the transcriptomic profiles coherently revealed that PW had opposite immunomodulatory effects depending on the presence of the TLR stimuli.

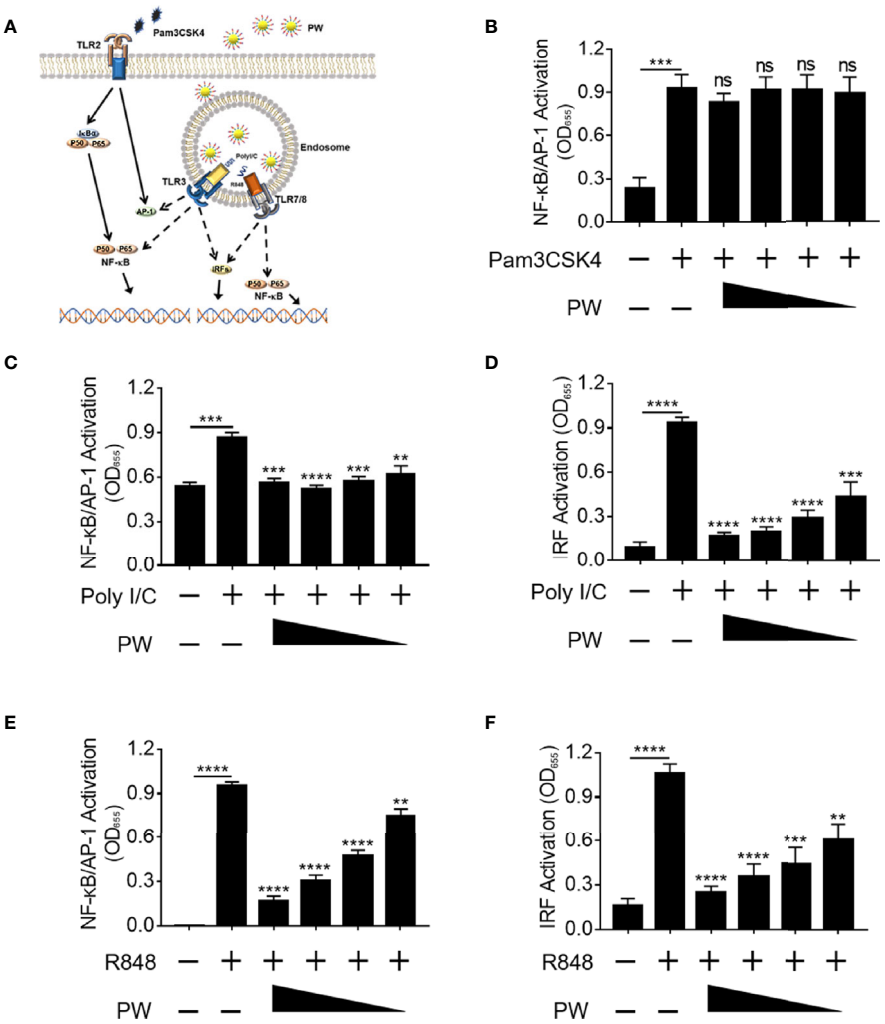

FIGURE 3 | Preferential inhibition of endosomal TLR signaling by PW in THP-1 reporter cells and their derived macrophages. **(A)** Illustration of the effects of PW on the cell surface TLR2 and the endosomal TLRs 3 and 7/8 signaling. **(B)** PW could not inhibit NF-κB/AP-1 activation induced by the TLR2 ligand Pam3CSK4 (10 ng/mL) in THP-1 reporter cell-derived macrophages. The inhibition of NF-κB/AP-1 **(C)** and IRF **(D)** by PW in TLR3 signaling stimulated by the Poly I/C (50 μg/mL) in THP-1 reporter cell-derived macrophages. The inhibitory effect of PW on the activation of NF-κB/AP-1 **(E)** and IRF **(F)** induced by the TLR7/8 ligand R848 (10 μg/mL) in THP-1 reporter cells. The concentrations of PW used: 200, 100, 50 and 25 nM; N ≥ 3, ns, not significant, $^{**}p < 0.01$, $^{***}p < 0.001$, $^{****}p < 0.0001$.

The Mechanism(s) of Actions of the Novel Immunomodulatory Activities of PW

We previously found that the inhibitory activity of the peptide-GNP hybrid P12 on TLR signaling was through the modulation of the endosomal pH (11). We expected that PW may have a similar mechanism as well. The uptake experiment by the confocal microscopy indeed showed that PW was internalized by macrophages (**Figure 5A**). To elucidate which internalization pathways were involved in the PW uptake, different chemical inhibitors were used to specifically inhibit the uptake pathway. It was found that the micropinocytosis inhibitors wortmannin and CytoD could significantly reduce the uptake of PW (**Figure 5B**), suggesting that PW was internalized through the micropinocytosis. As expected, the internalized PW at higher concentrations (100 and 200 nM) could block the endosomal acidification probed by the endosomal pH indicator (pHrodo red), where the dimmer fluorescence signals indicated a higher endosomal pH; the same phenomenon was seen with the well-known pH modulator chloroquine (CHQ) serving as a positive control (**Figures 5C, D**). These results suggested that the endosomal pH modulation contributed to the observed concentration dependent inhibition of TLR signaling by PW.

In addition to endosomal pH modulation, there may be other mechanisms of action of PW due to its unique opposite immunomodulatory activity. Based on the above discovery (**Figures 2**, **4**), we hypothesized that the inhibitory effects of PW on the TLR signaling may be primed by the PW treatment, in analogy to the LPS tolerance effects (17). To test this

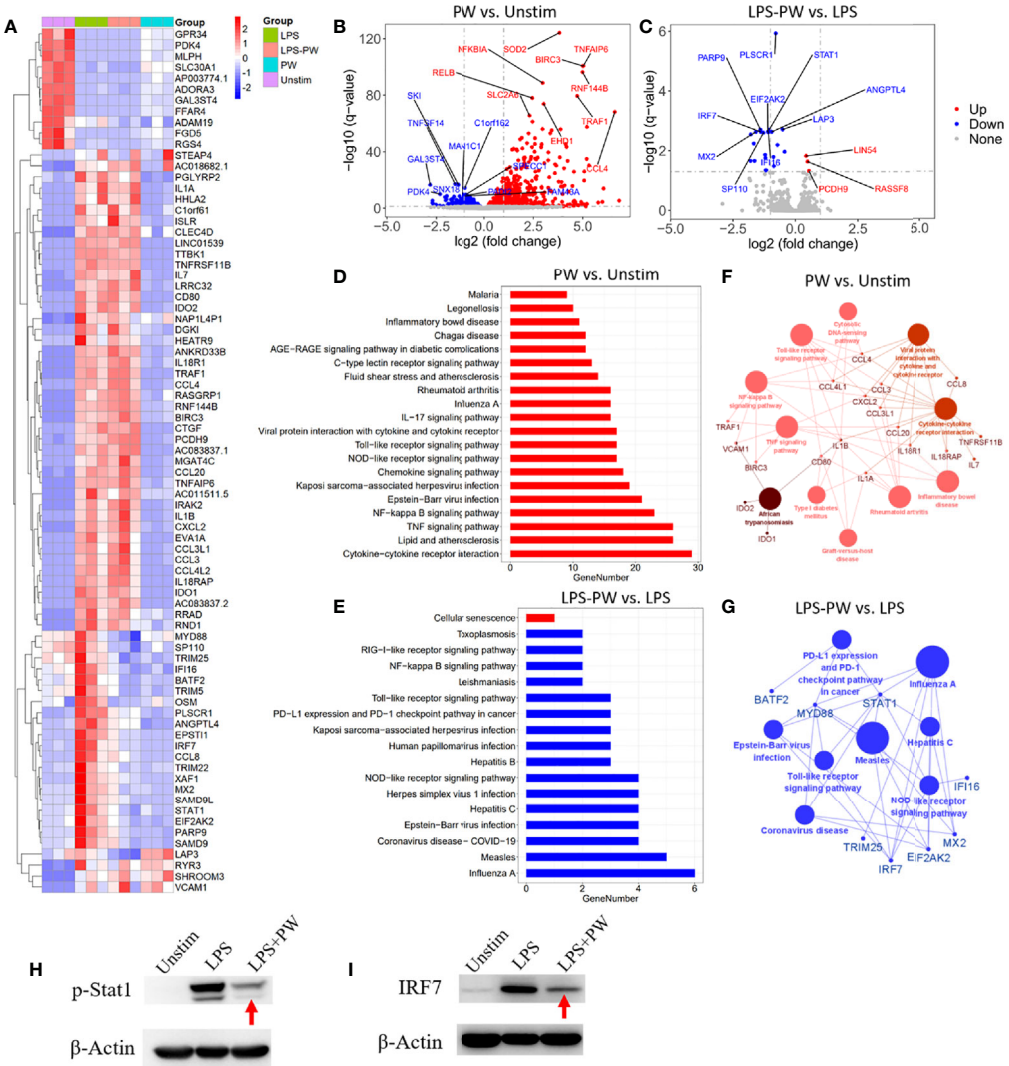

FIGURE 4 | Transcriptome analysis by RNA-Seq defining the immunomodulatory activities of PW in THP-1-derived macrophages. **(A)** The heatmap of the top 79 differentially expressed genes (DEGs) among the four experimental groups: LPS stimulation (LPS), LPS with PW treatment (LPS-PW), PW treatment only (PW) and unstimulated control (Unstim); each with three biological replicates; top 57 DEGs of adjusted p-value < 0.05 and ||log2 (fold change)|| > 2 were identified for PW vs. Unstim group, and 22 DEGs with adjusted p-value < 0.05 and |log2 (fold change)| > 0.5 were shown for LPS-PW vs. LPS group. **(B, C)** Volcano plots showing all the gene expression pattern and highlighting the top 10 up- or down-regulated DEGs in PW vs. Unstim group **(B)** and LPS-PW vs. LPS group **(C)**; the red, blue and gray color represents up-regulated, down-regulated and non-significant genes, respectively; the threshold line setting for adjusted p-value = 0.05 and ||log2 (fold change)| = 1. **(D, E)** KEGG pathway enrichment analysis for PW vs. Unstim **(D)** and LPS-PW vs. LPS **(E)**; all the pathways were significantly enriched with an adjusted p-value < 0.05; the red and blue color represents up-regulated and down-regulated pathways, respectively. **(F G)** Interaction analysis of pathways and related genes by ClueGO for PW vs. Unstim group **(F)** and LPS-PW vs. LPS group **(G)**; the red and blue color represents up-regulated and down-regulated pathways and genes, respectively; the cut-off p-value = 0.05. **(H, I)** Immunoblotting confirming the inhibition of STAT1 activation (phosphorylation of STAT1, p-STAT1) at 2h **(H)** and IRF7 expression at 24 h **(I)** by PW under LPS stimulation; β-actin as the internal control. PW = 100 nM, LPS = 10 ng/mL, N ≥ 3.

hypothesis, we pre-treated the reporter cell-derived macrophages with PW (100 nM) for different time periods (6, 12, 24 and 48 h), followed by the removal of PW and stimulation with LPS for 24 h to assess the activation of NF-κB/AP-1 and IRF (**Figure 6A**). Interestingly, we found that the PW pre-treatment (for up to 24 h) could inhibit the LPS-induced NF-κB/AP-1 activation; the inhibitory effects diminished and disappeared with longer pre-treatment (48 h) (**Figure 6B**). However, PW pre-treatment appeared to have shorter (6 h) and less priming effects on inhibition of the LPS-induced IRF activation (**Figure 6C**). These results revealed that although PW alone could trigger some inflammatory responses in the macrophages, such reaction may also activate certain regulatory signaling that could last for up to 48 h of priming for the second strike of strong inflammatory signals.

There are many negative regulators reported in controlling the TLR signaling cascades driving NF-κB activation, including SOCS1/3, A20, CYLD and SHP1 (18, 19). Among them,

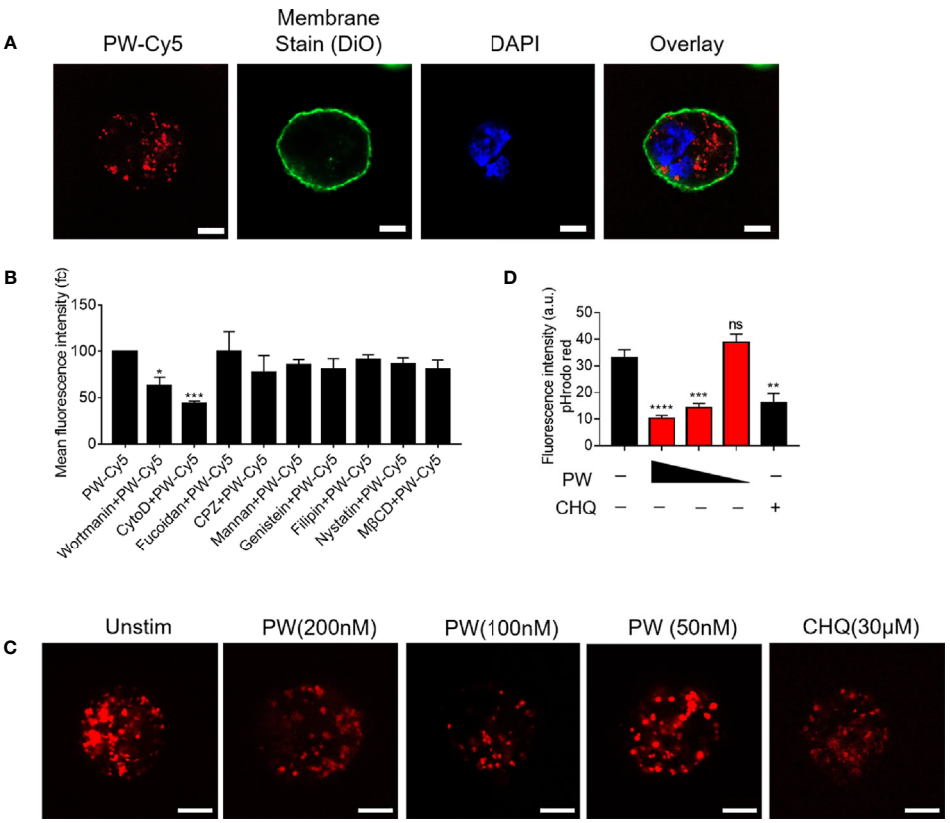

FIGURE 5 | The uptake of PW in THP-1-derived macrophages and the modulation of the endosomal pH. **(A)** Confocal images of macrophages treated with Cy5 labeled PW (PW-Cy5, red) for 5 h with the cell membrane stained with DiO (green) and the nucleus stained with DAPI (blue). **(B)** The quantitative analysis of PW-Cy5 in the macrophages with the pre-treatment of various endocytic pathway inhibitors for 5 h in comparison with the no inhibitor control by flow cytometry; N ≥ 3. **(C)** Confocal images of macrophages treated with PW (200, 100 and 50 nM) and the well-known pH modulator chloroquine (CHQ, 30 μM); cells were simultaneously treated with the endosomal pH indicator pHrodo red dextran (10 μg/mL, red); scale bar = 5 μm. **(D)** Quantitative analysis of the pHrodo red fluorescence signals as an indicator of endosomal pH; over 30 cells were quantified from three independent experiments; the fluorescence intensity is reversely proportional to the pH. *p < 0.05, **p < 0.01, ***p < 0.001, ****p < 0.0001; ns, not significant.

interleukin-1 receptor-associated kinase 3 (IRAK3 or IRAK-M) is a well-known one inhibiting TLR signaling, especially present in the monocytes and macrophages (20). It has been reported to participate in the signaling establishing LPS tolerance of macrophages (21). Thus, we speculated that IRAK-M may be involved in the inhibitory mechanisms of PW on TLR signaling. Interestingly, we found that PW could significantly elevate the expression of IRAK-M in the absence or presence of LPS stimulation (**Figure 6D**). The up-regulation of IRAK-M by PW was specific to the presence of WW region in the peptide sequence, as replacing WW with FF, LL, II, AA, SS, or TT (**Figure 6E**) could not induce the expression of IRAK-M (**Figures 6F, G**). This WW specific induction of IRAK-M expression was correlated well with the NF-κB activation by PW (**Figure 6H**). We also examined the time course of IRAK-M expression upon PW treatment and found that the IRAK-M expression increased with time and reached the maximum expression at 48 h, but significantly deceased at 72 h (**Figure 6I**). This time course of IRAK-M expression, to our surprise, had nice correlation with the observed priming effects of PW on inhibiting LPS-induced NF-κB activation (**Figure 6B**), where no inhibitory effect was seen at the condition of 48 h pre-treatment of PW with 24 h stimulation of LPS, at which the IRAK-M expression significantly dropped 72 h after PW treatment. These observations indicated that the inhibition of NF-κB by PW treatment might be also associated with the up-regulation of IRAK-M, while the inhibition of IRF by PW was primarily governed by the endosomal pH modulation.

Next, we aimed to address how PW induced IRAK-M expression. It was found that IRAK-M expression is regulated by JNK activation (22). When the macrophages were treated with the JNK inhibitor (SP600125), the IRAK-M expression induced by PW was down-regulated (**Figure 6J** and **Supplementary Figure S3**), confirming that JNK activation participated in the IRAK-M expression. To further explore how the PW-induced IRAK-M expression was triggered at the cell surface, we examined the mannose receptor as it has been reported to be utilized by a Trp containing protein to induce IRAK-M expression in macrophages (23, 24). We pretreated the THP-1-derived macrophages with an optimized concentration of the mannose receptor ligand mannan

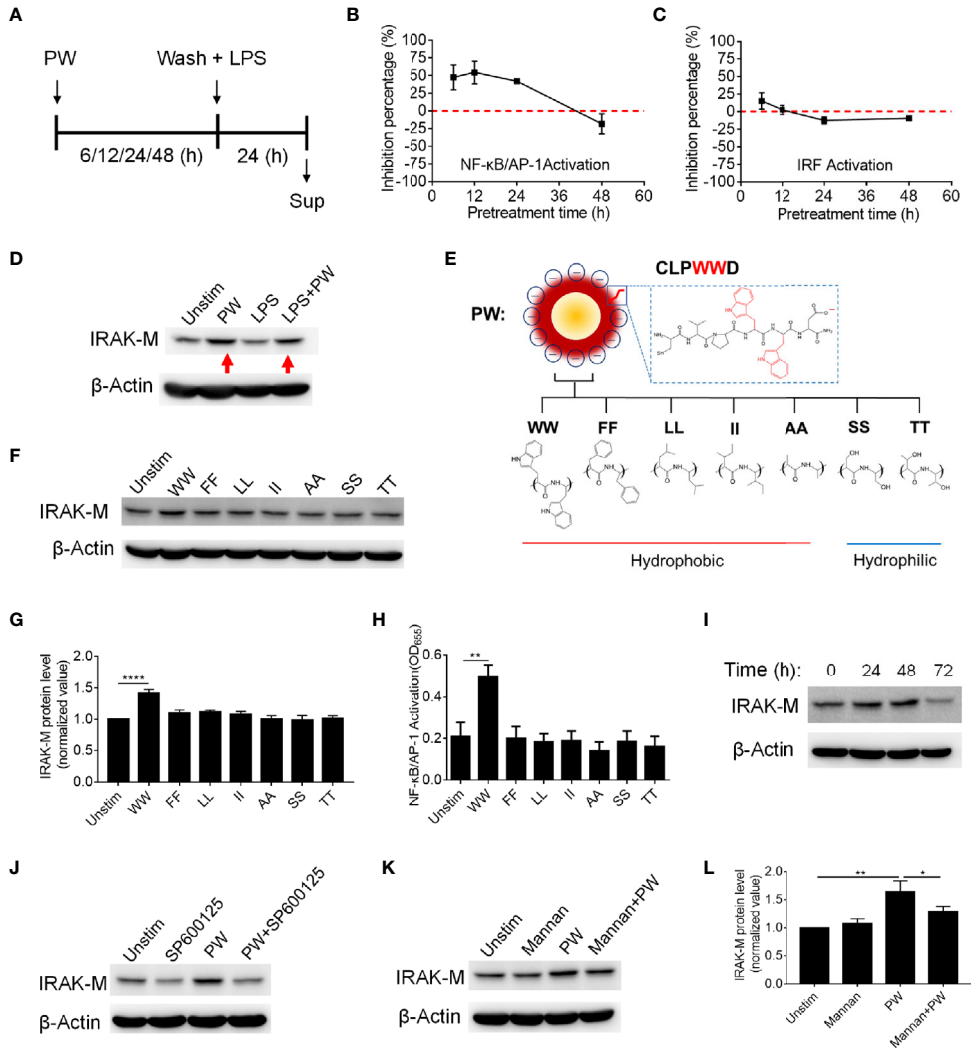

FIGURE 6 | The priming effects of PW on the TLR4 inhibition in relationship with the tryptophan dependent expression of IRAK-M in THP-1-derived macrophages. **(A)** The scheme of PW priming (100 nM) for different time periods (6, 12, 24 and 48 h) followed by LPS stimulation (10 ng/mL) for 24 h. **(B, C)** The time effect of PW pre-treatment on its inhibitory capacity on the activation of NF-κB/AP-1 **(B)** and IRF **(C)** upon LPS stimulation. **(D)** Immunoblotting showing the IRAK-M expression at 24 h induced by PW (100 nM) in the absence and presence of LPS (10 ng/mL) stimulation; β-actin as the internal control. **(E)** A scheme showing the mutation of two adjacent tryptophan residues (WW) in the peptide coating of PW to other two hydrophobic amino acids: phenylalanine (FF), leucine (LL), isoleucine (II) and alanine (AA) or hydrophilic amino acids: serine (SS) and threonine (TT). **(F)** The effect of the mutated hybrids (100 nM) displaying different amino acid residues on the IRAK-M expression at 24 h by immunoblotting; β-actin as the internal control. **(G)** Quantification of the IRAK-M expression in **(F)**. **(H)** The effect of the mutated hybrids (100 nM) on the NF-κB/AP-1 activation in the THP-1 reporter cell-derived macrophages. **(I)** The time course of IRAK-M expression induced by PW (100 nM); β-actin as the internal control. **(J)** Immunoblotting showing the IRAK-M expression at 24 h induced by PW (100 nM) in the absence and presence of SP600125 (10 μM); β-actin as the internal control. **(K)** Immunoblotting showing the IRAK-M expression at 24 h induced by PW (100 nM) with/without the pretreatment of mannan (5 μg/mL) for 0.5 h; β-actin as the internal control. **(L)** Quantification of the IRAK-M expression in **(K)**. N ≥ 3, *p < 0.05, **p < 0.01, ****p < 0.0001.

(**Supplementary Figure S4**) to block the interaction of PW with the receptor without activating it. Interestingly, the up-regulation of IRAK-M by PW was significantly reduced (**Figures 6K, L**) with the pretreatment of mannan at a low concentration (5 μg/mL), suggesting that the mannose receptor was involved in the PW-induced IRAK-M expression. These results provide better understanding of the Trp displaying nanodevices-induced IRAK-M expression and the subsequent effects on the TLR inhibition.

The Therapeutic Efficacy of PW in LPS-Induced ALI Mouse Model

We have demonstrated that PW was able to inhibit TLR signaling pathways and exhibit anti-inflammatory activity *in vitro*. Next, we employed a mouse model of LPS-induced ALI to examine the therapeutic activities of PW *in vivo*. PW (1.25 nmol/kg) was administered by intratracheal injection 2 h before the LPS (10 mg/kg) challenge through the same route, and the bronchoalveolar

lavage fluid (BALF) and lung tissues were collected for the analysis of lung inflammation and injury 24 h after LPS challenge (**Figure 7A**). We found that the PW treatment was able to reduce the LPS-induced lung inflammation by decreasing the total cell and neutrophil counts in the BALF (**Figures 7B, C**) and increasing the anti-inflammatory cytokine IL-10 in the BALF (**Figure 7D**), and reducing the ratio of wet-to-dry lung (W/D ratio) indicating the severity of pulmonary edema (**Figure 7E**). It is worth noting that PW treatment itself did not induce severe inflammatory responses *in vivo*. The cytospin images of the BALF cells revealed that PW was preferentially accumulated in the alveolar macrophages, indicating its targeting ability to macrophages (**Supplementary Figure S5**).

The lung injury and inflammation were also evaluated by histopathological analyses of both peribronchiolar and perivascular inflammatory infiltration on H&E stained lung tissue sections (**Figure 8A**). PW treatment attenuated LPS-induced ALI as quantified by the injury scores of the 5 histological features (**Figure 8B**): the alveolar neutrophils (**Figure 8C**), interstitial neutrophils (**Figure 8D**), hyaline membranes (**Figure 8E**), proteinaceous debris (**Figure 8F**) and alveolar septal thickening (**Figure 8G**). Note that the PW treatment alone could slightly increase the injury score, especially the alveolar and interstitial neutrophils as well as the proteinaceous debris scores, but much less than the LPS group. Overall, PW was able to alleviate LPS-induced ALI in mice although the hybrid alone may prime some mild inflammatory responses in the lung.

In addition to LPS-induced ALI, we also established a mouse model of Poly I/C-induced acute lung inflammation to investigate the therapeutic effect of PW on excessive TLR3 activation. PW (1.25 nmol/kg) was given intratracheally 2 h before Poly I/C (2.5 mg/kg) challenge twice at 0 and 24 h through the same route; the BALF or lung tissue was collected 24 h after the second Poly I/C challenge (**Supplementary Figure S6A**). We found that the Poly I/C challenge caused moderate inflammatory infiltration (compared with the LPS challenge) to the lung, and the PW treatment was able to decrease the number of total cells and neutrophils in the BALF (**Supplementary Figures S6B, C**). Similarly, PW treatment could also reduce the lung injury score from the histopathological analyses (**Supplementary Figures S6D, E**). Specifically, the PW treatment reduced the number of alveolar and interstitial neutrophils, hyaline membrane, protein fragments and alveolar septum thickening (**Supplementary Figures S6F–J**).

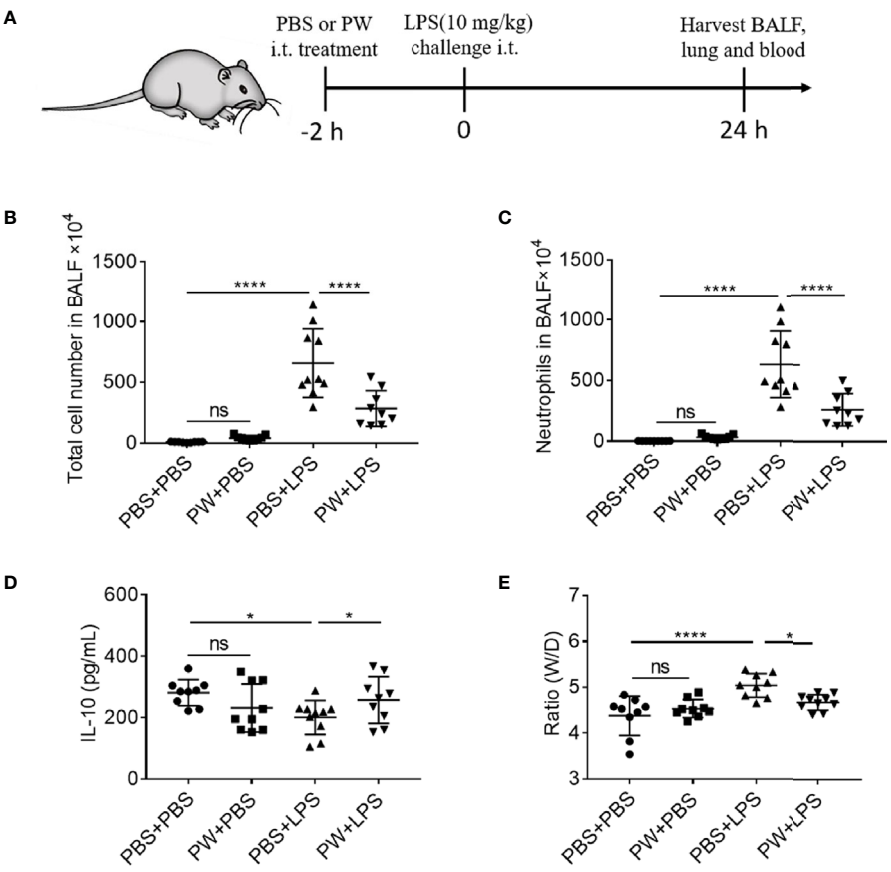

FIGURE 7 | The inhibitory effect of PW on the lung inflammation in LPS-induced ALI mice. **(A)** The scheme of the LPS-induced ALI mouse model; PW (1.25 nmol/kg) was intratracheally administered 2 h before the LPS (10 mg/kg) challenge through the same route for 24 h; the BALF was collected for the analysis of the total number of cells **(B)** and the neutrophils **(C)** infiltrated in the lung. **(D)** The level of the anti-inflammatory cytokine IL-10 in the BALF. **(E)** The pulmonary edema assessed by the lung W/D ratio. N ≥ 9 per group; ns, not significant, *p < 0.05, ****p < 0.0001.

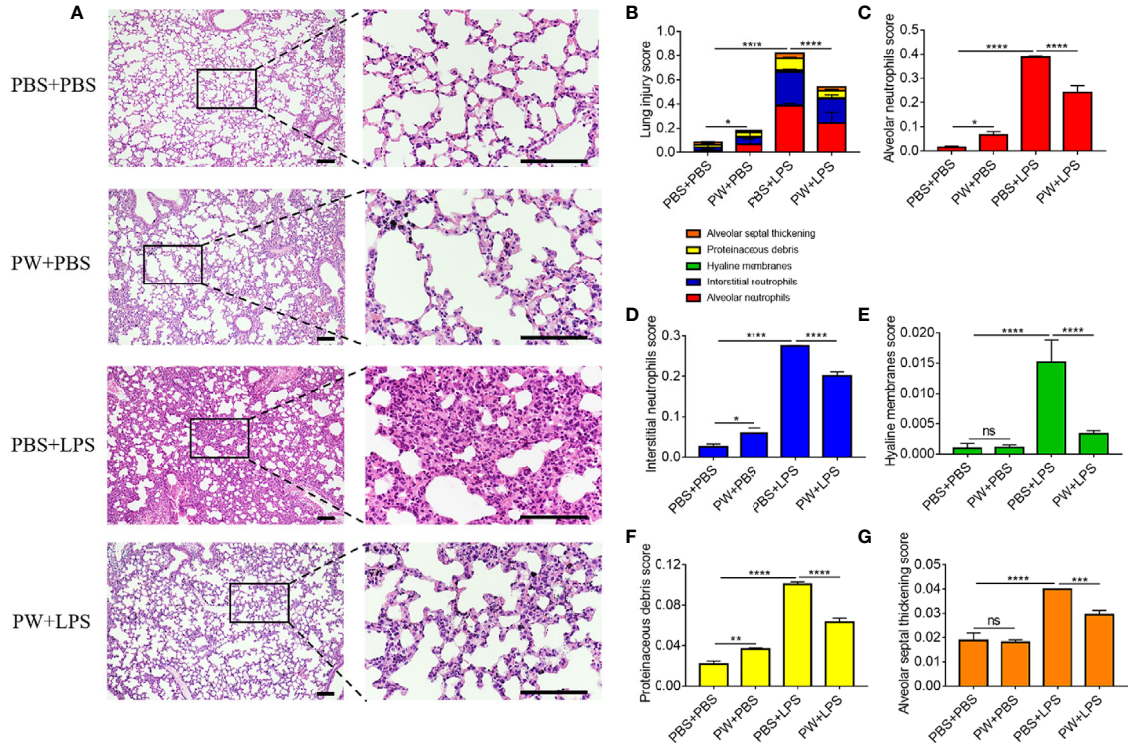

FIGURE 8 | The protective effect of PW on the histopathological damages of the lung in LPS-induced ALI mice. **(A)** The images of lung sections stained with H&E; the scale bar = 100 μm. **(B)** The lung injury score based on the 5 pathophysiological characteristics: the alveolar neutrophils **(C)**, interstitial neutrophils **(D)**, hyaline membranes **(E)**, proteinaceous debris **(F)** and alveolar septal thickening **(G)**. N ≥ 9 per group; ns, not significant, *p < 0.05, **p < 0.01, ***p < 0.001, ****p < 0.0001.

These results suggested that PW could alleviate TLR3 activation-mediated lung inflammation in mice, making PW a potent anti-inflammatory agent targeting multiple TLR signaling pathways for treating ALI.

DISCUSSION

Multiple lines of evidences have demonstrated that macrophages play a central role in the initiation, progression and resolution of inflammation in various disease conditions. Regulation of macrophage activation and its inflammatory responses would provide a promising therapeutic strategy to intervene such detrimental conditions. Nanodevices can naturally target macrophages through endocytosis and phagocytosis owing to their nanoscale property, making them a new class of versatile and effective agents to modulate the biological function of macrophages. In this study, we showed that a special class of Trp-containing hexapeptide-coated GNPs, PW, could trigger minute pro-inflammatory responses of macrophages; however, these nano-hybrids inhibited multiple TLR signaling pathways and exhibited potent anti-inflammatory activities *in vitro* and *in vivo* under the strike of strong inflammatory stimuli. This unique activity of PW could be attributed to the two arms of mechanistic actions: the blocking of endosomal acidification to inhibit TLR signaling, and the up-regulation of IRAK-M expression to dampen NF-κB activation in macrophages. The latter might contribute to the observed priming effect of PW for protection of macrophages from a subsequent insult by TLR stimulation in analogy to the known endotoxin tolerance effect. The Trp-containing peptide-GNP hybrids by design represented a novel immunomodulatory nanodevice that could be applied to manage the dysregulated innate immune responses for treating inflammatory conditions as in ALI and its severe form of acute respiratory distress syndrome (ARDS).

Nanodevice-Based Immune Modulation of Macrophages

TLRs are one major class of pathogen recognition receptors (PRRs) responsible for mounting innate immune responses in the host defense against infections or non-infectious insults (25). Excessive activation of TLR is associated with many inflammatory disorders, and hence regulating TLR signaling has become an attractive intervention strategy. Herein, we discovered that a peptide-decorated nanodevice (PW) that displays tryptophan residues on the surface could inhibit multiple TLR pathways including TLR4, TLR3 and TLR7/8 (**Figures 2** and **3**), and the production of pro-inflammatory cytokines (IL-6, IL-12/IL-23p40, TNF-α and MCP-1). Interestingly, PW did not affect TLR2 signaling, suggesting that PW preferentially acted on endosomal-related TLR signaling. The ability of inhibiting multiple TLR pathways makes PW a

potent nano-inhibitor to regulate multifactorial, overwhelming inflammatory reactions in complex diseases like ALI/ARDS.

It was surprising to us that PW alone had mild pro-inflammatory activity on NF-κB activation (**Figures 2**, **4**). This unique property of PW appeared to rely on the tryptophan residues displaying on the nanodevice. When replacing WW residues in the peptide coating on PW to either other hydrophobic amino acids (FF, LL, II, AA) or hydrophilic ones (SS, TT), these nano-hybrids did not activate NF-κB (**Figure 6H**). Moreover, neither the peptides alone nor the bare GNPs induced the activation of NF-κB (**Supplementary Figure S1**). Thus, the specific presence of the membrane anchoring amino acid tryptophan on the GNP surface imparts the nano-hybrid novel activity to mildly activate macrophages. Such an action on the contrary primed macrophages to lower the response for the subsequent inflammatory stimulation (see below IRAK-M).

On the other hand, the uptake of PW in macrophages could significantly modulate the endosomal pH, which in turn inhibited the TLR signaling (**Figure 5**). It has been found that the acidification process of endosomes/lysosomes can regulate many signaling events (26). For TLR4 signaling, the TRIF-dependent signal transduction requires the trafficking of TLR4 from the cell surface to the endosomes/lysosomes (27). During the trafficking process from early endosomes to late endosomes or lysosomes, the microenvironment changes accordingly including acidification in order to convey the signals to trigger corresponding cellular responses. Blockade of the endosomal/lysosomal acidification process is thus expected to affect the endosomal TLR signaling. PW would presumably behave like our previously developed anti-inflammatory nanoparticle P12, which can act like a proton sponge to sequester protons due to the negative charge of the aspartate (with side chain pKa of ~3.9) on the nanoparticles, consequently blocking the normal acidification process in the endosomes/lysosomes and inhibiting the endosomal TLR signaling.

Different from small molecule inhibitors, PW-based nanodevices have many advantages on TLR signaling modulation for basic and translation research. First, these nanodevices have targeting capability to phagocytic immune cells. Second, they can be easily traced based on the characteristics of the GNPs. Third, they can have preferred biodistribution and pharmacokinetic profiles by design. More importantly, the priming effect of PW and its TLR inhibitory activity resemble many phenomena reported in trained immunity, where exogenous or endogenous stimuli can prime the immune system to lunch a proper response (stronger or weaker) to the second attack (28). Therefore, these nanodevice-based TLR modulators could provide novel ideas to train our immune system to manage the detrimental inflammatory responses in many diseases.

The Negative Regulator IRAK-M in TLR Signaling and the Potential Mechanism(s) of PW-Mediated Priming Effects on TLR Inhibition

IRAK-M, a member of the IRAK family lacking kinase activity, is one of the important negative regulators of TLR signaling (20). It is mainly expressed in myeloid cells and regulates the immune homeostasis and tolerance (29, 30). IRAK-M negatively regulates NF-κB activation by competitively binding to IRAK1/4 to block the kinase activity, and hence consequently inhibits the downstream signaling cascades (31). Therefore, the induction of IRAK-M expression could limit the pathological damages caused by overactivation of the inflammatory signaling. In our studies, we found that PW could particularly elevate IRAK-M expression in macrophages (**Figure 6**), which was governed by the tryptophan (W) residues on the nanodevices as replacing the two tryptophan (WW) residues in PW with other amino acids (FF, LL, II, AA, SS and TT) abolished such an effect (**Figures 6E–G**). The up-regulation of IRAK-M by PW may explain the observed priming effect of PW on the TLR inhibition. In fact, mice with IRAK-M deficiency exhibited enhanced inflammatory responses to infection (32). Furthermore, compared with wild-type mice, the IRAK-M knockout mice had more inflammatory cell infiltration and higher pro-inflammatory cytokine production in the lung in response to OVA challenge (33). These evidences suggest that IRAK-M is essential in maintaining the immune homeostasis during inflammatory responses.

The expression of IRAK-M in macrophages can be induced by various endogenous and exogenous soluble factors, as well as inter- or intracellular signaling molecules. These molecules include molecular patterns of pathogen products such as LPS, flagellin, peptidoglycan (PGN) and CpG (34). Actually, IRAK-M induction is a very common phenomenon in endotoxin tolerance, a protective mechanism in which cells or organisms enter into a transient unresponsive state upon exposure to low dose of endotoxin, so they are unable to respond to a second challenge of endotoxin (17). Although many other factors, such as prostaglandin E2 (PGE2), GM-CSF, IL-13, pulmonary surfactant protein A and surfactant lipids as well as glucocorticoids, can up-regulate the expression of IRAK-M in macrophages (35, 36), currently to our knowledge there is no report on nanoparticle-induced IRAK-M expression except PW in our study (**Figure 6**).

Although the entry of PW into macrophages was primarily through micropinocytosis (**Figure 5B**), we found that the mannose receptor (MR) was involved in PW-induced IRAK-M expression. It has been found that a protein toxin released from the gram-positive bacteria of *Streptococcus pneumoniae*, pneumolysin (PLY), interacts with the mannose receptor depending on its tryptophan motif (23, 24). Binding of PLY to the mannose receptor C type 1 (MRC-1/CD206) on the mouse alveolar macrophages can reduce TLR signaling and pro-inflammatory cytokine production as well as infiltration of neutrophiles to the lung (24). Other studies also reported that the MR agonists, mannose-capped lipoarabinomannans (Man-LAMs), could inhibit LPS-induced IL-12 production through IRAK-M induction in mouse macrophages (37, 38). Herein, we showed that PW-mediated IRAK-M expression in macrophages was dependent on the tryptophan residues, and the MR was involved in the phenomenon (**Figures 6E–L**). More experiments with genetic tools are required in the future to confirm the specific role of IRAK-M induction in the observed TLR inhibition and anti-inflammatory activities of PW.

Trp-Displaying Nanodevices as a New Type of Immunomodulatory Nanotherapeutics for Treating ALI/ARDS

ALI/ARDS is a life-threatening condition with respiratory failure characterized by uncontrolled, rapid, widespread inflammation in the lungs (39). There are currently no effective pharmacological treatments for ALI/ARDS. Studies have shown that in the early stage of ALI/ARDS, alveolar macrophages (AM) and pattern recognition receptors (PRRs) on the AM surface, especially TLRs, contribute to the initiation of inflammatory responses (40, 41). Therefore, effective regulation of TLR signaling of lung macrophages may provide a promising strategy to treat ALI/ARDS. In this study, the developed PW could specifically target lung macrophages to attenuate TLR signaling and decrease pro-inflammatory cytokine production in two ALI mouse models (LPS and Poly I/C challenge) (**Figures 7**, **8**, and **Figure S6**). The potent inhibitory activity of PW on multiple TLR pathways, together with its macrophage targeting ability and tryptophan-specific regulatory function makes PW a promising therapeutic agent to treat ALI/ARDS. Nevertheless, PW is not biodegradable, and the development of new forms of PW is required for future clinical translation.

CONCLUSIONS

In conclusion, we developed a Trp-displaying nanodevice, PW, with unique immunomodulatory activities. PW was made by modifying GNPs with a peptide containing two Trp residues in the sequence. PW itself induced mild pro-inflammatory responses but exhibited potent anti-inflammatory activities with the presence of inflammatory stimuli through inhibiting multiple TLR (3, 4 and 7/8) signaling cascades in macrophages. This inhibitory activity was primarily attributed to the modulation of the endosomal pH and hence preferentially affecting the endosomal TLR signaling. Very interestingly, the PW alone could induce the expression of the negative regulator IRAK-M in the TLR signaling, which depended on the presence of Trp residues. The up-regulation of IRAK-M may contribute to the priming effect of PW on the inhibition of subsequent stimulation by LPS. The therapeutic effects of PW were assessed on two mouse models of LPS- and Poly I/C-induced ALI. It was found that PW pre-treatment was able to reduce the inflammatory cells infiltration, particularly neutrophils, and increase the anti-inflammatory cytokine IL-10 level in the BALF as well as decrease the lung injury and edema. This study defined a new design principle of using the membrane anchoring amino acid Trp to enable nanodevice-based TLR inhibitors with novel immunomodulatory capability, which served as a new class of anti-inflammatory therapeutics for treating inflammatory diseases such as ALI/ARDS.

DATA AVAILABILITY STATEMENT

The original contributions presented in the study are publicly available. This data can be found here: https://www.ncbi.nlm.nih.gov/geo/query/acc.cgi?acc=GSE181851.

ETHICS STATEMENT

The animal study was reviewed and approved by The Animal Care and Use Committee at Tianjin Medical University.

AUTHOR CONTRIBUTIONS

HY and SYF conceived the study and designed the research. HY, SYF, and LS wrote the manuscript. LS synthesized and purified the nanoparticles, and assessed their anti-inflammatory effects *in vitro* and *in vivo*. RW performed RNA-seq experiment and analysis. CW assisted cell culture and the animal experiments. JG conducted confocal microscopy experiments. HM performed TEM imaging. LS, RW, and JG analyzed the results and generated the figures. All authors contributed to the article and approved the submitted version.

FUNDING

This work was supported by the National Natural Science Foundation of China (No. 81770070 for HY and No. 81971549 for SYF), the Natural Science Foundation of Tianjin Municipal Science and Technology Commission (20JCYBJC00040 for HY) and the starting fund from Tianjin Medical University.

ACKNOWLEDGMENTS

We acknowledged Yuan Liu for providing liposomes and assistance with TEM imaging.

SUPPLEMENTARY MATERIAL

The Supplementary Material for this article can be found online at: https://www.frontiersin.org/articles/10.3389/fimmu.2021.750128/full#supplementary-material

REFERENCES

1. Fam SY, Chee CF, Yong CY, Ho KL, Mariatulqabtiah AR, Tan WS. Stealth Coating of Nanoparticles in Drug-Delivery Systems. *Nanomater (Basel)* (2020) 10(4):787. doi: 10.3390/nano10040787
2. Pelaz B, del Pino P, Maffre P, Hartmann R, Gallego M, Rivera-Fernandez S, et al. Surface Functionalization of Nanoparticles With Polyethylene Glycol: Effects on Protein Adsorption and Cellular Uptake. *ACS Nano* (2015) 9 (7):6996–7008. doi: 10.1021/acsnano.5b01326
3. Larson TA, Joshi PP, Sokolov K. Preventing Protein Adsorption and Macrophage Uptake of Gold Nanoparticles via a Hydrophobic Shield. *ACS Nano* (2012) 6(10):9182–90. doi: 10.1021/nn3035155
4. Belhadj Z, He B, Deng H, Song S, Zhang H, Wang X, et al. A Combined "Eat Me/Don't Eat Me" Strategy Based on Extracellular Vesicles for Anticancer Nanomedicine. *J Extracell Vesicles* (2020) 9(1):1806444. doi: 10.1080/20013078.2020.1806444
5. Rodriguez PL, Harada T, Christian DA, Pantano DA, Tsai RK, Discher DE. Minimal "Self" Peptides That Inhibit Phagocytic Clearance and Enhance

Delivery of Nanoparticles. *Science* (2013) 339(6122):971–5. doi: 10.1126/science.1229568
6. Wang Z, Li J, Cho J, Malik AB. Prevention of Vascular Inflammation by Nanoparticle Targeting of Adherent Neutrophils. *Nat Nanotechnol* (2014) 9 (3):204–10. doi: 10.1038/nnano.2014.17
7. Chung CH, Jung W, Keum H, Kim TW, Jon S. Nanoparticles Derived From the Natural Antioxidant Rosmarinic Acid Ameliorate Acute Inflammatory Bowel Disease. *ACS Nano* (2020) 14(6):6887–96. doi: 10.1021/acsnano.0c01018
8. Bayyurt B, Tincer G, Almacioglu K, Alpdundar E, Gursel M, Gursel I. Encapsulation of Two Different TLR Ligands Into Liposomes Confer Protective Immunity and Prevent Tumor Development. *J Control Release* (2017) 247:134–44. doi: 10.1016/j.jconrel.2017.01.004
9. Guo J, Li D, Tao H, Li G, Liu R, Dou Y, et al. Cyclodextrin-Derived Intrinsically Bioactive Nanoparticles for Treatment of Acute and Chronic Inflammatory Diseases. *Adv Mater* (2019) 31(46):e1904607. doi: 10.1002/adma.201904607
10. Yang H, Fung SY, Xu S, Sutherland DP, Kollmann TR, Liu M, et al. Amino Acid-Dependent Attenuation of Toll-Like Receptor Signaling by Peptide-Gold Nanoparticle Hybrids. *ACS Nano* (2015) 9(7):6774–84. doi: 10.1021/nn505634h
11. Yang H, Kozicky L, Saferali A, Fung SY, Afacan N, Cai B, et al. Endosomal pH Modulation by Peptide-Gold Nanoparticle Hybrids Enables Potent Anti-Inflammatory Activity in Phagocytic Immune Cells. *Biomaterials* (2016) 111:90–102. doi: 10.1016/j.biomaterials.2016.09.032
12. Wang L, Zhang H, Sun L, Gao W, Xiong Y, Ma A, et al. Manipulation of Macrophage Polarization by Peptide-Coated Gold Nanoparticles and its Protective Effects on Acute Lung Injury. *J Nanobiotechnol* (2020) 18(1):38. doi: 10.1186/s12951-020-00593-7
13. Xiong Y, Gao W, Xia F, Sun Y, Sun L, Wang L, et al. Peptide-Gold Nanoparticle Hybrids as Promising Anti-Inflammatory Nanotherapeutics for Acute Lung Injury: In Vivo Efficacy, Biodistribution, and Clearance. *Adv Healthc Mater* (2018) 7(19):e1800510. doi: 10.1002/adhm.201800510
14. de Jesus AJ, Allen TW. The Role of Tryptophan Side Chains in Membrane Protein Anchoring and Hydrophobic Mismatch. *Biochim Biophys Acta* (2013) 1828(2):864–76. doi: 10.1016/j.bbamem.2012.09.009
15. Fu Z, Zhou X, Xing D. Sensitive Colorimetric Detection of Listeria Monocytogenes Based on Isothermal Gene Amplification and Unmodified Gold Nanoparticles. *Methods* (2013) 64(3):260–6. doi: 10.1016/j.ymeth.2013.08.003
16. Matute-Bello G, Downey G, Moore BB, Groshong SD, Matthay MA, Slutsky AS, et al. An Official American Thoracic Society Workshop Report: Features and Measurements of Experimental Acute Lung Injury in Animals. *Am J Respir Cell Mol Biol* (2011) 44(5):725–38. doi: 10.1165/rcmb.2009-0210ST
17. Biswas SK, Lopez-Collazo E. Endotoxin Tolerance: New Mechanisms, Molecules and Clinical Significance. *Trends Immunol* (2009) 30(10):475–87. doi: 10.1016/j.it.2009.07.009
18. Yang L, Seki E. Toll-Like Receptors in Liver Fibrosis: Cellular Crosstalk and Mechanisms. *Front Physiol* (2012) 3:138. doi: 10.3389/fphys.2012.00138
19. Rothschild DE, McDaniel DK, Ringel-Scaia VM, Allen IC. Modulating Inflammation Through the Negative Regulation of NF-kappaB Signaling. *J Leukoc Biol* (2018) 103:(6). doi: 10.1002/JLB.3MIR0817-346RRR
20. Kobayashi K, Hernandez LD, Galan JE, Janeway CA Jr, Medzhitov R. IRAK-M Is a Negative Regulator of Toll-Like Receptor Signaling. *Cell* (2002) 110 (2):191–202. doi: 10.1016/S0092-8674(02)00827-9
21. Xiong Y, Medvedev AE. Induction of Endotoxin Tolerance In Vivo Inhibits Activation of IRAK4 and Increases Negative Regulators IRAK-M, SHIP-1, and A20. *J Leukoc Biol* (2011) 90(6):1141–8. doi: 10.1189/jlb.0611273
22. Jin P, Bo L, Liu Y, Lu W, Lin S, Bian J, et al. Activator Protein 1 Promotes the Transcriptional Activation of IRAK-M. *BioMed Pharmacother* (2016) 83:1212–9. doi: 10.1016/j.biopha.2016.08.024
23. Subramanian K, Iovino F, Tsikourkitoudi V, Merkl P, Ahmed S, Berry SB, et al. Mannose Receptor-Derived Peptides Neutralize Pore-Forming Toxins and Reduce Inflammation and Development of Pneumococcal Disease. *EMBO Mol Med* (2020) 12(11):e12695. doi: 10.15252/emmm.202012695
24. Subramanian K, Neill DR, Malak HA, Spelmink L, Khandaker S, Dalla Libera Marchiori G, et al. Pneumolysin Binds to the Mannose Receptor C Type 1 (MRC-1) Leading to Anti-Inflammatory Responses and Enhanced Pneumococcal Survival. *Nat Microbiol* (2019) 4(1):62–70. doi: 10.1038/s41564-018-0280-x
25. Gao W, Xiong Y, Li Q, Yang H. Inhibition of Toll-Like Receptor Signaling as a Promising Therapy for Inflammatory Diseases: A Journey From Molecular to Nano Therapeutics. *Front Physiol* (2017) 8:508. doi: 10.3389/fphys.2017.00508
26. Bonam SR, Wang F, Muller S. Lysosomes as a Therapeutic Target. *Nat Rev Drug Discov* (2019) 18(12):923–48. doi: 10.1038/s41573-019-0036-1
27. Ciesielska A, Matyjek M, Kwiatkowska K. TLR4 and CD14 Trafficking and its Influence on LPS-Induced Pro-Inflammatory Signaling. *Cell Mol Life Sci* (2021) 78(4):1233–61. doi: 10.1007/s00018-020-03656-y
28. Netea MG, Dominguez-Andres J, Barreiro LB, Chavakis T, Divangahi M, Fuchs E, et al. Defining Trained Immunity and its Role in Health and Disease. *Nat Rev Immunol* (2020) 20(6):375–88. doi: 10.1038/s41577-020-0285-6
29. van 't Veer C, van den Pangaart PS, van Zoelen MA, de Kruif M, Birjmohun RS, Stroes ES, et al. Induction of IRAK-M Is Associated With Lipopolysaccharide Tolerance in a Human Endotoxemia Model. *J Immunol* (2007) 179(10):7110–20. doi: 10.4049/jimmunol.179.10.7110
30. Flannery S, Bowie AG. The Interleukin-1 Receptor-Associated Kinases: Critical Regulators of Innate Immune Signalling. *Biochem Pharmacol* (2010) 80(12):1981–91. doi: 10.1016/j.bcp.2010.06.020
31. Zhou H, Yu M, Fukuda K, Im J, Yao P, Cui W, et al. IRAK-M Mediates Toll-Like Receptor/IL-1r-Induced NFkappaB Activation and Cytokine Production. *EMBO J* (2013) 32(4):583–96. doi: 10.1038/emboj.2013.2
32. Seki M, Kohno S, Newstead MW, Zeng X, Bhan U, Lukacs NW, et al. Critical Role of IL-1 Receptor-Associated Kinase-M in Regulating Chemokine-Dependent Deleterious Inflammation in Murine Influenza Pneumonia. *J Immunol* (2010) 184(3):1410–8. doi: 10.4049/jimmunol.0901709
33. Zhang M, Chen W, Zhou W, Bai Y, Gao J. Critical Role of IRAK-M in Regulating Antigen-Induced Airway Inflammation. *Am J Respir Cell Mol Biol* (2017) 57(5):547–59. doi: 10.1165/rcmb.2016-0370OC
34. Hubbard LL, Moore BB. IRAK-M Regulation and Function in Host Defense and Immune Homeostasis. *Infect Dis Rep* (2010) 2(1):e9. doi: 10.4081/idr.2010.e9
35. Miyata M, Lee JY, Susuki-Miyata S, Wang WY, Xu H, Kai H, et al. Glucocorticoids Suppress Inflammation via the Upregulation of Negative Regulator IRAK-M. *Nat Commun* (2015) 6:6062. doi: 10.1038/ncomms7062
36. Nguyen HA, Rajaram MV, Meyer DA, Schlesinger LS. Pulmonary Surfactant Protein A and Surfactant Lipids Upregulate IRAK-M, a Negative Regulator of TLR-Mediated Inflammation in Human Macrophages. *Am J Physiol Lung Cell Mol Physiol* (2012) 303(7):L608–616. doi: 10.1152/ajplung.00067.2012
37. Pathak SK, Basu S, Bhattacharyya A, Pathak S, Kundu M, Basu J. Mycobacterium Tuberculosis Lipoarabinomannan-Mediated IRAK-M Induction Negatively Regulates Toll-Like Receptor-Dependent Interleukin-12 P40 Production in Macrophages. *J Biol Chem* (2005) 280(52):42794–800. doi: 10.1074/jbc.M506471200
38. Nigou J, Zelle-Rieser C, Gilleron M, Thurnher M, Puzo G. Mannosylated Lipoarabinomannans Inhibit IL-12 Production by Human Dendritic Cells: Evidence for a Negative Signal Delivered Through the Mannose Receptor. *J Immunol* (2001) 166(12):7477–85. doi: 10.4049/jimmunol.166.12.7477
39. Matthay MA, Zemans RL, Zimmerman GA, Arabi YM, Beitler JR, Mercat A, et al. Acute Respiratory Distress Syndrome. *Nat Rev Dis Primers* (2019) 5 (1):18. doi: 10.1038/s41572-019-0069-0
40. Aggarwal NR, King LS, D'Alessio FR. Diverse Macrophage Populations Mediate Acute Lung Inflammation and Resolution. *Am J Physiol Lung Cell Mol Physiol* (2014) 306(8):L709–725. doi: 10.1152/ajplung.00341.2013
41. Takeuchi O, Akira S. Pattern Recognition Receptors and Inflammation. *Cell* (2010) 140(6):805–20. doi: 10.1016/j.cell.2010.01.022

Conflict of Interest: The authors declare that the research was conducted in the absence of any commercial or financial relationships that could be construed as a potential conflict of interest.

Publisher's Note: All claims expressed in this article are solely those of the authors and do not necessarily represent those of their affiliated organizations, or those of the publisher, the editors and the reviewers. Any product that may be evaluated in this article, or claim that may be made by its manufacturer, is not guaranteed or endorsed by the publisher.

frontiers in Immunology

ORIGINAL RESEARCH
published: 04 November 2021
doi: 10.3389/fimmu.2021.751683

Innate Memory Reprogramming by Gold Nanoparticles Depends on the Microbial Agents That Induce Memory

Benjamin J. Swartzwelter[1,2†], Sara Michelini[2], Tobias Frauenlob[2], Francesco Barbero[3], Alessandro Verde[1†], Anna Chiara De Luca[1†], Victor Puntes[3,4,5], Albert Duschl[2], Jutta Horejs-Hoeck[2], Paola Italiani[1] and Diana Boraschi[1,6,7]*

[1] Institute of Biochemistry and Cell Biology (IBBC), National Research Council (CNR), Napoli, Italy, [2] Department Biosciences, Paris Lodron University of Salzburg (PLUS), Salzburg, Austria, [3] Institut Català de Nanociència i Nanotecnologia (ICN2), Consejo Superior de Investigaciones Científicas (CSIC) and The Barcelona Institute of Science and Technology (BIST), Barcelona, Spain, [4] Vall d'Hebron Research Institute (VHIR), Barcelona, Spain, [5] Institució Catalana de Recerca I Estudis Avançats (ICREA), Barcelona, Spain, [6] Stazione Zoologica Anton Dohrn, Napoli, Italy, [7] Shenzhen Institute of Advanced Technology (SIAT), Chinese Academy of Sciences (CAS), Shenzhen, China

Innate immune memory, the ability of innate cells to react in a more protective way to secondary challenges, is induced by exposure to infectious and other exogeous and endogenous agents. Engineered nanoparticles are particulate exogenous agents that, as such, could trigger an inflammatory reaction in monocytes and macrophages and could therefore be also able to induce innate memory. Here, we have evaluated the capacity of engineered gold nanoparticles (AuNPs) to induce a memory response or to modulate the memory responses induced by microbial agents. Microbial agents used were in soluble *vs*. particulate form (MDP and the gram-positive bacteria *Staphylococcus aureus*; β-glucan and the β-glucan-producing fungi *C. albicans*), and as whole microrganisms that were either killed (*S. aureus*, *C. albicans*) or viable (the gram-negative bacteria *Helicobacter pylori*). The memory response was assessed *in vitro*, by exposing human primary monocytes from 2-7 individual donors to microbial agents with or without AuNPs (primary response), then resting them for 6 days to allow return to baseline, and eventually challenging them with LPS (secondary memory response). Primary and memory responses were tested as production of the innate/inflammatory cytokine TNFα and other inflammatory and anti-inflammatory factors. While inactive on the response induced by soluble microbial stimuli (muramyl dipeptide -MDP-, β-glucan), AuNPs partially reduced the primary response induced by whole microorganisms. AuNPs were also unable to directly induce a memory response but could modulate stimulus-induced memory in a circumscribed fashion, limited to some agents and some cytokines. Thus, the MDP-induced tolerance in terms of TNFα production was further exacerbated by co-priming with AuNPs, resulting in a less inflammatory memory response. Conversely, the *H. pylori*-induced tolerance was downregulated by AuNPs only relative to the anti-inflammatory cytokine IL-10, which would lead to an overall more inflammatory memory response. These effects of AuNPs may depend on a differential

OPEN ACCESS

Edited by:
David Pozo,
University of Seville, Spain

Reviewed by:
Umut Can Kucuksezer,
Istanbul University, Turkey
Mario M. D'Elios,
University of Florence, Italy

***Correspondence:**
Diana Boraschi
diana.boraschi@ibbc.cnr.it
Paola Italiani
paola.italiani@ibbc.cnr.it

†Present address:
Benjamin J. Swartzwelter,
Department of Microbiology, Immunology & Pathology, Colorado State University, Fort Collins, CO, United States
Alessandro Verde,
Institute for Experimental Endocrinology and Oncology, "G. Salvatore" (IEOS), Second Unit, Consiglio Nazionale Delle Ricerche (CNR), Napoli, Italy
Anna Chiara De Luca,
Institute for Experimental Endocrinology and Oncology, "G. Salvatore" (IEOS), Second Unit, Consiglio Nazionale Delle Ricerche (CNR), Napoli, Italy

Specialty section:
This article was submitted to Molecular Innate Immunity, a section of the journal Frontiers in Immunology

Received: 01 August 2021
Accepted: 14 October 2021
Published: 04 November 2021

Citation:
Swartzwelter BJ, Michelini S, Frauenlob T, Barbero F, Verde A, De Luca AC, Puntes V, Duschl A, Horejs-Hoeck J, Italiani P and Boraschi D (2021) Innate Memory Reprogramming by Gold Nanoparticles Depends on the Microbial Agents That Induce Memory. Front. Immunol. 12:751683. doi: 10.3389/fimmu.2021.751683

interaction/association between the reactive particle surfaces and the microbial components and agents, which may lead to a change in the exposure profiles. As a general observation, however, the donor-to-donor variability in memory response profiles and reactivity to AuNPs was substantial, suggesting that innate memory depends on the individual history of exposures.

Keywords: innate immunity, innate memory, nanoparticles, microbial agents, monocytes

INTRODUCTION

Immunological memory was long considered a distinctive trait of adaptive immunity, resulting in the capacity to mount a more rapid and more effective specific immune response to infectious challenges (1). It is however evident that organisms that only display innate immunity, the most ancient non-specific defensive system, can develop an immunological memory that allows them to resist better to various environmental pathogens and stressful events (*e.g.*, heat, wounds) (2–4). Higher vertebrates maintain an efficient innate immunity, in parallel to adaptive responses, and it is now evident that priming/exposure to microbial/stressful agents generates "innate memory" in innate immune cells, such as monocytes and macrophages. The innate memory is at least partially non-specific and allows for a more protective reaction to subsequent challenges (2, 3, 5–7).

The first type of innate memory described in mammals is known as "endotoxin tolerance" and results in a less potent secondary response to gram-negative endotoxin or other bacterial challenges, aiming at attaining sufficient protection while avoiding the substantial damage to the host tissues and organs that can be caused by a full innate/inflammatory response, which includes the deadly endotoxin shock (8–11). In other cases, *e.g.*, in the case of exposure to the tuberculosis vaccine BCG or to the fungal β-glucan, the memory response results in a potentiated reaction ("trained immunity") (6, 12). The innate memory responses, both tolerance and potentiation, are based on epigenetic and metabolic modifications, rather than in a general shift in gene transcription, and they should be understood as a medium-term functional reprogramming aimed at enhanced host defense (lasting several months to years in mammals) (6, 13–16). However, anomalous innate memory has been proposed to contribute to the development of immune/inflammatory diseases, such as autoimmune syndromes and chronic inflammatory diseases (6, 17). Which substances activate innate immune memory, in which direction (protective *vs.* detrimental, tolerance *vs.* potentiation) and how different agents might differentially modulate innate memory is still largely unexplored. Innate memory-inducing substances should be considered both from a safety perspective, in which excessive inflammation or immune suppression can be detrimental, but also for their therapeutic potential, to down-regulate or up-regulate excessive or insufficient innate immunity in different disease conditions.

Several microbial stimuli have been described for their memory inducing capacity. In addition to the aforementioned BCG, endotoxin (lipopolysaccharide -LPS-) and β-glucan, agents such as muramyl dipeptide (MDP) and *Candida albicans* have each demonstrated the capacity to alter the secondary reactivity of monocytes or macrophages (18–20). Recently, several studies have examined whether engineered nanoparticles are also capable of inducing or modulating innate immune memory. While pristine graphene could induce a potentiated status in murine macrophages (21), gold nanoparticles (AuNPs) failed to independently induce a memory response in human monocytes, although they seem able to modulate in different directions the innate memory induced by microbial agents (22–26).

In this context, here we have evaluated the capacity of AuNPs to modulate the innate memory response of human primary monocytes primed with different microbial agents in soluble *vs.* particulate forms (MDP and the gram-positive bacteria Staphylococcus aureus; β-glucan and the β-glucan-producing fungi C. albicans) and with a live microbial agent (the gram-negative bacterium Helicobacter pylori), using a realistic *in vitro* model based on human primary monocytes. The results show that AuNPs are unable per se to induce an inflammatory reaction or to induce innate memory in monocytes, but can partially affect the stimulus-induced cell activation.

MATERIALS AND METHODS

AuNP Synthesis and Characterization

AuNP Synthesis

AuNPs were synthesized as previously described by Bastús *et al.* (27). Briefly, 150 mL of sodium citrate 2.2 mM was brought to a boil under reflux, followed by rapid addition of 1 mL of $HAuCl_4$ 25 mM. AuNP "seeds" were formed in this manner, and sequential addition of $HAuCl_4$ achieved the desired particle size. All reagents were obtained from Sigma-Aldrich® (Merck KGaA, St. Louis, MO, USA).

AuNP Characterization

Transmission Electron Microscopy and Scanning Electron Microscopy

NP characterization images were obtained by STEM (scanning transmission electron microscopy) using a FEI Magellan XHR microscope (FEI, Hillsboro, OR, USA) in transmission mode with an acceleration of 20 kV, as previously described (22). AuNP samples were stabilized with polyvinylpyrrolidone (55 kDa) (28) and drop cast onto a carbon-coated TEM grid.

After drying, samples were imaged and particle size was assessed using an ImageJ macro. Scanning Electron Microscopy (SEM) was conducted on a JEOL 6700F scanning electron microscope (JEOL, Peabody, MA, USA) as described previously (29).

UV-vis Spectroscopy

To assess particle stability and uniformity of size, UV-vis spectra of the AuNP suspensions were obtained using a Shimadzu UV-2400 spectrophotometer (SSI, Kyoto, Japan) with a range of 300-700 nm. Samples were measured at room temperature, and milliQ water was used as a reference.

Dynamic Light Scattering

Particle ζ-potential and hydrodynamic diameter were determined by laser doppler velocimetry and dynamic light scattering (DLS), respectively, using a Malvern Zetasizer Nano ZS instrument (Malvern Panalytical Ltd., Malvern, UK) with a light source wavelength of 632.8 nm and a fixed scattering angle of 173° (at 25°C).

Atomic Force Microscopy

AFM measurements were performed with XE-70 microscope (Park Systems, Suwon, South Korea). The instrument is equipped with two flexure scanners (XY plane and Z) both for probe tips and samples. Scans were performed on an area up to 15x15 μm^2 with a topographic resolution below 1 nm (30). AFM images were acquired after deposition of AuNPs (10 µL at 1022 µg/mL) on a quartz slide by drop-casting.

Evaluation of Endotoxin Contamination

The presence of endotoxin contamination in NP samples was assessed with the Limulus Amoebocyte Lysate assay (LAL). The chromogenic Pyrochrome LAL assay (Associates of Cape Cod, Inc.; East Falmouth, MA, USA) was conducted at NP concentrations determined be to below the threshold for optical interference, following a protocol optimized for NPs (31), and sample absorbance was assessed using a Cytation 3 imaging reader (BioTek, Winooski, VT, USA). Endotoxin levels were expressed as endotoxin units per milligram of AuNPs (EU/mg).

Human Monocyte Isolation

Primary human monocytes were isolated from buffy coats of 20 healthy anonymous donors (provided by the blood bank of Salzburg, Austria, following overnight refrigeration), with cells from 4-8 buffy coats used for each primary stimulus. The study was conducted in accordance with the Declaration of Helsinki, and under Austrian national guidelines. According to Austrian regulations, no informed consent is required if blood cells derived from anonymous healthy donors, discarded after plasmapheresis (buffy coats) are used, therefore no additional approval by the national ethics committee was necessary. Peripheral blood mononuclear cells were obtained by Ficoll-Paque gradient density separation (GE Healthcare, Bio-Sciences AB, Uppsala, Sweden). Monocytes were further isolated by $CD14^+$ magnetic microbead separation (Miltenyi Biotec, Bergisch Gladbach, Germany) following the manufacturer's instructions. The resulting cell suspension was monitored for purity by differential counting on Wright-Giemsa-stained cytosmears (Diff-Quik; Medion Diagnostics, Düdingen, Switzerland) examined by optical microscopy. Cell viability was assessed by trypan blue dye exclusion. Only cell isolations with at least 95% purity and 95% viability were used.

Human Monocyte Primary Stimulation and Innate Memory Response

AuNP Biocorona Formation

Before addition into cell culture, AuNPs were pre-incubated in 50% inactivated human AB serum (Sigma-Aldrich) at 37°C for 1 h, in order to obtain the formation of a bio-corona of serum proteins and other components on the particle surface thereby ensuring particle stability in culture. However, being this a soft corona, it still allowed for interaction of the reactive particle surface with microbial agents and cells in culture (32, 33). The serum-AuNP mixture was added directly to culture wells (34), adjusting particle and serum concentration to the desired values.

Monocyte Primary Innate Response

Freshly isolated monocytes were suspended in culture medium (RPMI-1640 + Glutamax-I; GIBCO by Life Technologies, Paisley, UK) supplemented with 100 U/mL penicillin/streptomycin (Sigma-Aldrich). Cells ($1x10^5$/well) were added to 96 well flat bottom plates (Corning® Costar®; Corning Inc. Life Sciences, Oneonta, NY, USA). Cells were exposed to β-glucan (extracted from *C. albicans*; 2 µg/mL; a generous gift from Charles Dinarello, University of Colorado, Denver CO, USA), MDP (10 µg/mL; InvivoGen, San Diego, CA, USA), heat-killed *S. aureus* (ratio with monocytes 1:1; strain ATCC 6538, InvivoGen), heat-killed *Candida albicans* (ratio 0.1:1; strain ATCC 10231, InvivoGen), or live *H. pylori* (at MOI 0.2, 1, 5; WT strain p12, cultured in-house as described previously) (35). *H. pylori* CFUs were determined by spectrophotometric measurement of bacterial culture turbidity (OD_{600}; BioPhotometer plus, Eppendorf, Hamburg, Germany), following an in-house CFU calibration curve.

Cell stimulation was performed in the presence or absence of 20 µg/mL AuNPs. The final serum concentration of each well was adjusted to 5%. The primary monocyte response to stimuli was assessed as cytokine analysis in the 24 h supernatants. For stimulation with *H. pylori*, antibiotics were absent during the primary stimulation to ensure bacterial integrity during the primary activation/memory induction phase. Antibiotics were added into the culture medium for both the resting and challenge phases, to avoid unwanted activation by residual bacteria and to maintain the same culture conditions as for other stimuli.

Monocyte Memory Innate Response

After the primary response and supernatant collection, cells were rested in fresh culture medium for 6 days, with medium changes on days 4 and 6. A resting period of 6 days was sufficient for the complete extinction of monocyte activation induced by the different stimuli, based on the production of inflammation-related factors. That monocytes were no longer activated was assessed by measuring cytokine production in the 6-day

supernatant (representing the cytokine production from day 4 to 6; data not shown) and by challenging the primed cells with culture medium alone (see first column on the left "challenged by medium" in all the figures reporting innate memory results). At day 7, cells were exposed to fresh culture medium alone of containing 5 ng/mL of LPS (from *Escherichia coli* O55:B5; Sigma-Aldrich). Supernatants were collected after 24 h for cytokine analysis.

Cytokine Analysis

Production of TNFα and IL-1Ra was measured in the culture supernatants by ELISA (R&D Systems, Inc., Minneapolis, MN, USA). All other cytokines and chemokines were measured using a ProcartaPlex multiplex assay (Thermo Fisher Scientific, Waltham, MA, USA). The lower detection limits for the assays used was: TNFα, 15.6 pg/mL; IL-6, 9.4 pg/mL; IL-1Ra, 93.8 pg/mL; IL-10, 7.1 pg/mL; MCP-1, 15.0 pg/mL; IL-1α, 9.5 pg/mL; MIP-1α, 8.9 pg/mL; MIP-1β, 110.1 pg/mL; GROα, 3.0 pg/mL; IP-10, 23.4 pg/mL; IL-8, 31.2 pg/mL. Two ELISA replicates were run for each sample, and each experimental condition was tested with duplicate samples.

Statistical Analysis

Cytokine levels are reported as ng/10^6 plated monocytes. Graphical presentations and statistical analysis were obtained using Graphpad Prism 9 (GraphPad Inc., La Jolla, CA, USA). Data are shown as averages of biological triplicates or as averages of technical replicates of biological duplicates. Statistical analysis was conducted using one-way ANOVA with the Fisher's LSD *post hoc* test for multiple comparisons. The Shapiro-Wilk normality test was conducted on each data set prior to ANOVA, to ensure normal distributions.

RESULTS AND DISCUSSION

AuNP Characterization

In this study, we used gold nanoparticles (AuNPs in 2.2 mM sodium citrate) of an average diameter of 51 ± 4 nm (**Figures 1A–E**). Particle size and uniformity was confirmed by UV-vis (a single peak found at 531 nm), while DLS revealed a hydrodynamic size of 59 ± 16 nm, and a ζ-potential of about -39 ± 3 mV. The stock concentration following synthesis was 278 μg/mL (corresponding to a particle concentration of $2x10^{11}$ NPs/mL, to 1.4 mM Au, and to a surface area of $1.7x10^3$ mm^2/mL), with an endotoxin contamination (determined by LAL assay) of 3.97 EU/mg (**Figure 1A**). Endotoxin may activate monocytes at concentrations above 0.1 EU/mL; our preparation thus allowed for a NP working concentration in culture of 20 μg AuNPs/mL, containing 0.079 EU/mL of endotoxin, which is below the endotoxin activation threshold (36, 37). Prior to addition into culture, AuNP were incubated in 50% AB serum, to better mimic the physiological conditions of NP interaction with human immune cells (38). Formation of a serum-dependent biocorona on the NP surface avoided particle aggregation in culture medium (32, 39). The presence of AuNPs within cells was assessed by TEM 6 days after monocyte exposure to NPs for 24 h (**Figure 1E**). Particles could be observed within endosomes, but not free in the cytosol or within nuclei. This is in agreement with the notion that particles are endocytosed and kept within vesicles for eventual degradation, implying a mechanism of silent, non-inflammatory elimination of foreign/anomalous materials. The absence of AuNPs in the cytoplasm suggests that the particles are unable to destabilize the vesicle membrane and, consequently, to induce the activation of cytoplasmic inflammasomes by released lysosomal enzymes and mitochondrial ROS. Importantly, despite the lack of inflammatory activation, the mechanism of silent elimination was reported as able to "prime" macrophages and induce a protective innate memory *vs.* subsequent challenges (40). At this timepoint, no appreciable differences were noted in intracellular NP number, size and distribution across all experimental conditions (not shown), and no morphological alterations in monocytes were observed (**Figure 1F**).

Effect of AuNPs on the Primary Innate Response Induced by Soluble *vs.* Particulate Microbial Stimuli

We aimed to determine whether the presence of AuNPs might interfere with the induction of innate immune memory by microbial stimuli. In particular, we wanted to examine possible differential effects on innate memory induced by particulate stimuli (whole microorganisms) or by microbial molecules. Freshly isolated human blood monocytes were exposed for 24 h *in vitro* to culture medium alone or containing one of four microbial agents: the bacterial surface molecule muramyl dipeptide (MDP, 10 μg/mL); heat-killed gram-positive *Staphylococcus aureus* (*S. aureus*, ratio 1:1 with monocyte); the fungal polysaccharide β-glucan (2 μg/mL) and heat-killed *Candida albicans (C. albicans*, at a ratio 0.1:1 with monocytes). Concentrations were selected based on preliminary experiments and literature data as able to induce a significant but suboptimal innate immune activation (19, 41, 42; data not shown).

The direct, primary response of monocytes to microbial stimuli was evaluated in the absence or in the presence of AuNPs (20 μg/mL), and assessed in the 24-h supernatant as production of innate/inflammatory cytokines and chemokines. The size of AuNPs was chosen based upon preliminary data using AuNPs of different sizes, which suggested that 50 nm AuNPs were the best for observing effects on innate memory (23). The concentration was selected as the highest non-toxic and endotoxin-free concentration (data not shown).

Figure 2 shows the primary response of monocytes in terms of production of the inflammatory cytokine TNFα, measured in monocytes from 2-4 individual donors. As expected, cells exposed to culture medium alone or containing the endotoxin-free AuNPs did not produce appreciable levels of TNFα (<0.3 ng/10^6 monocytes). Stimulation of monocytes for 24 h with bacterial MDP or killed gram-positive *S. aureus* resulted in a substantial production of TNFα, which was not overall significantly impacted by the presence of AuNPs, although a decrease in the response to *S. aureus* was evident for cells of 3 out of 4 donors (**Figures 2A, B**). Cells were also stimulated with *C. albicans*-

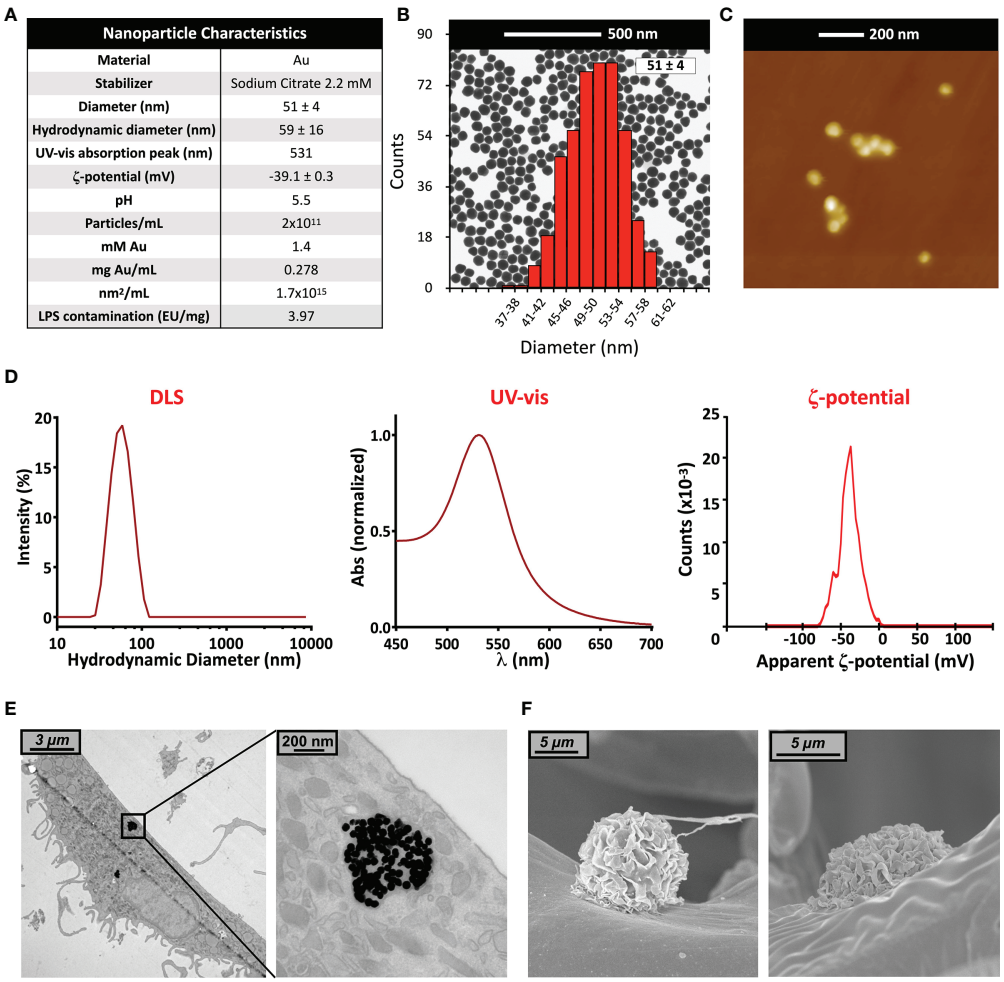

FIGURE 1 | Gold nanoparticle characterization. **(A)** Summary of characteristics of the AuNP batch used in this study; **(B)** TEM image and size distribution (calculated *via* ImageJ); **(C)** Atomic Force Microscopy image; **(D)** UV-vis spectrum, hydrodynamic size distribution calculated by DLS, and ζ-potential; **(E)** TEM and **(F)** SEM images of human primary monocytes, pre-exposed to AuNP for 24 h and then cultured for 6 additional days.

derived β-glucan and with the whole killed *C. albicans* organisms. Both fungal agents also induced TNFα production, although this increase did not attain statistical significance for β-glucan (only two subjects could be tested; **Figure 2C**). Co-exposure of monocytes to *C. albicans* and AuNPs caused a significant suppression of TNFα production in cells from all donors (**Figure 2D**). To investigate whether the AuNP effect observed for *C. albicans*-stimulated TNFα production was common to other *C. albicans*-induced factors, we examined the production of the inflammatory cytokine IL-6, the anti-inflammatory factor IL-1Ra and the chemokine MCP-1/CCL2, and found that AuNPs did not affect the stimulus-induced production of any of them (**Supplementary Figure 1**).

These results confirm previous observations that AuNPs do not have a substantial impact on the innate/inflammatory response of human monocytes to microbial stimuli, but that a partial reduction of the response to whole microorganisms can be observed in the majority of donors. Notably, individual effects can be observed on cells from many donors, these effects being variable (increase or decrease of the response) depending on the donor and irrespective of the inflammatory agent. Only in the case of *C. albicans* was a similar decrease observed in all donors, thus reaching statistical significance (**Figure 2D**).

Effect of AuNPs on the Memory Innate Response Induced by Soluble *vs.* Particulate Microbial Stimuli

Following primary activation, cells were rested for 6 days. This allows monocytes sufficient time to return to quiescence, prior to restimulation. Cell number and morphology following resting appeared consistent (by visual inspection) across wells from different primary conditions. After resting, cells were challenged with either medium alone or 5 ng/mL of LPS, in order to observe whether the previous exposure to inflammatory agents resulted in development of an innate immune memory (an increased or decreased response compared to control

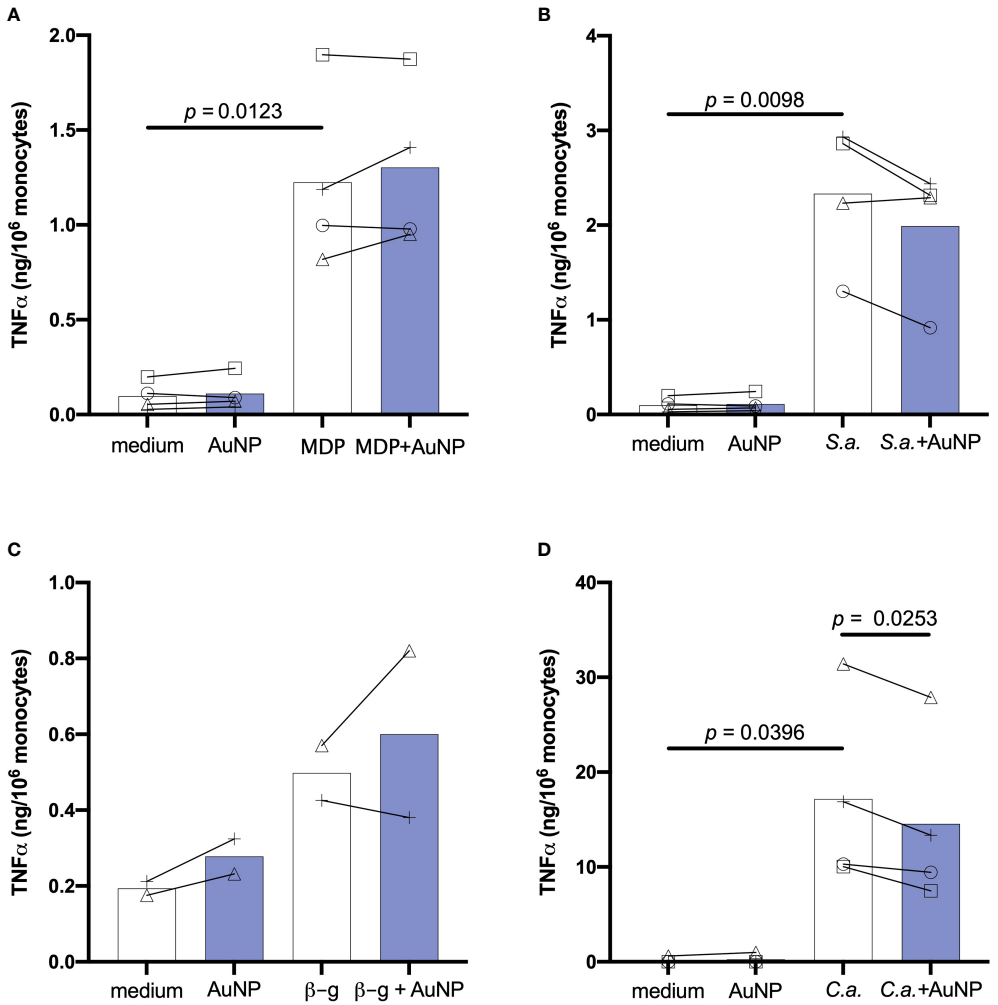

FIGURE 2 | Effect of AuNPs on the primary response of monocytes exposed to soluble or particulate microbial stimuli. $CD14^+$ monocytes were exposed to MDP (10 μg/mL) **(A)**, *S. aureus* (ratio 1:1; *S.a.*) **(B)**, β-glucan (2 μg/mL; β-g) **(C)** or **(C)** *albicans* (ratio 0.1:1; *C.a.*) **(D)** for 24 h in the presence or absence of AuNPs (20 μg/mL, indicated by blue bars). The inflammatory response is reported in terms of production of TNFα (ng/10^6 monocytes). Values from individual donors are depicted concurrent with mean cytokine production. Relevant *p* values are indicated when < 0.05. n = 4 **(A, B, D)**, n = 2 **(C)**.

unprimed cells). The *in vitro* model adopted for assessing memory induction is depicted in **Figure 3**. Challenge with medium alone resulted in TNFα levels below the detection limit of the assay for all primed cells, indicating that cells had returned to baseline TNFα production (**Figure 4**; medium-challenged cells are grouped into one bar that includes every priming condition tested). Restimulation with LPS induced significant production of TNFα, which was comparable between medium- and AuNP-primed cells, suggesting that pre-exposure to AuNPs was unable to induce a consistent memory response. It should be however noted that, while the average production is not statistically different between control and AuNP-primed monocytes, at the individual level there are cases in which AuNP-primed cells respond to challenge with an increased TNFα production, others in which there is a decrease, and others in which there is no change (see for instance the four donors in **Figure 4C**). This again underlines the need for an individual profiling of innate and memory responses, in order to predict reactivity to future challenges. Such profiling should include the production of a number of inflammatory and anti-inflammatory factors in response to different microbial challenges, in order to assess the overall balance between inflammation and anti-inflammation (26). The memory response of MDP-primed cells was of tolerance type, relative to TNFα production, with a decreased production of the inflammatory cytokine compared to medium-primed cells. Also in this case, the global difference was not statistically significant (p=0.0956), due to the interindividual variability (with monocytes from 1 out of 4 donors showing no change). Cells primed with MDP + AuNPs showed a significant tolerance at restimulation, compared to cells primed with either stimulus alone, confirming the tendency to tolerance observed with single priming agents (**Figure 4A**). Restimulation of cells primed with *S. aureus* (which contains MDP as part of its surface structure)

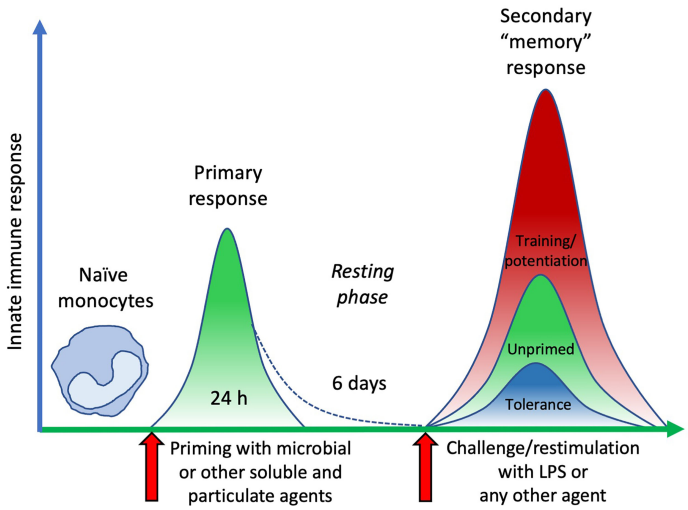

FIGURE 3 | The time course of an *in vitro* model of innate immune memory. Fresh naïve monocytes are activated by exposure in culture to different stimuli for 24 h (primary response). After elimination of stimuli, cell activation subsides with time (in our *in vitro* model 6 days are sufficient), during which period cells return to a resting status. Upon restimulation, cells that were not previously exposed to activating agents (unprimed) develop a secondary response of a given intensity. Conversely, cells that were previously primed and activated can react to restimulation with a secondary "memory" response, either more powerful (training/potentiation) or reduced (tolerance), compared to unprimed cells.

demonstrated that, similar to MDP, *S. aureus* is a potent inducer of innate memory in the direction of tolerance (**Figure 4B**). Unlike the memory effect upon MDP priming, AuNPs had no effect on *S. aureus*-driven tolerance. The difference in the effect of AuNPs on memory induced by MDP *vs*. the entire *S. aureus* bacteria might be ascribed to the different mechanisms of primary cell activation (which then initiate the epigenetic and metabolic reprogramming responsible for the establishment of memory), MDP mainly acting through NOD2 in the cytoplasm after receptor-independent endocytosis/transport through membrane channels (43, 44), while the whole bacteria principally interact with the plasma membrane through lipoteichoic acid activation of TLR2, thereby initiating an MyD88-dependent signaling pathway (45, 46). The metabolic cost and pathway involvement of bacterial phagocytosis compared to uptake of soluble factors most likely also contribute to the different memory profiles generated by *S. aureus* and MDP, although this remains unstudied to date (47). Thus, the presence of AuNPs, which are endocytosed, may have interfered with the MDP-dependent mechanism of memory generation, while unable to affect the memory mechanisms initiated extracellularly by *S. aureus*.

Upon challenge, cells primed with the fungal agents β-glucan and *C. albicans* did not demonstrate an innate memory response, as their TNFα production did not differ from that medium-primed (**Figures 4C, D**). In both cases, the presence of AuNPs at priming did not have any effect on the secondary response at challenge. To make sure that the lack of memory induction was not restricted to the production of a single inflammatory factor, in the case of *C. albicans* priming we also assessed the production of another inflammatory cytokine (IL-6), two anti-inflammatory factors (IL-10 and IL-1Ra) and six chemokines (three CC chemokines: MCP-1/CCL2, MIP-1α/CCL3 and MIP-1β/CCL4; and three CXC chemokines: GROα/CXCL1, IP-10/CXCL10 and IL-8/CXCL8) (**Supplementary Figure 2**). Two of these factors (IL-1Ra and CCL2/MCP-1) were spontaneously produced at high levels, and their levels were not increased in response to the LPS challenge. Similar to TNFα, priming with *C. albicans* did not induce memory (either potentiation or decrease of the secondary response) in terms of production of any of these factors. Likewise, the presence of AuNPs at priming did not have any significant effect (**Supplementary Figure 2**).

In all cases, again it should be noted that the interindividual variability is high and that, while the average values are not statistically different, the individual effects can be substantial both as decrease and increase of the memory response in the presence of AuNPs.

Effect of AuNPs on Primary and Memory Innate Responses Induced by Live Bacteria

Previous data suggest that the impact of AuNPs on innate memory induced by bacteria may vary depending on whether bacteria (BCG in this specific case) are viable or not (23). We have therefore also tested the effect of AuNPs on responses induced by a live microorganism, the gram-negative *H. pylori*, so as to compare such effect with those induced by killed microorganisms (*S. aureus* and *C. albicans*). Monocytes were primed *in vitro* for 24 h by live *H. pylori* at three concentrations (at MOI 0.2, 1 and 5) in the absence or presence of AuNPs. Primary stimulation with *H. pylori* revealed a potent dose-dependent induction of TNFα production (**Figure 5**), which was significantly suppressed by the presence of AuNPs, with the most robust suppression present at the lowest *H. pylori* dose (MOI 0.2). Thus, similar to what was observed with live BCG (23) and, to a lower extent, with killed whole bacteria

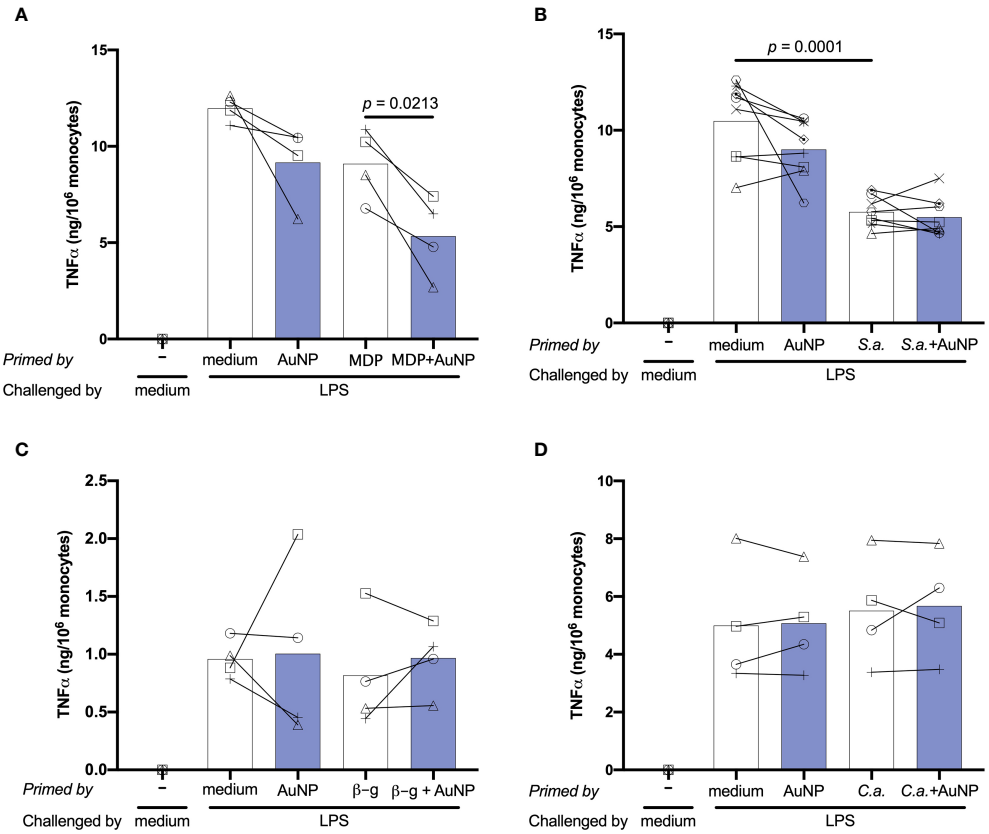

FIGURE 4 | Effect of AuNPs on the memory response of monocytes primed by soluble or particulate microbial stimuli. $CD14^+$ monocytes were primed with MDP **(A)**, *S. aureus* **(B)**, β-glucan **(C)** or *C. albicans* **(D)** for 24 h in the presence or absence of AuNPs (20 μg/mL, indicated by blue bars), then washed and rested for 6 days. Cells were then challenged with LPS (5 ng/mL) for 24 h, and supernatants collected for cytokine measurement. The inflammatory response is reported in terms of production of TNFα (ng/10^6 monocytes), and individual donor values are depicted concurrent with mean cytokine production. *p* values are indicated when < 0.05 for the comparisons between unprimed and primed groups and priming with and without NPs, n = 4 **(A, C, D)**, n = 8 **(B)**.

(**Figures 2B, D**), AuNPs are capable of interfering with the primary innate response induced by live *H. pylori*.

Induction of innate immune memory by *H. pylori* was assessed using the same *in vitro* model described previously for soluble and particulate microbial stimuli. Following 6 days of resting, control and primed cells were challenged with 5 ng/ml of LPS for 24 h. To better assess the memory induction by *H. pylori* and the AuNP impact, in addition to TNFα we have examined several other important inflammation-related cytokines and chemokines. Results in **Figure 6** show the memory response of *H. pylori*-primed cells in terms of production of two key inflammatory factors, TNFα and IL-6, and of two anti-inflammatory cytokines, IL-1Ra and IL-10. Additional factors are reported in **Supplementary Figure 2**. Only the results at *H. pylori* MOI 0.2 are shown, since no substantial differences were observed at higher concentrations. Upon challenge with LPS, cells primed with medium exhibited elevated production of all cytokines and chemokines measured, except IL-1Ra and MCP-1, whose baseline levels were already high (**Figure 6** and **Supplementary Figure 3**). Overall, the secondary response of cells primed with AuNPs was not significantly different from that of medium-primed cells, although again different behaviors were evident between donors. The memory response of *H. pylori*-primed cells revealed a potent induction of an innate immune tolerance in terms of TNFα, IL-6, IL-10 and the CXC chemokine IP-10, though not for IL-1α, IL-1Ra and in all the other chemokines tested (**Figure 6** and **Supplementary Figure 3**). The presence of AuNPs during priming with *H. pylori* did not alter the *H. pylori*-induced memory effect on any of the cytokines and chemokines tested, with the exception of the anti-inflammatory cytokine IL 10. In this case, the *H. pylori*-induced tolerance was significantly enhanced by AuNPs (**Figure 6D**), an effect evident at all *H. pylori* priming concentrations (data not shown).

Thus, monocytes exposed to live *H. pylori* can mount a potent inflammatory response that primes cells towards a generally less potent secondary memory response, in terms of production of two inflammatory factors (TNFα and IL-6), an anti-inflammatory cytokine (IL-10) and the chemokine IP-10. That *H. pylori* priming may affect the production of four different cytokines suggests different levels of epigenetic/metabolic reprogramming, likely dependent on the multiplicity of its cell activation modes. In fact, *H. pylori* can interact with TLR2 on the cell membrane,

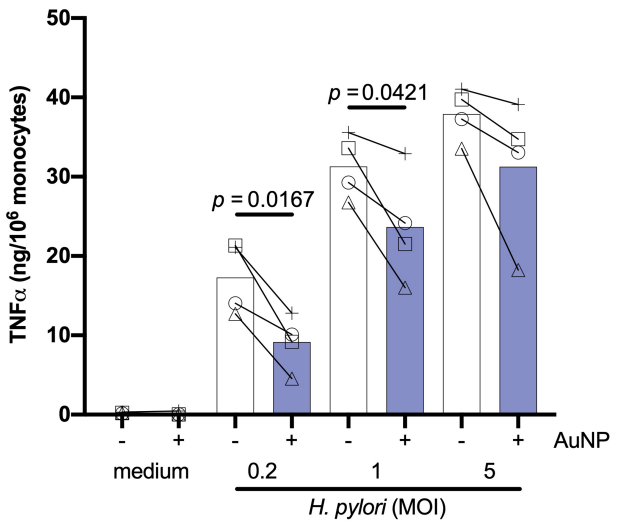

FIGURE 5 | Effect of AuNPs on the primary response of monocytes to live *H. pylori*. $CD14^+$ monocytes were stimulated with medium alone or containing live *H. pylori* (MOI: 0.2, 1, 5) for 24 h in the presence or absence of AuNPs (20 μg/mL, indicated by blue bars). The inflammatory response is reported in terms of production of TNFα (ng/10^6 monocytes). Values from individual donors are depicted concurrent with mean cytokine production. *p* values are indicated when < 0.05 for the comparison between stimulation with or without NPs, n = 4.

possibly through Hsp60 (48–50), while its LPS has very limited inflammatory activity and does not trigger a significant TLR4-mediated inflammation (51–53). Of note, the *cag* pathogenicity island (*cag*PAI), which mediates *H. pylori* pathogenesis in gastric epithelial cells, is less important in macrophages and dendritic cells (50, 54). *H. pylori* can induce inflammatory activation of innate cells (53, 55–57), possibly through the non-enzymatic interaction of secreted urease with receptors/acceptors on the cell membrane (55, 56), promote the macrophage M1 inflammatory phenotype through NOD1 (58), and survive for at least 24 hours within phagolysosomes after ingestion thereby inducing potent ROS production (59–61). By inducing phosphorylation of the NFκB p65 subunit at Ser-537, also the integrin-like kinase (ILK) promotes *H. plyori*-induced TNFα production (62). All these mechanisms of inflammatory activation will likely induce a multitude of different metabolic and epigenetic changes resulting in a complex innate memory profile. The tolerance memory response observed for TNFα and IL-6, two cytokines mainly dependent on the activation of the NFκB pathway, suggests that the TLR2-dependent priming may be principally involved. Conversely, the effects on IL-10 and IP-10, two factors that largely depend on interferon activation, are more likely mediated by other mechanisms, including the NOD1 pathway through the TRAF3-dependent induction of IRF3 and 7 and the production of type I IFN (63–70), which in turn activates the JAK/STAT signaling pathway (71). In this perspective, the capacity of AuNPs to interfere with *H. pylori*-induced memory, which is evident only in the case of IL-10, suggests that AuNPs may increase the *H. pylori* effect through production of type I IFN.

CONCLUSIONS

The aim of this study was to assess whether engineered AuNPs, a nanomaterial with wide applications in many fields including medicine and generally considered safe, are able to modulate the innate immune/inflammatory responses of human subjects. This would contribute on one side to the implementation of a more thorough safety evaluation of AuNPs and, on the other hand, it could open the way to a targeted use of this nanomaterial for the therapeutic modulation of innate immunity/inflammation in several immune-related and inflammatory diseases. In particular, this study has addressed innate memory, *i.e.*, the ability of monocytes/macrophages to activate a more protective reaction to a challenge when previously exposed to the same or a different infectious agent (6, 7, 9–17). Following previous studies showing that endotoxin-free Au and other NPs are essentially unable to induce innate/inflammatory responses and innate memory *per se*, but could at least in part modulate the memory induced by microbial agents (21–26, 72), here we have examined if the nature of the memory-inducing microbial agents could determine the capacity of AuNPs to interfere with the development of innate memory. To study innate memory, we have taken advantage of a realistic *in vitro* model, based on human primary monocytes exposed to microbial agents and to AuNPs coated with human serum. Based on our preliminary findings, we can draw the following conclusions and formulate the following hypotheses:

1. AuNPs generally decrease the inflammatory activation of monocytes induced by whole microorganisms, both killed (*C. albicans*, *S. aureus*) and viable (*H. pylori* in this study, BCG in ref. 23). Conversely, monocyte activation induced by microbial molecules (β-glucan and MDP in this study, LPS in refs. 22, 23, 25, 26) is not consistently affected by co-exposure to AuNPs. This may be ascribed to a possible interference of AuNPs (which are readily and abundantly taken up by monocytes and stored in endosomal vesicles) with the intracellular trafficking of phagocytosed microorganisms and the phagocytosis-dependent signaling pathways (47).
2. The capacity of AuNPs to modulate innate memory induced by microbial agents seems to be specifically restricted to some agents and to some of the memory response parameters (production levels of different cytokines), and appears to be independent of the effect on the primary response. In fact, AuNPs increase the tolerance memory effect induced by MDP on the inflammatory cytokine TNFα, whereas no effect of the primary response to MDP could be observed. In the case of *H. pylori*, while AuNPs could significantly decrease the TNFα primary response, no effect on the tolerance memory response was evident for the same cytokine, while a significant decrease of the IL-10 memory response was observed. Since IL-10 is an anti-inflammatory factor, its decrease would result in an overall increase of inflammation. The circumscribed effects of AuNPs on the memory production of some cytokines in response to some microbial agents could be explained as interference with distinct mechanisms of cell activation and reprogramming, although experimental evidence is currently missing. The physical interaction between AuNPs and microbial agents at

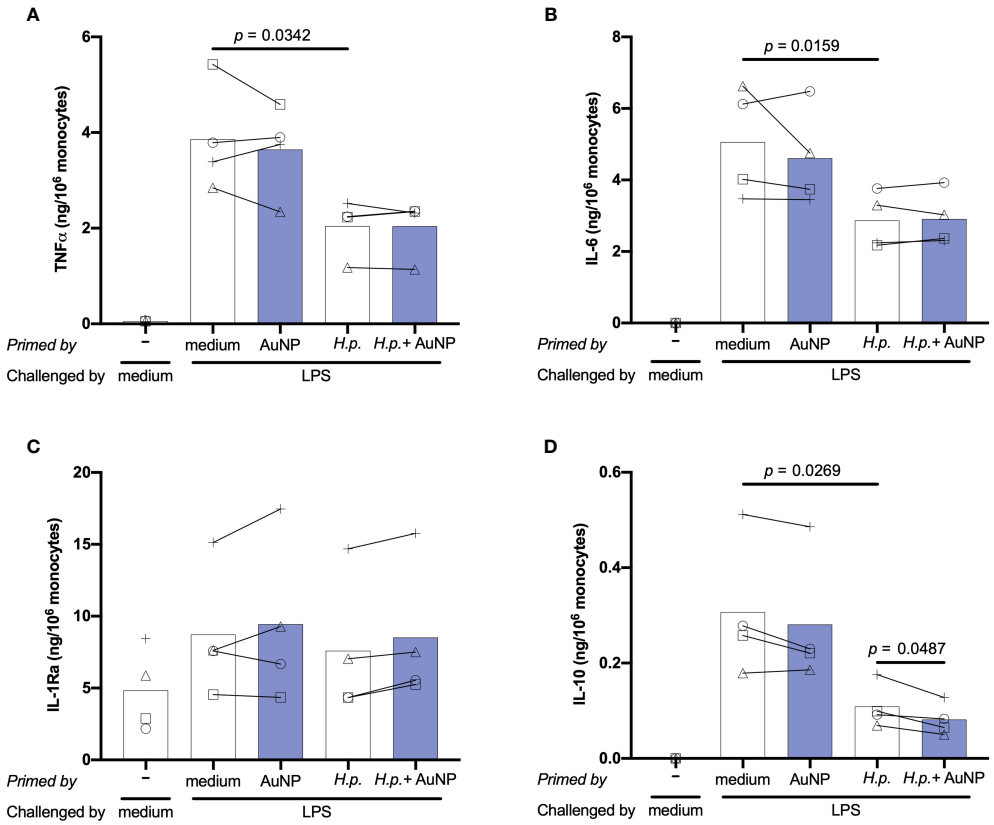

FIGURE 6 | Effect of AuNPs on the memory response of monocytes primed by live (*H*) *pylori*. CD14$^+$ monocytes were exposed to medium or *H. pylori* (at MOI 0.2) for 24 h in the presence or absence of AuNPs (20 μg/mL, indicated by blue bars), then washed and rested for 6 days. After resting, cells were challenged with LPS (5 ng/mL) for 24 h, supernatants were collected and examined for the production of TNFα **(A)**, IL-6 **(B)**, IL-1Ra **(C)** and IL-10 **(D)**. Values from individual donors are depicted concurrent with mean cytokine production. *p* values are indicated when < 0.05 for the comparisons between unprimed and primed groups and priming with and without NPs, n = 4. .

priming may lead to a different recognition/activation profile and trigger distinct epigenetic or metabolic pathways responsible of memory establishment.

3. The most striking observation made in this study, which confirms previous reports, is that opposite innate memory responses can be induced by the same agents and in the same conditions in monocytes from different subjects. Thus, the same microbial agent, alone or in combination with AuNPs, can cause potentiation, tolerance or no effect on cells from different donors. This suggests two considerations: first, it is not possible to classify the effects of NPs on innate memory in general terms; second, in order to know whether some NPs (to be used in medical applications) may have a detrimental effect on a patient, it is necessary to obtain a personalized innate memory profile.

DATA AVAILABILITY STATEMENT

The original contributions presented in the study are included in the article/**Supplementary Material**. Further inquiries can be directed to the corresponding author.

AUTHOR CONTRIBUTIONS

VP and FB synthesized and characterised the nanomaterials. BS, SM, TF, AV, and AL contributed to the experimental work. BS and SM planned the study. AD, JH-H, PI, and DB evaluated the results and monitored the experimental work. BS and DB wrote the manuscript. BS prepared the figures and performed the statistical analysis. All authors contributed to the article and approved the submitted version.

FUNDING

This work was supported by the EU Commission H2020 projects PANDORA (GA 671881) and ENDONANO (GA 812661), the Italian MIUR InterOmics Flagship projects MEMORAT and MAME, the Italian MIUR/PRIN-20173ZECCM, the Priority program ACBN (Allergy Cancer BioNano Research Centre) of the University of Salzburg, the Cancer Cluster Salzburg, the Research Grant from the University of Salzburg, and the Austrian Science Fund (FWF) Grant Nr. P 29941.

ACKNOWLEDGMENTS

We thank Marinella Pirozzi (EuroBioImaging facility at CNR) for the TEM images of NP uptake, and the Bioimaging Unit of the Stazione Zoologica Anton Dohrn for providing technical assistance for SEM images. We thank Charles A. Dinarello (University of Denver) for generously providing β-glucan, and Iris Gratz (Paris-Lodron University of Salzburg) for generously providing heat-killed *C. albicans*.

SUPPLEMENTARY MATERIAL

The Supplementary Material for this article can be found online at: https://www.frontiersin.org/articles/10.3389/fimmu.2021.751683/full#supplementary-material

Supplementary Figure 1 | Effect of AuNPs on the primary response of monocytes to killed *C. albicans*. CD14+ monocytes were stimulated with medium or *C. albicans* (ratio 0.1:1) for 24 h in the presence or absence of AuNPs (20 μg/mL, indicated by blue bars). The inflammatory response is reported in terms of production of IL-6 **(A)**, IL-1Ra **(B)** and MCP-1/CCL2 **(C)** and expressed as ng/106 monocyte. Values from individual donors are depicted concurrent with mean cytokine production. Relevant p values are indicated when < 0.05. n = 4.

Supplementary Figure 2 | Effect of AuNPs on the memory response of monocytes primed by *C. albicans*. CD14+ monocytes were exposed to medium or *C. albicans* (ratio 0.1:1) for 24 h in the presence or absence of AuNPs (20 μg/mL, indicated by blue bars), then washed and rested for 6 days. After resting, cells were challenged with LPS (5 ng/mL) for 24 h. Supernatants were collected and cytokine production measured: IL-6 **(A)**, IL-10 **(B)**, IL-1Ra **(C)** MCP-1/CCL2 **(D)**, MIP-1/CCL3 **(E)**, MIP-1b/CCL4 **(F)**, GROa/CXCL1 **(G)**, IP-10/CXCL10 **(H)**, IL-8/CXCL8 **(I)**. Individual donor values are depicted concurrent with mean cytokine production (ng/106 monocytes). n = 4.

Supplementary Figure 3 | Effect of AuNPs on the memory response of monocytes primed by *H. pylori*. CD14+ monocytes were exposed to medium or *H. pylori* (at MOI 0.2) for 24 h in the presence or absence of AuNPs (20 μg/mL, indicated by blue bars), then washed and rested for 6 days. After resting, cells were challenged with LPS challenge (5 ng/mL) for 24 h, and supernatant were collected for evaluation of cytokines and chemokines: IL-1a **(A)**, IL-8/CXCL8 **(B)**, MCP-1/CCL2 **(C)**, MIP-1a/CCL3 **(D)**, MIP-1b//CCL4 **(E)**, IP-10/CXCL10 **(F)**. Individual donor values are depicted concurrent with mean cytokine production (ng/106 monocytes). Relevant p values are indicated when < 0.05. n = 4.

REFERENCES

1. Murphy K, Weaver C. *Janeway's Immunobiology*. New York, NY: Garland Science (2016).
2. Milutinovic B, Kurtz J. Immune Memory in Invertebrates. *Semin Immunol* (2016) 28:328–42. doi: 10.1016/j.smim.2016.05.004
3. Reimer-Michalski EM, Conrath U. Innate Immune Memory in Plants. *Semin Immunol* (2016) 28:319–27. doi: 10.1016/j.smim.2016.05.006
4. Melillo D, Marino R, Italiani P, Boraschi D. Innate Immune Memory in Invertebrate Metazoans: A Critical Appraisal. *Front Immunol* (2018) 9:1915. doi: 10.3389/fimmu.2018.01915
5. Kurtz J. Specific Memory Within Innate Immune Systems. *Trends Immunol* (2005) 26:186–92. doi: 10.1016/j.it.2005.02.001
6. Netea MG, Joosten LA, Latz E, Mills KH, Natoli G, Stunnenberg HG, et al. Trained Immunity: A Program of Innate Immune Memory in Health and Disease. *Science* (2016) 352:aaf1098. doi: 10.1126/science.aaf1098
7. Arts RJW, Moorlag S, Novakovic B, Li Y, Wang SY, Oosting M, et al. BCG Vaccination Protects Against Experimental Viral Infection in Humans Through the Induction of Cytokines Associated With Trained Immunity. *Cell Host Microbe* (2018) 23:89–100.e5. doi: 10.1016/j.chom.2017.12.010
8. Beeson PB. Development of Tolerance to Typhoid Bacterial Pyrogen and its Abolition by Reticulo-Endothelial Blockade. *Proc Soc Exp Biol Med* (1946) 61:248–50. doi: 10.3181/00379727-61-15291P
9. Fan H, Cook JA. Molecular Mechanisms of Endotoxin Tolerance. *J Endotoxin Res* (2004) 10:71–84. doi: 10.1177/09680519040100020301
10. Cavaillon JM, Adib-Conquy M. Bench-To-Bedside Review: Endotoxin Tolerance as a Model of Leukocyte Reprogramming in Sepsis. *Crit Care* (2006) 10:233. doi: 10.1186/cc5055
11. Foster SL, Hargreaves DC, Medzhitov R. Gene-Specific Control of Inflammation by TLR-Induced Chromatin Modifications. *Nature* (2007) 447:972–8. doi: 10.1038/nature05836
12. Uthayakumar D, Paris S, Chapat L, Freyburger L, Poulet H, De Luca K. Non-Specific Effects of Vaccines Illustrated Through the BCG Example: From Observations to Demonstrations. *Front Immunol* (2018) 9:2869. doi: 10.3389/fimmu.2018.02869
13. Kleinnijenhuis J, Quintin J, Preijers F, Joosten LA, Ifrim DC, Saeed S, et al. Bacille Calmette-Guerin Induces NOD2-Dependent Nonspecific Protection From Reinfection via Epigenetic Reprogramming of Monocytes. *Proc Natl Acad Sci USA* (2012) 109:17537–42. doi: 10.1073/pnas.1202870109
14. Boraschi D, Italiani P. Innate Immune Memory: Time for Adopting a Correct Terminology. *Front Immunol* (2018) 9:799. doi: 10.3389/fimmu.2018.00799
15. Netea MG, Dominguez-Andres J, Barreiro LB, Chavakis T, Divangahi M, Fuchs E, et al. Defining Trained Immunity and its Role in Health and Disease. *Nat Rev Immunol* (2020) 20:375–88. doi: 10.1038/s41577-020-0285-6
16. Riksen NP, Netea MG. Immunometabolic Control of Trained Immunity. *Mol Asp Med* (2020) 77:100897. doi: 10.1016/j.mam.2020.100897
17. Arts RJW, Joosten LAB, Netea MG. The Potential Role of Trained Immunity in Autoimmune and Autoinflammatory Disorders. *Front Immunol* (2018) 9:298. doi: 10.3389/fimmu.2018.00298
18. Krahenbuhl J, Sharma S, Ferraresi R, Remington J. Effects of Muramyl Dipeptide Treatment on Resistance to Infection With Toxoplasma Gondii in Mice. *Infect Immun* (1981) 31:716–22. doi: 10.1128/iai.31.2.716-722.1981
19. Quintin J, Saeed S, Martens JHA, Giamarellos-Bourboulis EJ, Ifrim DC, Logie C, et al. Candida Albicans Infection Affords Protection Against Reinfection via Functional Reprogramming of Monocytes. *Cell Host Microbe* (2012) 12:223–32. doi: 10.1016/j.chom.2012.06.006
20. Mourits VP, Koeken VA, De Bree LCJ, Moorlag SJ, Chu WC, Xu X, et al. BCG-Induced Trained Immunity in Healthy Individuals: The Effect of Plasma Muramyl Dipeptide Concentrations. *J Immunol Res* (2020) 2020:5812743. doi: 10.1155/2020/5812743
21. Lebre F, Boland JB, Gouveia P, Gorman AL, Lundahl MLE, Lynch RI, et al. Pristine Graphene Induces Innate Immune Training. *Nanoscale* (2020) 12:11192–200. doi: 10.1039/c9nr09661b
22. Italiani P, Boraschi D. Induction of Innate Immune Memory by Engineered Nanoparticles: A Hypothesis That may Become True. *Front Immunol* (2017) 8:734. doi: 10.3389/fimmu.2017.00734
23. Swartzwelter BJ, Barbero F, Verde A, Mangini M, Pirozzi M, De Luca AC, et al. Gold Nanoparticles Modulate BCG-Induced Innate Immune Memory in Human Monocytes by Shifting the Memory Response Towards Tolerance. *Cells* (2020) 9:284. doi: 10.3390/cells9020284
24. Italiani P, Della Camera G, Boraschi D. Induction of Innate Immune Memory by Engineered Nanoparticles in Monocytes/Macrophages: From Hypothesis to Reality. *Front Immunol* (2020) 11:566309. doi: 10.3389/fimmu.2020.566309
25. Swartzwelter BJ, Verde A, Rehak ,L, Madej M, Puntes V, De Luca AC, et al. Interaction Between Macrophages and Nanoparticles: *In Vitro* 3D Cultures for the Realistic Assessment of Inflammatory Activation and Modulation of Innate Memory. *Nanomaterials* (2021) 11:207. doi: 10.3390/nano11010207
26. Della Camera G, Madej MP, Ferretti A, La Spina R, Li Y, Corteggio A, et al. Personalised Profiling of Innate Immune Memory Induced by Nano-Imaging Particles in Human Monocytes. *Front Immunol* (2021) 12:692165. doi: 10.3389/fimmu.2021.692165
27. Bastús NG, Comenge J, Puntes V. Kinetically Controlled Seeded Growth Synthesis of Citrate-Stabilized Gold Nanoparticles of Up to 200 Nm: Size Focusing *Versus* Ostwald Ripening. *Langmuir* (2011) 27:11098–105. doi: 10.1021/la201938u
28. Alijagic A, Barbero F, Gaglio D, Napodano E, Benada O, Kofroňová O, et al. Gold Nanoparticles Coated With Polyvinylpyrrolidone and Sea Urchin

Extracellular Molecules Induce Transient Immune Activation. *J Hazard Mater* (2021) 402:123793. doi: 10.1016/j.jhazmat.2020.123793
29. Bozzola JJ. Conventional Specimen Preparation Techniques for Scanning Electron Microscopy of Biological Specimens. *Methods Mol Biol* (2007) 369:449–66. doi: 10.1007/978-1-59745-294-6_22
30. Managò S, Zito G, Rogato A, Casalino M, Esposito E, De Luca AC, et al. Bioderived Three-Dimensional Hierarchical Nanostructures as Efficient Surface-Enhanced Raman Scattering Substrates for Cell Membrane Probing. *ACS Appl Mater Interfaces* (2018) 10:12406–16. doi: 10.1021/acsami.7b19285
31. Li Y, Italiani P, Casals E, Tran N, Puntes VF, Boraschi D. Optimising the Use of Commercial LAL Assays for the Analysis of Endotoxin Contamination in Metal Colloids and Metal Oxide Nanoparticles. *Nanotoxicology* (2015) 9:462–73. doi: 10.3109/17435390.2014.948090
32. Casals E, Pfaller T, Duschl A, Oostingh GJ, Puntes V. Time Evolution of the Nanoparticle Protein Corona. *ACS Nano* (2010) 4:3623–32. doi: 10.1021/nn901372t
33. Casals E, Puntes VF. Inorganic Nanoparticle Biomolecular Corona: Formation, Evolution and Biological Impact. *Nanomed (Lond)* (2012) 7:1917–30. doi: 10.2217/nnm.12.169
34. Piella J, Bastús NG, Puntes V. Size-Dependent Protein–Nanoparticle Interactions in Citrate-Stabilized Gold Nanoparticles: The Emergence of the Protein Corona. *Bioconjugate Chem* (2017) 28:88–97. doi: 10.1021/acs.bioconjchem.6b00575
35. Sarajlic M, Neuper T, Vetter J, Schaller S, Klicznik MM, Gratz IK, et al. *H. Pylori* Modulates DC Functions *via* T4SS/Tnfα/P38-Dependent SOCS3 Expression. *Cell Commun Signal* (2020) 18:1–13. doi: 10.1186/s12964-020-00655-1
36. Oostingh GJ, Casals E, Italiani P, Colognato R, Stritzinger R, Ponti J, et al. Problems and Challenges in the Development and Validation of Human Cell-Based Assays to Determine Nanoparticle-Induced Immunomodulatory Effects. *Part Fibre Toxicol* (2011) 8:8. doi: 10.1186/1743-8977-8-8
37. Li Y, Italiani P, Casals E, Valkenborg D, Mertens I, Baggerman G, et al. Assessing the Immunosafety of Engineered Nanoparticles With a Novel *In Vitro* Model Based on Human Primary Monocytes. *ACS Appl Mater Interfaces* (2016) 8:28437–47. doi: 10.1021/acsami.6b06278
38. Barbero F, Russo L, Vitali M, Piella J, Salvo I, Borrajo ML, et al. Formation of the Protein Corona: The Interface Between Nanoparticles and the Immune System. *Semin Immunol* (2017) 34:52–60. doi: 10.1016/j.smim.2017.10.001
39. Li Y, Shi Z, Radauer-Preiml I, Andosch A, Casals E, Luetz-Meindl U, et al. Bacterial Endotoxin (Lipopolysaccharide) Binds to the Surface of Gold Nanoparticles, Interferes With Biocorona Formation and Induces Human Monocyte Inflammatory Activation. *Nanotoxicology* (2017) 11:1157–75. doi: 10.1080/17435390.2017.1401142
40. Weavers H, Evans IR, Martin P, Wood W. Corpse Engulfment Generates a Molecular Memory That Primes the Macrophage Inflammatory Response. *Cell* (2016) 165:1658–71. doi: 10.1016/j.cell.2016.04.049
41. Saeed S, Quintin J, Kerstens HH, Rao NA, Aghajanirefah A, Matarese F, et al. Epigenetic Programming of Monocyte-to-Macrophage Differentiation and Trained Innate Immunity. *Science* (2014) 345:1251086. doi: 10.1126/science.1251086
42. Ifrim DC, Quintin J, Joosten LA, Jacobs C, Jansen T, Jacobs L, et al. Netea MGl. Trained Immunity or Tolerance: Opposing Functional Programs Induced in Human Monocytes After Engagement of Various Pattern Recognition Receptors. *Clin Vaccine Immunol* (2014) 21:534–45. doi: 10.1128/CVI.00688-13
43. Girardin SE, Boneca IG, Viala J, Chamaillard M, Labigne A, Thomas G, et al. Nod2 Is a General Sensor of Peptidoglycan Through Muramyl Dipeptide (MDP) Detection. *J Biol Chem* (2003) 278:8869–72. doi: 10.1074/jbc.C200651200
44. Al Nabhani Z, Dietrich G, Hugot J-P, Barreau F. Nod2: The Intestinal Gate Keeper. *PloS Pathog* (2017) 13:e1006177. doi: 10.1371/journal.ppat.1006177
45. Takeuchi O, Hoshino K, Akira S. Cutting Edge: TLR2-Deficient and MyD88-Deficient Mice are Highly Susceptible to *Staphylococcus* Aureus Infection. *J Immunol* (2000) 165:5392–6. doi: 10.4049/jimmunol.165.10.5392
46. Mullaly SC, Kubes P. The Role of TLR2 *In Vivo* Following Challenge With *Staphylococcus Aureus* and Prototypic Ligands. *J Immunol* (2006) 177:8154–63. doi: 10.4049/jimmunol.177.11.8154
47. Swartzwelter BJ, Fux AC, Johnson L, Swart E, Hofer S, Hofstätter N, et al. The Impact of Nanoparticles on Innate Immune Activation by Live Bacteria. *Int J Mol Sci* (2020) 21:9695. doi: 10.3390/ijms21249695
48. Takenaka R, Yokota K, Ayada K, Mizuno M, Zhao Y, Fujinami Y, et al. *Helicobacter Pylori* Heat-Shock Protein 60 Induces Inflammatory Responses Through the Toll-Like Receptor-Triggered Pathway in Cultured Human Gastric Epithelial Cells. *Microbiology* (2004) 150:3913–22. doi: 10.1099/mic.0.27527-0
49. Zhao Y, Yokota K, Ayada K, Yamamoto Y, Okada T, Shen L, et al. Helicobacter Pylori Heat-Shock Protein 60 Induces Interleukin-8 via a Toll-Like Receptor (TLR) 2 and Mitogen-Activated Protein (MAP) Kinase Pathway in Human Monocytes. *J Med Microbiol* (2007) 56:154–64. doi: 10.1099/jmm.0.46882-0
50. Neuper T, Frauenlob T, Sarajlic M, Posselt G, Wessler S, Horejs-Hoeck J. TLR2, TLR4 and TLR10 Shape the Cytokine and Chemokine Release of *H. Pylori*-Infected Human DCs. *Int J Mol Sci* (2020) 21:3897. doi: 10.3390/ijms21113897
51. Muotiala A, Helander IM, Pyhälä L, Kosunen TU, Moran A. Low Biological Activity of *Helicobacter Pylori* Lipopolysaccharide. *Infect Immun* (1992) 60:1714–6. doi: 10.1128/iai.60.4.1714-1716.1992
52. Mandell L, Moran AP, Cocchiarella A, Houghton J, Taylor N, Fox JG, et al. Intact Gram-Negative Helicobacter Pylori, Helicobacter Felis, and Helicobacter Hepaticus Bacteria Activate Innate Immunity via Toll-Like Receptor 2 But Not Toll-Like Receptor 4. *Infect Immun* (2004) 72:6446–54. doi: 10.1128/IAI.72.11.6446-6454.2004
53. Algood HMS, Cover TL. *Helicobacter Pylori* Persistence: An Overview of Interactions Between *H. Pylori* and Host Immune Defenses. *Clin Microbiol Rev* (2006) 19:597–613. doi: 10.1128/CMR.00006-06
54. Maeda S, Akanuma M, Mitsuno ,Y, Hirata Y, Ogura K, Yoshida H, et al. Distinct Mechanism of Helicobacter Pylori-Mediated NF-κb Activation Between Gastric Cancer Cells and Monocytic Cells. *J Biol Chem* (2001) 276:44856–64. doi: 10.1074/jbc.M105381200
55. Harris P, Mobley H, Perez-Perez G, Blaser M, Smith P. *Helicobacter Pylori* Urease Is a Potent Stimulus of Mononuclear Phagocyte Activation and Inflammatory Cytokine Production. *Gastroenterology* (1996) 111:419–25. doi: 10.1053/gast.1996.v111.pm8690207
56. Scopel-Guerra A, Olivera-Severo D, Staniscuaski F, Uberti AF, Callai-Silva N, Jaeger N, et al. The Impact of Helicobacter Pylori Urease Upon Platelets and Consequent Contributions to Inflammation. *Front Microbiol* (2017) 8:2447. doi: 10.3389/fmicb.2017.02447
57. Fehlings M, Drobbe L, Moos V, Renner Viveros P, Hagen J, Beigier-Bompadre M, et al. Comparative Analysis of the Interaction of *Helicobacter Pylori* With Human Dendritic Cells, Macrophages, and Monocytes. *Infect Immun* (2012) 80:2724–34. doi: 10.1128/IAI.00381-12
58. Suarez G, Romero-Gallo J, Piazuelo MB, Sierra JC, Delgado AG, Washington MK, et al. Nod1 Imprints Inflammatory and Carcinogenic Responses Toward the Gastric Pathogen Helicobacter Pylori. *Cancer Res* (2019) 79:1600–11. doi: 10.1158/0008-5472.CAN-18-2651
59. Allen L-AH, Schlesinger LS, Kang B. Virulent Strains of *Helicobacter Pylori* Demonstrate Delayed Phagocytosis and Stimulate Homotypic Phagosome Fusion in Macrophages. *J Exp Med* (2000) 191:115–28. doi: 10.1084/jem.191.1.115
60. Zheng PY, Jones NL. Helicobacter Pylori Strains Expressing the Vacuolating Cytotoxin Interrupt Phagosome Maturation in Macrophages by Recruiting and Retaining TACO (Coronin 1) Protein. *Cell Microbiol* (2003) 5:25–40. doi: 10.1046/j.1462-5822.2003.00250.x
61. Basu M, Czinn SJ, Blanchard TG. Absence of Catalase Reduces Long-Term Survival of Helicobacter Pylori in Macrophage Phagosomes. *Helicobacter* (2004) 9:211–6. doi: 10.1111/j.1083-4389.2004.00226.x
62. Ahmed AU, Sarvestani ST, Gantier MP, Williams BR, Hannigan GE. Integrin-Linked Kinase Modulates Lipopolysaccharide- and Helicobacter Pylori-Induced Nuclear Factor κb-Activated Tumor Necrosis Factor-α Production via Regulation of P65 Serine 536 Phosphorylation. *J Biol Chem* (2014) 289:27776–93. doi: 10.1074/jbc.M114.574541
63. Padovan E, Spagnoli GC, Ferrantini M, Heberer M. IFN-α2a Induces IP-10/CXCL10 and MIG/CXCL9 Production in Monocyte-Derived Dendritic Cells and Enhances Their Capacity to Attract and Stimulate CD8+ Effector T Cells. *J Leukoc Biol* (2002) 71:669–76. doi: 10.1189/jlb.71.4.669
64. Buttmann M, Berberich-Siebelt F, Serfling E, Rieckmann P. Interferon-β is a Potent Inducer of Interferon Regulatory Factor-1/2-Dependent IP-10/CXCL10 Expression in Primary Human Endothelial Cells. *J Vasc Res* (2007) 44:51–60. doi: 10.1159/000097977
65. Watanabe T, Asano N, Fichtner-Feigl S, Gorelick PL, Tsuji Y, Matsumoto Y, et al. NOD1 Contributes to Mouse Host Defense Against *Helicobacter Pylori*

via Induction of Type I IFN and Activation of the ISGF3 Signaling Pathway. *J Clin Invest* (2010) 120:1645–62. doi: 10.1172/JCI39481

66. Lin L, Hou J, Ma F, Wang P, Liu X, Li N, et al. Type I IFN Inhibits Innate IL-10 Production in Macrophages Through Histone Deacetylase 11 by Downregulating microRNA-145. *J Immunol* (2013) 191:3896–904. doi: 10.4049/jimmunol.1203450
67. McNab FW, Ewbank J, Howes A, Moreira-Teixeira L, Martirosyan A, Ghilardi N, et al. Type I IFN Induces IL-10 Production in an IL-27–Independent Manner and Blocks Responsiveness to IFN-γ for Production of IL-12 and Bacterial Killing in Mycobacterium Tuberculosis–Infected Macrophages. *J Immunol* (2014) 193:3600–12. doi: 10.4049/jimmunol.1401088
68. Fan Y-H, Roy S, Mukhopadhyay R, Kapoor A, Duggal P, Wojcik GL, et al. Role of Nucleotide-Binding Oligomerization Domain 1 (NOD1) and its Variants in Human Cytomegalovirus Control *In Vitro* and *In Vivo*. *Proc Nat Acad Sci USA* (2016) 113:E7818–27. doi: 10.1073/pnas.1611711113
69. Neuper T, Ellwanger K, Schwarz H, Kufer TA, Duschl A, Horejs-Hoeck J. NOD1 Modulates IL-10 Signalling in Human Dendritic Cells. *Sci Rep* (2017) 7:1–12. doi: 10.1038/s41598-017-00691-x
70. Ernst O, Glucksam-Galnoy Y, Bhatta B, Athamna M, Ben-Dror I, Glick Y, et al. Exclusive Temporal Stimulation of IL-10 Expression in LPS-Stimulated Mouse Macrophages by cAMP Inducers and Type I Interferons. *Front Immunol* (2019) 10:1788. doi: 10.3389/fimmu.2019.01788
71. Majoros A, Platanitis E, Kernbauer-Hölzl E, Rosebrock F, Müller M, Decker T. Canonical and Non-Canonical Aspects of JAK–STAT Signaling: Lessons From Interferons for Cytokine Responses. *Front Immunol* (2017) 8:29. doi: 10.3389/fimmu.2017.00029
72. Ferrari Barbosa MM, Kanno AI, Farias LP, Madej M, Sipos G, Sbrana S, et al. Primary and Memory Response of Human Monocytes to Vaccines: Role of Nanoparticulate Antigens in Inducing Innate Memory. *Nanomaterials* (2021) 11:931. doi: 10.3390/nano11040931

Conflict of Interest: The authors declare that the research was conducted in the absence of any commercial or financial relationships that could be construed as a potential conflict of interest.

Publisher's Note: All claims expressed in this article are solely those of the authors and do not necessarily represent those of their affiliated organizations, or those of the publisher, the editors and the reviewers. Any product that may be evaluated in this article, or claim that may be made by its manufacturer, is not guaranteed or endorsed by the publisher.

frontiers in Immunology

ORIGINAL RESEARCH
published: 26 November 2021
doi: 10.3389/fimmu.2021.753472

Pharmacological Activation of cGAS for Cancer Immunotherapy

*Kyle M. Garland[1], Jonah C. Rosch[1], Carcia S. Carson[2], Lihong Wang-Bishop[1], Ann Hanna[3], Sema Sevimli[1], Casey Van Kaer[4], Justin M. Balko[3,5], Manuel Ascano[6] and John T. Wilson[1,2,5,7,8,9]**

[1] Department of Chemical and Biomolecular Engineering, Vanderbilt University, Nashville, TN, United States, [2] Department of Biomedical Engineering, Vanderbilt University, Nashville, TN, United States, [3] Department of Medicine, Vanderbilt University Medical Center, Nashville, TN, United States, [4] Department of Bioengineering, Northeastern University, Boston, MA, United States, [5] Vanderbilt-Ingram Cancer Center, Vanderbilt University Medical Center, Nashville, TN, United States, [6] Department of Biochemistry, Vanderbilt University Medical Center, Nashville, TN, United States, [7] Vanderbilt Institute for Infection, Immunology, and Inflammation, Vanderbilt University Medical Center, Nashville, TN, United States, [8] Vanderbilt Center for Immunobiology, Vanderbilt University Medical Center, Nashville, TN, United States, [9] Vanderbilt Institute of Chemical Biology, Vanderbilt University Medical Center, Nashville, TN, United States

OPEN ACCESS

Edited by:
David Pozo,
University of Seville, Spain

Reviewed by:
Xin Li,
China Agricultural University, China
Chun-Jen Chen,
National Taiwan University, Taiwan

***Correspondence:**
John T. Wilson
john.t.wilson@vanderbilt.edu

Specialty section:
This article was submitted to Molecular Innate Immunity, a section of the journal Frontiers in Immunology

Received: *04 August 2021*
Accepted: *29 October 2021*
Published: *26 November 2021*

Citation:
Garland KM, Rosch JC, Carson CS, Wang-Bishop L, Hanna A, Sevimli S, Van Kaer C, Balko JM, Ascano M and Wilson JT (2021) Pharmacological Activation of cGAS for Cancer Immunotherapy. Front. Immunol. 12:753472. doi: 10.3389/fimmu.2021.753472

When compartmentally mislocalized within cells, nucleic acids can be exceptionally immunostimulatory and can even trigger the immune-mediated elimination of cancer. Specifically, the accumulation of double-stranded DNA in the cytosol can efficiently promote antitumor immunity by activating the cGAMP synthase (cGAS) / stimulator of interferon genes (STING) cellular signaling pathway. Targeting this cytosolic DNA sensing pathway with interferon stimulatory DNA (ISD) is therefore an attractive immunotherapeutic strategy for the treatment of cancer. However, the therapeutic activity of ISD is limited by several drug delivery barriers, including susceptibility to deoxyribonuclease degradation, poor cellular uptake, and inefficient cytosolic delivery. Here, we describe the development of a nucleic acid immunotherapeutic, NanoISD, which overcomes critical delivery barriers that limit the activity of ISD and thereby promotes antitumor immunity through the pharmacological activation of cGAS at the forefront of the STING pathway. NanoISD is a nanoparticle formulation that has been engineered to confer deoxyribonuclease resistance, enhance cellular uptake, and promote endosomal escape of ISD into the cytosol, resulting in potent activation of the STING pathway *via* cGAS. NanoISD mediates the local production of proinflammatory cytokines *via* STING signaling. Accordingly, the intratumoral administration of NanoISD induces the infiltration of natural killer cells and T lymphocytes into murine tumors. The therapeutic efficacy of NanoISD is demonstrated in preclinical tumor models by attenuated tumor growth, prolonged survival, and an improved response to immune checkpoint blockade therapy.

Keywords: cancer, cGAS/STING pathway, endosomal escape, immunotherapy, innate immune agonist, intratumoral, nanoparticles, nucleic acid therapy

INTRODUCTION

Nucleic acid sensing is a fundamental part of the innate immune system that can galvanize immune responses against pathogens and diseased cells (1). During cellular homeostasis, DNA is largely sequestered from the cytosol inside the nucleus and mitochondria (2). Accordingly, the abnormal accumulation of DNA inside the cytosol is indicative of cellular distress. The aberrant presence of such "danger signals" within the cytosol can trigger various pattern recognition receptors (PRRs) and lead to a myriad of immunological responses (3). Moreover, the physiochemical properties of cytosolic DNA (*e.g.* nucleotide sequence, base pair (BP) length, *etc.*) can drastically influence the nature of the resultant immune response by modulating PRR activation (4).

The stimulator of interferon genes (STING) cellular signaling pathway is a major DNA sensing pathway that bridges the gap between innate and adaptive immunity. The STING protein is located on the endoplasmic reticulum (5) and is directly activated by cyclic dinucleotides (CDNs) (6), such as the endogenous second messenger, 2′3′-cyclic guanosine monophosphate–adenosine monophosphate (cGAMP) (7). Molecules of cGAMP are produced intracellularly by cGAMP synthase (cGAS) when the enzyme detects double-stranded DNA (dsDNA) in the cytosol (7–10). Notably, the recognition of cytosolic dsDNA by cGAS is independent of nucleotide sequence (11), and therefore this DNA sensing pathway is broadly applicable to a vast number of microbial infections as well as the detection of self dsDNA leakage resulting from cellular malfunction, a common feature of many precancerous cells.

STING activation results in the local production of type-I interferons (IFN-I) and various other proinflammatory cytokines, the specific profile of which depends on cellular context as well as the type, intensity, and duration of the stimulant (12). This dynamic cytokine response generally creates an inflammatory microenvironment, which in certain settings, can promote robust cellular immune responses towards pathogens and diseases (13). Notably, localized STING signaling has been identified as critical for the spontaneous induction of antitumor immunity (14). Indeed, STING knockout (KO) mice (*i.e.* *Tmem173*$^{-/-}$) exhibit defective tumor control in some murine tumor models and demonstrate a significantly reduced therapeutic response to immune checkpoint blockade (ICB) therapy relative to wildtype mice (14). Moreover, these preclinical findings have corresponded with clinical data from human cancer patients that has positively correlated cGAS/STING activation with the presence of tumor infiltrating T lymphocytes (*i.e.* T cells) (15) as well as T cell–inflamed tumors with increased overall survival (16) and responsiveness to ICB therapy (17, 18).

Under the proper conditions, STING signaling can mediate cancer cell death either directly (19, 20) or indirectly by supporting cytotoxic T lymphocyte (CTL) (21) and natural killer (NK) cell (22, 23) responses. Additionally, the STING pathway is iatrogenically activated by many of the classical cancer therapies (*e.g.* radiation, certain chemotherapies, *etc.*) and may contribute to enhanced therapeutic responses in such cases (24, 25). Indeed, in murine tumor models, antitumor immune responses generated by STING signaling are essential to achieving maximum therapeutic efficacy in response to radiotherapy (26). These discoveries have collectively motivated the development of synthetic STING pathway agonists for applications in cancer immunotherapy.

Numerous preclinical studies using synthetic STING agonists have now shown that targeted activation of the STING pathway within established murine tumors can shift the immune profile of an immunosuppressive tumor microenvironment (TME) toward an immunogenic state that is conducive to productive antitumor immunity and to enhancing the therapeutic efficacy of multiple immunotherapeutic modalities (21, 27, 28). Accordingly, many synthetic STING agonists are currently being explored as cancer therapeutics in human clinical trials (29, 30). However, it is worth noting that all of the STING pathway agonists currently in clinical development are direct activators of the STING protein or inhibit antagonists of the pathway (28). Compared to the STING protein, cGAS has been relatively underappreciated as a druggable target for cancer immunotherapy (31), despite the potential of a cGAS-targeting therapeutic to more closely mimic endogenous STING signaling by simulating natural, endogenous DNA sensing.

There are many drug delivery challenges that must be overcome to activate cGAS with interferon stimulatory DNA (ISD), which may explain why the development of cGAS agonists has been remarkably limited thus far. Efficient cytosolic delivery of ISD is critical to the pharmacological activation of cGAS, yet freely administered ISD experiences negligible cellular uptake and is quickly cleared and degraded (32). Furthermore, cGAS possesses several DNA-length dependencies that affect both the activation of the pathway (33) and the strength of STING signaling (*i.e.* the amount of STING-driven gene expression) (34). Here, we have engineered a nucleic acid immunotherapeutic, NanoISD, which can target cGAS and exploit the DNA sensing pathway in the context of local cancer immunotherapy *via* the cytosolic delivery of noncoding, immunostimulatory dsDNA.

The well-established, endosomolytic polymer, poly [(DMAEMA)-*block*-(PAA-*co*-DMAEMA-*co*-BMA)] (D-PDB) (35–51) was used to electrostatically complex dsDNA into environmentally responsive nanoparticles capable of achieving cytosolic delivery. The DNA/polymer complexes were characterized using a library of synthetic ISD to study the effects of both N/P charge ratio (*i.e.* molar amount of protonated amines on the polymer corona / molar amount of phosphates on the nucleic acid backbone) and dsDNA composition on nanoparticle stability, transfection efficiency, cGAS activation, and antitumor immunity. *In vitro* screening of various DNA/nanoparticle complexes resulted in the identification of an optimized cGAS adjuvant, a phosphorothioate-capped 95-BP dsDNA/D-PDB complex, termed NanoISD. NanoISD is a nanoparticle formulation that confers deoxyribonuclease resistance, cellular uptake, endosomal escape, and potent activation of the STING pathway *via* cGAS (**Figure 1**). Notably, the direct injection of NanoISD into murine tumors triggers the production of proinflammatory cytokines, which leads to the tumor infiltration

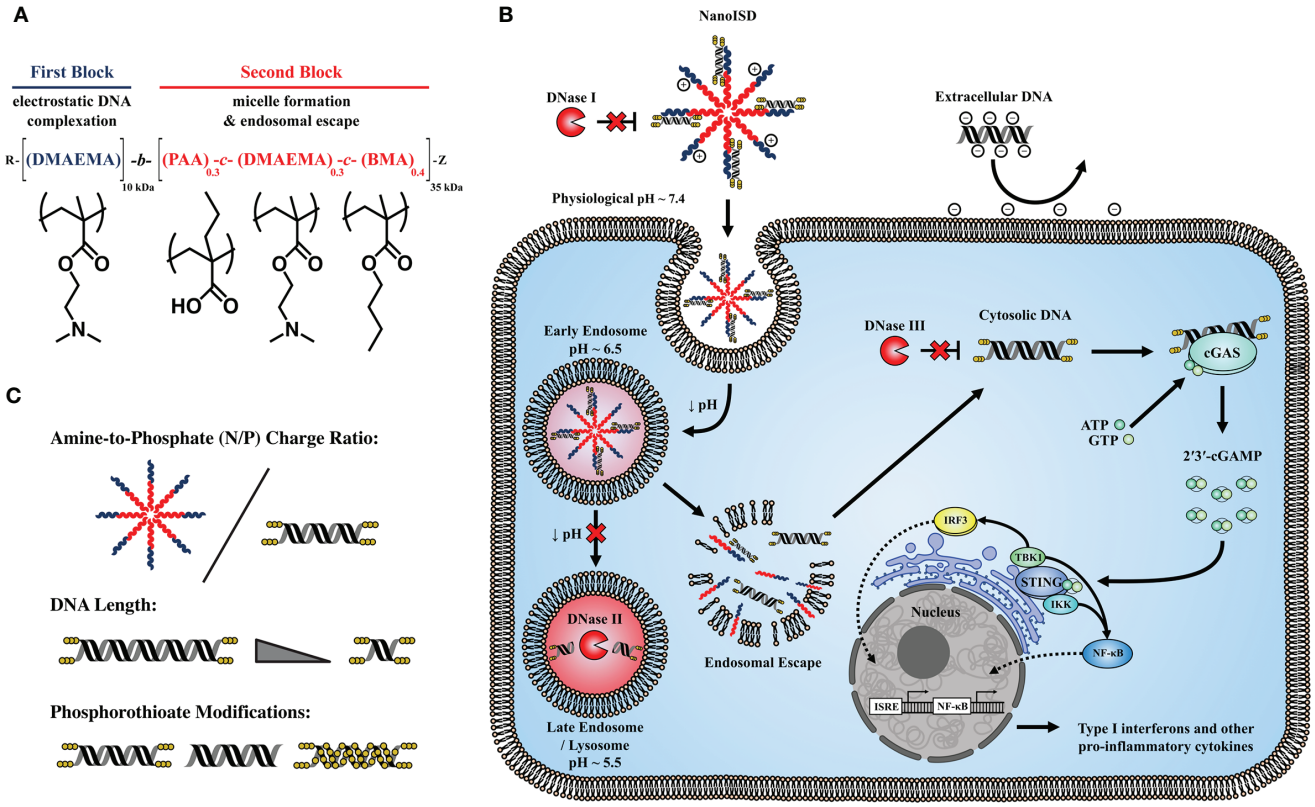

FIGURE 1 | NanoISD – A nanoscale activator of the cGAS/STING pathway. NanoISD is fabricated *via* the self-assembly of an optimized interferon stimulatory DNA (ISD) sequence in complex with endosome-destabilizing polymer nanoparticles. **(A)** Chemical composition of poly[(DMAEMA)-*block*-(PAA-*co*-DMAEMA-*co*-BMA)] (D-PDB). **(B)** Schematic representation of NanoISD activating cytosolic cGAS by evading major deoxyribonuclease and mediating cellular uptake and endosomal escape. **(C)** Design variables explored for DNA/polymer complexes include N/P charge ratio, dsDNA length, and degree and location of phosphorothioate backbone modifications.

of both NK cells and T lymphocytes. Finally, the therapeutic efficacy of NanoISD is demonstrated in preclinical tumor models by attenuated tumor growth, increased survival, and an improved therapeutic response to ICB therapy.

RESULTS AND DISCUSSION

Engineering DNA/Polymer Nanoparticles for Intracellular Activation of cGAS

A library of synthetic ISD was created with a distinct set of design principles intended to yield structurally optimized cGAS ligands (**Supplementary Figure 1**). The library contains 4 dsDNA sequences of different lengths (*i.e.* 20-BP, 45-BP, 70-BP, and 95-BP dsDNA). To the extent possible, based on the designated dsDNA length, the individual ISD strands comprise poly(AC) and poly(AAC) repeats, which are each 20 nucleotides in length and are interspersed with random sequence spacers that are each 5 nucleotides in length. This unique composition of the ISD sequences should provide enough footing to minimize strand slippage. Additionally, the individual ISD strands exhibit positive free energies for secondary structure formation and are therefore not disposed to hairpins and self-dimerization. Moreover, the ISD has melting temperatures that are sufficiently high to maintain double-stranded morphologies at biologically relevant temperatures (*i.e.* 37°C). Lastly, the synthetic ISD sequence contains three terminal phosphorothioate bonds (*i.e.* "caps") on both ends of each complementary DNA strand to inhibit exonuclease degradation, a known feature of such modifications (52).

To overcome the delivery barriers that limit the activity of ISD, we employed a diblock copolymer, D-PDB, which has previously been used primarily for the cytosolic delivery of small-interfering RNA (siRNA) (35–51). Under a physiological pH of ~ 7.4, D-PDB self-assembles into colloidally stable, nanoparticle micelles with a cationic corona that can electrostatically load nucleic acids. In response to the decrease in endosomal pH that follows cellular uptake, these nanoparticles disassemble. The hydrophobic moieties of the polymer become accessible and then disrupt the endosomal membrane, whereupon the exogenous nucleic acid cargo escapes from the endosome into the cytosol of the cell. While nuclear localization is required for most applications of intracellular DNA delivery (*e.g.* gene therapy), DNA delivery to the cytosol is adequate and perhaps better for pharmacologically targeting cGAS, since the

PRR is primarily activated by DNA within the cytosol (8). Thus, in terms of maximizing cGAS activation, D-PDB has potential to be advantageous relative to nanocarriers that are designed to deliver their nucleic acid cargo to the nucleus of cells.

To determine an ideal N/P charge ratio (*i.e.* molar amount of protonated amines on the polymer corona / molar amount of phosphates on the nucleic acid backbone) for the ISD and polymer, polymeric micelles of D-PDB were complexed with varying concentrations of phosphorothioate-capped 95-BP dsDNA, one of the ISD molecules from the starting library. The resultant complexes were then analyzed *in vitro via* agarose gel electrophoresis, dynamic light scattering (DLS), and reporter cell assays for IFN-I production (**Figure 2**).

Agarose gel electrophoresis was run to determine the N/P charge ratio at which complete complexation is achieved (**Figure 2A**). Consistent with previous findings for D-PBD with shorter double-stranded RNA molecules (35, 50), it was determined that N/P charge ratios of 1 and greater enabled complete loading of the phosphorothioate-capped 95-BP dsDNA. Conversely, an N/P charge ratio of 0.5 exhibited incomplete complexation, as demonstrated by the migration of unbound DNA, which formed a band corresponding to that of the free DNA.

DLS was subsequently performed to characterize the size and polydispersity of the complexes (**Figure 2B**). DLS analysis demonstrated that uncomplexed D-PDB micelles are ~ 45-60 nm in diameter and that loading phosphorothioate-capped 95-BP dsDNA at an N/P charge ratio of 4 results in slightly larger nanoparticles that are ~ 60-90 nm in diameter. As the N/P charge ratio was lowered, the measured hydrodynamic size significantly increased to micrometer diameters that are indicative of particle aggregation. Notably, larger particles (*i.e.* greater than 100 nm) are not ideal for *in vivo* cancer applications, since particle permeability and distribution within tumors are known to decrease with increasing particle size (53).

To determine the *in vitro* activity of the complexes, a reporter cell assay for cellular IFN-I production was utilized (**Figure 2C**). The reporter cells stably express a secreted luciferase downstream of interferon-stimulated response elements, and therefore luminescence can be used to track relative IFN-I production. RAW-Dual murine macrophages were treated with phosphorothioate-capped 95-BP dsDNA/D-PDB complexes that were formulated at different N/P charge ratios. Supernatants were collected 24 hours after the cells were treated, and the relative IFN-I production was quantified *via* luminescence. Notably, immunostimulatory activity was detected from all of the complexes. A maximum efficacy of ~ 275,000 Relative Light Units (RLU) was consistent for N/P charge ratios of 4, 2, and 1. Alternatively, the maximum efficacy for the N/P charge ratio of 0.5 over the same concentration range was substantially lower at ~ 170,000 RLU, which is likely due to the incomplete loading of the DNA that was observed in the agarose gel assay. Additionally, half-maximal effective concentration (EC_{50}) values were determined for each dose response curve to allow for the comparison of *in vitro* potency. The calculated EC_{50} values for the N/P charge ratios of 4, 2, 1, and 0.5 were 22 nM, 22 nM, 15 nM, and 3 nM, respectively. Since *in vitro* potency is inversely related to EC_{50} values, the potency is greater for the N/P charge ratios of 1 and 0.5, both of which also exhibit larger sizes as determined by DLS. The apparent increase in potency accompanied by an increase in particle size is consistent with a recent report that larger, micrometer-sized polyplexes enhance *in vitro* transfection efficiency relative to compositionally-equivalent nanometer-sized polyplexes due to increased gravitational sedimentation (54). Interestingly, we characterized a second ISD library of relatively larger PCR-amplified dsDNA (**Supplementary Figure 2**) with D-PDB and found that the effects of N/P charge ratio on particle complexation, size, and activity were well conserved with dsDNA up to at least 5000-BP in length (**Supplementary Figure 3**). Based on these initial *in vitro* characterizations of the complexes, an N/P charge ratio of 4 was selected for all complexes used in the subsequent studies.

The degree of cGAS activation is directly proportional to the length of dsDNA recognized by cGAS (34, 55), yet larger molecular weight dsDNA can also compromise the colloidal stability of non-viral vectors (56) and thereby limit transfection efficiency. Moreover, there exist DNA-length thresholds for cGAS activation that are species-specific due to some small variations in the amino acid composition of the protein (33). For *in vitro* cell-based assays, a minimum dsDNA length of ~ 45-BP is required to activate human cGAS (hcGAS) (33), whereas dsDNA as low as ~ 20-BP in length can activate murine cGAS (mcGAS) (57, 58). Thus, the entire library of variable-length, synthetic ISD was evaluated, so that the molecular weight (*i.e.* BP length) of the ISD in complex with D-PDB micelles could be optimized.

DLS analysis of D-PDB and the synthetic ISD library revealed that while keeping the N/P charge ratio consistent at 4, particle size slightly increased as the BP length of the DNA increased (**Supplementary Figure 4**). This relationship was also observed for D-PDB complexed to the second ISD library of larger PCR-amplified dsDNA, though size appeared to plateau at ~ 140 nm in diameter once a dsDNA length of 1250-BP was reached (**Supplementary Figure 5**). For the N/P charge ratio of 4, colloidal stability of the complexes was lost when dsDNA length reached 10,000-BP, as evident from the complex's nonuniform and highly polydisperse size range.

Reporter cell assays for IFN-I production were again utilized to evaluate *in vitro* activity of the complexes. RAW-Dual murine macrophages (**Figure 2D**), THP1-Dual human monocytes (**Figure 2E**), and A549-Dual adenocarcinomic human alveolar basal epithelial cells (**Figure 2F**) were all treated with each of the varied-length, synthetic ISD complexed to D-PDB over a range of ISD concentrations to generate dose response curves. The endogenous STING ligand, 2′3′-cGAMP was used as a positive control for IFN-I induction, and free D-PDB (*i.e.* not loaded with dsDNA) was used as a vehicle control. Additionally, free phosphorothioate-capped 95-BP dsDNA was used as a negative control to demonstrate the importance of the polymeric drug delivery vehicle. Maximum efficacy and EC_{50} values for each of the treatments can be found in the supplementary information (**Supplementary Figure 6**). Consistent with previous observations that cGAS is activated in a dsDNA length dependent manner (34),

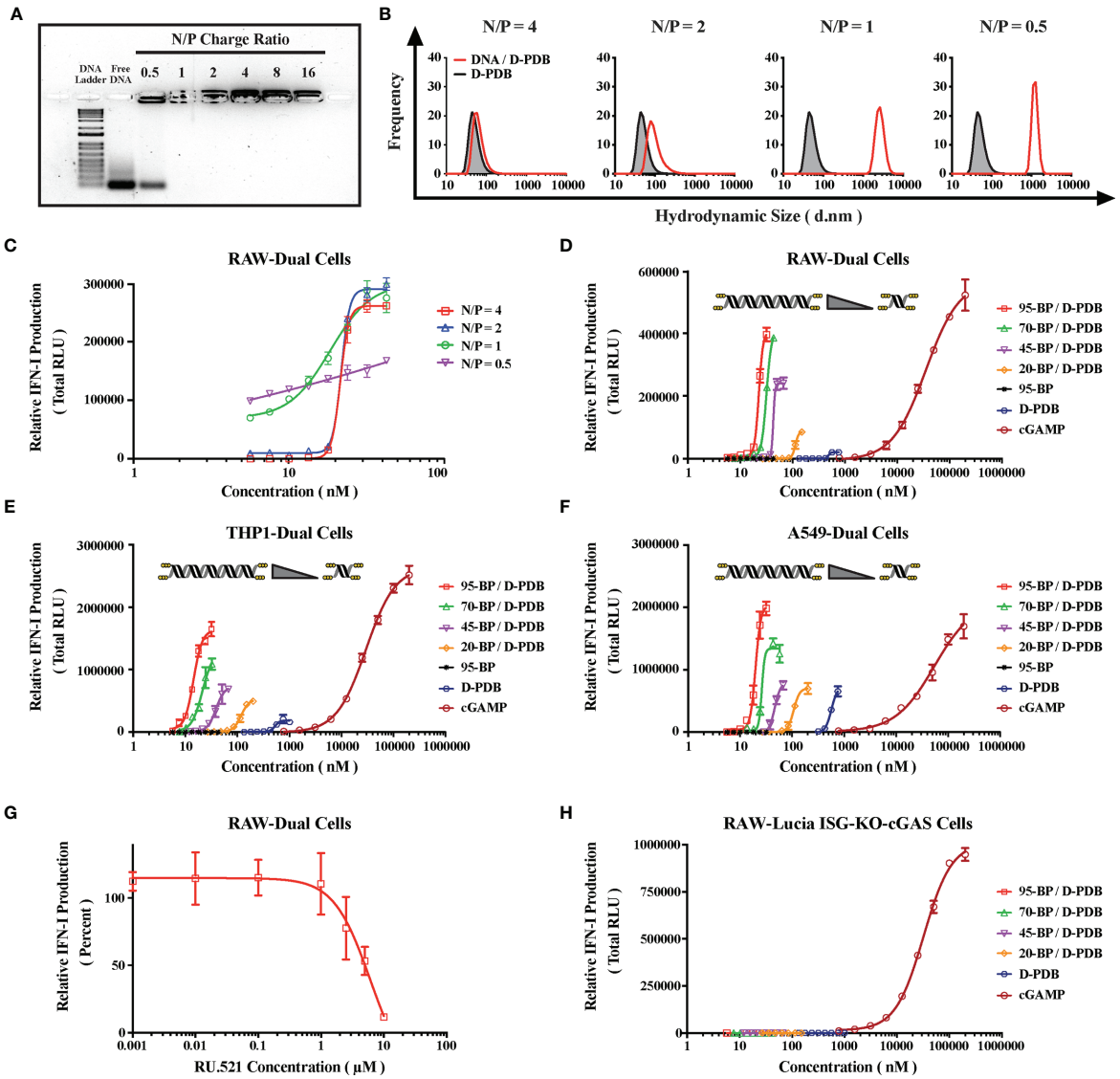

FIGURE 2 | Engineering DNA/Polymer Nanoparticles for Intracellular Activation of cGAS. **(A)** Agarose gel image. DNA Ladder refers to the TrackIt™ 1 Kb Plus DNA Ladder, and Free DNA refers to uncomplexed phosphorothioate-capped 95-BP dsDNA. Lanes comprise 1 μg DNA mixed with the indicated amount of D-PDB. **(B)** DLS analysis of phosphorothioate-capped 95-BP dsDNA/D-PDB complexes at varying N/P charge ratios. Frequency indicates the number-based particle size distribution. Hydrodynamic size indicates the particle diameter in nm. **(C)** RAW-Dual reporter cell assay of phosphorothioate-capped 95-BP dsDNA/D-PDB complexes at varying N/P charge ratios. **(D)** RAW-Dual reporter cell assay of synthetic, variable-length ISD library complexed to D-PDB at an N/P charge ratio of 4, and indicated experimental controls were used. **(E)** THP1-Dual reporter cell assay of synthetic, variable-length ISD library complexed to D-PDB at an N/P charge ratio of 4, and indicated experimental controls were used. **(F)** A549-Dual reporter cell assay of synthetic, variable-length ISD library complexed to D-PDB at an N/P charge ratio of 4, and indicated experimental controls were used. **(G)** Dose response of the cGAS inhibitor, RU.521 in RAW-Dual reporter cells. After a 4 hour incubation with RU.521, cells were treated with 25 nM phosphorothioate-capped 95-BP dsDNA complexed to D-PDB at an N/P charge ratio of 4. **(H)** RAW-Lucia ISG-KO-cGAS reporter cell assay of synthetic, variable-length ISD library complexed to D-PDB at an N/P charge ratio of 4, and indicated experimental controls were used. The dose response curves for free D-PDB are positioned along the x-axis in terms of the molar amount of polymer chains rather than molar amount of loaded dsDNA, and each dose response that utilized the polymer was administered using equivalent D-PDB concentrations.

both the potency and efficacy of the complexes generally increased with increasing BP length of the dsDNA cargo in all three reporter cell lines. Interestingly, free D-PDB demonstrated a small but significant dose response, suggesting that the polymer has an intrinsic capacity for stimulating some degree of IFN-I production.

In accordance with the established dsDNA length thresholds for species-specific cGAS activation, the phosphorothioate-capped 20-BP dsDNA complexed to D-PDB (*i.e.* 20-BP/D-PDB) enhanced maximum efficacy relative to that of free D-PDB in the murine RAW-Dual reporter cells (*i.e.* ~ 85,000 *vs.* ~

20,000 RLU, respectively) and did not affect baseline efficacy in the human A549-Dual reporter cells (*i.e.* both treatments ~ 70,000 RLU). However, in the human THP1-Dual reporter cells, the 20-BP/D-PDB treatment did slightly outperform free D-PDB in terms of maximum efficacy (*i.e.* ~ 50,000 RLU *vs.* ~ 20,000 RLU, respectively), despite the 20-BP dsDNA being shorter than the empirically established threshold for human cGAS activation (*i.e.* ~ 45-BP) (33). This subtle discrepancy may be due to cell line–specific phenomenon coupled with the phosphorothioate modifications of the ISD, as the threshold established in previous reports was determined using unmodified dsDNA (59, 60).

The role of cGAS in the immunostimulatory activity of the compounds was investigated in the RAW-Dual reporter cells by pretreating the cells with a dose response of the established small molecule inhibitor of cGAS, RU.521 (33, 61, 62) (**Figure 2G**). Four hours after incubation with RU.521, the cells were treated with the EC75 concentration of 95-BP/D-PDB (*i.e.* 25 nM), a treatment known to be consistently active. Analysis of the supernatant 24 hours after treatment revealed that the cGAS-specific inhibitor was able to significantly diminish the IFN-I signal at the higher concentrations, suggesting that the observed activity of the DNA/polymer complexes is indeed cGAS-dependent. Notably, RU.521 exhibited a half-maximal inhibitory concentration (IC_{50}) value of ~ 5 μM.

To further explore the dependence of cGAS on the activity of the treatments, RAW-Lucia ISG-KO-cGAS reporter cells, which do not express cGAS, were treated with each of the varied-length, synthetic ISD complexed to D-PDB (**Figure 2H**). Free D-PDB and cGAMP were again used as controls for the experiment. While cGAMP, which activates STING downstream of cGAS, retained its IFN-I activity, no activity was detected from DNA/polymer complexes, suggesting that the activity from those treatments observed in the wildtype reporter cells were largely, if not entirely, cGAS-dependent. These findings also suggest that if alternative IFN-inducing DNA sensors, such as IFI204 (*e.g.* the murine ortholog of IFI16), are involved in the response to the DNA/polymer complexes, they must operate as dependent cofactors of cGAS. Interestingly, the activity of free D-PDB was also completely abolished in the RAW-Lucia ISG-KO-cGAS reporter cells. While D-PDB is unlikely to be a direct cGAS ligand, D-PDB may indirectly activate cGAS in the wildtype reporter cells by inducing the cytosolic accumulation of mitochondrial DNA. Indeed, cationic nanocarriers have been linked to toll-like receptor 9 (TLR9) (*i.e.* a PRR for unmethylated DNA rich in CpG motifs) and STING activation *via* their intrinsic capacity for mitochondrial damage and the subsequent release of mitochondrial DNA (63, 64).

Similar cGAS-dependent activity in the RAW-Dual reporter cells was also demonstrated for the larger PCR-amplified dsDNA library complexed to D-PDB (**Supplementary Figure 7**). The DNA length–dependent trends were conserved for the larger PCR-amplified dsDNA library in the wildtype reporter cells, though the maximum efficacy of the DNA/polymer complexes did saturate at ~ 615,000 RLU when a dsDNA length of 625-BP was reached. Additionally, the colloidally unstable 10,000-BP/D-PDB complexes exhibited a reduced maximum efficacy of ~ 470,000 RLU over the same concentration range, which could be attributed to its extensive polydispersity of size. Furthermore, the synthetic phosphorothioate-capped 95-BP dsDNA complexed to D-PDB, which had a maximum efficacy of ~ 1,000,000 RLU, drastically outperformed all of the PCR-amplified dsDNA complexed to D-PDB in terms of maximum efficacy, which is likely a consequence of its exonuclease resistance and highlights the importance of such modifications for enhancing cGAS activation.

The starting ISD library used for the experiments in **Figure 2** comprised synthetic dsDNA molecules that were produced *via* solid-phase phosphoramidite-based synthesis, which can accommodate routine, scalable production of dsDNA up to ~ 95-BP in length as well as the molecular modification of dsDNA (65, 66). Conversely, PCR-mediated amplification of dsDNA utilizes polymerase-based synthesis that does not allow for site-specific DNA modification outside of the primer sequence, and therefore PCR-mediated amplification of dsDNA is not readily amenable to phosphorothioate-capping. Accordingly, the synthetic, phosphorothioate-capped 95-BP dsDNA became the lead cGAS ligand. Thus, the nanoparticle complex of D-PDB and the phosphorothioate-capped 95-BP dsDNA at an N/P charge ratio of 4, herein referred to as NanoISD, was employed as a potent cGAS adjuvant for the subsequent studies investigating its utility in cancer immunotherapy.

NanoISD Exhibits Deoxyribonuclease Resistance

Mammalian cells constitutively express many deoxyribonucleases (DNases) to prevent the potentially inflammatory accumulation of DNA outside of protective organelles. Notably, DNA present in systemic circulation, lysosomes, and cytosols is degraded by DNase I, DNase II (*i.e.* Acid DNase), and DNase III (*i.e.* TREX1), respectively (67–70). The inhibition of such nucleases can allow immunostimulatory dsDNA to remain intact for an extended period of time during delivery, which can lead to improved functionality. Notably, the length of cytosolic dsDNA directly influences the rate and extent of cGAS activation and thereby the amount of cGAMP produced (34). Thus, when dsDNA strands are not rapidly broken down into smaller fragments, they can exploit the length-dependence of the protein to promote maximal STING signaling. As the stability of DNA is essential for cGAS activation, the deoxyribonuclease resistance of NanoISD was evaluated (**Figure 3**).

Both free phosphorothioate-capped 95-BP dsDNA and NanoISD were incubated with three different concentrations of the endonuclease, DNase I (**Figure 3A**). 15 ng/mL was selected as it is the physiological level of DNase I in human serum (71), 100 ng/mL was selected as it is the concentration of recombinant human DNase I that can mediate the effective removal of DNA from blood circulation (72), and 2500 ng/mL was selected as an extreme high-dose control. Following incubation with DNase I, samples were heat-inactivated, and SDS was added to break apart the complexes. The samples were then run on a gel along with free

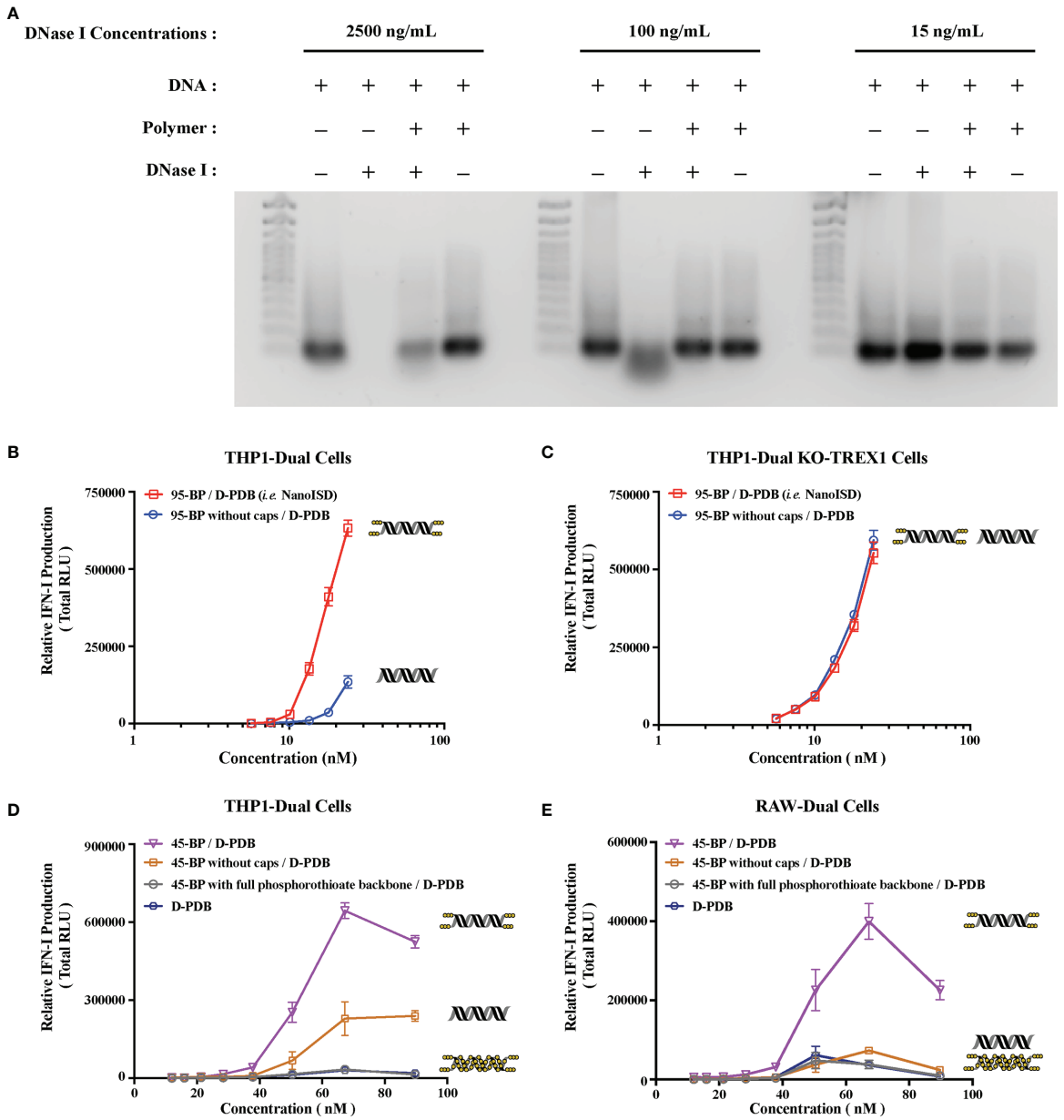

FIGURE 3 | NanoISD Exhibits Deoxyribonuclease Resistance. **(A)** Agarose gel image. Lanes are as indicated. The TrackIt™ 100 bp DNA Ladder was used for reference. The DNA used in these studies was the phosphorothioate-capped 95-BP dsDNA at a concentration of 1 μg DNA/lane, and the polymer used was D-PDB at an N/P charge ratio of 4. **(B)** THP1-Dual reporter cell assay of 95-BP dsDNA with and without phosphorothioate caps complexed to D-PDB at an N/P charge ratio of 4. **(C)** THP1-Dual KO-TREX1 reporter cell assay of 95-BP dsDNA with and without phosphorothioate caps complexed to D-PDB at an N/P charge ratio of 4. **(D)** THP1-Dual reporter cell assay of synthetic 45-BP dsDNA complexed to D-PDB at an N/P charge ratio of 4, and D-PDB was used as an experimental control. Each 45-BP/D-PDB treatment comprised DNA with varying levels of phosphorothioate incorporation as indicated. **(E)** RAW-Dual reporter cell assay of synthetic 45-BP dsDNA complexed to D-PDB at an N/P charge ratio of 4, and D-PDB was used as an experimental control. Each 45-BP/D-PDB treatment comprised DNA with varying levels of phosphorothioate incorporation as indicated. The dose response curves for free D-PDB are positioned along the x-axis corresponding to their equivalent dsDNA-loaded treatments, as each dose response that utilized the polymer was administered using equivalent D-PDB concentrations.

phosphorothioate-capped 95-BP dsDNA and NanoISD that were not exposed to DNase I. While free phosphorothioate-capped 95-BP dsDNA was susceptible to degradation by the higher concentrations of DNase I, NanoISD exhibited marked protection of its DNA cargo from deoxyribonuclease degradation, which is likely due to polymer-mediated steric hindrance of the nuclease (*i.e.* nanoparticle packaging).

Since cGAS activation is greatly dependent on the length, concentration, and persistence of dsDNA in the cytosol, a particularly important negative regulator of the STING

pathway is the exonuclease, TREX1 (*i.e.* DNase III). Indeed, it was recently discovered that DNA oxidized by reactive oxygen species (ROS) can significantly impede the exonuclease activity of TREX1, and such TREX1 inhibition was found to significantly potentiate STING signaling (73). Accordingly, the inhibition of TREX1 has recently been proposed as an immunotherapeutic strategy for the treatment of cancer (74).

The phosphorothioate caps of the synthetic ISD were implemented to boost immunostimulatory activity by obstructing the TREX1-mediated degradation of dsDNA that limits STING pathway activation. To further test the deoxyribonuclease resistance of the chemically modified ISD, reporter cell assays for IFN-I production were once again utilized. Phosphorothioate-capped 95-BP dsDNA and 95-BP dsDNA without caps were complexed with D-PDB micelles and incubated with THP1-Dual cells (**Figure 3B**) and THP1-Dual KO-TREX1 cells (**Figure 3C**).

In the wildtype reporter cells, the efficacy and potency of NanoISD were both significantly increased relative to D-PDB loaded with 95-BP dsDNA without phosphorothioate caps. As the caps inhibit TREX1 activity, it is likely that they enable a prolonged presence of the dsDNA in the cytosol and thereby enhance cGAS activation. This theory is supported by the finding that phosphorothioate caps on a 45-BP dsDNA also enhanced activity relative to 45-BP dsDNA without caps when delivered with D-PDB micelles to wildtype reporter cells (**Figures 3D, E**). Notably, it was also demonstrated that complete phosphorothioate modification of the dsDNA backbone rendered 45-BP dsDNA inactive, which is consistent with previous observations that phosphodiester bonds on dsDNA are required for cGAS activation (59, 75). One possible future opportunity for further enhancing the efficacy and potency of the ISD might involve incorporating intermittent phosphorothioate modifications along the DNA strands, which could potentially improve the deoxyribonuclease resistance and stability of the DNA while also maintaining a capacity for cGAS oligomerization/activation. The distance between each modification would likely need to be optimized to avoid deleterious effects on cGAS activation.

Moreover, in the TREX1 (*i.e.* DNase III) KO reporter cells, the efficacy and potency of the nanoparticles loaded with dsDNA lacking phosphorothioate caps were insignificantly different from that of NanoISD (**Figure 3C**), suggesting that in the wildtype reporter cells, TREX1 is mainly responsible for the reduced *in vitro* activity of the nanoparticles carrying unprotected dsDNA. Thus, in addition to the deoxyribonuclease resistance afforded by nanoparticle packaging, deoxyribonuclease activity was found to be further inhibited through the chemical modification of the synthetic dsDNA.

Notably, the IFN-I activity of the synthetic ISD library in the THP1-Dual reporter cells is entirely lost when delivered with the non-endosomolytic polymer, poly[(DMAEMA)-*block*-(BMA)] (D-B) at a consistent DNA concentration and N/P charge ratio (**Supplementary Figure 8**). D-B forms micelles that do not disassemble at low pH, and accordingly the polymer does not facilitate the cytosolic delivery of nucleic acid (50), which is necessary for cGAS activation. Conversely, D-PDB mediates endosomal escape at the onset of endosomal acidification due to the composition of the polymer (35) and the resultant loss of particle morphology under minimally acidic conditions (*e.g.* pH ~ 6.5), which leads to endosomal membrane disruption (50). Therefore, the dsDNA cargo loaded on D-PDB is likely released into the cytosol before endosomes can fully acidify. Since DNase II is mostly active under highly acidic conditions (*e.g.* pH ~ 5.5) (76), it is probable that the enzyme has a reduced opportunity to degrade the ISD when delivered with D-PDB. Indeed, the observed cGAS activation from NanoISD treatment is evidence that the dsDNA ligands are not appreciably degraded by DNase II in lysosomes. Thus, the chemical and physical composition of NanoISD as well as its intrinsic delivery route protect its cGAS ligand from three major deoxyribonucleases and thereby constitute NanoISD as an exceptionally potent cGAS adjuvant.

NanoISD Enhances Cellular Uptake and Immunostimulatory Activity of ISD *In Vitro*

DNA by itself does not readily pass through the negatively-charged plasma membrane of cells due to the relatively large, negatively-charged, and hydrophilic nature of DNA (77). However, when ISD is complexed at an N/P charge ratio of 4 with D-PDB micelles that exhibit a positive surface charge of +16.27 mV, the resultant DNA-loaded nanoparticles also exhibit a positive surface charge (**Supplementary Figure 9**) and can be efficiently endocytosed by DC2.4 dendritic cells *in vitro* as determined by flow cytometry analysis of fluorescently-labeled phosphorothioate-capped 95-BP dsDNA (*i.e.* Cy5-DNA) (**Figure 4A**). It is likely that the overall positive surface charge of NanoISD (*i.e.* +14.87 mV) afforded by D-PDB drives the cellular uptake of the nanoparticles, especially since free fluorescently-labeled D-PDB (*i.e.* NIR-D-PDB) is also efficiently endocytosed (**Figure 4B**). The positive charge of NanoISD does however dictate that the therapeutic be administered locally, as positively charged nanoparticles are typically poorly tolerated when administered systemically (78). There are many advantages to using local administration, especially for the delivery of a cancer immunotherapeutic (79). Indeed, while the direct injection of many classical cancer therapeutics (*e.g.* various chemotherapies) into solid tumors often results in therapeutic responses that are limited to the treated tumors, the local administration of a cancer immunotherapeutic can generate a systemic immune response with potential to clear untreated metastatic tumors (*i.e.* abscopal effect). Additionally, D-PDB treatment also confers a minor but significant degree of toxicity relative to cells treated with phosphate buffered saline (PBS) (**Figure 4C**). Notably, some toxicity may actually be beneficial in the context of killing cancer cells following local administration (80) and releasing tumor antigens, which can then be processed by APCs to promote the cancer immunity cycle (81).

The activation of APCs is a key feature of many innate immune agonists and is essential for cancer immunotherapies that are aimed at promoting antitumor T cells (82). Since STING pathway activation has been linked to APC maturation and T cell activation (83, 84), NanoISD was evaluated for its ability to promote APC maturation. Murine bone marrow-derived

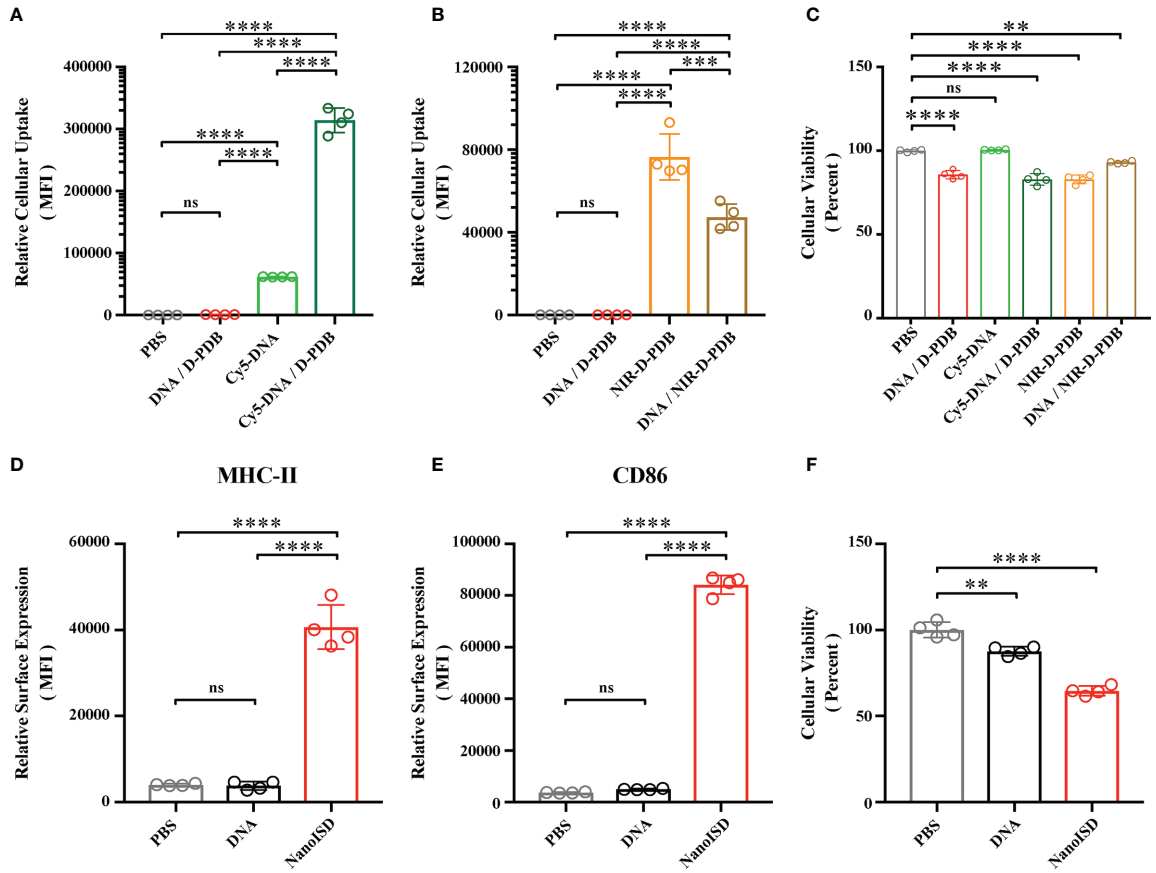

FIGURE 4 | NanoISD Enhances Cellular Uptake and Immunostimulatory Activity of ISD *In Vitro*. **(A)** Flow cytometry analysis on the cellular uptake of 45 nM DNA (*i.e.* Cy5-labeled phosphorothioate-capped 95-BP dsDNA). Flow cytometry was conducted 4 hours after indicated treatment. The median fluorescence intensity (MFI) of Cy5-labeled DNA was quantified. **(B)** Flow cytometry analysis on the cellular uptake of 1.1 μM D-PDB (*i.e.* NIR-D-PDB), which corresponds to 45 nM DNA for a N/P charge ratio of 4. Flow cytometry was conducted 4 hours after indicated treatment. The MFI of NIR-664-labeled D-PDB was quantified. **(C)** Cellular viability determined 4 hours after indicated treatment as assessed by DAPI staining. Percent viable is relative to cells treated with PBS. **(D)** Flow cytometry analysis of the BMDC maturation marker, MHC-II conducted 24 hours after treatment of either PBS, 45 nM DNA (*i.e.* phosphorothioate-capped 95-BP dsDNA), or NanoISD at a dose corresponding to 45 nM. The MFI of anti-MHC-II-APC-Cy7 was quantified. **(E)** Flow cytometry analysis of the BMDC maturation marker, CD86 conducted 24 hours after treatment of either PBS, 45 nM DNA (*i.e.* phosphorothioate-capped 95-BP dsDNA), or NanoISD at a dose corresponding to 45 nM. The MFI of anti-CD86-PE-Cy7 was quantified. **(F)** Cellular viability determined 24 hours after indicated treatment as assessed by DAPI staining. Percent viable is relative to cells treated with PBS. A one-way ANOVA with Tukey test was used for statistical analysis. ****p < 0.0001, ***p < 0.005, **p < 0.01. ns, not significant.

dendritic cells (BMDCs) were treated with either PBS, DNA (*i.e.* phosphorothioate-capped 95-BP dsDNA), or NanoISD. Markers of BMDC maturation (*i.e.* cell surface expression of CD86 and MHC-II) were quantified *via* flow cytometry 24 hours post treatment. It was determined that NanoISD evokes significantly enhanced maturation *in vitro* as compared to PBS-treated BMDCs and DNA-treated BMDCs (**Figures 4D, E**). Additionally, viability of the BMDCs after NanoISD treatment was comparable to that of the DC2.4 cells treated with the same concentration of NanoISD (**Figure 4F**).

NanoISD Enhances Delivery and Immunostimulatory Activity of ISD *In Vivo*

By packaging dsDNA into cationic nanoparticles, it was hypothesized that NanoISD would address the rapid clearance of dsDNA by promoting local cellular uptake at the site of injection. To evaluate this, NanoISD and free ISD were injected subcutaneously into mice and the *in vivo* retention was evaluated *via* IVIS imaging using both fluorescently-labeled phosphorothioate-capped 95-BP dsDNA (*i.e.* Cy5-DNA) and fluorescently-labeled D-PDB (*i.e.* NIR-D-PDB) (**Figures 5A, B**). As anticipated, the free ISD was rapidly cleared from the injection site (*i.e.* half-life < 6 hours). Interestingly, D-PDB was retained at the injection site for an extended timeframe (*i.e.* half-life ~ 50 days) and also dramatically enhanced the retention of the dsDNA (*i.e.* half-life ~ 50 days).

The intratumoral retention of the fluorescently-labeled phosphorothioate-capped 95-BP dsDNA (*i.e.* Cy5-DNA) with and without the polymeric carrier (*i.e.* D-PDB) was then investigated using a murine orthotopic tumor model of 4T1 breast cancer (**Figures 5C, D**). Consistent with the subcutaneous

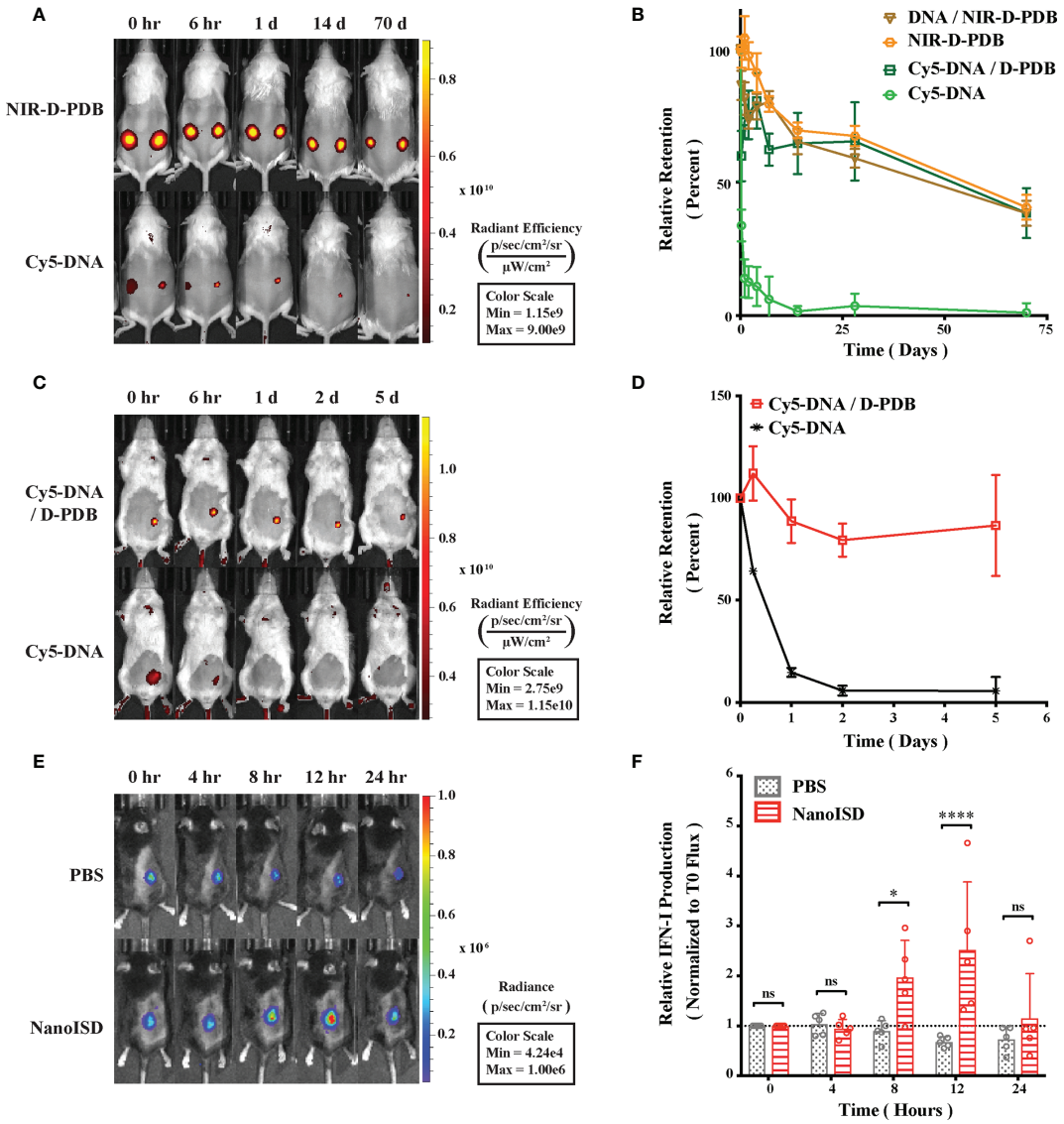

FIGURE 5 | NanoISD Enhances Delivery and Immunostimulatory Activity of ISD *In Vivo*. **(A)** Representative fluorescence IVIS images evaluating the subcutaneous retention of NanoISD in CD-1 mice. D-PDB labeled with NIR-664-iodoacetamide (*i.e.* NIR-D-PDB) was used to track the polymer, and phosphorothioate-capped 95-BP dsDNA labeled with Cy5 (*i.e.* Cy5-DNA) was used to track the DNA. On the left flank of each mouse, individual uncomplexed agents were administered, and on the right flank of each mouse, complexes at an N/P charge ratio of 4 with the indicated fluorescent agent were administered. A subcutaneous injection was given as a single 100 µL dose of 2 µg DNA and/or 36 µg of polymer. **(B)** Retention profiles of NIR-D-PDB and Cy5-DNA either uncomplexed or complexed with unlabeled counterparts following subcutaneous administration in CD-1 mice. **(C)** Representative fluorescence IVIS images evaluating the tumor retention of NanoISD in BALB/cJ mice bearing orthotopic 4T1 tumors. Phosphorothioate-capped 95-BP dsDNA labeled with Cy5 (*i.e.* Cy5-DNA) was used to track the DNA. Cy5-DNA was administered by itself or in complex with D-PDB at an N/P charge ratio of 4. An intratumoral injection was given as a single 100 µL dose of 2 µg DNA. **(D)** Retention profiles of Cy5-DNA complexed to D-PDB and free Cy5-labeled DNA following intratumoral administration into orthotopic 4T1 breast tumors growing in BALB/c mice. **(E)** Representative luminescence IVIS images evaluating tumor IFN activity in C57BL/6J mice bearing B16.F10 IFN-LUC tumors. An intratumoral injection was given as a single 100 µL dose of either PBS or NanoISD at a dose corresponding to 2 µg DNA. **(F)** Longitudinal analysis of IFN activity following treatment. A two-way ANOVA with Sidak test was used for statistical analysis. ****$p < 0.0001$, *$p < 0.05$. ns, not significant.

retention data, the free ISD dispersed quickly (*i.e.* half-life ~ 12 hours), and the ISD complexed to the polymer (*i.e.* NanoISD) exhibited sustained retention (*i.e.* half-life > 5 days). The matching pharmacokinetic clearance profiles of free D-PDB and the ISD complexed to D-PDB is consistent with prolonged *in vivo* association of the two species. Additionally, this finding is disparate with previous data that has consistently reported a short retention profile (*e.g.* half-life < 1 day) for siRNA complexed to the same polymer (42, 47, 48, 51). This discrepancy is likely attributable to the higher valency of the polymer interaction with the significantly larger dsDNA cargo and/or the extra deoxyribonuclease resistance afforded by the

phosphorothioate caps of the dsDNA. Notably, the local delivery of many innate immune agonists (*e.g.* CpG DNA, CDN STING agonists, *etc.*) results in widespread dissemination that can cause systemic inflammation and contribute to relatively low dose-limiting toxicities (85–87), while the enhanced local retention of NanoISD inherently limits the escape of nanoparticles into systemic circulation and therefore reduces the potential for systemic toxicity.

B16.F10 murine melanoma cells, which had been previously engineered to express luciferase upon IFN induction (*i.e.* B16.F10 IFN-LUC cells) (88), were next employed to assess whether the immunostimulatory activity of NanoISD was conserved in the non-immune, cancer cells and if so, to identify the *in vivo* kinetics of signaling. By quantifying luminescence *via* IVIS imaging following exposure to the substrate, D-luciferin, it was established that an *in vitro* treatment of NanoISD could activate luciferase production (*i.e.* IFN production) in the melanoma reporter cells, suggesting that the immunostimulatory capacity of the dsDNA was indeed conserved in the B16.F10 cell line (**Supplementary Figure 10**).

An intravital kinetics study of IFN production was subsequently performed to study the pharmacodynamics of NanoISD (**Figures 5E, F**). Mice were subcutaneously inoculated with the B16.F10 IFN-LUC cells, and when the tumors were ~ 50 mm^3, mice were given a single intratumoral injection of either PBS or NanoISD. At preselected timepoints, mice were administered D-luciferin, and luminescence was measured 15 minutes thereafter. The longitudinal IVIS imaging confirmed *in vivo* IFN production with peak protein production occurring 12 hours post treatment. The level of *in vivo* IFN signaling returned to baseline at 24 hours post treatment despite the extended local retention profile of NanoISD. Therefore, though NanoISD is likely still present and intact within the tumor, we suspect that over time other factors, such as inhibitory pathways within cells or extracellular exclusion (*e.g.* fibrotic entrapment), might inactivate the nanoparticle complex and/or locally down regulate IFN signaling. Moreover, cancer cell stress or death induced by the treatment may also contribute to the decreased IFN signal over time, especially since the cancer cells are serving as the IFN reporter. Regardless, the acute IFN activity of NanoISD *in vivo* motivates the use of a therapeutic dosing regimen involving multiple injections spaced days apart [*e.g.* every three days (*q3d*)].

NanoISD Reprograms the Immune Profile of the Tumor Microenvironment

The immunological effects of intratumorally administered NanoISD were initially quantified by measuring changes in the gene expression of certain signature cytokines for STING pathway activation. B16.F10 tumors were harvested 6 hours after a single intratumoral treatment of either PBS, D-PDB, or NanoISD, and the relative mRNA levels of *Ifnb1*, *Cxcl10*, *Tnf*, and *Il6* in the tumor were determined *via* quantitative polymerase chain reaction (qPCR) (**Figure 6A**). The relative gene expression of these proinflammatory molecules was significantly elevated as compared to that of tumors treated with either PBS or free D-PDB, which is in accordance with STING pathway activation in the TME (89). Free D-PDB also exhibited increased *Ifnb1* expression, though not to the extent of NanoISD treatment, which is consistent with the *in vitro* activity assays that indicated that the D-PDB polymer acts as a weak cGAS adjuvant.

NanoString gene expression analysis was subsequently performed to provide a more robust transcriptomic analysis of the immune response in the treated tumors (**Figure 6B**). Using a slight variation of a gene expression panel that had been previously developed for myeloid cell characterization (90), exact mRNA levels were quantified for 43 different immunomodulatory cytokines. As determined by one-way ANOVA main effect, a single intratumoral NanoISD treatment upregulated the myeloid activation markers of the panel relative to PBS treatment (*i.e.* $p = 0.0376$) and D-PDB treatment (*i.e.* $p = 0.0596$). Notably, cytokines involved in myeloid recruitment (*i.e. Cxcl1*, *Cxcl2*, *Cxcl3*), myeloid differentiation (*i.e. Csf1*, *Csf2*, *Csf3*), and T cell recruitment (*i.e. Cxcl9*, *Cxcl10*, *Cxcl11*, *Cxcl12*) were markedly upregulated in the TME after NanoISD treatment. Additionally, D-PDB treatment was insignificantly different from PBS treatment (*i.e.* $p = 0.9809$) with regard to the myeloid activation markers of the panel. These results from the NanoString study further support the qPCR findings and provide additional insight into the immune profile of the treated tumors, demonstrating that a proinflammatory phenotype is indeed induced by intratumorally administered NanoISD.

To characterize the immunocellular changes within the TME that were likely to follow the local cytokine response, flow cytometry was conducted on B16.F10 tumors 48 hours after the final injection of a three treatment *q3d* dosing regimen (**Figure 6C**). Cell populations of interest were quantified using a myeloid cell panel (**Supplementary Figure 11**) and a T cell panel (**Supplementary Figure 12**). No marked changes occurred for the tumor populations of macrophages (*i.e.* $CD45^+$ $CD11b^+$ $F4/80^+$), dendritic cells (*i.e.* $CD45^+$ $CD11c^+$ $MHC\text{-}II^+$), monocytic myeloid-derived suppressor cells (m-MDSCs) (*i.e.* $CD45^+$ $CD11b^+$ $Ly6C^+$), granulocytic MDSCs (g-MDSCs) (*i.e.* $CD45^+$ $CD11b^+$ $Ly6G^+$ SSC^{hi}), and neutrophils (*i.e.* $CD45^+$ $CD11b^+$ $Ly6G^+$, SSC^{lo}). However, the relative concentrations of NK cells (*i.e.* $CD45^+$ $NK1.1^+$), total T cells (*i.e.* $CD45^+$ $CD3^+$), and $CD8^+$ T cells (*i.e.* $CD45^+$ $CD3^+$ $CD8^+$) within the tumor were significantly elevated following NanoISD treatment, consistent with the established effects of STING pathway activation in tumors (14, 22, 23, 26). Thus, NanoISD can also propagate the adaptive arm of the cancer immunity cycle *via* the initial activation of innate immunity.

In addition to altering the migration and proliferation of lymphoid-derived immune cells, STING activation can also lead to improved cytotoxic immune responses by repolarizing immunosuppressive M2-like macrophages to M1-like macrophages that can promote antitumor immunity (91, 92). Thus, while not assessed in this work, it is possible that NanoISD also induces the M1-like phenotype in tumor macrophages, thereby further enhancing the antitumor immunity that is stimulated by NanoISD. Future work could study exactly how NanoISD affects macrophage polarization and the importance of such effects.

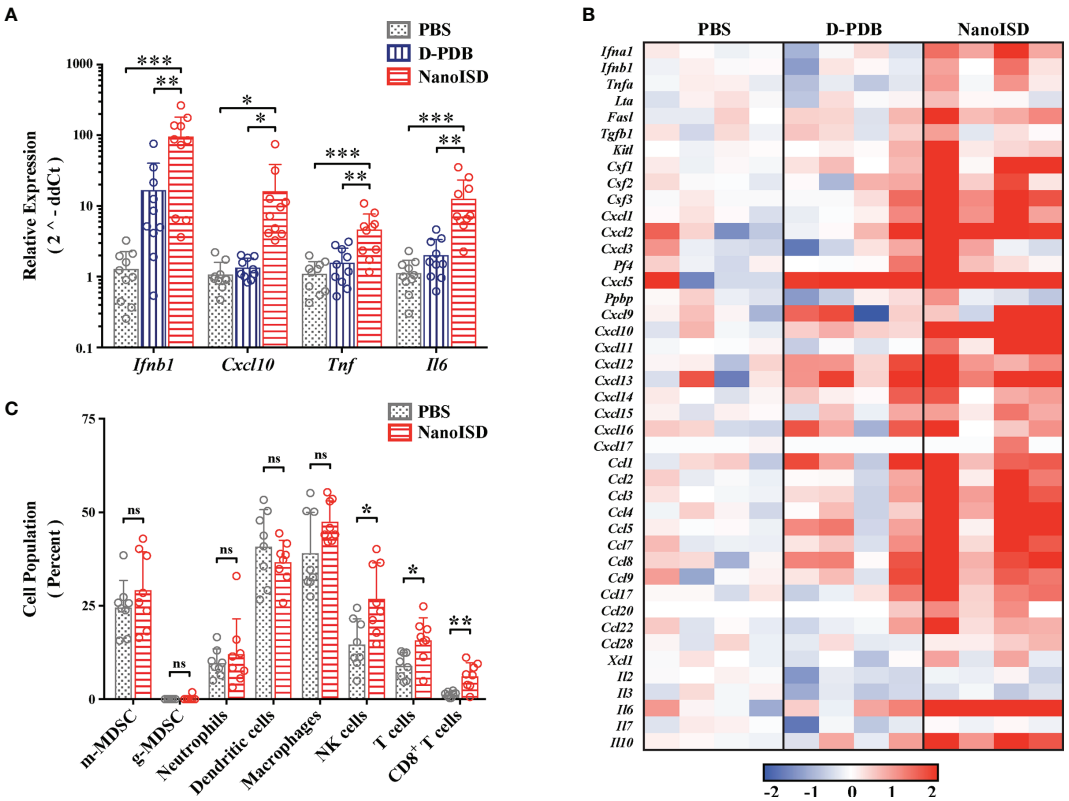

FIGURE 6 | NanoISD Reprograms the Immune Profile of the Tumor Microenvironment. **(A)** Quantitative polymerase chain reaction (qPCR) analysis of B16.F10 tumors 6 hours following a single 100μL intratumoral treatment of either PBS, D-PDB, or NanoISD at a dose corresponding to 2 μg DNA. A one-way ANOVA with Tukey test was used for statistical analysis. **(B)** NanoString analysis of B16.F10 tumors 6 hours following a single 100μL intratumoral treatment of either PBS, D-PDB, or NanoISD at a dose corresponding to 2 μg DNA. Data is presented as log2 fold change relative to PBS treatment. **(C)** Flow cytometry analysis of the cellular composition of B16.F10 tumors treated intratumorally with 100 μL of either PBS or NanoISD at a dose corresponding to 2 μg DNA. Tumors were harvested 48 hours after the third intratumoral injection of a *q3d* dosing regimen. Data is presented as percent of $CD45^+$ live cells. A two-way ANOVA with Sidak test was used for statistical analysis. ***$p < 0.005$, **$p < 0.01$, *$p < 0.05$. ns, not significant.

NanoISD Exerts Antitumor Effects

Cancer therapy studies were conducted in murine tumor models to establish the therapeutic effect of NanoISD. Initially, the antitumor effects of NanoISD and free D-PDB were investigated in a poorly immunogenic B16 model of melanoma that has been engineered to express the foreign antigen, OVA (*i.e.* B16-OVA) in order to increase its antigenicity and therefore potential to respond to cancer immunotherapies. Mice bearing B16-OVA murine melanoma tumors were intratumorally treated with either PBS, D-PDB, or NanoISD for a total of three injections administered *q3d* (**Supplementary Figure 13**). Notably, NanoISD significantly restricted tumor growth and prolonged survival relative to both free D-PDB and PBS, which is consistent with a previous finding that phosphorothioate-capped dsDNA delivered intratumorally with a cationic transfection agent can mediate antitumor immune effects in the B16-OVA tumor model (93). Additionally, while D-PDB acts as a weak cGAS adjuvant, the free polymer did not demonstrate therapeutic efficacy *in vivo*, suggesting that the intrinsic effects of the D-PDB are insufficient to initiate STING-driven antitumor immune programs in the TME.

NanoISD was subsequently explored as a therapeutic treatment for the less immunogenic tumor models, B16.F10 murine melanoma and MC38 murine colon cancer, both of which lack the expression of a foreign antigen (**Figure 7**). Treatments were again intratumorally administered *q3d* for a total of four injections. Relative to PBS-treated controls, the NanoISD treatment attenuated tumor growth (**Figures 7A, C**), prolonged murine survival (**Figures 7B, D**), and was well-tolerated by mice as demonstrated by insignificant differences in total mouse weight over time (**Supplementary Figure 14**). Furthermore, in the B16.F10 model, NanoISD treatment performed comparably to the well-established innate immune activator, CpG DNA when administered at the same dose (*i.e.* 2 μg DNA) (**Figures 7C, D**).

TLR9 agonists can function in a similar manner to that of cGAS/STING pathway agonists by promoting the cancer immunity cycle. Indeed, CpG DNA can induce B16 tumor regression in mice *via* NK cell-dependent, tumor antigen-specific T cell cross-priming (94). Accordingly, CpG DNA is also currently being investigated in human clinical trials for the

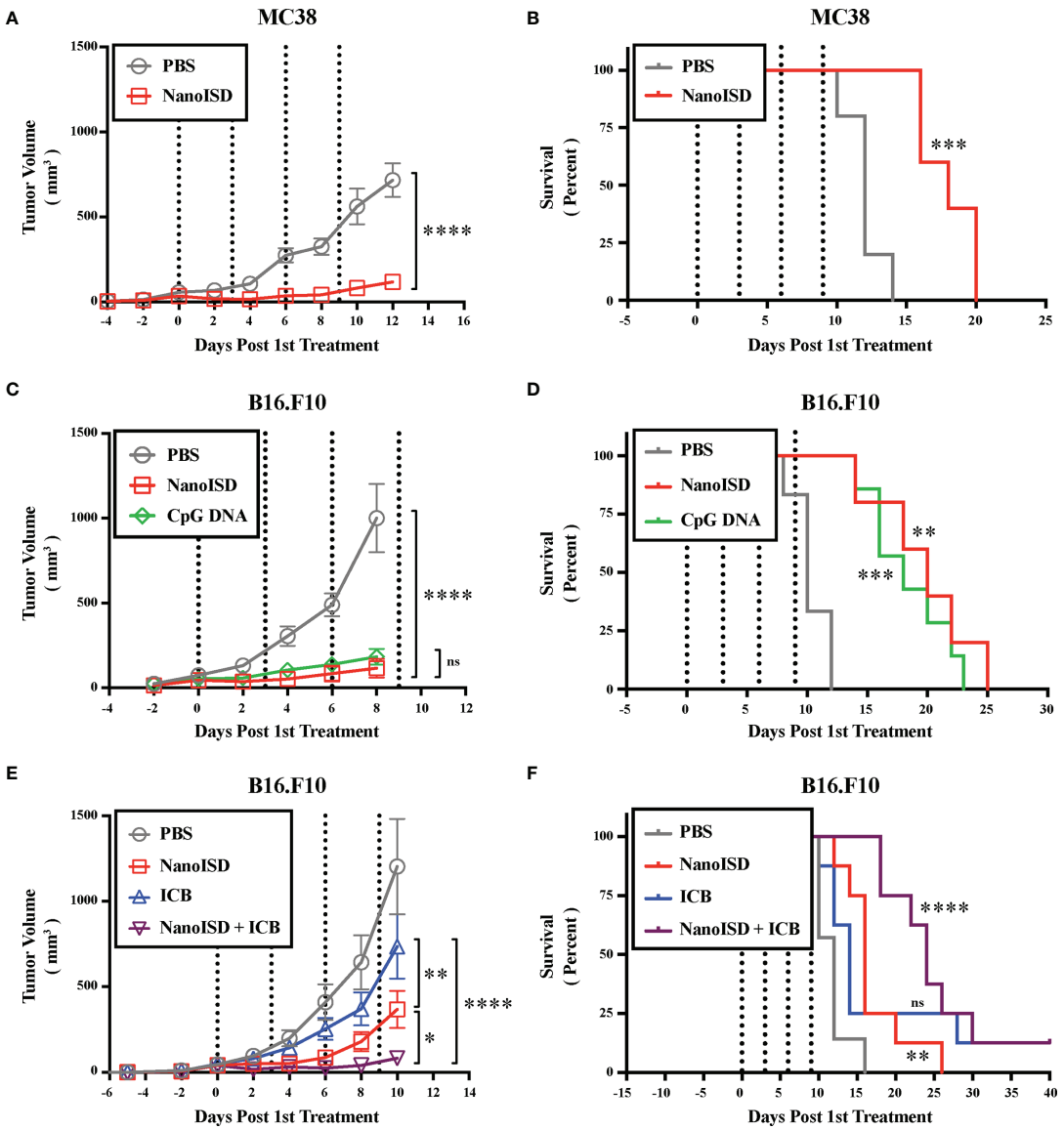

FIGURE 7 | NanoISD Exerts Antitumor Effects. **(A)** Tumor growth plot for MC38 tumors intratumorally treated with 100 µL of either PBS or NanoISD at a dose corresponding to 2 µg DNA (n = 5 per treatment group). Treatments were administered four times *q3d* as indicated by the dotted lines. Tumor growth curves were truncated to the first day that a mouse in any treatment group reached the study endpoint. A two-way ANOVA with Sidak test was used for statistical analysis. The statistical analysis presented is for the final day shown (*i.e.* day 12). **(B)** Kaplan-Meier survival curve for MC38 tumors intratumorally treated with 100 µL of either PBS or NanoISD. Log rank (Mantel-Cox) test was used for statistical analysis. **(C)** Tumor growth plot for B16.F10 tumors intratumorally treated with 100 µL of either PBS, CpG DNA (*i.e.* ODN 1826), or NanoISD (n = 5 or greater per treatment group). Both the CpG DNA and NanoISD doses corresponded to 2 µg DNA. Treatments were administered four times *q3d* as indicated by the dotted lines. Tumor growth curves were truncated to the first day that a mouse in any treatment group reached the study endpoint. A two-way ANOVA with Tukey test was used for statistical analysis. The statistical analysis presented is for the final day shown (*i.e.* day 8). **(D)** Kaplan-Meier survival curve for B16.F10 tumors intratumorally treated with 100 µL of either PBS, CpG DNA (*i.e.* ODN 1826), or NanoISD. Log rank (Mantel-Cox) test was used for statistical analysis. **(E)** Tumor growth plot for B16.F10 tumors treated with 100 µL of either PBS, ICB (*i.e.* anti-PD-1 + anti-CTLA-4 monoclonal antibody therapy), NanoISD, or NanoISD + ICB (n = 8 per treatment group). NanoISD and PBS were administered intratumorally, while ICB was administered intraperitoneally. The NanoISD dose corresponded to 2 µg DNA. The ICB treatment corresponded to 100 µg of both anti-PD-1 and anti-CTLA-4 monoclonal antibodies. Treatments were administered four times *q3d* as indicated by the dotted lines. Tumor growth curves were truncated to the first day that a mouse in any treatment group reached the study endpoint. A two-way ANOVA with Tukey test was used for statistical analysis. The statistical analysis presented is for the final day shown (*i.e.* day 10). **(F)** Kaplan-Meier survival curve for B16.F10 tumors treated with 100 µL of either PBS, ICB (*i.e.* anti-PD-1 + anti-CTLA-4 monoclonal antibody therapy), NanoISD, or NanoISD + ICB (*i.e.* anti-PD-1 + anti-CTLA-4 monoclonal antibody therapy). Log rank (Mantel-Cox) test was used for statistical analysis. ****p < 0.0001, ***p < 0.005, **p < 0.01, *p < 0.05. ns, not significant.

treatment of cancer and they have recently demonstrated great potential for overcoming PD-1 blockade resistance in humans with advanced melanoma (95). However, CpG DNA relies on the cellular expression of TLR9, which is mostly restricted to plasmacytoid dendritic cells and B cells in humans (96). Alternatively, both the cGAS and STING proteins are rather ubiquitously expressed in mammalian cells (97–99). Moreover, TLR9 signaling can only occur in cells that are directly exposed to CpG DNA, while STING signaling can locally propagate from cell-to-cell *via* endogenous cGAMP transfer following DNA-induced cGAS activation (100–102). Thus, the cGAS/STING pathway might represent a more accessible pathway for promoting antitumor immunity *via* cytosolic DNA sensing. Regardless, cGAS/STING pathway agonists increase the arsenal of potential immunotherapeutic treatments, which can dramatically enhance overall patient outcomes by providing more opportunities for application-specific treatments. For example, CpG-based immunotherapy can impair the antitumor activity of BRAF inhibitors in a B cell–dependent manner when used in combination to treat cancer (103), whereas STING agonists can actually sensitize melanoma cells to BRAF inhibitors (104) and might thereby improve therapeutic efficacy in such a scenario.

To determine the impact of NanoISD treatment on the therapeutic response to ICB treatment (*i.e.* combined anti-PD-1 and anti-CTLA-4 monoclonal antibody therapy), B16.F10-bearing mice were treated with either PBS, NanoISD, ICB, or a combination of NanoISD and ICB for a total of four injections administered *q3d* (**Figures 7E, F**). Notably, the NanoISD treatment outperformed the ICB treatment, and the combination treatment of NanoISD and ICB was most effective at inhibiting the growth of treated tumors, indicating that NanoISD treatment can indeed improve therapeutic responses to murine ICB therapy. We note that there is still much room for improvement regarding the therapeutic efficacy of NanoISD, as the treatment in combination with ICB resulted in only one complete response (*i.e.* complete tumor elimination), matching that of ICB alone.

Since NanoISD consists of a self-assembling multi-phasic structure and is highly amenable to the integration of reactive handles (105), it should support various chemical and biomolecular engineering strategies to co-deliver multiple therapeutic agents (*e.g.* potentiators of the cGAS/STING pathway). One potential strategy for increasing the efficacy of NanoISD could include coupling NanoISD treatment with MEK inhibition or CXCR2 inhibition in order to block the expression and/or function of potentially undesirable cytokines (*e.g.* CXCL1 and CXCL2) that can enhance MDSC activity (90) and thereby reduce immune-mediated tumor clearance. Indeed, such a strategy has been previously employed to alleviate certain immunosuppressive effects of STING signaling that can accompany STING agonists and radiotherapy (106).

Other future considerations for NanoISD might involve further improving upon the design of the cGAS ligand and/or the cytosolic delivery agent as well as exploring strategies that could enable intravenous administration and/or tumor targeting of the cGAS agonist.

One variable not examined in this work is whether NanoISD activates other intracellular DNA sensors, such as AIM2, which can limit the magnitude of STING signaling upon *in vitro* stimulation (107). Future studies could investigate whether AIM2 is involved in the response to NanoISD. We note that it is unlikely that AIM2 plays a large role in the response to NanoISD, since the BP length threshold for robust AIM2 activation *in vitro* (*i.e.* ~ 150-BP) is greater than that of the optimized cGAS ligand (*i.e.* 95-BP) (4). However, if AIM2 is involved in the response to NanoISD, strategies could be employed to reduce AIM2 activation with the goal of enhancing STING signaling.

In this work, D-PDB was employed because of its previous success as a vehicle for the cytosolic delivery of immunostimulatory nucleic acids. Indeed, in multiple murine tumor models, an intratumoral treatment regimen of D-PDB loaded with immunostimulatory 5′ triphosphate RNA demonstrated significant therapeutic efficacy by promoting the activation of RIG-I (*i.e.* another cytosolic PRR that can drive antitumor immunity) (49, 50). While the work in this paper demonstrates that D-PDB can also be used to induce a therapeutic response *via* the cytosolic delivery of ISD and the pharmacological activation of cGAS, it is possible that other nanocarriers may elicit enhanced ISD delivery and improved therapeutic responses. Thus, future work aimed at improving therapeutic efficacy could explore the comparison of other nanocarriers for the cytosolic delivery of the optimized ISD (*i.e.* phosphorothioate-capped 95-BP dsDNA).

Lastly, we note that NanoISD may also have utility in other therapeutic areas (*e.g.* vaccinations for infectious diseases), as the DNA/polymer complex is a versatile adjuvant that can indiscriminately generate a local proinflammatory response, which can be advantageous for treating various diseases.

CONCLUSION

Through an iterative experimental screen, the nucleic acid immunotherapeutic, NanoISD was engineered to trigger local cGAS/STING signaling *via* DNA-induced activation of the cGAS enzyme within the cytosol. The effects of formulation conditions (*i.e.* N/P charge ratio), DNA molecular weight (*i.e.* BP length), and DNA composition (*i.e.* phosphorothioate modifications) were investigated using a rationally designed synthetic ISD library in combination with a pH-responsive, endosome-destabilizing polymeric delivery vehicle. This yielded a potent nanoparticulate cGAS adjuvant that can evade major deoxyribonucleases, enhance cellular uptake, promote cytosolic delivery *via* endosomal escape, and trigger the cGAS/STING pathway in a cGAS-directed manner. Furthermore, NanoISD induces proinflammatory cytokine production, prompts the maturation of antigen presenting cells, promotes the tumor infiltration of NK cells and $CD8^+$ T cells, reduces tumor burden, and enhances responses to ICB therapy. Thus, NanoISD represents a novel immunostimulant with clear indications for the treatment of immunologically cold cancers.

MATERIALS AND METHODS

Polymer Synthesis and Characterization

Reversible addition-fragmentation chain transfer (RAFT) polymerization was employed to synthesize the amphiphilic diblock copolymer, *poly*[dimethylaminoethyl methacrylate]$_{10kDa}$-*block*-[(propylacrylic acid)$_{0.3}$-*co*-(dimethylaminoethyl methacrylate)$_{0.3}$-*co*-(butyl methacrylate)$_{0.4}$]$_{35kDa}$ [*p*(DMAEMA)$_{10kDa}$-*bl*-(PAA$_{0.3}$-*co*-DMAEMA$_{0.3}$-*co*-BMA$_{0.4}$)$_{35kDa;}$ D-PDB] as previously described (36). Briefly, the chain transfer agent (CTA) and mass initiator for the RAFT polymerizations were 4-cyano-4-(ethylsulfanylthiocarbonyl)sulfanylpentanoic acid (ECT; Boron Molecular) and 2,2'-azobis(4-methoxy-2,4-dimethyl valeronitrile) (V-70; Wako Chemicals), respectively. An analytical mass balance (XSE205DU DualRange; Mettler Toledo) was used for all mass measurements. Inhibitors were removed from monomer stocks by gravity filtration in columns that were packed with aluminum oxide.

For the first block of the polymer, filtered dimethylaminoethyl methacrylate (DMAEMA) was added to measured CTA in a glass vial with a target degree of polymerization of 100. A mass initiator stock was prepared by dissolving the initiator in the reaction solvent, dioxane. An appropriate amount of the mass initiator stock was added to the solution of CTA and DMAEMA at a molar ratio of 100:1:0.05 representing total monomer, CTA, and initiator, respectively. Additional dioxane was then added to the reaction vessel to attain a 40 wt% monomer solution. The solution was sealed and purged with nitrogen gas for 30 minutes on ice and then allowed to react at 40°C in an oil bath.

The reaction was stopped after 22 hours by opening the reaction vessel and exposing the mixture to air. The resultant polymer was then purified by precipitation into cold pentane and subsequent dialysis. The crude product was precipitated six times by transferring the polymer solution into cold pentane. Centrifugation (5000 rpm, 5 min, 4°C) was used to pellet the polymer mixture, and the supernatant was then discarded. Small volumes of acetone were added to dissolve the pelleted polymer, thereby enabling the polymer to be transferred to new precipitation tubes. The polymer mixture was then collected in a 3.5 MWCO SnakeSkin™ dialysis membrane (Cat. No. 68035; Thermo Fisher Scientific) and further purified *via* membrane dialysis against pure acetone (3x), half-acetone and half deionized water (2x), and then pure deionized water (2x) for 4 hour intervals each. Following dialysis, poly(DMAEMA) was frozen at -80°C for 5 hours and then lyophilized for 3 days.

For the second block of the polymer, poly(DMAEMA) was used as a macroCTA (mCTA). Filtered DMAEMA, PAA, and BMA (at a molar ratio of 30:30:40) were added to measured mCTA in a glass vial with a target degree of polymerization of 450. PAA was synthesized using diethyl propylmalonate as the precursor as previously described (108). A mass initiator stock was prepared by dissolving the initiator in the reaction solvent, N,N-dimethylacetamide (DMAC). An amount of the mass initiator stock was added to the solution of mCTA and monomers at a molar ratio of 450:1:0.4 representing total monomer, mCTA, and initiator, respectively. Note that a greater Initiator/CTA ratio is required to get PAA to incorporate into the polymer chains. Additional DMAC was then added to the reaction vessel to attain a 40 wt% mCTA and monomer solution. The solution was sealed and purged with nitrogen gas for 30 minutes on ice and then allowed to react at 40°C in an oil bath.

The reaction was stopped after 24 hours by opening the reaction vessel and exposing the mixture to air. The resultant polymer was then purified by precipitation into cold pentane:ether (80:20) and subsequent dialysis. The crude product was precipitated six times by transferring the polymer solution into cold pentane:ether (80:20). Centrifugation (5000 rpm, 5 min, 4°C) was used to pellet the polymer mixture and remove the supernatant. Again, small volumes of acetone were added to dissolve the pelleted polymer, thereby enabling the polymer to be transferred to new precipitation tubes. The polymer mixture was then collected in a 10 MWCO SnakeSkin™ dialysis membrane (Cat. No. 68100; Thermo Fisher Scientific) and further purified *via* membrane dialysis against pure acetone (3x), half-acetone and half deionized water (2x), and then pure deionized water (2x) for 4 hour intervals each. Following dialysis, poly(DMAEMA) was frozen at -80°C for 5 hours and then lyophilized for 3 days. All lyophilized polymer was stored at -20°C prior to use.

^{1}H NMR Spectroscopy ($CDCl_3$ with TMS, 400 MHz) was used to calculate the experimental degree of polymerization, polymer composition, and theoretical molecular weight of the polymers (**Supplementary Figure 15**). Subsequently, the experimental molecular weight and a polydispersity index were measured by gel permeation chromatography (GPC) (mobile phase HPLC-grade dimethylformamide (DMF) containing 0.1% LiBr) with inline light scattering (Wyatt Technology) and refractive index (Agilent) detectors (**Supplementary Figure 16**). The ASTRA V Software (Wyatt Technology) was used for all GPC-related calculations. Additionally, The *poly*(dimethylaminoethyl methacrylate)$_{10kDa}$-*block*-(butyl methacrylate)$_{34kDa}$ (*p*DMAEMA$_{10kDa}$-*bl*- BMA$_{34kDa;}$ D-B) polymer was previously prepared (50).

Near-infrared D-PDB (NIR-D-PDB) was created by labeling D-PDB with NIR-664-iodoacetamide (CAS 149021-66-9; Santa Cruz) at a molar ratio of 1:1. Briefly, 72 µL of a 12.5 mg/mL stock of NIR-664-iodoacetamide dissolved in methanol was added to 50 mg of D-PDB dissolved in 1 mL methanol. The mixture was vortexed, and the reaction was allowed to proceed at room temperature overnight while continuously stirring and protected from light. The mixture was then transferred to a 3.5 MWCO SnakeSkin™ dialysis membrane (Cat. No. 68035; Thermo Fisher Scientific) and purified *via* membrane dialysis against pure methanol (3x), half-methanol and half deionized water (2x), and then pure deionized water (2x) for 4 hour intervals each, all the while kept at 4°C and protected from light. Following dialysis, the sample was run through a PD-10 desalting column (17085101; Cytiva) into H_2O. The fully purified sample was frozen at -80°C for 5 hours and then lyophilized for 2 days. NIR-D-PDB was stored at -20°C prior to use.

Preparation of ISD Libraries

The synthetic library of phosphorothioate-capped dsDNA (**Supplementary Figure 1**) and other associated DNA sequences

were purchased as a duplex from Integrated DNA Technologies (IDT) unless otherwise specified. The second ISD library of PCR-amplified dsDNA (**Supplementary Figure 2**) was prepared as follows. The 10,183-BP lentiGuide-Puro plasmid (Plasmid #52963; Addgene) was used to generate custom BP length dsDNA PCR products. In brief, the lentiGuide-Puro agar stab was spread over standard 0.5 mg/mL puromycin agar plates and placed in a 37°C bacteria incubator overnight. The following day, individual bacteria colonies were isolated and placed in liquid LB broth with 0.5 mg/mL puromycin, swirled, loosely covered with sterile cap, and left to incubate at 37°C for 12 hours. Bacteria growths were purified with the QIAprep Miniprep kit (Cat. No. 27104; Qiagen), resuspended in sterile H_2O, and DNA concentration was quantified by ultraviolet–visible (UV-Vis) spectroscopy (Nanodrop 2000 Spectrophotometer; Thermo Fisher Scientific).

Forward and reverse primers were designed using the NCBI Primer Blast tool for dsDNA sequences of variable BP length (*i.e.* 95, 156, 313, 625, 1250, 2500, 5000, and 10000 BP). For the PCR-amplification of each length of dsDNA, individual reactions were set up with 4 μL of 5x Phusion GC Buffer, 0.4 μL of 10 mM dNTPs (D7295; MilliporeSigma), 1 μL of 10 μM forward primer, 1 μL of 10 μM reverse primer, 0.6 μL of DMSO, 0.2 μL of Phusion® High-Fidelity DNA Polymerase (M0530; New England Biolabs), 4 μL of 1 ng/μL (4 ng) of lentiGuide-Puro plasmid template DNA (Plasmid #52963; Addgene), and 8.8 μL of H_2O, per 20 μL reaction. Thermocycling conditions were 98°C for 30 seconds, followed by 35 cycles of 98°C for 10 seconds, 54°C for 30 seconds, 72°C for 30 seconds per kb of PCR length, followed by 72°C for 10 minutes. PCR products were concentrated using standard ethanol precipitation and clear bands were observed on a 2% agarose gel for each PCR length. Each PCR-amplified product was stored at -20°C prior to use.

Nanoparticle Formulation

Lyophilized D-PDB was dissolved in ethanol to 50 mg/mL. Aliquots of this polymer stock were then diluted in phosphate buffer (pH 7.0, 100 mM) to a concentration of 10 mg/mL, allowing the polymer chains to self-assemble into micelles. The 10 mg/mL polymer solution was then concentrated into PBS (pH 7.4; Gibco) through 4 cycles of centrifugal filtration with Amicon® Ultra 0.5 mL Centrifugal Filter Units (Ultracel® - 3K, Regenerated Cellulose 3,000 NMWL; MilliporeSigma) following manufacturer's instructions. The final concentrated polymer solution was collected, and an aliquot was taken to determine the polymer concentration relative to a standard curve. Using a 96-well plate (REF 655180; Greiner Bio-One), the polymer concentration was calculated from UV-vis spectroscopy (Synergy H1 Multi-Mode Microplate Reader; Biotek) based on absorbance at 310 nm. The micelle solution was diluted to 1 mg/mL with PBS and passed through a 0.2 μm Whatman® Puradisc polyethersulfone sterile filter (WHA67801302; MilliporeSigma). A fixed amount of the sterile-filtered polymer stock was then added to an aqueous solution containing a set amount of nucleic acid, which corresponded to the desired N/P charge ratio. Again, note that the first block of the diblock copolymer composed of poly (DMAEMA) is estimated to exhibit 50% protonation at pH 7.4 for the purposes of determining N/P ratios. Upon the addition of the polymer micelles to the nucleic acid, the solution was rapidly mixed by pipetting and then incubated at room temperature for 20 minutes to allow for complete electrostatic complexation.

Nanoparticle Physical Characterization

Hydrodynamic size of the polymeric micelles and DNA/polymer complexes was measured *via* digital light scattering (DLS) using either the Zetasizer Nano ZS instrument (Malvern Panalytical) or the Litesizer 500 instrument (Anton Paar) as indicated in figure captions. Additionally, the zeta potential of the polymeric micelles and DNA/polymer complexes was determined using the Zetasizer Nano ZS instrument (Malvern Panalytical). Polymer concentrations were normalized to 1 mg/mL and samples were run at physiological pH 7.4. DNA concentrations correspond to the N/P charge ratios, which were set to 4 unless otherwise indicated.

2% agarose gels were prepared by dissolving 3 grams of UltraPure™ Agarose powder (16500100; Thermo Fisher Scientific) in 150 mL of 1x TAE buffer that had been diluted with deionized H_2O from a 10x TAE buffer stock (REF 46010CM; Corning). The mixture was microwaved in 30 second intervals until the agarose was fully dissolved. The solution was then cast into a gel. DNA and DNA/polymer complexes were then prepared. For the DNase I activity experiment, the indicated concentrations of DNase I (M0303; New England Biolabs) were incubated with the indicated samples for 15 minutes at 37°C. The resultant mixtures and controls were then incubated at 75°C for 15 minutes to heat-inactivate the DNase I, and a volume of 10% sodium dodecyl sulfate (SDS) (RGE3230; K-D Medical) was subsequently added to the mixtures and controls such that a final concentration of 1% SDS was achieved, which allowed for decomplexation of the DNA from the polymer. All of the samples were mixed with a volume of glycerol such that a final concentration of 5% glycerol was achieved prior to gel loading. Samples were loaded into wells of the agarose gel at a concentration of 1 μg DNA/lane. Polymer concentrations correspond to the indicated N/P charge ratio. The TrackIt™ 100 bp DNA Ladder (Cat. No. 10488058; Thermo Fisher Scientific), the TrackIt™ 1 Kb Plus DNA Ladder (Cat. No. 10488085; Thermo Fisher Scientific), or the NEB 1 kb DNA Ladder (N3232; New England Biolabs) were used for references as indicated in figure captions. Gel electrophoresis was then performed at 120 V for 45 minutes. Gels were subsequently stained with SYBR Safe dye (S33102; Thermo Fisher Scientific) for 30 minutes while protected from light and then imaged with a Digital ChemiDoc MP system (Bio-Rad).

Cell Lines

All cell lines were maintained according to supplier specifications and/or technical data sheets. RAW-Dual cells (InvivoGen) and RAW-Lucia ISG-KO-cGAS cells (InvivoGen) were cultured in Dulbecco's Modified Eagle Medium (DMEM; Gibco) supplemented with 2 mM $_L$-glutamine, 4.5 g/L glucose, 10% heat-inactivated fetal bovine serum (HI-FBS; Gibco), 100 U ml^{-1} penicillin/100 μg ml^{-1} streptomycin (Gibco), and 100 μg/mL Normocin. For the continual selection of these cell lines, Zeocin

was added on every other cell passage at a concentration of 200 μg/mL. THP1-Dual cells (InvivoGen) and THP1-Dual KO-TREX1 cells (InvivoGen) were cultured in Roswell Park Memorial Institute (RPMI) 1640 Medium (Gibco) supplemented with 2 mM $_L$-glutamine, 25 mM HEPES, 10% heat-inactivated fetal bovine serum (HI-FBS; Gibco), 100 U ml^{-1} penicillin/100 μg ml^{-1} streptomycin (Gibco), and 100 μg/mL Normocin. For the continual selection of these cell lines, Blasticidin and Zeocin were added after every cell passage at concentrations of 10 μg/mL and 100 μg/mL, respectively. A549-Dual cells (InvivoGen) were cultured in Dulbecco's Modified Eagle Medium (DMEM; Gibco) supplemented with 2 mM $_L$-glutamine, 4.5 g/L glucose, 10% heat-inactivated fetal bovine serum (HI-FBS; Gibco), 100 U ml^{-1} penicillin/100 μg ml^{-1} streptomycin (Gibco), and 100 μg/mL Normocin. For the continual selection of this cell line, Blasticidin and Zeocin were added after every cell passage at concentrations of 10 μg/mL and 100 μg/mL, respectively. DC2.4 cells were cultured in Roswell Park Memorial Institute (RPMI) 1640 Medium (Gibco) supplemented with 2 mM $_L$-glutamine, 1× non-essential amino acids (Cellgro), 10 mM HEPES (Invitrogen), 50 μM 2-mercaptoethanol (Gibco), 10% heat-inactivated fetal bovine serum (HI-FBS; Gibco), and 100 U ml^{-1} penicillin/100 μg ml^{-1} streptomycin (Gibco). 4T1 cells (ATCC) were cultured in Dulbecco's Modified Eagle Medium (DMEM; Gibco) supplemented with 2 mM $_L$-glutamine, 4.5 g/L glucose, 10% heat-inactivated fetal bovine serum (HI-FBS; Gibco), and 100 U ml^{-1} penicillin/100 μg ml^{-1} streptomycin (Gibco). B16.F10 cells (ATCC) were cultured in Dulbecco's Modified Eagle Medium (DMEM; Gibco) supplemented with 2 mM $_L$-glutamine, 4.5 g/L glucose, 10% heat-inactivated fetal bovine serum (HI-FBS; Gibco), and 100 U ml^{-1} penicillin/100 μg ml^{-1} streptomycin (Gibco). B16.F10 IFN-LUC cells were cultured in Dulbecco's Modified Eagle Medium (DMEM; Gibco) supplemented with 2 mM $_L$-glutamine, 4.5 g/L glucose, 10% heat-inactivated fetal bovine serum (HI-FBS; Gibco), and 100 U ml^{-1} penicillin/100 μg ml^{-1} streptomycin (Gibco). Puromycin was added after every cell passage at a concentration of 10 μg/mL. B16-OVA cells were cultured in Dulbecco's Modified Eagle Medium (DMEM; Gibco) supplemented with 2 mM $_L$-glutamine, 4.5 g/L glucose, 10% heat-inactivated fetal bovine serum (HI-FBS; Gibco), and 100 U ml^{-1} penicillin/100 μg ml^{-1} streptomycin (Gibco). For the continual selection of this cell line, Geneticin (G418; Gibco) was added after every cell passage at a concentration of 500 μg/mL. MC38 cells were cultured in Dulbecco's Modified Eagle Medium (DMEM; Gibco) supplemented with 2 mM $_L$-glutamine, 0.1 mM non-essential amino acids (Cellgro), 10 mM HEPES (Invitrogen), 1 mM sodium pyruvate, 10% heat-inactivated fetal bovine serum (HI-FBS; Gibco), 100 U ml^{-1} penicillin/100 μg ml^{-1} streptomycin (Gibco), and 50 μg/mL gentamicin sulfate (Gibco). All cells lines were tested for Mycoplasma contamination and kept in a humidified environment with 5% CO at 37°C.

In Vitro Reporter Cell Assays

96-well plates (REF 655180; Greiner Bio-One) were used for screening the DNA/polymer complexes. Reporter cells were seeded at 50,000 cells/well in 100 μL media. When cells became ~ 80% confluent, treatments were administered in 100 μL PBS. Results were collected 24 hours after treatment. Quanti-Luc™ and Quanti-Blue™ (InvivoGen) assays were performed on cell supernatants following manufacturer's instructions. Luminescence and absorbance were quantified *via* plate reader (Synergy H1 Multi-Mode Microplate Reader; Biotek). Luminescence measurements were performed using white, opaque-bottom 96-well plates (REF 655073; Greiner Bio-One), and absorbance measurements were performed using standard, clear 96-well plates (REF 655180; Greiner Bio-One). The signal for each sample concentration was determined using 3 biological replicates, each with 3 technical replicates. For the *in vitro* IVIS assay with the B16.F10 IFN-LUC cells, black 96-well plates (REF 655096; Greiner Bio-One) were used, and luminescence measurements were performed on an IVIS Lumina III (PerkinElmer) 5 minutes after the addition of Pierce™ D-Luciferin, Monopotassium Salt (88293; Thermo Fisher Scientific) reconstituted in PBS, such that the final concentration of D-luciferin was 150 μg/mL. The *in vitro* IVIS experiment included 3 biological replicates without technical replicates. All reporter cell measurements were normalized by subtracting the average value of a PBS-treated negative control group. All bell-shaped dose response curves were truncated at their plateau. The EC_{50} and IC_{50} values were calculated for each of the dose responses using curve fitting analysis in the GraphPad Prism software.

In Vitro Cellular Uptake Study

DC2.4 cells were seeded in 12-well plates (REF 665180; Greiner Bio-One) at 4 x 10^5 cells/well and allowed to adhere overnight. Treatments of either PBS, DNA/D-PDB, Cy5-DNA, Cy5-DNA/D-PDB, NIR-D-PDB, or DNA/NIR-D-PDB were administered to the cells for 4 hours at 37°C with 5% CO_2. Doses were set at 45 nM DNA (*i.e.* theoretical EC_{50} value for NanoISD in RAW-Dual cells normalized to surface area of the tissue culture area on the 12-well plate) and/or the corresponding concentration of polymer for an N/P charge ratio of 4. Following incubation, cells were trypsinized, washed, and resuspended with flow cytometry staining buffer (FACS buffer) (*i.e.* PBS + 2% FBS) supplemented with 1 μg/mL DAPI. Cells were then analyzed using an Amnis CellStream Luminex flow cytometer. Each treatment was performed with 4 technical replicates. Cellular uptake was also analyzed at 24 hours post treatment, and similar results were observed (*data not shown*).

In Vitro BMDC Maturation Study

Bone marrow cells were harvested from femurs and tibias of 6-8 week-old female C57BL/6J mice by flushing them with cold PBS. Cells were centrifuged for 5 minutes at 450 x g and resuspended in complete BMDC culture media (*i.e.* RPMI 1640 medium supplemented with 10% HI FBS, 1% Pen-Strep (*i.e.* 100 U/mL penicillin and 100 μg/mL streptomycin), 2 mM L-glutamine, 10 mM HEPES, 1 mM sodium pyruvate, 1x non-essential amino acids, 50 μM β-mercaptoethanol, and 20 ng/mL GM-CSF). The cell suspension was passed through a 70 μM sterile cell strainer (22363548; Fisherbrand™; Thermo Fisher Scientific), and the

cells were then seeded in 100x15 mm non-tissue-culture-treated petri dishes (REF 351029; Corning) and incubated at 37°C with 5% CO_2. Fresh complete BMDC culture media was added on days 3, 5, and 7. On day 8, the percentage of $CD11c^+$ cells (*i.e.* BMDCs) was confirmed to be greater than 80% as measured with by flow cytometry using anti-CD11c-FITC (Clone N418; BioLegend), and the BMDCs were then seeded in 12-well plates (REF 665180; Greiner Bio-One) at 6 x 10^5 cells/well. Treatments of PBS, 45 nM phosphorothioate-capped 95-BP dsDNA (*i.e.* DNA), 2 μM MPLA, and 45 nM NanoISD (*i.e.* theoretical EC_{50} value for NanoISD in RAW-Dual cells normalized to surface area of the tissue culture area on the 12-well plate) were administered to the BMDCs for 24 hours at 37°C with 5% CO_2. Following incubation, cells were scrapped, washed with FACs buffer, incubated with Fc-block (anti-CD16/CD32, Clone 2.4G2; Tonbo) for 15 minutes at 4°C, and then stained with antibodies against the markers of DC activation, anti-CD86-PE/Cy7 (Clone GL-1; BioLegend) and anti-MHC-II-APC/Cy7 (Clone M5.114.15.2; BioLegend) for 1 hour at 4°C. Cells were then washed 2x in FACS buffer, resuspended using FACS buffer supplemented with 1 μg/mL DAPI, and analyzed using an Amnis CellStream Luminex flow cytometer. Each treatment was performed with 4 technical replicates, and the experiment was conducted 3 times with similar results.

In Vivo Imaging Experiments

All *in vivo* imaging was performed on the IVIS Lumina III (PerkinElmer). Mice were anesthetized with isoflurane gas and shaved around the injection site as necessary. For all *in vivo* retention experiments, fluorescence was recorded longitudinally as indicated, and corresponding fluorophore-specific filter pairs were used. For the subcutaneous retention study, 6-8 week-old CD-1 mice (Charles River Laboratories) were administered a single 100 μL subcutaneous injection of either PBS, Cy5-DNA, Cy5-DNA/D-PDB, NIR-D-PDB, or DNA/NIR-D-PDB on each rear flank. Individual uncomplexed fluorescent agents were administered on the left flank of the mice, and the complexes at an N/P charge ratio of 4 with the indicated fluorescent agent were administered on the right flank of the mice. Each treatment contained 2 μg DNA and/or the corresponding amount of polymer for an N/P charge ratio of 4. For the intratumoral retention study, 6-8 week-old BALB/c mice (The Jackson Laboratory) were orthotopically inoculated with 4T1 tumors by injecting 1 x 10^6 cells suspended in 100 μL of a 1:1 mixture of PBS and Type 2 Cultrex Basement Membrane Extract (3532-005-02; R&D Systems) into the left inguinal mammary fat pad. When tumors were ~ 100 mm^3, the mice were administered a single 100 μL intratumoral injection of either PBS, Cy5-labeled phosphorothioate-capped 95-BP dsDNA (*i.e.* Cy5-DNA), or Cy5-DNA/D-PDB. Each treatment contained 2 μg DNA and/or the corresponding amount of polymer for an N/P charge ratio of 4.

For the *in vivo* IFN activity experiment, 6-8 week-old C57BL/6 mice (The Jackson Laboratory) were inoculated with B16.F10 IFN-LUC tumors by subcutaneously injecting 1 x 10^6 cells suspended in 100 μL of PBS into the rear right flank. When tumors were ~ 100 mm^3, the mice were administered a single 100 μL intratumoral injection of either PBS or NanoISD at a 2 μg DNA dose. Luminescence was recorded at set time points (*i.e.* 0, 4, 8, 12, and 24 hours). For each timepoint, the mice were administered a dorsal subcutaneous 150 μL injection of 30 mg/mL Pierce™ D-Luciferin, Monopotassium Salt (88293; Thermo Fisher Scientific) reconstituted in PBS, and a luminescence image was captured 15 minutes thereafter.

Quantitative RT-PCR and NanoString Analysis

6-8 week-old C57BL/6 mice (The Jackson Laboratory) were inoculated with B16.F10 tumors by subcutaneously injecting 1 x 10^6 cells suspended in 100 μL of PBS into the rear right flank. When tumors were ~ 200 mm^3, the mice were administered a single 100 μL intratumoral injection of either PBS, D-PDB, or NanoISD at a 2 μg DNA dose. 6 hours after the intratumoral injection, mice were euthanized and tumors were harvested. Tumors were then homogenized using TissueLyser II (Qiagen), and tumor RNA was isolated using the RNeasy® Plus Mini Kit (Qiagen).

For the qPCR analysis of gene expression, 1 μg of the tumor RNA was reverse transcribed by an iScript cDNA synthesis kit (Bio-Rad) following the manufacturer's instructions. The qPCR was conducted on the generated cDNA using a Bio-Rad CFX Connect Real-time System, with the threshold cycle number determined by Bio-Rad CFX manager software V.3.0. The following TaqMan gene expression kits (Thermo Fisher Scientific) were used following the manufacturer's instructions: mouse *Ifnb1* (Mm00439552_s1); mouse *Cxcl10* (Mm00445235_m1); mouse *Tnf* (Mm00443258_m1); mouse *Il6* (Mm00446190_m1); mouse *Ppib* (Mm00478295_m1). Reactions for each gene were performed in technical duplicate for ten biological samples per treatment group, and the threshold cycle numbers were averaged. Gene expression was normalized to the house-keeping gene, *Ppib* and then normalized to the PBS treatment values using the 2^{-ddCt} method of analysis.

For the NanoString analysis of gene expression, 100 ng of mRNA isolated from tumor tissue was hybridized to a myeloid panel of target-specific fluorescent barcodes. The hybridized samples were analyzed on the NanoString nCounter MAX Analysis system. Subsequent data processing was performed using the NanoString nSolver data analysis software.

In Vivo Tumor Therapy Experiments

6-8 week-old C57BL/6 mice (The Jackson Laboratory) were inoculated with B16-OVA, B16.F10, or MC38 tumors by subcutaneously injecting 1 x 10^6 cells suspended in 100 μL of PBS into the rear right flank. When tumors were ~ 50 mm^3, the mice were given four 100 μL intratumoral injections administered *q3d* with treatments of either PBS, D-PDB, CpG DNA (*i.e.* ODN 1826), or NanoISD at a 2 μg DNA dose. For the therapy study with ICB, certain mice were also given four 100 μL intraperitoneal injections on the same days as the intratumoral treatments (*i.e.* administered *q3d*) with a treatment of the monoclonal antibodies, anti-PD-1 (RMP1-14, BE0146; Bio X Cell) and anti-CTLA-4 (9d9, BE0164; Bio X Cell). Tumor volume, total murine mass, and murine well-being were

recorded *qod* for the duration of the study. The study endpoint for maximum tumor volume (*i.e.* survival) was 1500 mm^3.

Flow Cytometry

6-8 week-old C57BL/6 mice (The Jackson Laboratory) were inoculated with B16.F10 tumors by subcutaneously injecting 1 x 10^6 cells suspended in 100 µL of PBS into the rear right flank. When tumors were ~ 50 mm^3, the mice were given three 100 µL intratumoral injections administered *q3d* with treatments of either PBS or NanoISD at a 2 µg DNA dose. 48 hours after the final intratumoral injection, mice were euthanized and tumors were harvested. The tumors were then mechanically dissociated with an OctoMACS separator, and digested in a solution of 125 µg ml−1 Deoxyribonuclease I (Worthington) and 500 µg ml−1 Collagenase III (Worthington) in RPMI 1640 media for 30 minutes at 37°C. The digested tumors were strained through a 70 µM sterile cell strainer (22363548; Fisherbrand™; Thermo Fisher Scientific) and treated with ACK Lysing Buffer (Gibco).

The remaining tumor cells were washed and diluted to a concentration of 1×10^7 cells/mL in FACS buffer supplemented with 50 nM dasatinib, and the cell suspension was aliquoted into a 96-well plate (REF 655180; Greiner Bio-One). 100 µl was add to each well with the number of wells filled corresponding to the number of flow cytometry tests to be performed. After another wash with FACS buffer supplemented with 50 nM dasatinib, the plated cells were incubated with Fc-block (anti-CD16/CD32, Clone 2.4G2; Tonbo) for 15 minutes at 4°C. The relevant fluorescent antibodies were then added for each flow cytometry test, and the cells were incubated for 45 minutes at 4°C while protected from light. Cells were washed twice, suspended in FACS buffer supplemented with 1 µg/mL DAPI, and then analyzed using a 5-laser LSRII flow cytometer (BD).

The samples were stained with the fluorescent antibodies of either a myeloid panel or T cell panel. The following antibodies were used for the myeloid panel: anti-CD45.2-APC (20-0454-U025; Tonbo), anti-CD11b-PerCp-Cy5.5 (550993; BD BioSciences), anti-NK-1.1-PE (108707; BioLegend), anti-F4/80-PE/Cy7 (123113; BioLegend), anti-MHC-II-APC/Cy7 (107628; BioLegend), anti-CD11c-PE/Cy5 (117316; BioLegend), anti-Ly-6G-A488 (127625; BioLegend), and anti-Ly-6C-BV605 (128035; BioLegend). The following antibodies were used for the T cell panel: anti-CD45.2-APC (20-0454-U025; Tonbo), anti-CD3e-PE/Cy7 (552774; BD BioSciences), and anti-CD8a-PE/Cy5 (100710; BioLegend). DAPI was used to discriminate live *versus* dead cells. Representative gating for each panel can be found in the Supplementary Information (**Supplementary Figures 11, 12**).

Statistical Analysis

The significance for each experiment was determined as indicated in the corresponding figure caption. Statistical analyses were performed using GraphPad Prism software, version 7.0c. The plotted values represent the experimental means, and the error bars represent one standard deviation (SD), except for those in the tumor growth plots, which represent one standard error of the mean (SEM). ****$p < 0.0001$, ***$p < 0.005$, **$p < 0.01$, *$p < 0.05$.

DATA AVAILABILITY STATEMENT

The original contributions presented in the study are publicly available. This data can be found at https://www.ncbi.nlm.nih.gov/geo/under the following accession numbers: GSE183144, GPL30574 and GSM5552035-GSM555204.6.

ETHICS STATEMENT

All animal experiments were reviewed and approved by the Vanderbilt University Institutional Animal Care and Use Committee (IACUC), and all surgical and experimental procedures were performed in accordance with the regulations and guidelines of the Vanderbilt University IACUC. All mice were maintained at the animal facilities of Vanderbilt University under pathogen-free conditions.

AUTHOR CONTRIBUTIONS

Conceptualization was performed by KG and JW. Methodology was done by KG, JR, CC, and SS. Formal analysis was performed by KG. Experiments were performed by KG, CC, LW-B, AH, and CK. Resources were provided by JR, CC, SS, JB, MA, and JW. Data visualization and figure preparation was done by KG. The original draft was written by KG. The manuscript was reviewed and/or edited by JR, CC, LW-B, AH, SS, CK, JB, MA, and JW. Funding was acquired by JW. All authors contributed to the article and approved the submitted version.

FUNDING

This research was supported by grants from the National Science Foundation CBET-1554623 (JW), a Vanderbilt Ingram Cancer Center (VICC) Ambassador Discovery Grant (JW), an American Cancer Society Institutional Research Grant (IRG-58-009-56 to JW), the Congressionally-Directed Medical Research Program (W81XWH-161-0063 to JW), and a Stand Up To Cancer Innovative Research Grant, Grant Number SU2C-AACR-IRG 20-17 (JW). Stand Up To Cancer (SU2C) is a program of the Entertainment Industry Foundation. Research grants are administered by the American Association for Cancer Research, the scientific partner of SU2C. CC acknowledges a National Science Foundation Graduate Research Fellowship under grant numbers DGE-1445197 and DGE-1937963. CK was supported by the Vanderbilt Institute for Infection, Immunology, and Immunity (VI4) Summer Research Scholars Program - Class of 2019.

ACKNOWLEDGMENTS

We thank Prof. Craig Duvall (Vanderbilt University) for the use of GPC and IVIS imaging equipment, Prof. Carlos Silvera Batista (Vanderbilt University) for the use of their Anton Paar Litesizer 500 instrument, the Vanderbilt Institute of Nanoscale Science and Engineering (VINSE) for the use of their Malvern Zetasizer Nano ZS instrument, and the VUMC Flow Cytometry Shared

Resource, supported by the Vanderbilt Ingram Cancer Center (P30 CA68485) and the Vanderbilt Digestive Disease Research Center (DK058404), for the use of flow cytometers, and the 2019 VI4 Summer Research Scholars Program for providing CK with the opportunity to participate in academic research.

SUPPLEMENTARY MATERIAL

The Supplementary Material for this article can be found online at: https://www.frontiersin.org/articles/10.3389/fimmu.2021.753472/full#supplementary-material

REFERENCES

1. Schlee M, Hartmann G. Discriminating Self From Non-Self in Nucleic Acid Sensing. *Nat Rev Immunol* (2016) 16(9):566–80. doi: 10.1038/nri.2016.78
2. Roers A, Hiller B, Hornung V. Recognition of Endogenous Nucleic Acids by the Innate Immune System. *Immunity* (2016) 44(4):739–54. doi: 10.1016/j.immuni.2016.04.002
3. Iurescia S, Fioretti D, Rinaldi M. Nucleic Acid Sensing Machinery: Targeting Innate Immune System for Cancer Therapy. *Recent Pat Anticancer Drug Discov* (2018) 13(1):2–17. doi: 10.2174/1574892812666171030163804
4. Emming S, Schroder K. Tiered DNA Sensors for Escalating Responses. *Science* (2019) 365(6460):1375–6. doi: 10.1126/science.aay2701
5. Ishikawa H, Barber GN. STING Is an Endoplasmic Reticulum Adaptor That Facilitates Innate Immune Signalling. *Nature* (2008) 455(7213):674–8. doi: 10.1038/nature07317
6. Danilchanka O, Mekalanos JJ. Cyclic Dinucleotides and the Innate Immune Response. *Cell* (2013) 154(5):962–70. doi: 10.1016/j.cell.2013.08.014
7. Zhang X, Shi H, Wu J, Zhang X, Sun L, Chen C, et al. Cyclic GMP-AMP Containing Mixed Phosphodiester Linkages is an Endogenous High-Affinity Ligand for STING. *Mol Cell* (2013) 51(2):226–35. doi: 10.1016/j.molcel.2013.05.022
8. Sun L, Wu J, Du F, Chen X, Chen ZJ. Cyclic GMP-AMP Synthase Is a Cytosolic DNA Sensor That Activates the Type I Interferon Pathway. *Science* (2013) 339(6121):786–91. doi: 10.1126/science.1232458
9. Wu J, Sun L, Chen X, Du F, Shi H, Chen C, et al. Cyclic GMP-AMP Is an Endogenous Second Messenger in Innate Immune Signaling by Cytosolic DNA. *Science* (2013) 339(6121):826–30. doi: 10.1126/science.1229963
10. Diner EJ, Burdette DL, Wilson SC, Monroe KM, Kellenberger CA, Hyodo M, et al. The Innate Immune DNA Sensor cGAS Produces a Noncanonical Cyclic Dinucleotide That Activates Human STING. *Cell Rep* (2013) 3(5):1355–61. doi: 10.1016/j.celrep.2013.05.009
11. Ablasser A, Chen ZJ. cGAS in Action: Expanding Roles in Immunity and Inflammation. *Science* (2019) 363(6431):eaat8657. doi: 10.1126/science.aat8657
12. Hooy RM, Sohn J. The Allosteric Activation of cGAS Underpins Its Dynamic Signaling Landscape. *Elife* (2018) 7:e39984. doi: 10.7554/eLife.39984
13. Dubensky TW Jr., Kanne DB, Leong ML. Rationale, Progress and Development of Vaccines Utilizing STING-Activating Cyclic Dinucleotide Adjuvants. *Ther Adv Vaccines* (2013) 1(4):131–43. doi: 10.1177/2051013613501988
14. Woo SR, Fuertes MB, Corrales L, Spranger S, Furdyna MJ, Leung MY, et al. STING-Dependent Cytosolic DNA Sensing Mediates Innate Immune Recognition of Immunogenic Tumors. *Immunity* (2014) 41(5):830–42. doi: 10.1016/j.immuni.2014.10.017
15. An X, Zhu Y, Zheng T, Wang G, Zhang M, Li J, et al. An Analysis of the Expression and Association With Immune Cell Infiltration of the cGAS/STING Pathway in Pan-Cancer. *Mol Ther Nucleic Acids* (2019) 14:80–9. doi: 10.1016/j.omtn.2018.11.003
16. Bruni D, Angell HK, Galon J. The Immune Contexture and Immunoscore in Cancer Prognosis and Therapeutic Efficacy. *Nat Rev Cancer* (2020) 20(11):662–80. doi: 10.1038/s41568-020-0285-7
17. Petitprez F, Meylan M, de Reynies A, Sautes-Fridman C, Fridman WH. The Tumor Microenvironment in the Response to Immune Checkpoint Blockade Therapies. *Front Immunol* (2020) 11:784. doi: 10.3389/fimmu.2020.00784
18. Liu R, Yang F, Yin JY, Liu YZ, Zhang W, Zhou HH. Influence of Tumor Immune Infiltration on Immune Checkpoint Inhibitor Therapeutic Efficacy: A Computational Retrospective Study. *Front Immunol* (2021) 12:685370. doi: 10.3389/fimmu.2021.685370
19. Murthy AMV, Robinson N, Kumar S. Crosstalk Between cGAS-STING Signaling and Cell Death. *Cell Death Differ* (2020) 27(11):2989–3003. doi: 10.1038/s41418-020-00624-8
20. Wang-Bishop L, Wehbe M, Shae D, James J, Hacker BC, Garland K, et al. Potent STING Activation Stimulates Immunogenic Cell Death to Enhance Antitumor Immunity in Neuroblastoma. *J Immunother Cancer* (2020) 8(1):e000282. doi: 10.1136/jitc-2019-000282
21. Corrales L, Glickman LH, McWhirter SM, Kanne DB, Sivick KE, Katibah GE, et al. Direct Activation of STING in the Tumor Microenvironment Leads to Potent and Systemic Tumor Regression and Immunity. *Cell Rep* (2015) 11(7):1018–30. doi: 10.1016/j.celrep.2015.04.031
22. Marcus A, Mao AJ, Lensink-Vasan M, Wang L, Vance RE, Raulet DH. Tumor-Derived cGAMP Triggers a STING-Mediated Interferon Response in Non-Tumor Cells to Activate the NK Cell Response. *Immunity* (2018) 49(4):754–63.e4. doi: 10.1016/j.immuni.2018.09.016
23. Nicolai CJ, Wolf N, Chang IC, Kirn G, Marcus A, Ndubaku CO, et al. NK Cells Mediate Clearance of CD8(+) T Cell-Resistant Tumors in Response to STING Agonists. *Sci Immunol* (2020) 5(45):eaaz2738. doi: 10.1126/sciimmunol.aaz2738
24. Yum S, Li M, Chen ZJ. Old Dogs, New Trick: Classic Cancer Therapies Activate cGAS. *Cell Res* (2020) 30(8):639–48. doi: 10.1038/s41422-020-0346-1
25. Storozynsky Q, Hitt MM. The Impact of Radiation-Induced DNA Damage on cGAS-STING-Mediated Immune Responses to Cancer. *Int J Mol Sci* (2020) 21(22):8877. doi: 10.3390/ijms21228877
26. Deng L, Liang H, Xu M, Yang X, Burnette B, Arina A, et al. STING-Dependent Cytosolic DNA Sensing Promotes Radiation-Induced Type I Interferon-Dependent Antitumor Immunity in Immunogenic Tumors. *Immunity* (2014) 41(5):843–52. doi: 10.1016/j.immuni.2014.10.019
27. Wang H, Hu S, Chen X, Shi H, Chen C, Sun L, et al. cGAS is Essential for the Antitumor Effect of Immune Checkpoint Blockade. *Proc Natl Acad Sci USA* (2017) 114(7):1637–42. doi: 10.1073/pnas.1621363114
28. Flood BA, Higgs EF, Li S, Luke JJ, Gajewski TF. STING Pathway Agonism as a Cancer Therapeutic. *Immunol Rev* (2019) 290(1):24–38. doi: 10.1111/imr.12765
29. Marloye M, Lawler SE, Berger G. Current Patent and Clinical Status of Stimulator of Interferon Genes (STING) Agonists for Cancer Immunotherapy. *Pharm Pat Anal* (2019) 8(4):87–90. doi: 10.4155/ppa-2019-0013
30. Le Naour J, Zitvogel L, Galluzzi L, Vacchelli E, Kroemer G. Trial Watch: STING Agonists in Cancer Therapy. *Oncoimmunology* (2020) 9(1):1777624. doi: 10.1080/2162402X.2020.1777624
31. Ding C, Song Z, Shen A, Chen T, Zhang A. Small Molecules Targeting the Innate Immune Cgasstingtbk1 Signaling Pathway. *Acta Pharm Sin B* (2020) 10(12):2272–98. doi: 10.1016/j.apsb.2020.03.001
32. Vanpouille-Box C, Hoffmann JA, Galluzzi L. Pharmacological Modulation of Nucleic Acid Sensors - Therapeutic Potential and Persisting Obstacles. *Nat Rev Drug Discov* (2019) 18(11):845–67. doi: 10.1038/s41573-019-0043-2
33. Zhou W, Whiteley AT, de Oliveira Mann CC, Morehouse BR, Nowak RP, Fischer ES, et al. Structure of the Human cGAS-DNA Complex Reveals Enhanced Control of Immune Surveillance. *Cell* (2018) 174(2):300–311.e11. doi: 10.1016/j.cell.2018.06.026
34. Luecke S, Holleufer A, Christensen MH, Jonsson KL, Boni GA, Sorensen LK, et al. cGAS Is Activated by DNA in a Length-Dependent Manner. *EMBO Rep* (2017) 18(10):1707–15. doi: 10.15252/embr.201744017
35. Convertine AJ, Benoit DS, Duvall CL, Hoffman AS, Stayton PS. Development of a Novel Endosomolytic Diblock Copolymer for siRNA Delivery. *J Control Release* (2009) 133(3):221–9. doi: 10.1016/j.jconrel.2008.10.004
36. Convertine AJ, Diab C, Prieve M, Paschal A, Hoffman AS, Johnson PH, et al. pH-Responsive Polymeric Micelle Carriers for siRNA Drugs. *Biomacromolecules* (2010) 11(11):2904–11. doi: 10.1021/bm100652w

37. Palanca-Wessels MC, Convertine AJ, Cutler-Strom R, Booth GC, Lee F, Berguig GY, et al. Anti-CD22 Antibody Targeting of pH-Responsive Micelles Enhances Small Interfering RNA Delivery and Gene Silencing in Lymphoma Cells. *Mol Ther* (2011) 19(8):1529–37. doi: 10.1038/mt.2011.104
38. Nelson CE, Gupta MK, Adolph EJ, Shannon JM, Guelcher SA, Duvall CL. Sustained Local Delivery of siRNA From an Injectable Scaffold. *Biomaterials* (2012) 33(4):1154–61. doi: 10.1016/j.biomaterials.2011.10.033
39. Arany S, Xu Q, Hernady E, Benoit DS, Dewhurst S, Ovitt CE. Pro-Apoptotic Gene Knockdown Mediated by Nanocomplexed siRNA Reduces Radiation Damage in Primary Salivary Gland Cultures. *J Cell Biochem* (2012) 113 (6):1955–65. doi: 10.1002/jcb.24064
40. Arany S, Benoit DS, Dewhurst S, Ovitt CE. Nanoparticle-Mediated Gene Silencing Confers Radioprotection to Salivary Glands *In Vivo*. *Mol Ther* (2013) 21(6):1182–94. doi: 10.1038/mt.2013.42
41. Li H, Yu SS, Miteva M, Nelson CE, Werfel T, Giorgio TD, et al. Matrix Metalloproteinase Responsive, Proximity-Activated Polymeric Nanoparticles for siRNA Delivery. *Adv Funct Mater* (2013) 23(24):3040–52. doi: 10.1002/adfm.201202215
42. Nelson CE, Kim AJ, Adolph EJ, Gupta MK, Yu F, Hocking KM, et al. Tunable Delivery of siRNA From a Biodegradable Scaffold to Promote Angiogenesis *In Vivo*. *Adv Mater* (2014) 26(4):607–14, 506. doi: 10.1002/adma.201303520
43. Li H, Miteva M, Kirkbride KC, Cheng MJ, Nelson CE, Simpson EM, et al. Dual MMP7-Proximity-Activated and Folate Receptor-Targeted Nanoparticles for siRNA Delivery. *Biomacromolecules* (2015) 16(1):192–201. doi: 10.1021/bm501394m
44. Horev B, Klein MI, Hwang G, Li Y, Kim D, Koo H, et al. pH-Activated Nanoparticles for Controlled Topical Delivery of Farnesol to Disrupt Oral Biofilm Virulence. *ACS Nano* (2015) 9(3):2390–404. doi: 10.1021/nn507170s
45. Martin JR, Nelson CE, Gupta MK, Yu F, Sarett SM, Hocking KM, et al. Local Delivery of PHD2 siRNA From ROS-Degradable Scaffolds to Promote Diabetic Wound Healing. *Adv Healthc Mater* (2016) 5(21):2751–7. doi: 10.1002/adhm.201600820
46. Zhou J, Horev B, Hwang G, Klein MI, Koo H, Benoit DS. Characterization and Optimization of pH-Responsive Polymer Nanoparticles for Drug Delivery to Oral Biofilms. *J Mater Chem B* (2016) 4(18):3075–85. doi: 10.1039/C5TB02054A
47. Wang Y, Malcolm DW, Benoit DSW. Controlled and Sustained Delivery of siRNA/NPs From Hydrogels Expedites Bone Fracture Healing. *Biomaterials* (2017) 139:127–38. doi: 10.1016/j.biomaterials.2017.06.001
48. Wang Y, Zhang S, Benoit DSW. Degradable Poly(Ethylene Glycol) (PEG)-Based Hydrogels for Spatiotemporal Control of siRNA/Nanoparticle Delivery. *J Control Release* (2018) 287:58–66. doi: 10.1016/j.jconrel.2018.08.002
49. Elion DL, Jacobson ME, Hicks DJ, Rahman B, Sanchez V, Gonzales-Ericsson PI, et al. Therapeutically Active RIG-I Agonist Induces Immunogenic Tumor Cell Killing in Breast Cancers. *Cancer Res* (2018) 78(21):6183–95. doi: 10.1158/0008-5472.CAN-18-0730
50. Jacobson ME, Wang-Bishop L, Becker KW, Wilson JT. Delivery of 5'-Triphosphate RNA With Endosomolytic Nanoparticles Potently Activates RIG-I to Improve Cancer Immunotherapy. *Biomater Sci* (2019) 7(2):547–59. doi: 10.1039/C8BM01064A
51. Garland KM, Sevimli S, Kilchrist KV, Duvall CL, Cook RS, Wilson JT. Microparticle Depots for Controlled and Sustained Release of Endosomolytic Nanoparticles. *Cell Mol Bioeng* (2019) 12(5):429–42. doi: 10.1007/s12195-019-00571-6
52. Putney SD, Benkovic SJ, Schimmel PR. A DNA Fragment With an Alpha-Phosphorothioate Nucleotide at One End is Asymmetrically Blocked From Digestion by Exonuclease III and can be Replicated *In Vivo*. *Proc Natl Acad Sci USA* (1981) 78(12):7350–4. doi: 10.1073/pnas.78.12.7350
53. Cabral H, Matsumoto Y, Mizuno K, Chen Q, Murakami M, Kimura M, et al. Accumulation of Sub-100 Nm Polymeric Micelles in Poorly Permeable Tumours Depends on Size. *Nat Nanotechnol* (2011) 6(12):815–23. doi: 10.1038/nnano.2011.166
54. Pezzoli D, Giupponi E, Mantovani D, Candiani G. Size Matters for *In Vitro* Gene Delivery: Investigating the Relationships Among Complexation Protocol, Transfection Medium, Size and Sedimentation. *Sci Rep* (2017) 7:44134. doi: 10.1038/srep44134
55. Du M, Chen ZJ. DNA-Induced Liquid Phase Condensation of cGAS Activates Innate Immune Signaling. *Science* (2018) 361(6403):704–9. doi: 10.1126/science.aat1022
56. Kreiss P, Cameron B, Rangara R, Mailhe P, Aguerre-Charriol O, Airiau M, et al. Plasmid DNA Size Does Not Affect the Physicochemical Properties of Lipoplexes But Modulates Gene Transfer Efficiency. *Nucleic Acids Res* (1999) 27(19):3792–8. doi: 10.1093/nar/27.19.3792
57. Karayel E, Burckstummer T, Bilban M, Durnberger G, Weitzer S, Martinez J, et al. The TLR-Independent DNA Recognition Pathway in Murine Macrophages: Ligand Features and Molecular Signature. *Eur J Immunol* (2009) 39(7):1929–36. doi: 10.1002/eji.200939344
58. Li X, Shu C, Yi G, Chaton CT, Shelton CL, Diao J, et al. Cyclic GMP-AMP Synthase is Activated by Double-Stranded DNA-Induced Oligomerization. *Immunity* (2013) 39(6):1019–31. doi: 10.1016/j.immuni.2013.10.019
59. Stetson DB, Medzhitov R. Recognition of Cytosolic DNA Activates an IRF3-Dependent Innate Immune Response. *Immunity* (2006) 24(1):93–103. doi: 10.1016/j.immuni.2005.12.003
60. Andreeva L, Hiller B, Kostrewa D, Lassig C, de Oliveira Mann CC, Jan Drexler D, et al. cGAS Senses Long and HMGB/TFAM-Bound U-Turn DNA by Forming Protein-DNA Ladders. *Nature* (2017) 549(7672):394–8. doi: 10.1038/nature23890
61. Vincent J, Adura C, Gao P, Luz A, Lama L, Asano Y, et al. Small Molecule Inhibition of cGAS Reduces Interferon Expression in Primary Macrophages From Autoimmune Mice. *Nat Commun* (2017) 8(1):750. doi: 10.1038/s41467-017-00833-9
62. Wiser C, Kim B, Vincent J, Ascano M. Small Molecule Inhibition of Human cGAS Reduces Total cGAMP Output and Cytokine Expression in Cells. *Sci Rep* (2020) 10(1):7604. doi: 10.1101/2020.03.30.016535
63. Wei X, Shao B, He Z, Ye T, Luo M, Sang Y, et al. Cationic Nanocarriers Induce Cell Necrosis Through Impairment of Na(+)/K(+)-ATPase and Cause Subsequent Inflammatory Response. *Cell Res* (2015) 25(2):237–53. doi: 10.1038/cr.2015.9
64. Liu L, Liu Y, Xu B, Liu C, Jia Y, Liu T, et al. Negative Regulation of Cationic Nanoparticle-Induced Inflammatory Toxicity Through the Increased Production of Prostaglandin E2 via Mitochondrial DNA-Activated Ly6C (+) Monocytes. *Theranostics* (2018) 8(11):3138–52. doi: 10.7150/thno.21693
65. Kosuri S, Church GM. Large-Scale De Novo DNA Synthesis: Technologies and Applications. *Nat Methods* (2014) 11(5):499–507. doi: 10.1038/nmeth.2918
66. Shivalingam A, Brown T. Synthesis of Chemically Modified DNA. *Biochem Soc Trans* (2016) 44(3):709–15. doi: 10.1042/BST20160051
67. Pandey S, Kawai T. Chapter 5 - Host DNA Induced Inflammation and Autoimmune Diseases. In: Ishii KJ, Tang CK, editors. *Biological DNA Sensor*. Amsterdam: Academic Press (2014). p. 103–32.
68. Baranovskii AG, Buneva VN, Nevinsky GA. Human Deoxyribonucleases. *Biochem (Mosc)* (2004) 69(6):587–601. doi: 10.1023/B:BIRY.0000033731.50496.01
69. Benmerzoug S, Ryffel B, Togbe D, Quesniaux VFJ. Self-DNA Sensing in Lung Inflammatory Diseases. *Trends Immunol* (2019) 40(8):719–34. doi: 10.1016/j.it.2019.06.001
70. Wang Q, Liu X, Zhou Q, Wang C. Cytosolic Sensing of Aberrant DNA: Arming STING on the Endoplasmic Reticulum. *Expert Opin Ther Targets* (2015) 19(10):1397–409. doi: 10.1517/14728222.2015.1067303
71. Napirei M, Karsunky H, Zevnik B, Stephan H, Mannherz HG, Moroy T. Features of Systemic Lupus Erythematosus in Dnase1-Deficient Mice. *Nat Genet* (2000) 25(2):177–81. doi: 10.1038/76032
72. Prince WS, Baker DL, Dodge AH, Ahmed AE, Chestnut RW, Sinicropi DV. Pharmacodynamics of Recombinant Human DNase I in Serum. *Clin Exp Immunol* (1998) 113(2):289–96. doi: 10.1046/j.1365-2249.1998.00647.x
73. Gehrke N, Mertens C, Zillinger T, Wenzel J, Bald T, Zahn S, et al. Oxidative Damage of DNA Confers Resistance to Cytosolic Nuclease TREX1 Degradation and Potentiates STING-Dependent Immune Sensing. *Immunity* (2013) 39(3):482–95. doi: 10.1016/j.immuni.2013.08.004
74. Hemphill WO, Simpson SR, Liu M, Salsbury FRJr., Hollis T, Grayson JM, et al. TREX1 as a Novel Immunotherapeutic Target. *Front Immunol* (2021) 12:660184. doi: 10.3389/fimmu.2021.660184
75. Steinhagen F, Zillinger T, Peukert K, Fox M, Thudium M, Barchet W, et al. Suppressive Oligodeoxynucleotides Containing TTAGGG Motifs Inhibit cGAS Activation in Human Monocytes. *Eur J Immunol* (2018) 48(4):605–11. doi: 10.1002/eji.201747338

76. Counis MF, Torriglia A. Acid DNases and Their Interest Among Apoptotic Endonucleases. *Biochimie* (2006) 88(12):1851–8. doi: 10.1016/j.biochi.2006.07.008
77. Roberts TC, Langer R, Wood MJA. Advances in Oligonucleotide Drug Delivery. *Nat Rev Drug Discov* (2020) 19(10):673–94. doi: 10.1038/s41573-020-0075-7
78. de la Harpe KM, Kondiah PPD, Choonara YE, Marimuthu T, du Toit LC, Pillay V. The Hemocompatibility of Nanoparticles: A Review of Cell-Nanoparticle Interactions and Hemostasis. *Cells* (2019) 8(10):1209. doi: 10.3390/cells8101209
79. Melero I, Castanon E, Alvarez M, Champiat S, Marabelle A. Intratumoural Administration and Tumour Tissue Targeting of Cancer Immunotherapies. *Nat Rev Clin Oncol* (2021) 18:558–76. doi: 10.1038/s41571-021-00507-y
80. Peynshaert K, Manshian BB, Joris F, Braeckmans K, De Smedt SC, Demeester J, et al. Exploiting Intrinsic Nanoparticle Toxicity: The Pros and Cons of Nanoparticle-Induced Autophagy in Biomedical Research. *Chem Rev* (2014) 114(15):7581–609. doi: 10.1021/cr400372p
81. Chen DS, Mellman I. Oncology Meets Immunology: The Cancer-Immunity Cycle. *Immunity* (2013) 39(1):1–10. doi: 10.1016/j.immuni.2013.07.012
82. Waldman AD, Fritz JM, Lenardo MJ. A Guide to Cancer Immunotherapy: From T Cell Basic Science to Clinical Practice. *Nat Rev Immunol* (2020) 20(11):651–68. doi: 10.1038/s41577-020-0306-5
83. Skrnjug I, Guzman CA, Rueckert C. Cyclic GMP-AMP Displays Mucosal Adjuvant Activity in Mice. *PloS One* (2014) 9(10):e110150. doi: 10.1371/journal.pone.0110150
84. Gutjahr A, Papagno L, Nicoli F, Kanuma T, Kuse N, Cabral-Piccin MP, et al. The STING Ligand cGAMP Potentiates the Efficacy of Vaccine-Induced CD8+ T Cells. *JCI Insight* (2019) 4(7):e125107. doi: 10.1172/jci.insight.125107
85. Bourquin C, Anz D, Zwiorek K, Lanz AL, Fuchs S, Weigel S, et al. Targeting CpG Oligonucleotides to the Lymph Node by Nanoparticles Elicits Efficient Antitumoral Immunity. *J Immunol* (2008) 181(5):2990–8. doi: 10.4049/jimmunol.181.5.2990
86. Liu H, Moynihan KD, Zheng Y, Szeto GL, Li AV, Huang B, et al. Structure-Based Programming of Lymph-Node Targeting in Molecular Vaccines. *Nature* (2014) 507(7493):519–22. doi: 10.1038/nature12978
87. Li S, Luo M, Wang Z, Feng Q, Wilhelm J, Wang X, et al. Prolonged Activation of Innate Immune Pathways by a Polyvalent STING Agonist. *Nat BioMed Eng* (2021) 5(5):455–66. doi: 10.1038/s41551-020-00675-9
88. Shae D, Becker KW, Christov P, Yun DS, Lytton-Jean AKR, Sevimli S, et al. Endosomolytic Polymersomes Increase the Activity of Cyclic Dinucleotide STING Agonists to Enhance Cancer Immunotherapy. *Nat Nanotechnol* (2019) 14(3):269–78. doi: 10.1038/s41565-018-0342-5
89. Zheng J, Mo J, Zhu T, Zhuo W, Yi Y, Hu S, et al. Comprehensive Elaboration of the cGAS-STING Signaling Axis in Cancer Development and Immunotherapy. *Mol Cancer* (2020) 19(1):133. doi: 10.1186/s12943-020-01250-1
90. Franklin DA, Sharick JT, Ericsson-Gonzalez PI, Sanchez V, Dean PT, Opalenik SR, et al. MEK Activation Modulates Glycolysis and Supports Suppressive Myeloid Cells in TNBC. *JCI Insight* (2020) 5(15):e134290. doi: 10.1172/jci.insight.134290
91. Cheng N, Watkins-Schulz R, Junkins RD, David CN, Johnson BM, Montgomery SA, et al. A Nanoparticle-Incorporated STING Activator Enhances Antitumor Immunity in PD-L1-Insensitive Models of Triple-Negative Breast Cancer. *JCI Insight* (2018) 3(22):e120638. doi: 10.1172/jci.insight.120638
92. Downey CM, Aghaei M, Schwendener RA, Jirik FR. DMXAA Causes Tumor Site-Specific Vascular Disruption in Murine Non-Small Cell Lung Cancer, and Like the Endogenous Non-Canonical Cyclic Dinucleotide STING Agonist, 2'3'-cGAMP, Induces M2 Macrophage Repolarization. *PloS One* (2014) 9(6):e99988. doi: 10.1371/journal.pone.0099988
93. Ahn J, Xia T, Rabasa Capote A, Betancourt D, Barber GN. Extrinsic Phagocyte-Dependent STING Signaling Dictates the Immunogenicity of Dying Cells. *Cancer Cell* (2018) 33(5):862–73.e5. doi: 10.1016/j.ccell.2018.03.027
94. Liu C, Lou Y, Lizee G, Qin H, Liu S, Rabinovich B, et al. Plasmacytoid Dendritic Cells Induce NK Cell-Dependent, Tumor Antigen-Specific T Cell Cross-Priming and Tumor Regression in Mice. *J Clin Invest* (2008) 118(3):1165–75. doi: 10.1172/JCI33583
95. Ribas A, Medina T, Kirkwood JM, Zakharia Y, Gonzalez R, Davar D, et al. Overcoming PD-1 Blockade Resistance With CpG-A Toll-Like Receptor 9 Agonist Vidutolimod in Patients With Metastatic Melanoma. *Cancer Discov* (2021) candisc.0425.2021. doi: 10.1158/2159-8290.CD-21-0425
96. Hornung V, Rothenfusser S, Britsch S, Krug A, Jahrsdorfer B, Giese T, et al. Quantitative Expression of Toll-Like Receptor 1-10 mRNA in Cellular Subsets of Human Peripheral Blood Mononuclear Cells and Sensitivity to CpG Oligodeoxynucleotides. *J Immunol* (2002) 168(9):4531–7. doi: 10.4049/jimmunol.168.9.4531
97. Uhlen M, Fagerberg L, Hallstrom BM, Lindskog C, Oksvold P, Mardinoglu A, et al. Proteomics. Tissue-Based Map of the Human Proteome. *Science* (2015) 347(6220):1260419. doi: 10.1126/science.1260419
98. Uhlen M, Zhang C, Lee S, Sjostedt E, Fagerberg L, Bidkhori G, et al. A Pathology Atlas of the Human Cancer Transcriptome. *Science* (2017) 357(6352):eaan2507. doi: 10.1126/science.aan2507
99. Verrier ER, Langevin C. Cyclic Guanosine Monophosphate-Adenosine Monophosphate Synthase (cGAS), a Multifaceted Platform of Intracellular DNA Sensing. *Front Immunol* (2021) 12:637399. doi: 10.3389/fimmu.2021.637399
100. Ablasser A, Schmid-Burgk JL, Hemmerling I, Horvath GL, Schmidt T, Latz E, et al. Cell Intrinsic Immunity Spreads to Bystander Cells via the Intercellular Transfer of cGAMP. *Nature* (2013) 503(7477):530–4. doi: 10.1038/nature12640
101. Zhou C, Chen X, Planells-Cases R, Chu J, Wang L, Cao L, et al. Transfer of cGAMP Into Bystander Cells via LRRC8 Volume-Regulated Anion Channels Augments STING-Mediated Interferon Responses and Anti-Viral Immunity. *Immunity* (2020) 52(5):767–81.e6. doi: 10.1016/j.immuni.2020.03.016
102. Lahey LJ, Mardjuki RE, Wen X, Hess GT, Ritchie C, Carozza JA, et al. LRRC8A:C/E Heteromeric Channels Are Ubiquitous Transporters of cGAMP. *Mol Cell* (2020) 80(4):578–91.e5. doi: 10.1016/j.molcel.2020.10.021
103. Huang L, Wang Z, Liu C, Xu C, Mbofung RM, McKenzie JA, et al. CpG-Based Immunotherapy Impairs Antitumor Activity of BRAF Inhibitors in a B-Cell-Dependent Manner. *Oncogene* (2017) 36(28):4081–6. doi: 10.1038/onc.2017.35
104. Chipurupalli S, Ganesan R, Dhanabal SP, Kumar MS, Robinson N. Pharmacological STING Activation Is a Potential Alternative to Overcome Drug-Resistance in Melanoma. *Front Oncol* (2020) 10:758. doi: 10.3389/fonc.2020.00758
105. Knight FC, Gilchuk P, Kumar A, Becker KW, Sevimli S, Jacobson ME, et al. Mucosal Immunization With a pH-Responsive Nanoparticle Vaccine Induces Protective CD8(+) Lung-Resident Memory T Cells. *ACS Nano* (2019) 13(10):10939–60. doi: 10.1021/acsnano.9b00326
106. Liang H, Deng L, Hou Y, Meng X, Huang X, Rao E, et al. Host STING-Dependent MDSC Mobilization Drives Extrinsic Radiation Resistance. *Nat Commun* (2017) 8(1):1736. doi: 10.1038/s41467-017-01566-5
107. Corrales L, Woo SR, Williams JB, McWhirter SM, Dubensky TW Jr, Gajewski TF. Antagonism of the STING Pathway via Activation of the AIM2 Inflammasome by Intracellular DNA. *J Immunol* (2016) 196(7):3191–8. doi: 10.4049/jimmunol.1502538
108. Ferritto M, Tirrell DA, Macromolecular Syntheses. In: D.A. Tirrell, editor. *Poly(2-Ethylacrylic Acid)*, vol. 11. Hattiesburg, Mississippi: MRG Polymer Press (1992) Library of Congress Catalog Card Number: 63–18627.

Conflict of Interest: The authors declare that the research was conducted in the absence of any commercial or financial relationships that could be construed as a potential conflict of interest.

Publisher's Note: All claims expressed in this article are solely those of the authors and do not necessarily represent those of their affiliated organizations, or those of the publisher, the editors and the reviewers. Any product that may be evaluated in this article, or claim that may be made by its manufacturer, is not guaranteed or endorsed by the publisher.

frontiers in Immunology

REVIEW
published: 07 March 2022
doi: 10.3389/fimmu.2022.818538

Myeloid Responses to Extracellular Vesicles in Health and Disease

Priya Makhijani[1,2] *and Tracy L. McGaha*[1,2*]

[1] Department of Immunology, University of Toronto, Toronto, ON, Canada, [2] Tumor Immunotherapy Program, Princess Margaret Cancer Center, University Health Network, Toronto, ON, Canada

Extracellular vesicles are mediators of cell-cell communication playing a key role in both steady-state and disease conditions. Extracellular vesicles carry diverse donor-derived cargos, including DNA, RNA, proteins, and lipids that induce a complex network of signals in recipient cells. Due to their ability to capture particulate matter and/or capacity to polarize and orchestrate tissue responses, myeloid immune cells (e.g., dendritic cells, macrophages, etc.) rapidly respond to extracellular vesicles, driving local and systemic effects. In cancer, myeloid-extracellular vesicle communication contributes to chronic inflammation, self-tolerance, and therapeutic resistance while in autoimmune disease, extracellular vesicles support inflammation and tissue destruction. Here, we review cellular mechanisms by which extracellular vesicles modulate myeloid immunity in cancer and autoimmune disease, highlighting some contradictory results and outstanding questions. We will also summarize how understanding of extracellular vesicle biology is being utilized for novel therapeutic and diagnostic applications.

Keywords: macrophage, extracellular vesicle, cancer, autoimmune disease, inflammation

OPEN ACCESS

Edited by:
David Pozo,
University of Seville, Spain

Reviewed by:
Lei Shi,
Georgia State University, United States
Sherri L. Christian,
Memorial University of Newfoundland, Canada

****Correspondence:***
Tracy L. McGaha
tmcgaha@uhnresearch.ca

Specialty section:
This article was submitted to Molecular Innate Immunity, a section of the journal Frontiers in Immunology

Received: *19 November 2021*
Accepted: *15 February 2022*
Published: *07 March 2022*

Citation:
Makhijani P and McGaha TL (2022) Myeloid Responses to Extracellular Vesicles in Health and Disease. Front. Immunol. 13:818538. doi: 10.3389/fimmu.2022.818538

1 INTRODUCTION

Extracellular vesicles (EVs) are phospholipid bilayer-bound particles shown to be produced by all tested cell types. These cell-derived vesicles are released into the extracellular space accumulating in tissue, circulation and other fluids (1). Studies on EV cargo, subtype heterogeneity, and cell responses have shown they play diverse roles in health and disease. EV cargos include protein, DNA, mRNA, non-coding RNA and lipids from the donor cell, with specific cargo enrichment depending on cell status and EV subtype (2). The three most examined subtypes of EVs are apoptotic bodies (ABs), ectosomes and exosomes, though novel EV subtypes are still being identified. EVs can elicit potent autocrine, paracrine, and systemic responses in many cell types including in macrophages, endothelial cell, and lymphocytes (3). EV responses have been shown to regulate physiological processes including inflammation and tissue regeneration (3). Therefore, EVs are increasingly recognized as key mediators of intra- and inter-cellular communication, akin to cytokine signals. However, unlike most cytokines, EVs are highly stable and carry diverse cargo allowing EVs to drive complex responses both locally and at distant sites. Responses to EVs are dictated by many factors including capture mechanisms and physiological context. EVs are internalized *via* multiple mechanisms including receptor-mediated and lipid-raft mediated endocytosis, phagocytosis, and pinocytosis (3). Depending on route of internalization, EV cargo is delivered to different cellular compartments driving rapid recycling, interaction with endosomal receptors, and/or antigen

presentation leading to different responses (4). EV responses *via* cell surface receptor interactions have also been reported, especially in cells that are poor at EV capture. For example, exosomal PD-L1 binds to PD-1 on the surface of T cells and TIM-4 has been shown to interact with phosphatidylserine on ABs, both driving immune suppression (5, 6).

In this review, we focus on EV responses in myeloid cells. Myeloid cells (e.g., macrophages, neutrophils, dendritic cells) are a key component of innate and adaptive immunity outnumbering other immune cells in most tissues. Importantly, myeloid cells can readily capture particulate materials and are key drivers and modulators of inflammation and tissue repair. Therefore, myeloid cells are likely highly responsive to EVs, driven by their receptor expression and/or capacity for phagocytosis and pinocytosis. Physiological context has become an important consideration in understanding EV responses, dictating which cargos are loaded into EVs as well as how recipient cells respond, including their capacity for uptake and stress or activation status (7). As such, EVs can serve opposing roles in autoimmunity and cancer depending on the inflammatory context. At steady-state innate cells capture EVs maintaining homeostasis and self-tolerance. In cancer, these mechanisms may function to dampen immune surveillance and promote chronic inflammation (8). EVs also play a progressive role as their systemic accumulation increases as we will later see in the example of metastasis. In autoimmunity, we see that the same EV cargo can promote the breakdown of immune tolerance driven by the inflammatory milieu.

Understanding how EVs drive physiological processes and identifying representative EV cargo signatures in pathological states is being utilized for therapeutic targeting and disease diagnosis. However, the role of EVs is only partially understood as the field of EV research is currently still in its infancy, and requires refinement in limitations of detection and isolation (1) as well as resolving contradictory results. The excitement around uncovering new biological mechanisms driven by these small particles, however, is generating rapid progress in the field. Here, we will examine what is known regarding mechanistic interactions between EV cargo and myeloid cells—defining a paradigm for understanding the mixed responses to EV cargo. We will also comment on the viability of therapeutic opportunities EVs generate, including inhibitory targeting of biogenesis and transfusion of EVs with an artificial therapeutic load and as vaccines.

2 EV HETEROGENEITY

There are currently three well described subtypes of EVs, differentiated by size and the cell processes responsible for their production. Apoptotic bodies are the largest and most studied class of EVs produced as a result of programmed cell death (2). Ectosomes and exosomes are smaller on average, jointly called small EVs (sEVs), and are produced by living cells. Differentiating the two sEVs, ectosomes are shed directly from the cell surface while exosomes (the smaller of the two sEV categories) originate from the cellular lumen bearing protein markers of their endocytic origin (9). The first EVs to be reported were ABs (50nm-5μm), as apoptosis was being closely studied in the 1960s (10). Microparticles (MPs, 50nm-1μm), also referred to as ectosomes, were first described in 1967 in the context of platelets and blood coagulation (11). The smallest EVs, exosomes (30-150nm) were first identified in the early 1980s (12, 13) in the study of transferrin receptor loss during reticulocyte maturation. These two sEV subtypes collectively were shown to be produced by healthy living cells of nearly all types—with EV dysfunction observed under cellular stress (14). The details of EV biogenesis have been recently reviewed elsewhere (3) and will not be covered here. Although the intracellular origin of the each EV subtype can be tracked, attempts to describe EV biogenesis and heterogeneity is confounded by overlapping size and biomarker criteria (2). Moreover, new classes of EVs are continually being identified including exophers (15), cytokine vesicles (16) and midbody remnants (17). The lack of consistent nomenclature in the field and biomarker oversimplification has driven pragmatic researchers to choose simpler terms like small and large EV to broadly understand biological functions.

2.1 Classical and Non-Classical EV Subtypes

Correctly characterizing and naming EVs is necessary for understanding each EV's distinct physiological role. In a recent review, Kalluri and LeBleu streamline EVs into two categories, EVs shed from the plasma membrane of the cell as ectosomes, and EVs originating from intracellular compartments as exosomes (9). While this system works for such classical EVs, other particles must be included as non-classical subtypes (**Figure 1**). Specifically, this taxonomic classification of EVs does not fully capture EV heterogeneity, especially pertaining to large EVs. While some large EVs like oncosomes (<10μm), shed from the membrane of amoeboid tumor cells, fit into their system as ectosomes, ABs and exophers do not (18). ABs can neither be characterized as large or small EVs because of their wide size range nor as ectosomes or exosomes produced by live cells because they are formed out of complete cell components from dying cells. Also, the 4 μm exophers described recently in cardiomyocytes (15) and neurons (19), though containing intracellular mitochondrial components are too large to meet the exosome biogenesis criteria. Since exosome production involves formation of intraluminal vesicles (ILVs), exosomes are limited to ILV size between 30nm and 150nm (2). Further, Nicolás-Ávila et al. predict that production of exophers is related to autophagy dependant waste removal of abnormal mitochondria and protein, while exosomes are considered active agents of cell communication—although this has proven difficult to confirm. The authors also highlight that exophers are unrelated to ABs since apoptosis is not expected in quiescent cardiomyocytes or neurons. To enable accurate classification of such particles and to attribute responses correctly, we must include both exophers and ABs into the taxonomy of EVs. Inclusive criteria allow better resolution between particles, prevent misclassification, and can improve our understanding of complex EV responses.

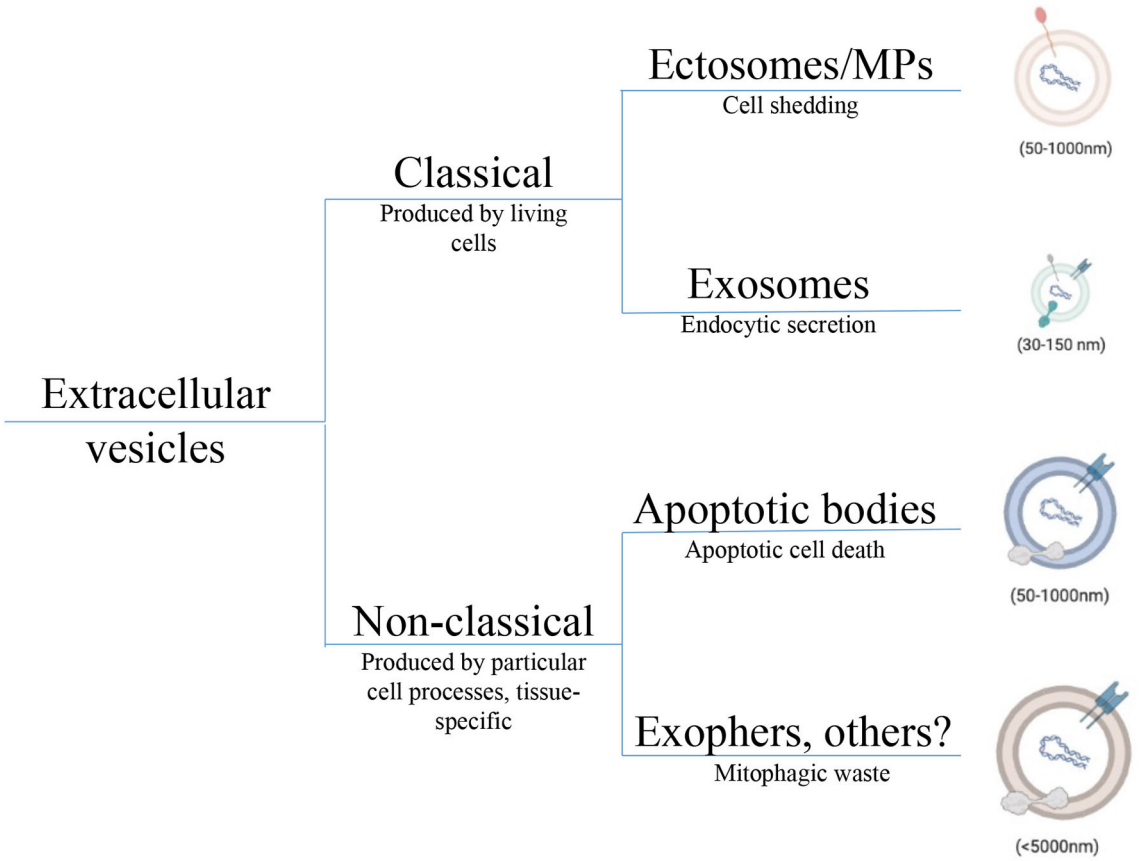

FIGURE 1 | Taxonomic tree depicting EV heterogeneity. Diversity in EV populations can be grouped into classical and non-classical subtypes. Classical EVs are produced by health living cells; either shed from the cell surface as ectosomes, also called microparticles, or derived from inside the cell as exosomes. Although exosomes and ectosomes carry similar cargos including proteins, lipids, and nucleic acids, species of endocytic origin (e.g., HSPs, mtDNA) are only expected in exosomes. Non-classical EVs tend to be larger and correspond to a wide array of cell processes and include species like apoptotic bodies from dying cells, exophers released from neurons and cardiomyocytes as metabolic waste, and oncosomes derived from certain tumor cells. Non-classical subtyping allows for a better understanding of novel EVs that do not fit classical criteria preventing their misclassification. Cargos in each non-classical EV subtype are distinct but not fully understood. EV, Extracellular vesicle; HSP, Heat shock protein; mtDNA, Mitochondrial DNA.

To create consistency across different EV subtypes, the minimal information for studies of extracellular vesicles (MISEV) 2018 statement recommended the use thorough biomarker characterization of EVs (20). However, authors also acknowledge that defining EVs by biomarkers that reflect their biogenesis also leads to significant overlap between EV subtypes. Importantly, this limits tracking of EVs *in vivo* resulting in a lack of knowledge on rates of production and physiologically relevant EV concentrations. Consequently, most studies rely on *in vitro* derived EVs from a single cell or body fluid source used for treatment *in vitro* or for *in vivo* transfer. EV isolation methods rely on size- and density-based ultracentrifugation, size-exclusion columns, polyethylene glycol precipitation or microfluids-based immunoprecipitation, with each method yielding a partially pure EV population (1). Although small (s) EVs and be easily separated from large (l)EVs using these isolation methods, sEV isolation results in co-precipitation of other species in biofluid or media (16, 21). Heterogenous EV preparations confound our understanding of EV cargo signatures as well as cellular responses to EV treatment. More sophisticated isolation procedures, definitive biomarkers, basic biogenesis research, and nanoscale experimentation will be required for progress in this field. In the meantime, these limitations must be considered while studying the role EVs play in physiological processes.

3 TUMOR EVS AND MYELOID-DRIVEN INFLAMMATION

The heterogeneous cell populations in solid tumors and hematological malignancies produce a diversity of EV populations, changing by disease stage and therapeutic intervention. Understanding the diversity of EV populations within the tumor microenvironment (TME) as well as their nuanced effects on tumor pathology has been confounded by

isolation and biomarker limitations. However, extensive characterization of immune responses to EVs in multiple cancer models have revealed the key role EVs play in chronic inflammation and immune tolerance. Innate immune cells are often abundant in the TME and express a wide array of receptors that capture or interact with EV particles suggesting that EVs regulate immunity by impacting innate immune function in the local tumor milieu. Supporting this prediction, studies have shown blocking EV production by tumor cells correlates with decreased overall immune responses in the TME (5) and increased myeloid cell infiltration, suppressive polarization, and differentiation (22–24) In this section, we will describe known molecular mechanisms of tumor EVs driven dysfunction in myeloid immune cells promoting chronic inflammation and immune tolerance in the tumor.

3.1 EV Dysfunction in the Tumor Microenvironment

Addressing the role EVs play in tumor pathophysiology begins with understanding the nature of EV production in the TME. While increased plasma EV concentration in cancer patients compared to healthy donors has been reported for many tumor types (25), production of EVs by the tumor and tumor-associated cells cannot be directly confirmed with current methodology. However, several studies suggest that tumor-associated cells produce higher levels of EVs with unique molecular signatures. EV biogenesis genes like Rab27 are upregulated in tumors and associated with poor prognosis (26). Further, hypoxia (27–30) and the cytokine milieu (e.g. IFNγ, TGFβ) in the TME modulate EV biogenesis and cargo loading (31). Basal levels of stress (7, 14) and therapeutic interventions like radiation (32) can also alter EV levels and composition. The normal response to stress *via* the tumor suppressor p53 was shown to drive exosome biogenesis *via* the TSAP6 protein, suggesting abnormal exosome production by p53 mutated tumor cells (33). Activating KRAS mutations, found in many different tumor types, have been shown to control miRNA loading into exosomes. McKenzie et al. found lower levels of *let-7a* miRNA packaged into exosomes when Ago2 is phosphorylated by the activated KRAS (34). *Let-7a* miRNA has been show to target KRAS with decreased levels been reported in KRAS and BRAF tumors (35). Furthermore, high levels of *let-7a* were shown to promote anti-tumor microglia activation (36), suggesting a role for exosomes on innate myeloid cell responses. Together, tumor mutations and TME stimuli may drive a unique EV signature impacting systemic and local tumor immune responses.

3.2 EVs and the Tumor Wound Hypothesis

Tumor promoting inflammation and immune suppression in the TME has been understood by drawing parallels between the tumor and a healing wound (37). In the "tumor wound" concept, the TME hijacks wound healing mechanisms driving immunosuppressive and reparative stages of inflammation without resolution stage, resulting in a chronic wound-like state. In injured tissue damaged cells release a wide range of damage-associate molecular patterns (DAMPs) including heat shock proteins (HSPs), Glypicans, HMGB1, mitochondrial DNA (mtDNA) driving the production of alarmins (IL-1, IL-33) and other effectors that recruit and activate immune effectors *via* pattern-recognition receptors (PRRs) (38). In the TME, tumor-derived DAMPs can include mitochondrial components released due to the Warburg effect, miRNA and HSPs released due to genetic mutations and other factors like hypoxia. These DAMPs have been widely reported in tumor EVs across many tumor models (**Table 1**) and can drive inflammation in the tumor. In the healing wound, other signals from the unvascularized repairing tissue, hypoxia for example, drive a switch from acute inflammation to tolerance, where alternatively activated myeloid cells promote the immunosuppressive, pro-angiogenic and fibrotic stages of wound healing. A growing tumor is similarly supported by the suppression of anti-tumor immunity, angiogenesis and fibrosis. The mechanisms that sustain tumor growth in an unresolving state are not fully understood. However, the continuous exposure to EV-DAMPs to myeloid cells poised for particle capture, may contribute to tumor promoting inflammation. The signalling pathways stimulated upon EV exposure point to a key role of EV-mediated induction of tumor promoting inflammation.

TABLE 1 | Examples of EV cargo effects on signalling in myeloid cells.

Cargo	Species	Function on myeloid immune cells
DNA	gDNA Micronuclei (39)	Cytoplasmic STING activation in dendritic cells
	mitoDNA (40)	Endosomal TLR9-mediated suppressive macrophage polarization
RNA	miRNA (41)	STAT3-mediated MDSC activation
	Y-RNA (42)	TLR7 mediated PDL-1 upregulation in monocytes
	dsRNA (43)	TLR3-mediated neutrophil recruitment at metastatic sites
	lncRNA-HOTAIRM1 (44)	MDSC expansion *via* STAT3
Mitochondria	Cardiac autophagy (15)	Phagocytic clearance by macrophage supports tissue homeostasis
Lipids	Phosphatidylserine (45)	Receptor-mediated regulatory macrophage polarization
Cytokines	TGF-β1 (46)	Dendritic cell driven T cell suppression
Self-antigen	MART1 (47)	Delivery of tumor antigen to activated dendritic cells
Checkpoint molecules	PDL1 (5)	Delivery of PDL1 to myeloid cells leads to systemic T cell exhaustion
Integrins	Tissue specific integrin signature (48)	Integrins prime Kuppfer cells for liver metastasis
Microbiome components	Gram negative cell wall components (49)	TLR-4 ligands in bacterial EVs activate innate immune cells

3.2.1 Vesicular TLR-Ligand Driven Inflammation

Myeloid cells express a battery of pattern-recognition receptors including Toll-like receptors (TLR), retinoic-acid inducible gene (RIG-I), and stimulator of interferon genes (STING) that are highly responsive to DAMPs allowing rapid immune reactivity to tissue injury (50). In the tumor, EV-DAMPs have been shown to engage both plasma membrane-localized TLRs (e.g., TLR2 and TLR4) and endosomal TLRs (e.g. TLR3, 7, and 9) driving potent responses *via* the transcription factor, NFκB (51). In breast cancer, palmitoylated proteins in tumor EVs can act as TLR2 ligands leading to upregulation of proinflammatory cytokines and chemokines including CCL2, IL-6 and GCSF in macrophages (52). TLR2 ligand, HMGB-1 was also found in lung cancer and shown to drive NF-κB-dependent metabolic reprogramming of macrophages at metastatic sites (53). Also using a lung cancer model, Fabbri et al. demonstrated that exosomal miRNAs (i.e. miR-21 and miR-29a) induce IL-6 and TNFα in macrophages *via* a TLR7-NFκB dependent mechanism promoting inflammation and metastasis (54). Similarly, exosomal RNA can activate TLR3 promoting neutrophil recruitment at metastatic sites *via* induced expression of CXCL chemokines (43). To offer further insight into which RNA species are EV associated, an atlas of vesicular and non-vesicular RNA from healthy biofluids was recently published (55). In pancreatic cancer, sEVs from were shown to carry genomic dsDNA (56) that act as a TLR-9 ligand activating myeloid cells (57). However, Jeppesen et al. showed that genomic dsDNA-TLR9 ligands are secreted from tumor cells independent of exosomes, while HSP-TLR2 and RNA-TLR7 ligands are enriched in sEVs (21). Jeppesen et al. argue that genomic DNA (gDNA) does not exist in the same subcellular location for endosomal loading required for exosome biogenesis. However, gDNA may become exosome associated, adhering to positively charged EVs prior to capture by donor cells. The presence of double stranded mitochondrial DNA (mtDNA) is less controversial due to subcellular location. MtDNA has been observed in breast and prostate cancer EVs at higher concentrations that noncancer epithelia (58). Although transfer of mt-DNA between cell types is likely EV-mediated, most researchers have studied the role of mt-DNA alone. Mt-DNA has been shown to induce TLR9-mediated NF-κB activation driving regulatory polarization in macrophages in liver cancer (59) as well as activation of neutrophils in various forms of injury (60). Further, non-immune cancer-associated fibroblasts were also shown respond to mt-DNA *via* TLR-9 contributing to therapeutic resistance to taxanes (40). In addition to inflammatory modulation, mutations in tumor mt-DNA can also regulate mitochondrial metabolism in recipient cells (61) but have not been well-studied in the context of myeloid immunity. Size-based EV isolation procedures leading to the co-precipitation of non-vesicular nucleic acids and other molecules will confound data on EV-mediated gene induction until more specific isolation methods are found.

DAMP-TLR activation in myeloid cells can drive both pro-inflammatory and regulatory responses *via* mechanisms that are not fully understood. One hypothesis is that pro-inflammatory effectors are expected to drive pleiotropic effects on immune cells and other cells of the body, supporting both inflammatory and suppressive responses in a context dependent manner. In the context of macrophages in chronic conditions, experts have encouraged a spectrum polarization model over the dichotomous M1-M2 model, which better describes acute conditions. This integrative spectrum model also allows for a better understanding of chronic inflammation driven by tumor EVs. Interestingly, EV studies described here show upregulation of both pro- and anti-inflammatory cytokines and effectors in myeloid cells pointing to concomitant responses to mixed EV cargo. Secondly, chronic exposure to TLR ligands drives negative feedback mechanisms that lead to reduced inflammatory cytokine and increased regulatory cytokine production. Repeat treatments with DNA drive tolerance in macrophages *via* TLR-9 as seen by reduced TNFα production (62), mimicking the chronic nature of EV responses. This chronic exposure to TLR ligands is also expected to dictate hematopoietic outcomes starting in the bone marrow, driving a myeloid differentiation bias leading to reduced lymphoid to myeloid ratios in blood (63), with trained immunity being a common feature of aging and cancer pathophysiology (64).

3.2.2 STAT3 Driven Inflammation

Upon TLR activation of NFκB transcriptional program a further activation of STAT3 is driven by autocrine IL-6 stimulation, in turn amplifying the overall inflammatory response (65). Chalmin et al. demonstrated the TLR2 ligand Hsp70, found on the exosome surface, activates STAT3 in MDSCs *via* autocrine action of IL-6 (66). These activated MDSCs produce IL-10 and upregulate arginase 1 activity inhibiting T cell proliferation. The EV-driven IL-6-STAT3 axis was also shown to keep bone marrow precursors in an immature state inhibiting the differentiation to mature DCs capable of anti-tumor responses (24). A STAT3 regulatory signature was also observed in monocytes treated with glioblastoma exosomes correlating with increased interferon-ɣ production (67). A similar TLR2/4-STAT3 response driven by HSPs was seen in bone marrow-derived dendritic cells (BMDCs) promoting a pro-tumor IL-6, PGE-2, IL-1, and TNF response after exosome treatment (68).

EVs have also been shown to control the NFκB-STAT3 axis *via* the action of specific miRNA cargo. Both NFκB-driven and exosomal *miR-21a* was shown to silence PDCD4, a tumor suppressor and IL-6 inhibitor, promoting the expansion of MDSCs in a IL-6/STAT3 dependant manner in lung cancer (69). Exosomal *miR-106b* found in colorectal cancer also suppresses PDCD4 driving both IL-6/STAT3 and mTOR signalling to promoting regulatory polarization in tumor macrophages (70). The exosomal *miR-222-3p* in ovarian cancer, has been shown to silence SOCS3 in monocytes promoting a STAT3-mediated regulatory signature in macrophages including Arg1 and CD206 expression (71). It is not clear whether the concentration of miRNA in sEVs can reach a local concentration capable of eliciting an immune response (72) or whether tumor derived sEVs may be continuously produced eliciting a cumulative response over time.

3.3 EVs and Pre-Metastatic Niche Formation

EV-macrophage interactions have been implicated in the priming of the metastatic niche in several studies. In Hoshino et al., exosomes from tumor cell lines with a liver metastatic ability were compared to non-metastatic lines and were shown to carry integrin $\alpha_v\beta_5$. This allowed preferential binding to liver-specific cells including $CD169^+$ Kupffer macrophages, driving an inflammatory phenotype *via* integrin-mediated Src phosphorylation and upregulation of s100 and fibronectin genes (48). Similarly, in Costa-Silva et al., migration inhibitory factor (MIF) found in pancreatic cancer exosomes was taken up by Kupffer macrophages driving TGFβ and fibronectin production priming the liver for metastasis (73). In Peinado et al., the receptor tyrosine kinase MET found in melanoma exosomes was captured by bone marrow progenitors driving vasculogenesis and promoting metastasis in a systemic fashion (74). Another group studying brain metastasis, showed that *miR-19a* carried from astrocyte exosomes to tumor cells led to reduction of PTEN and increased CCL2 *via* NFκB in tumor cells driving suppressive myeloid infiltration (75). Interestingly, injection of melanoma EVs drove downregulation of IFNAR1 in monocytes at distant sites driving lung metastasis *via* fibronectin deposition (76). This downregulation of IFNAR was thought to dependent on p38 expression driven by exosomal mRNA mediated TLR3-NFκB activation (43, 76). Albeit *via* differing mechanisms, these studies all support the pathogenic role of distant EV-mediated cell-cell communication in tumor metastasis.

3.4 Modulating the Interferon Response

Activation of TLRs in myeloid cells *via* DAMPs drives both NFκB and interferon regulatory factor (IRF) signalling. However, several studies suggest tumor EVs may inhibit interferon (IFN) expression and IFN responses. In an elegant approach, Gao et al. injected tumor derived exosomes into mice infected with both DNA and RNA viruses to examine EV-driven immune suppression. The data showed that exosome-delivered epidermal growth factor receptor (EGFR) reduced INFβ expression in macrophages after viral infection (77). Mechanistically, this was the result of tumor EV-EGFR driven Mitogen-Activated Protein Kinase Kinase Kinase 2 (MEKK2) phosphorylation, inhibiting IRF3 dimerization and IFN production. Similarly, hepatocarcinoma EVs containing interferon induced transmembrane Protein 2 (IFITM2) reduced IFNα production by HBV infected dendritic cells (78) while exosome delivered IRF2 (IRF2 is a repressor of Type I IFN signaling) limited IFNα/β production in macrophages. EVs can also directly reduce cellular responsiveness to IFN stimulation. For example, melanoma EVs can directly down-regulate interferon alpha and beta receptor 1 (IFNAR1) in myeloid cells *via* p38 activation dampening responsiveness to IFN stimulation (76). IFNAR downregulation was also required for maintaining suppressive activation in MDSCs (79). Thus, cumulatively the data suggests EV exposure can have wide ranging impact on IFN response influencing initial stimulation and downstream IFN-induced transcriptional programs.

EVs produced by tumors also contain self-associated molecular patterns (SAMPs) that potentially modulate tumor inflammation by molecular pathways that are distinct from those described above (80). The siglec-family self-pattern recognition receptors (SPRRs) bind to self-sialic acid residues abundant on EVs (81). Hypersialyation has been reported in both solid tumors and hematological malignancies (82) with sialic acid enrichment on tumor EVs (83). These surface glycans are required for EV internalization by many cell types (83). For example, CD169 (also known as Siglec-1 or sialoadhesin) is an exosome endocytic receptor for macrophages by binding α2,3-linked sialic acids (84). CD169 is expressed on sentinel macrophages at key interfaces in the body (blood-spleen, fetal-maternal, lung-air, etc). In peripheral lymphoid organs, $CD169^+$ macrophages play a key role in orchestrating the response to particulate antigens including ABs and virus particles (85–87). Infection with vesicular stomatitis virus (VSV) induced CD169 upregulation and recruitment of a DAP12/SHP2/TRIM27 complex (88). This inhibitory complex ubiquitinated and degraded TBK1, inhibiting IRF3 phosphorylation and downregulating the type I IFN response (88). Because CD169 is an IFN stimulated gene (ISG) this mechanism may be a negative feedback loop, promoting tolerance to self-sialic acids. Supporting this concept, in a mouse model of HIV, CD169 deletion lead to better control of viral load with increased IFN-I production (86). Other siglec family receptors (e.g. Siglec-H, Siglec-G and Siglec-10) also contain immunoreceptor tyrosine-based inhibitory motifs (ITIMs) or recruit adaptor proteins with ubiquitinase activity, with the exception of CD33 and Siglec-H which have activating function (82). Binding of EV sialic acids to siglecs may similarly attenuate IFN responses, modifying the overall effect of EV-DAMP signalling *via* TLR (89, 90). Specifically, myeloid siglec-7 and siglec-9 have been shown to reduce HLA-DR and CD86 expression upon engagement with tumor-derived sialic acids promoting T cell suppression in the pancreatic TME (91). $Siglec^+$ macrophages were also found in the bone marrow, controlling HSC (92) and erythrocyte egress (93).

These studies collectively show that EVs package both DAMPs and other endogenous immunity-inducing structures driving diverse responses in myeloid immune cells (**Figure 2**). While one signal from DAMPs provides activation of TLR-STAT-NFκB pathways resulting in inflammatory cytokine production, a second signal from self-patterns and other cargo inhibits the IFN-I response attenuating inflammation and self-antigen presentation. This results in a unique EV response that promotes the breakdown of immune surveillance in cancer and prevents autoimmunity under homeostatic conditions.

4 AUTOIMMUNE EVS PROMOTE INFLAMMATION AND TISSUE DESTRUCTION

In cancer studies the popularity of the term "exosome" has resulted in its use as a generic descriptor of EVs despite its specific endocytic definition that precludes other EVs (94). In the field of autoimmunity, outside of apoptotic bodies that have been widely

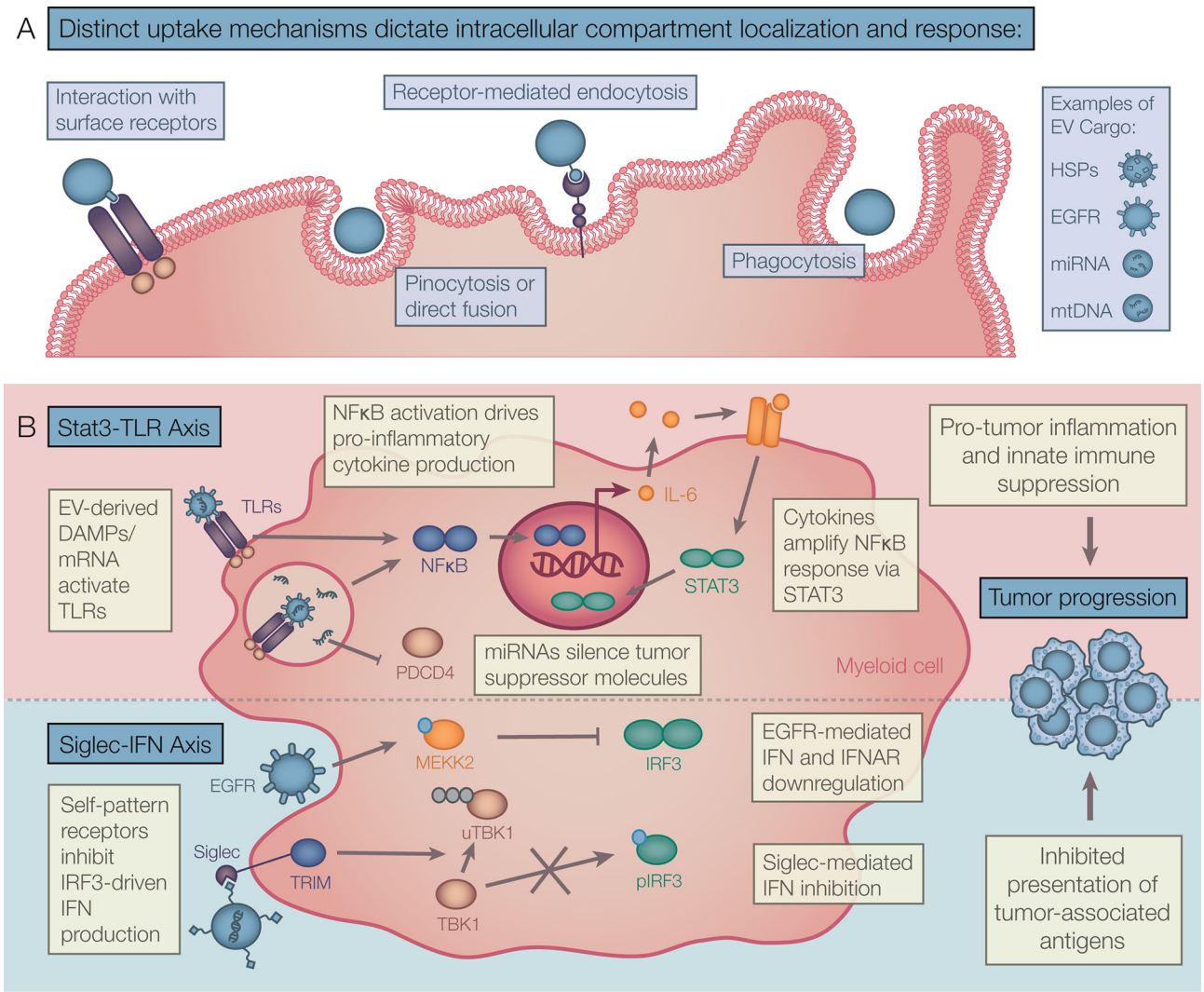

FIGURE 2 | Theoretical framework for tumor EV driven myeloid responses. **(A)** EV capture mechanisms include binding directly to cell surface receptors, direct fusion, and internalization by pinocytosis, receptor-mediated endocytosis, and phagocytosis. Distinct capture mechanisms deliver EV cargo to compartment-specific receptors driving diverse EV responses in recipient myeloid cells. **(B)** A range of tumor EV cargos act together to drive tumor promoting inflammation. Chronic interaction with EV-DAMPs and other effectors activate NF-κB and STAT3 signalling resulting in accumulation of late-stage cytokines. Also, self-molecular patterns and other effectors found in EVs attenuate type I IFN production and/or response. These signals can modulate acute inflammation and presentation of tumor antigens. EV, Extracellular vesicle; DAMPs, Danger-associated molecular patterns; NF-κB, Nuclear factor Kappa B; STAT, Signal transducer and activator of transcription; IFN, Interferon.

studied, the term microparticle (MP) is more prevalent in the study of sEVs. Because *in vitro* derived MPs mainly use lower centrifugation speeds, these studies capture larger vesicles, enriching the ectosomal or cell shedding EV phenotype. MPs also lack endocytic markers like chaperone HSPs and are enriched in phosphatidylserine (95). Exosomes, have also been studied in autoimmunity, however, the role they play distinct from other sEV subtypes is not clear.

Many of the same EV cargo components have been found in cancer and autoimmunity. Similar to observations in cancer EVs, higher levels of EVs have been reported in Sjögren's syndrome, systemic lupus erythematosus (SLE) and rheumatoid arthritis (RA) compared to healthy individuals (96, 97). Here too, the presence of DAMPs in EVs drives inflammation in a TLR-dependent manner. The focus in autoimmune disease has been on the TLR7 and TLR9 ligands DNA and RNA which are abundant in sEVs and apoptotic bodies found at high concentrations in circulation (98). We have previously reviewed the systemic effects of ABs in SLE (99), and will focus on the role of sEVs in this review. Exosomal *miR-let-7b* found in RA synovial fluid, promoted TLR7 activity in myeloid cells of inflamed joints, stimulating production of IL-1β and IL-6 (100). Further, removal of DNA from EVs by circulating DNASE1L3 prevents autoimmunity in healthy mice, while in lupus, DNASE1L3 null mutations and the presence of anti-DNA autoantibodies

protects against DNA degradation promoting inflammation in a TLR-MyD88-dependent, STING-independent mechanism (101). HMGB1 has also been found in autoimmune EVs and functions to promote inflammation *via* TLR4 in myeloid cells (102). In these studies, sources of EVs were varied, arising from platelets, endothelial cells, fibroblasts, and dying lymphocytes. A similar mechanism was also observed in scleroderma (103). EVs were also found as immune-complexes (ICs) with the anti-DNA/RNA autoantibodies characteristic of RA and SLE, promoting complement-driven, TLR-mediated DC inflammatory activation (104). EVs were also shown to contain citrullinated self-proteins contributing to the formation of inflammatory immune complexes in SLE and RA, driving monocyte and macrophage activation (105, 106). In lupus, ICs were required for a metabolic switch to glycolysis in macrophages leading to production of IL1 and ROS (107), further exasperating autoimmunity.

In type 1 diabetes (T1D) pancreatic β-cell specific destruction is triggered, rather than the systemic tissue destruction seen in SLE. Because EV release occurs prior to immune β-cell destruction, EVs may play a role in disease initiation. Using *in vitro* derived EVs from MSC-like cells from the NOD pancreas, Rahman et al. show that the intrinsic endoplasmic reticulum stress in cells of the pre-diabetic pancreas controls EV cargo driving DC-mediated priming of autoreactive T and B cells *via* IFNγ upon EV treatment (108). Moreover, the T1D autoantigens glutamic acid decarboxylase 65 (GAD65), zinc transporter 8 (ZnT8), and β-cell resident glucose transporter 2 (Glut2) were found within T1D islet EVs (109), supporting both the EV delivery of self-antigen as well as auto-antibody-EV immune complex driven myeloid cell activation *via* F_c receptors. Micro RNA species have also shown to play a key role in T1D pathogenesis. In addition to targeting many metabolic genes, the exosomal *miR-29* derived from β-cells, also found in tumor exosomes, also induces TLR7-MyD88 dependent inflammatory cytokine production, including IFN-I responses (110). Exosomal *miR-29* has also been found at higher levels in type 2 diabetes, driving metabolic reprogramming of macrophages *via* TRAF3 promoting systemic insulin resistance (111). Like observations in cancer and systemic autoimmune diseases, EVs appear to largely promote inflammation in T1D. However, EV-driven protection from autoimmunity has also been reported. AhR ligands found in EVs and other endogenous sources, attenuate autoimmunity in cases of EAE and lupus (98, 112).

The inflammatory context in autoimmunity and cancer lead to myeloid responses to the same EV cargo to both break tolerance and suppress immune responses *via* mechanisms that remain elusive. Studies on differences in EV concentration and IFN induction by autoimmune EVs versus tumor EVs may offer insights into how this is achieved.

5 EVS AND THERAPEUTIC OPPORTUNITIES

The most readily apparent application for EVs is their potential as diagnostic tools. Since they contain biomarkers of cell status, EVs from blood, ascites, and urine can potentially be utilized to serve as a liquid biopsy diagnostic differentiating healthy from diseased states. Targets including metabolic peptides, nucleotide species including circulating tumor (ct)DNA, autoantibody immune complexes and microbiome-derived EV cargo are being actively explored for diagnostic purposes (25, 113). Though finding EV biomarkers that differentiate related disease states have proven difficult, this line of investigation may be useful for both cancer and systemic autoimmune conditions (114, 115). A thorough review of EV cargo biomarkers being investigated for diagnostic application can be found elsewhere (116).

As detailed in this review, EVs promote inflammation and disease pathophysiology by variety of different mechanisms. Therefore, the inhibition of EV biogenesis using small molecules agents is being explored as a therapeutic opportunity in both cancer and autoimmunity. Small molecules including GW4869 and dimethyl amerlioride, as well as siRNA against proteins in EV biogenesis pathways, have been used extensively for research and hold promise in targeting pro-tumor inflammation driven by EV-DAMPs. However, each of these molecules have exhibited off-target effects on cellular physiology; for example, GW4869 which targets neutral sphingomyelinase (N-SMase) can also have effects on autophagy (117). Datta et al. have validated novel exosome inhibitors using prostate cancer cells, identifying natural small molecules like Forskolin and antibiotics like Manumycin A as blockers of exosome biogenesis (118). Rab-GTPase inhibitors, along with other anti-tumor functions on tumor growth and cytokine secretion, can also antagonize EV biogenesis and can be used therapeutically (119). The design and delivery of siRNA against proteins involved in biogenesis like Rab27a/b in the case of exosomes may allow for more specific targeting than small molecule inhibitors (120). However, to identify the best therapeutic target with the fewest off-target effects, a more comprehensive understanding of both EV responses and biogenesis pathways is required.

The targeting of EV capture and response by myeloid immune cells is another strategy to attenuate chronic inflammation in both cancer and autoimmunity. As described earlier, the siglec-sialic acid axis may antagonize IFN-mediated tumor destruction. Several anti-siglec antibodies are being investigated including anti-siglec-7 and anti-siglec-33 which target NK cells and immature myeloid cells respectively attenuating their regulatory function (121). Targeting other siglecs and scavenger receptors may lead to the abrogation of EV capture or facilitate delivery of therapeutical active EV cargo. EV-CD169 interactions in macrophages also drive antigen presentation in the context of infection and chemotherapy (86, 87). Capitalizing on this observation, Edgar et al. show that liposomes containing antigens targeted to CD169 *via* decoration with sialic acid residues induces CD4 T cell responses, but requires liposome loading with high-doses of TLR7-IFN promoting adjuvant for cytolytic CD8 T cell responses (122). The myeloid responses to EV-DAMPs can be inhibited *via* the targeting of the TLR-NFκB pathways. Though this is promising in autoimmunity, in cancer TLR agonism is being investigated in the clinic due to its ability to promote tolerance to the tumor (123). However, TLR4 driven myeloid tolerance has also been blamed for paclitaxel

resistance which acts as a TLR4 agonist (124). Inhibiting this pathway in cancer may involve timing where, as a neoadjuvant strategy, EV-DAMP driven NFκB activation can be inhibited temporarily prior to T cell activation or chemotherapy. Lastly, to promote MHC loading of tumor neoantigen in APCs after EV capture, an interesting recycling regulator Rab17 (shown to prevent presentation of AB derived self-antigens) could be targeted to promote tumor-specific immune destruction (125). Because EV-myeloid cell interactions are also part of homeostatic processes, targeting EV biogenesis, capture and responses to EVs may drive off-target effects that remain to be fully understood in *in vivo* disease contexts.

Furthermore, the administration of bioactive EVs is being investigated in various therapeutic strategies. The use of EVs for delivery is advantageous over liposomes with the ability to easily disguise as self in the body. Moreover, EVs decorated with integrins can target specific tissue sites allowing for specific delivery of therapeutic cargo (48). In mice, exosomes loaded with IL-12 (exoIL2) were shown to promote an antitumor T cell response, superior to the recombinant cytokine alone due to the improved pharmacokinetics (126). Because IFN signalling in APCs drives antigen presentation and cross presentation to both CD8+ and CD4+ T cells (127), therapeutic administration of large doses of EVs loaded with STING agonist dinucleotides (exoSTING) is being explored to promote adaptive anti-tumor immune responses. Jang et al. showed that exoSTING exerts tumor control by targeting APCs preferentially which induces antitumor T cell responses with long-term memory T cell induction (128). Although STING and RIG-I activation has been reported in dendritic cells, and other cells stimulated by EVs (129, 130), it may be attenuated downstream by Siglec-TBK1-dependant mechanisms *in vivo*. Limiting IFN-driven antigen presentation in response to DAMP-containing EVs may be an evolutionary mechanism to limit excessive self-peptide presentation and autoimmunity, also serving to limit tumor neoantigen presentation. Modulating the dose of EVs and additional modifications to such therapeutically administered EVs, like sialidase treatment might circumvent regulatory immune responses. In autoimmunity, these administered EVs can functions as decoys to autoantibodies. Casella et al. showed that EVs from oligodendrocytes contain myelin and related antigens and can be used to subvert myelin destruction in a model of multiple sclerosis (131). The applications for decorating or loading EVs with many different cell-targeting or immunomodulatory agents suggest EVs could be utilized as versatile payload delivery agents.

EVs have also been explored as cell-free anti-tumor vaccines. Specifically, vaccination with exosomes derived from tumor antigen loaded DCs reduced tumor burden by induction of anti-tumor T cell responses (132). DC-derived sEVs can carry whole tumor associated antigens (TAAs), TAA peptide-loaded MHC/HLA, and co-stimulatory signals significantly improving vaccination efficacy compared to whole tumor lysate vaccination (133). However, the requirement of MHC molecules for functionality/immune responses to DC-derived EVs (DEX) is not clear. For example, Hiltbrunner et al. reported that whole antigen in the absence of MHCI and II is sufficient to induce a DEX-mediated T cell response suggesting internalization and antigen processing are the key relevant components for EV-driven immune responses (134). Supporting this prediction, DEX loaded with antigen can drive stronger *in vivo* T cell responses than DC-EVs from an ectosomal origin, suggesting an involvement of the endocytic compartment in the efficacy of DEX (135). The clinical success of DEX as vaccines will likely require large, non-physiological doses of EV particles which necessitated the large-scale culture of donor-matched DCs potentially limiting this approach. In contrast to DEX, the application of the more readily available tumor EVs is currently limited to DC vaccines primed with tumor EVs. Andre et al. show that exosomes isolated from melanoma ascites contain TAAs like MART1 and gp100, and when used to stimulate donor-matched dendritic cells promote antigen-specific T cell activation and cytolytic function *in vitro* (47). Further. the *in vivo* injection of DCs treated with *in vitro* tumor cell-derived EVs into tumor-bearing mice was reported to drive tumor rejection in a T cell-dependent manner (136). These DC vaccine strategies are similarly challenged with the culture and dosing of DCs at therapeutic concentration as well as HLA-matching of both EVs and DCs required to induce the desired anti-tumor response. The pre-dominantly immunosuppressive role for tumor EVs is supported by a large body of literature and suggests the direct use of tumor-derived exosomes as TAA containing vaccines may not be a readily applicable approach given our current level of understanding.

6 CONCLUSION

Extracellular vesicles take on a wide heterogeneity of subtypes and relay a specific molecular signature from their cell of origin. The effects of a diverse EV cargo on myeloid immune cells are revealing their role in inflammation and diseases of immune dysregulation including cancer and autoimmunity. In the tumor, context dependant mechanisms drive a pro-tumor inflammation both locally and at metastatic sites promoting a breakdown of immune surveillance, whereas in autoimmunity, mechanistically similar EV signals promote a breakdown of tolerance and autoimmune pathology. Importantly, EVs are potent modulators of the IFN response which may provide protective function preventing autoimmunity, but also provide a significant barrier to anti-cancer immunity. EVs are more biologically complex compared to other cell-cell communication systems (e.g., cytokines) and this complexity has provided a barrier to our understanding, but also opportunities to harness EV biology for therapy. In this vein, the clinical application of EVs is numerous including disease diagnosis/prognosis, engineered delivery of therapeutic cargo, and administration of anti-tumor vaccines. Ultimately, these therapeutic strategies hold great promise but require much more research for safe and effective execution. In the final analysis, although great strides towards the understanding of EVs have been made, this burgeoning field

promises to reveal novel cellular mechanisms involved in health and disease.

AUTHOR CONTRIBUTIONS

PM and TM conceived the manuscript. All authors contributed to the article and approved the submitted version.

ACKNOWLEDGMENTS

This work was supported by NIH grants R01AR067763, R01CA190449, the Terry Fox Research Institute New Frontiers Program, and Canadian Institutes of Health Research Project Grants (TM). We would like to thank Dr. Kieran Manion for assistance with figure preparation.

REFERENCES

1. Cocozza F, Grisard E, Martin-Jaular L, Mathieu M, Théry C. SnapShot: Extracellular Vesicles. *Cell* (2020) 182:262–262.e1. doi: 10.1016/j.cell.2020.04.054
2. Colombo M, Raposo G, Théry C. Biogenesis, Secretion, and Intercellular Interactions of Exosomes and Other Extracellular Vesicles. *Annu Rev Cell Dev Biol* (2014) 30:255–89. doi: 10.1146/annurev-cellbio-101512-122326
3. Mathieu M, Martin-Jaular L, Lavieu G, Théry C. Specificities of Secretion and Uptake of Exosomes and Other Extracellular Vesicles for Cell-to-Cell Communication. *Nat Cell Biol* (2019) 21:9–17. doi: 10.1038/s41556-018-0250-9
4. Horibe S, Tanahashi T, Kawauchi S, Murakami Y, Rikitake Y. Mechanism of Recipient Cell-Dependent Differences in Exosome Uptake. *BMC Cancer* (2018) 18:47. doi: 10.1186/s12885-017-3958-1
5. Poggio M, Hu T, Pai C-C, Chu B, Belair CD, Chang A, et al. Suppression of Exosomal PD-L1 Induces Systemic Anti-Tumor Immunity and Memory. *Cell* (2019) 177:414–27.e13. doi: 10.1016/j.cell.2019.02.016
6. Wong K, Valdez PA, Tan C, Yeh S, Hongo J-A, Ouyang W. Phosphatidylserine Receptor Tim-4 Is Essential for the Maintenance of the Homeostatic State of Resident Peritoneal Macrophages. *Proc Natl Acad Sci* (2010) 107:8712–7. doi: 10.1073/pnas.0910929107
7. Harmati M, Gyukity-Sebestyen E, Dobra G, Janovak L, Dekany I, Saydam O, et al. Small Extracellular Vesicles Convey the Stress-Induced Adaptive Responses of Melanoma Cells. *Sci Rep* (2019) 9:15329. doi: 10.1038/s41598-019-51778-6
8. Willms E, Cabañas C, Mäger I, Wood MJA, Vader P. Extracellular Vesicle Heterogeneity: Subpopulations, Isolation Techniques, and Diverse Functions in Cancer Progression. *Front Immunol* (2018) 9:738. doi: 10.3389/fimmu.2018.00738
9. Kalluri R, LeBleu VS. The Biology, Function, and Biomedical Applications of Exosomes. *Science* (2020) 367:640–1. doi: 10.1126/science.aau6977
10. Kerr JF, Wyllie AH, Currie AR. Apoptosis: A Basic Biological Phenomenon With Wide-Ranging Implications in Tissue Kinetics. *Br J Cancer* (1972) 26:239–57. doi: 10.1038/bjc.1972.33
11. Wolf P. The Nature and Significance of Platelet Products in Human Plasma. *Br J Haematol* (1967) 13:269–88. doi: 10.1111/j.1365-2141.1967.tb08741.x
12. Harding C, Heuser J, Stahl P. Receptor-Mediated Endocytosis of Transferrin and Recycling of the Transferrin Receptor in Rat Reticulocytes. *J Cell Biol* (1983) 97:329–39. doi: 10.1083/jcb.97.2.329
13. Pan BT, Johnstone RM. Fate of the Transferrin Receptor During Maturation of Sheep Reticulocytes *In Vitro*: Selective Externalization of the Receptor. *Cell* (1983) 33:967–78. doi: 10.1016/0092-8674(83)90040-5
14. Fleshner M, Crane CR. Exosomes, DAMPs and miRNA: Features of Stress Physiology and Immune Homeostasis. *Trends Immunol* (2017) 38:768–76. doi: 10.1016/j.it.2017.08.002
15. Nicolás-Ávila JA, Lechuga-Vieco AV, Esteban-Martínez L, Sánchez-Díaz M, Díaz-García E, Santiago DJ, et al. A Network of Macrophages Supports Mitochondrial Homeostasis in the Heart. *Cell* (2020) 183:94–109.e23. doi: 10.1016/j.cell.2020.08.031
16. Fitzgerald W, Freeman ML, Lederman MM, Vasilieva E, Romero R, Margolis L. A System of Cytokines Encapsulated in ExtraCellular Vesicles. *Sci Rep* (2018) 8:8973. doi: 10.1038/s41598-018-27190-x
17. Rai A, Greening DW, Xu R, Chen M, Suwakulsiri W, Simpson RJ. Secreted Midbody Remnants Are a Class of Extracellular Vesicles Molecularly Distinct From Exosomes and Microparticles. *Commun Biol* (2021) 4:400. doi: 10.1038/s42003-021-01882-z
18. Morello M, Minciacchi VR, de Candia P, Yang J, Posadas E, Kim H, et al. Large Oncosomes Mediate Intercellular Transfer of Functional microRNA. *Cell Cycle Georget Tex* (2013) 12:3526–36. doi: 10.4161/cc.26539
19. Melentijevic I, Toth ML, Arnold ML, Guasp RJ, Harinath G, Nguyen KC, et al. C. Elegans Neurons Jettison Protein Aggregates and Mitochondria Under Neurotoxic Stress. *Nature* (2017) 542:367–71. doi: 10.1038/nature21362
20. Théry C, Witwer KW, Aikawa E, Alcaraz MJ, Anderson JD, Andriantsitohaina R, et al. Minimal Information for Studies of Extracellular Vesicles 2018 (MISEV2018): A Position Statement of the International Society for Extracellular Vesicles and Update of the MISEV2014 Guidelines. *J Extracell Vesicles* (2018) 7:1535750. doi: 10.1080/20013078.2018.1535750
21. Jeppesen DK, Fenix AM, Franklin JL, Higginbotham JN, Zhang Q, Zimmerman LJ, et al. Reassessment of Exosome Composition. *Cell* (2019) 177:428–445.e18. doi: 10.1016/j.cell.2019.02.029
22. Bobrie A, Krumeich S, Reyal F, Recchi C, Moita LF, Seabra MC, et al. Rab27a Supports Exosome-Dependent and -Independent Mechanisms That Modify the Tumor Microenvironment and can Promote Tumor Progression. *Cancer Res* (2012) 72:4920–30. doi: 10.1158/0008-5472.CAN-12-0925
23. Liu Y, Xiang X, Zhuang X, Zhang S, Liu C, Cheng Z, et al. Contribution of MyD88 to the Tumor Exosome-Mediated Induction of Myeloid Derived Suppressor Cells (MDSC) (95.16). *J Immunol* (2010) 184:95.16–6. doi: 10.2353/ajpath.2010.090777
24. Yu S, Liu C, Su K, Wang J, Liu Y, Zhang L, et al. Tumor Exosomes Inhibit Differentiation of Bone Marrow Dendritic Cells. *J Immunol Baltim Md 1950* (2007) 178:6867–75. doi: 10.4049/jimmunol.178.11.6867
25. Melo SA, Luecke LB, Kahlert C, Fernandez AF, Gammon ST, Kaye J, et al. Glypican1 Identifies Cancer Exosomes and Facilitates Early Detection of Cancer. *Nature* (2015) 523:177–82. doi: 10.1038/nature14581
26. Kren N, Michaud D, Bagchi S, Greene K, Pylayeva-Gupta Y. Rab27a Plays a Dual Role in Metastatic Propensity of Pancreatic Cancer. *Sci Rep* (2020) 10:7390. doi: 10.1038/s41598-020-64248-1
27. King HW, Michael MZ, Gleadle JM. Hypoxic Enhancement of Exosome Release by Breast Cancer Cells. *BMC Cancer* (2012) 12:421. doi: 10.1186/1471-2407-12-421
28. Li L, Li C, Wang S, Wang Z, Jiang J, Wang W, et al. Exosomes Derived From Hypoxic Oral Squamous Cell Carcinoma Cells Deliver miR-21 to Normoxic Cells to Elicit a Prometastatic Phenotype. *Cancer Res* (2016) 76:1770–80. doi: 10.1158/0008-5472.CAN-15-1625
29. Parolini I, Federici C, Raggi C, Lugini L, Palleschi S, De Milito A, et al. Microenvironmental pH Is a Key Factor for Exosome Traffic in Tumor Cells. *J Biol Chem* (2009) 284:34211–22. doi: 10.1074/jbc.M109.041152
30. Xu J, Zhang J, Zhang Z, Gao Z, Qi Y, Qiu W, et al. Hypoxic Glioma-Derived Exosomes Promote M2-Like Macrophage Polarization by Enhancing Autophagy Induction. *Cell Death Dis* (2021) 12:1–16. doi: 10.1038/s41419-021-03664-1
31. Zhang Q, Fu L, Liang Y, Guo Z, Wang L, Ma C, et al. Exosomes Originating From MSCs Stimulated With TGF-β and IFN-γ Promote Treg Differentiation. *J Cell Physiol* (2018) 233:6832–40. doi: 10.1002/jcp.26436
32. Ni J, Bucci J, Malouf D, Knox M, Graham P, Li Y. Exosomes in Cancer Radioresistance. *Front Oncol* (2019) 9:869. doi: 10.3389/fonc.2019.00869
33. Lespagnol A, Duflaut D, Beekman C, Blanc L, Fiucci G, Marine J-C, et al. Exosome Secretion, Including the DNA Damage-Induced P53-Dependent Secretory Pathway, Is Severely Compromised in TSAP6/Steap3-Null Mice. *Cell Death Differ* (2008) 15:1723–33. doi: 10.1038/cdd.2008.104
34. McKenzie AJ, Hoshino D, Hong NH, Cha DJ, Franklin JL, Coffey RJ, et al. KRAS-MEK Signaling Controls Ago2 Sorting Into Exosomes. *Cell Rep* (2016) 15:978–87. doi: 10.1016/j.celrep.2016.03.085

35. Wang X-R, Luo H, Li H-L, Cao L, Wang X-F, Yan W, et al. Overexpressed Let-7a Inhibits Glioma Cell Malignancy by Directly Targeting K-Ras, Independently of PTEN. *Neuro Oncol* (2013) 15:1491–501. doi: 10.1093/neuonc/not107
36. Buonfiglioli A, Efe IE, Guneykaya D, Ivanov A, Huang Y, Orlowski E, et al. Let-7 MicroRNAs Regulate Microglial Function and Suppress Glioma Growth Through Toll-Like Receptor 7. *Cell Rep* (2019) 29:3460–71.e7. doi: 10.1016/j.celrep.2019.11.029
37. Hanahan D, Weinberg RA. Hallmarks of Cancer: The Next Generation. *Cell* (2011) 144:646–74. doi: 10.1016/j.cell.2011.02.013
38. Foster DS, Jones RE, Ransom RC, Longaker MT, Norton JA. The Evolving Relationship of Wound Healing and Tumor Stroma. *JCI Insight* (2018) 3: E9991. doi: 10.1172/jci.insight.99911
39. Yokoi A, Villar-Prados A, Oliphint PA, Zhang J, Song X, Hoff PD, et al. Mechanisms of Nuclear Content Loading to Exosomes. *Sci Adv* (2019) 5: eaax8849. doi: 10.1126/sciadv.aax8849
40. Haldar S, Mishra R, Billet S, Thiruvalluvan M, Placencio-Hickok VR, Madhav A, et al. Cancer Epithelia-Derived Mitochondrial DNA is a Targetable Initiator of a Paracrine Signaling Loop That Confers Taxane Resistance. *Proc Natl Acad Sci* (2020) 117:8515–23. doi: 10.1073/pnas.1910952117
41. Huber V, Vallacchi V, Fleming V, Hu X, Cova A, Dugo M, et al. Tumor-Derived microRNAs Induce Myeloid Suppressor Cells and Predict Immunotherapy Resistance in Melanoma. *J Clin Invest* (2018) 128:5505–16. doi: 10.1172/JCI98060
42. Haderk F, Schulz R, Iskar M, Cid LL, Worst T, Willmund KV, et al. Tumor-Derived Exosomes Modulate PD-L1 Expression in Monocytes. *Sci Immunol* (2017) 2. doi: 10.1126/sciimmunol.aah5509
43. Liu Y, Gu Y, Han Y, Zhang Q, Jiang Z, Zhang X, et al. Tumor Exosomal RNAs Promote Lung Pre-Metastatic Niche Formation by Activating Alveolar Epithelial TLR3 to Recruit Neutrophils. *Cancer Cell* (2016) 30:243–56. doi: 10.1016/j.ccell.2016.06.021
44. Thakuri BKC, Zhang J, Zhao J, Nguyen LN, Nguyen LNT, Khanal S, et al. LncRNA HOTAIRM1 Promotes MDSC Expansion and Suppressive Functions Through the HOXA1-Mir124 Axis During HCV Infection. *Sci Rep* (2020) 10:22033. doi: 10.1038/s41598-020-78786-1
45. Matsumura S, Minamisawa T, Suga K, Kishita H, Akagi T, Ichiki T, et al. Subtypes of Tumour Cell-Derived Small Extracellular Vesicles Having Differently Externalized Phosphatidylserine. *J Extracell Vesicles* (2019) 8. doi: 10.1080/20013078.2019.1579541
46. Huang F, Wan J, Hao S, Deng X, Chen L, Ma L. TGF-β1-Silenced Leukemia Cell-Derived Exosomes Target Dendritic Cells to Induce Potent Anti-Leukemic Immunity in a Mouse Model. *Cancer Immunol Immunother* (2017) 66:1321–31. doi: 10.1007/s00262-017-2028-5
47. Andre F, Schartz NE, Movassagh M, Flament C, Pautier P, Morice P, et al. Malignant Effusions and Immunogenic Tumour-Derived Exosomes. *Lancet* (2002) 360:295–305. doi: 10.1016/S0140-6736(02)09552-1
48. Hoshino A, Costa-Silva B, Shen T-L, Rodrigues G, Hashimoto A, Mark MT, et al. Tumour Exosome Integrins Determine Organotropic Metastasis. *Nature* (2015) 527:329–35. doi: 10.1038/nature15756
49. Tulkens J, De Wever O, Hendrix A. Analyzing Bacterial Extracellular Vesicles in Human Body Fluids by Orthogonal Biophysical Separation and Biochemical Characterization. *Nat Protoc* (2020) 15:40–67. doi: 10.1038/s41596-019-0236-5
50. Brubaker SW, Bonham KS, Zanoni I, Kagan JC. Innate Immune Pattern Recognition: A Cell Biological Perspective. *Annu Rev Immunol* (2015) 33:257–90. doi: 10.1146/annurev-immunol-032414-112240
51. Abu N, Rus Bakarurraini NAA, Nasir SN. Extracellular Vesicles and DAMPs in Cancer: A Mini-Review. *Front Immunol* (2021) 12:740548. doi: 10.3389/fimmu.2021.740548
52. Chow A, Zhou W, Liu L, Fong MY, Champer J, Van Haute D, et al. Macrophage Immunomodulation by Breast Cancer-Derived Exosomes Requires Toll-Like Receptor 2-Mediated Activation of NF-κB. *Sci Rep* (2014) 4:5750. doi: 10.1038/srep05750
53. Morrissey SM, Zhang F, Ding C, Montoya-Durango DE, Hu X, Yang C, et al. Tumor-Derived Exosomes Drive Immunosuppressive Macrophages in a Pre-Metastatic Niche Through Glycolytic Dominant Metabolic Reprogramming. *Cell Metab* (2021) 33(10):2040–58. doi: 10.1016/j.cmet.2021.09.002
54. Fabbri M, Paone A, Calore F, Galli R, Gaudio E, Santhanam R, et al. MicroRNAs Bind to Toll-Like Receptors to Induce Prometastatic Inflammatory Response. *Proc Natl Acad Sci USA* (2012) 109:E2110–6. doi: 10.1073/pnas.1209414109
55. Murillo OD, Thistlethwaite W, Rozowsky J, Subramanian SL, Lucero R, Shah N, et al. exRNA Atlas Analysis Reveals Distinct Extracellular RNA Cargo Types and Their Carriers Present Across Human Biofluids. *Cell* (2019) 177:463–77.e15. doi: 10.1016/j.cell.2019.02.018
56. Kahlert C, Melo SA, Protopopov A, Tang J, Seth S, Koch M, et al. Identification of Double-Stranded Genomic DNA Spanning All Chromosomes With Mutated KRAS and P53 DNA in the Serum Exosomes of Patients With Pancreatic Cancer*. *J Biol Chem* (2014) 289:3869–75. doi: 10.1074/jbc.C113.532267
57. Haas T, Metzger J, Schmitz F, Heit A, Müller T, Latz E, et al. The DNA Sugar Backbone 2′ Deoxyribose Determines Toll-Like Receptor 9 Activation. *Immunity* (2008) 28:315–23. doi: 10.1016/j.immuni.2008.01.013
58. Sansone P, Savini C, Kurelac I, Chang Q, Amato LB, Strillacci A, et al. Packaging and Transfer of Mitochondrial DNA *via* Exosomes Regulate Escape From Dormancy in Hormonal Therapy-Resistant Breast Cancer. *Proc Natl Acad Sci* (2017) 114:E9066–75. doi: 10.1073/pnas.1704862114
59. Bao D, Zhao J, Zhou X, Yang Q, Chen Y, Zhu J, et al. Mitochondrial Fission-Induced mtDNA Stress Promotes Tumor-Associated Macrophage Infiltration and HCC Progression. *Oncogene* (2019) 38:5007–20. doi: 10.1038/s41388-019-0772-z
60. Zhang Q, Raoof M, Chen Y, Sumi Y, Sursal T, Junger W, et al. Circulating Mitochondrial DAMPs Cause Inflammatory Responses to Injury. *Nature* (2010) 464:104–7. doi: 10.1038/nature08780
61. Petros JA, Baumann AK, Ruiz-Pesini E, Amin MB, Sun CQ, Hall J, et al. mtDNA Mutations Increase Tumorigenicity in Prostate Cancer. *Proc Natl Acad Sci USA* (2005) 102:719–24. doi: 10.1073/pnas.0408894102
62. Dalpke AH, Lehner MD, Hartung T, Heeg K. Differential Effects of CpG-DNA in Toll-Like Receptor-2/-4/-9 Tolerance and Cross-Tolerance. *Immunology* (2005) 116:203–12. doi: 10.1111/j.1365-2567.2005.02211.x
63. Esplin BL, Shimazu T, Welner RS, Garrett KP, Nie L, Zhang Q, et al. Chronic Exposure to a TLR Ligand Injures Hematopoietic Stem Cells. *J Immunol* (2011) 186:5367–75. doi: 10.4049/jimmunol.1003438
64. Mitroulis I, Ruppova K, Wang B, Chen L-S, Grzybek M, Grinenko T, et al. Modulation of Myelopoiesis Progenitors Is an Integral Component of Trained Immunity. *Cell* (2018) 172:147–61.e12. doi: 10.1016/j.cell.2017.11.034
65. Ji Z, He L, Regev A, Struhl K. Inflammatory Regulatory Network Mediated by the Joint Action of NF-kB, STAT3, and AP-1 Factors Is Involved in Many Human Cancers. *Proc Natl Acad Sci* (2019) 116:9453–62. doi: 10.1073/pnas.1821068116
66. Chalmin F, Ladoire S, Mignot G, Vincent J, Bruchard M, Remy-Martin J-P, et al. Membrane-Associated Hsp72 From Tumor-Derived Exosomes Mediates STAT3-Dependent Immunosuppressive Function of Mouse and Human Myeloid-Derived Suppressor Cells. *J Clin Invest* (2010) 120:457–71. doi: 10.1172/JCI40483
67. Gabrusiewicz K, Li X, Wei J, Hashimoto Y, Marisetty AL, Ott M, et al. Glioblastoma Stem Cell-Derived Exosomes Induce M2 Macrophages and PD-L1 Expression on Human Monocytes. *OncoImmunology* (2018) 7: e1412909. doi: 10.1080/2162402X.2017.1412909
68. Shen Y, Guo D, Weng L, Wang S, Ma Z, Yang Y, et al. Tumor-Derived Exosomes Educate Dendritic Cells to Promote Tumor Metastasis *via* HSP72/HSP105-TLR2/TLR4 Pathway. *Oncoimmunology* (2017) 6. doi: 10.1080/2162402X.2017.1362527
69. Zhang X, Li F, Tang Y, Ren Q, Xiao B, Wan Y, et al. miR-21a in Exosomes From Lewis Lung Carcinoma Cells Accelerates Tumor Growth Through Targeting PDCD4 to Enhance Expansion of Myeloid-Derived Suppressor Cells. *Oncogene* (2020) 39:6354–69. doi: 10.1038/s41388-020-01406-9
70. Yang C, Dou R, Wei C, Liu K, Shi D, Zhang C, et al. Tumor-Derived Exosomal microRNA-106b-5p Activates EMT-Cancer Cell and M2-Subtype TAM Interaction to Facilitate CRC Metastasis. *Mol Ther* (2021) 29(6):2088–107. doi: 10.1016/j.ymthe.2021.02.006
71. Ying X, Wu Q, Wu X, Zhu Q, Wang X, Jiang L, et al. Epithelial Ovarian Cancer-Secreted Exosomal miR-222-3p Induces Polarization of Tumor-Associated Macrophages. *Oncotarget* (2016) 7:43076–87. doi: 10.18632/oncotarget.9246

72. Chevillet JR, Kang Q, Ruf IK, Briggs HA, Vojtech LN, Hughes SM, et al. Quantitative and Stoichiometric Analysis of the microRNA Content of Exosomes. *Proc Natl Acad Sci USA* (2014) 111:14888–93. doi: 10.1073/pnas.1408301111
73. Costa-Silva B, Aiello NM, Ocean AJ, Singh S, Zhang H, Thakur BK, et al. Pancreatic Cancer Exosomes Initiate Pre-Metastatic Niche Formation in the Liver. *Nat Cell Biol* (2015) 17:816–26. doi: 10.1038/ncb3169
74. Peinado H, Alečković M, Lavotshkin S, Matei I, Costa-Silva B, Moreno-Bueno G, et al. Melanoma Exosomes Educate Bone Marrow Progenitor Cells Toward a Pro-Metastatic Phenotype Through MET. *Nat Med* (2012) 18:883–91. doi: 10.1038/nm.2753
75. Zhang L, Zhang S, Yao J, Lowery FJ, Zhang Q, Huang W-C, et al. Microenvironment-Induced PTEN Loss by Exosomal microRNA Primes Brain Metastasis Outgrowth. *Nature* (2015) 527:100–4. doi: 10.1038/nature15376
76. Ortiz A, Gui J, Zahedi F, Yu P, Cho C, Bhattacharya S, et al. An Interferon-Driven Oxysterol-Based Defense Against Tumor-Derived Extracellular Vesicles. *Cancer Cell* (2019) 35:33–45.e6. doi: 10.1016/j.ccell.2018.12.001
77. Gao L, Wang L, Dai T, Jin K, Zhang Z, Wang S, et al. Tumor-Derived Exosomes Antagonize Innate Antiviral Immunity. *Nat Immunol* (2018) 19:233–45. doi: 10.1038/s41590-017-0043-5
78. Shi Y, Du L, Lv D, Li H, Shang J, Lu J, et al. Exosomal Interferon-Induced Transmembrane Protein 2 Transmitted to Dendritic Cells Inhibits Interferon Alpha Pathway Activation and Blocks Anti–Hepatitis B Virus Efficacy of Exogenous Interferon Alpha. *Hepatology* (2019) 69:2396–413. doi: 10.1002/hep.30548
79. Alicea-Torres K, Sanseviero E, Gui J, Chen J, Veglia F, Yu Q, et al. Immune Suppressive Activity of Myeloid-Derived Suppressor Cells in Cancer Requires Inactivation of the Type I Interferon Pathway. *Nat Commun* (2021) 12:1717. doi: 10.1038/s41467-021-22033-2
80. van de Wall S, Santegoets KCM, van Houtum EJH, Büll C, Adema GJ. Sialoglycans and Siglecs Can Shape the Tumor Immune Microenvironment. *Trends Immunol* (2020) 41:274–85. doi: 10.1016/j.it.2020.02.001
81. Lübbers J, Rodríguez E, van Kooyk Y. Modulation of Immune Tolerance *via* Siglec-Sialic Acid Interactions. *Front Immunol* (2018) 9:2807. doi: 10.3389/fimmu.2018.02807
82. Crocker PR, Paulson JC, Varki A. Siglecs and Their Roles in the Immune System. *Nat Rev Immunol* (2007) 7:255–66. doi: 10.1038/nri2056
83. Christianson HC, Svensson KJ, van Kuppevelt TH, Li J-P, Belting M. Cancer Cell Exosomes Depend on Cell-Surface Heparan Sulfate Proteoglycans for Their Internalization and Functional Activity. *Proc Natl Acad Sci* (2013) 110:17380–5. doi: 10.1073/pnas.1304266110
84. Saunderson SC, Dunn AC, Crocker PR, McLellan AD. CD169 Mediates the Capture of Exosomes in Spleen and Lymph Node. *Blood* (2014) 123:208–16. doi: 10.1182/blood-2013-03-489732
85. Ravishankar B, Shinde R, Liu H, Chaudhary K, Bradley J, Lemos HP, et al. Marginal Zone CD169+ Macrophages Coordinate Apoptotic Cell-Driven Cellular Recruitment and Tolerance. *Proc Natl Acad Sci* (2014) 111:4215–20. doi: 10.1073/pnas.1320924111
86. Gummuluru S, Ramirez N-GP, Akiyama H. CD169-Dependent Cell-Associated HIV-1 Transmission: A Driver of Virus Dissemination. *J Infect Dis* (2014) 210:S641–7. doi: 10.1093/infdis/jiu442
87. Barral P, Polzella P, Bruckbauer A, van Rooijen N, Besra GS, Cerundolo V, et al. CD169+ Macrophages Present Lipid Antigens to Mediate Early Activation of Invariant NKT Cells in Lymph Nodes. *Nat Immunol* (2010) 11:303–12. doi: 10.1038/ni.1853
88. Zheng Q, Hou J, Zhou Y, Yang Y, Xie B, Cao X. Siglec1 Suppresses Antiviral Innate Immune Response by Inducing TBK1 Degradation *via* the Ubiquitin Ligase TRIM27. *Cell Res* (2015) 25:1121–36. doi: 10.1038/cr.2015.108
89. Loschko J, Heink S, Hackl D, Dudziak D, Reindl W, Korn T, et al. Antigen Targeting to Plasmacytoid Dendritic Cells *via* Siglec-H Inhibits Th Cell-Dependent Autoimmunity. *J Immunol* (2011) 187:6346–56. doi: 10.4049/jimmunol.1102307
90. Chen G-Y, Brown NK, Zheng P, Liu Y. Siglec-G/10 in Self-Nonself Discrimination of Innate and Adaptive Immunity. *Glycobiology* (2014) 24:800–6. doi: 10.1093/glycob/cwu068
91. Rodriguez E, Boelaars K, Brown K, Eveline Li RJ, Kruijssen L, Bruijns SCM, et al. Sialic Acids in Pancreatic Cancer Cells Drive Tumour-Associated Macrophage Differentiation *via* the Siglec Receptors Siglec-7 and Siglec-9. *Nat Commun* (2021) 12:1270. doi: 10.1038/s41467-021-21550-4
92. Chow A, Lucas D, Hidalgo A, Méndez-Ferrer S, Hashimoto D, Scheiermann C, et al. Bone Marrow CD169+ Macrophages Promote the Retention of Hematopoietic Stem and Progenitor Cells in the Mesenchymal Stem Cell Niche. *J Exp Med* (2011) 208:261–71. doi: 10.1084/jem.20101688
93. Chow A, Huggins M, Ahmed J, Hashimoto D, Lucas D, Kunisaki Y, et al. CD169^{+} Macrophages Provide a Niche Promoting Erythropoiesis Under Homeostasis and Stress. *Nat Med* (2013) 19:429–36. doi: 10.1038/nm.3057
94. Witwer KW, Théry C. Extracellular Vesicles or Exosomes? On Primacy, Precision, and Popularity Influencing a Choice of Nomenclature. *J Extracell Vesicles* (2019) 8. doi: 10.1080/20013078.2019.1648167
95. Latham SL, Tiberti N, Gokoolparsadh N, Holdaway K, Olivier Couraud P, Grau GER, et al. Immuno-Analysis of Microparticles: Probing at the Limits of Detection. *Sci Rep* (2015) 5:16314. doi: 10.1038/srep16314
96. Turpin D, Truchetet M-E, Faustin B, Augusto J-F, Contin-Bordes C, Brisson A, et al. Role of Extracellular Vesicles in Autoimmune Diseases. *Autoimmun Rev* (2015) 15:174–83. doi: 10.1016/j.autrev.2015.11.004
97. Sellam J, Proulle V, Jüngel A, Ittah M, Miceli Richard C, Gottenberg J-E, et al. Increased Levels of Circulating Microparticles in Primary Sjögren's Syndrome, Systemic Lupus Erythematosus and Rheumatoid Arthritis and Relation With Disease Activity. *Arthritis Res Ther* (2009) 11:R156. doi: 10.1186/ar2833
98. Shinde R, Hezaveh K, Halaby MJ, Kloetgen A, Chakravarthy A, da Silva Medina T, et al. Apoptotic Cell-Induced AhR Activity Is Required for Immunological Tolerance and Suppression of Systemic Lupus Erythematosus in Mice and Humans. *Nat Immunol* (2018) 19:571–82. doi: 10.1038/s41590-018-0107-1
99. McGaha TL, Karlsson MCI. Apoptotic Cell Responses in the Splenic Marginal Zone: A Paradigm for Immunologic Reactions to Apoptotic Antigens With Implications for Autoimmunity. *Immunol Rev* (2016) 269:26–43. doi: 10.1111/imr.12382
100. Kim S, Chen Z, Essani AB, Elshabrawy HA, Volin MV, Volkov S, et al. Identification of a Novel Toll-Like Receptor 7 Endogenous Ligand in Rheumatoid Arthritis Synovial Fluid That Can Provoke Arthritic Joint Inflammation. *Arthritis Rheumatol Hoboken NJ* (2016) 68:1099–110. doi: 10.1002/art.39544
101. Sisirak V, Sally B, D'Agati V, Martinez-Ortiz W, Özçakar ZB, David J, et al. Digestion of Chromatin in Apoptotic Cell Microparticles Prevents Autoimmunity. *Cell* (2016) 166:88–101. doi: 10.1016/j.cell.2016.05.034
102. Harris HE, Andersson U, Pisetsky DS. HMGB1: A Multifunctional Alarmin Driving Autoimmune and Inflammatory Disease. *Nat Rev Rheumatol* (2012) 8:195–202. doi: 10.1038/nrrheum.2011.222
103. Ryu C, Walia A, Ortiz V, Sun H, Winkler J, Kanyo J, et al. Herzog, Bioactive Plasma Mitochondrial DNA Is Associated With Disease Progression in Scleroderma-Associated Interstitial Lung Disease. *Arthritis Rheumatol* (2020) 72:1905–15. doi: 10.1002/art.41418
104. Uccellini MB, Avalos AM, Marshak-Rothstein A, Viglianti GA. Toll-Like Receptor-Dependent Immune Complex Activation of B Cells and Dendritic Cells. *Methods Mol Biol Clifton NJ* (2009) 517:363–80. doi: 10.1007/978-1-59745-541-1_22
105. Burbano C, Villar-Vesga J, Orejuela J, Muñoz C, Vanegas A, Vásquez G, et al. Potential Involvement of Platelet-Derived Microparticles and Microparticles Forming Immune Complexes During Monocyte Activation in Patients With Systemic Lupus Erythematosus. *Front Immunol* (2018) 9:322. doi: 10.3389/fimmu.2018.00322
106. Burbano C, Villar-Vesga J, Vásquez G, Muñoz-Vahos C, Rojas M, Castaño D. Proinflammatory Differentiation of Macrophages Through Microparticles That Form Immune Complexes Leads to T- and B-Cell Activation in Systemic Autoimmune Diseases. *Front Immunol* (2019) 10:2058. doi: 10.3389/fimmu.2019.02058
107. Jing C, Castro-Dopico T, Richoz N, Tuong ZK, Ferdinand JR, Lok LSC, et al. Macrophage Metabolic Reprogramming Presents a Therapeutic Target in Lupus Nephritis. *Proc Natl Acad Sci* (2020) 117:15160–71. doi: 10.1073/pnas.2000943117
108. Rahman MJ, Regn D, Bashratyan R, Dai YD. Exosomes Released by Islet-Derived Mesenchymal Stem Cells Trigger Autoimmune Responses in NOD Mice. *Diabetes* (2014) 63:1008–20. doi: 10.2337/db13-0859

109. Hasilo CP, Negi S, Allaeys I, Cloutier N, Rutman AK, Gasparrini M, et al. Presence of Diabetes Autoantigens in Extracellular Vesicles Derived From Human Islets. *Sci Rep* (2017) 7:5000. doi: 10.1038/s41598-017-04977-y
110. Salama A, Fichou N, Allard M, Dubreil L, De Beaurepaire L, Viel A, et al. MicroRNA-29b Modulates Innate and Antigen-Specific Immune Responses in Mouse Models of Autoimmunity. *PloS One* (2014) 9. doi: 10.1371/journal.pone.0106153
111. Sun Y, Zhou Y, Shi Y, Zhang Y, Liu K, Liang R, et al. Expression of miRNA-29 in Pancreatic β Cells Promotes Inflammation and Diabetes *via* TRAF3. *Cell Rep* (2021) 34:108576. doi: 10.1016/j.celrep.2020.108576
112. Quintana FJ, Murugaiyan G, Farez MF, Mitsdoerffer M, Tukpah A-M, Burns EJ, et al. An Endogenous Aryl Hydrocarbon Receptor Ligand Acts on Dendritic Cells and T Cells to Suppress Experimental Autoimmune Encephalomyelitis. *Proc Natl Acad Sci USA* (2010) 107:20768–73. doi: 10.1073/pnas.1009201107
113. Chronopoulos A, Kalluri R. Emerging Role of Bacterial Extracellular Vesicles in Cancer. *Oncogene* (2020) 39:6951–60. doi: 10.1038/s41388-020-01509-3
114. Lucien F, Lac V, Billadeau DD, Borgida A, Gallinger S, Leong HS. Glypican-1 and Glycoprotein 2 Bearing Extracellular Vesicles do Not Discern Pancreatic Cancer From Benign Pancreatic Diseases. *Oncotarget* (2019) 10:1045–55. doi: 10.18632/oncotarget.26620
115. Mobarrez F, Vikerfors A, Gustafsson JT, Gunnarsson I, Zickert A, Larsson A, et al. Microparticles in the Blood of Patients With Systemic Lupus Erythematosus (SLE): Phenotypic Characterization and Clinical Associations. *Sci Rep* (2016) 6:36025. doi: 10.1038/srep36025
116. Jayaseelan VP. Emerging Role of Exosomes as Promising Diagnostic Tool for Cancer. *Cancer Gene Ther* (2020) 27:395–8. doi: 10.1038/s41417-019-0136-4
117. Back MJ, Ha HC, Fu Z, Choi JM, Piao Y, Won JH, et al. Activation of Neutral Sphingomyelinase 2 by Starvation Induces Cell-Protective Autophagy *via* an Increase in Golgi-Localized Ceramide. *Cell Death Dis* (2018) 9:1–18. doi: 10.1038/s41419-018-0709-4
118. Datta A, Kim H, McGee L, Johnson AE, Talwar S, Marugan J, et al. High-Throughput Screening Identified Selective Inhibitors of Exosome Biogenesis and Secretion: A Drug Repurposing Strategy for Advanced Cancer. *Sci Rep* (2018) 8:8161. doi: 10.1038/s41598-018-26411-7
119. Qin X, Wang J, Wang X, Liu F, Jiang B, Zhang Y. Targeting Rabs as a Novel Therapeutic Strategy for Cancer Therapy. *Drug Discov Today* (2017) 22:1139–47. doi: 10.1016/j.drudis.2017.03.012
120. Li X, Wang H, Ni Q, Tang Z, Ni J, Xu L, et al. Effects of Silencing Rab27a Gene on Biological Characteristics and Chemosensitivity of Non-Small Cell Lung Cancer. *Oncotarget* (2017) 8:94481–92. doi: 10.18632/oncotarget.21782
121. Murugesan G, Weigle B, Crocker PR. Siglec and Anti-Siglec Therapies. *Curr Opin Chem Biol* (2021) 62:34–42. doi: 10.1016/j.cbpa.2021.01.001
122. Edgar LJ, Kawasaki N, Nycholat CM, Paulson JC. Targeted Delivery of Antigen to Activated CD169+ Macrophages Induces Bias for Expansion of CD8+ T Cells. *Cell Chem Biol* (2019) 26:131–6.e4. doi: 10.1016/j.chembiol.2018.10.006
123. Petroni G, Buqué A, Zitvogel L, Kroemer G, Galluzzi L. Immunomodulation by Targeted Anticancer Agents. *Cancer Cell* (2021) 39:310–45. doi: 10.1016/j.ccell.2020.11.009
124. Kelly MG, Alvero AB, Chen R, Silasi D-A, Abrahams VM, Chan S, et al. TLR-4 Signaling Promotes Tumor Growth and Paclitaxel Chemoresistance in Ovarian Cancer. *Cancer Res* (2006) 66:3859–68. doi: 10.1158/0008-5472.CAN-05-3948
125. Yin C, Kim Y, Argintaru D, Heit B. Rab17 Mediates Differential Antigen Sorting Following Efferocytosis and Phagocytosis. *Cell Death Dis* (2016) 7: e2529. doi: 10.1038/cddis.2016.431
126. Lewis ND, Sia CL, Kirwin K, Haupt S, Mahimkar G, Zi T, et al. Exosome Surface Display of IL12 Results in Tumor-Retained Pharmacology With Superior Potency and Limited Systemic Exposure Compared With Recombinant IL12. *Mol Cancer Ther* (2021) 20:523–34. doi: 10.1158/1535-7163.MCT-20-0484
127. Spadaro F, Lapenta C, Donati S, Abalsamo L, Barnaba V, Belardelli F, et al. IFN-α Enhances Cross-Presentation in Human Dendritic Cells by Modulating Antigen Survival, Endocytic Routing, and Processing. *Blood* (2012) 119:1407–17. doi: 10.1182/blood-2011-06-363564
128. Jang SC, Economides KD, Moniz RJ, Sia CL, Lewis N, McCoy C, et al. ExoSTING, an Extracellular Vesicle Loaded With STING Agonists, Promotes Tumor Immune Surveillance. *Commun Biol* (2021) 4:1–17. doi: 10.1038/s42003-021-02004-5
129. Kitai Y, Kawasaki T, Sueyoshi T, Kobiyama K, Ishii KJ, Zou J, et al. DNA-Containing Exosomes Derived From Cancer Cells Treated With Topotecan Activate a STING-Dependent Pathway and Reinforce Antitumor Immunity. *J Immunol* (2017) 198:1649–59. doi: 10.4049/jimmunol.1601694
130. Nabet BY, Qiu Y, Shabason JE, Wu TJ, Yoon T, Kim BC, et al. Exosome RNA Unshielding Couples Stromal Activation to Pattern Recognition Receptor Signaling in Cancer. *Cell* (2017) 170:352–66.e13. doi: 10.1016/j.cell.2017.06.031
131. Casella G, Rasouli J, Boehm A, Zhang W, Xiao D, Ishikawa LLW, et al. Oligodendrocyte-Derived Extracellular Vesicles as Antigen-Specific Therapy for Autoimmune Neuroinflammation in Mice. *Sci Transl Med* (2020) 12: eaba0599. doi: 10.1126/scitranslmed.aba0599
132. Zitvogel L, Regnault A, Lozier A, Wolfers J, Flament C, Tenza D, et al. Eradication of Established Murine Tumors Using a Novel Cell-Free Vaccine: Dendritic Cell-Derived Exosomes. *Nat Med* (1998) 4:594–600. doi: 10.1038/nm0598-594
133. Gu X, Erb U, Büchler MW, Zöller M. Improved Vaccine Efficacy of Tumor Exosome Compared to Tumor Lysate Loaded Dendritic Cells in Mice. *Int J Cancer* (2015) 136:E74–84. doi: 10.1002/ijc.29100
134. Hiltbrunner S, Larssen P, Eldh M, Martinez-Bravo M-J, Wagner AK, Karlsson MCI, et al. Exosomal Cancer Immunotherapy Is Independent of MHC Molecules on Exosomes. *Oncotarget* (2016) 7:38707–17. doi: 10.18632/oncotarget.9585
135. Wahlund CJE, Güclüler G, Hiltbrunner S, Veerman RE, Näslund TI, Gabrielsson S. Exosomes From Antigen-Pulsed Dendritic Cells Induce Stronger Antigen-Specific Immune Responses Than Microvesicles *In Vivo*. *Sci Rep* (2017) 7:17095. doi: 10.1038/s41598-017-16609-6
136. Wolfers J, Lozier A, Raposo G, Regnault A, Théry C, Masurier C, et al. Tumor-Derived Exosomes Are a Source of Shared Tumor Rejection Antigens for CTL Cross-Priming. *Nat Med* (2001) 7:297–303. doi: 10.1038/85438

Conflict of Interest: The authors declare that the research was conducted in the absence of any commercial or financial relationships that could be construed as a potential conflict of interest.

Publisher's Note: All claims expressed in this article are solely those of the authors and do not necessarily represent those of their affiliated organizations, or those of the publisher, the editors and the reviewers. Any product that may be evaluated in this article, or claim that may be made by its manufacturer, is not guaranteed or endorsed by the publisher.

frontiers in Immunology

HYPOTHESIS AND THEORY
published: 17 March 2022
doi: 10.3389/fimmu.2022.750175

How Does Immunomodulatory Nanoceria Work? ROS and Immunometabolism

Lena M. Ernst[1] *and Victor Puntes*[1,2,3,4]*

[1] Vall d'Hebron Research Instiute (VHIR), Barcelona, Spain, [2] Instiut Català de Nanociència I Nanotecnologia (ICN2), CSIC, The Barcelona Institute of Science and Technology (BIST), Universitat Autònoma de Barcelona (UAB), Barcelona, Spain, [3] Institució Catalana de Recerca I Estudis Avançats (ICREA), Barcelona, Spain, [4] Networking Research Centre for Bioengineering, Biomaterials, and Nanomedicine (CIBER-BBN), Instituto de Salud Carlos III, Madrid, Spain

Dysregulation of the immune system is associated with an overproduction of metabolic reactive oxygen species (ROS) and consequent oxidative stress. By buffering excess ROS, cerium oxide (CeO_2) nanoparticles (NPs) (nanoceria) not only protect from oxidative stress consequence of inflammation but also modulate the immune response towards inflammation resolution. Immunomodulation is the modulation (regulatory adjustment) of the immune system. It has natural and human-induced forms, and it is part of immunotherapy, in which immune responses are induced, amplified, attenuated, or prevented according to therapeutic goals. For decades, it has been observed that immune cells transform from relative metabolic quiescence to a highly active metabolic state during activation(1). These changes in metabolism affect fate and function over a broad range of timescales and cell types, always correlated to metabolic changes closely associated with mitochondria number and morphology. The question is how to control the immunochemical potential, thereby regulating the immune response, by administering cellular power supply. In this regard, immune cells show different general catabolic modes relative to their activation status, linked to their specific functions (maintenance, scavenging, defense, resolution, and repair) that can be correlated to different ROS requirements and production. Properly formulated, nanoceria is highly soluble, safe, and potentially biodegradable, and it may overcome current antioxidant substances limitations and thus open a new era for human health management.

Keywords: nanoparticles, nanoceria, inflammation, macrophages, immunemetabolism, metabolism, ROS - reactive oxygen species, entropy

OPEN ACCESS

Edited by:
David Pozo,
University of Seville, Spain

Reviewed by:
Dr. Sanjay Singh,
U.P. Pandit Deen Dayal Upadhyaya Veterinary University, India
Sanjay Singh,
National Institute of Animal Biotechnology (NIAB), India

***Correspondence:**
Victor Puntes
victor.puntes@vhir.org

Specialty section:
This article was submitted to Molecular Innate Immunity, a section of the journal Frontiers in Immunology

Received: *30 July 2021*
Accepted: *18 February 2022*
Published: *17 March 2022*

Citation:
Ernst LM and Puntes V (2022) How Does Immunomodulatory Nanoceria Work? ROS and Immunometabolism. Front. Immunol. 13:750175. doi: 10.3389/fimmu.2022.750175

INTRODUCTION

Inflammation and oxidative stress (OS), mediated by reactive oxidant species (ROS) overproduction, are strictly interconnected (1). ROS refers to various biogenic free radical molecules resulting from natural metabolism characterized by being highly oxidant. These free radicals are involved in different critical physiological processes, such as gene expression, signal transduction, growth regulation, and, significantly, inflammation, where high ROS concentrations are not only needed for the activation of inflammatory pathways but also to sustain the energetic demands of an inflammatory response (2). Therefore, from a theoretical point of view, antioxidant

substances can both protect from oxidative stress (OS) and facilitate the resolution of pathogenic inflammation by inhibiting ROS-dependent inflammatory reactions and returning to homeostatic balance (3, 4).

The role of antioxidant substances became popular in the second half of the 20th century when Linus Pauling (1954 and 1962 Nobel laureate) developed the so-called orthomolecular medicine based on nutritional supplementation and high doses of ascorbic acid (5, 6). It resurfaced again in the 90s due to a large human study suggesting that vitamin E supplements could be associated with a reduced risk of heart diseases (7). During this period, other pre-clinical and epidemiological works also reported beneficial effects of antioxidant substances against chronic inflammation, neurodegeneration, and cancer (8). Subsequently, antioxidant therapies were evaluated in placebo-controlled trials involving tens of thousands of patients. Despite the pathophysiologic, epidemiologic, and mechanistic compelling evidence, these clinical trials have been, to date, mostly negative. This has been attributed to the non-drug-likeness of available antioxidant substances (9). These substances have high unspecific uncontrolled reactivity, poor solubility, and hence limited absorption profiles, low bioavailability, and low concentrations at the target site (10, 11). This has given rise to a pessimistic view of antioxidant therapies. Today, only a few antioxidant substances have reached clinical use. These include N-acetylcysteine for acetaminophen overdose, Edaravone for ischemic stroke, alpha-lipoic acid for diabetic neuropathy, some flavonoids (polyphenolic compounds present in dietary plants) for chronic venous insufficiency, as well as baicalein and catechins for osteoarthritis. Unfortunately, these treatments have not been fully satisfactory, and as a result, new approaches are being explored.

In these circumstances, new antioxidant mineral substances like nanoceria, displaying minimal toxicity to normal tissues while providing cellular protection from ROS-dependent oxidative damage, have attracted considerable attention as a potential therapeutic tool in preventing and treating oxidative stress-related diseases. With its mild but permanent ROS scavenging capacities and good pharmacology, nanoceria may overcome previous limitations and finally enable full antioxidant therapies in human health. Nanoceria has already demonstrated its ability to restrict inflammation in a large number of pathologies, based on their ability to reduce ROS levels and, consequently, most inflammatory mediators (12). Over the last decade, the beneficial effects of nanoceria treatment have been reported in various pre-clinical models, including cardiac diseases, diabetes, retinal diseases, gastrointestinal inflammation, liver inflammation, and cancer. In neurology, beneficial effects have been reported in pre-clinical models of Alzheimer's disease, Parkinson's disease, multiple sclerosis, traumatic brain injury, and brain ischemia, all conditions associated with high ROS production and neuroinflammation, reviewed in (13).

The underlying hypothesis is that by scavenging excess ROS, tissue is protected, metabolism is controlled, immune activation suffocated, and resolution of inflammation allowed. Thus, to understand how nanoceria works inside a biological system as an anti-inflammatory and immunomodulatory substance, it is essential to know how immune cells employ different metabolic pathways to sustain their energetic needs. For that, we focus on ROS production as a cause and consequence of inflammation and nanoceria ROS scavenging capacities. To propose a mechanism of action that results in effective and beneficial ROS scavenging and buffering, we need first to review the basics of metabolism and ROS production and immunometabolism, from a chemist's point of view. Then we describe the nanoceria ROS reactivity towards unpaired electrons and free radicals. Finally, we consider pharmacological and production aspects for the proper development of medical formulations based on nanoceria.

A BRIEF OVERVIEW ON METABOLISM, MITOCHONDRIA, AND ROS

In our body, nutrients and oxygen are transformed into energy, water, carbon dioxide, and other by-products as ROS. The amounts of O_2 consumed, and CO_2 produced reflect the body's metabolism and metabolized nutrients (14). In biological systems, energy is mainly provided by the controlled oxidation of carbohydrates and fatty acids, where the oxidizer is the limiting reagent. From a chemical point of view, oxidation of nutrients corresponds to the irreversible exothermic reaction of materials called fuels, consisting mainly of carbon and hydrogen, with an oxydizer. These oxidation reactions are more complex than they may seem. Initially, carbohydrates and fatty acids decompose to react with oxygen, forming unstable highly oxidant compounds called free radicals (ROS in our case). Then, these free radicals take C and H electrons, and most of the heat is released. Oxidation is completed when stable products are formed. It is interesting to note that incomplete oxidation leads to the release of highly reactive intermediates in the form of free radicals.

These nutrient oxidation chemical reactions are a fundamental part of metabolism. Metabolism can be divided into catabolism, the energy sourcing, extracting it from chemical bonds, breaking large molecules into smaller ones, and anabolism, the synthesis of complex molecules from simpler ones, using part of the produced energy. Regarding catabolism, three different basic catabolic pathways exist depending on the employed fuel (glucose or fatty acids derived from carbohydrates and lipids); oxidizer (O_2/ROS), and combustion mode (aerobic or anaerobic). The produced energy is stored in the form of ATP (indeed, in the form of ATP/ADP gradients (15)) and heat. These pathways can be referred to as aerobic glycolysis, anaerobic glycolysis, and fatty acid oxidation.

Glycolysis is relatively efficient in aerobic conditions (high ATP production and low ROS production) and very inefficient in anaerobic conditions, where a lot of glucose is consumed, and a lot of ROS produced. In fatty acid oxidation (FAO), processing one palmitic molecule efficiently produces 129 ATP molecules, compared with 2 ATP molecules produced per molecule of glucose during anaerobic glycolysis, or 36 ATP molecules per

molecule of glucose during aerobic glycolysis. FAO is accompanied by a slight non-pathological ROS overproduction when compared to aerobic glycolysis. Regarding power (*energy per unit time*), anaerobic glycolysis can produce ATP 100 times faster (16) than aerobic, thus providing the highest power to cells. FAO delivers energy at intermediate rates. These different catabolic pathways allow adjustments for the different cellular energetic requirements and needs, and as a consequence, biological responses can be controlled by targeting the energy supply. The following is important for our hypothesis: biological oxidation rate is adjusted by ROS concentration rather than oxygen concentration, which is more stable (constant) inside the body than ROS, and therefore the relevance of antioxidant substances.

These different cellular metabolic pathways can be observed by the lactate production, the expression of glucose transporters at the cell membrane, or mitochondria number and morphology (See **Figure 1** and **Table 1**). Mitochondria have been described as *cell power-houses*, converting nutrients in the form of glucose or fatty acids into energy in the form of ATP, and ROS. Mitochondria can rapidly adjust to the cell metabolic needs, and play a central role in bioenergetic and biosynthetic pathways. Increased energy demand is met by mitochondrial reproduction and fusion. In contrast, a decrease in energy demand results in the removal of superfluous mitochondria through fission and mitophagy.

It has been described that ROS generate from the leakage of electrons in the mitochondria transport chain. Under normal conditions, the potentially harmful effects of ROS are successfully restrained by protective and reparative mechanisms. Natural antioxidant defenses may remove ROS either in a highly specific manner, e.g., by catalase, SOD, or glutathione peroxidases, or in a less specific way, with small molecules such as ascorbate, glutathione, alkaloids, or carotenoids (1).

From a chemical engineering perspective, mitochondria could be described as an internal combustion engine (17), transforming oxygen and organic fuels into energy and oxidized products such as CO_2, H_2O, and H_2O_2 (ROS). H_2O_2 exists in equilibrium with hydroxyl species (a model ROS), and it is a common source of free radicals. Therefore, for intervening in the operating mode of an internal combustion engine, one can either address the fuel supply (*e.g.*, ketogenic diets are known to both be anti-inflammatory and to restrict anaerobic glycolysis (18)), or the excess oxidizer (mainly ROS), *i.e.*, the target of antioxidant substances.

Changes in mitochondria membrane potential parallel mitochondrial morphology (oval, spherical, or elongated/branched), which determines oxygen supply rate and, consequently, activity (19). A high mitochondria surface-to-volume ratio (elongated/branched) allows the oxidation of high dense fuels as FA. A low surface-to-volume ratio (spherical) will result in the lack of oxygen and the production of highly reactive oxidation intermediates. Consequently, considering the mitochondria as an internal combustion engine where the oxygen is supplied through the membrane to the fuel inside it, the surface-to-volume ratio is directly proportional to the oxygen provision rate. Thus, higher mitochondrial membrane polarization implies a higher surface-to-volume ratio and higher oxygen provision to the fuel for oxidation. Mitochondria display an oval shape most of the time, providing a sufficient O_2 supply for pyruvate oxidation in the TCA cycle and OXPHOS. In contrast, reduced O_2 supply in spherical mitochondria, when the surface-to-volume ratio is minimal, induces incomplete oxidation (anaerobic glycolysis)

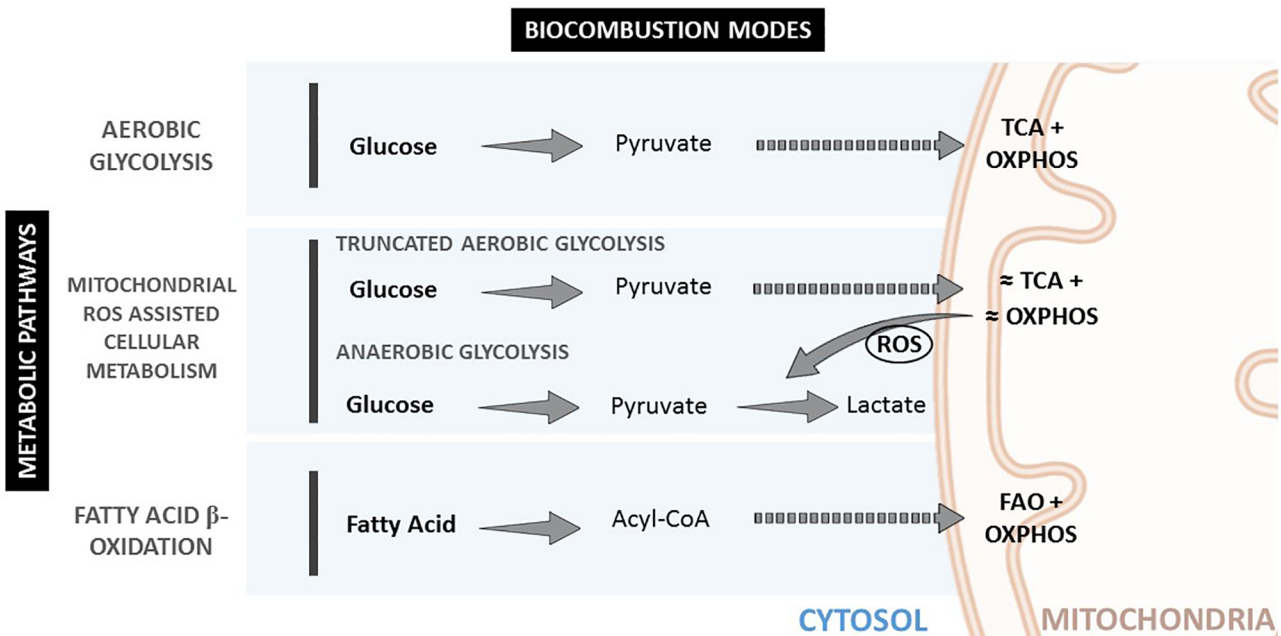

FIGURE 1 | Metabolic pathways and biocombustion modes inside the cell.

TABLE 1 | The three different mitochondria operating modes.

CATABOLIC PATHWAY	*Fuel*	*Oxidizer*	*Oxydation mode*	*Mitochondria shape*	*Mitochondria S-to-V ratio*	*Power suppy*	*ROS production*
Aerobic Glycolysis	Glucose	Oxygen	Aerobic	Elongate	Medium	Low	Basal
Mitochondrial ROS assisted cellular metabolism	Glucose	Oxygen &ROS	Anaerobic/ truncated aerobic glycolysis	Spherical	Low	High	High
Fatty Acid β-oxidation	Fatty Acid	Oxygen	Aerobic	Hyperfused	High	Medium	Medium

and excessive ROS production, decreasing the cell redox potential and igniting the pyruvate in the cytoplasm. Later, mitochondria can fuse and expand their surface, increasing polarization and creating elongated and branched structures with a higher surface-to-volume ratio, allowing for FA consumption.

Accordingly, mitochondria reduce their number and surface area (depolarize) when the cell power requirement is high. In this case, glucose is fully oxidized and directly in the cytoplasm at high rates. This can be clearly observed in the connection between glucose transport and mitochondrial mode of work in conditions of OS (1), where stimulation of cellular glucose uptake is frequently concomitant to inflammation. Therefore, during anaerobic glycolysis, a high glycolytic flux and impaired oxidative phosphorylation are associated with increased ROS levels (20, 21). Interestingly, glucose uptake has also been described as an anti-ROS mechanism since excess mitochondrial ROS is consumed, burning the extra uptake of glucose (22). This is consistent with the fact that the oxidizer is the limiting reagent, and then the oxidizer concentration can be decreased by increasing the fuel supply. When ROS levels are too high and/or remain increased during a prolonged time, a vicious circle of ROS-stimulated glucose uptake and glucose-stimulated ROS production can be triggered. This pathological cycle can be broken by restoring mitochondrial ROS production to normal levels, a phenomenon that has stimulated interest in antioxidant therapies.

Antioxidant therapies should not eliminate all ROS. Under normal conditions, the potentially harmful effects of ROS are successfully restrained by protective and reparative mechanisms. Compartmented controlled ROS levels act as signaling molecules to mediate localized events *via* the oxidative modification of redox-sensitive mediators, which are needed at low doses for many normal biological functions, such as DNA replication and repair. However, they become toxic at high concentrations when the antioxidant cell defenses are overwhelmed. High ROS concentration induces OS, damaging phospholipids and DNA, inducing cell alterations, provoking mutations, and cell death. Consistently, abnormal ROS overproduction has been involved, directly or indirectly, in the pathogenesis and progression of many diseases, to the point that it is fair to ask if there is any disease without associated abnormal ROS production. And the answer seems to be no (23, 24).

ROS are highly reactive free radicals and, therefore, short-lived molecules, and can therefore be used by the cell to produce rapid and local responses. They are also challenging to target since they are highly *mutable* and quickly transform into different free radicals. Free radicals propagate in chain reactions. Thus, once a reactive free radical is generated, it can react with stable molecules forming new free radicals. For example, the unpaired electron transfer from O to N and S molecules produces reactive nitrogen species and reactive sulfur species, all highly oxidant. Chain termination occurs when two free radical species react with each other to form a stable, non-radical adduct. This, as discussed below, can be promoted by nanoceria. In addition, ROS, in the form of H_2O_2, easily cross biological membranes escaping their compartment and leaking into the tissue, diffusing in and outside cells.

All this is especially critical regarding the immune system (25), where the different immune responses have clearly different energetic needs and power requirements, especially during inflammation (26). For decades, it has been observed that immune cells transform from relative metabolic quiescence to a highly active metabolic state during inflammation (1). Inflammation requires high power consumption. This encourages the immune system to increase the production of cytokines and chemokines, phagocytosis, immune cell recruitment and activation. These changes in essential metabolic processes affect fate and function over a broad range of different timescales and cell types, making the expression of inflammation in different organs and conditions complex. In contrast, its basal metabolic pathways are very conserved. Therefore, it is possible to target metabolic processes by scavenging ROS during an immune response, modulating thus immune activity.

Accordingly, macrophages, fundamental cells of the innate immune system responsible for detecting, categorizing and eliminating pathogens or aberrant cells, tissue repairing, development, and resolution of inflammation (27) follow the same metabolic trends. Macrophage functions can be grouped into three well-described macrophage functional phenotypes (also called cellular polarization) (28): M0 for resting, quiescent, macrophages; M1 for classical pro-inflammatory activation; and M2 for alternative activation when resolving an inflammatory reaction and promoting tissue repair (29). It has been independently and repeatedly observed that M0 works on aerobic glycolysis, M1 on anaerobic glycolysis, and M2 on FAO, providing different amounts of power and different ROS concentrations in each case (2) (**Figure 2**). Thus, changes in the basic macrophage metabolism occur following immune activation, shifting from reliance on aerobic glycolysis to increased anaerobic glycolysis, or FAO. The different macrophage polarization energy processing has been studied under the concept of immunometabolism (30).

The final question is how to modulate the immunochemical potential. As high ROS concentrations are needed to sustain anaerobic glycolysis, the cell response can be controlled by controlling ROS concentration. Modulating ROS should change the cell chemical potential, inducing metabolic adjustments and phenotypic changes towards inflammation resolution and homeostasis restoration in the case of macrophages. For that, ROS flooding the tissue and mutating have to be removed in many forms from everywhere, for a sufficiently long period of time, conditions that can only be achieved at unrealistically high doses with currently available substances and traditional molecular medicine.

THE NANOCERIA IMMUNOMODULATORY MECHANISM

Nanoceria has recently raised as an anti-inflammatory agent working very well in a wide variety of disease models. Indeed, cerium and other rare-earth compounds have been employed in medicine since the 19th century (31–33). The first reported use was that of Ce^{3+} oxalate as an antiemetic agent during pregnancy, reported by the Scottish doctor J.Y. Simpson in 1854. Subsequently, it came to be prescribed for other gastrointestinal disorders. Indeed, it gained unaccountably rapid and widespread popularity to treat sickness and coughing, and other nervous disorders such as chorea and epilepsy. Its fall into oblivion was almost as quick as it rose and for equally unclear reasons. It was said that: "Here, perhaps, is a good case of the right drug being used for the wrong reason" (34). Diversity of opinion regarding the therapeutic value of cerium oxalate has existed ever since. It is possible that the lack of a mechanistic description of its action, and the lack of standardized materials, were at the root of the controversy. Afterward, in the late 1950s, cerium oxide and phosphate tested in rats showed anti-inflammatory efficacy attributed to their dual valence state of oxidation (35). At these times, cerium and other lanthanide compounds found use as bio-imaging contrast agents in light and electron microscopy for the *in situ* detection of oxidase (36, 37) and phosphatase (38) activity since oxidized cerium precipitates in the form of highly electron-dense NPs. Later, in 1999, Telek et al. (39) used cerium chloride for the *in vivo* histological detection of oxygen-derived free radicals in inflammatory conditions, and observed anti-inflammatory effects. Although the precise mechanisms were not elucidated, the report hinted at a possible role of cerium precipitates in the observed decrease of ROS concentration. Besides, during the 20th century, nanoceria was extensively developed in the petrochemical and automobile industry as catalysts. Currently, nanoceria is also

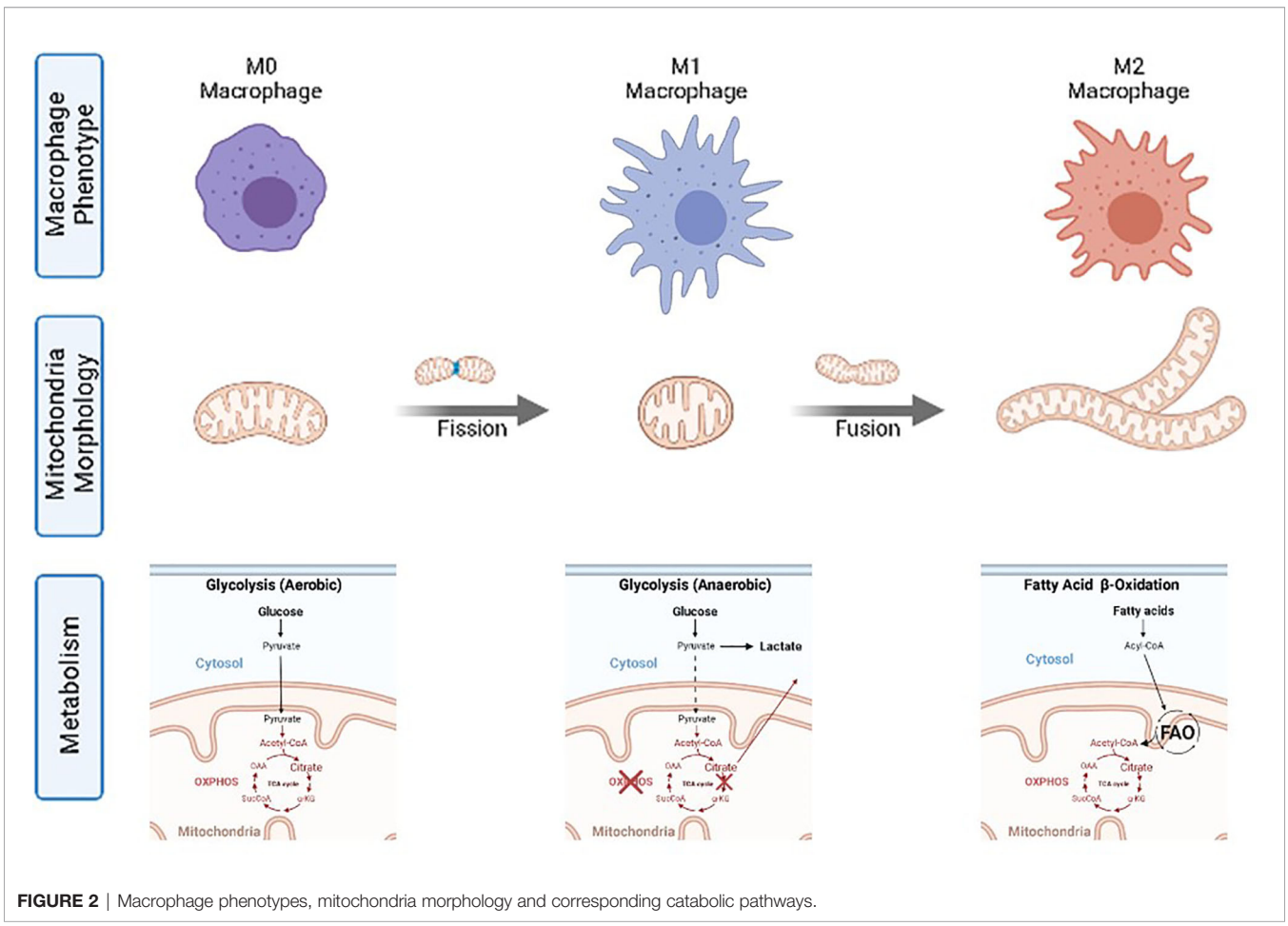

FIGURE 2 | Macrophage phenotypes, mitochondria morphology and corresponding catabolic pathways.

employed as a polishing agent, as a glass constituent to prevent solar discoloration, and in coatings to protect metallic materials from corrosion. Its promising past having been forgotten, the nanoceria biomedical potential was re-discovered in Virginia Tech less than two decades ago, when it was observed that nanoceria of less than 20 nm prolonged the lifespan of brain cell cultures for periods of up to 6–8 months (40). This finding was described by Professor Berverly Rzigalinski, and collaborators Sudipta Seal, David Bailey, and Swanand Patil, as "somewhat serendipitous", according to her words (41) since she was studying nanoceria as a drug carrier. Since then, many studies have been performed by them and others, and the potential therapeutical effects of nanoceria examined in many animal models of disease.

The first diseases subject to nanoceria treatment in pre-clinical models have been related to inflammation and diseases where antioxidants substances were previously assayed with positive results, from sepsis to age-related degeneration. Regarding sepsis, nanoceria has shown promising results regarding septic shock treatments where the mortality rate induced by LPS sepsis in rats decreased from 73% to 11% (34, 42, 43). Indeed, nanoceria has also been proposed to counteract the lethal effects of cytokine storms in COVID-19 patients (44). Regarding aging (45), nanoceria has shown significant protective effects in age-related diseases such as retinal degeneration (46), Alzheimer's, and Parkinson's (47, 48). Nanoceria has also demonstrated a positive impact in metabolic disorders, rather orphan of treatment, such as the metabolic syndrome or non-alcoholic fatty liver disease (NAFLD) (49), where ROS contribute to the initiation and progression of the disease. Another prominent example of metabolic disorder related to disease is cancer, illustrated by the Warburg effect and the metabolic reprogramming of cancer and other cells in tumor microenvironments, where anaerobic glycolysis is favored (44), suggesting that proliferation *contra naturam* costs extra energy. Another field where nanoceria could be beneficial is regenerative medicine. One of the biggest challenges in regenerative medicine and tissue engineering is to deal with inflammation. Typically, the tissue to reconstruct is under oxidative stress due to tissue damage that impedes proper regeneration. In this regard, in a partial hepatectomy animal model, rats treated with nanoceria showed a significant increase in liver regeneration compared with controls (50). Similarly, in an acetaminophen overdose experimental model, nanoceria and N-acetyl-cysteine treatments decreased early liver damage. However, only nanoceria was associated with a significant increment of hepatocellular proliferation (50).

The nanoceria chemical formula is commonly written as CeO_2 since its primary oxidation state is Ce^{4+}. Nevertheless, defects in the crystal structure are usually present at the nanoscale, and some Ce ions present a Ce^{3+} instead of a Ce^{4+} valance state. Having Ce^{3+} instead of Ce^{4+} induces a deficiency of positive charge, compensated with oxygen vacancies, usually occurring at the NP surface. The Ce^{3+} concentration in the NP, hence oxygen vacancies and redox activity, increases as the NP size decreases, achieving its maximum capacity and thermodynamic stability at diameters of a few (2 to 5) nm (50, 51). Notably, the nanoceria cubic fluorite crystal structure is preserved while Ce^{4+} is reduced to Ce^{3+} and oxygen vacancies formed. Consequently, Ce^{3+} can be easily re-oxidized (recycled) to Ce^{4+} and the vacancy covered, completing thus its catalytic loop.

The observed competitive nanoceria advantages, such as its electron sponge effect, catalytic behavior, and potential biodegradability, should be looked for in its electronic structure. Metallic cerium has an electronic configuration [Xe] $4f^15d^16s^2$, Ce^{3+} has an electronic configuration [Xe] $4f^15d^06s^0$, and Ce^{4+} has an electronic configuration [Xe] $4f^05d^06s^0$, indicating that the 4f electron is the labile one. The main difference of rare earths from other elements is to have these 4f orbitals, whose electrons are shielded by 4d and 5p orbitals. This orbital shield makes 4f electrons weakly bound to the nucleus, allowing for the Ce^{3+}/Ce^{4+} tautomery. Thus, the two oxidation states of the cerium element in the face-centered cubic crystal lattice make possible the formation and occupation of oxygen vacancies essential to its oxygen (electron) buffering capabilities, and thus its ability to act as a catalyst for both oxidation and reduction reactions.

Nanoceria has been described as an antioxidant and anti-inflammatory agent since it produces effects similar to those substances. By measuring the nanoceria electronic structure in real-time by X-ray absorption spectroscopy during the catalytic degradation of H_2O_2, a rapid uptake of electrons by the NPs was evidenced, followed by a later and slower release of these electrons, and corresponding pH modifications, in such a way that nanoceria was described as electron sponges (52). A labile unpaired electron from the free radical can be passivated by either pairing it with another electron (antioxidants provide this electron), or removing it (by antireducers), with opposite effects on pH. Thus, nanoceria is antireducer (Ce^{4+} to Ce^{3+}), and antioxidant (Ce^{3+} to Ce^{4+}) during recycling, providing a high capacity to remove excess ROS from its surroundings. Normally, substances that uptake electrons are called electron sinks or antireducers, rather than antioxidants, even if the ROS scavenging effects are similar. Such molecules, antireducers, are ubiquitous in nature, especially in the photosynthesis reaction chain, where the generation of ROS by-products is higher than during metabolism.

Taking the hydroxyl molecule as model ROS, the oxygen atom in the OH· molecule is surrounded by 7 electrons in its valence band, and it is unsatisfied, longing for 8 (the octet). This situation can be overcome if the unpaired electron is removed, and Ce^{4+} passes to Ce^{3+}, and the OH· becomes ½ O_2 plus the formation of H^+ (equation 1). Alternatively, the OH· molecule may get an electron from the nanoceria, and Ce^{3+} recycles to Ce^{4+}, and the OH· transforms into OH^- (equation 2). Thus, the nanoceria catalytic cycle, with corresponding pH modifications and oxygen generation, can be described as follows:

$$Ce^{4+}{}_{(s)} + OH\cdot_{(I)} -> Ce^{3+}{}_{(s)} + 1/2O_{2(g)} + H^+_{(I)} \quad (1)$$

$$Ce^{3+}{}_{(s)} + OH\cdot_{(I)} -> Ce^{4+}{}_{(s)} + OH^-{}_{(I)} \quad (2)$$

If we add the two equations:

$$2OH\cdot_{(I)} -> H_2O_{(l)} + 1/20_{2(g)} \quad (3)$$

Accordingly, when mixing nanoceria and H_2O_2, oxygen generation is clearly observed in the form of vigorous bubbling. Note that oxygen generation by nanoceria could be related to their observed pro-angiogenic properties (53).

However, we have to take two other equations into account. At low OH· concentration, reaction (2) can be outcompeted by (4):

$$Ce^{4+}{}_{(s)} + 1/2\ O_{2(g)} + H^+{}_{(I)} -> Ce^{4+}{}_{(s)} + OH\cdot_{(I)} \quad (4)$$

and the ROS scavenging activity stopped, or even its production promoted. Additionally, at low ROS and O_2 concentrations, the Ce^{3+} ion, which is soluble at pH below 8 (see Pourbaix diagram in SI), may dissolve away from the NP (indeed, it is the Ce^{4+} crystal structure that holds the Ce^{3+} soluble ions in the solid phase), and nanoceria slowly disintegrates, (equation 5).

$$Ce^{3+}{}_{(s)} -> Ce^{3+}{}_{(I)} \quad (5)$$

In other words, nanoceria can uptake a limited number of electrons maintaining their fluorite crystal structure and NP integrity. Due to the water solubility of Ce^{3+} ions and an increasing concentration of oxygen vacancies, if Ce^{3+} ions are not recycled to Ce^{4+}, at some point, the fluorite crystal structure cannot be maintained, and the NP disintegrates.

The combination of these equations makes nanoceria act as a redox buffer. Free radicals have to be continuously supplied to the NP surface to allow their combination into more stable species. When the ROS concentration is low, and this condition cannot be fulfilled anymore, the NP loses its catalytic activity, and reactions 1 and 4 combine instead of 1 and 2. This ROS concentration threshold needed to trigger nanoceria activity is apparently found to be between M1 and M2 phenotypes. In such a way that during M1 polarization, ROS is efficiently scavenged by nanoceria, but no nanoceria activity or biological effect has been observed when cells are expressing an M0 or M2 phenotype. Indeed, it has been recurrently observed that the use of nanoceria enables the expression of M2 polarization and increased production of SOD, Arginase, or NOS synthetases (54), well known M2 enzymes and cytokines, employed to protect the cell from OS. This is probably not because nanoceria promotes M2 polarization. This is simply because when M1 polarization is stopped, M2 is allowed to take control of the produced damage and repair the tissue. In the opposite direction, nanoceria ROS buffering capacity increases with ROS concentration up to NP surface saturation. Taking into account that ROS have to arrive, absorb, react and desorb from the NP surface, surface saturation will determine the highest ROS concentration it can be managed at once. Consequently, the nanoceria scavenging reaction rate will be constant while ROS is in excess (according to the NP surface). This reaction rate will diminish as ROS concentration decreases until it stops, corresponding to homeostatic concentrations of ROS. This buffering capacity is at the origin of their immunomodulatory properties.

Nanoceria biodegradation can also be described with the above equations. Cerium oxide is known to be a non-biodegradable material. However, in its nanometric form, at neutral pH and low oxygen concentration, nanoceria in water thermodynamically prefers to stay in the Ce^{3+} soluble valence state rather than in the Ce^{4+} insoluble valence state (see Pourbaix diagram in SI (55)). Thus, during the catalytic cycle, an "activated" state, Ce^{3+}, can leak from the NP and swim away. Consequently, *in vivo*, nanoceria can degrade into innocuous Ce^{3+} ions, expulsed from the body through the urine. The degradation of nanoceria during its biological action was reported for the first time in 2014, after observing how intracellular antioxidants dissolve man-made antioxidant nanoparticles and proposing to use the redox vulnerability of nanoceria to develop a responsive drug delivery system (56). Recent data show how nanoceria distributes, accumulates, and is expulsed from healthy mice after intravenous injection (54). At few hours after injection, the NPs are accumulated in the liver and spleen. From this point, the cerium concentration progressively decreases following an exponential decay where half of the dose has been expulsed in 6 weeks. During this experiment, cerium was found in urine and feces (57). Probably ions in the first case and NPs in the second, expulsed through the hepatobiliary route. This degradation of nanoceria can be promoted by increasing the reducing environment, decreasing pH (as in endolysosomes), and complexing molecules that absorb Ce^{3+} ions in solution and remove them from the equilibrium. As a final consideration, the smaller the NP, the higher their dissolution rate. Regarding nanoceria excretion, it is worthy to mention the observed excretion of nanoceria coated with dextran when administered orally as a computed tomography contrast agent for imaging the gastrointestinal tract in a mice model of Inflammatory Bowel Disease (58).

PHARMACOLOGICAL DEVELOPMENT OF NANOCERIA

These last two decades have started building a pharmacokinetic model for nanoceria, its behavior in physiological media, administration, biodistribution, degradation, and excretion. Still, today, the pharmacological knowledge on the subject is premature, mainly due to material uncertainty. First, NPs for medicine should be monodisperse, biocompatible, small, and highly dispersible in physiological media, with engineered surfaces to escape from phagocytosis (59). The traditional industrial basic precipitation employed for the preparation of nanoceria is normally continued by a calcination step to fully oxidize Ce^{3+} to Ce^{4+} and fully dehydrate $Ce(OH)_4$ into CeO_2. Nanoceria prepared in these conditions sinters and grows, losing its therapeutical properties, and needs high temperature to be activated, which is common in its industrial applications. Interestingly, current procedures for preparing nanoceria for medical applications by basic precipitation yield small colloidal $Ce^{+3/+4}$ hydroxide/oxide NPs that can be employed in biology. The Ce^{3+}/Ce^{4+} ratio is not always specified in the scientific

literature despite being highly dependent on the NP size, preparation technique, NP history, and surface state. It can be determined by some characterization techniques, including X-ray photoelectron spectroscopy (XPS) (60), X-ray absorption spectroscopy (52), and UV-visible absorption spectroscopy (UV/VIS) (61).

We recommend the use of $CeCl_3$ as cerium precursor instead of $Ce(NO_3)_3$ when using TMAOH as the base (chosen because of the stabilizing effect of TMA^+ counterions) since the presence of nitrate in the synthesis process may derivate in nitrosamine contaminants which are of serious concerns for the regulatory agencies. In this respect, the "FDA guidance for industry on drug products, including biological products, that contain nanomaterials" (62) can be of great help in developing medical nanoceria. Related to that, a paper indicating how to carry pre-clinical studies on nanoceria harmonized with FDA regulations has recently been published (63). It is expected that nanoceria will have to follow the path other metal oxide inorganic NPs have followed, such as Fe_3O_4 NPs, approved as a contrast agent for MRI (Resovist®), as iron supply in the case of iron-deficiency anemia (Feromuxytol®) or as hyperthermia agent to treat neuroblastoma (Nanotherm®).

Special attention must be given to size, parental (as-synthesized), and eventually, aggregated (when dispersed). Aggregation, especially in physiological media, corresponds to the NP natural tendency to reduce surface area and consequently surface energy. Size is critical for both the catalytic activity of nanoceria and their pharmacological properties. This is because the number of oxygen vacancies increases with reducing the size and surface accesses increases for non-aggregate NPs, and because size is a major parameter of the administration, biodistribution, metabolization, and excretion profile of NPs (57).

The biodistribution of NPs is different from traditional small drugs designed to cross biological barriers and membranes, and distribute across the body. Nanoceria follows the main principles of NP biodistribution which depends on size, hydrophilicity, and surface charge (64). The initial observation is how reducing NP size extends blood circulating times and reaches good levels of homogeneous distribution in tissues (65). For neutral and negatively charged small inorganic NPs, depending on the portal of entry, different organs can be targeted. Normally, after i.v. administration, NPs accumulate in the liver (90%) and spleen (9%) after a few hours of blood circulation (66). However, NPs smaller than 6 nm can be rapidly cleared through the urinary tract (67). To avoid this, small nanoceria can be conjugated to different biomolecules, such as albumin (54), to prevent aggregation and avoid renal clearance. The reported most prolonged half-life in blood for nanoceria has been about 4 hours after injection (68). It is also feasible to target the lymph nodes after intramuscular injection, or the eye, the skin, and the gastrointestinal tract, by oral and topical administration. If injected into a tumor or the brain, NPs tend to remain inside the organ. It is also essential to consider that body barriers controlling NP dispersion are altered during the course of disease. Two significant cases are worthy of mention. First is the enhanced penetration and retention effect of NPs into solid tumors, described by Maeda *et al.* in 2002 (69), where due to abnormal angiogenesis, blood vessels supplying nutrients to solid tumors have defects in their tiling, and large pores (hundreds of nm) are formed, making the tumor accessible to nanocarriers, which together with poor lymphatic drainage, facilitate their accumulation (indeed albumin act as a nanometric carrier for cisplatin favoring its accumulation in tumors) (70). Second is the increase of barrier permeability during inflammation, as in the case of neuroinflammation, granting access to the brain to NPs after i.v. or i.p. injection (68, 71). All in all means that nanoceria can be designed to passively reach and stay in different organs for an extended period of time, depending on NP features, medical state, and administration route.

At the cellular level, NPs distribution has also been well described (72). For many different materials such as gold or iron oxide, NPs are found to be densely aggregated in endosomes persistent during the experimental times. The same is observed with nanoceria (54). In these cases, one would say that the nanoceria will not be functional because it is kept away from the cytoplasm, and this is true; however, as ROS can cross the phospholipid bilayers in the form of H_2O_2, the aggregate nanoceria can perform its task scavenging cytoplasmatic ROS that enters the endosome. Hypothetically, if long-lasting and functional, these structures could be pictorially called *ceriasomes*, a nanoceria highly loaded (hundreds of NPs) endosome which scavenges free radicals as soon as they enter, as artificial intracellular OS protective organelles. Besides, nanoceria permeation out of the endosome can increase during endosomal acidification if it loses its surface charge and become non-charged (depending on lysosome pH, nanoceria concentration, and nanoceria isoelectric point). In addition, proton-sponge-like effects due to its basic oxide surface may contribute to endosomal disruption. Nevertheless, this appears to happen only eventually. Therefore, most nanoceria will remain in endosomal vesicles inside the cytoplasm, acting as a ROS scavenging organelle.

These studies are, in part, possible thanks to the easy traceability of cerium. As a xenobiotic element, its background presence in the body is negligible, making it possible to trace its presence to attomolar concentrations by inductively coupled plasma mass spectroscopy (ICPMS). Additionally, thanks to its high Z number, it gives strong contrast, not only in optical and electron microscopies but also to X-ray (58). These aspects are not shared by conventional drugs that "disappear" as soon as they enter the body, and complex chemical and biochemical resolution-limited techniques must be employed.

Regarding dosing, nanoceria has been administered formulated with BSA (54), PEG (71), sodium citrate and EDTA (68), or a series of drugs (73). In most cases, aggregates of few tens nm have been employed, however, works with non aggregated NPs showed better biodistribution and increased biocompatibility. In any case, despite formulation and aggregation state, successful nanoceria applications work at concentrations of a few micrograms (50 to 250 μg) per gram of tissue, administered in single injections at concentrations of about 1 to 10 mg/ml, which in the case of 3 nm NPs corresponds to $9.25x10^{15}$ NPs/ml to $9.25x10^{16}$ NPs/ml. It is normally administered up to 1 mg nanoceria per Kg of animal, in

200 (mice) or 300 (rat) microliter volumes (**Table 2**, see an extended version in the SI, which includes formulation and administration route, among others).

Nanosafety

Since the seminal work of Vicky Colvin in 2003 (56), nanosafety has been one of the most significant issues when discussing NP medical, industrial, and customer applications. Since then, a great effort has been dedicated to studying the detrimental aspects of NPs. Initial results were sometimes puzzling and confusing. In this regard, Prof. Harald Krug, in a 2014 review article (83), analyzing about 10.000 nanotoxicology papers, revealed that most of the nanotoxicity studies "do not offer a clear statement on the safety of nanomaterials and, on the contrary, most of them are either self-contradictory or arrive at completely erroneous conclusions." Indeed, it has been observed that at realistic doses in a controlled manner, NPs show no significant increased toxicity compared to their molecular or bulk counterparts. The reported toxicity often has to be attributed to NPs aggregation and NPs association with toxic moieties (endotoxin, surfactants, or allergens) rather than the NPs themselves, leading to apparently contradictory data. Nanoceria is an illustrative case (84). While it is reported many times to be beneficial in protecting against oxidative stress and irradiation damage, other studies, mainly related to the toxicity of nanoceria in the industrial dry form (nanometric aggregate powders), show *in vitro* and *in vivo* toxicity (81). Similarly, while some studies show anti-inflammatory effects of nanoceria taken up by hepatocytes (54), others report liver macrophage (Kupffer cells) uptake and pro-inflammatory effects (85). This often results from the challenging dispersibility of inorganic NPs in physiological media that too often leads to NP aggregation and sedimentation, losing their beneficial properties. *In vitro* studies showed how the nanoceria ROS scavenging capacity increased with nanoceria concentration until it was lost when NPs aggregated at higher concentrations and started being pro-inflammatory (54). Interestingly, the therapeutic doses are far from these toxic doses (10 to 100 times). Large aggregates are easily detected by the immune system, and often a pro-inflammatory response is triggered, making the medical use of NPs complicated because of material uncertainty. Ji et al. demonstrated the importance of controlling NPs size, shape, and aggregation state. Inflammatory immune response and toxicity were only reported when using high aspect ratio nanoceria nanowires at high doses and aggregation state. Besides, it is important to note that some toxic ingredients coming from the NP formulation or derived from chemicals employed during NP preparation can misreport NP toxicity (83). An example is the work of Dowding et al. where a similar nanoceria synthesis process was done, but using different bases [NH_4OH or hexamethylenetetramine (HMTA)] (86). Results showed that HMTA-nanoceria NPs were readily taken into endothelial cells and reduced cell viability at a 10-fold lower concentration than the other NPs, which showed no toxicity. Finally, a paper was published recently on a woman who drank a large amount of nanoceria-based polishing powder by mistake (87). The product was not described, but this industrial nanoceria is a mix of NP aggregates at a relatively high pH. The observed transient toxic effects could be related to the basic pH of the preparation and the presence of Ce^{3+} soluble species in the formulation. Besides, observed coagulation disorders had been previously described with Ce^{3+} at high doses because of their interference with Ca^{2+} homeostasis (88).

Therefore, well-described, pure, monodisperse, and highly dispersible in physiological media nanoceria is mandatory for this promising material meaningful and controlled use for therapy. One strategy to avoid nanoceria toxicity due to aggregation when dispersed in physiological media is pre-albuminization before injection (54). The albumin has not to be firmly bound to the NP. Its mere presence prevents NP aggregation by interacting with its surface. Once injected, NPs dilute in the bloodstream, or tissue, putting away aggregation risk.

Finally, cerium is affordable, abundant as silver (not in veins though, which makes its mining complicated), and nanoceria is easy to produce following green chemistry principles -at RT with simple reagents having recyclable basic waters as by-product. It is stable in simple storage conditions, and of universal use (the same NPs perform well in different disease models). Additionally, it is xenobiotic, which makes it easily traceable by imaging and spectroscopic techniques such as X-ray or mass spectroscopy, facilitating its preclinical studies. Thus, nanoceria and other nanozymes may represent a new era for medicine, where the ability to buffer excess ROS allows for better general population health (anti-aging, anti-tumoral and anti-inflammatory).

Summarizing, the relationship between metabolism and disease has been extensively explored during the past decade. Understanding how cells use energy to perform their functions has attracted attention concerning diseases such as obesity, diabetes, cancer, and neurodegeneration. Indeed, pathological inflammation is at the origin and progression of many diseases, from chronic, inducing accelerated aging and oncogenesis, to acute, such as ischemia, cytokine storms, and anaphylaxis. Antioxidant substances have shown promising immunomodulation in pre-clinical and epidemiological studies, and their mechanism has been observed in detail. However, they are still poorly translated to the clinic. The inconsistencies between the mechanistic and

TABLE 2 | Dosing of nanoceria in different *in vivo* studies.

Study #	1 (74)	2 (75)	3 (76)	4 (77)	5 (78)	6 (79)	7 (68)	8 (80)	9 (81)	10 (82)	11 (71)
Size* (nm)	3	1, 3	10	No data	3	1-2.5	2.4	3	10	No data	3.3
Dose (μg/g)	No Data	No Data	0.05, 0.5, 5, 50	0.1	30, 100	10, 6	10, 20, 30	20	0.05, 0.5	0.05, 0.5, 5	0.1, 0.3, 0.5, 0.7, 1, 1.5

**parental size, independently of aggregation state.*

epidemiological studies, and the clinical trials, indicate the poor pharmacological properties of currently available substances and the need for new approaches and strategies. Today, nanoceria, catalytic mild antioxidant NPs, may provide the required pharmacokinetics and overcome previous limitations, unleashing the power of antioxidant prevention and therapy.

Cerium is a rare earth element that accumulates oxygen vacancies in its nanometric oxide form capable of catalytically removing excess ROS in metabolic imbalance situations. Indeed, nanoceria act as a redox buffer, promoting immunomodulation without immune suppression. Nanoceria displays a good safety profile to normal tissues while providing cellular protection from various forms of ROS and irradiation. Thanks to its catalytic nature, nanoceria can be used at low doses for a prolonged time (before NPs are degraded, dissolved, and excreted). Small nanoceria in the neutral pH and low oxidant conditions inside the body slowly dissolves in few months as the insoluble Ce^{4+} is progressively reduced to soluble Ce^{3+} ions, excreted through the urine. Nanoceria is redox selective (only degrades ROS at high concentrations) but not ROS selective (degrades any form of ROS). Indeed, it is selective to a high concentration of unpaired electrons regardless of the atomic orbital carrying them. When adequately formulated (endotoxin-free, stable, soluble), no harmful effects have been observed in *in vitro* and *in vivo* models at applicable doses. Of note, cerium compounds (cerium oxalate and cerium nitrate) were used in the past, among others, as antiemetic agents during pregnancy. Nanoceria formulation and dose will have to be developed case by case since tissue environment, and the metabolic and immune status depends on the studied tissue and medical condition. For example, the brain, despite its high consumption of glucose and tendency to suffer from oxidative stress, it is short in endogenous antioxidant defenses. Or like pregnancy, which starts with the immune system activating an M1 polarization to follow up with an M2 polarization from placentation up to delivery.

DATA AVAILABILITY STATEMENT

The original contributions presented in the study are included in the article/**Supplementary Material**. Further inquiries can be directed to the corresponding author.

AUTHOR CONTRIBUTIONS

LM and VP developed the hypothesis, search the literature, wrote the manuscript and approved it for publication.

SUPPLEMENTARY MATERIAL

The Supplementary Material for this article can be found online at: https://www.frontiersin.org/articles/10.3389/fimmu.2022.750175/full#supplementary-material

REFERENCES

1. Liemburg-Apers DC, Willems PHGM, Koopman WJH, Grefte S. Interactions Between Mitochondrial Reactive Oxygen Species and Cellular Glucose Metabolism. *Arch Toxicol* (2015) 89:1209–26. doi: 10.1007/s00204-015-1520-y
2. Viola A, Munari F, Sánchez-Rodríguez R, Scolaro T, Castegna A. The Metabolic Signature of Macrophage Responses. *Front Immunol* (2019) 10:1462. doi: 10.3389/fimmu.2019.01462
3. Arulselvan P, Fard MT, Tan WS, Gothai S, Fakurazi S, Norhaizan ME, et al. Role of Antioxidants and Natural Products in Inflammation. *Oxid Med Cell Longev* (2016) 2016:5276130. doi: 10.1155/2016/5276130
4. Liguori I, Russo G, Curcio F, Bulli G, Aran L, Della-Morte D, et al. Oxidative Stress, Aging, and Diseases. *Clin Interv Aging* (2018) 13:757–72. doi: 10.2147/CIA.S158513
5. Pauling L. Vitamin C and the Common Cold. *Can Med Assoc J* (1971) 105:448. doi: 10.1001/jama.1971.03180280086025
6. *Vitamin C and the Common Cold* (1970). Available at: https://www.worldcat.org/title/vitamin-c-and-the-common-cold/oclc/107441 (Accessed June 6, 2021). WorldCat.org.
7. Knekt P, Reunanen A, Jävinen R, Seppänen R, Heliövaara M, Aromaa A. Antioxidant Vitamin Intake and Coronary Mortality in a Longitudinal Population Study. *Am J Epidemiol* (1994) 139:1180–9. doi: 10.1093/oxfordjournals.aje.a116964
8. *Natural Antioxidants in Human Health and Disease - Google Llibres* . Available at: https://books.google.es/books?hl=ca&lr=&id=GYUXAAAAQBAJ&oi=fnd&pg=PP1&dq=antioxidant+cancer+inflammation+neuro*&ots=vR9knTlVcL&sig=j30lop6HKgW1D_FwKzmVbyceSiw#v=onepage&q&f=false (Accessed June 30, 2021).
9. Steinhubl SR. Why Have Antioxidants Failed in Clinical Trials? *Am J Cardiol* (2008) 101:S14–9. doi: 10.1016/j.amjcard.2008.02.003
10. Firuzi O, Miri R, Tavakkoli M, Saso L. Antioxidant Therapy: Current Status and Future Prospects. *Curr Med Chem* (2012) 18:3871–88. doi: 10.2174/092986711803414368
11. Benfeito S, Oliveira C, Soares P, Fernandes C, Silva T, Teixeira J, et al. Antioxidant Therapy: Still in Search of the "Magic Bullet." *Mitochondrion* (2013) 13:427–35. doi: 10.1016/j.mito.2012.12.002
12. Xu C, Qu X. Cerium Oxide Nanoparticle: A Remarkably Versatile Rare Earth Nanomaterial for Biological Applications. *NPG Asia Mater* (2014) 6:e90–0. doi: 10.1038/am.2013.88
13. Casals E, Zeng M, Parra-Robert M, Fernández-Varo G, Morales-Ruiz M, Jiménez W, et al. Cerium Oxide Nanoparticles: Advances in Biodistribution, Toxicity, and Preclinical Exploration. *Small* (2020) 16:1907322. doi: 10.1002/smll.201907322
14. Willner D, Weissman C. Carbon Dioxide Production, Metabolism, and Anesthesia. In: *Capnography*, *2nd ed*. Cambridge: Cambridge University Press. (2011). p. 239–49. doi: 10.1017/CBO9780511933837.026
15. Klingenberg M, Rottenberg H. Relation Between the Gradient of the ATP/ADP Ratio and the Membrane Potential Across the Mitochondrial Membrane. *Eur J Biochem* (1977) 73:125–30. doi: 10.1111/j.1432-1033.1977.tb11298.x
16. Liberti MV, Locasale JW. The Warburg Effect: How Does it Benefit Cancer Cells? *Trends Biochem Sci* (2016) 41:211. doi: 10.1016/J.TIBS.2015.12.001
17. Magnasco MO. Molecular Combustion Motors. *Phys Rev Lett* (1994) 72:2656. doi: 10.1103/PhysRevLett.72.2656
18. Shen Y, Kapfhamer D, Minnella AM, Kim JE, Won SJ, Chen Y, et al. Bioenergetic State Regulates Innate Inflammatory Responses Through the Transcriptional Co-Repressor CtBP. *Nat Commun* (2017) 8:1–13. doi: 10.1038/s41467-017-00707-0
19. Karbowski M, Youle RJ. Dynamics of Mitochondrial Morphology in Healthy Cells and During Apoptosis. *Cell Death Differ* (2003) 10:870–80. doi: 10.1038/sj.cdd.4401260
20. Zhou J, Deo BK, Hosoya K, Terasaki T, Obrosova IG, Brosius FC, et al. Increased JNK Phosphorylation and Oxidative Stress in Response to Increased Glucose Flux Through Increased GLUT1 Expression in Rat Retinal Endothelial Cells. *Investig Ophthalmol Vis Sci* (2005) 46:3403–10. doi: 10.1167/iovs.04-1064

21. Talior I, Yarkoni M, Bashan N, Eldar-Finkelman H. Increased Glucose Uptake Promotes Oxidative Stress and PKC-δ Activation in Adipocytes of Obese, Insulin-Resistant Mice. *Am J Physiol - Endocrinol Metab* (2003) 285:295–02. doi: 10.1152/ajpendo.00044.2003
22. Brand KA, Hermfisse U. Aerobic Glycolysis by Proliferating Cells: A Protective Strategy Against Reactive Oxygen Species 1. *FASEB J* (1997) 11:388–95. doi: 10.1096/fasebj.11.5.9141507
23. Yang S, Lian G. ROS and Diseases: Role in Metabolism and Energy Supply. *Mol Cell Biochem* (2020) 467:1. doi: 10.1007/s11010-019-03667-9
24. Di Meo S, Reed TT, Venditti P, Victor VM. Role of ROS and RNS Sources in Physiological and Pathological Conditions. *Oxid Med Cell Longev* (2016) 2016:1245049. doi: 10.1155/2016/1245049
25. Van Anders G, Klotsa D, Ahmed NK, Engel M, Glotzer SC. Understanding Shape Entropy Through Local Dense Packing. *Proc Natl Acad Sci U.S.A.* (2014) 111:E4812–21. doi: 10.1073/pnas.1418159111
26. deS Breda CN, Davanzo GG, Basso PJ, Saraiva Câmara NO, Moraes-Vieira PMM. Mitochondria as Central Hub of the Immune System. *Redox Biol* (2019) 26:101255. doi: 10.1016/j.redox.2019.101255
27. Chaplin DD. Overview of the Immune Response. *J Allergy Clin Immunol* (2010) 125:S3–S23. doi: 10.1016/j.jaci.2009.12.980
28. Italiani P, Boraschi D. From Monocytes to M1/M2 Macrophages: Phenotypical vs. Functional Differentiation. *Front Immunol* (2014) 5:514. doi: 10.3389/fimmu.2014.00514
29. Andersson SGE, Karlberg O, Canbäck B, Kurland CG, Whatley FR, van der Giezen M, et al. On the Origin of Mitochondria: A Genomics Perspective. *Philos Trans R Soc B: Biol Sci (Royal Society)* (2003) 358:165–79. doi: 10.1098/rstb.2002.1193
30. O'Neill LAJ, Kishton RJ, Rathmell J. A Guide to Immunometabolism for Immunologists. *Nat Rev Immunol* (2016) 16:553–65. doi: 10.1038/nri.2016.70
31. *The Medical Times and Gazette. New Ser.:V.19* (1859). HathiTrust Digital Library | HathiTrust Digital Library. Available at: https://babel.hathitrust.org/cgi/pt?id=hvd.32044103088555&view=1up&seq=288 (Accessed June 1, 2021).
32. Simpson JY. Note on the Therapeutic Action of the Salts of Cerium. *Mon J Med Sci* (1854) 10:563.
33. Baehr G, Wessler H. The Use of Cerium Oxalate for the Relief of Vomiting: An Experimental Study of the Effects of Some Salts of Cerium, Lanthanum, Praseodymium, Neodymium and Thorium. *Arch Intern Med* (1909) II:517–31. doi: 10.1001/archinte.1909.00050110014002
34. Rice KM, Bandarupalli VVK, Manne NDPK, Blough ER. Spleen Data: Cerium Oxide Nanoparticles Attenuate Polymicrobial Sepsis Induced Spenic Damage in Male Sprague Dawley Rats. *Data Br* (2018) 18:740–6. doi: 10.1016/j.dib.2018.03.073
35. Van Noorden CJF, Frederiks WM. Cerium Methods for Light and Electron Microscopical Histochemistry. *J Microsc* (1993) 171:3–16. doi: 10.1111/j.1365-2818.1993.tb03354.x
36. Veenhuis M, Bonga SEW. Cytochemical Localization of Catalase and Several Hydrogen Peroxide-Producing Oxidases in the Nucleoids and Matrix of Rat Liver Peroxisomes. *Histochem J* (1979) 11:561–72. doi: 10.1007/BF01012539
37. Vaughn KC, Duke SO, Duke SH, Henson CA. Ultrastructural Localization of Urate Oxidase in Nodules of Sesbania Exaltata, Glycine Max, and Medicago Sativa. *Histochemistry* (1982) 74:309–18. doi: 10.1007/BF00493430
38. Veenhuis M, Van Dijken JP, Harder W. A New Method for the Cytochemical Demonstration of Phosphatase Activities in Yeasts Based on the Use of Cerous Ions. *FEMS Microbiol Lett* (1980) 9:285–91. doi: 10.1111/j.1574-6968.1980.tb05654.x
39. Telek G, Scoazec JY, Chariot J, Ducroc R, Feldmann G, Rozé C. Cerium-Based Histochemical Demonstration of Oxidative Stress in Taurocholate-Induced Acute Pancreatitis in Rats: A Confocal Laser Scanning Microscopic Study. *J Histochem Cytochem* (1999) 47:1201–12. doi: 10.1177/002215549904700912
40. Rzigalinski BA, Bailey D, Chow L, Kuiry SC, Patil S, Merchant S, et al. Cerium Oxide Nanoparticles Increase the Lifespan of Cultured Brain Cells and Protect Against Free Radical and Mechanical Trauma. *FASEB J* (2003) 17.
41. Rzigalinski BA. Nanoparticles and Cell Longevity. *Techonology Cancer Res Treat* (2005) 4:651–9. doi: 10.1177/153303460500400609
42. Cox GM, Harrison TS, McDade HC, Taborda CP, Heinrich G, Casadevall A, et al. Superoxide Dismutase Influences the Virulence of Cryptococcus Neoformans by Affecting Growth Within Macrophages. *Infect Immun* (2003) 71:173–80. doi: 10.1128/IAI.71.1.173-180.2003
43. Hashem RM, Rashd LA, Hashem KS, Soliman HM. Cerium Oxide Nanoparticles Alleviate Oxidative Stress and Decreases Nrf-2/HO-1 in D-GALN/LPS Induced Hepatotoxicity. *BioMed Pharmacother* (2015) 73:80–6. doi: 10.1016/j.biopha.2015.05.006
44. Allawadhi P, Khurana A, Allwadhi S, Joshi K, Packirisamy G, Bharani KK. Nanoceria as a Possible Agent for the Management of COVID-19. *Nano Today* (2020) 35:100982. doi: 10.1016/j.nantod.2020.100982
45. Finkel T, Holbrook NJ. Oxidants, Oxidative Stress and the Biology of Ageing. *Nature* (2000) 408:239–47. doi: 10.1038/35041687
46. Chen J, Patil S, Seal S, McGinnis JF. Rare Earth Nanoparticles Prevent Retinal Degeneration Induced by Intracellular Peroxides. *Nat Nanotechnol* (2006) 1:142–50. doi: 10.1038/nnano.2006.91
47. D'Angelo B, Santucci S, Benedetti E, Di Loreto S, Phani R, Falone S, et al. Cerium Oxide Nanoparticles Trigger Neuronal Survival in a Human Alzheimer Disease Model By Modulating BDNF Pathway. *Curr Nanosci* (2009) 5:167–76. doi: 10.2174/157341309788185523
48. Pinna A, Malfatti L, Galleri G, Manetti R, Cossu S, Rocchitta G, et al. Ceria Nanoparticles for the Treatment of Parkinson-Like Diseases Induced by Chronic Manganese Intoxication. *RSC Adv* (2015) 5:20432–9. doi: 10.1039/C4RA16265J
49. Carvajal S, Perramón M, Oró D, Casals E, Fernández-Varo G, Casals G, et al. Cerium Oxide Nanoparticles Display Antilipogenic Effect in Rats With non-Alcoholic Fatty Liver Disease. *Sci Rep* (2019) 9:1–20. doi: 10.1038/s41598-019-49262-2. 2019 91.
50. Córdoba-Jover B, Arce-Cerezo A, Ribera J, Pauta M, Oró D, Casals G, et al. Cerium Oxide Nanoparticles Improve Liver Regeneration After Acetaminophen-Induced Liver Injury and Partial Hepatectomy in Rats. *J Nanobiotechnol* (2019) 17:1–12. doi: 10.1186/S12951-019-0544-5. 2019 171.
51. Reed K, Cormack A, Kulkarni A, Mayton M, Sayle D, Klaessig F, et al. Exploring the Properties and Applications of Nanoceria: Is There Still Plenty of Room at the Bottom? *Environ Sci Nano* (2014) 1:390–405. doi: 10.1039/C4EN00079J
52. Cafun J-D, Kvashnina KO, Casals E, Puntes VF, Glatzel P. Absence of Ce3+ Sites in Chemically Active Colloidal Ceria Nanoparticles. *ACS Nano* (2013) 7:10726–32. doi: 10.1021/nn403542p
53. Das S, Singh S, Dowding JM, Oommen S, Kumar A, Sayle TXT, et al. The Induction of Angiogenesis by Cerium Oxide Nanoparticles Through the Modulation of Oxygen in Intracellular Environments. *Biomaterials* (2012) 33:7746–55. doi: 10.1016/J.BIOMATERIALS.2012.07.019
54. Oró D, Yudina T, Fernández-Varo G, Casals E, Reichenbach V, Casals G, et al. Cerium Oxide Nanoparticles Reduce Steatosis, Portal Hypertension and Display Anti-Inflammatory Properties in Rats With Liver Fibrosis. *J Hepatol* (2016) 64:691–8. doi: 10.1016/j.jhep.2015.10.020
55. Channei D, Phanichphant S, Nakaruk A, Mofarah SS, Koshy P, Sorrell CC. Aqueous and Surface Chemistries of Photocatalytic Fe-Doped CeO2 Nanoparticles. *Catal* (2017) 7:45. doi: 10.3390/CATAL7020045
56. Muhammad F, Wang A, Qi W, Zhang S, Zhu G. Intracellular Antioxidants Dissolve Man-Made Antioxidant Nanoparticles: Using Redox Vulnerability of Nanoceria to Develop a Responsive Drug Delivery System. *ACS Appl Mater Interfaces* (2014) 6:19424–33. doi: 10.1021/am5055367
57. Poon W, Zhang YN, Ouyang B, Kingston BR, Wu JLY, Wilhelm S, et al. Elimination Pathways of Nanoparticles. *ACS Nano* (2019) 13:5785–98. doi: 10.1021/ACSNANO.9B01383
58. Naha PC, Hsu JC, Kim J, Shah S, Bouché M, Si-Mohamed S, et al. Dextran-Coated Cerium Oxide Nanoparticles: A Computed Tomography Contrast Agent for Imaging the Gastrointestinal Tract and Inflammatory Bowel Disease. *ACS Nano* (2020) 14:10187–97. doi: 10.1021/ACSNANO.0C03457
59. Ernst LM, Casals E, Italiani P, Boraschi D, Puntes V. The Interactions Between Nanoparticles and the Innate Immune System From a Nanotechnologist Perspective. *Nanomater* (2021) 11:2991. doi: 10.3390/NANO11112991. 2021, Vol 11, Page 2991.
60. Garcia X, Soler L, Divins NJ, Vendrell X, Serrano I, Lucentini I, et al. Ceria-Based Catalysts Studied by Near Ambient Pressure X-Ray Photoelectron Spectroscopy: A Review. *Catal* (2020) 10:286. doi: 10.3390/CATAL10030286. 2020, Vol 10, Page 286.
61. Manoharan D. Optical Properties of Nano-Crystalline Cerium Dioxide Synthesized by Single Step Aqueous Citrate-Nitrate Gel Combustion Method. *Artic Asian J Chem* (2013) 25:9045–49. doi: 10.14233/ajchem.2013.14984
62. Fda, Cder, Yeaton and Ayse. *Drug Products, Including Biological Products, That Contain Nanomaterials - Guidance for Industry*. Available at: https://www.fda.gov/Drugs/GuidanceComplianceRegulatoryInformation/Guidances/default.htm (Accessed July 6, 2021).

63. Ghorbani M, Izadi Z, Jafari S, Casals E, Rezaei F, Aliabadi A, et al. Preclinical Studies Conducted on Nanozyme Antioxidants: Shortcomings and Challenges Based on US FDA Regulations. *Futur Med* (2021) 16:1133–51. doi: 10.2217/NNM-2021-0030
64. McNeil SE. Nanoparticle Therapeutics: A Personal Perspective. *Wiley Interdiscip Rev Nanomed Nanobiotechnol* (2009) 1:264–71. doi: 10.1002/WNAN.6
65. Hoshyar N, Gray S, Han H, Bao G. The Effect of Nanoparticle Size on *In Vivo* Pharmacokinetics and Cellular Interaction. *Nanomedicine* (2016) 11:673. doi: 10.2217/NNM.16.5
66. Tsoi KM, Macparland SA, Ma XZ, Spetzler VN, Echeverri J, Ouyang B, et al. Mechanism of Hard-Nanomaterial Clearance by the Liver. *Nat Mater* (2016) 15:1212–21. doi: 10.1038/nmat4718
67. Soo Choi H, Liu W, Misra P, Tanaka E, Zimmer JP, Itty Ipe B, et al. Renal Clearance of Quantum Dots. *Nat Biotechnol* (2007) 25:1165–70. doi: 10.1038/nbt1340
68. Heckman KL, Decoteau W, Estevez A, Reed KJ, Costanzo W, Sanford D, et al. Custom Cerium Oxide Nanoparticles Protect Against a Free Radical Mediated Autoimmune Degenerative Disease in the Brain. *ACS Nano* (2013) 7:10582–96. doi: 10.1021/nn403743b
69. Maeda H, Wu J, Sawa T, Matsumura Y, Hori K. Tumor Vascular Permeability and the EPR Effect in Macromolecular Therapeutics: A Review. *J Control Release* (2000) 65:271–84. doi: 10.1016/S0168-3659(99)00248-5
70. Comenge J, Sotelo C, Romero F, Gallego O, Barnadas A, Parada TGC, et al. Detoxifying Antitumoral Drugs *via* Nanoconjugation: The Case of Gold Nanoparticles and Cisplatin. *PloS One* (2012) 7:47562. doi: 10.1371/journal.pone.0047562
71. Kim CK, Kim T, Choi I-Y, Soh M, Kim D, Kim Y-J, et al. Ceria Nanoparticles That can Protect Against Ischemic Stroke. *Angew Chemie Int Ed* (2012) 51:11039–43. doi: 10.1002/anie.201203780
72. Sousa De Almeida M, Susnik E, Drasler B, Taladriz-Blanco P, Petri-Fink A, Rothen-Rutishauser B. Understanding Nanoparticle Endocytosis to Improve Targeting Strategies in Nanomedicine. *Chem Soc Rev* (2021) 50:5397–434. doi: 10.1039/D0CS01127D
73. Bao Q, Hu P, Xu Y, Cheng T, Wei C, Pan L, et al. Simultaneous Blood–Brain Barrier Crossing and Protection for Stroke Treatment Based on Edaravone-Loaded Ceria Nanoparticles. *ACS Nano* (2018) 12:6794–805. doi: 10.1021/ACSNANO.8B01994
74. Kwon HJ, Cha MY, Kim D, Kim DK, Soh M, Shin K, et al. Mitochondria-Targeting Ceria Nanoparticles as Antioxidants for Alzheimer's Disease. *ACS Nano* (2016) 10:2860–70. doi: 10.1021/ACSNANO.5B08045
75. Wahba SMR, Darwish AS, Kamal SM. Ceria-Containing Uncoated and Coated Hydroxyapatite-Based Galantamine Nanocomposites for Formidable Treatment of Alzheimer's Disease in Ovariectomized Albino-Rat Model. *Mater Sci Eng C* (2016) 65:151–63. doi: 10.1016/j.msec.2016.04.041
76. Dillon CD, Billings M, Hockey KS, Delagarza L, Rzigalinski BA. Cerium Oxide Nanoparticles Protect Against MPTP-Induced Dopaminergic Neurodegeneration In A Mouse Model For Parkinson's Disease. *NSTI-Nanotech* (2011) 3:451–4.
77. Hegazy MAE, Maklad HM, Abd Elmonsif DA, Elnozhy FY, Alqubiea MA, Alenezi FA, et al. The Possible Role of Cerium Oxide (CeO2) Nanoparticles in Prevention of Neurobehavioral and Neurochemical Changes in 6-Hydroxydopamine-Induced Parkinsonian Disease. *Alexandria J Med* (2017) 53:351–60. doi: 10.1016/J.AJME.2016.12.006
78. Kwon HJ, Kim D, Seo K, Kim YG, Han SI, Kang T, et al. Ceria Nanoparticle Systems for Selective Scavenging of Mitochondrial, Intracellular, and Extracellular Reactive Oxygen Species in Parkinson's Disease. *Angew Chemie Int Ed* (2018) 57:9408–12. doi: 10.1002/anie.201805052
79. *Ceria Nanopartciles Reduce Disease Severity in a Mouse Model of Multiple Sclerosis – TechConnect Briefs* . Available at: https://briefs.techconnect.org/papers/ceria-nanopartciles-reduce-disease-severity-in-a-mouse-model-of-multiple-sclerosis/ (Accessed July 21, 2021).
80. DeCoteau W, Heckman KL, Estevez AY, Reed KJ, Costanzo W, Sandford D, et al. Cerium Oxide Nanoparticles With Antioxidant Properties Ameliorate Strength and Prolong Life in Mouse Model of Amyotrophic Lateral Sclerosis. *Nanomed Nanotechnol Biol Med* (2016) 12:2311–20. doi: 10.1016/J.NANO.2016.06.009
81. Bailey ZS, Nilson E, Bates JA, Oyalowo A, Hockey KS, Sajja VSSS, et al. Cerium Oxide Nanoparticles Improve Outcome After *In Vitro* and *In Vivo* Mild Traumatic Brain Injury. *J Neurotrauma* (2016) 37:142–62. doi: 10.1089/neu.2016.4644. neu.2016.4644.
82. Hicks HJ, Jackson P, Willner J, Whiting M. Post-Injury Administration of Cerium Oxide Nanoparticles: A Dose-Response Study. (2013).
83. Krug HF. Nanosafety Research-Are We on the Right Track? *Angew Chemie Int Ed* (2014) 53:12304–19. doi: 10.1002/anie.201403367
84. Casals E, Gusta MF, Piella J, Casals G, Jiménez W, Puntes V. Intrinsic and Extrinsic Properties Affecting Innate Immune Responses to Nanoparticles: The Case of Cerium Oxide. *Front Immunol* (2017) 8:970. doi: 10.3389/fimmu.2017.00970
85. Hirst SM, Karakoti A, Singh S, Self W, Tyler R, Seal S, et al. Bio-Distribution and *In Vivo* Antioxidant Effects of Cerium Oxide Nanoparticles in Mice. *Environ Toxicol* (2013) 28:107–18. doi: 10.1002/tox.20704
86. Dowding JM, Das S, Kumar A, Dosani T, McCormack R, Gupta A, et al. Cellular Interaction and Toxicity Depend on Physicochemical Properties and Surface Modification of Redox-Active Nanomaterials. *ACS Nano* (2013) 7:4855–68. doi: 10.1021/NN305872D/SUPPL_FILE/NN305872D_SI_001.PDF
87. Lu YQ. Coagulation Disorders Following an Accidental Ingestion of Cerium Dioxide Nanoparticles. *Environ Toxicol Pharmacol* (2021) 82:103560. doi: 10.1016/J.ETAP.2020.103560
88. Environmental Protection Agency. Toxicological Review of Cerium Oxide and Cerium Compounds: In Support of Summary Information on the Integrated Risk Information System (IRIS). *Fed Regist* (2009).

Conflict of Interest: The authors declare that the research was conducted in the absence of any commercial or financial relationships that could be construed as a potential conflict of interest.

Publisher's Note: All claims expressed in this article are solely those of the authors and do not necessarily represent those of their affiliated organizations, or those of the publisher, the editors and the reviewers. Any product that may be evaluated in this article, or claim that may be made by its manufacturer, is not guaranteed or endorsed by the publisher.

frontiers | Frontiers in Immunology

ORIGINAL RESEARCH
published: 14 April 2022
doi: 10.3389/fimmu.2022.826164

Peptides-Coated Oncolytic Vaccines for Cancer Personalized Medicine

Sara Feola[1,2,3,4], *Salvatore Russo*[1,2,3,4†], *Beatriz Martins*[1,2,3,4†], *Alessandra Lopes*[5], *Gaëlle Vandermeulen*[5], *Vinciane Fluhler*[1,2,3,4], *Camilla De Giorgi*[1,2,3,4], *Manlio Fusciello*[1,2,3,4], *Sari Pesonen*[6], *Erkko Ylösmäki*[1,2,3,4], *Gabriella Antignani*[1,2,3,4], *Jacopo Chiaro*[1,2,3,4], *Firas Hamdan*[1,2,3,4], *Michaela Feodoroff*[1,2,3,4], *Mikaela Grönholm*[1,2,3,4] and *Vincenzo Cerullo*[1,2,3,4,7*]

[1] Drug Research Program (DRP) ImmunoViroTherapy Lab (IVT), Division of Pharmaceutical Biosciences, Faculty of Pharmacy, University of Helsinki, Helsinki, Finland, [2] Helsinki Institute of Life Science (HiLIFE), University of Helsinki, Helsinki, Finland, [3] Translational Immunology Program (TRIMM), Faculty of Medicine Helsinki University, University of Helsinki, Helsinki, Finland, [4] Digital Precision Cancer Medicine Flagship (iCAN), University of Helsinki, Helsinki, Finland, [5] Advanced Drug Delivery and Biomaterials, Louvain Drug Research Institute, Université Catholique de Louvain, Brussels, Belgium, [6] Valo Therapeutics, Helsinki, Finland, [7] Department of Molecular Medicine and Medical Biotechnology, Naples University "Federico II", Naples, Italy

OPEN ACCESS

Edited by:
David Pozo,
University of Seville, Spain

Reviewed by:
Cristian Smerdou,
University of Navarra, Spain
Vladimir Mulens-Arias,
Pompeu Fabra University, Spain

***Correspondence:**
Vincenzo Cerullo
vincenzo.cerullo@helsinki.fi

[†]*These authors have contributed equally to this work*

Specialty section:
This article was submitted to Molecular Innate Immunity, a section of the journal Frontiers in Immunology

Received: *30 November 2021*
Accepted: *23 March 2022*
Published: *14 April 2022*

Citation:
Feola S, Russo S, Martins B, Lopes A, Vandermeulen G, Fluhler V, De Giorgi C, Fusciello M, Pesonen S, Ylösmäki E, Antignani G, Chiaro J, Hamdan F, Feodoroff M, Grönholm M and Cerullo V (2022) Peptides-Coated Oncolytic Vaccines for Cancer Personalized Medicine. Front. Immunol. 13:826164. doi: 10.3389/fimmu.2022.826164

Oncolytic Viruses (OVs) work through two main mechanisms of action: the direct lysis of the virus-infected cancer cells and the release of tumor antigens as a result of the viral burst. In this sc.enario, the OVs act as *in situ* cancer vaccines, since the immunogenicity of the virus is combined with tumor antigens, that direct the specificity of the anti-tumor adaptive immune response. However, this mechanism in some cases fails in eliciting a strong specific T cell response. One way to overcome this problem and enhance the priming efficiency is the production of genetically modified oncolytic viruses encoding one or more tumor antigens. To avoid the long and expensive process related to the engineering of the OVs, we have exploited an approach based on coating OVs (adenovirus and vaccinia virus) with tumor antigens. In this work, oncolytic viruses encoding tumor antigens and tumor antigen decorated adenoviral platform (PeptiCRAd) have been used as cancer vaccines and evaluated both for their prophylactic and therapeutic efficacy. We have first tested the oncolytic vaccines by exploiting the OVA model, moving then to TRP2, a more clinically relevant tumor antigen. Finally, both approaches have been investigated in tumor neo-antigens settings. Interestingly, both genetically modified oncolytic adenovirus and PeptiCRAd elicited T cells-specific anti-tumor responses. However, *in vitro* cross-representation experiments, showed an advantage of PeptiCRAd as regards the fast presentation of the model epitope SIINFEKL from OVA in an immunogenic rather than tolerogenic fashion. Here two approaches used as cancer oncolytic vaccines have been explored and characterized for their efficacy. Although the generation of specific anti-tumor T cells was elicited in both approaches, PeptiCRAd retains the advantage of being rapidly adaptable by coating the adenovirus with a different set of tumor antigens, which is crucial in personalized cancer vaccines clinical setting.

Keywords: oncolytic viruses, cancer vaccines, personalized medicine, PeptiCRAd, tumor antigens

INTRODUCTION

Cancer Immunotherapy reprograms a patient´s immune system to generate, stimulate, and sustain specific anti-tumor responses, targeting cancer cells for destruction (1). In the case of a cell-mediated response, the crosstalk between the innate and adaptive arms is essential for generating an optimal anti-tumor T-cell cytotoxic response. In particular, the antigen-presenting cells (APCs), mainly dendritic cells (DCs), are the first players in the frontline of an anti-tumor immune response. Indeed, DCs capture, process, and present tumor antigens (TAs) within the MHC-I complex, priming and/or activating the T-cell response that in turn recognizes and destroys malignant cells (2). All together these elements are key regulators in evoking anti-tumor immune response and so far, a plethora of strategies have been developed to exploit each one of these steps as cancer therapeutic approaches (3). Among the different cancer immunotherapeutic strategies, cancer vaccines based on synthetic peptides have been extensively used to guide the immune response specifically to the eradication of cancer (4, 5). Tumor peptide vaccines have the potential of dramatic anti-tumoral effects due to both strong and anti-tumor-specific immune activation (6); furthermore, immunopeptidomic pipelines to capture the MHC-I peptides landscape is growing and a new avenue to patient´s tailored therapy is on the way (7–9). However, tumor peptides vaccines are still facing major impediments that need to be addressed to reach clinical efficacy (10) and up to date no *in vivo* peptide-based cancer vaccine has obtained FDA approval (10). The main limitations are due to the immunosuppressive tumor microenvironment, self-tolerance, and tumor heterogenicity (10). To overcome these disadvantages and to unleash tumor peptides vaccines' full potential, several attempts in the field have been made, either combining tumor peptides with adjuvants as Polyinosinic: polycytidylic acid (Poly ICLC) or using genetic-based strategies (i.e., DNA/RNA based vaccines), reaching some level of pre-clinical success but still, a lot of progress needs to be made (10, 11).

Moreover, the breakthrough of immune checkpoint inhibitors (ICIs) targeting programmed death receptor-1 (PD-1), its ligand PD-L1, and cytotoxic T cell-associated antigen 4 (CTL-A4), has increased the full potential of different immune therapeutic cancer treatments, opening new opportunities (12, 13). Indeed, ICIs take the break off of the immune system, unleashing the anti-tumor immune response and/or revitalizing exhausted T-cells (14). The use of ICIs has prolonged the survival of patients affected by highly immunogenic tumors such as metastatic melanoma and lung cancers (15–17); however, the majority of patients still fail to respond to therapy as the effectiveness of ICIs depends on a pre-existing anti-tumor immune response within the TME that can be boosted and/or re-activated by ICIs (18). Thus, combinatorial approaches are needed to induce and/or increase immune components infiltration, turning an immunologically "cold" tumor into a "hot" one (19). Oncolytic virotherapy has been proposed as a platform for the recruitment of immune cells in the TME. Indeed, Oncolytic Viruses (OVs) are a class of viruses genetically modified or naturally occurring able to infect and replicate selectively in cancer cells (20). They are an emerging class of immunotherapeutic agents as in the last decades it became clear that beyond the direct oncolysis, the OVs own a second and more important mechanism of action based on inducing immunogenic cell death (ICD) that ultimately activate the immune system (20, 21). Upon oncolytic cell burst, tumor-associated antigens (TAA) and eventually neoantigens (TNA) are released and ingested by DCs that in turn prime and activate specific anti-tumor T cells. Moreover, the oncolytic cell burst promotes immunogenic cell death (ICD), with the release of several cellular factors known as damage-associated molecular patterns (DAMPs) such as calreticulin (ecto-CRT), secreted adenosine triphosphate (ATP) and high mobility group box 1 protein (HMGB1), enhancing the anti-tumor immunity (22–24). In addition to that, OV mediated cell lysis is combined with the accumulation of viral components such as nucleic acid (DNA, dsRNA, ssRNA, and 5′-triphosphate RNA), proteins and capsid components named pathogen-associated molecular patterns (PAMPS) (20, 22). In turn, DAMPs and PAMPs license the DCs to bolster the generation of an immunogenic response instead of a tolerogenic one (21).Nevertheless, the anti-viral T cells response is predominant in the immune reaction, with only a minor component of this latter being a specific anti-tumor response.

To take full advantage of the natural immunogenicity of OVs for one side and to exploit the specificity of tumor peptide vaccines to guide the tumor response for cancer´s eradication on the other side, genetically modified OVs expressing tumor antigens (TA) has been extensively produced and tested. However, expensive and time-consuming protocols are required to generate OVs encoding one or more TAs and these requirements are not compatible with patient-tailored treatment; additionally, as the viral genome encodes the TAs, their production demands robust infection and therefore the final vaccinal outcome depends on the unpredictable and highly variable intrinsic sensitivity of each tumor to OVs (25). To avoid this main disadvantage and to increase the anti-tumor immune response, PeptiCRAd a technology that consists of an oncolytic adenovirus (OAd) decorated with MHC-I tumor peptides has been developed and is currently being explored as a cancer therapeutic vaccine. The technology uses poly-lysine tail-peptides that through electrostatic interactions bind the adenoviral capsid; a reaction takes only 15 minutes (26).

In this work, we aimed to investigate and compare OVs encoding TAs and PeptiCRAd with main regards to their cancer prophylactic and therapeutic efficacy. Herein, we have generated an oncolytic adenovirus (OAd) encoding either the model protein chicken ovalbumin (OVA) or the more clinically relevant tumor antigen murine tyrosinase-related protein 2 (TRP_2); then we have carefully characterized the T-cell immune profile in mice pre-immunized either with the OAd encoding the TAs or with PeptiCRAd. Next, we have challenged the therapeutic efficacy of PeptiCRAd and cloned viruses by treating mice bearing the established B16.OVA tumor model. Finally, we have moved to a more complex and clinically relevant

setting to mimic the heterogeneous tumor profile. To this end, we have generated OAd encoding previously described neoantigens in the poor immunogenic model B16F1 (27) to compare the anti-tumor efficacy of PeptiCRAd coated with the same set of neoantigen.

In this study, we have shown that PeptiCRAd technology is as efficient as OAd engineered to express TAs; however, translated in a clinical scenario, PeptiCRAd retains the advantage of being easily adaptable for personalized cancer therapy, bypassing the need of engineering cancer-specific patient OVs.

MATERIAL AND METHODS

Cell Lines and Reagents

Human lung carcinoma cell line A549, human triple-negative breast cancer cell line MDA-MB-436, and human ovarian cancer SKOV-3 cell line were cultured in DMEM supplemented with 10% FBS (Gibco), 1% glutamine (GIBCO), 100 µg/ml streptomycin, and 100 U/ml penicillin (Life Technologies, California). Human epithelial colorectal adenocarcinoma CACO-2 cell line was cultured in DMEM supplemented with 20% FBS, 1% glutamine, 100 µg/ml streptomycin, and 100 U/ml penicillin. Murine colon cancer cell line CT26 was cultured in RPMI supplemented with 10% FBS, 1% glutamine, 100 µg/ml streptomycin, and 100 U/ml penicillin. Murine triple-negative breast cancer cell line 4T1 was cultured in RPMI high glucose. Human melanoma cell line SK-MEL2 was cultured in EMEM supplemented with 10% FBS, 1% glutamine, 100 µg/ml streptomycin, and 100 U/ml penicillin. Murine dendritic cell line JAWSII was cultured in alpha MEM supplemented with 20% FBS, 1% glutamine, 100 µg/ml streptomycin, and 100 U/ml penicillin. All the cell lines were purchased from ATCC. B16F1, a melanoma cell line from C57BL/6 mice, was kindly provided by Professor Veronique Preat (Université Catholique de Louvain, Belgium). B16F1 was cultured in MEM complete medium, containing 10%FBS, 100 µg/ml streptomycin, and 100 U/ml penicillin.

B16.OVA, a mouse melanoma cell line expressing chicken OVA, was kindly provided by Professor Richard Vile (Mayo Clinic, Rochester, MN, USA). B16.OVA cells were cultured in RPMI with 10% FBS, 1% L-glutamine, 1% penicillin/streptomycin, and 5 mg/mL Geneticin (Life Technologies). The cells were cultivated at 37°C, 5% CO_2 in a humidified atmosphere. The following peptides were used through the study and were purchased from Zhejiang Ontores Biotechnologies (Zhejiang, China):

DSGSPFPAAVILRDALHMARGLKYLHQ(PbK),

PSKPSFQEFVDWENVSPELNSTDQPFL (Kif18b), EFKHIKAFDRTFADNPGPMVRPWQSAS(Cpsf3l),

WNRQLYPEWTEAQRL (gp100) SVYDFFVWL (TRP2), KKKKKDSGSPFPAAVILRDALHMARGLKYLHQ (PbK),

KKKKKKKKKKPSKPSFQEFVDWENVSPELNSTDQPFL (Kif18b)

KKKKKEFKHIKAFDRTFADNPGPMVRPWQSAS (Cpsf3l)

KKKKKKWNRQLYPEWTEAQRL (gp100)

KKKKKKSVYDFFVWL (TRP2)

SIINFEKL (OVA)

KKKKKKSIINFEKL (OVA)

IFN-γ ELISpot

IFN-γ ELISpot assays were performed using a commercially available mouse ELISpot reagent set (ImmunoSpot, Bonn Germany) and 20 ng/uL of each peptide was tested in *in vitro* stimulations of $3x10^5$ splenocytes for each well at 37 °C for 72h. Spots were counted using an ELISpot reader system (ImmunoSpot, Bonn Germany).

INF-γ/IL-10 FluoroSpot

INF-γ/IL-10 FluoroSpot was performed using a commercially available mouse FluoroSpot reagent set (Mabtech, Nacka Strand, Sweden) and 20 ng/uL of each peptide was tested in *in vitro* stimulations of $3x10^5$ splenocytes for each well at 37 °C for 72h. Spots were counted using a FluoroSpot reader system (Nacka Strand, Sweden).

Quantification Assay for Ad-OVA

Human lung carcinoma A549 cells, human TNBC MDA-MB-436 cells, and human epithelial colorectal adenocarcinoma CACO-2 were infected with 10MOI, and the supernatant was collected at 24h post-infection. Murine TNBC 4T1 cells and murine CT26 colon cell line were infected with 500 MOI and the supernatant was collected at 48h and72h post-infection. The Human lung carcinoma A549 cell line was infected with 10 MOI and the cell pellet was collected at 48h post-infection. The cell lysate and the supernatants were analyzed for the presence of OVA by ELISA (ABIN2537475, Antibodies) according to the manufacturer´s instructions.

PeptiCRAd Complex Formation

The PeptiCRAd complex was prepared by mixing the oncolytic adenovirus and each peptide with a polyK tail. We mixed polyK-extended epitopes with Ad5/3D24 for 15 minutes at room temperature before treatments with the PeptiCRAd complexes. More details about the stability and formation of the complex can be found in our previous study (26).

Cross-Presentation Experiment

Murine dendritic JAWS-II cells were infected with 250 MOI of different viruses (Ad5/3-D24, Ad5/3-CMV-OVA, and PeptiCRA-SIINFEKL). One well was left uninfected as control. After 4 hours of incubation, the medium was changed and at 24h and 48h post-infection the cells were stained.

Animal Experiment

All animal experiments were reviewed and approved by the Experimental Animal Committee of the University of Helsinki and the Provincial Government of Southern Finland (license number ESAVI/11895/2019). 4-6 weeks old female C57BL/6JOlaHsd mice were obtained from Envigo (Laboratory, Bar Harbor, Maine UK).

For the prophylactic experiment, mice (n=10 per group) were allocated in different groups according to the treatment and each

mouse was subcutaneously injected with $1x10^9$ VP (viral particle). The prime and boosting were done respectively on days 1,2,3 and 10 and the mice were sacrificed on day 14. For the B16.OVA tumor-bearing mice experiment, $3x10^5$ B16.OVA cells were injected subcutaneously. Details about the schedule of the treatment can be found in the figure legends. For the B16F1 tumor-bearing mice experiment, $1x10^5$ and 0.5 $x10^5$cells were injected subcutaneously on the right and left flank of the mice respectively.

The viral dose was $1x10^9$ VP/tumor complexed with 20 μg of a single peptide or with 4 μg+4 μg 4 μg+4 μg +4 μg mixture of five peptides.

Oncolytic Adenovirus

In this study, the virus Ad-OVA, Ad-TRP2, and Ad-Epitopes were used and they were generated according to Hamdan et al. (28). Briefly, Ad-OVA, Ad-TRP2, and Ad-Epitopes are conditionally replicating adenovirus serotype 5 with adenovirus 3 fiber knob modification and 24-base pair deletion of the gene E1A. The CR1-alpha and gp19Kgenes of the E3A region were replaced with human cytomegalovirus (CMV) promoter region and OVA (Ad-OVA), murine TRP2 (Ad-TRP2), or five epitopes (Ad-Epitopes). The five epitopes are expressed as single peptides separated through a linker of arginine. The cloning cassette have been inserted in E3 adenoviral region. A rabbit β-globin polyadenylation signal was added. The VP concentration was measured at 260nm, and infections units (IU) were determined by immunocytochemistry (ICC) by staining the hexon protein in infected A549 cells.

Cell Viability Assays

Human SK-MEL-2 cells, human lung carcinoma A549 cells, human TNBC MDA-MB-436 cells, murine TNBC 4T1 cells, and murine melanoma B16.OVA and B16F1 cells were infected with various amounts of Ad-OVA, Ad-TRP2, Ad-Epitopes, and Ad5/3-D24 or left uninfected. Cells were analyzed for their viability3 and 5 days postinfection with the CellTiter 96 AqueousOne Solution MTS Reagent (Promega), according to the manufacturer's instructions, and a multi-well plate reader (Varioskan Flash; Thermo Labsystems) was used to determine the absorbance of the samples.

Flow Cytometry

The following antibodies were used in the cross-presentation experiments: TruStain Fcblock anti-mouse CD16/32 (101320; BioLegend), FITC-CD11c (117306; Biolegend), APC-H2Kb-bound SIINFEKL (141606; Biolegend), APC/Cy7-CD40 (124637; Biolegend), PerCP/Cy5.5- ICAM_1 (116123; Biolegend), BV510-CD86 (563077; BD), PE/Cy7-MHC-II (107629; Biolegend), V450-CD80 (12519; BD). The following antibodies were used for the immunological analysis in the *in vivo* animal experiments: FITC-CD8 (553062; BD), PE-CD4 (100408; Biolegend), APC-CXCR3 (562266; BD), PerCP/Cy5.5-CD3 (100732; Biolegend), PE-CXCR3 (155903); FITC-CD8 (11083782); PerCP/Cy5.5-CD3 (100328);. Flow cytometric analyses were performed using Fortessa LSR Flow Cytometer (BD Biosciences) or BD Accuri C6 Plus (BD Bioscience). FlowJo software v.10 (FlowJo) was used for the data analysis.

qPCR Analysis

B16F1 cell lines were collected 48 hours after infection and the RNA was extracted by using the Rneasy Plus Mini kit (74134, Qiagen), according to the protocol provided by the manufacturer. The RNA extraction quality was checked by electrophoresis in 1% agarose gel. The RNA samples were reverse-transcribed by SuperScript-IV Reverse Transcriptase (18091050, Invitrogen) and random hexamers as primers, according to the protocol provided by the manufacturer. The reverse transcription products were used as DNA templates for PCR reactions. The Real-Time PCR was performed using StepOnePlus _Real Time PCR system (Applied Biosystems). The qPCR experiment was designed as C_T comparative experiment (ΔC_T). As the fluorescent dye, SYBR Green was used (SYBR_Green PCR master mix, A25742, Applied Biosystem). Two reaction master mixes were prepared for two pairs of primers to amplify murine GAPDH and the epitopes, following the protocol provided by the manufacturer. 10 ng of cDNA as template and 200 nM of the primers were used for each reaction.

RT-PCR

Human lung adenocarcinoma A549 cells and murine TNBC 4T1 cells were infected with 5 and 100 MOI of Ad5/3-D24, Ad5/3-D24-CMV-TRP2, and Ad5/3-D24-CMV-OVA. pCMV-OVA was transfected as well as control with Lipofectamine (Lipofectamine 2000) according to the manufacturer's instructions The cells were collected 48 hours post-infection and the RNA was extracted by using the RNeasy Plus Mini kit (74134, Qiagen), according to the protocol provided by the manufacturer. The RNA samples were reverse-transcribed by SuperScript-IV Reverse Transcriptase (18091050, Invitrogen) and random hexamers as primers, according to the protocol provided by the manufacturer. The reverse transcription products were used as DNA templates for PCR reactions.

Statistical Analysis

Statistical analysis was performed using GraphPad Prism 9.0 software (GraphPad Software Inc.). Details about the statistical tests for each experiment can be found in the corresponding figure legends.

RESULTS

In Vitro Characterization of Oncolytic Adenovirus Encoding Model Tumor Antigens

The use of OVs encoding TAs has been extensively explored as cancer vaccines to take full advantage of both viral immunogenicity and tumor peptides that direct the specificity of the anti-tumor adaptive immune response. However, the vaccinal outcome heavily depends on the viral infectivity and consequently viral replication as each tumor owns a different sensitivity to OVs. To bypass this

limitation, we wanted to investigate whether the PeptiCRAd technology, based on OAd decorated with tumor antigens, could be considered a legitimate alternative cancer vaccine to OAd encoding TAs. To this end, we needed to generate OAds encoding TAs to be used for comparative studies. Therefore, we cloned OAds encoding the tumor model chicken ovalbumin (OVA) and the more relevant tumor antigen murine tyrosinase-related protein 2 (TRP_2) by applying GAMER-Ad protocol according to Hamdan et al. (28). Briefly, the region E3 was removed and replaced with the gene of interest (GOI) contained in E3 deleted of gp19K and 7.1K (**Figure 1A**). After constructing the adenovectors expressing the GOI, we digested and transfected the construct in A549, and we waited for the viral plaque formation. Once the plaques appeared, the viruses were harvested and purified. Next, we proceeded with an extensive validation of the generated novel OAd encoding TAs. First, we assessed whether the oncolytic fitness or replication of the viruses was affected upon the insertion of the GOI in the viral genome. The viruses have a 24-bp deletion in the E1A region conditioning such viruses to replicate only in Retinoblastoma (Rb)-deficient cells as the majority of human cancer cell lines are. Moreover, the OAd used through the study is serotype 5 with adenovirus 3 fiber knob modification, allowing the infection of a wider range of cells unrestrictedly to CAR receptor expression (29). Hence, lung carcinoma cells (A549), ovarian cancer cells (SKOV3), triple-negative breast cancer cells (MDA-MB-436), melanoma cells (SKMEL-2) were infected with unarmed Ad5/3Δ24, AdOVA, and AdTRP2 viruses. Oncolysis was observed at days 3 (**Supplementary Figures 1A–D**) and 5 (**Supplementary Figures 2A–D**) post-infection in a dose-dependent fashion. In all the analyzed cell lines, the oncolysis levels of the cloned viruses resembled those of the unmodified virus, indicating that the transgene did not affect oncolytic potency or virus replication. To further corroborate this, two murine cell lines, B16.OVA and 4T1 were also investigated. Human adenoviruses serotype can infect murine cell lines but are unable to replicate. As expected, no cell death was observed with either murine cell line when infected with the unmodified, AdOVA and AdTRP2 viruses, at day 3 (**Supplementary Figures 1E, F**) and day 5 (**Supplementary Figures 2E, F**) post-infection, showing that

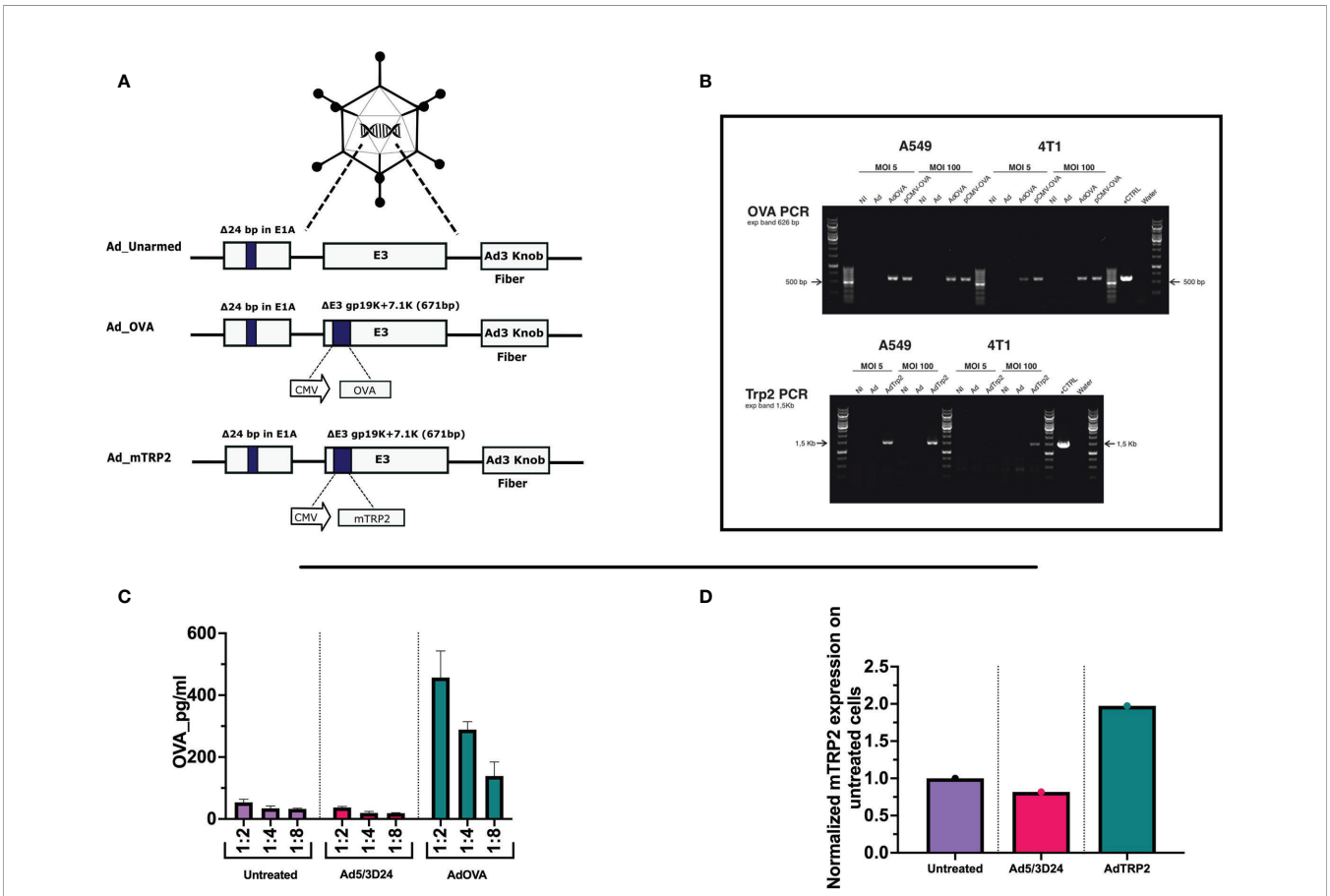

FIGURE 1 | Generation and characterization of AdOVA and AdTRP2 **(A)** Schematic representation of oncolytic adenovirus delta 24 (Ad5/3-D24) constructs with modifications in E1, E3, and fiber region. Both unarmed (Ad_unarmed) and armed (Ad_OVA and Ad_mTRP2) bear a deletion of 24bp in the E1A gene. Additionally, AdOVA (Ad_OVA) and AdTRP2 (Ad_mTRP2) contains an expression cassette under CMV promoter in E3 region. **(B)** Reverse-transcribed PCR reaction with specific primers for OVA and mTRP2 on cDNA derived from A549 and 4T1 infected with 5 and 100 MOI. **(C, D)** A549 cells were infected with 10MOI and the cell lysate was collected at 48h and OVA and TRP2 levels were checked by ELISA and the data are depicted as bar plots.

oncolytic fitness or replication was unaltered in the cloned viruses. We then investigated the transgene expression at both RNA and protein levels. Reverse transcription PCR confirmed the presence of mRNA expression for OVA in one human cell line (A549) and one murine cell line (4T1) infected with 5 and 100 MOI of AdOVA (**Figure 1B**). The presence of TRP_2 was confirmed in A549 at both 5 and 100MOI, whereas in 4T1, we detected the presence of 4T1 at 100MOI (**Figure 1B**). Moreover, the cell lysate from A549 infected with the cloned viruses was investigated for the presence of OVA and TRP_2. The analysis showed the expression at the protein level for both OVA (**Figure 1C**) and TRP_2 (**Figure 1D**). Moreover, the supernatant of human A549, MDA-MB-436, and CACO2 cell lines infected with AdOVA confirmed the protein expression of OVA (**Supplementary Figures 3A-C**); the results were confirmed in murine 4T1 and CT26 cell line AdOVA infected at 48h and 72h post-infection (**Supplementary Figures 3D, E**). Overall, the data confirmed that the insertion of the GOI in the viral genome permitted normal oncolytic activity and that the viruses expressed the transgene as demonstrated at both mRNA and protein levels, granting their use for further comparative analysis.

Peptides-Coated Platform Showed Immunogenic Activity Comparable to OAd Encoding TAs in *In Vitro* and *In Vivo* Studies

After the generation and characterization of AdOVA and AdTRP2, we used them as a benchmark as we carefully sought to characterize the immunological effects of PeptiCRAd. First, a comparative immunogenic analysis of PeptiCRAd and the cloned viruses was performed as regards APCs activation and antigen presentation. To this end, we used the murine dendritic cell line JAWS-II. As Ovalbumin is broadly studied and several tools are available for research purposes, the first comparative analysis was done exploiting AdOVA and the PeptiCRAd counterpart. Hence, JAWS-II cells were pulsed either with AdOVA or PeptiCRAd coated with the OVA epitope SIINFEKL; cells incubated with peptide or virus alone were used as controls. Then we stained the cells at 24h and 48h post-incubation with a monoclonal antibody specific for the OVA peptide SIINFEKL complexed with H2Kb. An example of the gating strategy is shown in **Supplementary Figure 4**. To determine whether the DCs were presenting the antigen in a tolerogenic or stimulatory manner, activation markers (CD80, CD86, MHC-II, CD40) were included in the analysis as well. Interestingly, at 24h post-incubation, H2Kb bound to SIINFEKL and the co-stimulatory factor CD86 were upregulated in JAWS-II treated either with PeptiCRAd-SIINFEKL or with AdOVA (**Figure 2A**). Instead, CD40 (**Supplementary Figure 5A**), CD80 (**Supplementary Figure 5B**), MHC-II (**Supplementary Figure 5C**) and the adhesion molecule ICAM-I (**Supplementary Figure 5D**) showed comparable expression among the different treatment groups. Additionally, we observed that in PeptiCRAd-SIINFEKL treated DCs the level of H2Kb bound to SIINFEKL and CD86 were higher compared to JAWS-II treated with AdOVA. Indeed, in DCs treated with PeptiCRAD-SIINFEKL, the expression of the H2Kb bound to SIINFEKL and CD86 markers were already high at 24h post-incubation, whereas AdOVA induced comparable levels of the H2Kb bound to SIINFEKL and CD86 at 48h post-incubation (**Figure 2B**). These results match the different kinetics of peptides versus proteins, with the first being directly available to DCs presentation and the latter depending on the vector expression and protein processing. Moreover, at 48h post-incubation CD40 (**Supplementary Figure 5E**), CD80 (**Supplementary Figure 5F**), MHC-II (**Supplementary Figure 5G**), and the adhesion molecule ICAM-I (**Supplementary Figure 5H**) showed similar expression

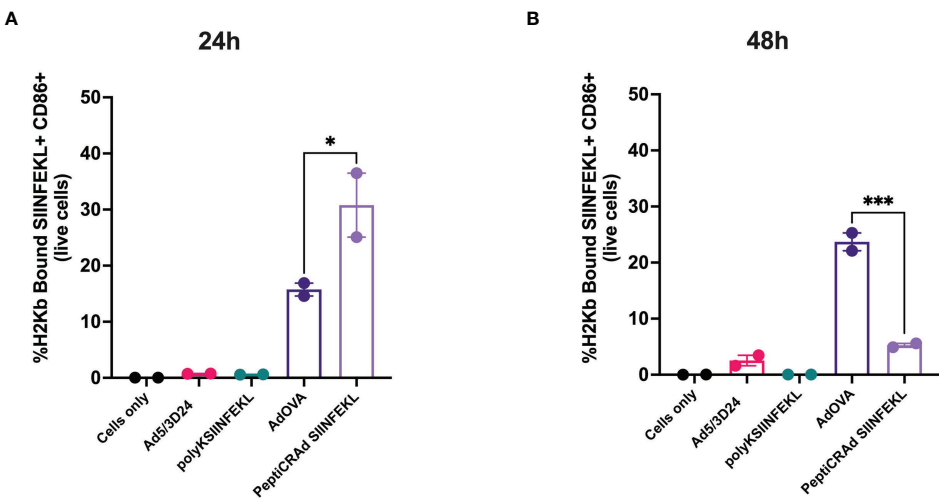

FIGURE 2 | DCs cross-present antigen in an immunogenic fashion upon stimulation with Ad encoding TAs or PeptiCRAd. Mouse dendritic cell line JAWS II was pulsed with Ad5/3Δ24, peptide alone (polyKSIINFEKL), AdOVA, PeptiCRAd-SIINFEKL or left unpulsed (cells only). The viruses were used at 250 MOI. Flow cytometry analysis was used to determine the cross-presentation at 24h **(A)** and 48h **(B)** post incubation. CD86 was used to measure DCs activation and an antibody specific for OVA peptide SIINFEKL complexed with H2Kb to detect the antigen presentation. The data are depicted as bar plot mean ± SEM. Statistical analysis was performed with ordinary One-way ANOVA (ns $P > 0.05$, *$P \leq 0.05$, **$P \leq 0.01$, ***$P \leq 0.001$, $P \leq 0.0001$).

pattern among the different treatment groups, whereas CD80 (**Supplementary Figure 5F**) was upregulated in the adenovirus treated cells. Next, as we wanted to characterize the *in vivo* efficacy of PeptiCRAd as a prophylactic vaccine in comparison to Ad encoding TAs, mice were immunized by subcutaneous direct injection of Ad-OVA and AdTRP2 and with counterpart coated peptide technology according to the schematic depicted in **Figure 3A**. Spleens were harvested at the end of the pre-immunization procedure and the T cell-specific immune response was functionally characterized by IFN-γ ELISPOT assay upon stimuli such as SIINFEKL and TRP2. Our data showed that both cloned viruses and PeptiCRAd induced T cell-specific response (**Figures 3B, C**) *in vivo*, confirming the stimulatory activity observed in *in vitro* experimental settings. Overall, the first set of results showed that peptide-coated oncolytic vaccine PeptiCRAd activates APCs that in turn prime and induce specific T cell response well in line with the established outcome of OAd encoding TAs used as cancer therapeutic vaccine.

Peptide-Coated Cancer Vaccine and OAd Encoding TAs Showed Similar Therapeutic Activity in a Syngeneic Mouse Model of B16.OVA Melanoma

As aforementioned, PeptiCRAd and OAd encoding TAs exerted similar immunological activity in both *in vivo* and *in vitro* experimental settings. These data prompted us to assess the therapeutic efficacy of PeptiCRAd compared to OAd encoding

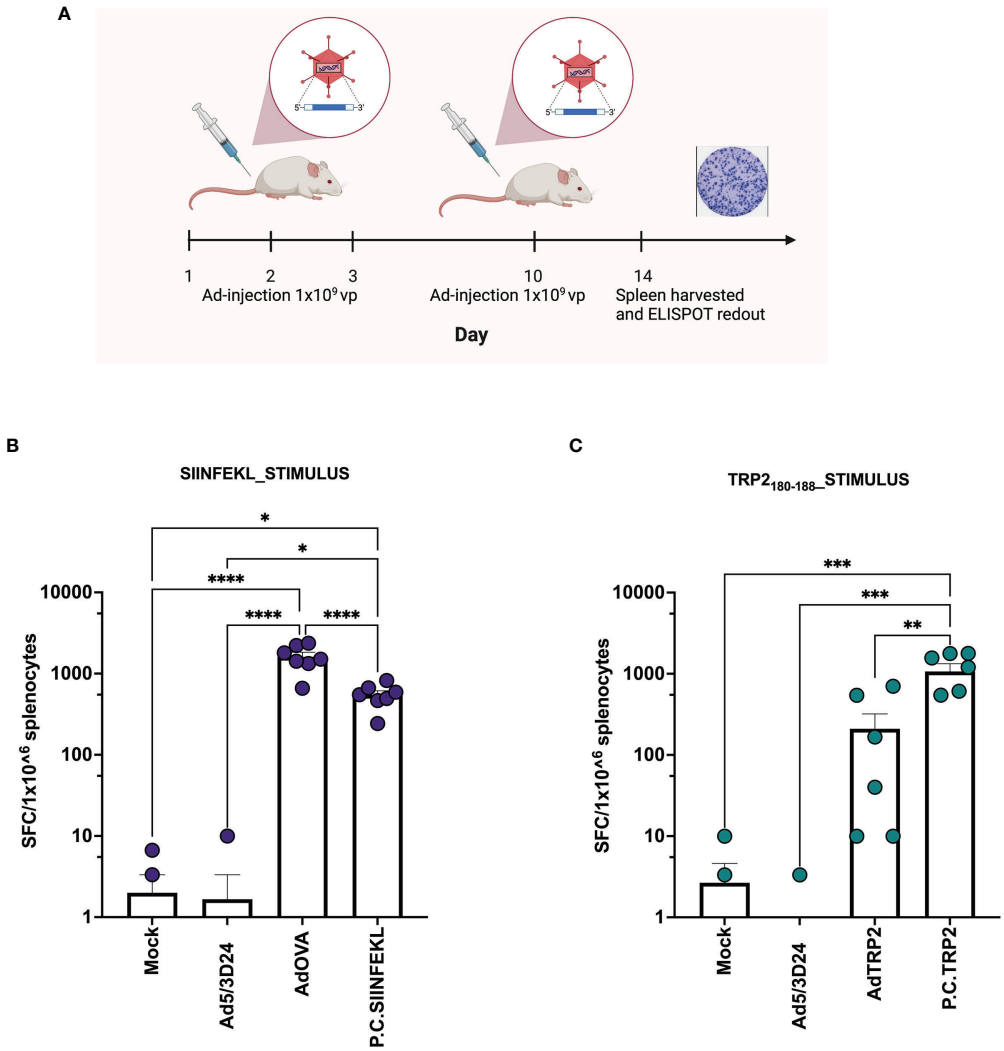

FIGURE 3 | Ad encoding TAs and PeptiCRAd show *in vivo* prophylactic efficacy. **(A)** Schematic representation of the schedule followed during the vaccination procedure. The mice have been subcutaneously injected with Ad5/3Δ24, PeptiCRAd (P.C. SIINFEKL, P.C. TRP2), cloned viruses (AdOVA, AdTRP2) or PBS (Mock) at day 1,2,3 and 10. The spleens were harvested at day 14. **(B, C)** IFN-γ ELISpot was performed on harvested splenocytes and individual response to SIINFEKL **(B)** and TRP2 **(C)** for each mouse is reported as IFN-γ spot forming cells (SFC)/10^6 splenocytes. The data are depicted as bar plot and mean + SEM is shown. (P.C.=PeptiCRAd) and the statistical analysis was performed with ordinary One-way ANOVA (ns $P > 0.05$, *$P \leq 0.05$, **$P \leq 0.01$, ***$P \leq 0.001$, ****$P \leq 0.0001$). Created with BioRender BioRender.com.

TAs in a poorly immunogenic tumor model. To this end, immunocompetent C57Bl/6 mice were subcutaneously injected with the syngeneic B16.OVA melanoma tumor cells in the right flank. When the tumors were established, the mice were intratumorally treated either with AdTRP2 or the PeptiCRAd counterpart. Mice injected only with PBS (Mock) and Ad5/3Δ24 groups were used as controls; the viral dose used was $1x10^9$ VP/tumor. PeptiCRAd and AdTRP2 improved tumor growth control (**Figure 4A**) as depicted also in the single tumor growth per mouse per each treatment group, with 63% and 86% of responders respectively in AdTRP2 and PeptiCRAd treated mice (**Figure 4B**). Next, we sought to investigate the immunological modulation due to different therapeutic regimens. First, we observed an increase in the CD8+ T cell population in spleens of mice treated with PeptiCRAd (**Figure 4C**) compared to other groups; to dissect the functional profile of those CD8+ T cells, an INF-γ ELISPOT assay was performed on the spleen of the treated mice; upon TRP2 stimulus the production of IFN-γ increased significantly in PeptiCRAd treated mice, highlighting systemic generation of specific anti-tumor T cells following PeptiCRAd treatment (**Figure 4D**). Moreover, CD8+ T cells showed an increasing trend within the tumor microenvironment (**Figure 4E**) in all the groups that underwent adenovirus-based treatment (Ad5/3Δ24, AdTRP2, and PeptiCRAd); however, a tendency in increased effector phenotype CXCR3+ among the CD8+ T cells was reported only in PeptiCRAd treated group (**Figure 4F**).

Overall, the data confirmed that PeptiCRAd technology could be a valid alternative to OAd encoding TAs; from an immunological point of view, PeptiCRAd elicited specific anti-tumor T cells response in secondary lymphoid organs, additionally inducing an increased tumor infiltration of effectors phenotype CD8+T cells.

PeptiCRAd as Prophylactic Vaccine-Induced Specific Anti-Tumor Immune Response Addressing Tumor Heterogeneity

After demonstrating that PeptiCRAd technology could be used as a treatment alternative to OAd encoding TAs as regard both prophylactic and therapeutic efficacy by exploiting the tumor model antigens OVA and TRP2, we aimed to challenge our technology to address the complex tumor heterogeneity. Indeed, upon mutations, the immunopetidomic landscape of cancer cells changes and novel mutated epitopes named tumor neo-antigens (TNAs) are presented within the MHC-I complex (30). These latter are preferential targets for cancer treatment as they bypass the negative T-cell clonal selection (31). Moreover, to engage both arms of adaptive immune response (CD8 and CD4), we included in the subsequent experimental setting also MHC-II restricted epitopes. Hence, we sought to investigate whether PeptiCRAd could exert immunological modulation also in the context of MHC-I and MHC-II TNAs, benchmarking our technology by using OAd encoding TNAs. To this end, we have first generated an OAd encoding five different neo-epitopes (AdEpitopes) previously described in the B16F1 melanoma model (PbK, Kif18b, Cpsf3l, gp100, and TRP_2) (27). Briefly, to generate the AdEpitopes we used the GAMER-Ad protocol described in Hamdan et al. (28), removing the region E3 and replacing it with the GOI a poly-epitopes construct contained in E3 deleted of gp19K and 7.1K (**Figure 5A**). To assess whether the insertion of the transgene could interfere with the oncolytic activity of the cloned virus, we infected the human lung (A549) cancer cell line, the human triple-negative breast (MDA-MB-436) cancer cell line, the human ovarian (SKOV3) cancer cell line and the human melanoma (SKMEL-2) cancer cell line with different amount of MOI and we checked the cell viability at day 3 (**Supplementary Figures 6A-D**) and 5 (**Supplementary Figures 7A–D**) post-infection. The cloned virus showed oncolytic activity accordingly to MOI concentration, resembling the unarmed OAd (Ad5/3D24) and thus confirming that the presence of the GOI in the viral genome was compatible with the adenoviral replication and oncolytic activity. Additionally, two murine cell lines (4T1 and CT26) were infected at different MOI and the cell viability was checked as well at day 3 (**Supplementary Figures 6E, F**) and 5 (**Supplementary Figures 7E, F**) post-infection. The cell viability was stable during the infection, confirming that human OAd oncolytic activity is restricted to the human setting. Next, we analyzed the expression of GOI in the B16F1 cell line infected with 5 MOI of the cloned virus. Cells not infected and cells infected with unarmed virus (Ad5/3Δ24) were used as control. RNA was extracted from B16F1, and real-time quantitative reverse transcriptase-polymerase chain reaction (qRT-PCR) was performed; the results confirmed the presence of the transgene in the transfected cells at RNA level (**Figure 5B**). Next, we wanted to assess the prophylactic activity of PeptiCRAd decorated with the neoepitopes in comparison to the cloned virus. Hence, mice were pre-immunized either with the cloned virus or with PeptiCRAd counterpart, and the spleens were harvested at the end of the pre-immunization protocol to investigate the T cell response induced following the different regiments administrated. The IFN-γ ELISPOT assay showed specific TRP2 T-cell response in both PeptiCRAd and AdEpitopes preimmunized mice (**Figure 5C**) and interestingly PeptiCRAd inducted a statistically higher amount of specific T cells compared to AdEpitopes (**Figure 5C**); even though the adenoviral T-cells response was observed in all the groups adeno pre-immunized (Ad5/3Δ24, AdEpitopes and PeptiCRAd), the anti-viral response elicited in both AdEpitopes and in PeptiCRAd was statically lower compared to Ad5/3Δ24 (**Figure 5C**). This suggests that both approaches shifted the immune response from being mainly antiviral to being mainly tumor-antigenic specific, with PeptiCRAd showing the best performance in switching the immune response from antiviral to antigen-specific T cells (**Figure 5C**). Upon antigenic stimulation, we also detected the level of IL-10 in the cultures of splenocytes; a high release of IL-10 was observed in PeptiCRAd treated group upon TRP2 stimulus, suggesting that CD8+T cells were highly activated and cytolytic (32) (**Figure 5D**). Upon adeno stimulation, the highest production

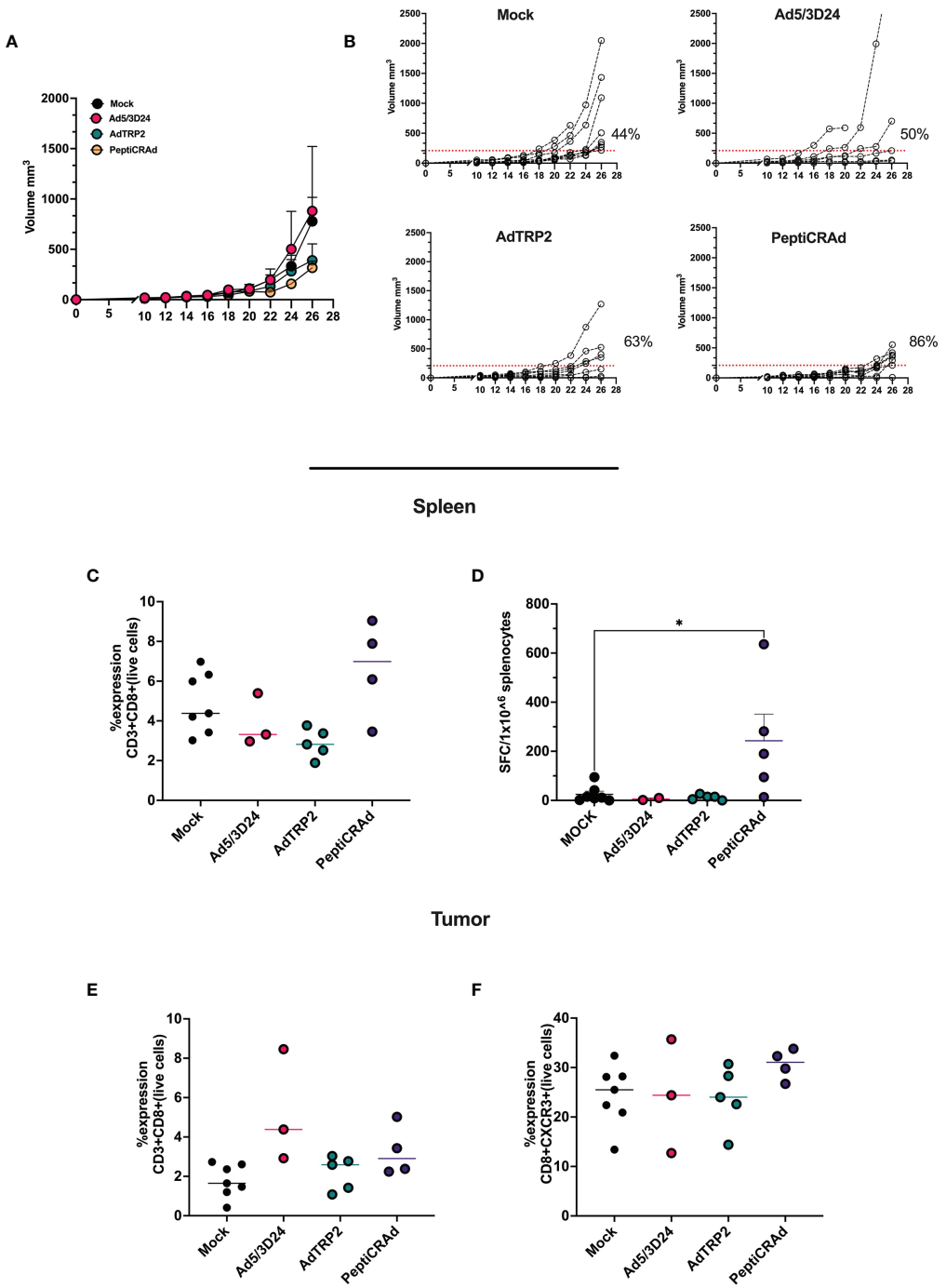

FIGURE 4 | Intratumorally administration of PeptiCRAd induced tumor regression and immunological modulation **(A)** Ad5/3Δ24, AdTRP2 or PeptiCRAd was given intratumorally at 9,11,13 and 15 days post tumor implantation. The tumor growth was followed until the end of the experiment and the tumor size is presented as the mean ± SEM. Statistically difference was assessed with two-way ANOVA (ns $P > 0.05$, *$P \leq 0.05$, **$P \leq 0.01$, ***$P \leq 0.001$, $P \leq 0.0001$). (Mock n=9, Ad5/3Δ24 n=6 AdTRP2 n=8 or PeptiCRAd n=7) **(B)** Single tumor growth for single mouse for each treatment group is depicted. A threshold of 209 mm^3 was set to define the percentage of mice responding to the different therapies (red dotted line). The percentage of responders in each treatment group is shown on the right side of the dotted line. (The threshold was defined as the median of the tumor size at the last day of the experiment in the Ad5/3Δ24 treated group). **(C)** Flow cytometry analysis of spleens from treated mice showing the frequency of CD8+T cells. Data are expressed as single dot for each mouse and median is reported **(D)** IFN-γ ELISpot was performed on harvested splenocytes and individual response to TRP2 for each mouse is reported as IFN-γ spot forming cells (SFC)/10^6 splenocytes. The data are depicted as dot plot and mean ± SEM is shown. Statistical analysis was performed with ordinary One-way ANOVA (ns $P > 0.05$, *$P \leq 0.05$, **$P \leq 0.01$, ***$P \leq 0.001$, $P \leq 0.0001$). The frequency of CD8+ **(E)** and CD8+CXCR3+ **(F)** was analyzed in TME through flow cytometry analysis and the data are shown as single dot for each mouse and median is reported.

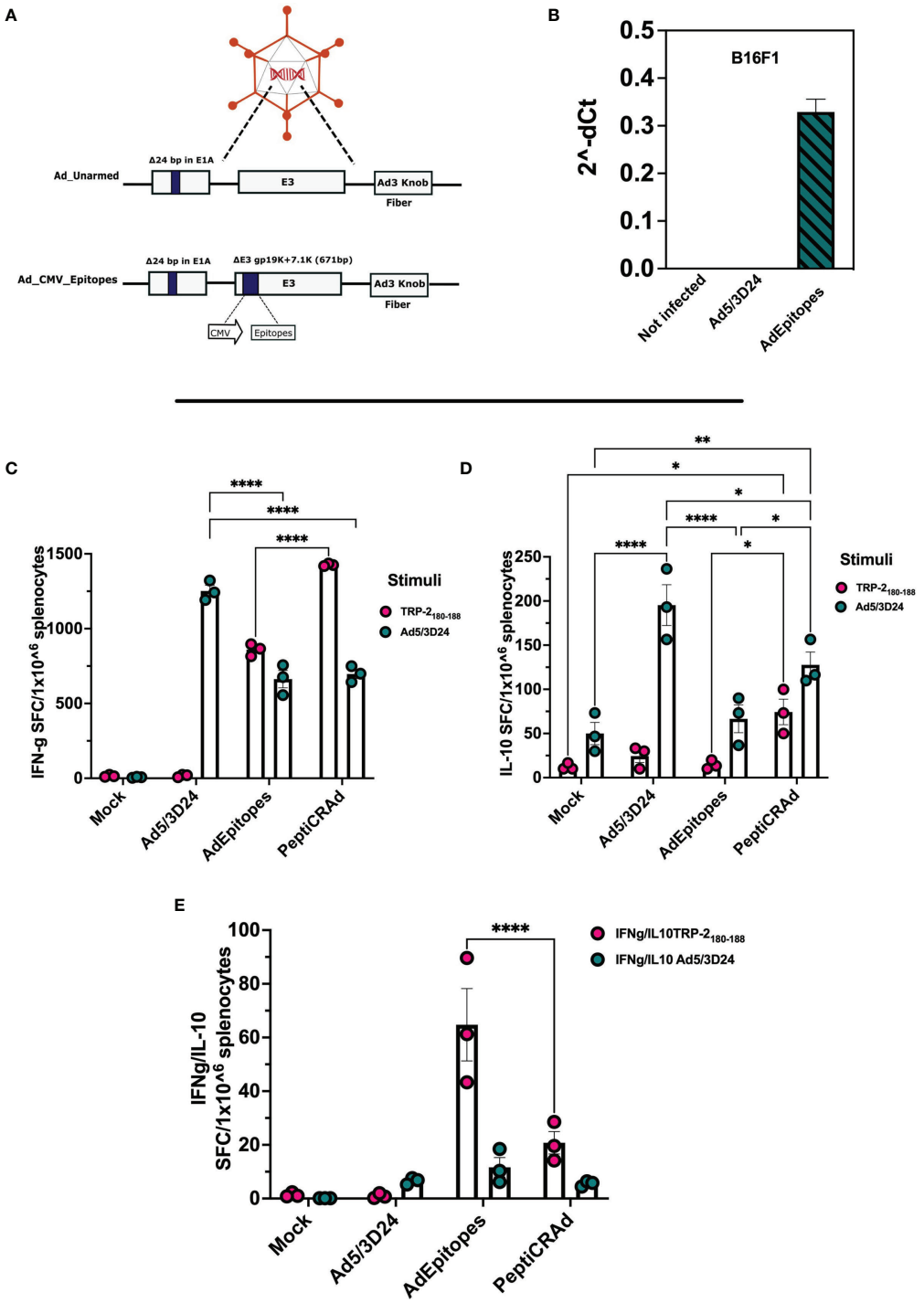

FIGURE 5 | Generation and characterization of AdEpitopes **(A)** Schematic representation of oncolytic adenovirus delta 24 (Ad5/3-D24) constructs with modifications in E1, E3, and fiber region. Both unarmed (Ad_unarmed) and armed (Ad_CMV_Epitopes) bear a deletion of 24bp in the E1A gene. Additionally, AdEpitopes (Ad_CMV_Epitopes) contains an expression cassette under CMV promoter in E3 region. **(B)** Real-time PCR was performed in B16F1 infected with 5MOI of AdEpitopes, Ad5/3Δ24 or left untreated (not infected) and the fold gene expression is analyzed as 2^{-dCt}.The data are represented ad bar blot and mean ± SEM. **(C)** IFN-γ ELISpot was performed on harvested splenocytes from mice treated with Ad5/3Δ24, AdEpitopes or PBS (Mock). The individual response to TRP2 (pink) and Ad5/3Δ24 (green) is reported as IFN-γ spot forming cells (SFC)/10^6 splenocytes. **(D)** IL-10 FluoroSpot evaluated the level of IL-10 released upon stimulation with TRP2 (pink) and Ad5/3Δ24 (green) in splenocytes harvested from mice immunized with Ad5/3Δ24, AdEpitopes or PBS (Mock). **(E)** The ratio IFN-γ/IL-10 spot forming cells is depicted and TRP2 (pink) and Ad5/3Δ24 (green). The data are shown as bar and dot plot for each technical replicate, and mean ± SEM. Significance was assessed with ordinary One-way ANOVA (ns $P > 0.05$, *$P \leq 0.05$, **$P \leq 0.01$, ***$P \leq 0.001$, ****$P \leq 0.0001$).

of IL-10 was instead reported in the Ad5/3Δ24 treated group, well in line with the previous observation that either AdEpitopes or PeptiCRAd shifted the immune response from mainly anti-viral to mainly anti-tumoral (**Figure 5D**). Strictly, the ratio IFN-γ/IL-10 was increased in AdEpitopes treated mice upon TRP2 stimulation compared to PeptiCRAd (**Figure 5E**), suggesting that PeptiCRAd induced more activated and cytolytic CD8+T cells compared to AdEpitopes as both IFN-γ and IL-10 showed upregulation in PepitCRAd (**Figure 5E**). The data demonstrated that we have first generated an OAd encoding TNAs that we used in turn to benchmark PeptiCRAd with main regard to its prophylactic efficacy. The results showed similar immune efficacy in eliciting a specific anti-tumor response, highlighting however that PeptiCRAd could induce more activated and cytolytic immunophenotypes in the CD8+ T cells population compared to AdEpitopes.

PeptiCRAd Monotherapy Created a Systemic Anti-Tumor Immune Response Controlling the Tumor Growth of Distant Untreated Cancer Lesions in a Poorly Immunogenic Melanoma Model

We have demonstrated that PeptiCRAd technology elicited a specific anti-tumor immune response at a similar magnitude to cloned viruses regarding its prophylactic activity. Next, we wanted to assess whether PeptiCRAd could work as a therapeutic approach also in the context of TNAs. To this end, immunocompetent C57Bl/6 mice were subcutaneously injected with the syngeneic B16F1 melanoma cells in the right and left flanks. When the tumors were established, AdEpitopes or PeptiCRAd counterpart were injected intratumorally only in the right tumors. Mock and Ad5/3Δ24 were used as controls; the viral dose used was $1x10^9$ VP/tumor. At the end of the experiment, AdEpitopes and PeptiCRAd showed tumor growth control in the treated lesions with the same efficacy of Ad5/3Δ24 (**Figure 6A**) as depicted also in the single tumor growth per each mouse per each treatment group (**Figures 6B–E**), indicating local anti-tumor activity due mainly to Ad5/3Δ24. However, both AdEpitopes and PeptiCRAd counterparts, but not Ad5/3Δ24 slowed down the tumor growth of the not-injected lesion (left side) (**Figure 6A**), highlighting that both approaches elicited systemic anti-tumor specific response. These observations prompted us to further investigate the immune components within the untreated lesions (left side). First, we observed a statically relevant increased infiltration of CD8+ T cells in both AdEpitopes and PeptiCRAd treated mice (**Figures 7A, B**); moreover, as both approaches also engaged MHC-II restricted epitopes, accordingly a tendency in increased CD4+T (**Figure 7C**) cells was also observed. The migratory marker CXCR3 was in general downregulated in the CD8+T cells population, whereas PeptiCRAd statically increased the CXCR3+CD8+T cells within the TME of the untreated lesions (**Figure 7D**).

Altogether, the data confirmed that PeptiCRAd monotherapy effectively exerts anti-tumoral activity in the context of TNAs through modulation of the immune response, in particular modulating the adaptive immune response (CD4+ and CD8+ T cell population). PeptiCRAd acted as efficiently as a traditional OAd encoding TNAs, acting as de facto cancer vaccines.

In conclusion, we have exploited a "plug-and-play" technology named PeptiCRAd, based on decorating OVs (OAd) with tumor peptides to elicit specific anti-tumor T cell response and we have carefully analyzed this technology in comparison to conventional oncolytic cancer vaccines. Indeed, we combined the viral immunogenicity with tumor peptides to guide the immune response specifically to the eradication of cancer. Compared to conventional OAd encoding tumor antigens, PeptiCRAd showed comparable efficacy in both prophylactic and therapeutic profiles. Moreover, PeptiCRAd showed anti-tumor efficacy in the context of TNAs, generating a systemic anti-tumor response to the same extent as the counterpart conventional cancer OV. However, PeptiCRAd retains the advantage of being rapidly adapted by coating the adenovirus with a new set of tumor antigens, a crucial key in personalized cancer vaccines clinical setting and therefore PeptiCRAd can be considered a valid alternative to OAd encoding TAs.

DISCUSSION

In this work, we have investigated PeptiCRAd, a "plug-and-play" technology based on OAd coated with tumor peptides to assess its prophylactic and therapeutic efficacy in comparison to conventional OAd encoding TAs, that currently represent one of the most exploited platforms in the field for cancer vaccines due to its immunogenicity and tumor cell lysis capability (33). PeptiCRAd consists of an OAd coated through electrostatic interactions with positively charged MHC-I restricted tumor peptides (poly-lysine tail-peptides) (26). The reaction requires only 15 minutes and several studies have shown its anti-tumor efficacy and immunological modulation in different contexts and tumor models such as murine triple-negative breast cancer (34), as a cancer therapeutic platform for immunopeptidomic pipelines (7, 35), as a tool to explore viral mimicry to tumor antigens for cancer immunotherapy (36), as a platform to exploit pre-existing immunity to pathogens for boosting anti-tumoral CD8 T cell response (37) or to decorate with tumor peptides OAd encoding immunostimulatory molecules (38). However, we have never compared our cancer vaccine platform with traditional approaches in the field such as OAd genetically modified to encode TAs. Therefore, here we have aimed to confront the immunological modulation and anti-tumor profile of PeptiCRAd with OAd encoding TAs. To mimic clinically relevant context, we have generated and characterized *in-house* OAd encoding TAs. As the production of novel OAd encoding TAs requires validation and characterization procedure, for each cloned OAd we have always investigated the oncolytic activity and the transgene expression at both RNA and protein level whenever it was technically possible. Indeed, the manufacture of cancer therapeutic vaccines is still facing the limitation of identifying a delivery system that is cost-effective and timely convenient (39, 40). In contrast, PeptiCRAd is a

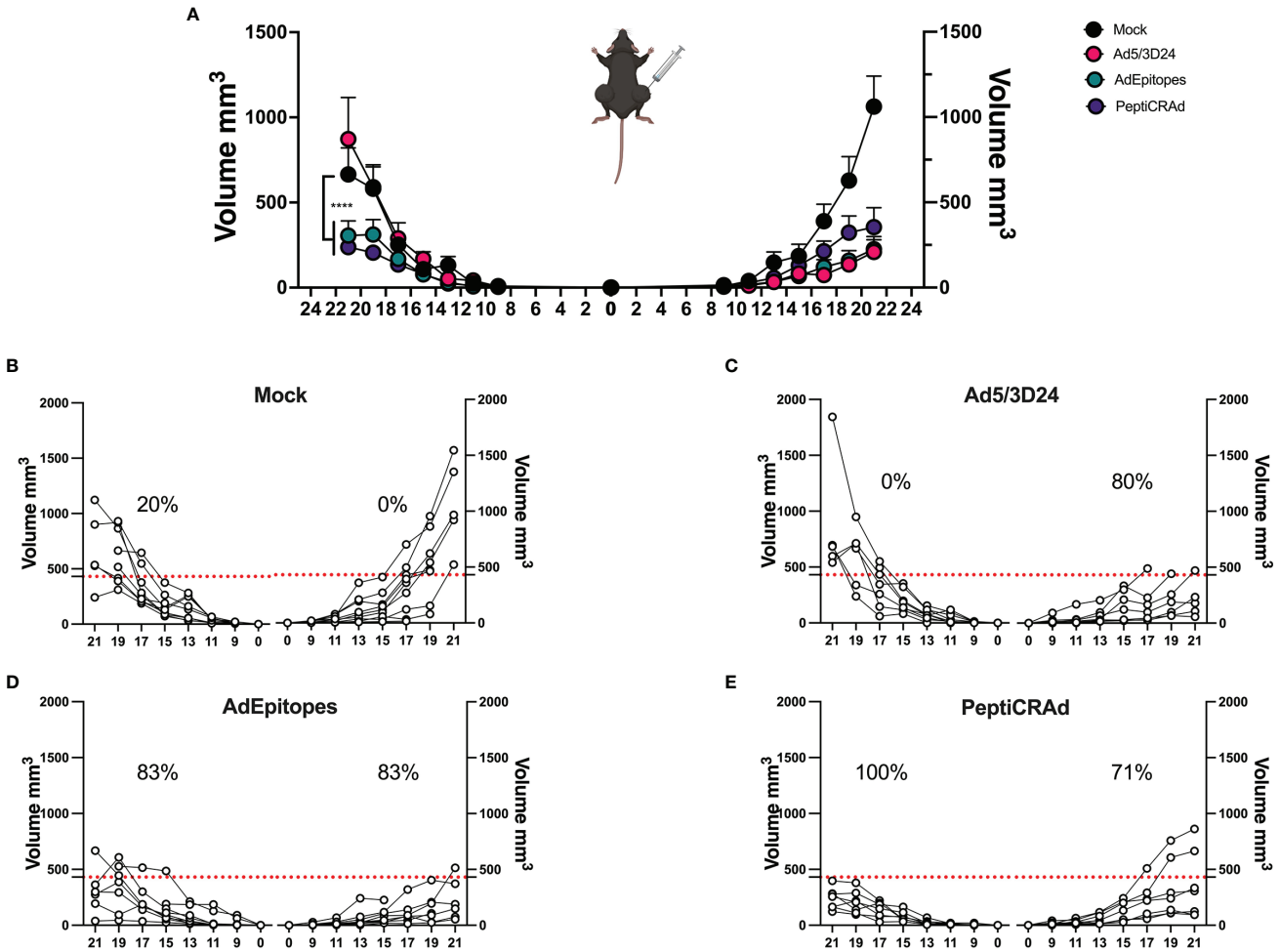

FIGURE 6 | PeptiCRAd elicited local and systemic antitumor response in a poor immunogenic tumor melanoma model. **(A)** Immunocompetent C57Bl/6 mice were subcutaneously injected with the syngeneic tumor model B16.F1 in the left ($0.5x10^4$ cells) and right flank ($1x10^5$). Ad5/3Δ24, AdEpitopes and PeptiCRAd were intratumorally administrated four times, two days apart starting from day 9. The B16F1 tumor growth was followed until the end of the experiment and the tumor size is presented as the mean ± SEM and statistically difference was assessed with two-way ANOVA; (ns $P > 0.05$, *$P \leq 0.05$, **$P \leq 0.01$, ***$P \leq 0.001$, ****$P \leq 0.0001$). **(B–E)** Single tumor growth for single mouse for Mock **(B)**, Ad5/3Δ24 **(C)**, AdEpitopes **(D)** and PeptiCRAd **(E)** is shown. A threshold of 431 mm^3 was set to define the percentage of mice responding to the different therapies (red dotted line) for right and left tumors. The percentage of responders in each treatment group is shown on the top of the dotted line. The threshold was defined as the median of the tumor size at the last day of the experiment in Ad5/3Δ24 treated group. (Mock n=9, Ad5/3 Δ24n=9, AdEpitopes n= 9, PeptiCRAd n=8).

cloning-free technology that relies on coating OAd with tumor peptides, making it easily adaptable to personalized cancer medicine. Additionally, upon advancements in manufacturing and manipulation, the peptides are relatively less expensive and due to their synthetic nature, batch-to-batch variation is avoided (41). However, the immunogenicity of peptides is limited, and several strategies have been explored to enhance their efficacy (42, 43). PeptiCRAd offers a solution for both time-demanding vaccine platform development and the weak immunogenicity of peptide-based therapy thanks to fast electrostatic interaction and the adenoviral immunostimulatory properties. Through this work, we have adopted two main strategies for the comparative analysis: *in vitro* stimulation of murine dendritic cell line and *in vivo* murine vaccination studies. The proof of concept has exploited the tumor antigen OVA because several tools and specific antibodies are available for the downstream detection of this antigen; the *in vitro* study highlighted that both AdOVA and PeptiCRAd have elicited the presentation of TAs in an immunogenic fashion as shown by the contemporaneity expression of H2Kb-bound to SIINFEKL and upregulation of CD86 molecule; in details, PeptiCRAd induced immunogenic modulation already 24h post-infection, whereas AdOVA required 48h. The different kinetic is explained by the nature of the two platforms. The cloned virus´ antigen expression relies on the translation of the construct, in contrast, PeptiCRAd directly delivers the peptides to DCs, priming the APCs faster and avoiding issues related to the genetic expression of TAs.

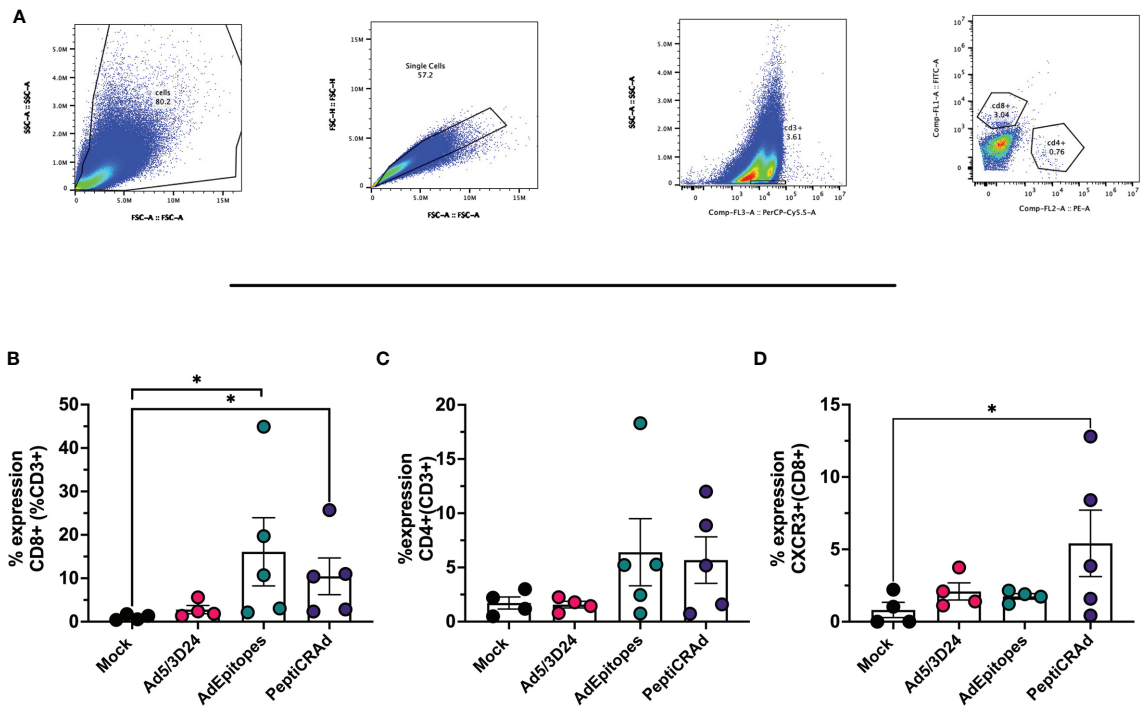

FIGURE 7 | PeptiCRAd induced immune infiltration in distant not treated cancer lesions. **(A)** A representative gating strategy for the flow cytometry analysis of the untreated tumors is showed. **(B–D)** The immunological T cell profile was investigated in untreated lesions by flow cytometry. The frequency of CD8+ **(B)**, of CD4+ **(C)** and CXCR3+ (CD8+) **(D)** T cells is shows. All the data are plotted as dot plot for each tumor and for each treatment group as mean± SEM. The significance was assessed by One way ANOVA and Tukey's correction (ns P > 0.05, *P ≤ 0.05, **P ≤ 0.01, ***P ≤ 0.001, P ≤ 0.0001).

Indeed, a well-known bottleneck in the application of OVs encoding TAs as cancer therapeutic vaccines is that transgene expression depends on viral genome replication. Indeed, this latter requires robust viral infection and ultimately the vaccination depends on the unpredictable and highly variable intrinsic sensitivity of each tumor to OVs (25). Once we showed that the priming of DCs in *in vitro* experimental settings was comparable at least under a quality point of view between AdOVA and PeptiCRAd, we needed to further explore the licensing and generation of antigen-specific T cells upon DC activation. To this end, the adaptive immune response was assessed in *in vivo* by preimmunization of mice. The functional characterization of T cell response confirmed that vaccination with PeptiCRAd could induce antigen-specific T-cells response to the same extent as cloned viruses and, most importantly, our proof of concept has shown the same results also with the clinically relevant tumor antigen $TRP2_{180\text{-}188}$. However, to compare the anti-tumoral efficacy with OAd encoding TAs, our technology was used as a therapeutic approach for the treatment of tumor-bearing mice. The tumor growth was slowed down in PeptiCRAd as well as in AdTRP2, confirming that our technology has activated DCs that in turn have primed and generated specific T-cells response; these latter have then exercised anti-tumor activity. The first part of our work has confirmed that our technology worked similarly to a conventional adeno-based cancer vaccine. Next, we have moved to a more relevant clinical scenario, involving the use of TNAs for cancer therapeutic approaches. Indeed, in cancer immunotherapy TNAs have gained momentum, becoming the preferential target of several therapeutic strategies. TNAs are selectively expressed in cancer cells, minimizing immune tolerance as well as autoimmune reactions (44); additionally, TNAs are more likely to engage CD8+ T-cell response and in this sense, the cancer immunotherapy could exploit personalized treatments, taking into account cancer patients' mutanome for a rational design of cancer therapeutic vaccine (45–47). To answer this need, we have applied our technology for the targeting of five TNAs found in the murine cell line B16F1, as previously described (27). Herein, we have generated an OAd encoding the five TNAs and then performed an *in vivo* characterization in mice to test both the prophylactic and the therapeutic efficacy. The prophylactic results have confirmed the efficacy of both approaches in generating specific T- cell response and, interestingly, the detection of IL-10 in mice pre-immunized with PeptiCRAd indicated highly activated and cytolytic CD8+ T-cells (32). This observation was well in line with the anti-tumor effect observed in mice bearing the tumor melanoma B16F1. Interestingly, both AdEpitopes and PeptiCRAd controlled the tumor growth of both the injected and not-injected lesions. This effect is known as "abscopal effect" and it indicated the generation of a systemic specific anti-tumor response able to eradicate distant lesions (48). The

data were then confirmed by subsequent immunological analysis, showing an increased infiltration of effector CD8+ T cells within the TME.

In summary, PeptiCRAd could serve as a platform for cancer oncolytic vaccines, as we showed that the immunological profile and the anti-tumor activity are comparable to conventional cloned-based adenoviral platform vaccines. In addition, PeptiCRAd offers an easy and time-effective solution for the generation of therapeutic vaccines. Secondly, the antigen is delivered as a peptide and it is readily available to APCs, meaning that the issues related to genetic expression are avoided. Third, PeptiCRAd can be easily customized depending on the patient´s specific mutations and tumor development. Finally, as OAd is decorated with peptides, the viral genome can be modified to express transgenes such as immunostimulatory molecules (i.e.GM-CSF). Ultimately, we could combine in a single platform, viral immunogenicity with a specific antitumor response guided by the peptides and an enhanced immune activation due to the expression of immunostimulatory molecules encoded in the viral genome.

DATA AVAILABILITY STATEMENT

The original contributions presented in the study are included in the article/**Supplementary Material**. Further inquiries can be directed to the corresponding author.

ETHICS STATEMENT

All animal experiments were reviewed and approved by the Experimental Animal Committee of the University of Helsinki and the Provincial Government of Southern Finland (license number ESAVI/11895/2019).

AUTHOR CONTRIBUTIONS

SF: conception and design, acquisition of data, analysis and interpretation of data, drafting of manuscript. SR: conception and design, acquisition of data, analysis and interpretation of data, drafting of manuscript. BM: conception and design, analysis and interpretation of data, drafting of manuscript. AL: acquisition of data, analysis and interpretation of data. GV: acquisition of data, analysis and interpretation of data. VF: revising of manuscript. CG.: analysis and interpretation of data. MF: interpretation of data, revising of manuscript. SP: interpretation of data, revising of manuscript. EY: analysis and interpretation of data, revising of manuscript. MiF: analysis and interpretation of data, revising of manuscript. SP: interpretation of data, revising manuscript. GA: interpretation of data, revising manuscript. JC: interpretation of data, revising of manuscript. FH: interpretation of data, revising of manuscript. MF: conception and design, interpretation of data, revising of manuscript. MG: conception and design, interpretation of data, revising of manuscript. VC: conception and design, acquisition of data, analysis and interpretation of data, drafting of manuscript. All authors contributed to the article and approved the submitted version.

FUNDING

This work has been supported by the European Research Council under the European Union's Horizon 2020 Framework program (H2020)/ERC-CoG-2015 Grant Agreement No. 681219, the Helsinki Institute of Life Science (HiLIFE), the Jane and Aatos Erkko Foundation (decision 19072019), the Cancer Society of Finland (Syöpäjärjestöt).

ACKNOWLEDGMENTS

We thank all the participants for their support and advice. Moreover, flow cytometry analysis was performed at the HiLife Flow Cytometry Unit, University of Helsinki.

SUPPLEMENTARY MATERIALS

The Supplementary Material for this article can be found online at: https://www.frontiersin.org/articles/10.3389/fimmu.2022.826164/full#supplementary-material

REFERENCES

1. Waldman AD, Fritz JM, Lenardo MJ. A Guide to Cancer Immunotherapy: From T Cell Basic Science to Clinical Practice. *Nat Rev Immunol* (2020) 20 (11):651–68. doi: 10.1038/s41577-020-0306-5
2. Chen DS, Mellman I. Oncology Meets Immunology: The Cancer-Immunity Cycle. *Immunity* (2013) 39(1):1–10. doi: 10.1016/j.immuni.2013.07.012
3. Kumar AR, Devan AR, Nair B, Vinod BS, Nath LR. Harnessing the Immune System Against Cancer: Current Immunotherapy Approaches and Therapeutic Targets. *Mol Biol Rep* (2021) 48(68):1–21. doi: 10.1007/s11033-021-06752-9
4. Melief CJ, van der Burg SH. Immunotherapy of Established (Pre)Malignant Disease by Synthetic Long Peptide Vaccines. *Nat Rev Cancer* (2008) 8(5):351–60. doi: 10.1038/nrc2373
5. Rabu C, Rangan L, Florenceau L, Fortun A, Charpentier M, Dupre E, et al. Cancer Vaccines: Designing Artificial Synthetic Long Peptides to Improve Presentation of Class I and Class II T Cell Epitopes by Dendritic Cells. *Oncoimmunology* (2019) 8 (4):e1560919. doi: 10.1080/2162402X.2018.1560919
6. Zhang L, Huang Y, Lindstrom AR, Lin TY, Lam KS, Li Y. Peptide-Based Materials for Cancer Immunotherapy. *Theranostics* (2019) 9(25):7807–25. doi: 10.7150/thno.37194
7. Feola S, Chiaro J, Martins B, Russo S, Fusciello M, Ylösmäki E, et al. A Novel Immunopeptidomic-Based Pipeline for the Generation of Personalized Oncolytic Cancer Vaccines. *eLife* (2022) 11:e71156. doi: 10.7554/eLife.71156
8. Bassani-Sternberg M, Braunlein E, Klar R, Engleitner T, Sinitcyn P, Audehm S, et al. Direct Identification of Clinically Relevant Neoepitopes Presented on Native Human Melanoma Tissue by Mass Spectrometry. *Nat Commun* (2016) 7:13404. doi: 10.1038/ncomms13404

9. Chong C, Muller M, Pak H, Harnett D, Huber F, Grun D, et al. Integrated Proteogenomic Deep Sequencing and Analytics Accurately Identify non-Canonical Peptides in Tumor Immunopeptidomes. *Nat Commun* (2020) 11 (1):1293. doi: 10.1038/s41467-020-14968-9
10. Stephens AJ, Burgess-Brown NA, Jiang S. Beyond Just Peptide Antigens: The Complex World of Peptide-Based Cancer Vaccines. *Front Immunol* (2021) 12:696791. doi: 10.3389/fimmu.2021.696791
11. Nelde A, Rammensee HG, Walz JS. The Peptide Vaccine of the Future. *Mol Cell Proteom* (2021) 20:100022. doi: 10.1074/mcp.R120.002309
12. Sharma P, Wagner K, Wolchok JD, Allison JP. Novel Cancer Immunotherapy Agents With Survival Benefit: Recent Successes and Next Steps. *Nat Rev Cancer* (2011) 11(11):805–12. doi: 10.1038/nrc3153
13. Sharma P, Allison JP. The Future of Immune Checkpoint Therapy. *Science* (2015) 348(6230):56–61. doi: 10.1126/science.aaa8172
14. Pardoll DM. The Blockade of Immune Checkpoints in Cancer Immunotherapy. *Nat Rev Cancer* (2012) 12(4):252–64. doi: 10.1038/nrc3239
15. Van Allen EM, Miao D, Schilling B, Shukla SA, Blank C, Zimmer L, et al. Genomic Correlates of Response to CTLA-4 Blockade in Metastatic Melanoma. *Science* (2015) 350(6257):207–11. doi: 10.1126/science.aad0095
16. Rizvi NA, Hellmann MD, Snyder A, Kvistborg P, Makarov V, Havel JJ, et al. Cancer Immunology. Mutational Landscape Determines Sensitivity to PD-1 Blockade in non-Small Cell Lung Cancer. *Science* (2015) 348(6230):124–8. doi: 10.1126/science.aaa1348
17. Tang T, Huang X, Zhang G, Hong Z, Bai X, Liang T. Advantages of Targeting the Tumor Immune Microenvironment Over Blocking Immune Checkpoint in Cancer Immunotherapy. *Signal Transduct Target Ther* (2021) 6(1):72. doi: 10.1038/s41392-020-00449-4
18. Rotte A. Combination of CTLA-4 and PD-1 Blockers for Treatment of Cancer. *J Exp Clin Cancer Res* (2019) 38(1):255. doi: 10.1186/s13046-019-1259-z
19. Liu YT, Sun ZJ. Turning Cold Tumors Into Hot Tumors by Improving T-Cell Infiltration. *Theranostics* (2021) 11(11):5365–86. doi: 10.7150/thno.58390
20. Ylosmaki E, Cerullo V. Design and Application of Oncolytic Viruses for Cancer Immunotherapy. *Curr Opin Biotechnol* (2020) 65:25–36. doi: 10.1016/j.copbio.2019.11.016
21. Kaufman HL, Kohlhapp FJ, Zloza A. Oncolytic Viruses: A New Class of Immunotherapy Drugs. *Nat Rev Drug Discovery* (2015) 14(9):642–62. doi: 10.1038/nrd4663
22. Guo ZS, Liu Z, Bartlett DL. Oncolytic Immunotherapy: Dying the Right Way is a Key to Eliciting Potent Antitumor Immunity. *Front Oncol* (2014) 4:74. doi: 10.3389/fonc.2014.00074
23. Bartlett DL, Liu Z, Sathaiah M, Ravindranathan R, Guo Z, He Y, et al. Oncolytic Viruses as Therapeutic Cancer Vaccines. *Mol Cancer* (2013) 12(1):103. doi: 10.1186/1476-4598-12-103
24. Huang B, Sikorski R, Kirn DH, Thorne SH. Synergistic Anti-Tumor Effects Between Oncolytic Vaccinia Virus and Paclitaxel are Mediated by the IFN Response and HMGB1. *Gene Ther* (2011) 18(2):164–72. doi: 10.1038/gt.2010.121
25. Roy DG, Geoffroy K, Marguerie M, Khan ST, Martin NT, Kmiecik J, et al. Adjuvant Oncolytic Virotherapy for Personalized Anti-Cancer Vaccination. *Nat Commun* (2021) 12(1):2626. doi: 10.1038/s41467-021-22929-z
26. Capasso C, Hirvinen M, Garofalo M, Romaniuk D, Kuryk L, Sarvela T, et al. Oncolytic Adenoviruses Coated With MHC-I Tumor Epitopes Increase the Antitumor Immunity and Efficacy Against Melanoma. *Oncoimmunology* (2016) 5(4):e1105429. doi: 10.1080/2162402X.2015.1105429
27. Lopes A, Feola S, Ligot S, Fusciello M, Vandermeulen G, Preat V, et al. Oncolytic Adenovirus Drives Specific Immune Response Generated by a Poly-Epitope pDNA Vaccine Encoding Melanoma Neoantigens Into the Tumor Site. *J Immunother Cancer* (2019) 7(1):174. doi: 10.1186/s40425-019-0644-7
28. Hamdan F, Martins B, Feodoroff M, Giannoula Y, Feola S, Fusciello M, et al. GAMER-Ad: A Novel and Rapid Method for Generating Recombinant Adenoviruses. *Mol Ther Methods Clin Dev* (2021) 20:625–34. doi: 10.1016/j.omtm.2021.01.014
29. Kanerva A, Mikheeva GV, Krasnykh V, Coolidge CJ, Lam JT, Mahasreshti PJ, et al. Targeting Adenovirus to the Serotype 3 Receptor Increases Gene Transfer Efficiency to Ovarian Cancer Cells. *Clin Cancer Res* (2002) 8(1):275–80.
30. Schumacher TN, Schreiber RD. Neoantigens in Cancer Immunotherapy. *Science* (2015) 348(6230):69–74. doi: 10.1126/science.aaa4971
31. McGranahan N, Furness AJ, Rosenthal R, Ramskov S, Lyngaa R, Saini SK, et al. Clonal Neoantigens Elicit T Cell Immunoreactivity and Sensitivity to Immune Checkpoint Blockade. *Science* (2016) 351(6280):1463–9. doi: 10.1126/science.aaf1490
32. Trandem K, Zhao J, Fleming E, Perlman S. Highly Activated Cytotoxic CD8 T Cells Express Protective IL-10 at the Peak of Coronavirus-Induced Encephalitis. *J Immunol* (2011) 186(6):3642–52. doi: 10.4049/jimmunol.1003292
33. Zhao Y, Liu Z, Li L, Wu J, Zhang H, Zhang H, et al. Oncolytic Adenovirus: Prospects for Cancer Immunotherapy. *Front Microbiol* (2021) 12:707290. doi: 10.3389/fmicb.2021.707290
34. Feola S, Capasso C, Fusciello M, Martins B, Tahtinen S, Medeot M, et al. Oncolytic Vaccines Increase the Response to PD-L1 Blockade in Immunogenic and Poorly Immunogenic Tumors. *Oncoimmunology* (2018) 7(8):e1457596. doi: 10.1080/2162402X.2018.1457596
35. Peltonen K, Feola S, Umer HM, Chiaro J, Mermelekas G, Ylosmaki E, et al. Therapeutic Cancer Vaccination With Immunopeptidomics-Discovered Antigens Confers Protective Antitumor Efficacy. *Cancers (Basel)* (2021) 13(14):3408. doi: 10.3390/cancers13143408
36. Chiaro J, Kasanen HHE, Whalley T, Capasso C, Gronholm M, Feola S, et al. Viral Molecular Mimicry Influences the Antitumor Immune Response in Murine and Human Melanoma. *Cancer Immunol Res* (2021) 9(8):981–93. doi: 10.1158/2326-6066.CIR-20-0814
37. Tahtinen S, Feola S, Capasso C, Laustio N, Groeneveldt C, Ylosmaki EO, et al. Exploiting Preexisting Immunity to Enhance Oncolytic Cancer Immunotherapy. *Cancer Res* (2020) 80(12):2575–85. doi: 10.1158/0008-5472.CAN-19-2062
38. Ylosmaki E, Ylosmaki L, Fusciello M, Martins B, Ahokas P, Cojoc H, et al. Characterization of a Novel OX40 Ligand and CD40 Ligand-Expressing Oncolytic Adenovirus Used in the PeptiCRAd Cancer Vaccine Platform. *Mol Ther Oncolytics* (2021) 20:459–69. doi: 10.1016/j.omto.2021.02.006
39. Blass E, Ott PA. Advances in the Development of Personalized Neoantigen-Based Therapeutic Cancer Vaccines. *Nat Rev Clin Oncol* (2021) 18(4):215–29. doi: 10.1038/s41571-020-00460-2
40. Sahin U, Tureci O. Personalized Vaccines for Cancer Immunotherapy. *Science* (2018) 359(6382):1355–60. doi: 10.1126/science.aar7112
41. Thundimadathil J. Cancer Treatment Using Peptides: Current Therapies and Future Prospects. *J Amino Acids* (2012) 2012:967347. doi: 10.1155/2012/967347
42. Garetto S, Sizzano F, Brusa D, Tizzani A, Malavasi F, Matera L. Binding of Prostate-Specific Membrane Antigen to Dendritic Cells: A Critical Step in Vaccine Preparation. *Cytotherapy* (2009) 11(8):1090–100. doi: 10.3109/14653240903164971
43. Akhtar NH, Pail O, Saran A, Tyrell L, Tagawa ST. Prostate-Specific Membrane Antigen-Based Therapeutics. *Adv Urol* (2012) 2012:973820. doi: 10.1155/2012/973820
44. Yarchoan M, Johnson BA3rd, Lutz ER, Laheru DA, Jaffee EM. Targeting Neoantigens to Augment Antitumour Immunity. *Nat Rev Cancer* (2017) 17 (9):569. doi: 10.1038/nrc.2017.74
45. Martin SD, Coukos G, Holt RA, Nelson BH. Targeting the Undruggable: Immunotherapy Meets Personalized Oncology in the Genomic Era. *Ann Oncol* (2015) 26(12):2367–74. doi: 10.1093/annonc/mdv382
46. Marty R, Kaabinejadian S, Rossell D, Slifker MJ, van de Haar J, Engin HB, et al. MHC-I Genotype Restricts the Oncogenic Mutational Landscape. *Cell* (2017) 171 (6):1272–83e15. doi: 10.1016/j.cell.2017.09.050
47. Laumont CM, Vincent K, Hesnard L, Audemard E, Bonneil E, Laverdure JP, et al. Noncoding Regions are the Main Source of Targetable Tumor-Specific Antigens. *Sci Transl Med* (2018) 10(470). doi: 10.1126/scitranslmed.aau5516
48. Ngwa W, Irabor OC, Schoenfeld JD, Hesser J, Demaria S, Formenti SC. Using Immunotherapy to Boost the Abscopal Effect. *Nat Rev Cancer* (2018) 18(5):313–22. doi: 10.1038/nrc.2018.6

Conflict of Interest: VC is a co-founder and shareholder at VALO Therapeutics. SP is an employee and a shareholder at VALO Therapeutics.

The remaining authors declare that the research was conducted in the absence of any commercial or financial relationships that could be construed as a potential conflict of interest.

Advantages of publishing in Frontiers

OPEN ACCESS
Articles are free to read for greatest visibility and readership

FAST PUBLICATION
Around 90 days from submission to decision

HIGH QUALITY PEER-REVIEW
Rigorous, collaborative, and constructive peer-review

TRANSPARENT PEER-REVIEW
Editors and reviewers acknowledged by name on published articles

Frontiers
Avenue du Tribunal-Fédéral 34
1005 Lausanne | Switzerland

Visit us: www.frontiersin.org
Contact us: frontiersin.org/about/contact

REPRODUCIBILITY OF RESEARCH
Support open data and methods to enhance research reproducibility

DIGITAL PUBLISHING
Articles designed for optimal readership across devices

FOLLOW US
@frontiersin

IMPACT METRICS
Advanced article metrics track visibility across digital media

EXTENSIVE PROMOTION
Marketing and promotion of impactful research

LOOP RESEARCH NETWORK
Our network increases your article's readership